UNIVERSITY OF LIVERPOOL

Inhibiting *Plasmodium Falciparum* IspD, a MEP Pathway Enzyme as a Novel Target for the Development of Antimalarial Chemotherapeutics

Thesis submitted in accordance with the requirements of the

University of Liverpool

For the degree of

Doctor in Philosophy

By

Matthew J Pye

September 2017

Declaration

This thesis is the result of my own work. The results contained within this thesis unless otherwise stated are my own. The material contained within this document has not been presented, or is currently being presented either wholly or in part of any other degree or qualification.

Matthew J Pye

This research was carried out at the University of Liverpool Department of Chemistry Laboratories, and Paediatric Department at Washington University School of Medicine in St. Louis.

Acknowledgements

Throughout my time at the University of Liverpool I have had a challenging but very happy time. I would like to thank all the people that have made both my undergraduate degree and my PhD a pleasurable experience. In particular I would like to thank everybody that gave me advice on work, research or otherwise, and to all the people that were there for me during the difficult times.

I would like to thank my supervisors Dr Neil Berry and Professor Paul O'Neill, firstly for giving me the opportunity to work with them on very interesting research; and secondly for all of their advice, help and support throughout my PhD, without their help this research and my growth as a chemist, would not have been possible. I would also like to thank Dr Audrey Odom and her group for carrying out biological testing on all of our compounds. Many thanks go to all members of the Robert Robinson Laboratories 4th floor both past and present who made me feel very welcome, for all of their support, and for all the good times we have shared. Finally I also want to thank the analytical service team whose generous time enabled me to obtain the results within my PhD.

There are many people I would like to thank and I apologise that I cannot name everybody here. I would like to give special thanks to the following people. Dr Sitthivut Charoensutthivarakul (Nham) who always made time for me, with help with research, as a friend. His knowledge, advice and friendship was, and always will be invaluable to me. I would also like to acknowledge my long time university friends Christopher Riley and Paul McGillan whom I have shared great experiences with, I would like to thank them for all the pub trips, mad ones, coffees, chill time, and of course, all of their help both personal and work related. I want to thank Marta Fernandez-Gimenez again whom I have shared many great experiences with, including all the dinners, all the pints and all the coffees. She could always make me smile and I am forever grateful to have developed such a strong friendship with her over the past 4 years. I also want to thank Dr María Pin Nó for her unwavering friendship, and for putting up with me during the late nights we were in the labs when I wanted a chat; her dedication to her work was always an inspiration to me during my time here. Similarly I would also like to thank Dr Teresa Almeida again for her unwavering friendship, and for frequently cooking me dinner whenever I worked late, both María's and Teresa's kindness were always appreciated it and it got me through many a long day. Finally, I would like to thank Dr Konstantin Luzyanin for being a great friend, mentor and for all his support regarding NMR. A very special thanks goes to my parents and family, my parents have always been very supportive, have always stayed positive and have truly kept me going. My family have been incredible, patient and understanding. They have stuck by me and I would never have made it so far without their immeasurable input. I hope that this thesis and this work does everyone both friends and family proud.

Abstract

Malaria remains one of the world's most widespread and deadly parasitic diseases, killing hundreds of thousands of people per year, most of whom are children under the age of 5 years old. There have been great efforts to deliver novel effective antimalarial chemotherapies over the recent decades, however, the development of such therapies remains a significant challenge. The ability of the malaria parasite to rapidly acquire resistance to chemotherapies makes the disease an ever-present threat to populations living in endemic areas. The emergence of resistance to all current frontline therapies is a fundamental issue. Thus far, all of the successful therapies target the same small number of clinically validated pathways, however, as the same pathway is targeted resistance to the new therapy develops within a matter of years or even months.

More recently, focus has turned to the development of therapies targeting novel pathways and enzymes to circumvent the resistance problem. This research focuses on the inhibition of the methyl erythritol phosphate (MEP) pathway for the chemical interruption of isoprenoid biosynthesis in the malaria parasite. Isoprenoids have a large number of crucial biological roles within all living organisms, however, their synthesis in mammals is enzymatically distinct from the MEP pathway. This potentially allows for the species specific targeting of isoprenoid biosynthesis, thereby making the MEP pathway a highly attractive target for antimalarial drug development. Fosmidomycin has been found to effectively target the second enzyme in the MEP pathway IspC, validating the pathway as amenable to small molecule inhibition. Here, our goal is to target the next pathway enzyme IspD, with the aim of developing a lead candidate to be taken forward as an effective antimalarial therapeutic.

Extensive structure activity relationships (SAR) were carried out on 3 chemotypes: MMV008138 a tetrahydro-β-carboline was recently elucidated to possess potent *Pf*IspD activity; and we were successful in our SAR studies to deliver 2 new compounds that possessed an improved cellular potency (*Pf*3D7 EC_{50} 248 nM (n = 1) and 275 ± 10.5 nM n = 4) one of which possessed an improved pharmacokinetic profile. A targeted HTS identified a 1,2-benzo[*d*]isothiazol-3(2*H*)-one as a potent inhibitor of *Pf*IspD, which is believed to operate through covalent modification of the IspD active site. SAR yielded 4 compounds with improved *Pf*IspD activity (*Pf*IsPD IC_{50} <300 nM) over the hits in the HTS screen, however, cellular potency requires further investigation. Finally, a second HTS screen identified a benzothiazine chemotype as another potent inhibitor of *Pf*IspD. A compound set was synthesised, however, activity of all analogues did not match that of the HTS.

Publications

Molecular interactions between *Plasmodium falciparum* IspD and the Malaria Box inhibitor, (1*R*, 3*S*)-MMV008138

Leah Imlay, Kathryn Price, Matthew Pye, Chandrakala Pidathala, Raman Sharma, Alexandre Lawrenson, Neil Berry, Paul O'Neill, and Audrey Odom John.

Manuscript in preparation.

SAR and DMPK investigations of (1*R*, 3*S*)-MMV008138 a recently discovered inhibitor of *Plasmodium falciparum* IspD

Matthew Pye, Kathryn Price, Chandrakala Pidathala, Alexandre Lawrenson, Raman Sharma, Leah Imlay, Audrey Odom John, Paul O'Neill, and Neil Berry.

Manuscript in preparation

Abbreviations

2D	2-dimensional
Å	Angström
Ac-CoA	Acetyl Coenzyme A
ACN	Acetonitrile
ACT	Artemisinin combination therapy
ADME	Absorption, distribution, metabolism, excretion
ADP	Adeonsine diphosphate
Ar	Argon
Ar	Aromatic
At	*Arabidopsis thaliana*
ATP	Adeonsine triphosphate
AZ	AstraZeneca
B-	Basic site
BITZ	Benzoisothiazolinone
Boc	^{t}Butyloxycarbonyl
BTZ	Benzothiazine
CDC	Center of Disease Control
$CDCl_3$	Deuterated chloroform
CMP	Cytosinne monophosphate
CDPME	4-diphosphocytidyl-2-*C*-methyl-D-erythritol
CDPMEP	4-diphosphocytidyl-2-*C*-methyl-D-erythritol-2-phosphate
CI	Chemical ionisation
cMEPP	2-*C*-methyl-D-erythritol-2, 4-cyclodiphosphate
CTP	Cytosine triphosphate
Cys	Cysteine
CYP	Cytochrome P
CQ	Chloroquine
DCM	Dichloromethane
DCE	Dichloroethane
DDT	Dichlorodiphenyltrichloroethane
DHA	Dihydroartemisinin
DHFR	Dihydrofolate reductase
DHFS	Dihydrofolate synthase
DHPS	Dihydropteroate synthase
DHODH	Dihydroorotate dehydrogenase
DIPEA	Diisopropylethylamine
DMAP	4-Dimethylaminopyridine
DMAPP	Dimethylallyll pyrophosphate (or diphosphate)
DMF	Dimethyl formamide
DMPK	Drug metabolism and pharmacokinetic
DMSO	Dimethyl sulfoxide
DNA	Deoxyribonucleic acid
DTT	Dithiothreitol
dUMP	Deoxyuridine monophosphate
dTMP	Deoxythymidine monophosphate
DXP	1-Deoxy-D-xyulose 5-phosphate
DXS	DXP synthase
ED	Entner-Doudoroff
EDC.HCl	*N*-(3-Dimethylaminopropyl)-*N*'-ethylcarbodiimide hydrochloride

EPR	Electron paramagnetic resonance
ESI	Electrospray ionisation
Et_2O	Diethyl ether
EtOAc	Ethyl acetate
FOS	Fosmidomycin
G	Glyoxylate
G6PD	Glucose-6-phosphate dehydrogenase deficiency
GAP	Glyceraldehyde-3-phosphate
GGPP	Genarylgenaryl pyrophosphate
GHMP	Galacto-homoserine-mevalonate-phosphomevalonate kinase
GP	Glycerate3-phosphate
GSH	Glutathione
GSK	GlaxoSmithKline
GTP	Guanosine triphosphate
HATU	1-[Bis(dimethylamino)methylene]-1*H*-1,2,3-triazolo[4,5-*b*]pyridinium 3-oxid hexafluorophosphate
Heps	Hepatocytes
H. halobium	*Halobacterium halobium*
H. influenza	*Haemophilus influenzae*
His	Histidine
HMG-CoA	(*S*)-3-hydroxy-3-methylglutaryl CoA
HMGPP	4-hydroxy-3-methyl-2-(*E*)-butenyl-4-diphosphate
HMGR	HMG-CoA reductase
HOBT	Hydroxybenzotriazole
HPLC	High performance liquid chromatography
HTS	High throughput screen
IP	Isopentyl-5-phosphate
IPK	Isopentyl phosphate kinase
IPP	Isoentyl pyrophosphate (or diphosphate)
IR	Infra-red
IRS	Indoor residual spray
ITN	Insecticide treated net
KDPG	2-Keto-3-deoxy-6-phosphogluconate
LCMS	Liquid chromatography – mass spectrometry
MDD	Mevalonate diphosphate decarboxylase
MDP	Mevalonate-5-diphosphate
ME	Methyl erythritol
MeOD	Deuterated methanol
MEP	2-*C*-methyl-D-erythritol-4-phosphate
MEP	Methyl erythritol phosphate
Mics	Microsomes
MK	Mevalonate kinase
MMV	Medicines for Malaria Venture
MP	Mevalonate-5-phosphate
mRNA	Messenger ribonucleic acid
MRSA	Methicillin-resistant *Staphylococcus aureus*
Mt	*Mycobacterium tuberculosis*
MVA	Mevalonate
MVADP	Phosphomevalonate decarboxylase
NAD	Nicotinamide adenine dinucleotide (oxidised)
NADH	Nicotinamide adenine dinucleotide (reduced)

NADP	Nicotinamide adenine dinucleotide phosphate (oxidised)
NADPH	Nicotinamide adenine dinucleotide phosphate (reduced)
NMR	Nuclear magnetic resonance
NOE	Nuclear Overhauser effect
NOESY	2D nuclear Overhauser effect spectroscopy
PABA	*para*-aminobenzoate
Pf	*Plasmodium falciparum*
***Pf*CRT**	*Plasmodium falciparum chloroquine resistance transporter*
***Pf*NDH2**	*Plasmodium falciparum NADH : ubiquinone reductase*
PMK	Phosphomevalonate kinase
PP	Pyrophosphate (or diphosphate)
^{cyc}Pr	Cyclopropyl
Pv	*Plasmodium vivax*
RT	Room temperature
SAR	Structure activity relationship
SET	Single electron transfer
TCAMs	Tres-Cantos antimalarial set
TFA	Trifluoro acetic acid
THF	Tetrahydrofuran
ThDP	Thiamine diphosphate
TLC	Thin Layer Chromatography
Tol	Toluene
TCA	Tricarboxylic acid
THBC	Tetrahydro-β-carboline
TMS	Trimethylsilyl
TS	Thymidylate synthase
Ts	Tosyl
UMP	Uridine monophosphate
WHO	World Health Organisation
Z. mobilis	*Zymomonas mobilis*

Contents

Chapter 1:

Introduction to Malaria

Chapter 2:

Optimisation of a Novel *Plasmodium Falciparum* IspD Inhibitor MMV008138

Chapter 3:

Development of Ebsulfur, Ebselen and Benzothiazine Analogues as Inhibitors of *Pf*IspD

Appendix

Chapter 1: Introduction to Malaria and the Methyl Erythritol Phosphate (MEP) Pathway

1.1 Introduction

1.1.1 Global Impact

Despite the concerted efforts over several decades to generate effective antimalarial therapies, malaria remains one of the world's most widespread and deadly parasitic diseases, killing approximately 438,000 people per annum, most of whom are children under the age of five.[1]

The World Health Organisation in 2015 estimated that 212 million people were diagnosed with malaria worldwide, with 90 % of incidence occurring in Africa.[1] Clearly the African continent holds an overwhelming share of the malaria burden, and this causes great economic strain on the countries within this region that suffer from deep poverty.[1] The prevention and treatment of the disease within African countries is responsible for approximately 40 % of all public health spending, increasing further the poverty and economic burden on this region, eventually resulting in the poorest areas being unable to afford prevention and / or treatment methods for the disease.[1,2]

Other malaria endemic areas include central and south East Asia, and the Americas (Figure 1.1). Current estimates predict that half of the world's population, 3.3 billion people, are at risk of contracting the disease. This combined with the issues mentioned above, highlights the need for continued preventative and control strategies in order to reduce both the incidence and mortality rates.[1]

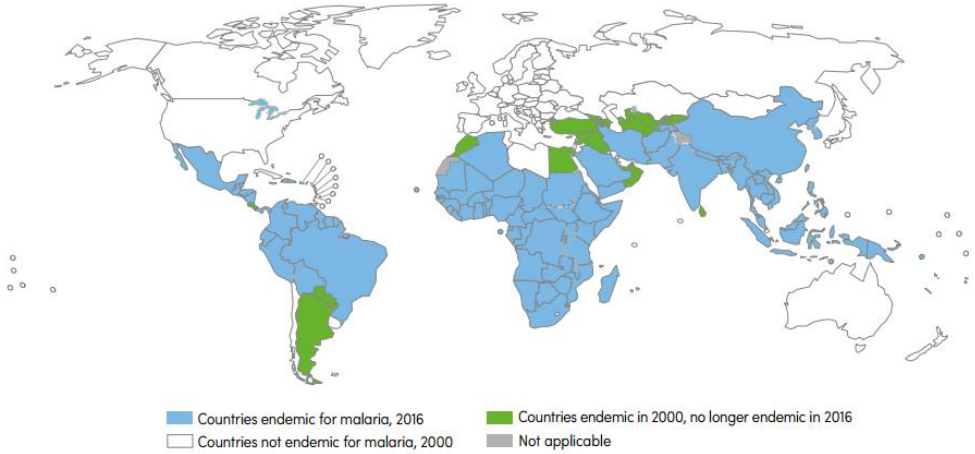

Figure 1.1. Global Distribution of Malaria. Figure reproduced from World Malaria Report 2016. Geneva: World Health Organization; 2016. Permission of use allowed by Creative Commons Licence: CC BY-NC-SA 3.0 IGO.[1]

The malaria parasite is a vector-borne disease caused by the eukaryotic single celled protozoan organism belonging to the genus *Plasmodium* (*Phylum Apicomplexia*).[1] It is transmitted through the bite of a female A*nopheles* mosquito when she takes a blood meal. The malaria parasite

is found in regions where these mosquitos flourish, such as in warm tropical climates including sub-Saharan Africa, south East Asia, and the regions of Americas.[1]

There are five main species of malaria that infect humans; these are *Plasmodium falciparum*, *P. vivax*, *P. malariae*, *P. ovale*, *P. knowlesi*.[1,3] Of these five strains, *P. falciparum*, and *P. vivax* are the most challenging to control, causing the vast majority of malarial infection.[1,4] *P. falciparum* is recognised as the most deadly of these protozoa due to its prevalence throughout Africa, and its widely documented mortality rates.[1] *P. vivax* on the other hand, has higher rates of incidence outside of Africa; it is responsible for approximately 16 million cases per annum and as a result, is a significant cause of mortality outside of the African continent.[1,5]

1.2 General Life Cycle of *Plasmodium*

The *Plasmodium* life cycle is one of complexity allowing for the parasite to evade host immune defence systems.[6,7] As malaria is vector borne, it requires two hosts for its survival and within these hosts there are a total of three key cycles, one of which is a sexual stage which takes place within the mosquito, whist the other two cycles are asexual and take place within the human host. The whole life cycle is displayed in Figure 1.2 and discussed below.

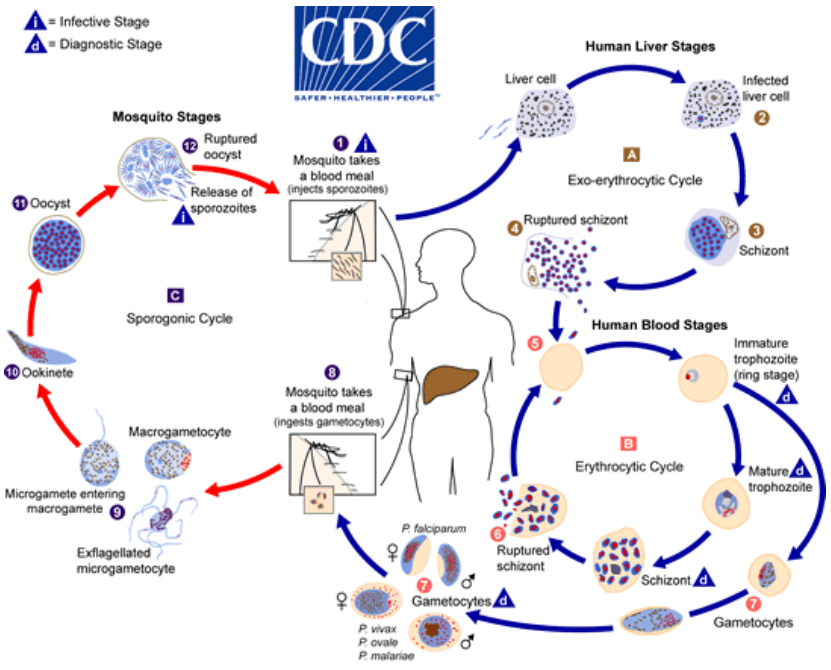

Figure 1.2. The Malaria Life cycle image reproduced from the Center of Disease Control and Prevention (CDC). Image is in the public domain and free of copyright restrictions. CDC - DPDx/ Alexander J. da Silva Melanie Moser.[8]

Liver stage: When an infected mosquito takes a blood meal she injects infective sporozoites from the salivary glands into the human host blood stream; the parasite then rapidly travels through the blood to the liver within 30 minutes of infection, initiating the liver stage. Sporozoites infect liver

cells, where they evade human immune defence systems, mature into schizonts and then replicate asexually into thousands of merozoites. The liver cells become overloaded with parasites, rupture, and release infective merozoites into the blood stream. A process that takes between 6 – 16 days.[9–15]

Blood stage: Merozoites proceed to invade red blood cells beginning the blood stage cycle. Asexual division occurs in the red blood cell causing the parasites to propagate. During this stage the parasite matures, first into trophozoites, also known as the ring form, then into schizonts. This stage digests the host's haemoglobin as a source of amino acids for replication. The schizonts produce approximately 20 merozoites, which then burst through the red blood cell upon schizont rupture ready to infect new red blood cells; this stage takes approximately two days. It is this cycle that causes the clinical manifestations of malaria to take place. Most drugs target the parasite at this stage of its life cycle. After numerous cycles, some of the parasites diverge into male and female gametocytes, which are up taken by another mosquito when she takes a blood meal. The gametocytogenesis stage takes 10 – 12 days, and begins the sexual stage if the parasite life cycle.[6,7,11,15,16]

Mosquito stage: Once the mosquito takes a blood meal the gametocytes are ingested into the mosquito gut and form gametes. The gametes undergo sexual fertilisation and form a zygote followed by an ookinete. This penetrates a cell wall in the gut and develops into an oocyst. The oocyst produces many sporozoites and eventually ruptures allowing the sporozoites to migrate to the salivary glands. The cycle up to this stage takes about 10 – 18 days and the mosquito can be infective for up to two months. The mosquito can then infect a new human host when she takes a blood meal.[15,17,18]

Malaria affects numerous systems within the body. After initial infection, the clinical manifestations of malaria begin to become apparent generally after 10 – 20 days, which are due to the blood stage of the parasite.[1] The early symptoms of malaria infection include fever-like symptoms, such as headache, cough, nausea, aches, and often paroxysm of fever, these symptoms are referred to as uncomplicated malaria which can be caused by all strains of *Plasmodium*.[19,20] In the case of *P. falciparum*, the disease can quickly proceed to complicated malaria if left untreated.[1] Symptoms include vomiting, diarrhoea, anaemia, renal failure, hypoglycaemia and severe respiratory distress all of which can lead to death. Further to this, complicated *P. falciparum* infection can progress to form cerebral malaria, symptoms include headaches, coma, and ultimately death.[20] Though *P. falciparum* is well known to be the most lethal of strains, there is increasing evidence that *P. vivax* mortality is underestimated.[21–28] *P. vivax* has a slightly different life cycle and possesses a dormant liver stage; if these dormant liver stage parasites (hypnozoites) are not eliminated completely, malaria symptoms can relapse weeks, or even months after treatment. Both strains should be treated as serious, and both strains are becoming difficult to treat due to the emergence of drug resistance.[5,29–33]

1.3 Malaria Prevention and Treatment

1.3.1 Vector Control

Vector control is an integral part in reducing incident rates in the fight against malaria. Between 2000 – 2015 case incidence has dropped globally by 41 %, and 21 % between 2010 – 2015, this can in part be attributed to effective vector control.[1] There are three strategies for the protection of individuals in high risk areas; indoor residual spray (IRS), insecticide treated nets (ITN), and vaccines.[1] The insecticide dichlorodiphenyltrichloroethane (DDT) (**1**) (Figure 1.3), was the first efficacious IRS in successfully reducing malaria transmission worldwide.[34] Unfortunately, however, the fallout from using **1** led to extensive environmental damage particularly to birds.[34–36] The compound is highly lipophilic and resistant to metabolism, meaning it has a long half-life, and has a risk of bioaccumulation.[34,37] **1** was classified as being probably carcinogenic to humans, these factors, coupled with emerging mosquito resistance to the compound, eventually led to the substance use being banned.[34,37,38]

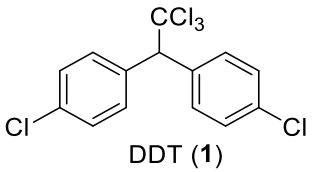

DDT (**1**)

Figure 1.3. DDT (1).

Other IRSs with a better safety profile have been introduced such as pyrethroid insecticides which, though more expensive than **1**, are the only insecticide recommended by the WHO for use as both IRSs and on ITNs.[1,39] Once again, however, resistance is emerging for pyrethroids and eventually new insecticides will need to be developed to continue to aid a fall in incidence rates.[1,40] The effectiveness of IRSs and ITNs has been substantial, in sub-Saharan Africa the proportion of the population sleeping under an ITN or protected by an IRS has risen to 51 % in 2015, compared with 37 % in 2010, this has led to both a reduction in incidence rates, along with a reduction in mortality rates, highlighting the importance of this strategy as a preventive method.[1]

The development of a working vaccine against malaria would be a significant feat in aiding the prevention of the disease. A number of vaccine development projects are currently on-going, however, only one vaccine, RTS,S/AS01, has completed phase III clinical trials. After administration of the required four doses, RTS,S/AS01 demonstrated a reduction of incidence of uncomplicated malaria by 39 %, and severe malaria by 31 % in children ages 5 – 17 months. In 2018, a pilot scale vaccination is due to begin, which if successful, could begin wide scale use of this vaccine as another weapon in the arsenal of malarial preventative measures.[1]

1.3.2 Antimalarial Chemotherapy

Indeed, whilst vector control is providing aid in high risk areas where malaria is a burden, it is only a prevention strategy, and until a viable vaccine is fully developed, drug chemotherapy will remain crucial in the fight against malaria both as a preventative measure and as a treatment option. This following section will discuss past and current antimalarial therapeutics categorised by class and mode of action.

1.3.2.1 Quinolines

It is true that most of the most efficacious antimalarial therapeutics are, or have been, derived or inspired from natural products. Often in drug discovery programmes it is ill-advised to use natural products as starting points for drug optimisation, due to the poor drug like properties of these compounds, difficulty in isolation, and often highly complex synthetic routes, where isolation is a not an option. Ultimately these issues mean that natural product use can be very cost ineffective. Despite this, malaria treatment has been largely successful utilising natural products as a basis for further candidate development.[41]

The first mainstream antimalarial compound quinine (**2**) (Figure 1.4), is a compound belonging to the quinoline class. Indeed quinine is a natural product, and is isolated from the bark of the Andean *Cinchona* tree. It was the only known antimalarial drug for over 300 years and was discovered almost 400 years ago, even with this long history of use, it remains an efficacious treatment in many regions where malaria is prevalent.[42]

Quinine is a type of alkaloid and was first isolated by Pelletier and Caventou in 1820.[42] It is a chiral 4-aminoalcohol-quinoline, can be considered as a small molecule (Mr <500 $gmol^{-1}$), and shows some favourable physiochemical properties. The limitation of quinine from natural sources is associated with the difficulty in isolation of large enough quantities to fulfil the demand for the drug. Attempts towards the total synthesis of quinine was first described by Woodward and von Doering in 1945, however, the synthesis was too complicated for commercial use and also non-stereoselective.[43,44] It was not until the beginning of the 21st century that the first stereoselective synthesis of quinine was successfully achieved by Stork, since then, in 2004, Kobayashi and Jacobsen have independently also synthesised the enantiopure molecule.[45–47]

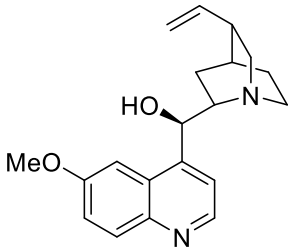

Quinine (**2**)

Figure 1.4. Quinine (2).

Due to the difficulty in both synthesis and isolation of quinine, efforts shifted to the synthesis of simpler alternatives to cope with the demand for antimalarial therapeutics. The discovery of methylene blue (**3**) (Figure 1.5) in 1891 by Ehrlich, which was advantageous due to its simple synthesis, cost effectiveness, and accessibility to large scale synthesis.[42,48] This prompted the development of the second synthetic antimalarial, pamaquine also known as plasmoquine (**4**) (Figure 1.5) by German scientists in the 1920s.[49] Pamaquine belongs to the 8-aminoquinoline template and was efficacious treatment at preventing *P. vivax* relapse, the first compound of its kind to accomplish such a feat.[50–52] Pamaquine (**4**) shows activity against the liver stage of the parasite and hypnozoites. It was also moderately active against the blood stage of *P. vivax* and *P. malariae*, however, inactive against blood stage *P. falciparum* infection.[50–52] Despite this, it was very effective against the sexual stage of the *P. falciparum*, more specifically, it showed potent gametocytocidal activity.[52] However, though these are promising results, toxicity issues were found with this class of chemotype. It was later identified that toxicity was particularly observed with glucose-6-phosphate dehydrogenase deficient (G6PD) patients, who suffer from haemolytic anaemia if they take this drug.[50–52]

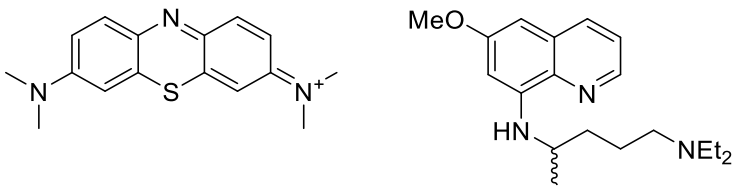

Methylene blue (**3**) (±) Pamaquine (**4**)

Figure 1.5. Methylene blue (3), Pamaquine (4).

It was believed that the basic side chain of pamaquine was important for compound efficacy, this led to the synthesis and discovery of Mepacrine (**5**) (Figure 1.6) by Bayer.[41,48] Although not a quinoline this aminoacridine does share a similar structure and was found to be efficacious against the parasite, but showed no advantages over quinine in terms of safety and physiochemical profile.[41,48] Bayer therefore decided to remove the acridine portion of the core, re-utilising the quinoline core of quinine, leading to the development of potentially the most efficacious compound for the eradication of the parasite, chloroquine (**6**) (Figure 1.6).

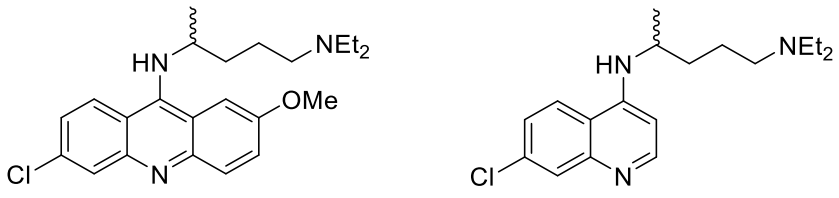

(±) Mepacrine (**5**) (±) Chloroquine (**6**)

Figure 1.6. Mepacrine (5), Chloroquine (6).

6 was used extensively as the main treatment for malaria for the decades following World War II due to its high efficacy, low production cost, high scalability and low rates of major side effects. This made chloroquine the gold standard for antimalarial chemotherapy.[41,42,48]

The mechanism of action of the 4-aminoquinoline / 4-aminoalcohol-quinoline template is believed to be the inhibition in the formation of hemozoin (**10**) (Figure 1.7). When the parasite is in the blood stage, it digests the protein portion of haemoglobin to obtain the essential amino acids it needs to survive and replicate. As a by-product, haem (**7**) is generated and can be autooxidised to a hematin monomer (**8**) both are toxic to the parasite. To circumvent the toxicity, the parasite dimerises **7** or **8** to a hematin dimer (**9**) which is crystallised to a non-toxic form known as hemozoin (**10**) within the parasitic food vacuole.[53–55] The 4-aminoquinoline drug class, is believed to complex with free haem, inhibiting the formation of haematin, and increasing the levels of toxic haem within the parasite, resulting in parasite death.[54,56–64]

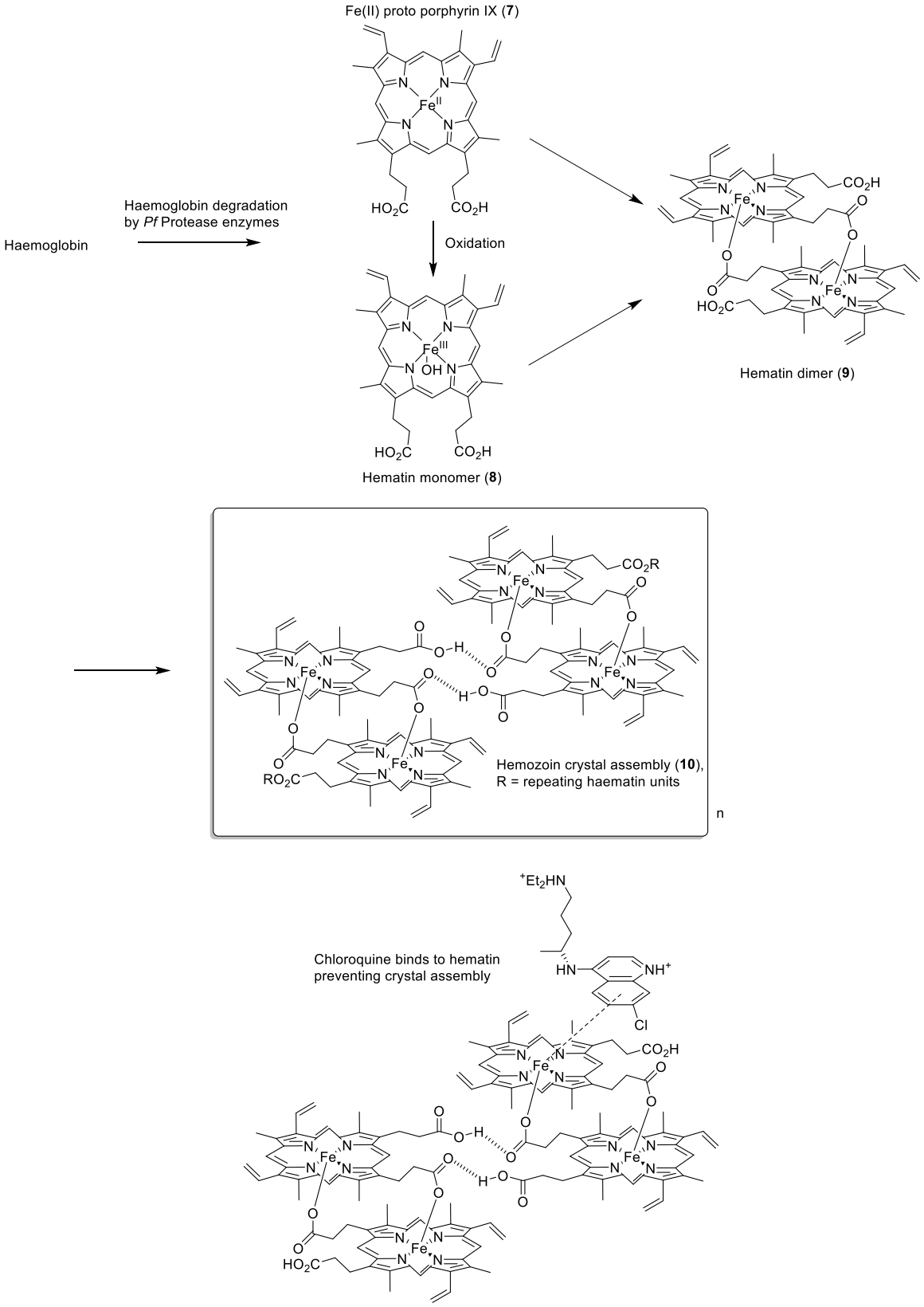

Figure 1.7. Inhibition of hemozoin (10) formation by chloroquine (6).

Unfortunately due to the over use of chloroquine (**6**), resistance to the drug developed in the late 1950s and early 1960s.[65] This resulted in the loss of efficacy of the drug, and **6** is now no longer

recommended for treatment of *P. falciparum*.[66] The generally accepted mechanism of resistance to **6** involves a point mutation in the *Plasmodium falciparum* chloroquine resistance transporter (*Pf*CRT) gene in which lysine76 is converted into threonine (K76T) in the protein chain.[67–70] **6** can exist in protonated and unprotonated forms at physiological pH, however, only the unprotonated form is membrane permeant. Upon administration, unprotonated **6** diffuses into the red blood cell, and then the parasite, before making its way to the parasite digestive vacuole.[54] This vacuole is acidic and protonates one or both of the basic nitrogen atoms in **6**, this removes the drugs ability to diffuse back out of the digestive vacuole, allowing for accumulation of the drug, here is where the drug binds to free haem, causing parasite death.[62,63] The *Pf*CRT is a transmembrane transporter protein found in the membrane of the digestive vacuole.[54,67] In chloroquine-sensitive strains of *P. falciparum*, the K76 amino acid residue is positively charged, which will repel the also positively charged chloroquine away from the transporter. In resistant strains, however, the mutation to T76 results in charge loss, allowing **6** to associate with the transporter, which facilitates the removal of the drug out of the digestive vacuole.[71–73] There have been efforts to develop chloroquine resistance reverser drugs, which has been successfully carried out *in vitro*. Common features of these compounds are two aromatic side chains believed to interact with the substrate binding site of *Pf*CRT, and a basic amino-alkyl chain which after protonation, is thought to restore the positive charge that repels chloroquine away from the transporter.[64] The mechanism of resistance is depicted in Figure 1.8.

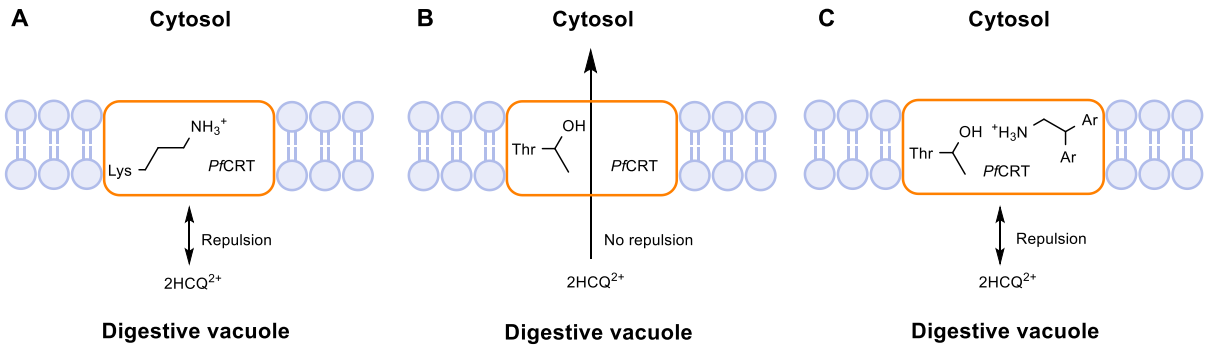

Figure 1.8. Chloroquine resistance transporter A) unmutated (chloroquine sensitive) B) mutated (chloroquine resistance) C) Chloroquine resistance reversed. $2HCQ^{2+}$ equals doubley protonated chloroquine

To overcome this resistance problem, new 4-aminoquinoline candidates were developed. Modifying the alkyl chain to an aromatic linker led to the development of amodiaquine (**11**) in the late 1940s, and it was discovered to be efficacious against chloroquine resistant strains in the early 1950s.[74–76] The main drawback of **11** is that its metabolites can show unacceptable levels of hepatoxicity in certain individuals (a proposed mechanism to hepatoxicty is depicted in Figure 1.9), this restricts its use as a prophylactic and treatment, however, it is still in use as part of an artemisinin combination therapy (ACT) with artesunate (**46**) (see **Section 1.3.2.5**).[66,75–77]

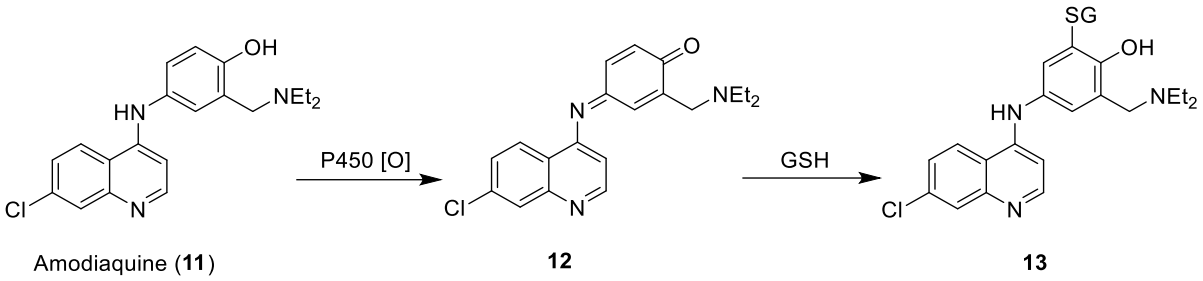

Amodiaquine (**11**) **12** **13**

Figure 1.9. Amodiaquine (11) and its proposed route to heptoxicity *via* P450 oxidation to compound 12, followed by reaction with glutathione forming compound 13.

In the 1960s a bis-4-aminoquinoline was developed which contains two quinoline cores, named piperaquine (**14**) (Figure 1.10).[78] Despite being very effective against both chloroquine sensitive and resistant strains, resistance to this drug developed quickly, and new alternatives needed to be found.[64,78] Though there is evidence of resistance, piperaquine is marketed as part of a combination therapy with dihydroartemisinin.

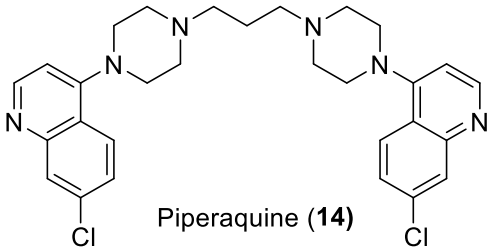

Piperaquine (**14**)

Figure 1.10. Piperaquine (14).

Mefloquine (**15**) (Figure 1.11) a 4-aminoalcohol-quinoline was discovered in the 1970s and due to urgent demand for new antimalarial chemotherapies; it was brought to market and administered without phase III trials. The drug, though carrying some health concerns, is currently still used as a treamtent option, as part of an ACT in combination with artesunate due to the drugs extensively long half-life.[64,79–81] More recently in the 1990s ferroquine (**16**) (Figure 1.11) has been developed which contains a ferrocene moiety within the basic side chain of the 4-aminoquinoline structure. It is highly active against chloroquine resistant strains and is currently undergoing phase II clinical trials.[64,82–85] In 2003, O'Neill *et al.* developed Isoquine (**17**) (Figure 1.11), a regioisomer of **11**, in order to circumvent potential metabolism to a toxic quinone-imine.[76] One of the *N*-ethyl groups was replaced with *N*-^{t}Bu, forming *N*-^{t}Bu-isoquine (**18**) (Figure 1.11), which displayed very good activity against chloroquine resistant strains, and entered phase I clinical trials.[76,86] Unfortunately, the compound did not progress further as it showed no advantage over **11** in terms of safety during these trials.[87]

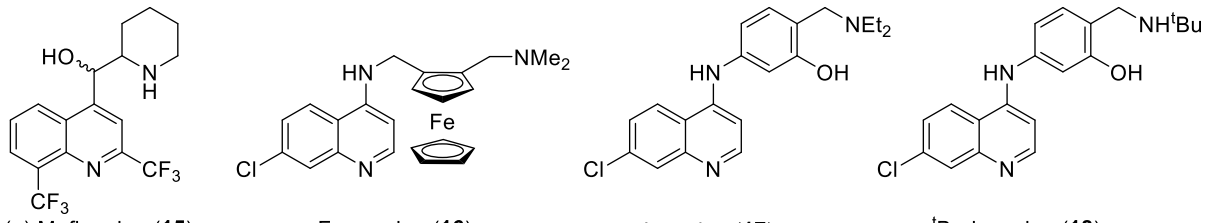

Figure 1.11. Mefloquine (15), ferroquine (16), isoquine (17), ^{t}Bu-isoquine (18).

After the success of pamaquine (**4**) against both liver and blood stages of the parasite, attention turned back to 8-aminoquinolines as a template for antimalarial candidate development. Simple removal of the ethyl groups of the terminal amine, resulted in the compound primaquine (**19**) (Figure 1.12).[52] **19** was discovered to be less toxic than **4**, and possessed improved efficacy against the liver stage of the parasite, particularly for *P. vivax*.[52,88] It is also effective against the blood stage of *P. vivax*, though interestingly, it is not effective for blood stage *P. falciparum*.[52,89–91] However, it is outstanding in clearing gametocytes of *P. vivax* and *P. falciparum* in a single dose (between 0.25 mg / kg and 7.5 mg / kg in combination with an artemisinin based drug), therefore it is recommended as a prophylactic, especially in regions suffering from high *P. vivax* incidence.[52,66,92] The downside to **19** is that it still toxic for G6PD deficient patients, causing hemolysis, and this population cannot take this drug.[50,52,93,94] To date **19** is the only marketed antimalarial that is able to clear the dormant liver stage parasites for *P. vivax*.[52] Another 8-aminoquinoline is currently undergoing phase III clinical trials, named tafenoquine (**20**) (Figure 1.12). **20**, like **19** and **4** is efficacious in the treatment of the liver stage of *P. vivax*, it has the advantage of a better safety profile, longer half-life and thus the potential for single dose cure. Once again, however, G6PD patients cannot take this drug due to the potential to cause hemolysis.[52,95–97]

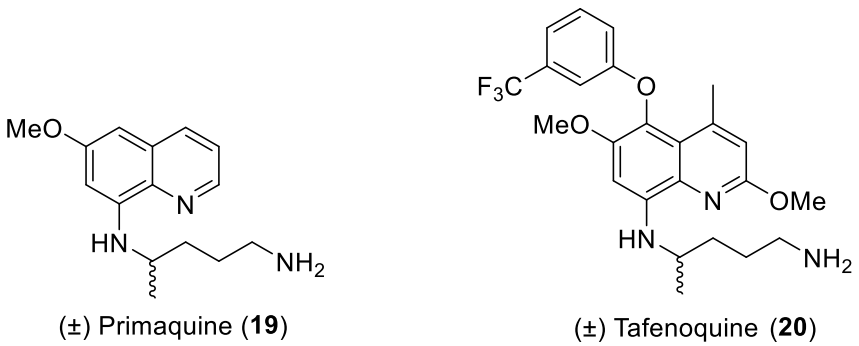

Figure 1.12. Primaquine (19) (left), tafenoquine (20) (right).

The exact mechanism of action of the 8-aminoquinoline template, is yet to be elucidated, at present **19** and likely **4**, are believed to act as prodrugs.[52] During metabolism, **19** can be oxidised at the 5-position of the quinoline ring, forming 5-hydroxy-primaquine (**21**), which is rapidly oxidised to the quinone-imine (**22**), before demethylation of the 6-OMe group forming **23** (Figure 1.13). This

compound could be responsible for its antimalarial activity, and likely the side effects associated with G6PD deficiency, but exactly how is still unknown, it should also be noted that other potentially active primaquine metabolites have been identified.[52,98] In the case of tafenoquine (**20**), one could envisage that this active metabolite can still be formed, as **20** harbours an O-aryl linker at this 5-position.

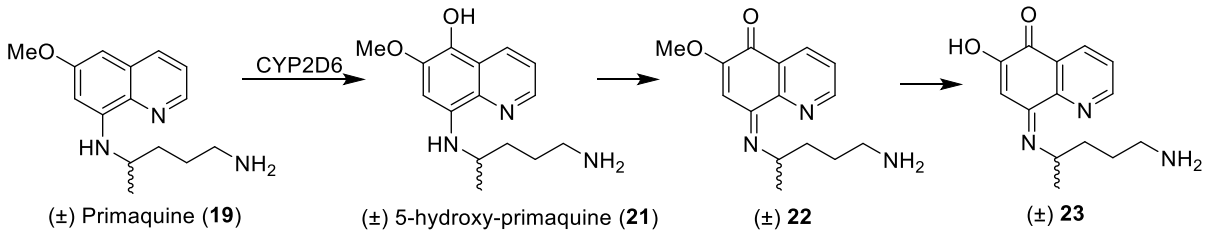

Figure 1.13. Routes to potential primaquine reactive metabolite(s).

1.3.2.2 Antifolate inhibitors

Dihydrofolate (**24**) (Figure 1.14) and folate-derived compounds are important cofactors involved in the supply of one carbon subunits for the essential biosynthesis of methionine, serine, glycine, and also nucleic acids, where the latter, is also needed for the generation of DNA.[99–102] Parasite growth and survival, is highly dependent on compound **24**. Humans lack the biosynthesis pathways necessary for production of **24**, and rely on folate intake from the diet.[99,101,102] Malaria, however, does have the ability to synthesise **24**, and it does so *via* the reaction of a phosphorylated pteridine compound (derived from a purine precursor) with *para*-aminobenzoate (PABA) to form dihydropteroate. L-glutamate is then coupled with dihydropteroate which completes the biosynthesis. Dihydropteroate synthase (DHPS) is the enzyme responsible for the coupling of PABA to the pteridine portion of the compound, and is an enzyme that humans lack, this makes it an attractive target for antimalarial therapeutics.[99,101–103]

24 itself is not biochemically active until it is reduced to tetrahydropteroate.[101] 5,10 Methyltetrahydropteroate, is used in the biosynthesis of nucleotides, more specifically, it transfers a methyl group to deoxyuridine monophosphate (dUMP) forming deoxythymidine monophosphate (dTMP).[99,101–103] This results in the formation of **24** which needs to be reduced back to tetrahydropteroate, this is done by the enzyme dihydrofolate reductase (DHFR).[99,101–103] This enzyme is present in humans and malaria, however, the structural differences between the two enzymes means the malarial form can be targeted safely.[104,105] It is also very sensitive to inhibition and so has been targeted for antimalarial drug development.[101] Inhibition of this enzyme results in dTMP biosynthesis cessation, resulting in the failure of parasitic DNA synthesis.[99–103]

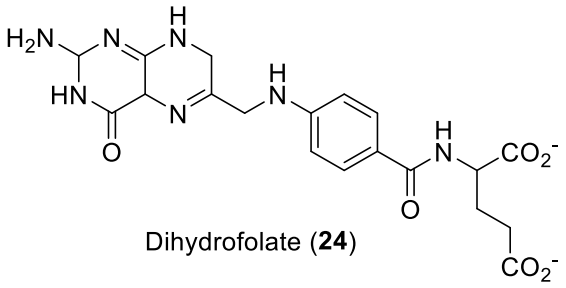

Figure 1.14. Dihydrofolate (24) structure.

Inhibitors targeting DHFR and DHPS enzymes are placed into different classes, for DHFR, inhibitors are termed class I, for DHPS, inhibitors are termed class II. The first inhibitor of DHFR (class I set) was proguanil (**25**) (Figure 1.15), discovered in the 1940s and demonstrated improved activity over quinine against avian malaria with an improved therapeutic index, which led to its use in humans.[105,106] The mechanism of action of **25** was elucidated after it was found to be a prodrug.[105,107] The compound is metabolised to cycloguanil (**26**) (Figure 1.15), which contains a triazine moiety, which was confirmed to target DHFR.[108] When used alone, this drug is recommended as a prophylactic, it can also be used as part of a combination based therapy, with chloroquine (**6**), or atovaquone (**39**).[109–112] The combination of atovaquone (**39**) with proguanil (**25**), is the only other method effective to clear parasites from the liver stage without the use of primaquine (**19**), however, this combination does not kill hypnozoites in the case of *P. vivax* and cannot be used to prevent relapsing malaria.[109,113]

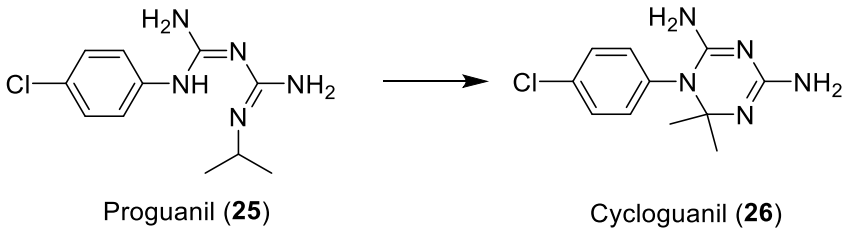

Figure 1.15. Proguanil (25) is metabolised to the active cycloguanil (26).

To optimise further the efficacy of **25**, structural activity relationship studies were undertaken, which led to the identification of chlorproguanil (**27**) (Figure 1.16). Also a prodrug, it was simply developed by incorporation of an extra chlorine atom within the phenyl portion of the drug. **27** is more potent than **25**, and has been used as part of a combination therapy with dapsone (**29**).[105]

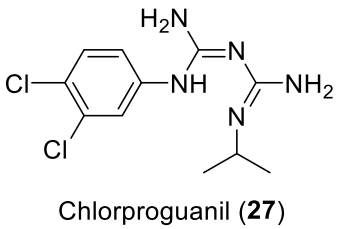

Figure 1.16. Chlorproguanil (27).

Pyrimethamine (**28**) (Figure 1.17), a compound sharing structural similarity to **26**, is a 2,4-diaminopyrimidine. First discovered in the late 1940s, it was believed due to this structural similarity, that this class of compounds could also show efficacy against the parasite, and the folate pathway.[105,114] This hypothesis indeed proved to be true, and **28** is one of the most widely used DHFR inhibitors. It is used in combination with sulfadoxine, providing potent antimalarial activity.[105]

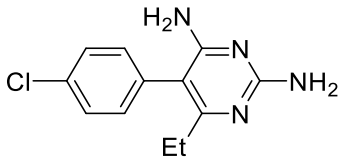

Pyrimethamine (**28**)

Figure 1.17. Pyrimethamine (28).

The class II set of inhibitors targeting DHPS, are mainly sulfa-drugs. These drugs compounds block the *de novo* synthesis of folate, which gained interest due to the parasite specificity of the DHPS enzyme. Unfortunately most of the drugs belonging to this class showed poor efficacy and high levels of toxicity, which ruled them out as a monotherapy.[105] Fortuitously, however, it was observed that the compounds show a synergistic effect when taken as part of a combination with class I inhibitors, leading to the development of antifolate combination therapies.[105]

The first compound showing activity against DHPS was dapsone (**29**) (Figure 1.18) and it is the most potent compound to date.[105] **29** was first discovered in 1908 as a result for a search of molecules to produce azo dyes. However, it was not until the 1930s that its antimicrobial effects were observed, when Buttle *et al*. and Fourneau *et al*. explored its chemotherapeutic effect against numerous pathogens. They observed that **29** was able to suppress the growth of pathogens including mycobacteria and crucially the malaria parasite.[105,115] It does possess high toxicity and development of the drug was halted.[116,117] It can be taken as part of a combination therapy with pyrimethamine (**28**), marketed as Maloprim. It has also been used, as stated above as part of a combination with chloroproguanil (**27**).[105]

Pyrimethamine (**28**) has also been combined with sulfadoxine (**30**) (Figure 1.18), which demonstrates a long half-life >80 hours, marketed as Fansidar.[118] Compared with Maloprim, Fansidar, shows a much better therapeutic window, as the half-life of dapsone (**29**) is approximately 24 hours, after this time, the drug synergy with pyrimethamine (**28**) begins to fall.[119,120] Therefore, Fansidar has been much more widely used.

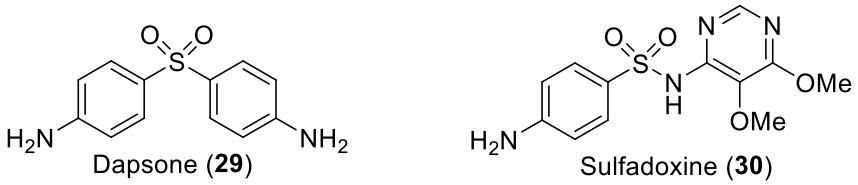

Figure 1.18. Dapsone (29), sulfadoxine (30).

Like the quinoline series of compounds, resistance has become a major issue concerning the efficacy of these drugs. A single point mutation in the DHFR enzyme at codon 108 serine (S) to asparagine (N) or threonine (T) (S108N/T) is sufficient in reducing efficacy of pyrimethamine (**28**) by 100 fold.[121–125] In order to circumvent the problem, novel antifolate inhibitors must be developed to address this issue.

A potential solution was found when the Walter Reed Army Institute of Research discovered WR99210 (**31**) (Figure 1.19), which showed good *in vitro* efficacy against pyrimethamine resistant strains with mutated DHFR. However, it suffered the drawback of having poor oral bioavailability, which gave hindered *in vivo* potency.[126,127] Yuthavong *et al.* reasoned this could be due to the basicity of the triazine moiety in the drug, to test the hypothesis they synthesised P65 (**32**) (Figure 1.19), a less basic 2,4-diaminopyrimidine mimic of **31**, which demonstrated improved oral bioavailability in rats, 83 % *vs* <1 %, and thus improved *in vivo* efficacy. Using structure based studies and X-ray crystallography; the group were able to develop a potent inhibitor of wild type, and 4-point mutated *Pf*DHFR, with greater affinity for this enzyme, than the human isoform, named P218 (**33)** (Figure 1.19). This resulted in the molecule potentially possessing a good safety profile; at present this drug is in phase I clinical trials.[127]

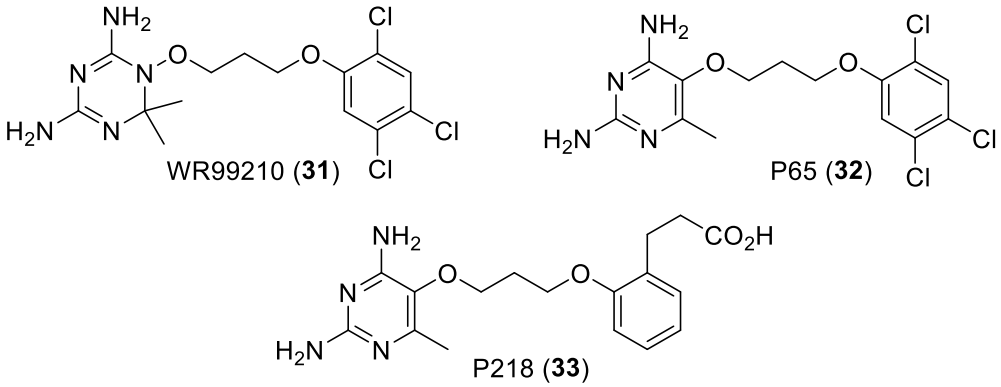

Figure 1.19. WR99210 (31), P65 (32), P218 (33).

1.3.2.3 Pyrimidine Biosynthesis Inhibitors

A closely related biosynthetic pathway to the folate pathway is the *de novo* biosynthesis of pyrimidines. The two pathways are linked *via* the enzyme thymidylate synthetase (TS), indeed TS is part of the bi-functional DHFR protein, also named DHFR-TS, a validated drug target.[103,128] The biosynthesis pathway contains six linear, enzyme-catalysed steps, starting from biacarbonate, glutamine, and adenosine triphosphate, finishing with uridine monophosphate (UMP).[103,129] The pathway though present in mammals can be targeted, as mammals have efficient pyrimidine salvage mechanisms to support DNA synthesis, whereas parasites have poor salvage ability.[130,131]

Whilst the first few enzymes of the pathway are poorly characterised, the fourth enzyme in the pathway dihydroorotate dehydrogenase (DHODH), responsible for the oxidation of dihydroorotate to orotate, has been of particular interest for small molecule inhibition.[130,132–136] It has been demonstrated that human DHODH and malaria DHODH have different binding sites for the same inhibitor leflunomide, meaning that the enzyme can be potentially targeted specifically.[137] Further to this, DHODH is linked to the electron transport chain in the malaria parasite by the ubiquinone co-enzyme.[136] The electron transport system is a validated target within the malaria parasite.[103,134,137,138] Thus it could be possible that inhibition of DHODH could show synergistic effects with both folate inhibitors, and electron transport inhibitors.

Numerous high-throughput screens (HTS) have been carried out and indeed inhibitors specifically targeting *Pf*DHODH have been successfully identified. These include, Genz 667348 (**34**), MMV020439 (**35**), MM007571 (**36**), DSM1 (**37**) and DSM265 (**38**) (Figure 1.20).[139–142] The most promising candidate came from the HTS that identified DSM1 (**37**), led by Phillips *et al*.[140] **37** had very good *in vitro* potency (*Pf*DHODH IC_{50} 47 ± 22 nM, *Pf*3D7 EC_{50} 79 ± 45 nM) but its main drawback was its poor pharmacokinetic profile, and thus, poor *in vivo* potency.[140] The group used structure-guided studies to optimise the molecule, which led to the development of DSM265.[143] This shows excellent *in vivo* potency and DMPK properties, it is currently in phase IIa clinical trials and if successful the molecule will be the first chemotype targeting DHODH.[144]

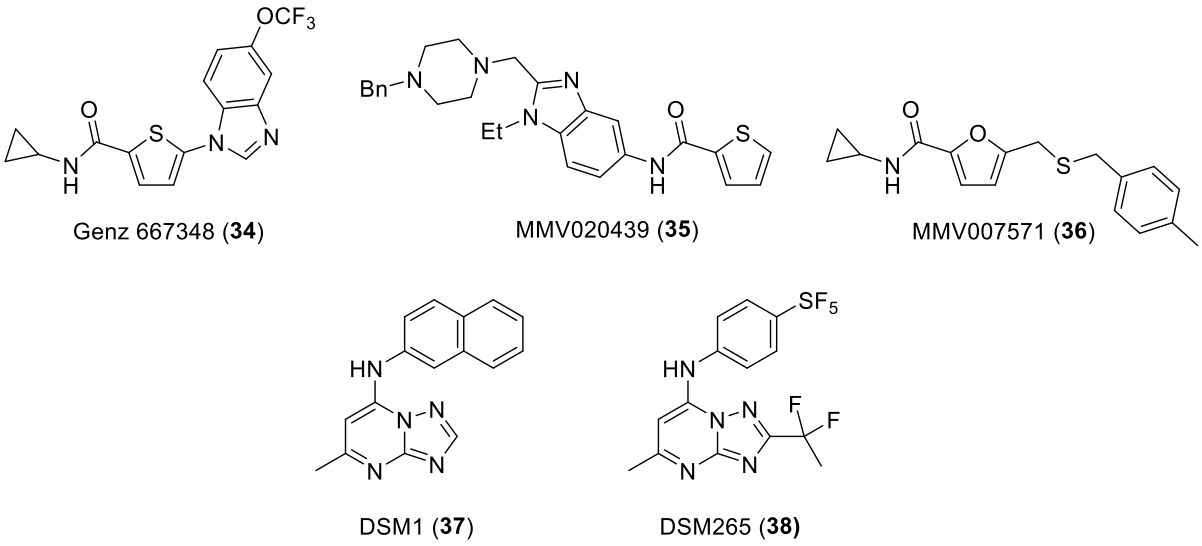

Figure 1.20. Inhibitors of *Pf*DHODH.

1.3.2.4 Cytochrome *bc*1 Inhibitors

The cytochrome *bc*1 complex is used as part of the mitochondrial electron transport chain, a crucial part of the respiratory cycle (Figure 1.21). The complex is used to transport protons across the mitochondrial membrane, into the intermembrane space. It does this *via* the oxidation of two ubiquinol molecules to two ubiquinone molecules followed by reduction of one bound ubiquinone molecule to ubiquinol. The net result is 4 protons are transported into the intermembrane space, while 2 protons are gained from the mitochondrial matrix. As mentioned in the previous section, the electron transport chain and pyrimidine biosynthesis are linked together, cytochrome *bc*1 provides the required ubiquinone molecule for DHODH for orotate production.[136]

Atovaquone (**39**) (Figure 1.22) a 2-hydroxynapthoquinone was the first commercially used *bc*1 inhibitor. Discovered first in the 1980s it demonstrated efficacy against the parasite, and was one of the few quinones found stable to human microsomes.[145] **39** acts as a competitive inhibitor of ubiquinol at the *bc*1 complex.[146] This results in two situations; first the electron transport chain is halted, as protons can no longer be passed into the mitochondrial intermembrane space, meaning that a proton gradient is no longer generated resulting in the loss of function of the ATP-synthase enzyme further down the chain.[147] Second, a pool of ubiquinone is no longer generated for the enzyme DHODH, resulting in the loss of pyrimidine biosynthesis.[148] The loss of mitochondrial function ultimately leads to parasite death.[148–153]

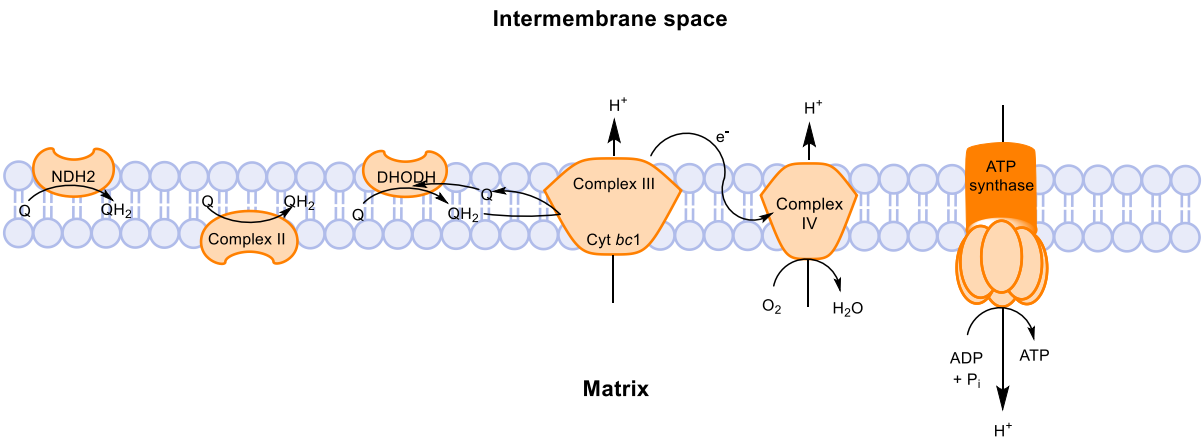

Figure 1.21. Simplified electron transport chain in malaria.

Resistance to **39** as a monotherapy developed quickly, and can be attributed to the single point mutations of leucine 271 to valine (L271V), lysine 272 to arginine (K272R), isoleucine 258 to methionine (I258M), phenylalanine 267 to isoleucine (F267I), or tyrosine to serine / cysteine / asparagine (Y268S/C/N).[64,149,154,155] This means that **39** is not recommended for use as a monotherapy or as a prophylaxis on its own, however, the same point mutation Y268/N has also emerged for malarone (atovaquone (**39**) / proguanil (**25**)).[149,156] The result is a 1000 fold loss of activity for any single point mutation.[154,157]

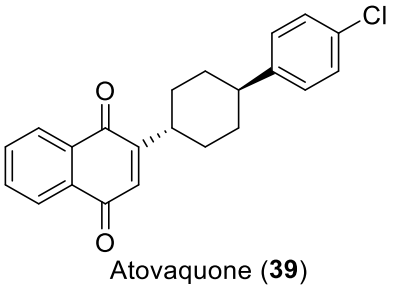

Figure 1.22. Atovaquone (39).

The emergence of resistance to **39** has led to the development of novel drug molecules against the electron transport chain. ELQ-300 (**40**) (Figure 1.23), a quinolone-3-diarylether, has been developed by Nilsen *et al*. in 2013.[147] It demonstrates good potency (PfDd2 IC_{50} 2.2 nM) and is active against liver, blood, and sexual stages of *P. falciparum* and *P. vivax*. It selectively targets the *bc*1 complex, and possesses good drug metabolism and pharmacokinetic (DMPK) properties, and despite poor aqueous solubility, it has good oral bioavailability in mice at efficacious doses (~100 % at 0.3 mg / kg).[147] Promisingly **40** shows synergy with **39**, which could help slow the resistance problem.[158] Whilst other enzymes of the electron transport chain have been targeted, nothing as of yet has reached clinical trials. At present ELQ-300 is the most promising lead, it was in preclinical development as of 2015.[159]

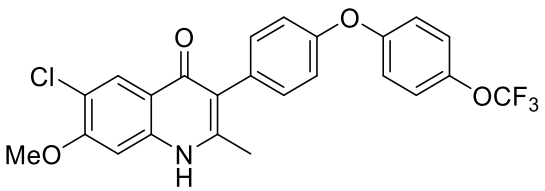

ELQ-300 (**40**)

Figure 1.23. ELQ-300 (40).

The O'Neill group were successful in the synthesis of another inhibitor of the electron transport chain, however, this time the specific target was not *bc*1, instead it was NADH : ubiquinone reductase (PfNDH2), involved in ubiquinol production. After high-throughput screening and medicinal chemistry optimisation two potent inhibitors of the enzyme were discovered, CK-2-68 (**41**) and SL-2-25 (**42**) (Figure 1.24). Both also showed potent antimalarial activity *in vitro* and *in vivo*, low toxicity and high metabolic stability. The drawback of the series was poor solubility of the compounds (<5 μM at pH 7.4) and as such did not pass preclinical development stage.[160,161]

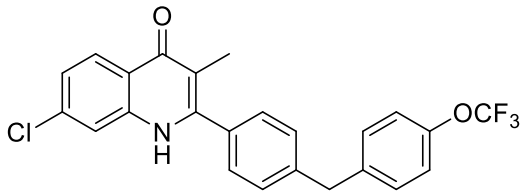

CK-2-68 (**41**)

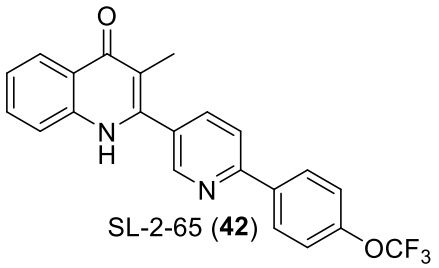

SL-2-65 (**42**)

Figure 1.24. CK-2-68 (41) and SL-2-25 (42).

1.3.2.5 Artemisinins and Endoperoxides

Artemisinin (**43**) and its derivatives (**44** – **46**) (Figure 1.25), often combined with another agent, are currently the frontline therapies against the malaria parasite. Like quinine (**2**) before it, artemisinin (**43**) is also a natural product. The molecule has an unusual structure; it is a sesquiterpene lactone and possesses an endoperoxide bridge as part of a 1,2,4-triozane ring. It is this trioxane moiety that acts as the warhead for antiparasitic activity.[41,162] **43** is isolated from the leaves of the Chinese plant, *Artemisia annua* also known as sweet wormwood.[4] For many years it was known that *Artemisia annua* leaves alleviated the symptoms of malaria, however, it was not until 1979 that the active compound was isolated and fully characterised.[163] **43** has demonstrated fast killing ability, *via* the destruction of the early-ring stages, which aids in the clearance of symptoms rapidly upon administration.[164–167] **43** in its natural form, however, suffers with the issue of poor oral bioavailability, and fast metabolism to inactive forms of the drug, which called for efforts to generate semi-synthetic derivatives.[168]

This led to the development of dihydroartemisinin (**44**) (DHA), which surprisingly, can be formed by reduction of the lactone to a lactol, without cleavage of the endoperoxide bridge when sodium borohydride is used as the reducing agent.[169] Though **44** showed improved potency, it still showed poor DMPK properties *in vivo*.[170] The hydroxy of the lactol was converted into its methoxy derivative, giving artemether (**45**), which demonstrated greater potency and stability, making it the most prescribed treatment from this class.[41,169] Another derivative artesunate (**46**), was also developed which has enhanced water solubility. **46** is used for intravenous administration when oral administration is not possible, as can be the case with severe and cerebral malaria.[41] Both **45**, and **46** are rapidly metabolised in the body to the active form of the drug DHA (**44**).[169]

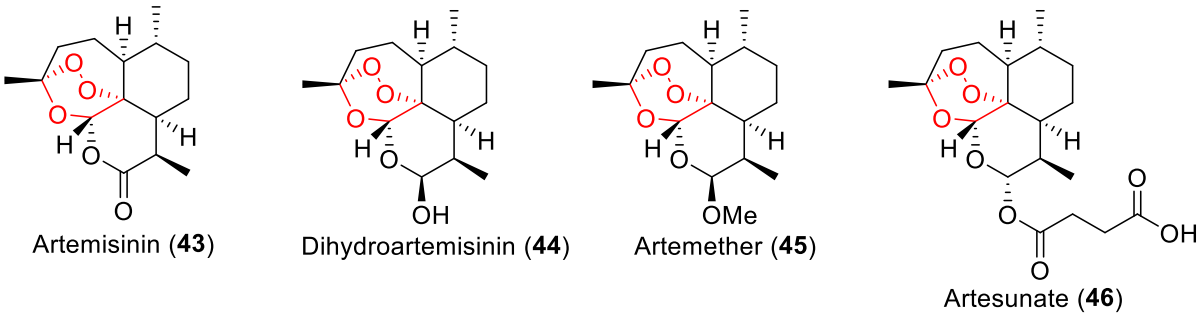

Figure 1.25. Artemisinin derivatives. Warhead highlighed in red. Artemisinin (43), dihydroartemisinin (44), artemeter (45), artesunate (46).

Despite the improvements to the DMPK properties with semi-synthetic derivatives, the artemisinin class still has a very short half-life in the body (15 – 60 minutes) and thus these compounds are normally administered as part of an artemisinin combination therapy (ACT).[41,171] This in itself holds two advantages, first, the dual mode of action allows for complete parasite clearance, the artemisinin compound, quickly kills most of the parasites, whilst the remaining, are killed by the other therapy, which is usually a compound possessing a long half-life and separate mode of action. Second, the dual, or sometimes triple use of therapy, is more likely to delay or halt the spread of resistance, as it is unlikely that the parasite will develop resistance mechanisms to both compounds at the same time, if resistance develops to one therapy, the resistant parasites will likely be killed by the other. It is due to this intelligent approach to a problem, which has led to ACTs becoming the frontline treatment of malaria.[172,173] ACTs are generally used for uncomplicated malaria, and are taken as part a of 3-day treatment regime *vs* 7 days as an artemisinin monotherapy. Even after 7 days, artemisinin monotherapy is known to cause recrudescence. The shorter ACT treatment regime not only aids in patient compliance to the treatment, but is also more likely to ensure complete parasite clearance.[172] The most frequently used combinations are artemether-lumefantrine, artesunate-amodiaquine, artesunate-mefloquine, and artesunate-sulfadoxine-pyrimethamine.[174–177]

The success of the artemisinin class of antimalarials is substantial, however, like quinine (**2**), it suffers the drawback of isolation from the natural source, resulting in poor cost ineffectiveness.[41] In addition to this, modifications to the structure are required to produce the efficacious semi-synthetic derivatives, further increasing costs. Attempts towards the total synthesis of **43** have been successfully carried out, but again, they are too complicated for commercial use.[178–187] Like with quinine (**2**) this has driven the development of fully synthetic analogues of artemisinin (**43**).

The exact mode of action of the artemisinin class is still widely debated.[162,188] It is generally accepted that it acts in a similar manner as chloroquine (**6**), blocking the formation of hemozoin (**10**).[189] Free Fe^{2+} generated from haemoglobin degradation, reduces the endoperoxide bridge thereby activating artemisinin, forming an oxygen-centred radical before rearranging to carbon centred radical (**47**).[190] These radicals have been shown to react with haem (**7**) directly forming (**48**) (Figure 1.26), which could block hemozoin (**10**) formation.[189,191] Recently, using biological probes and click chemistry, it has been demonstrated that **43** has a number of potential targets, *via* the alkylation of molecular targets in the glycolytic, haemoglobin degradation, antioxidant defence and protein synthesis pathways.[192,193] This therefore, could show that **43** has more than one mode of action. Although **43** and ACT resistance has emerged, this could be why it has not yet resulted in a failure of the drug, parasite desensitisation for now, can be overcome provided the partner drug remains effective, there is no evidence of full artemisinin resistance yet according to the WHO.[194]

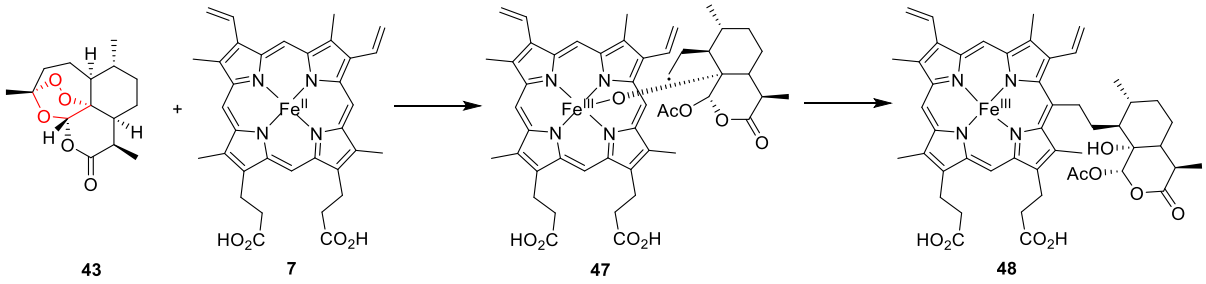

Figure 1.26. Haem adducts identified by mass spectrometry.[191]

The emergence of resistance and the need for cheaper derivatives of **43**, led to Vennerstrom *et al.* to utilise the trioxolane warhead for SAR studies. They developed a symmetrical trioxolane (**49**), fused at both sides by cyclohexane rings. The compound was inactive *in vivo* and suffered a lack of stability. Replacement of the cyclohexyl rings to adamantane rings (**50**) increased the stability of the molecule, but was also inactive *in vivo*, whilst replacement of only one of the cyclohexyl ring to adamantane led to both a potent, stable compound **51** (Figure 1.27).[195,196]

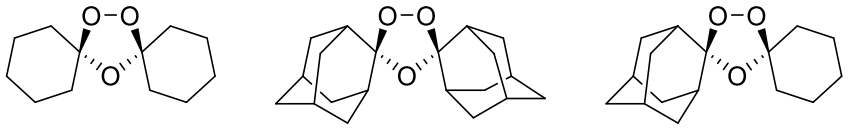

Figure 1.27. Vennestrom initial trioxolane SAR.[195,196]

To make the trioxolane series more drug-like, OZ277 (**52**) (Figure 1.28) was developed by Vennerstrom, which displayed improved DMPK properties.[196,197] **52** was the first synthetic peroxide to be used in the market, currently only on the Indian market as part of a three dose cure with piperaquine.[198] OZ439 (**53**) (Figure 1.28) was developed with a much-improved half-life over **52**, which gave the molecule hope for a single dose cure; it is currently in phase IIb clinical trials with the partner drug still to be determined.[198] It is also being explored by the MMV in combination with ferroquine and is also in phase IIb clinical trials.[199] **53** crucially, has demonstrated efficacy against artemisinin resistant strains.[200]

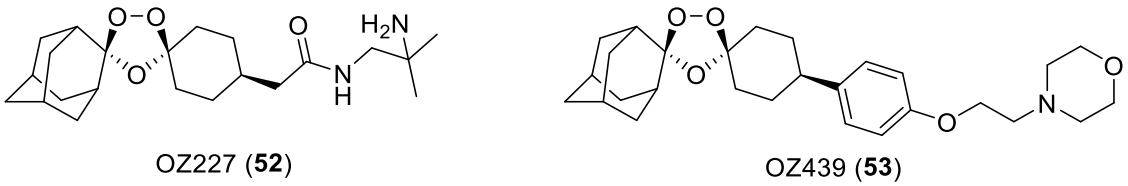

Figure 1.28. OZ277 (52) (left) and OZ439 (53) (right).[198]

O'Neill *et al.* have generated 1,2,4,5-tetraoxanes for potential use as antimalarial chemotherapy.[201–203] The tetraoxane moiety can stabilise the O-O bond by the anomeric effect,[204] and baring two peroxide bridges, the structure gives an opportunity for improved potency. The two most promising compounds to date are RKA182 (**54**) and E209 (**55**) (Figure 1.29), both of which show good potency against the parasite.[201–203] **54** had an extended half-life, good stability and maintained potency, but unfortunately was not able to deliver a single dose cure.[201–203] **55** is the next in development, which outperforms artesunate (**46**) with a 66 % cure rate at single oral doses of 30 mg / kg. It demonstrates low nanomolar activity against chloroquine sensitive strains of *P. falciparum*.[201]

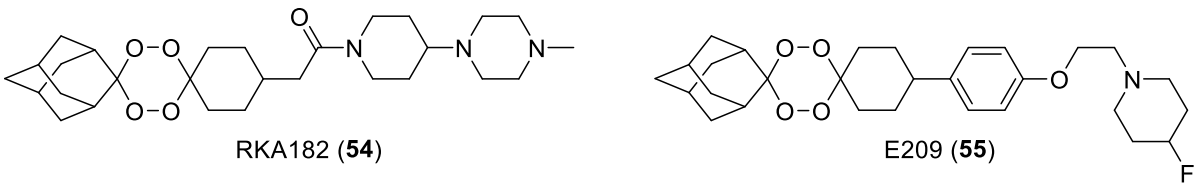

Figure 1.29. RKA182 (54) (left) E209 (55) (right).[201]

1.3.2.6 Selected Novel Targets in the Pipeline

The emergence of resistance to all current frontline therapies is a fundamental problem which could potentially derail all of the successful milestones antimalarial chemotherapy has accomplished to date. With the exception of DSM and DHODH inhibitors, all of the treatments acknowledged thus far, target the same clinically validated pathways through chemotype modification. This modification is usually a minor structural change that regains potency against drug resistant strains, the 4-aminoquinoline compounds exemplifies this. As such, resistance commonly develops to the new treatments within a matter of years, or even months.

Medicinal chemists have looked for novel pathways within the parasite to circumvent this problem, targeting an as of yet untargeted enzyme / protein, is more likely to develop resistance slowly. These new compounds offer renewed hope for the future of antimalarial chemotherapy, which was under severe threat with the emergence of artemisinin resistant strains located along the Thai-Cambodian border.[205]

Most of the current novel targets have been identified by whole cell high-throughput screening. A Novartis based screen identified imidazolopiperazines as an active chemotype against the parasite; the lead compound generated from information from this screen was KAF156 (**56**) (Figure 1.30).[206–208] It is a very effective compound, potentially delivering a radical cure, it is active across all stages of the *Plasmodium* life cycle and gives IC_{50} values of 6 nM against drug resistant blood stage parasites, furthermore it demonstrates a mouse *in vivo* ED_{50} of 0.6 mg / kg.[207] As of yet the target of the drug is not fully known, but is believed to be a protein with unknown function and is known as *Plasmodium falciparum* cyclic amine resistance locus (*Pf*CARL). This is thought to be the target as parasite resistance correlates with the accumulation of mutations in this protein. The compound has progressed to phase IIb clinical trials in combination with lumefantrine (MMV portfolio).[200]

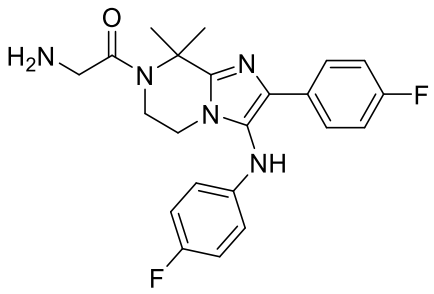

KAF156 (**56**)

Figure 1.30. KAF156 (56).[207]

Like KAF156 (**56**), MMV390048 (**57**) (Figure 1.31) (also known as MMV048) has demonstrated efficacy across all stages of the *Plasmodium* life cycle. It was discovered from a HTS that elucidated

the template belonging to 3,5-diaryl-2-aminoquinoline possessed antimalarial activity.[209] After SAR optimisation around the initial hit, the lead was discovered, with improved potency and a better DMPK profile, showing single oral dose cures of *P.berghei* at 30 mg / kg in the mouse model.[209] At the time of discovery the target was unknown, however, recently it has been identified to target PI 4 kinase.[210] **57** is currently entering phase IIa clinical trials (MMV portfolio).

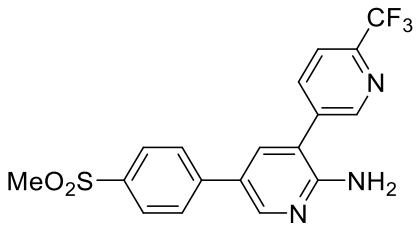

MMV048 (**57**)

Figure 1.31. MMV048 (57).[209]

Another example of a novel chemotype in the pipeline is DDD107498 (**58**) (Figure 1.32) now renamed to DDD498. The hit molecule was also identified from a whole cell screen and belongs to 2,6 disubstituted quinoline-4-carboxamide scaffold.[211] It showed promising potency of 120 nM against the parasite. Optimisation of the template generated not only a 100-fold increase in potency for the lead, but also enhanced DMPK properties, this coupled with an estimated low cost of goods shows good promise for the future of this compound.[211] The compound entered human trials in 2017 (MMV portfolio). The molecular target of **58** was found to be eEF2, responsible for mediating GTP-dependent translocation of the ribosome across mRNA, causing the ribosome to stall, which shuts down peptide synthesis.[211]

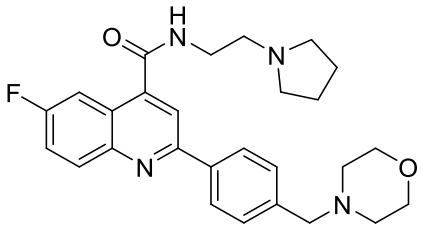

DDD498 (**58**)

Figure 1.32. DDD498 (58).[211]

Of the novel drug targets currently being addressed, perhaps the most exploited is the ATPase4 enzyme in the malaria parasite. Selected inhibitors include, but are not limited to, PA92 (**59**) (Figure 1.33), SJ733 (**60**) (Figure 1.33), and Cipargamin (**63**) previously KAE609 (Figure 1.34). ATPase4 acts as a sodium transporter in the parasite, and inhibition of this, leads to lethal levels of Na^+ building within the parasite causing parasite death.[212] PA92 (**59**) belongs to the imidazole family possessing a aryl substituted pyrazole, bound to the imidazole by an amide linker, it is fast killing and demonstrates

good physiochemical properties,[212,213] but suffers from a potential ames positive potential metabolite (MMV portolio). Currently it is in pre-clinical development. SJ733 (**60**) also is being pursued to be part of a single dose radical cure, and it too possesses good physiochemical properties, it is a novel chemotype that contains a dihydroisoquinalone core, the drawbacks are high cost of goods as it is a chiral molecule. Currently it is in phase I clinical trials.[212,214]

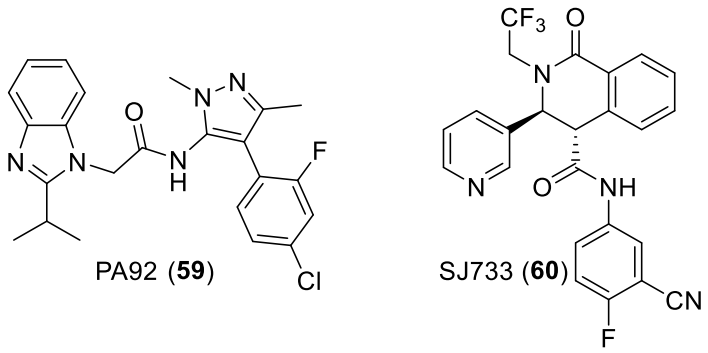

Figure 1.33. PA92 (59) (left), SJ733 (60) (right).[212–214]

The most successful compound to date inhibiting ATPase4 is Cipargamin (**63**) (Figure 1.34).[215–217] Developed by Novartis, it is a compound of noteworthy similarity to our hit chemotype discussed as part of this thesis. The molecule is a tetrahydro-β-carboline structure with a fused spiroindalone ring. The original hit (**61**) was identified from a HTS against the malaria parasite that showed efficacy against chloroquine resistant strains of the parasite.[215–218] The 7 membered C ring of the hit from the screen was changed to a 6 membered ring (**62**), which improved activity. The compound, however, suffered from poor metabolic stability, to circumvent this, halogens were incorporated into the A ring of the tetrahydro-β-carboline, which not only solved the metabolism problem, it also led to improved potency.[215–218] Since the lead compound (**63**) was discovered it has demonstrated an acceptable safety profile in humans and as a result has currently completed phase IIa clinical trials.[215–218]

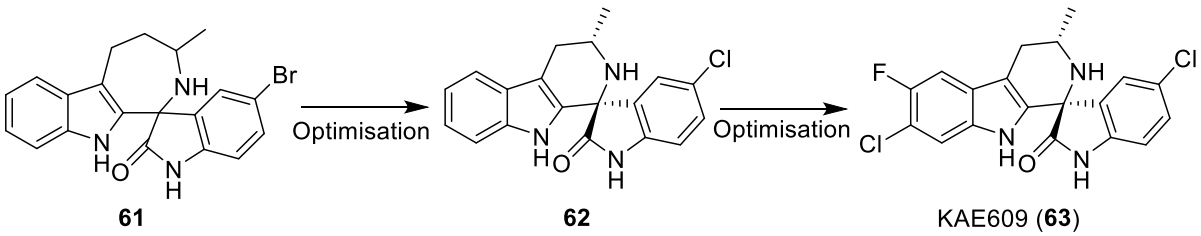

Figure 1.34. Route to the discovery of KAE609.[216–218]

1.4 Isoprenoid Biosynthesis and the Methyl Erythritol Phosphate (MEP) Pathway

The emergence of strains of *Plasmodium falciparum* that are resistant to frontline therapies is a threat to the efforts to eradicate the disease. Further to this, if widespread resistance occurs, the malaria burden will only be exacerbated and will likely lead to increased mortality rates worldwide.

To regain control, medicinal chemists are targeting novel pathways that are less likely to show resistance, with the ultimate aim of developing a candidate drug to be taken to market. The requirements for the novel drug candidate are; ideally single dose cure; low human toxicity, activity across all stages of the *Plasmodium* life cycle, and the ability to be taken as part of a combination therapy to hamper any potential resistance developing.[219]

During the extensive research efforts to find druggable novel pathways within the parasite, the methyl erythritol phosphate (MEP) pathway has emerged as another potential target due to its parasite specificity over mammalian systems. The MEP pathway is responsible for the biosynthesis of crucial isoprenoid precursors; therefore the inhibition of precursor development provides a unique opportunity to chemically interrupt numerous biological pathways within the parasite which require isoprenoids to function. The MEP pathway presents another potential tool for the eradication of the parasite as interruption of isoprenoid biosynthesis can result in a loss of parasite viability.

1.4.1 Isoprenoids

Isoprenoids are a diverse class of compounds that are essential natural products for all living organisms. The isoprenoid family consists of over 55,000 members; all of which are generated from the repeated head to tail (regular) or head to head / tail to tail (irregular) condensations of one or both of two precursors, isopentyl-pyrophosphate (IPP) (**90**) and dimethylallyl-pyrophosphate (DMAPP) (**91**).[220–223] These condensations coupled with the incorporation of functional groups leads to the generation of many cyclic, acyclic, chiral, or achiral molecules all belonging to the isoprenoid family.[221,224] Indeed isoprenoids show a large degree of structural diversity and are required for numerous biological processes including but not limited to, protein prenylation, protein degradation, apoptosis, transcription regulation, post translational modifications, cell wall biosynthesis, photosynthesis and regulation of the electron transport chain.[221,225,226] Some examples of isoprenoid derived compounds include terpenes, sterols, ubiquinone, pigments (e.g. chlorophyll), cholesterol, hormones, and natural fragrances.[225] The antimalarial drugs quinine (**2**) and artemisinin (**43**) are also biosynthesised from isoprenoid derived compounds.[227–229]

The IPP (**90**) and DMAPP (**91**) precursors are both generated biosynthetically within all living organisms; these 5 carbon isoprene units are responsible for the regulation and maintenance of many differing species specific biological processes and as such have gained interest from pharmaceutical industries.[225] Until relatively recently, it was believed that the mevalonate (MVA) pathway was used exclusively by all organisms for the generation of **90** and **91**. It was not until the 1990s when research by Rohmer and Arigoni independently discovered a completely distinct biosynthetic pathway named

the non-mevalonate pathway, alternatively known as the MEP pathway.[230–232] A comparison between both pathways is depicted below (Figure 1.35).[221]

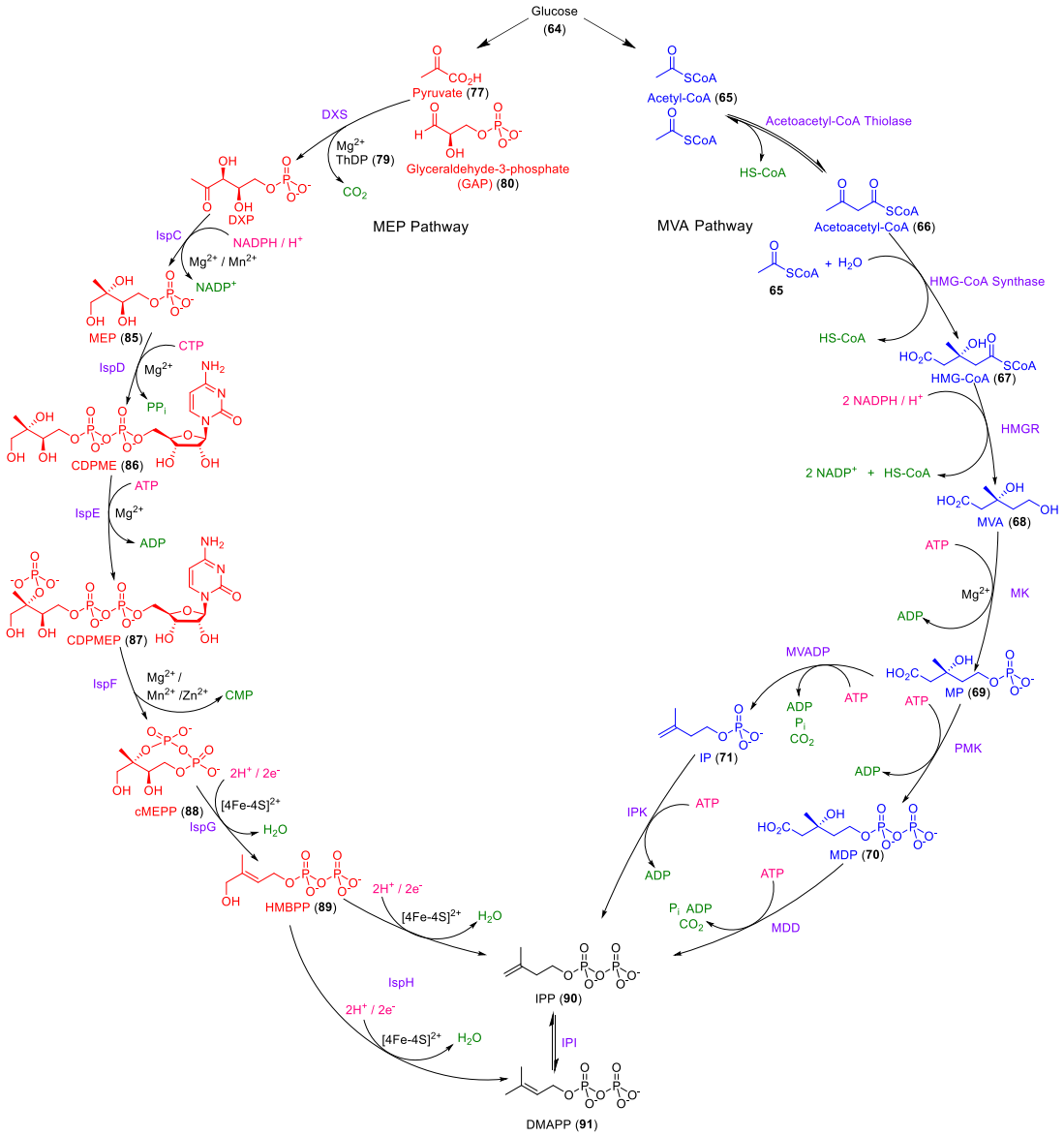

Figure 1.35. Comparative pathways for the production of DMAPP and IPP. Left (red) MEP pathway, right (blue) MVA pathway. Enzymes are highlighted in purple, cofactors are highlighted in pink, leaving groups are highlighted in green, metals are highlighted in black.

Once the MEP pathway was elucidated, efforts began to discover the distribution of the two independent pathways within living organisms.[232] These studies demonstrated that humans, mammals, archaebacteria, fungi and some plants species synthesise **90** and **91** *via* the MVA pathway, whereas the MEP pathway is responsible for precursor synthesis in green algae, plant species, numerous pathogenic bacteria, eubacteria, and crucially apicomplexan protozoa including *Plasmodium falciparum*.[232,233] Interestingly it has been demonstrated that in higher plants, both pathways are in operation together, with clear compartmentalisation; terpene and sterol production

occurs in the cytoplasm *via* the MVA pathway, whereas carotenoids and phytol are biosynthesised within plastid organelles *via* the MEP pathway.[233,234]

1.5 The Methyl Erythritol Phosphate (MEP) Pathway

1.5.1 Discovery

Though the MEP pathway was discovered within the last two decades, evidence for its existence dates back to the 1960s when it was observed that maize seedling-feeding experiments with ^{14}C radiolabelled CO_2 and MVA led to distinct labelling in specific terpenes. When labelled ^{14}C CO_2 is used alone, β-carotene and phytol where heavily labelled with ^{14}C whereas sterols and β-amyrin and the prenyl side chain of mitochondrial ubiquinone are only slightly labelled. Inversely when ^{14}C radiolabelled MVA (**68**) is used, sterols, β-amyrin and ubiquinone are heavily radiolabelled, whilst β-carotene and phytol are not. Whilst this was not direct evidence of an alternate pathway it did indicate that plastidic isoprenoids are synthesised within the chloroplast whereas sterols are synthesised outside of the chloroplast.[235,236] To explain this result it was proposed that, first; **68** may not be able to penetrate the chloroplast effectively, explaining why radiolabelled **68** preferentially led to cytoplasmic sterols and second; that IPP (**90**) and DMAPP (**91**) biosynthesis was segregated into plastid, mitochondrial, and cytoplasmic compartments.[235–237]

Further inconsistencies from the MVA pathway arose when it was demonstrated that the fungal metabolite mevinolin, a highly potent and specific inhibitor of the MVA pathway enzyme (*S*)-3-hydroxy-3-methyl-glutaryl-coenzyme A reductase (HMGR), was used against radish species.[238] As expected, the cytoplasmic sterol biosynthesis was inhibited, but curiously chloroplast derived terpenes were not. Again a possible explanation is that mevinolin could not penetrate the chloroplast effectively, thus no mevinolin could reach the potential HMGR enzyme in the chloroplast.[237,238] Another explanation was that chloroplasts do not use **68** for isoprenoid biosynthesis, but at the time no evidence existed to support this. With regards to mitochondrial ubiquinone, it was demonstrated that mevinolin also led to a reduction of total ubiquinone, and showed that its biosynthesis seemed to be reliant on the biosynthesis of IPP (**90**) from the cytoplasm, which is in contrast to chloroplast derived terpenes. Another curiosity is that no HMGR enzyme had ever been isolated from purified chloroplasts.[237,239] Following a similar experiment, further inconsistencies with the MVA pathway were found when addition of mevinolin also did not inhibit the growth of *E. coli*, which is devoid of chloroplasts, but mevinolin completely inhibited *H. halobium* growth.[240]

The identification of the alternative pathway began to be uncovered when work on the biosynthesis of bacterial hopanoids using C1 and C2 ^{13}C labelled acetate by Flesch and Rohmer again

found inconsistencies from the classical pathway.[241] Using C1 labelled acetate led to unexpected labelling of numerous positions within the hopanoid skeleton with ^{13}C. With C1 labelled acetate it is expected that two of the carbons in the isoprenic units contain ^{13}C if the MVA pathway is followed directly (Path A Figure 1.36, compounds **72** and **73**). Based on the retrosynthetic analysis of what was observed, only one carbon was labelled per isoprenic unit (Path B Figure 1.36, compounds **74** and **75**).[241]

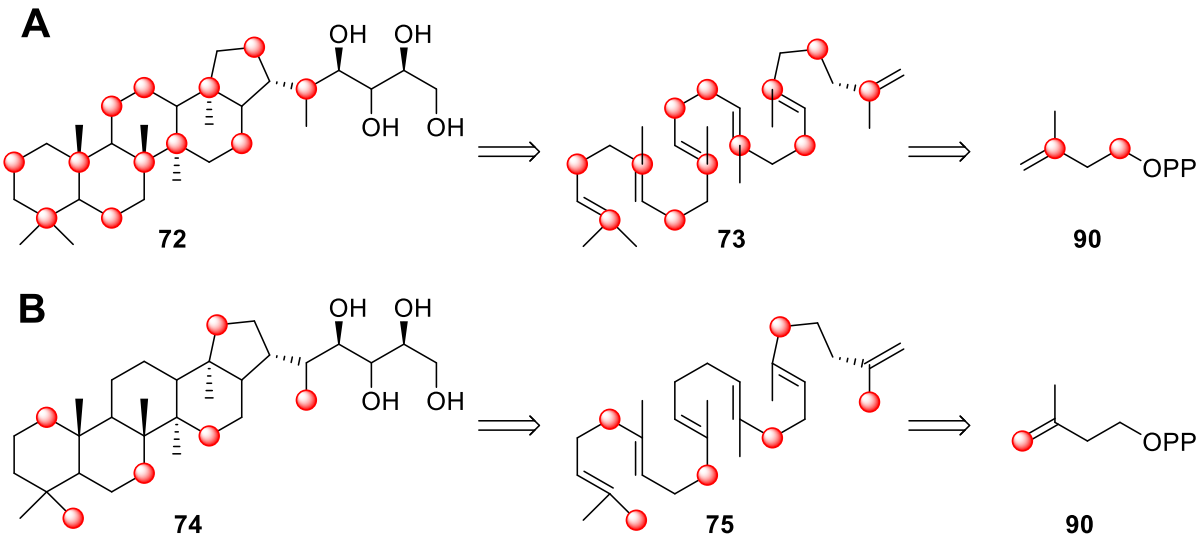

Figure 1.36. Labelling of hapanoid skeleton and retrosynthesis to IPP. A. Expected ^{13}C labelling patterns. B. Observed ^{13}C labelling patterns. ^{13}C labels are depicted as red spheres.[241]

It appeared at first glance that MVA (**68**) had been biosynthesised by an unlabelled pool of acetoacetate, and by one molecule of 2C ^{13}C acetate, which had been interconverted with respect to the starting 1C ^{13}C acetate, this interconversion can be achieved via the glyoxylate / tricarboxylic acid cycles (G / TCA cycles), gluconeogenesis and glucose metabolism *via* the Entner-Doudoroff (ED) pathway (these pathways will not be discussed in the scope of this thesis).[241] However, further studies using labelled glucose (**64**), pyruvate (**77**) and erythrose later uncovered that the isoprenic units of hopanoids and the prenyl side chains of ubiquinones still did not appear to follow the expected labelling patterns from an MVA pathway.[237,242]

It was identified that labelling patterns of a novel biosynthesis matched for numerous bacterium species including, *Alicyclobacillus acidocaldarius*, *Escherichia coli*, *Methylobacterium fujisawaense*, *Methylobacterium organophilium*, *Rhodopseudomonas acidophila*, *Rhodopseudomonas palustris* and *Zymomonas mobilis*. The incorporation of labelled glucose (**64**), acetate, pyruvate (**77**) and erythrose precursors into isoprenoids led to the identification of two new starting molecules; one possessing a two-carbon unit, and another possessing a three-carbon unit. The two-carbon unit was

identified to be derived from pyruvate (**77**) and the three-carbon unit was identified to be glyceraldehyde-3-phosphate (GAP) (**80**).[231,232,234,242]

The initial clues into the identity of the novel substrates came using labelled ^{13}C glucose (**64**) as a sole feeding source for the bacterium *Z. mobilis*. Glucose (**64**) is metabolised to pyruvate (**77**) and GAP (**80**) by the ED pathway, but in *Z. mobilis* pyruvate (**77**) is not converted into GAP (**80**).[232,243] This meant that labelling glucose (**64**) at each of its positions allowed determination of the GAP fragment, which must arise from the C4, C5, and C6 positions of glucose (**64**). It was clear from the labelling studies that the C1, C2 and C4 atoms of the isoprenic units came from GAP (**80**) corresponding to labelling positions C4 – 6 in glucose (**64**). In *Z. mobilis* pyruvate (**77**) is obtained equally by the metabolism of glucose (**64**) from either C1 – 3 positions, or C4 – 6 positions after further GAP (**80**) metabolism. Labelling the C2 / C5 position or C3 / C6 position of glucose (**64**) resulted in the respective labelling of positions C3 and C5 of the isoprenic units corresponding to the metabolism of GAP (**80**) to pyruvate (**77**). Finally labelling positions C1 and C4 of glucose (**64**) only leads labelling of position 4 of the isoprenic unit, which indicated that a decarboxylation of pyruvate (**77**) occurs, followed by condensation to the 3 carbon triose unit of GAP (**80**), this can be rationalised as C1 labelling will always be lost as CO_2 (Figure 1.37).[231,232,234,242]

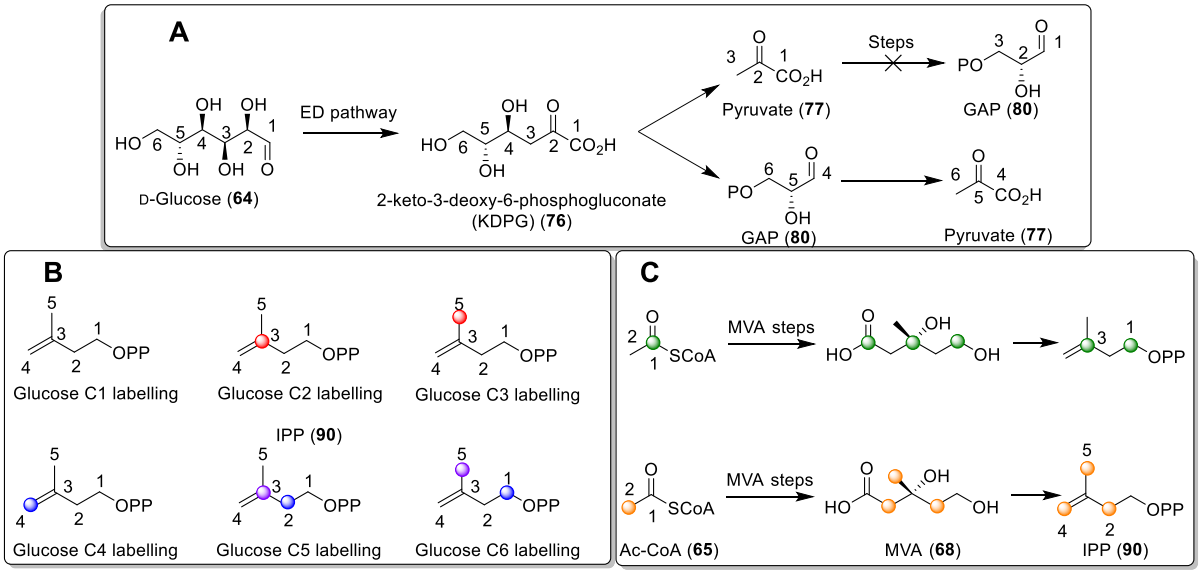

Figure 1.37. Labelling studies with *Z. mobilis*. A. *Z. mobilis* glucose metabolism, atom numbers are shown for clarity. B. Observed hopanoid labelling with glucose labelled at each respective position, singular isoprene building blocks rather than the hopanoid skeleton are shown for clarity. Labels arising from direct incorporation of pyruvate fragment (C2 and 3 from glucose) are shown in red, labels arising from GAP fragment directly (C4-6 in glucose) are shown in blue, labels arising from pyruvate after further GAP metabolism are shown in purple (C5 and 6 in glucose). C. Expected labelling of IPP if MVA pathway is followed directly, labelled 1C acetate is shown in green, labelled 2C acetate is shown in yellow.

It was proposed that decarboxylation of pyruvate followed by condensation with GAP (**80**) led to the formation of 1-deoxyxyluslose 5-phosphate (DXP) (**81**) and was thiamine diphosphate (ThDP) (**78**) dependent (Figure 1.38). This then yielded another curiosity, the same labelling studies identified

that the C1, C2, and C4 positions of IPP where derived from GAP (**80**), whilst positions C3 and C5 where derived from pyruvate (**77**), this led to the conclusion that a rearrangement must occur after DXP (**81**) formation (Figure 1.38).[231,242] From this it was discovered that the complete MEP pathway occurs *via* a 7 step enzyme sequence which at no point forms MVA (**68**) as an intermediate. All 7 enzymes involved in the pathway have been isolated and their functions are known, although the exact mechanism by which some enzymes carry out their substrate transformations remains a topic of debate.

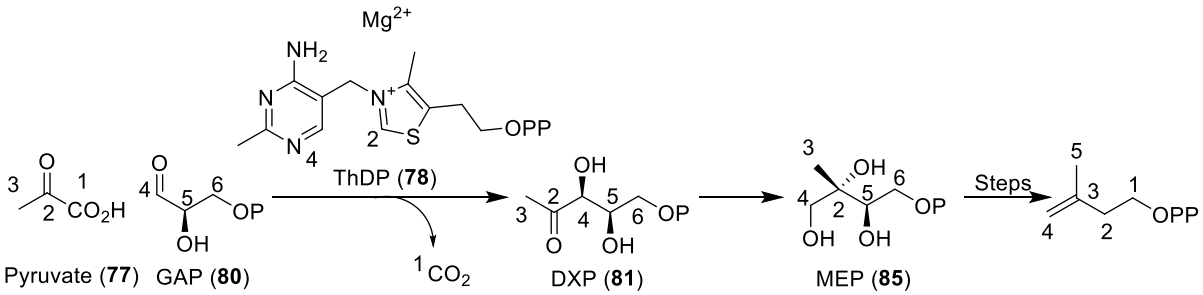

Figure 1.38. Proposed formation and rearrangement of DXP (81).

1.5.2 1-Deoxy-D-xylose 5-phosphate synthase (DXS)

DXS was the first enzyme of the MEP pathway discovered after the thiamine diphosphate (ThDP) (**78**) dependent reaction of pyruvate (**77**) with GAP (**80**) was uncovered.[233,242] The *E. coli* genome was examined for enzymes by searching for reactions involving the decarboxylation of pyruvate (**77**) with ThDP (**78**) dependence; eventually an enzyme was found that could accept **77**, **78** and **80** as substrates, which also converted the substrates to DXP (**81**).[244]

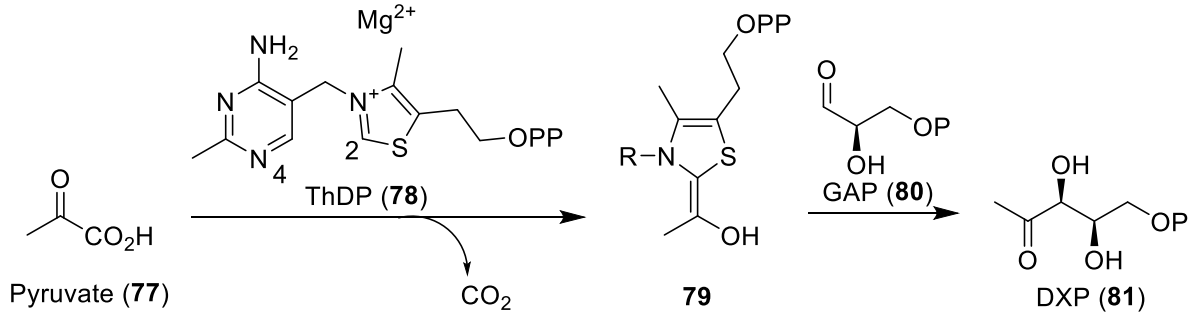

Figure 1.39. ThDP dependent formation of DXP (81).

The mechanism by which the enzyme acts is *via* an acyloin condensation. ThDP (**78**) is first activated *via* deprotonation of the C2 carbon atom forming a reactive ylide. Deprotonation is believed to occur either by, the N4 nitrogen of the aminopyrimidine ring, or by glutamate and arginine side chains (for *E. coli*) within the enzyme active site. The ylide can then attack the ketone group of pyruvate after substrate binding. The resulting iminium moiety then acts as an electron acceptor for

the decarboxylation step. This results in an enamine (**79**) that can then attack the aldehyde of GAP (**80**). A final deprotonation releases the ThDP ylide and results in the formation of deoxyxyulose 5-phosphate (DXP) (**81**) (Figure 1.39).[244–246]

1.5.3 1-Deoxy-D-xylose 5-phosphate reductisomerase (IspC)

After the formation of DXP (**81**) it was postulated that a rearrangement must occur due to the apparent migration of one of the carbons coming from the GAP unit *en-route* to the isoprenic building blocks.[231,242] It was believed that this rearrangement started from **81** as 2-*C*-methyl-D-erythritol-2,4-cyclodiphosphate (cMEPP) (**88**) had been identified in bacterial species and could be derived from 2-*C*-methyl-D-erythritol-4-phosphate (MEP) (**85**).[232,247,248] Therefore the formation of **85** was hypothesised to occur by the rearrangement and reduction of **81**. The enzyme responsible for the transformation was elucidated after observed incorporation of ^{2}H-labelled 2-*C*-methyl-D-erythritol (ME) into *E. coli* ubiquinone.[249] Research led by Seto *et al*. created *E. coli* K-12 mutants auxotrophic for MEP.[250] Transformation of these mutants with a genome fragment library of the same *E. coli* strain identified that the expression of the gene *yaeM* was able to rescue the *E. coli* mutants that were auxotrophic. The protein adduct created by this gene was isolated and demonstrated that it could catalyse the intramolecular rearrangement of **81** to 2-*C*-methyl-D-erythrose-4-phosphate (**84**) before reduction to MEP (**85**) which is dependent on NADPH as a cofactor. The enzyme was later named 1-deoxy-D-xylose 5-phosphate reductisomerase or IspC.[250]

The enzyme has a sequential reaction mechanism, first the NADPH co-factor, along with a divalent metal co-factor bind in the active site causing a conformational change on the protein that allows binding of DXP (**81**).[251] The isomerisation of **81** is then undertaken, however, the exact mechanism by which this is carried out is not fully understood; at present two mechanisms have been hypothesised.

The first hypothesised mechanism for the isomerisation of **81** is an α-ketol rearrangement which occurs by migration of the C3 – C4 bond onto the ketone of **81**, forming 2-*C*-methyl-D-erythrose-4-phosphate (**84**) (Figure 1.40). This rearrangement is thought to be mediated by protonation or coordination of the ketone group to the divalent metal cofactor allowing build-up of positive charge on the C2 atom of **81**.[251] The second hypothesised mechanism is a retro-aldol / aldol condensation. Deprotonation of the C4 hydroxyl group of **81** and retro-aldol cleavage of C3 – C4 bond yields hydroxyacetone enolate (**82**) and phosphoglycolaldehyde (**83**). An aldol condensation can then occur forming **84**.[251] Though it has not yet been proven which mechanism is in operation, it is generally believed that the α-ketol rearrangement is the likely mode of action of the enzyme, due to the difficult

requirements of substrate containment if the retro-aldol mechanism is followed.[252] It should be noted, however, that kinetic isotope effects support the retro-aldo proposal, but curiously the enzyme cannot accept **82** or **83** as exogenous substrates and cannot convert them to **84**.[251–254] **84** is finally reduced by the NADPH cofactor, releasing MEP (**85**) as the product, and $NADP^+$ as a by-product (Figure 1.40).

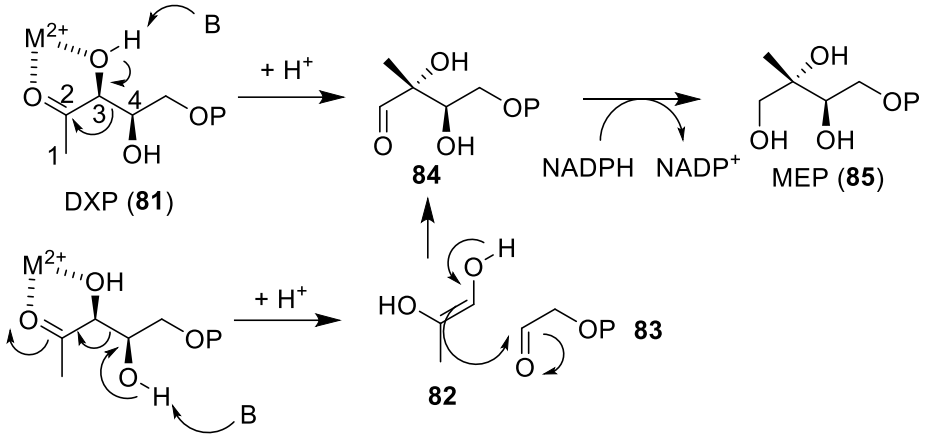

Figure 1.40. Proposed mechanisms for the formation of MEP (85).

1.5.4 2-*C*-methyl-D-erythritol-4-phosphate cytidyltransferase (IspD)

Plasmodium falciparum 2-*C*-methyl-d-erythritol-4-phosphate cytidyltransferase (IspD) is the main focus of the work described within this thesis, it has been less extensively examined than IspC, but has had over 20 reported crystal structures solved.[255] A structure for *Plasmodium falciparum*, however, has not yet been elucidated. The first IspD enzyme was discovered from *E. coli* quickly after the identification of IspC. C2 ^{14}C radiolabelled MEP (**85**) was added to *E. coli* cell extracts and a new radioactive product was observed, after NMR spectroscopy the product was identified to be 4-diphosphocytidyl-2-*C*-methyl-D-erythritol (CDPME) (**86**).[256] The addition of a cytidine-5-monophosphate (CMP) moiety to MEP (**85**) pointed towards the existence of a cytidyltransferase enzyme using cytidine-5-triphosphate (CTP) as substrate. CTP is not commonly found as a substrate and cofactor in comparison to adenosine triphosphate (ATP) and guanosine triphosphate (GTP), this coupled with the unusual MEP (**85**) substrate makes this enzyme particularly attractive to target for small molecule inhibition. The gene *ygbP* was discovered to be responsible for the production of the resulting IspD enzyme after a database search for enzymes responsible for the transfer of CTP onto another molecule with loss of pyrophosphate as a by-product.[256] Seto *et al*. also identified the *ygbP* gene by blocking the conversion of **85** in *E. coli*. After identification and expression of the gene followed by purification of the resultant enzyme, they showed that the enzyme converted MEP (**85**) into CDPME (**86**) in the presence of CTP (Figure 1.41).[257]

Catalytic activity was found to depend on the presence of a divalent metal ion, predominantly Mg^{2+}.[257] Like IspC the enzymatic mechanism occurs sequentially. First a divalent metal ion coordinates, this is followed by CTP and then MEP coordinates last.[258] Both CTP and MEP are bound by hydrogen bonding and ionic interactions, CTP is bound *via* a glycine-rich loop, the α and γ-phosphate groups of CTP are hydrogen bonded with the enzyme. The divalent metal ion is coordinated by all of the phosphate groups from both substrates. The exact mechanism of phosphate attack for IspD has not been determined, and there are numerous mechanisms by which the phosphate of MEP could attack the α-phosphate of CTP.[259–261] It has been proposed in the literature that attack of the phosphate of **85** onto the α-phosphate of CTP follows an associative in-line mechanism, this is proposed to form a negatively charged pentacoordinate transition state which is stabilised by positively charged lysine and arginine residues, along with the metal ion within the enzyme active site.[221,255,258,262]

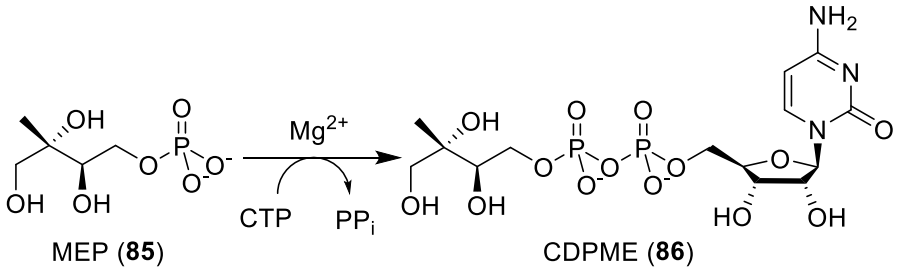

Figure 1.41. Formation of CDPME (86).

The IspD structure is similar to other cytidyltranferases, it exists as a homodimer with the monomer units existing as a single domain which adopts an α / β fold conformation.[258,262] This domain is connected to a subdomain known as the β arm of the protein, the two monomer β arms associate to form the dimer interface and is the location of active site, the interface is solvent exposed.[258,263] The *E. coli* IspD crystal structure with bound CDPME and Mg^{2+} is depicted below (Figure 1.42).[262]

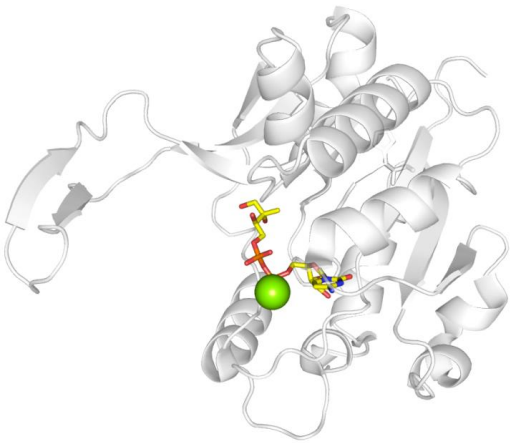

Figure 1.42. *E. coli* IspD crystal structure (PDB code: 1INI).[262] Protein rendered as white cartoon CDPME is coloured by element, yellow for carbon, red for oxygen, blue for nitrogen, and orange for phosphorous. Mg^{2+} is depicted as a green sphere. Image created in Pymol.[264]

1.5.5 4-Diphosphocytidyl-2-*C*-methyl-D-erythritol kinase (IspE)

The IspE enzyme is an ATP dependent member of the galacto-homoserine-mevalonate-phosphomevalonte kinase (GHMP) family.[255] It was discovered after the observation that the *E. coli ychB* gene followed the same pattern of occurrence as other genes that were possessed by organisms possessing other MEP pathway genes.[221] Expression of this gene followed by testing the enzyme in the presence of ATP and 2C ^{14}C radiolabelled CDPME (**86**) led to the formation of 4-diphosphocytidyl-2-*C*-methyl-D-erythritol-2-phosphate CDPMEP (**87**) (Figure 1.43).[265] Using a genetic engineering approach the same gene was identified by generating *E. coli* mutants deficient in biosynthetic steps from MEP (**85**) to IPP (**90**).[266]

The mechanism of the reaction has not been fully elucidated, but is proposed to be similar to that of IspD and other enzyme catalysed phospho-group transfers.[267–270] The C-2 hydroxyl group is deprotonated before nucleophilic attack on the ATP γ-phosphate group to yield the product **87** and ADP as a by-product.[221,270–272] Again the catalytic mechanism is believed to be sequential where the substrate binds first, followed by the cofactor.[221,273] The C-2 hydroxyl group is believed to be deprotonated by highly conserved aspartate and lysine residues after forming hydrogen bonds with them. It is postulated that the lysine residue is responsible for the stabilisation of negative charge build up in the transition state.[221,270–272] Although a divalent metal cation has been shown to be crucial for activity of this enzyme, no crystal structure to date has been isolated with this metal bound.[221]

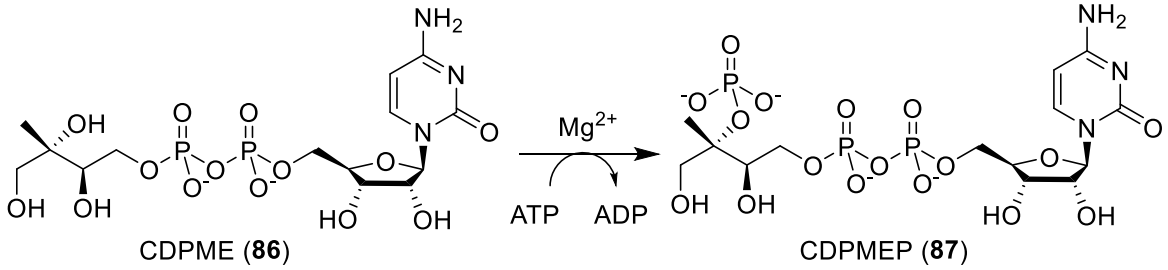

Figure 1.43. Formation of CDPMEP (87).

1.5.6 2-*C*-methyl-D-erythritol-2,4-cyclodiphosphate synthase (IspF)

IspF was discovered alongside the IspD enzyme as the *ygbP* gene belonging to IspD was coupled with the *ygbB*.[256] The *ygbB* gene was identified as a likely MEP pathway enzyme as it was distributed along all other MEP gene containing organisms. After the gene was expressed in *E. coli*, and the enzyme isolated and purified, IspF was found to convert CDPMEP (**87**) into the corresponding cMEPP (**88**) (Figure 1.44).[274] The structure of cMEPP had already been elucidated in numerous bacterial species confirming cMEPP as an intermediate within the MEP pathway.

The catalytic mechanism is dependent on two divalent metal cations in order to proceed, a Zn^{2+} metal ion coordinates to the β-phosphate, polarising it, promoting attack by the C-2 phosphate. Another metal cation either Mg^{2+} or Mn^{2+} help align the substrate and stabilise the build-up of negative charge before ring closure to the product (**88**) and loss of CMP.[275–277]

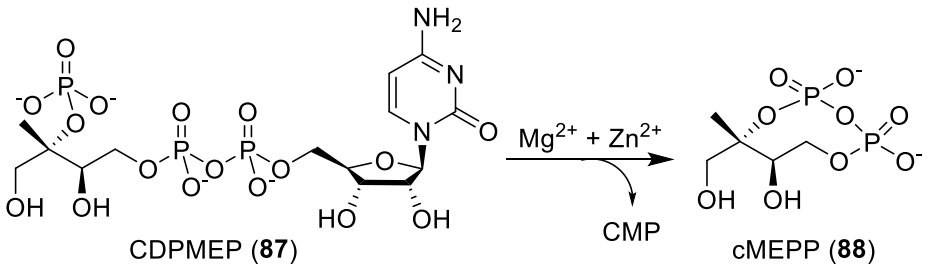

Figure 1.44. Formation of cMEPP (88).

1.5.7 4-Hydroxy-3-methyl-2-(*E*)-butenyl-4-diphosphate synthase (IspG)

The penultimate step of the MEP involves the conversation of cMEPP (**88**) into 4-hydroxy-3-methyl-2-(*E*)-butenyl-4-diphosphate (HMBPP) (**89**) (Figure 1.45). Again this distribution of the gene *gcpE* encoding for the enzyme was found in organisms possessing other MEP pathway genes, and led to the belief this was another gene involved in the MEP pathway.[278–280] ^{13}C labelled experiments with DXP (**81**) and overexpression of all current MEP genes and *gcpE* led to the identification of HMBPP (**89**) by NMR.[281] The enzyme corresponding to the gene was isolated and named IspG. The IspG enzyme in isolated form unexpectedly demonstrated poor activity, it was later elucidated that the enzyme likely possessed an $[4Fe\text{-}4S]^{2+}$ cluster, which is sensitive to air.[282] Protein purification in oxygen free conditions followed by activity studies led to the improved activity of the enzyme, whose role is the reductive dehydroxylation of cMEPP (**88**) into HMGPP (**89**).[283,284] Similar to IspC, the reaction mechanism of the IspG enzyme remains a matter of debate. Differing mechanisms have proposed the involvement of radical, carbocation, and carbanion intermediates.[285] The current accepted mechanism is complicated and is discussed elsewhere.[286–289]

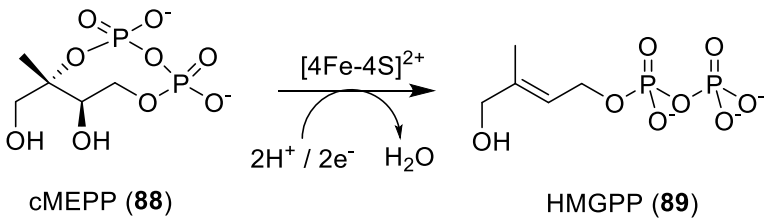

Figure 1.45. Formation of HMGPP (89).

1.5.8 4-Hydroxy-3-methyl-2-(*E*)-butenyl-4-diphosphate reductase (IspH)

The final step of the MEP pathway requires another reductive dehydroxylation reaction resulting in the formation of IPP (**90**) or DMAPP (**91**). The gene encoding for the final enzyme was *lytB*, and again this gene was believed to be involved in the MEP pathway after it was identified in organisms possessing other MEP pathway genes.[290] Adding insertions into the gene led to death in cyanobacterium, and also led to changes in the observed ratio of **90** and **91**.[291] In *E. coli* disruption of the gene also led to cell death.[292] Confirmation of the enzyme function was elucidated using ^{13}C labelled deoxyxyulose, the enzyme was found to convert **89** to both **90** and **91** in a ratio of 5 : 1 and the enzyme named IspH.[293] Similar to IspG, activity studies on IspH in air led to poor activity suggesting another $[4Fe\text{-}4S]^{2+}$ cluster, this was confirmed upon repeating the isolation and studies in oxygen free conditions, and using EPR.[294–297]

Again similar to IspG the enzymes mechanism for the conversion of HMBPP (**89**) to the products **90** and **91** (Figure 1.46) was complex and is a matter of debate. Proposed intermediates within the mechanism included radical, carbocation, carbanion, and ferraoxetane structures, but none could be identified definitively.[285,294–296] Isotopic labelling studies have aided a proposed mechanism which is described elsewhere.[298–300]

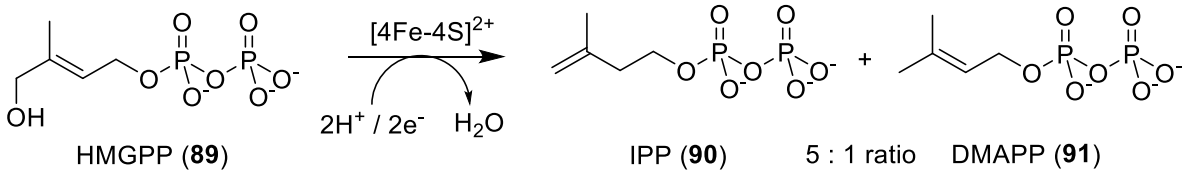

Figure 1.46. Formation of IPP (90) and DMAPP (91).

1.6 Targeting the MEP Pathway

The *P. falciparum* parasite belongs to a group of organisms of the phylum *Apicomplexa*, which can be identified by the existence of an additional plastid organelle known as the apicoplast.[301] The apicoplast is a relict plastid organelle; its heritage is similar to that of chloroplasts and mitochondria, as it contains its own unique DNA sequence. This plastid is derived from a secondary endosymbiotic origin; it was derived first from the invasion of a eukaryotic cell by a cyanobacterium, this was was subsequently engulfed by a second eukaryotic cell which preserved the first cell as a plastid.[302] A unique feature of the apicoplast is that it contains four cell membranes, and though derived from photosynthetic origin, has lost the ability to photosynthesise.[302]

The exact functions of the apicoplast within the malaria parasite are not fully known, however, it has been identified that the MEP pathway is localised within this organelle along with all of the

pathways constituent enzymes.[303,304] Interestingly the enzymes are not encoded by the apicoplast DNA, rather encoded by the parasite nucleus and then transported to the apicoplast where they carry out their function.[273] The biosynthesis of isoprenoids by the apicoplast is in operation during intraerythrocytic stage of the parasite and is essential for parasite survival.[305] Other known functions of the apicoplast include type II fatty acid biosynthesis and *de novo* haem biosynthesis, however, in contrast to the MEP pathway, these functions are essential to parasite survival at the mosquito and liver stages.[303,306] These plastid specific functions make the apicoplast an interesting organelle for drug development, indeed the antibiotic tetracycline which can be used for antimalarial chemotherapy is known to target the apicoplast, validating it as a drug target.[307] Further to this the MEP pathway has also been validated as a potential target for antimalarial chemotherapy since the discovery that fosmidomycin (**92**) (Figure 1.47) inhibits the second enzyme in the pathway IspC.

The MEP pathway is gaining interest for chemical interruption due to its parasite specificity over human hosts.[305] The pathway has been genetically validated in numerous organisms and is already being explored for the development of treatments of numerous antimicrobial diseases including malaria and tuberculosis.[255,308,309] Further to this the phylogenic exclusivity of the pathway to these organisms raises the potential to avoid unwanted drug side effects *via* inhibition of human isoprenoid biosynthesis, through the selective inhibition of the enzymes belonging to the pathway.

The seven steps belonging to the MEP pathway are all linear and each enzyme is highly substrate specific generating a specific product for the next enzyme. Chemical interruption of any of the enzymes should prove fatal to the parasite, as each specific step is fundamental for the continuation of the pathway and thus the *de novo* biosynthesis of isoprenoids.[273,310] To date there is no known alternate pathway for the generation of the intermediates of the MEP pathway in the malaria parasite. Though should they exist, an argument can be made to target the earlier stages of the pathway to avoid these problems, furthermore due to the linearity of the pathway, targeting earlier stages could lead to higher levels of parasite death.

The exact requirement for isoprenoids in malaria has not yet been fully elucidated due to the complexity of the parasite and its scavenging capabilities.[310] For example the parasite cannot synthesise certain isoprenoids, such as sterols and cholesterol, instead it requires uptake of these compounds from the host cells.[311] Thus inhibiting the MEP pathway will have no effect of sterol regulation. However, other isoprenoids have been identified that are synthesised *de novo* by the parasite due to the lack of scavenger pathways and have functions that are essential for parasite survival. These include, first; ubiquinone, which is synthesised *de novo* within the parasitic mitochondria and is reliant on the synthesis of IPP (**90**) and DMAPP (**91**). Ubiquinone is required for

the function of the DHODH enzyme discussed in **Section 1.3.2.3** and interruption of this causes cessation of pyrimidine biosynthesis.[310] Second; protein prenylation, a post-translational modification of proteins which is responsible for protein-protein interactions and is required for numerous processes such as DNA replication.[312] Third; carotenoids, which are thought to function as antioxidants in the parasite,[313] and fourth; the biosynthesis of dolicol, which is required for *N*-linked glycoslation and is essential for intraerythrocytic parasitic development.[313] The disruption in the available pool of **90** and **91** could potentially show fallout for all of the above mentioned pathways and therefore result in unrecoverable parasite death.

To summarise, the MEP pathway has emerged as a novel chemotherapeutic target for the development of new antimalarial drug therapies. The pathway is parasite specific with the constituent enzymes possessing a differing evolutionary background; this gives a unique opportunity to interrupt the biosynthesis of IPP (**90**) and DMAPP (**91**) without the issue of interrupting host biosynthesis due to the existence of an entirely distinct pathway, potentially circumventing toxicity issues. The pathway has been validated as a viable target since the identification of fosmidomycin (**92**) (Figure 1.47) as an efficacious inhibitor of the IspC enzyme (**Section 1.6.1**). It is a completely linear pathway with all seven of the enzymes having the potential to be targeted for small molecule inhibition, and due to its exclusivity, novel combination therapeutics could target numerous enzymes in the pathway in order to ensure complete parasitic clearance. The remainder of the chapter will give an overview of known inhibitors of IspC, known inhibitors of IspD and introduce our line of work on the IspD enzyme.

1.6.1 Inhibitors of IspC

IspC is the most extensively studied enzyme of the MEP pathway, this can in part be attributed to the discovery that fosmidiomycin (**92**) is a potent inhibitor of *P. falciparum* and *E. coli* IspC (Figure 1.47).[314] Despite the discovery of **92** and the numerous available crystal structures of IspC, the rational development of novel inhibitors is difficult, owing to the conformational change of the enzyme upon substrate or inhibitor binding.[315] Due to the flexibility of the active site, some inhibitors based on the fosmidomycin scaffold are hypothesised to possess a reversed binding mode in comparison to **92** itself, further complicating the target based design of inhibitors.[316]

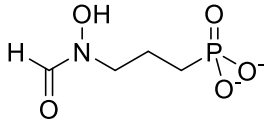

Fosmidomycin (**92**)

IC_{50} = 32 nM (*Pf*IspC)
IC_{50} = 290 ± 130 nM (*Pf*Dd2)
IC_{50} = 35 nM (*Ec*IspC)

Figure 1.47. Fosmidomycin (92).[304,314,317]

92 is a natural product isolated from *Streptomyces lavendulae* and was first identified in the 1980s, after which it was initially used as an antibiotic agent. It was later discovered to act as a substrate mimic of DXS *in vitro* against IspC where it acts as a competitive inhibitor.[318] **92** showed good promise during the early activity studies of the compound, demonstrating the ability to cure rodent malaria *P. vinckei* in mice and also demonstrated activity against multidrug resistant *P. falciparum* strains.[304] Both fosmidomycin (**92**) and its closely related acetyl analogue FR-900098 (**93**) (isolated from *S. rubellomurinus*) (Figure 1.48) have demonstrated high potency in the inhibition of the Dd2 strain of *P. falciparum* growth *in vitro*, with IC_{50} values of 290 ± 130 nM and 90 ± 20 nM, respectively.[304] Fosmidomycin (**92**) demonstrates an excellent safety profile with a half maximal lethal dose (LD_{50}) concentration of 11,000 $mgkg^{-1}$ in mice.[319] This impressive result confirms the MEP pathway can be selectively and safely targeted over the MVA pathway in mammals. Despite these promising activities the two drug molecules cannot be taken as part of a single dose regimen, they are highly polar, water soluble molecules. This results in a sub-optimal pharmacokinetic profile, showing in a poor *in vivo* half-life, poor oral bioavailability, rapid clearance from the parasite and high recrudescence rates.[320] Although fosmidomycin (**92**) is also a potent inhibitor of *M. tuberculosis* IspC *in vitro* it demonstrates little activity in the cellular assay, likely due to the inability of the drug to pass through the bacterial cell wall.[315] **92** progressed to clinical trials with clindamycin (**94**) (Figure 1.48) as a combination therapy in 2004, but was halted due to the lack of efficacy in children under the age of three coupled with high recrudescence rates.[321] It is currently in phase II clinical trials with piperaquine (**14**) as part of another combination therapy.[322]

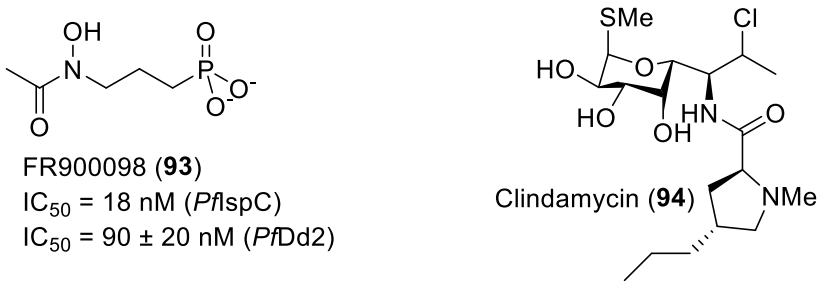

Figure 1.48. FR900098 (93) and clindamycin (94).[304,317]

Most of the inhibitors of IspC to date are based around the fosmidomycin scaffold, with attempts focused on boosting the lipophilicity to obtain better *in vivo* and pharmacokinetic profiles. Attempts have been made to replace the hydroxamate moiety of fosmidomycin (**92**) despite knowing that this functional group is required for strong cation binding in the active site.[317] However, the hydoxamate group can be rapidly metabolised *in vivo* either by hydrolysis, glucuronidation or sulfonation.[315] To date, replacement of either the hydroxamate, replacement of the phosphonate

group or modifications to the carbon backbone have mainly resulted in diminished metabolic stability or a loss of affinity.[323–325]

Promisingly a series of α-aryl substituents led to the development of **95** (Figure 1.49) with antimalarial potency greater than that of **92** against *Pf*Dd2.[326] Reverse fosmidomycin derivatives have also been synthesised which contain a hydroxamic acid moiety as the core.[327] Of these derivatives those possessing an aryl substituent α to the phosphate drove the development of **96** (Figure 1.49) which is a highly potent antimalarial compound that also possesses good activity against *E. coli*.[327] Research by Deng *et al.* identified a non-fosmidomycin like scaffold which displayed moderate activity against *E. coli* IspC. The novel chemotype is an aryl-substituted hydroxy-pyridinone scaffold **97** (Figure 1.49), the same group also identified a similar scaffold compound **98**, which displayed improved sub-micromolar activity against *E. coli* IspC (Figure 1.49).[316,328] These findings suggest that a thorough exploration of chemical space may be crucial to further discover new inhibitors of the IspC enzyme.

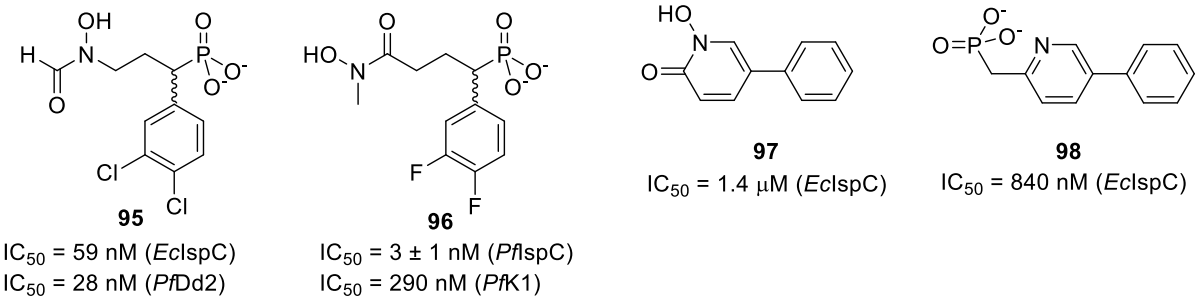

Figure 1.49. α-aryl inhibitors, reverse fosmidomycin, inhibitors, and novel scaffolds targeting IspC.[316,326–328]

1.6.2 Inhibitors of IspD

IspD has been much less studied than its IspC counterpart despite the number of available crystal structures. Fosmidomycin (**92**) is the only MEP pathway inhibitor to find its way into clinical trials and thus there is a vast array of unexplored opportunities to further develop novel chemotherapies to target the other constituent enzymes of the MEP pathway. The IspD enzyme is a cytidyltransferase, which is uncommon as CTP is not often found as a substrate for enzymatic transformations in comparison to ATP and GTP. The enzyme therefore possesses two unusual substrates, with the other substrate being MEP. These attributes potentially mean the enzyme can be targeted safely. This led us to our goal, which is to identify and design novel inhibitors of this enzyme in *P. falciparum*, with the ultimate aim of developing a lead candidate to be taken forward as an effective antimalarial therapeutic targeting the MEP pathway.

In a similar manner to fosmidomycin (**92**) the first known inhibitor of IspD was a demethylated structural mimic of the substrate MEP (**85**), known as erythritoyl 4-phosphate (**99**) with unspecified

configuration (Figure 1.50). Unlike fosmidomycin (**92**), the molecule showed very weak activity against both *E. coli*, with an IC_{50} value of 1.38 mM[329] Masini *et al.* demonstrated that the IspD active site is the most polar active site of all of the MEP pathway enzymes; furthermore the CTP binding site is exposed to solvent, which therefore means there is a significant challenge in the generation of substrate competitive inhibitors of this enzyme.[330]

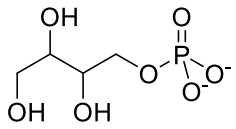

Erythritol 4-phosphate (**99**)
IC_{50} = 1.38 mM (*Ec*IspD)

Figure 1.50. Erythritol 4-phosphate (99).[329]

A diversity-based HTS was carried out by BASF for the purpose of identifying new herbicidal based molecules targeting *Arabidopsis thaliana* IspD, after it was discovered that IspD functionality was essential for plant survival.[331] From the screen the most active hit **100** (Figure 1.51) possessed a triazolopyrimidine scaffold with an unprecedented sub-micromolar IC_{50} activity of 140 ± 10 nM. The group led by Witschel, identified that based on the crystal structure of *A. thaliana* IspD there was no reasonable docking mode of the hit within the enzyme active site. The group decided to co-crystallise the hit with the enzyme, they successfully elucidated that the hit binds within an allosteric pocket proximal to the active site, causing a conformational change, decreasing the size of the active site and resulting in the failure of substrate binding.[331] Further optimisation of the template led to the development of the nitrile derivative of **101** with an IC_{50} value of 35 ± 7 nM (Figure 1.51).[331]

After the success of the triazolopyrimidines Kunfermann *et al.* carried out another HTS screen, which identified the highly halogenated marine alkaloids belonging to the pseudilin class, as inhibitors of the IspD enzyme.[332] The compounds were tested against *At*IspD and *Pv*IspD, interestingly in the case of *At*IspD the activity was shown to be dependent on the addition of divalent cations, in particular, Cd^{2+} which gave a 7-fold increase in activity for the hit molecule **102** with an IC_{50} of 1400 ± 200 nM (Figure 1.51).[332] The inhibitors were less potent against *Pv*IspD showing double-digit µM IC_{50} values with little dependence on cations. The crystal structure of *At*IspD was solved with the inhibitor and the Cd^{2+} metal ion bound within the same allosteric pocket as the triazolopyrimidines.[331,332] Unfortunately, this specific class of inhibitors was found to be cytotoxic to mammalian cells suggesting multiple molecular targets. Furthermore, the poorer activity associated with *Pv*IspD suggests that this allosteric pocket is structurally different or not present with other IspD homologues and thus is species specific.[332]

Another class of inhibitors was identified by BASF in their HTS of *At*IspD with a scaffold belonging to acetylated aminobenzothiazoles **103** (Figure 1.51). However, the activities where only in the low µM range and were not optimised, further to this the mechanism of action was not investigated.[333]

Recently a HTS screen of *Pf*IspD carried out by our research group(s) in collaboration with Biofocus, discovered a novel class of inhibitors belonging to the benzoisothiazolinone (BITZ) scaffold **104** (Figure 1.51). Unfortunately, due to the absence of *Pf*IspD enzyme crystal structures, exact binding modes could not be determined. In spite of this, the proposed mechanism of action is thought to proceed *via* the formation of a covalent adduct within the enzyme active site preventing substrate binding, this class of inhibitors is further investigated in Chapter 3 of this thesis.[334] Wu *et al.* also determined a tetrahydro-β-carboline chemotype as another inhibitor of *Pf*IspD named MMV008138 (**105**) (Figure 1.51).[335] **105** was initially found to possess potent antiplasmodial activity from a phenotypic screen of the of the GlaxoSmithKline (GSK) compound library.[336] The structure of **105** and other newly discovered antimalarial compounds were made available free of charge by the Medicines for Malaria Venture (MMV) as part of the malaria box programme.[337] The target of **105** was identified to be IspD after mutations in the *ygbP* gene led to resistance against the compound. Research from our group and Yao *et al*. from chemical rescue screens and activity studies have demonstrated that this compound is a potent *Pf*IspD inhibitor displaying low nM activity against the enzyme, and moderate nM activity against *Pf* whole cell assays.[338,339] Therefore this scaffold presents a highly promising opportunity for further development in order to develop a candidate drug targeting *Pf*IspD, and is discussed in Chapter 2 of this thesis.

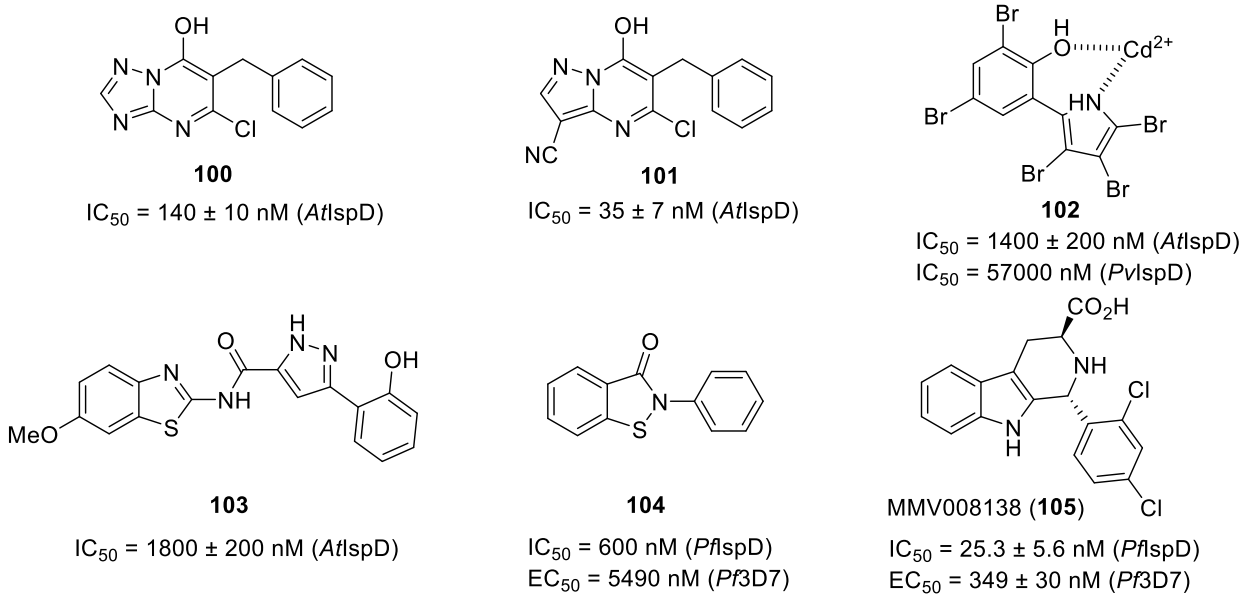

Figure 1.51. Inhibitors of IspD.[331–335]

1.7 Aim

The MEP pathway is responsible for the biosynthesis of crucial isoprenoid precursors IPP (**90**) and DMAPP (**91**) from which all isoprenoids are derived. Its absence from mammalian cells makes this particular pathway an attractive drug target as compounds can be designed to be enzyme selective, there-by reducing potential unwanted side effects. The chemical interruption of precursor development has the potential to shut down numerous parasitic biological functions which rely on the *de novo* synthesis of isoprenoids, were the loss of these crucial compounds could result in parasite death. This research focuses on the inhibition of specifically the *P. falciparum* homologue of the third enzyme in the MEP pathway IspD. The enzyme has been genetically validated and has been demonstrated to be druggable. The pathway itself has been validated as a drug target owing to the success of fosmidomycin, inhibiting the second enzyme of the MEP pathway IspC and the only MEP pathway inhibitor to be taken to clinical trials.

There are very few known inhibitors of IspD, and until recently there were no inhibitors with an IC_{50}, of sub 1 μM. This coupled with the unusual substrates for this enzyme made this particular enzyme of interest to us. As the MEP pathway is linear and IspD is an early enzyme, the inhibition of this upstream enzyme could have a greater potential to cause parasite death. Furthermore, the downstream IspF enzyme has been proposed to rely upon cMEPP and MEP to carry out potential regulatory functions for the MEP pathway.[340,341] Sustained levels of cMEPP have also been demonstrated to be essential for other biochemical processes as well; therefore the loss of function of IspD could ultimately also cause a loss of function of the MEP pathway as a whole along with other biochemical targets.[315] As the MEP pathway and IspD are novel biochemical targets, there is high potential that any compounds targeting IspD will have the potential to kill multidrug resistant strains of *P. falciparum* thus offering renewed hope for the eradication of the disease, and against the battle of *P. falciparum* strains now resistant to all frontline therapies.

The ultimate goal of this research is to identify and develop a novel lead candidate template through the guidance of SAR studies that has potent *in vitro* activity against *Pf*IspD and *P. falciparum* parasites. The strain of *P. falciparum* being used for this research is the 3D7 strain, which is chloroquine sensitive, but sulfadoxine resistant. Compounds of interest will be taken for studies on their *in vitro* pharmacokinetic profile, with identified leads taken forward to *in vivo* studies.

1.8. References

(1) World Health Organization. *World Malaria report*; **2016**, Geneva. License: CC BY-NC-SA 3.0 IGO. (Accessed 14th March **2017**)
(2) World Health Organization. *State of health financing in the African Region*; **2013**. (Accessed

14th March **2017**)
(3) Oddoux, O.; Debourgogne, A.; Kantele, A.; Kocken, C. H.; Jokiranta, T. S.; Vedy, S.; Puyhardy, J. M.; Machouart, M. *Eur. J. Clin. Microbiol. Infect. Dis.* **2011**, *30* (4), 597–601.
(4) Renslo, A. R. *ACS Med. Chem. Lett.* **2013**, *4* (12), 1126–1128.
(5) Global Malaria Progamme. *Control and Elimination of Plamodium Vivax Malaria - A Technical Brief*; **2015**, (Accessed 14th March **2017**).
(6) Florens, L.; Washburn, M. P.; Raine, J. D.; Anthony, R. M.; Grainger, M.; Haynes, J. D.; Moch, J. K.; Muster, N.; Sacci, J. B.; Tabb, D. L.; Witney, A. A.; Wolters, D.; Wu, Y.; *et al.* D. J. *Nature* **2002**, *419* (6906), 520–526.
(7) Greenwood, B. M.; Fidock, D. A.; Kyle, D. E.; Kappe, S. H. I.; Alonso, P. L.; Collins, F. H.; Duffy, P. E. *J. Clin. Invest.* **2008**, *118* (4).
(8) Center for Disease Control and Prevention (CDC), CDC - DPDx/ Alexander J. da Silva Melanie Moser, **2016**. (Accessed 15th March **2017**)
(9) Vaughan, A. M.; Aly, A. S. I.; Kappe, S. H. I. *Cell Press* **2008**, *4* (3), 209–218.
(10) Yamauchi Lucy M., L. M.; Coppi, A.; Snounou, G.; Sinnis, P. *Cell. Microbiol.* **2007**, *9* (5), 1215–1222.
(11) Silvie, O.; Mota, M. M.; Matuschewski, K.; Prudêncio, M. *Curr. Opin. Microbiol.* **2008**, *11* (4), 352–359.
(12) Kebaier, C.; Voza, T.; Vanderberg, J. *PLoS Pathog.* **2009**, *5* (4).
(13) Amino, R.; Thiberge, S.; Martin, B.; Celli, S.; Shorte, S.; Frischknecht, F.; Ménard, R. *Nat. Med.* **2006**, *12* (2), 220–224.
(14) Jones, M. K.; Good, M. F. *Nat. Med.* **2006**, *12* (2), 170–171.
(15) Tuteja, R. *FEBS J.* **2007**, *274* (18), 4670–4679.
(16) Cowman, A. F.; Crabb, B. S. *Cell* **2006**, *124* (4), 755–766.
(17) Pukrittayakamee, S.; Imwong, M.; Singhasivanon, P.; Stepniewska, K.; Day, N. J.; White, N. J. *Am. J. Trop. Med. Hyg.* **2008**, *79* (3), 378–384.
(18) Miller, L. H.; Baruch, D. I.; Marsh, K.; Doumbo, O. K. *Nature* **2002**, *415* (6872), 673–679.
(19) Weatherall, D. J.; Miller, L. H.; Baruch, D. I.; Marsh, K.; Doumbo, O. K.; Casals-Pascual, C.; Roberts, D. J. *Hematology Am. Soc. Hematol. Educ. Program* **2002**, 35–57.
(20) Bartoloni, A.; Zammarchi, L. *Mediterr. J. Hematol. Infect. Dis.* **2012**, *4* (1).
(21) Battle, K. E.; Gething, P. W.; Elyazar, I. R. F.; Moyes, C. L.; Sinka, M. E.; Howes, R. E.; Guerra, C. A.; Price, R. N.; Baird, K. J.; Hay, S. I. *The Global Public Health Significance of Plasmodium vivax*; Elsevier, **2012**; Vol. 80.
(22) Rogerson, S. J.; Carter, R. *PLoS Med.* **2008**, *5* (6), 0881–0889.
(23) Antinori, S.; Corona, A.; Ridolfo, A. L.; Galimberti, L.; Ricaboni, D.; Milazzo, L.; Corbellino, M. *Malar. J.* **2016**, *15* (1), 105.
(24) Antinori, S.; Milazzo, L.; Ridolfo, A. L.; Galimberti, L.; Corbellino, M. *Clin. Infect. Dis.* **2012**, *55* (11), 1581–1583.
(25) Alexandre, M. A.; Ferreira, C. O.; Siqueira, A. M.; Magalhães, B. L.; Mourão, M. P. G.; Lacerda, M. V.; Alecrim, M. das G. C. *Emerg. Infect. Dis.* **2010**, *16* (10), 1611–1614.
(26) Rodriguez-Morales, A. J.; Benítez, J. A.; Arria, M. *J. Trop. Pediatr.* **2008**, *54* (2), 94–101.
(27) Anstey, N. M.; Russell, B.; Yeo, T. W.; Price, R. N. *Cell Press* **2009**, *25* (5), 220–227.
(28) Price, R. N.; Tjitra, E.; Guerra, C. A.; Yeung, S.; White, N. J.; Anstey, N. M. *Am. Soc. Trop. Med. Hyg.* **2009**, *77* (61), 79–87.
(29) Shanks, G. D.; White, N. J. *Lancet Infect. Dis.* **2013**, *13* (10), 900–906.
(30) White, N. J. *Malar. J.* **2011**, *10* (1), 297.
(31) Mendis, K.; Sina, B. J.; Marchesini, P.; Carter, R. *Am. J. Trop. Med. Hyg.* **2001**, *64* (1–2 SUPPL.), 97–106.
(32) Gething, P. W.; Elyazar, I. R. F.; Moyes, C. L.; Smith, D. L.; Battle, K. E.; Guerra, C. A.; Patil, A. P.; Tatem, A. J.; Howes, R. E.; Myers, M. F.; George, D. B.; Horby, P.; *et al. PLoS Negl. Trop. Dis.* **2012**, *6* (9).

(33) Mueller, I.; Galinski, M. R.; Baird, J. K.; Carlton, J. M.; Kochar, D. K.; Alonso, P. L.; del Portillo, H. A. *Lancet Infect. Dis.* **2009**, *9* (9), 555–566.
(34) Sadasivaiah, S.; Tozan, Y.; Breman, J. G. *Am. J. Trop. Med. Hyg.* **2007**, *77* (SUPPL. 6), 249–263.
(35) Fry, D. M. *Environ. Health Perspect.* **1995**, *103* (SUPPL. 7), 165–171.
(36) Wurster CF Jr, Wurster DH, S. W. *Science (80-.).* **1965**, *148*, 90–91.
(37) Wolff, M. S.; Zeleniuch-jacquotte, A.; Dubin, N.; Toniolo, P. *Cancer Epidemiol. Biomarkers Prev.* **2000**, *9* (March), 271–277.
(38) IARC (International Agency for Research on Cancer). *IARC Monographs evaluate DDT, lindane, and 2,4-D*; **2015**. (Accessed 21st March **2017**).
(39) World Health Organization. *Safety of Pyrethroids for Public Health Use*; 2005. (Accessed 21st March **2017**).
(40) Greenwood, B. M.; Bojang, K.; Whitty, C. J. M.; Targett, G. A. T. *Lancet* **2005**, *365* (9469), 1487–1498.
(41) Fernández-Álvaro, E.; Hong, W. D.; Nixon, G. L.; O'Neill, P. M.; Calderón, F. *J. Med. Chem.* **2016**, *59* (12), 5587–5603.
(42) Foley, M.; Tilley, L. *Pharmacol. Ther.* **1998**, *79* (1), 55–87.
(43) Woodward, R. B.; Doering, W. E. *J. Nat. Prod.* **1944**, *66* (5), 849.
(44) Seeman, J. I. *Angew. Chemie - Int. Ed.* **2007**, *46* (9), 414–415.
(45) Raheem, I. T.; Goodman, S. N.; Jacobsen, E. N. *J. Am. Chem. Soc.* **2004**, *126* (3), 706–707.
(46) Igarashi, J.; Katsukawa, M.; Wang, Y. G.; Acharya, H. P.; Kobayashi, Y. *Tetrahedron Lett.* **2004**, *45* (19), 3783–3786.
(47) Stork, G.; Niu, D.; Fujimoto, R. a; Koft, E. R.; Balkovec, J. M.; Tata, J. R.; Dake, G. R. *J. Am. Chem. Soc.* **2001**, *123* (11), 3239–3242.
(48) Krafts, K.; Hempelmann, E.; Skórska-Stania, A. *Parasitol. Res.* **2012**, *111* (1), 1–6.
(49) Roehl, W. *Arch Schiffs-Tropenhyg* **1926**, *30* ((Suppl 3)), 311–318.
(50) Kondrashin, A.; Baranova, A. M.; Ashley, E. A.; Recht, J.; White, N. J.; Sergiev, V. P. *Malar. J.* **2014**, *13* (1), 1–15.
(51) Manifold, J. A. *J. R. Army Med. Corps* **1930**, *56* (6), 410–423.
(52) World Health Organization. *WHO Geneva* **2015**, *8* (3), 191. (Accessed 21st March **2017**).
(53) Slater, A. F. G.; Swiggard, W. J.; Orton, B. R.; Flitter, W. D.; Goldberg, D. E.; Cerami, A.; Henderson, G. B. *Proc. Natl. Acad. Sci. U. S. A.* **1991**, *88* (2), 325–329.
(54) Chinappi, M.; Via, A.; Marcatili, P.; Tramontano, A. *PLoS One* **2010**, *5* (11).
(55) Egan, T. J. *J. Inorg. Biochem.* **2008**, *102* (5–6), 1288–1299.
(56) Sullivan, D. J.; Matile, H.; Ridley, G.; Goldberg, D. E.; Ridley, R. G. **1998**, *273* (47), 31103–31107.
(57) Sullivan, D. J.; Gluzman, I. Y.; Russell, D. G.; Goldberg, D. E. *Proc. Natl. Acad. Sci. U. S. A.* **1996**, *93* (21), 11865–11870.
(58) Slater, A. F. G. *Pharmac. Ther* **1993**, *57*, 203–235.
(59) Pagola, S.; Stephens, P. W.; Bohle, D. S.; Kosar, a D.; Madsen, S. K. *Nature* **2000**, *404*, 307–310.
(60) Bray, P. G.; Mungthin, M.; Ridley, R. G.; Ward, S. A. *Mol. Pharmacol.* **1998**, *54* (1), 170–179.
(61) Bray, P. G.; Janneh, O.; Ward, S. a. *J Cell Biol* **1999**, *145* (2), 363–376.
(62) Yayon A, Cabantchik ZI, G. H. *EMBO J* **1984**, *3* (11), 2695–2700.
(63) Homewood, C. A.; Warhurst, D. C.; Peters, W.; Baggaley, V. C. *Nature* **1972**, *235* (5332), 50–52.
(64) Schlitzer, M. *ChemMedChem* **2007**, *2* (7), 944–986.
(65) Achan, J.; Talisuna, A. O.; Erhart, A.; Yeka, A.; Tibenderana, J. K.; Baliraine, F. N.; Rosenthal, P. J.; D'Alessandro, U. *Malar. J.* **2011**, *10* (1), 144.
(66) World Health Organization. *Guidelines For The Treatment of Malaria*; 2015. (Accessed 21st March **2017**)
(67) Fidock, D. A.; Nomura, T.; Talley, A. K.; Cooper, R. A.; Dzekunov, S. M.; Ferdig, M. T.; Ursos, L.

M.; Sidhu, A. B.; Naudé, B.; Deitsch, K. W.; Su, X. Z.; Wootton, J. C.; Roepe, P. D.; Wellems, T. E. *Mol. Cell* **2000**, *6* (4), 861–871.
(68) Bray, P. G.; Martin, R. E.; Tilley, L.; Ward, S. A.; Kirk, K.; Fidock, D. A. *Mol. Microbiol.* **2005**, *56* (2), 323–333.
(69) Wellems, T. E.; Plowe, C. V. *J.Infect.Dis.* **2001**, *184* (6), 770–776.
(70) Cooper, R. A.; Lane, K. D.; Deng, B.; Mu, J.; Patel, J. J.; Wellems, T. E.; Su, X.; Ferdig, M. T. *Mol. Microbiol.* **2007**, *63* (1), 270–282.
(71) Lehane, A. M.; Kirk, K. *Antimicrob. Agents Chemother.* **2008**, *52* (12), 4374–4380.
(72) Martin, R. E.; Kirk, K. *Mol. Biol. Evol.* **2004**, *21* (10), 1938–1949.
(73) Martin, R. E.; Marchetti, R. V; Cowan, A. I.; Howitt, S. M.; Bröer, S.; Kirk, K. *Science* **2009**, *325* (5948), 1680–1682.
(74) Johansson, T.; Jurva, U.; Grönberg, G.; Weidolf, L.; Masimirembwa, C. *Drug Metab. Dispos.* **2009**, *37* (3), 571–579.
(75) Gelb, M. H. *Curr. Opin. Chem. Biol.* **2007**, *11* (4), 440–445.
(76) O'Neill, P. M.; Mukhtar, A.; Stocks, P. A.; Randle, L. E.; Hindley, S.; Ward, S. A.; Storr, R. C.; Bickley, J. F.; O'Neil, I. A.; Maggs, J. L.; Hughes, R. H.; Winstanley, P. a; Bray, P. G.; Park, B. K. *J. Med. Chem.* **2003**, *46*, 4933–4945.
(77) Neftel, K. A.; Woodtly, W.; Schmid, M.; Frick, P. G.; Fehr, J. *Br. Med. J. (Clin. Res. Ed).* **1986**, *292* (6522), 721–723.
(78) Davis, T. M. E.; Hung, T.; Sim, I.; Karunajeewa, H. A.; Ilett, K. F. *Drugs* **2005**, *65* (1), 75–87.
(79) Adjuik, M.; Agnamey, P.; Babiker, A.; Borrmann, S.; Brasseur, P.; Cisse, M.; Cobelens, F.; Diallo, S.; Faucher, J. F.; Garner, P.; Gikunda, S.; Kremsner, P. G.; *et al. Lancet* **2002**, *359* (9315), 1365–1372.
(80) Congpuong, K.; Bualombai, P.; Banmairuroi, V.; Na-Bangchang, K. *Malar. J.* **2010**, *9*, 43.
(81) Croft, A. M. *J R Soc Med* **2007**, *100*, 170–174.
(82) Domarle, O.; Blampain, G.; Agnaniet, H.; Nzadiyabi, T.; Lebibi, J.; Brocard, J.; Maciejewski, L.; Biot, C.; Georges, A. J.; Millet, P. *Antimicrob. Agents Chemother.* **1998**, *42* (3), 540–544.
(83) Biot, C.; Glorian, G.; Maciejewski, L. A.; Brocard, J. S.; Domarle, O.; Blampain, G.; Millet, P.; Georges, A. J.; Lebibi, J. *J. Med.Chem.* **1997**, *40* (23), 3715–3718.
(84) Atteke, C.; Me Ndong, J. M.; Aubouy, A.; Maciejewski, L.; Brocard, J.; Lébibi, J.; Deloron, P. *J. Antimicrob. Chemother.* **2003**, *51* (4), 1021–1024.
(85) Delhaes, L.; Abessolo, H.; Biot, C.; Berry, L.; Delcourt, P.; Maciejewski, L.; Brocard, J.; Camus, D.; Dive, D. *Parasitol. Res.* **2001**, *87* (3), 239–244.
(86) O'Neill, P. M.; Park, B. K.; Shone, A. E.; Maggs, J. L.; Roberts, P.; Stocks, P. A.; Biagini, G. A.; Bray, P. G.; Gibbons, P.; Berry, N.; Winstanley, P. A.; Mukhtar, A.; *et al. J. Med. Chem.* **2009**, *52* (5), 1408–1415.
(87) O'Neill, P. M.; Barton, V. E.; Ward, S. A.; Chadwick, J. In *Treatment and Prevention of Malaria: Antimalarial Drug Chemistry, Action and Use*; **2012**; pp 19–44.
(88) Schmidt, L. H.; Alexander, S.; Allen, L.; Rasco, J. *Antimicrob. Agents Chemother.* **1977**, *12* (1), 51–60.
(89) Baird, J. K.; Wiady, I.; Sutanihardja, A.; Suradi; Purnomo; Basri, H.; Sekartuti; Ayomi, E.; Fryauff, D. J.; Hoffman, S. L. *Am. J. Trop. Med. Hyg.* **2002**, *66* (6), 659–660.
(90) Geary, T. G.; Divo, A. A.; Jensen, J. B. *Trans. R. Soc. Trop. Med. Hyg.* **1987**, *81* (3), 499–503.
(91) ARNOLD, J.; ALVING, A. S.; HOCKWALD, E. S.; CLAYMAN, C. B.; DERN, R. J.; BEUTLER, E.; FLANAGAN, C. L.; JEFFERY, G. M. *J. Lab. Clin. Med.* **1955**, *46* (3), 391–397.
(92) Pukrittayakamee, S.; Chotivanich, K.; Chantra, A.; Clemens, R.; Looareesuwan, S.; White, N. J. *Antimicrob. Agents Chemother.* **2004**, *48* (4), 1329–1334.
(93) Beutler, E.; Duparc, S. *Am. J. Trop. Med. Hyg.* **2007**, *77* (4), 779–789.
(94) Beutler, E. *Blood* **1959**, *14*, 103–109.
(95) Shanks, G.; Oloo, A.; Aleman, G.; Ohrt, C.; Klotz, F.; Braitman, D.; Horton, J.; Brueckner, R. *Clin Infect Dis* **2001**, *33* (12), 1968–1974.

(96) Ponsa, N.; Sattabongkot, J.; Kittayapong, P.; Eikarat, N.; Coleman, R. E. *Am. J. Trop. Med. Hyg.* **2003**, *69* (5), 542–547.
(97) Brueckner, R. P.; Lasseter, K. C.; Lin, E. T.; Schuster, B. G. *Am. J. Trop. Med. Hyg.* **1998**, *58* (5), 645–649.
(98) Pybus, B. S.; Sousa, J. C.; Jin, X.; Ferguson, J. A.; Christian, R. E.; Barnhart, R.; Vuong, C.; Sciotti, R. J.; Reichard, G. A.; Kozar, M. P.; Walker, L. A.; Ohrt, C.; Melendez, V. *Malar J* **2012**, *11*, 259.
(99) Nzila, A.; Ward, S. A.; Marsh, K.; Sims, P. F. G.; Hyde, J. E. *Trends Parasitol.* **2005**, *21* (6), 292–298.
(100) Nzila, A.; Ward, S. A.; Marsh, K.; Sims, P. F. G.; Hyde, J. E. *Trends Parasitol.* **2005**, *21* (7), 334–339.
(101) Metz, J. *Food Nutr Bull* **2007**, *28* (4 Suppl), S540-9.
(102) Hyde, J. E. *Acta Trop.* **2005**, *94*, 191–206.
(103) Krungkrai, S. R.; Krungkrai, J. *Asian Pac. J. Trop. Med.* **2016**, *9* (6), 525–534.
(104) Zhang, K.; Rathod, P. K. *Science* **2002**, *296* (5567), 545–547.
(105) Nzila, A. *J. Antimicrob. Chemother.* **2006**, *57* (6), 1043–1054.
(106) Curd, F. H. S.; Davey, D. G.; Rose, F. L. *Ann. Trop. Med. Parasitol.* **1945**, *39* (3–4), 208–216.
(107) Carrington, H. C.; Crowther, A. F.; Davey, D. G.; Levi, A. A.; Rose, F. L. *Nature*. 1951, p 1080.
(108) Burchall, J. J. *Mol. Pharmacol.* **1969**, *5* (1), 49–59.
(109) Kain, K. C. *BioDrugs* **2003**, *17* (Suppl. 1), 23–28.
(110) Kain, K. C.; Shanks, G. D.; Keystone, J. S. *Clin. Infect. Dis.* **2001**, *33* (2), 226–234.
(111) Shanks, G. D.; Kain, K. C.; Keystone, J. S. *Clin. Infect. Dis.* **2001**, *33* (3), 381–385.
(112) Peters, W. *Br. Med. J.* **1971**, *2* (5753), 95–98.
(113) Berman, J. D.; Nielsen, R.; Chulay, J. D.; Dowler, M.; Kain, K. C.; Kester, K. E.; Williams, J.; Whelen, A. C.; Shmuklarsky, M. J. *Trans R Soc Trop Med Hyg* **2001**, *95* (4), 429–432.
(114) FALCO, E. A.; GOODWIN, L. G.; HITCHINGS, G. H.; ROLLO, I. M.; RUSSELL, P. B.; *Br. J. Pharmacol.* **1951**, *6* (2), 185–200.
(115) BUTTLE, G. A. H.; STEPHENSON, D.; SMITH, S.; FOSTER, G. E. *Lancet* **1937**, 1331–1334.
(116) Sheehy, T.; Reba, R.; Neff, T.; Gaintner, J.; Tigertt, W. *Arch. Intern. Med.* **1967**, *119* (6), 561–566.
(117) Rieckmann, K. H.; Brewer, G. J.; Powell, R. D. *Trans. R. Soc. Trop. Med. Hyg.* **1968**, *62* (5), 649–653.
(118) Watkins, W. M.; Mosobo, M.; Watkins, W. M. *Trans. R. Soc. Trop. Med. Hyg.* **1993**, *87* (1), 75–78.
(119) Segal, H. E.; Chinvanthananond, P.; Laixuthai, B.; Pearlman, E. J.; Hall, A. P.; Phintuyothin, P.; Na-Nakorn, A.; Castaneda, B. F. *Trans. R. Soc. Trop. Med. Hyg.* **1975**, *69* (1), 139–142.
(120) Winstanley, P.; Watkins, W.; Muhia, D.; Szwandt, S.; Amukoye, E.; Marsh, K. *Trans. R. Soc. Trop. Med. Hyg.* **1997**, *91* (3), 322–327.
(121) Sridaran, S.; McClintock, S. K.; Syphard, L. M.; Herman, K. M.; Barnwell, J. W.; Udhayakumar, V. *Malar. J.* **2010**, *9*, 247.
(122) Warhurst, D. C. *Drug Discov. Ther.* **1998**, *3* (12), 538–546.
(123) Wu, Y.; Kirkman, L. A.; Wellems, T. E. *Proc. Natl. Acad. Sci. U. S. A.* **1996**, *93* (3), 1130–1134.
(124) Peterson, D. S.; Walliker, D.; Wellems, T. E. *Proc. Natl. Acad. Sci. U. S. A.* **1988**, *85* (23), 9114–9118.
(125) Abdul-Ghani, R.; Farag, H. F.; Allam, A. F. *Acta Trop.* **2013**, *125* (2), 163–190.
(126) Canfield, C. J.; Milhous, W. K.; Ager, A. L.; Rossan, R. N.; Sweeney, T. R.; Lewis, N. J.; Jacobus, D. P. *Am. J. Trop. Med. Hyg.* **1993**, *49* (1), 121–126.
(127) Yuthavong, Y.; Tarnchompoo, B.; Vilaivan, T.; Chitnumsub, P.; Kamchonwongpaisan, S.; Charman, S. A.; McLennan, D. N.; White, K. L.; Vivas, L.; *et al. Proc. Natl. Acad. Sci. U. S. A.* **2012**, *109* (42), 16823–16828.
(128) Yuthavong, Y.; Yuvaniyama, J.; Chitnumsub, P.; Vanichtanankul, J.; Chusacultanachai, S.; Tarnchompoo, B.; Vilaivan, T.; Kamchonwongpaisan, S. *Parasitology* **2005**, *130* (2005), 249–

259.
(129) Gao, G.; Nara, T.; Nakajima-Shimada, J.; Aoki, T. *J. Mol. Biol.* **1999**, *285* (1), 149–161.
(130) Krungkrai, J.; Krungkrai, S. R.; Phakanont, K. *Biochem. Pharmacol.* **1992**, *43* (6), 1295–1301.
(131) Pels Rijcken, W. R.; Overdijk, B.; van den Eijnden, D. H.; Ferwerda, W. *Biochem. J.* **1993**, *293*, 207–213.
(132) Krungkrai, J.; Cerami, a; Henderson, G. B. *Biochemistry* **1991**, *30* (7), 1934–1939.
(133) Seymour, K. K.; Lyons, S. D.; Phillips, L.; Rieckmann, K. H.; Christopherson, R. I. *Biochemistry* **1994**, *33* (17), 5268–5274.
(134) Phillips, M. a; Rathod, P. K. *Infect.Disord.Drug Targets.* **2010**, *10* (1871–5265 (Print)), 226–239.
(135) Heikkilä, T.; Ramsey, C.; Davies, M.; Galtier, C.; Stead, A. M. W.; Johnson, A. P.; Fishwick, C. W. G.; Boa, A. N.; McConkey, G. A. *J. Med. Chem.* **2007**, *50* (2), 186–191.
(136) Krungkrai, J. *Biochim. Biophys. Acta - Gen. Subj.* **1995**, *1243* (3), 351–360.
(137) Hurt, D. E.; Widom, J.; Clardy, J. *Acta Crystallogr. Sect. D Biol. Crystallogr.* **2006**, *62* (3), 312–323.
(138) Krungkrai, J.; Kanchanaphum, P.; Krungkrai, S. R. *Asian Pac. J. Trop. Med.* **2008**, *1* (1), 31–49.
(139) Baldwin, J.; Michnoff, C. H.; Malmquist, N. A.; White, J.; Roth, M. G.; Rathod, P. K.; Phillips, M. A. *J. Biol. Chem.* **2005**, *280* (23), 21847–21853.
(140) Phillips, M. A.; Gujjar, R.; Malmquist, N. A.; White, J.; El Mazouni, F.; Baldwin, J.; Rathod, P. K. *J. Med. Chem.* **2008**, *51* (12), 3649–3653.
(141) Booker, M. L.; Bastos, C. M.; Kramer, M. L.; Barker, R. H.; Skerlj, R.; Sidhu, A. B.; Deng, X.; Celatka, C.; Cortese, J. F.; Guerrero Bravo, J. E.; Crespo Llado, K. N.; *et al. J. Biol. Chem.* **2010**, *285* (43), 33054–33064.
(142) Dickerman, B. K.; Elsworth, B.; Cobbold, S. A.; Nie, C. Q.; McConville, M. J.; Crabb, B. S.; Gilson, P. R.; Dondorp, A. M.; Pillai, A. D.; Liu, J.; Istvan, E. S.; *et al. Sci. Rep.* **2016**, *6* (November), 37502.
(143) Coteron, J. M. *J. Med. Chem.* **2011**, *54*, 5540–5561.
(144) Phillips, M. A; Lotharius, J.; Marsh, K.; White, J.; Dayan, A.; White, K. L.; Njoroge, J. W.; El Mazouni, F.; Lao, Y.; Kokkonda, S.; Tomchick, D. R.; Deng, X.; Laird, T.; *et al. Sci. Transl. Med.* **2015**, *7* (296).
(145) Hudson, A. T.; Dickins, M.; Ginger, C. D.; Gutteridge, W. E.; Holdich, T.; Hutchinson, D. B.; Pudney, M.; Randall, A. W.; Latter, V. S. *Drugs Exp. Clin. Res.* **1991**, *17* (9), 427–435.
(146) Fry, M.; Pudney, M. *Biochem. Pharmacol.* **1992**, *43* (7), 1545–1553.
(147) Nilsen, A.; LaCrue, A. N.; White, K. L.; Forquer, I. P.; Cross, R. M.; Marfurt, J.; Mather, M. W.; Delves, M. J.; Shackleford, D. M.; Saenz, F. E.; Morrisey, J. M.; Steuten, J. *et al. Sci. Transl. Med.* **2013**, *5* (177), 177ra37.
(148) Capper, M. J.; O'Neill, P. M.; Fisher, N.; Strange, R. W.; Moss, D.; Ward, S. A.; Berry, N. G.; Lawrenson, A. S.; Hasnain, S. S.; Biagini, G. A.; Antonyuk, S. V.; O'Neill, P. M. *et al. Proc. Natl. Acad. Sci.* **2015**, *112* (3), 201416611.
(149) Nixon, G. L.; Moss, D. M.; Shone, A. E.; Lalloo, D. G.; Fisher, N.; O'Neill, P. M.; Ward, S. A.; Biagini, G. A. *J. Antimicrob. Chemother.* **2013**, *68* (5), 977–985.
(150) Srivastava, I. K.; Rottenberg, H.; Vaidya, A. B. *J. Biol. Chem.* **1997**, *272* (7), 3961–3966.
(151) Biagini, G. A.; Viriyavejakul, P.; O'Neill, P. M.; Bray, P. G.; Ward, S. A. *Antimicrob. Agents Chemother.* **2006**, *50* (5), 1841–1851.
(152) Painter, H. J.; Morrisey, J. M.; Mather, M. W.; Vaidya, A. B. *Nature* **2007**, *446* (7131), 88–91.
(153) Goodman, C. D.; Buchanan, H. D.; McFadden, G. I. *Trends Parasitol.* **2017**, *33* (3), 185–193.
(154) Srivastava, I. K.; Morrlsey, J. M.; Darrouzet, E.; Daldal, F.; Vaidya, A. B. *Mol. Microbiol.* **1999**, *33* (4), 704–711.
(155) Korsinczky, M.; Chen, N.; Kotecka, B.; Saul, A.; Rieckmann, K.; Cheng, Q. *Antimicrob. Agents Chemother.* **2000**, *44* (8), 2100–2108.
(156) Musset, L.; Bouchaud, O.; Matheron, S.; Massias, L.; Le Bras, J. *Microbes Infect.* **2006**, *8* (11),

2599–2604.
(157) Fisher, N.; Majid, R. A.; Antoine, T.; Al-Helal, M.; Warman, A. J.; Johnson, D. J.; Lawrenson, A. S.; Ranson, H.; O'Neill, P. M.; Ward, S. A.; Biagini, G. A. *J. Biol. Chem.* **2012**, *287* (13), 9731–9741.
(158) Stickles, A. M.; Smilkstein, M. J.; Morrisey, J. M.; Li, Y.; Forquer, I. P.; Kelly, J. X.; Pou, S.; Winter, R. W.; Nilsen, A.; Vaidya, A. B.; Riscoe, M. K. *Antimicrob. Agents Chemother.* **2016**, *60* (8), 4853–4859.
(159) Miley, G. P.; Pou, S.; Winter, R.; Nilsen, A.; Li, Y.; Kelly, J. X.; Stickles, A. M.; Mather, M. W.; Forquer, I. P.; Pershing, A. M.; White, K.; Shackleford, D.; Saunders, J.; *et al. Antimicrob. Agents Chemother.* **2015**, *59* (9), 5555–5560.
(160) Pidathala, C.; Amewu, R.; Pacorel, B.; Nixon, G. L.; Gibbons, P.; Hong, W. D.; Leung, S. C.; Berry, N. G.; Sharma, R.; Stocks, P. A.; Srivastava, A.; Shone, A. E. *et al. J. Med. Chem.* **2012**, *55* (5), 1831–1843.
(161) Leung, S. C.; Gibbons, P.; Amewu, R.; Nixon, G. L.; Pidathala, C.; Hong, W. D.; Pacorel, B.; Berry, N. G.; Sharma, R.; Stocks, P. A.; Srivastava, A.; Shone, A. E. *et al. J. Med. Chem.* **2012**, *55* (5), 1844–1857.
(162) Klonis, N.; Creek, D. J.; Tilley, L. *Curr. Opin. Microbiol.* **2013**, *16* (6), 722–727.
(163) Hsu, E. *Trans. R. Soc. Trop. Med. Hyg.* **2006**, *100* (6), 505–508.
(164) Pukrittayakamee, S.; Chantra, A.; Simpson, J. A.; Vanijanonta, S.; Clemens, R.; Looareesuwan, S.; White, N. J. *Antimicrob. Agents Chemother.* **2000**, *44* (6), 1680–1685.
(165) White, N. J. *Antimicrob. Agents Chemother.* **1997**, *41* (7), 1413–1422.
(166) Sanz, L. M.; Crespo, B.; De Cozar, C.; Ding, X. C.; Llergo, J. L.; Burrows, J. N.; Garcia-Bustos, J. F.; Gamo, F. J. *PLoS One* **2012**, *7* (2), e30949.
(167) Antoine, T.; Fisher, N.; Amewu, R.; O'Neill, P. M.; Ward, S. A.; Biagini, G. A. *J. Antimicrob. Chemother.* **2014**, *69* (4), 1005–1016.
(168) Cui, L.; Su, X. *Expert Rev. Anti. Infect. Ther.* **2009**, *7* (8), 999–1013.
(169) Lin, A. J.; Klayman, D. L.; Milhous, W. K. *J. Med. Chem.* **1987**, *30* (11), 2147–2150.
(170) Ilett, K. F.; Ethell, B. T.; Maggs, J. L.; Davis, T. M. E.; Batty, K. T.; Burchell, B.; Binh, T. Q.; Thi, L. E.; Thu, A. N. H.; Hung, N. C.; Pirmohamed, M.; Park, B. K.; Edwards, G. **2002**, *30* (9), 1005–1012.
(171) Morris, C. A; Duparc, S.; Borghini-Fuhrer, I.; Jung, D.; Shin, C.-S.; Fleckenstein, L. *Malar. J.* **2011**, *10*:263, 1–17.
(172) White, N. J. *Trends Parasitol.* **2004**, *113* (8), 1084–1092.
(173) Dondorp, A. M.; Yeung, S.; White, L.; Nguon, C.; Day, N. P. J.; Socheat, D.; von Seidlein, L. *Nat. Rev. Microbiol.* **2010**, *8* (4), 272–280.
(174) Eziefula, A. C. *Lancet Infect. Dis.* **2016**, *16* (10), 1086–1087.
(175) Elamin, S. B.; Malik, E. M.; Abdelgadir, T.; Khamiss, A. H.; Mohammed, M. M.; Ahmed, E. S.; Adam, I. *Malar. J.* **2005**, *4*, 41.
(176) Sirima, S. B.; Gansané, A. *Expert Opin. Investig. Drugs* **2007**, *16* (7), 1079–1085.
(177) Adjei, G. O.; Goka, B. Q.; Binka, F.; Kurtzhals, J. A. L. *Expert Rev. Anti. Infect. Ther.* **2009**, *7* (6), 669–681.
(178) Acton, N.; Roth, R. J. *J. Org. Chem.* **1992**, *57* (13), 3610–3614.
(179) Kopetzki, D.; Lévesque, F.; Seeberger, P. H. *Chem. - A Eur. J.* **2013**, *19* (17), 5450–5456.
(180) Paddon, C. J.; Westfall, P. J.; Pitera, D. J.; Benjamin, K.; Fisher, K.; McPhee, D.; Leavell, M. D.; Tai, a; Main, a; Eng, D.; Polichuk, D. R.; Teoh, K. H.; Reed, D. W.; *et al. Nature* **2013**, *496* (7446), 528–532.
(181) Yadav, J. S.; Satheesh Babu, R.; Sabitha, G. *Tetrahedron Lett.* **2003**, *44* (2), 387–389.
(182) Schmid, G.; Hofheinz, W. *J. Am. Chem. Soc.* **1983**, *105* (9), 624–625.
(183) Avery, M. A.; Chong, W. K. M.; Jennings-White, C. *J. Am. Chem. Soc.* **1992**, *114* (3), 974–979.
(184) Zhu, C.; Cook, S. P. *J. Am. Chem. Soc.* **2012**, *134* (33), 13577–13579.
(185) Dietrich, J. A.; Yoshikuni, Y.; Fisher, K. J.; Woolard, F. X.; Ockey, D.; McPhee, D. J.; Renninger,

N. S.; Chang, M. C. Y.; Baker, D.; Keasling, J. D. *ACS Chem. Biol.* **2009**, *4* (4), 261–267.
(186) Westfall, P. J.; Pitera, D. J.; Lenihan, J. R.; Eng, D.; Woolard, F. X.; Regentin, R.; Horning, T.; Tsuruta, H.; Melis, D. J.; Owens, A.; Fickes, S.; Diola, D.; Benjamin, K. R. *et al. Proc. Natl. Acad. Sci. U. S. A.* **2012**, *109* (3), E111-8.
(187) Ro, D.; Paradise, E. M.; Ouellet, M.; Fisher, K. J.; Newman, K. L.; Ndungu, J. M.; Ho, K. A.; Eachus, R. A.; Ham, T. S.; Kirby, J.; Chang, M. C. Y.; Withers, S. T.; Shiba, Y.; Sarpong, R.; Keasling, J. D. *Nature* **2006**, *440* (April), 3–6.
(188) O'Neill, P. M.; Barton, V. E.; Ward, S. A. *Molecules* **2010**, *15* (3), 1705–1721.
(189) Li, J.; Zhou, B. *Molecules* **2010**, *15* (3), 1378–1397.
(190) Mercer, A. E.; Copple, I. M.; Maggs, J. L.; O'Neill, P. M.; Park, B. K. *J. Biol. Chem.* **2011**, *286* (2), 987–996.
(191) Robert, A.; Coppel, Y.; Meunier, B. *Chem. Commun.* **2002**, *0*, 414–415.
(192) Ismail, H. M.; Barton, V.; Phanchana, M.; Charoensutthivarakul, S.; Wong, M. H. L.; Hemingway, J.; Biagini, G. A.; O'Neill, P. M.; Ward, S. A. *Proc. Natl. Acad. Sci.* **2016**, *113* (8), 2080–2085.
(193) Ismail, H. M.; Barton, V. E.; Panchana, M.; Charoensutthivarakul, S.; Biagini, G. A.; Ward, S. A.; O'Neill, P. M. *Angew. Chemie - Int. Ed.* **2016**, *55* (36), 10548.
(194) WHO. *Artemisinin and artemisinin-based combination therapy resistance*, No. October, 1–8. **2016**, (Accessed 23rd March **2017**).
(195) Dong, Y.; Chollet, J.; Matile, H.; Charman, S. A.; Chiu, F. C. K.; Charman, W. N.; Scorneaux, B.; Urwyler, H.; Santo Tomas, J.; Scheurer, C.; Snyder, C.; Dorn, A.; Wang, X.; *et al. J. Med. Chem.* **2005**, *48* (15), 4953–4961.
(196) Vennerstrom, J. L.; Arbe-Barnes, S.; Brun, R.; Charman, S. a; Chiu, F. C. K.; Chollet, J.; Dong, Y.; Dorn, A.; Hunziker, D.; Matile, H.; McIntosh, K.; Padmanilayam, M.; *et al. Nature* **2004**, *430* (7002), 900–904.
(197) Dong, Y.; Wittlin, S.; Sriraghavan, K.; Chollet, J.; Charman, S. A.; Charman, W. N.; Scheurer, C.; Urwyler, H.; Tomas, J. S.; Snyder, C.; Creek, D. J.; Morizzi, J.; Koltun, M. *et al. J. Med. Chem.* **2010**, *53* (1), 481–491.
(198) Dong, Y.; Wang, X.; Kamaraj, S.; Bulbule, V. J.; Chiu, F. C. K.; Chollet, J.; Dhanasekaran, M.; Hein, C. D.; Papastogiannidis, P.; Morizzi, J.; Shackleford, D. M.; *et al. J. Med. Chem.* **2017**, *60* (7), 2654−2668.
(199) Phyo, A. P.; Jittamala, P.; Nosten, F. H.; Pukrittayakamee, S.; Imwong, M.; White, N. J.; Duparc, S.; Macintyre, F.; Baker, M.; Möhrle, J. J. *Lancet Infect. Dis.* **2015**, 61–69.
(200) Wells, T. N. C.; van Huijsduijnen, R. H.; Van Voorhis, W. C. *Nat. Rev. Drug Discov.* **2015**, *14* (6), 424–442.
(201) O' Neill, P. M.; Sabbani, S.; Nixon, G. L.; Schnaderbeck, M.; Roberts, N. L.; Shore, E. R.; Riley, C.; Murphy, B.; McGillan, P.; Ward, S. A.; Davies, J.; Amewu, R. K. *Tetrahedron* **2016**, *72* (40), 6118–6126.
(202) O'Neill, P. M.; Amewu, R. K.; Nixon, G. L.; ElGarah, F. B.; Mungthin, M.; Chadwick, J.; Shone, A. E.; Vivas, L.; Lander, H.; Barton, V.; Muangnoicharoen, S.; Bray, P. G.; *et al. Angew. Chemie - Int. Ed.* **2010**, *49* (33), 5693–5697.
(203) Marti, F.; Chadwick, J.; Amewu, R. K.; Burrell-Saward, H.; Srivastava, A.; Ward, S. A.; Sharma, R.; Berry, N.; O'Neill, P. M. *Medchemcomm* **2011**, *2* (7), 661.
(204) Gomes, G. dos P.; Vil', V.; Terent'ev, A.; Alabugin, I. V. *Chem. Sci.* **2015**, *6* (12), 6783–6791.
(205) Müller, O.; Sié, A.; Meissner, P.; Schirmer, R. H.; Kouyaté, B. *Lancet* **2009**, *374* (9699), 1419.
(206) Nagle, A.; Wu, T.; Kuhen, K.; Gagaring, K.; Borboa, R.; Francek, C.; Chen, Z.; Plouffe, D.; Lin, X.; Caldwell, C.; Ek, J.; Skolnik, S.; Liu, F.; Wang, J.; Chang, J.; Li, C.; *et al. J. Med. Chem.* **2012**, *55* (9), 4244–4273.
(207) Kuhen, K. L.; Chatterjee, A. K.; Rottmann, M.; Gagaring, K.; Borboa, R.; Buenviaje, J.; Chen, Z.; Francek, C.; Wu, T.; Nagle, A.; Barnes, S. W.; Plouffe, D.; Lee, M. C. S.; *et al. Antimicrob. Agents Chemother.* **2014**, *58* (9), 5060–5067.

(208) Wu, T.; Nagle, A.; Kuhen, K.; Gagaring, K.; Borboa, R.; Francek, C.; Chen, Z.; Plouffe, D.; Goh, A.; Lakshminarayana, S. B.; Wu, J.; Ang, H. Q.; Zeng, P.; Kang, M. L. *et al. J. Med. Chem.* **2011**, *54* (14), 5116–5130.
(209) Younis, Y.; Douelle, F.; Feng, T. S.; Cabrera, D. G.; Manach, C. Le; Nchinda, A. T.; Duffy, S.; White, K. L.; Shackleford, D. M.; Morizzi, J.; Mannila, J. *et al. J. Med. Chem.* **2012**, *55* (7), 3479–3487.
(210) Ghidelli-Disse, S.; Lafuente-Monasterio, M. J.; Waterson, D.; Witty, M.; Younis, Y.; Paquet, T.; Street, L. J.; Chibale, K.; Gamo-Benito, F. J.; Bantscheff, M.; Drewes, G. *Malar. J.* **2014**, *13* (Suppl 1), P38.
(211) Baragaña, B.; Hallyburton, I.; Lee, M. C. S.; Norcross, N. R.; Grimaldi, R.; Otto, T. D.; Proto, W. R.; Blagborough, A. M.; Meister, S.; Wirjanata, G.; Ruecker, A.; *et al.Nature* **2015**, *522* (7556), 315–320.
(212) Spillman, N. J.; Kirk, K. *Int. J. Parasitol. Drugs Drug Resist.* **2015**, *5* (3), 149–162.
(213) Vaidya, A. B.; Morrisey, J. M.; Zhang, Z.; Das, S.; Daly, T. M.; Otto, T. D.; Spillman, N. J.; Wyvratt, M.; Siegl, P.; Marfurt, J.; Wirjanata, G.; Sebayang, B. F. *et al. Proc. Natl. Acad. Sci. U. S. A.* **2015**, *112* (42), E5764.
(215) Rottmann, M.; McNamara, C.; Yeung, B. K. S.; Lee, M. C. S.; Zou, B.; Russell, B.; Seitz, P.; Plouffe, D. M.; Dharia, N. V; Tan, J.; Cohen, S. B.; Spencer, K. R.; *et al. Science* **2010**, *329* (5996), 1175–1180.
(216) Smith, P. W.; Diagana, T. T.; Yeung, B. K. S. *Parasitology* **2014**, *141* (1), 66–76.
(217) Yeung, B. K. S.; Zou, B.; Rottmann, M.; Lakshminarayana, S. B.; Ang, S. H.; Leong, S. Y.; Tan, J.; Wong, J.; Keller-Maerki, S.; Fischli, C.; Goh, A.; Schmitt, E. K.; Krastel, P.; *et al. J. Med. Chem.* **2010**, *53* (14), 5155–5164.
(218) Turner, H. *Future Med. Chem.* **2016**, *8* (2), 227–238.
(219) Capuzzi, S. J.; Muratov, E. N.; Tropsha, A. *J. Chem. Inf. Model.* **2017**, *57* (3), 417–427.
(220) Thulasiram, H. V.; Erickson, H. K.; Poulter, C. D. *Science (80-.).* **2007**, *316* (5821), 73–76.
(221) Frank, A.; Groll, M. *Chem. Rev.* **2017**, *117* (8), 5675–5703.
(222) Ruzicka, L. *Experientia* **1953**, *9* (10), 357–367.
(223) Nes, W. D. *Chem. Rev.* **2011**, *111* (10), 6423–6451.
(224) Dickschat, J. S. *Nat. Prod. Rep.* **2011**, *28* (12), 1917.
(225) Oldfield, E.; Lin, F. Y. *Angew. Chemie - Int. Ed.* **2012**, *51* (5), 1124–1137.
(226) Gershenzon, J.; Dudareva, N. *Nat. Chem. Biol.* **2007**, *3* (7), 408–414.
(227) O'Connor, S. E.; Maresh, J. J. *Nat. Prod. Rep.* **2006**, *23* (4), 532.
(228) Leete, E. *Acc. Chem. Res.* **1969**, *2* (2), 59–64.
(229) Brown, G. D. *Molecules* **2010**, *15* (11), 7603–7698.
(230) Arigoni, D.; Sagner, S.; Latzel, C.; Eisenreich, W.; Bacher, a; Zenk, M. H. *Proc. Natl. Acad. Sci. U. S. A.* **1997**, *94* (20), 10600–10605.
(231) Rohmer, M.; Seemann, M.; Horbach, S.; Bringer-Meyer, S.; Sahm, H. *J. Am. Chem. Soc.* **1996**, *118* (11), 2564–2566.
(232) Rohmer, M.; Rohmer, M. *Nat. Prod. Rep.* **1999**, *16* (5), 565–574.
(233) Eisenreich, W.; Bacher, A.; Arigoni, D.; Rohdich, F. *Cell. Mol. Life Sci.* **2004**, *61* (12), 1401–1426.
(234) Rohmer, M. *Lipids* **2008**, *43* (12), 1095–1107.
(235) Treharne, K. J.; Mercer, E. I.; Goodwin, T. W. *Biochem. J.* **1966**, *99* (1), 239–245.
(236) Threlfall, D. R.; Griffiths, W. T.; Goodwin, T. W. *Biochem. J.* **1967**, *103* (3), 831–851.
(237) Lichtenthaler, H. K.; Rohmer, M.; Schwender, J. *Plant Physiol.* **1997**, *101*, 643–652.
(238) Bach, T. J.; Lichtenthaler, H. K. *physiol. plant* **1983**, *59*, 50–60.
(239) Kreuz, K.; Kleining, H. *Eur. J. Biochem.* **1984**, *141* (3), 531–535.
(240) Zhou, D.; White, R. H. *Biochem. J.* **1991**, *273 (Pt 3*, 627–634.
(241) Flesch, G.; Rohmer, M. *Eur. J. Biochem.* **1988**, *175* (2), 405–411.
(242) Rohmer, M.; Knani, M.; Simonin, P.; Sutter, B.; Sahm, H. *Biochem. J.* **1993**, *295* (2), 517–524.

(243) Sprenger, G. A. *FEMS Microbiol. Lett.* **1996**, *145*, 301–307.
(244) Sprenger, G. a; Schörken, U.; Wiegert, T.; Grolle, S.; de Graaf, a a; Taylor, S. V; Begley, T. P.; Bringer-Meyer, S.; Sahm, H. *Proc. Natl. Acad. Sci.* **1997**, *94* (24), 12857–12862.
(245) Lois, L. M.; Campos, N.; Putra, S. R.; Danielsen, K.; Rohmer, M.; Boronat, a. *Proc. Natl. Acad. Sci. U. S. A.* **1998**, *95* (5), 2105–2110.
(246) Jurgenson, C. T.; Begley, T. P.; Ealick, S. E. *Annu. Rev. Biochem.* **2009**, *78* (1), 569–603.
(247) Turner, D. L.; Santos, H.; Fareleira, P.; Pacheco, I.; LeGall, J.; Xavier, a V. *Biochem. J.* **1992**, *285 (Pt 2*, 387–390.
(248) Ostrovsky, D.; Shashkov, A.; Sviridov, A. *Biochem. J.* **1993**, No. 1988, 1987–1988.
(249) Duvold, T.; Calí, P.; Bravo, J. M.; Rohmer, M. *Tetrahedron Lett.* **1997**, *38* (35), 6181–6184.
(250) Takahashi, S.; Kuzuyama, T.; Watanabe, H.; Seto, H. *Proc. Natl. Acad. Sci.* **1998**, *95*, 9879–9884.
(251) Hoeffler, J. F.; Tritsch, D.; Grosdemange-Billiard, C.; Rohmer, M. *Eur. J. Biochem.* **2002**, *269* (18), 4446–4457.
(252) Lauw, S.; Illarionova, V.; Bacher, A.; Rohdich, F.; Eisenreich, W. *FEBS J.* **2008**, *275* (16), 4060–4073.
(253) Munos, J. W.; Pu, X.; Mansoorabadi, S. O.; Kim, H. J.; Liu, H. W. *J. Am. Chem. Soc.* **2009**, *131* (6), 2048–2049.
(254) Wong, U.; Cox, R. J. *Angew. Chemie - Int. Ed.* **2007**, *46* (26), 4926–4929.
(255) Hale, I.; O'Neill, P. M.; Berry, N. G.; Odom, A.; Sharma, R. *Medchemcomm* **2012**, *3* (4), 418–433.
(256) Rohdich, F.; Wungsintaweekul, J.; Fellermeier, M.; Sagner, S.; Herz, S.; Kis, K.; Eisenreich, W.; Bacher, a; Zenk, M. H. *Proc. Natl. Acad. Sci. U. S. A.* **1999**, *96*, 11758–11763.
(257) Kuzuyama, T.; Takagi, M.; Kaneda, K.; Seto, H. *Tetrahedron Lett.* **2000**, *41*, 703–706.
(258) Richard, S. B.; Lillo, A. M.; Tetzlaff, C. N.; Bowman, M. E.; Noel, J. P.; Cane, D. E. *Biochemistry* **2004**, *43* (38), 12189–12197.
(259) Kirby, A. J.; Nome, F. *Acc. Chem. Res.* **2015**, *48* (7), 1806–1814.
(260) Lowe, G. *Acc. Chem. Res.* **1983**, *16* (7), 244–251.
(261) Wilkie, J.; Gani, D. *J. Chem. Soc., Perkin Trans.* **1996**, *2*, 783.
(262) Richard, S. B.; Bowman, M. E.; Kwiatkowski, W.; Kang, I.; Chow, C.; Lillo, A. M.; Cane, D. E.; Noel, J. P. *Nat. Struct. Biol.* **2001**, *8*, 641–648.
(263) Kemp, L. E.; Bond, C. S.; Hunter, W. N. *Acta Crystallogr. - Sect. D Biol. Crystallogr.* **2003**, *59* (3), 607–610.
(264) Schrödinger, L. *PyMOL Molecular Graphics, Version~1.8*; **2015**.
(265) Lüttgen, H.; Rohdich, F.; Herz, S.; Wungsintaweekul, J.; Hecht, S.; Schuhr, C. a; Fellermeier, M.; Sagner, S.; Zenk, M. H.; Bacher, A.; Eisenreich, W. *Proc. Natl. Acad. Sci. U. S. A.* **2000**, *97* (3), 1062–1067.
(266) Kuzuyama, T.; Takagi, M.; Kaneda, K.; Watanabe, H. *Tetrahedron Lett.* **2000**, *41*, 2925–2928.
(267) Cheek, S.; Zhang, H.; Grishin, N. V. *J. Mol. Biol.* **2002**, *320* (4), 855–881.
(268) Lahiri, S. D.; Zhang, G.; Dunaway-Mariano, D.; Allen, K. N. *Science* **2003**, *299* (5615), 2067–2071.
(269) Knowles, J. *Science.* **2003**, *299* (5615), 2002–2003.
(270) Miallau, L.; Alphey, M. S.; Kemp, L. E.; Leonard, G. A.; McSweeney, S. M.; Hecht, S.; Bacher, A.; Eisenreich, W.; Rohdich, F.; Hunter, W. N. *Proc. Natl. Acad. Sci.* **2003**, *100* (16), 9173–9178.
(271) Wada, T.; Kuzuyama, T.; Satoh, S.; Kuramitsu, S.; Yokoyama, S.; Unzai, S.; Tame, J. R. H.; Park, S. Y. *J. Biol. Chem.* **2003**, *278* (32), 30022–30027.
(272) Sgraja, T.; Alphey, M. S.; Ghilagaber, S.; Marquez, R.; Robertson, M. N.; Hemmings, J. L.; Lauw, S.; Rohdich, F.; Bacher, A.; Eisenreich, W.; Illarionova, V.; Hunter, W. N. *FEBS J.* **2008**, *275* (11), 2779–2794.
(273) Hunter, W. N. *J. Biol. Chem.* **2007**, *282* (30), 21573–21577.
(274) Herz, S.; Wungsintaweekul, J.; Schuhr, C. A.; Hecht, S.; Luttgen, H.; Sagner, S.; Fellermeier, M.;

Eisenreich, W.; Zenk, M. H.; Bacher, A.; Rohdich, F. *Proc. Natl. Acad. Sci. U. S. A.* **2000**, *97* (6), 2486–2490.
(275) Steinbacher, S.; Kaiser, J.; Wungsintaweekul, J.; Hecht, S.; Eisenreich, W.; Gerhardt, S.; Bacher, A.; Rohdich, F. *J. Mol. Biol.* **2002**, *316*, 79–88.
(276) Kemp, L. E.; Bond, C. S.; Hunter, W. N. *Proc. Natl. Acad. Sci. U. S. A.* **2002**, *99* (10), 6591–6596.
(277) Richard, S. B.; Ferrer, J. L.; Bowman, M. E.; Lillo, A. M.; Tetzlaff, C. N.; Cane, D. E.; Noel, J. P. *J. Biol. Chem.* **2002**, *277* (10), 8667–8672.
(278) Altincicek, B.; Kollas, A.; Sanderbrand, S.; Wiesner, J.; Hintz, M.; Beck, E.; Jomaa, H. *Society* **2001**, *183* (8), 2411–2416.
(279) Baker, J.; Franklin, D. B.; Parker, J. *FEMS Microbiol. Lett.* **1992**, *94*, 175–180.
(280) Campos, N.; Rodríguez-Concepción, M.; Seemann, M.; Rohmer, M.; Boronat, A. *FEBS Lett.* **2001**, *488*, 170–173.
(281) Hecht, S.; Eisenreich, W.; Adam, P.; Amslinger, S.; Kis, K.; Bacher, A.; Arigoni, D.; Rohdich, F. *Proc. Natl. Acad. Sci. U. S. A.* **2001**, *98* (26), 14837–14842.
(282) Wolff, M.; Seemann, M.; Grosdemange-Billiard, C.; Tritsch, D.; Campos, N.; Rodriguez-Concepcion, M.; Boronat, A.; Rohmer, M. *Tetrahedron Lett.* **2002**, *43* (14), 2555–2559.
(283) Kollas, A. K.; Duin, E. C.; Eberl, M.; Altincicek, B.; Hintz, M.; Reichenberg, A.; Henschker, D.; Henne, A.; Steinbrecher, I.; Ostrovsky, D. N.; Hedderich, R.; Beck, E.; Jomaa, H.; Wiesner, J. *FEBS Lett.* **2002**, *532* (3), 432–436.
(284) Seemann, M.; Bui, B. T. S.; Wolff, M.; Tritsch, D.; Campos, N.; Boronat, A.; Marquet, A.; Rohmer, M. *Angew. Chemie - Int. Ed.* **2002**, *41* (22), 4337–4339.
(285) Wang, W.; Oldfield, E. *Angew. Chemie - Int. Ed.* **2014**, *53* (17), 4294–4310.
(286) Rekittke, I.; Jomaa, H.; Ermler, U. *FEBS Lett.* **2012**, *586* (19), 3452–3457.
(287) Xiao, Y.; Rooker, D.; You, Q.; Freel Meyers, C. L.; Liu, P. *ChemBioChem* **2011**, *12* (4), 527–530.
(288) Brandt, W.; Dessoy, M. A.; Fulhorst, M.; Gao, W.; Zenk, M. H.; Wessjohann, L. A. *ChemBioChem* **2004**, *5* (3), 311–323.
(289) Quitterer, F.; Frank, A.; Wang, K.; Rao, G.; O'Dowd, B.; Li, J.; Guerra, F.; Abdel-Azeim, S.; Bacher, A.; Eppinger, J.; Oldfield, E.; Groll, M. *J. Mol. Biol.* **2015**, *427* (12), 2220–2228.
(290) Altincicek, B.; Kollas, A. K.; Eberl, M.; Wiesner, J.; Sanderbrand, S.; Hintz, M.; Beck, E.; Jomaa, H. *FEBS Lett.* **2001**, *499* (1–2), 37–40.
(291) Cunningham, F. X. *J. Bacteriol.* **2000**, *182* (20), 5841–5848.
(292) Mcateer, S.; Coulson, A.; Mclennan, N.; Masters, M. **2001**, *183* (24), 7403–7407.
(293) Rohdich, F.; Hecht, S.; Gärtner, K.; Adam, P.; Krieger, C.; Amslinger, S.; Arigoni, D.; Bacher, A.; Eisenreich, W. *Proc. Natl. Acad. Sci. U. S. A.* **2002**, *99* (3), 1158–1163.
(294) Rohdich, F.; Zepeck, F.; Adam, P.; Hecht, S.; Kaiser, J.; Laupitz, R.; Gräwert, T.; Amslinger, S.; Eisenreich, W.; Bacher, A.; Arigoni, D. *Proc. Natl. Acad. Sci. U. S. A.* **2003**, *100* (4), 1586–1591.
(295) Wolff, M.; Seemann, M.; Tse Sum Bui, B.; Frapart, Y.; Tritsch, D.; Garcia Estrabot, A.; Rodríguez-Concepción, M.; Boronat, A.; Marquet, A.; Rohmer, M. *FEBS Lett.* **2003**, *541* (1–3), 115–120.
(296) Altincicek, B.; Duin, E. C.; Reichenberg, A.; Hedderich, R.; Kollas, A. K.; Hintz, M.; Wagner, S.; Wiesner, J.; Beck, E.; Jomaa, H. *FEBS Lett.* **2002**, *532* (3), 437–440.
(297) Adam, P.; Hecht, S.; Eisenreich, W.; Kaiser, J.; Grawert, T.; Arigoni, D.; Bacher, A.; Rohdich, F. *Proc. Natl. Acad. Sci. U. S. A.* **2002**, *99* (19), 12108–12113.
(298) Span, I.; Gräwert, T.; Bacher, A.; Eisenreich, W.; Groll, M. *J. Mol. Biol.* **2012**, *416* (1), 1–9.
(299) Seemann, M.; Janthawornpong, K.; Schweizer, J.; Böttger, L. H.; Ahrens-botzong, A.; Tambou, E. N.; Rotthaus, O.; Alfred, X.; Rohmer, M.; Schünemann, V. **2009**, *8* (15 mL), 1–6.
(300) Wang, K.; Saarlandes, U.; Bacher, A. **2012**, No. November 2016.
(301) McFadden, G. I.; Reith, M. E.; Munholland, J.; Lang-Unnasch, N. *Nature*. 1996, pp 482–482.
(302) Janouskovec, J.; Horak, A.; Obornik, M.; Lukes, J.; Keeling, P. J. *Proc. Natl. Acad. Sci.* **2010**, *107* (24), 10949–10954.
(303) Yeh, E.; DeRisi, J. L. *PLoS Biol.* **2011**, *9* (8).

(304) Jomaa, H.; Wiesner, J.; Sanderbrand, S.; Altincicek, B.; Weidemeyer, C.; Hintz, M.; Türbachova, I.; Eberl, M.; Zeidler, J.; Lichtenthaler, H. K.; Soldati, D.; Beck, E. *Science* **1999**, *285* (5433), 1573–1576.
(305) Cassera, M. B.; Gozzo, F. C.; D'Alexandri, F. L.; Merino, E. F.; Del Portillo, H. A.; Peres, V. J.; Almeida, I. C.; Eberlin, M. N.; Wunderlich, G.; Wiesner, J.; Jomaa, H.; Kimura, E. A.; Katzin, A. M. *J. Biol. Chem.* **2004**, *279* (50), 51749–51759.
(306) Wiley, J. D.; Merino, E. F.; Krai, P. M.; McLean, K. J.; Tripathi, A. K.; Vega-Rodríguez, J.; Jacobs-Lorena, M.; Klemba, M.; Cassera, M. B. *Eukaryot. Cell* **2015**, *14* (2), 128–139.
(307) Dahl, E. L.; Shock, J. L.; Shenai, B. R.; Gut, J.; DeRisi, J. L.; Rosenthal, P. J. *Antimicrob. Agents Chemother.* **2006**, *50* (9), 3124–3131.
(308) Hasan, S.; Daugelat, S.; Rao, P. S. S.; Schreiber, M. *PLoS Comput. Biol.* **2006**, *2* (6), 0539–0550.
(309) Odom, A. R.; Van Voorhis, W. C. *Mol. Biochem. Parasitol.* **2010**, *170* (2), 108–111.
(310) Odom, A. R. *PLoS Pathog.* **2011**, *7* (12), 1–3.
(311) Labaied, M.; Jayabalasingham, B.; Bano, N.; Cha, S. J.; Sandoval, J.; Guan, G.; Coppens, I. *Cell. Microbiol.* **2011**, *13* (4), 569–586.
(312) Maltese, W. A. *FASEB J.* **1990**, *4* (15), 3319–3328.
(313) Tonhosolo, R.; D'Alexandri, F. L.; de Rosso, V. V.; Gazarin, M. L.; Matsumura, M. Y.; Peres, V. J.; Merino, E. F.; Carlton, J. M.; Wunderlich, G.; Mercadante, A. Z.; Kimura, E. A.; Katzin, A. M. *J. Biol. Chem.* **2009**, *284* (15), 9974–9985.
(314) Yajima, S.; Hara, K.; Sanders, J. M.; Yin, F.; Ohsawa, K.; Wiesner, J.; Jomaa, H.; Oldfield, E. *J. Am. Chem. Soc.* **2004**, *126* (35), 10824–10825.
(315) Masini, T.; Hirsch, A. K. H. *J. Med. Chem.* **2014**, *57*, 9740–9763.
(316) Deng, L.; Endo, K.; Kato, M.; Cheng, G.; Yajima, S.; Song, Y. *ACS Med. Chem. Lett.* **2011**, *2* (2), 165–170.
(317) Gießmann, D.; Heidler, P.; Haemers, T.; Calenbergh, S. Van; Reichenberg, A.; Jomaa, H.; Weidemeyer, C.; Sanderbrand, S.; Wiesner, J.; Link, A. *Chem. Biodivers.* **2008**, *5*, 643–656.
(318) Wiesner, J.; Borrmann, S.; Jomaa, H. *Parasitol Res* **2003**, *90*, 71–76.
(319) Takashi, K.; Masashi, H.; Keiji, H.; Hidekazu, T. Hydroxyaminohydrocarbonphosphonic acids. US4206156 A, **1980**.
(320) Lell, B.; Ruangweerayut, R.; Wiesner, J.; Missinou, M. A.; Schindler, A.; Baranek, T.; Hintz, M.; Hutchinson, D.; Jomaa, H.; Kremsner, P. G. *Antimicrob. Agents Chemother.* **2003**, *47* (2), 735–738.
(321) Lanaspa, M.; Moraleda, C.; Machevo, S.; González, R.; Serrano, B.; Macete, E.; Cisteró, P. *Antimicrob. Agents Chemother.* **2012**, *56* (6), 2923–2928.
(322) Mishra, M.; Mishra, V. K.; Kashaw, V.; Iyer, A. K.; Kumar, S. *Eur. J. Med. Chem.* **2017**, *125*, 1300–1320.
(323) Woo, Y.; Fernandes, R. P. M.; Proteau, P. J. *Bioorganic Med. Chem.* **2006**, *14*, 2375–2385.
(324) Devreux, V.; Wiesner, J.; Goeman, J. L.; Eycken, J. Van Der; Jomaa, H.; Calenbergh, S. Van. *J. Med. Chem.* **2006**, *49*, 2656–2660.
(325) Andaloussi, M.; Lindh, M.; Björkelid, C.; Suresh, S.; Wieckowska, A.; Iyer, H.; Karlén, A.; Larhed, M. *Bioorg. Med. Chem. Lett.* **2011**, *21* (18), 5403–5407.
(326) Haemers, T.; Wiesner, J.; Poecke, S. Van; Goeman, J.; Henschker, D.; Beck, E.; Calenbergh, S. Van. *Bioorg. Med. Chem. Lett.* **2006**, *16*, 1888–1891.
(327) Behrendt, C. T.; Kunfermann, A.; Illarionova, V.; Matheeussen, A.; Pein, M. K.; Gr, T.; Kaiser, J.; Bacher, A.; Eisenreich, W.; Illarionov, B.; Fischer, M.; Maes, L.; Groll, M.; Kurz, T. *J. Med. Chem.* **2011**, *54*, 6796–6802.
(328) Deng, L.; Sundriyal, S.; Rubio, V.; Shi, Z.; Song, Y. *J. Med. Chem. Lett.* **2009**, *52*, 6539–6542.
(329) Wungsintaweekul, J. Enzymes of the Alternative Terpenoid Pathway in Escherichia coli, Technical University of Munich, 2001.
(330) Masini, T.; Kroezen, B. S.; Hirsch, A. K. H. *Drug Discov. Today* **2013**, *18* (23–24), 1256–1262.
(331) Witschel, M. C.; Hoffken, H. W.; Seet, M.; Parra, L.; Mietzner, T.; Thater, F.; *et al. Angew.*

Chemie - Int. Ed. **2011**, *50*, 7931–7935.
(332) Kunfermann, A.; Witschel, M.; Illarionov, B.; Martin, R.; Rottmann, M.; Hoffken, H. W.; Seet, M.; Eisenreich, W.; Knolker, H.; Fischer, M.; Bacher, A.; Groll, M.; Diederich, F. *Angew. Chemie - Int. Ed.* **2014**, *53*, 2235–2239.
(333) Witschel, M.; Rohl, F.; Niggeweg, R.; Newton, T. *Pest Manag. Sci.* **2013**, *69* (5), 559–563.
(334) Price, K. E.; Armstrong, C. M.; Imlay, L. S.; Hodge, D. M.; Pidathala, C.; Roberts, N. J.; Park, J.; Mikati, M.; Sharma, R.; Lawrenson, A. S.; Tolia, N. H.; Berry, N. G.; Neill, P. M. O.; John, A. R. O. *Nat. Publ. Gr.* **2016**, *6* (November), 1–12.
(335) Wu, W.; Herrera, Z.; Ebert, D.; Baska, K.; Cho, S. H.; Derisi, J. L.; Yeh, E. *Antimicrob. Agents Chemother.* **2015**, *59* (1), 356–364.
(336) Gamo, F.-J.; Sanz, L. M.; Vidal, J.; de Cozar, C.; Alvarez, E.; Lavandera, J.-L.; Vanderwall, D. E.; Green, D. V. S.; Kumar, V.; Hasan, S.; Brown, J. R.; Peishoff, C. E.; Cardon, L. R.; Garcia-Bustos, J. F. *Nature* **2010**, *465* (7296), 305–310.
(337) Spangenberg, T.; Burrows, J. N.; Kowalczyk, P.; McDonald, S.; Wells, T. N. C.; Willis, P. *PLoS One* **2013**, *8* (6).
(338) Imlay, L. S.; Armstrong, C. M.; Masters, M. C.; Li, T.; Price, K. E.; Edwards, R. L.; Mann, K. M.; Li, L. X.; Stallings, C. L.; Berry, N. G.; Neill, P. M. O.; Odom, A. R. *ACS Infect. Dis.* **2015**, *1*, 157–167.
(339) Yao, Z.; Krai, P. M.; Merino, E. F.; Simpson, M. E.; Slebodnick, C.; Belen, M.; Carlier, P. R. *Bioorg. Med. Chem. Lett.* **2015**, *25* (7), 1515–1519.
(340) Bitok, J. K.; Meyers, C. F. *ACS Chem. Biol.* **2012**, *7*, 1702–1710.
(341) Rivasseau, C.; Seemann, M.; Boisson, A.; Streb, P.; Gout, E.; Douce, R.; Rohmer, M.; Bligny, R. *Plant, Cell Environ.* **2009**, *32*, 82–92.

Chapter 2: Optimisation of a Novel *Plasmodium Falciparum* IspD Inhibitor MMV008138

2.1 Discovery of a Specific Stereoisomer of MMV008138 as an Inhibitor of *Pf*IspD

MMV008138, also known as 1-(2,4-dichlorophenyl)-2,3,4,9-tetrahydro-1*H*-pyrido[3,4-*b*]indole-3-carboxylic acid (**1**), was identified in 2010 as possessing antiplasmodial activity through phenotypic screening of the GlaxoSmithKline (GSK) compound library.[1] The structure of **1** (Figure 2.1) and other newly discovered antimalarial compounds were made available free of charge by the Medicines for Malaria Venture (MMV) as part of the malaria box programme.[2]

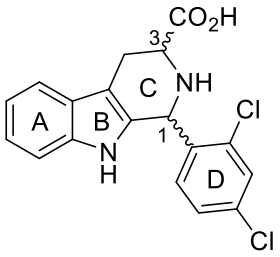

MMV008138 (**1**)

Figure 2.1. Structure of MMV008138 (1), each ring is labelled A, B, C and D.

From this discovery, Bowman *et al.* were successful in utilising a chemical rescue screen that identified compounds from the malaria box as possessing likely apicoplast activity.[3] This was achieved by examining the growth effect of IPP supplementation with active compounds. As mentioned in Chapter 1, the biosynthesis of IPP is localised within the apicoplast, therefore if parasite growth is rescued by IPP supplementation it is reasonable to assume the compound targets this organelle. Of all the compounds tested only MMV008138 (**1**) possessed both potent activity (<1000 nM), and led to parasite rescue when supplemented with IPP. **1** belongs to the tetrahydro-β-carboline (THBC) chemical scaffold and bares substituents at the C1 and C3 positions (Figure 2.1), this gives rise to 4 stereoisomers (Figure 2.2). Bowman examined MMV008138 (**1**) as a mixture of all stereoisomers, and determined that its specific IC_{50} activity was 350 nM *vs* the Dd2 strain for *Plasmodium falciparum*.[3]

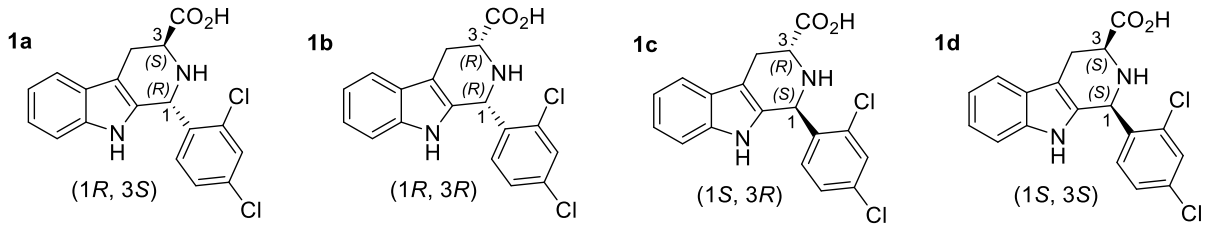

Figure 2.2. Structure of all stereoisomers of MMV008138 (1a – d). Positions bearing stereogenic centres are numbered accordingly with stereochemistry displayed.

Both Bowman and Wu *et al*. also gave evidence to support that the MEP pathway as the likely metabolic target within the apicoplast.[3,4] Bowman showed that parasites exposed to MMV008138 (**1**) suffered a loss of mitochondrial membrane potential, an observation that is seen when ubiquinone production is also inhibited. Fosmidomycin has already been demonstrated to inhibit ubiquinone

synthesis and targets the MEP pathway enzyme IspC, suggesting MMV008138 (**1**) possesses a similar mode of action.[3,5,6] Both research groups also compared the kinetics of fomidomycin and **1** with other apicoplast specific drugs such as doxycylicine and clindamycin.[3,4] These drugs exhibit a delayed death phenomenon from their mechanisms of action, interfering with the apicoplast genome development *via* the inhibition of transcription and translation.[7] Unlike doxycycline and clindamycin, both fosmidomycin and **1** exhibit immediate death characteristics.[3,4] Furthermore doxycycline, clindamycin, fosmidomycin and **1** all disrupt apicoplast morphology; this change in morphology is not rescued in parasites treated with doxycycline and clindamycin in the presence of exogenous IPP. In fosmidomycin and **1**, however, the apicoplast is fully rescued from IPP supplementation and parasites remain viable, again suggesting a mode of action on a direct metabolic pathway within the organelle.[3]

Wu and co-workers undertook research to confirm the molecular target of **1**. They first isolated all four diastereoisomers and found the (1*R*, 3*S*)-enantiomer (**1a**) to be the most potent, demonstrating an EC_{50} of 110 nM against *Pf*W2 strain, whilst the other diastereoisomers showed substantially reduced inhibition or no inhibition >50 µM (Table 2.1).[4]

Table 2.1. Inhibitory activities of each MMV008138 diastereoisomer against parasite growth (Dd2), both with and without IPP supplementation.

Stereoisomer	*Pf*Dd2 EC_{50} (µM)	*Pf*Dd2 EC_{50} (µM) + IPP rescue
(1*R*, 3*S*)-**1a**	0.11 (0.10 – 0.12)	>25
(1*R*, 3*R*)-**1b**	3.8 (2.7 – 5.3)	>25
(1*S*, 3*R*)-**1c**	18.6 (12.4 – 28.0)	>25
(1*S*, 3*S*)-**1d**	>50	>50

They then generated three separate populations of parasites that were drug resistant to **1a** and examined their genomes. Mutations were shared in the IspD coding gene suggesting that IspD was the target. To confirm if this was the case, non-mutated IspD was purified and its activity interrogated using a pyrophosphate release assay. Indeed the (1*R*, 3*S*)-enantiomer **1a** demonstrated potent activity against the enzyme displaying a potent IC_{50} value at 7.0 nM. These lines of evidence provide very good support that IspD is the molecular target (Table 2.2).[4]

Table 2.2. Inhibitory activities of each MMV008138 diastereoisomer against *Plasmodium falciparum* IspD.

Stereoisomer	*Pf*IspD EC_{50} (µM)
(1*R*, 3*S*)-**1a**	0.0071 (0.0061 – 0.0083)
(1*R*, 3*R*)-**1b**	0.17 (0.14 – 2.0)
(1*S*, 3*R*)-**1c**	2.5 (1.9 – 3.1)
(1*S*, 3*S*)-**1d**	>25

Interestingly the authors state that the compound has no activity against the *Plasmodium vivax* homologue of IspD and is specific to *Plasmodium falciparum*, which may be due to only a 31 % sequence similarity between the two homologues.[4] In contrast to this, however, the Odom group also purified *Pv*IspD and identified **1a** as an inhibitor with an IC_{50} value of 310 nM. Running the same screen with recombinant *Pf*IspD yielded an IC_{50} of 47 nM, indicating that *Plasmodium falciparum* is more sensitive to inhibition.[8] Although demonstrating the potential ability to kill both *Pf* and *Pv* strains of malaria, **1a** is not active against bacterial IspD homologues such as *M. tuberculosis*, or *E. coli* displaying no inhibition of these enzymes at >30 μM.[4,8] Furthermore the compound is also not active against the plant homologues as demonstrated by the observation that there is no activity against *A. thaliana* IspD at 1 mM.[4] The IspD homologues of the *Plasmodium* species therefore possibly have a distinct binding pocket that is susceptible to selective small molecule inhibition.

In order to confirm whether inhibition of *Pf*IspD leads to effective shutdown of the MEP pathway, the expected levels of *in vivo* MEP pathway metabolites should decrease further downstream after inhibition. Imlay and Odom demonstrated that administration of **1a** to *Plasmodium falciparum* led to a decrease in the levels of cMEPP within the parasite to just 12 % ± 4 of the control, a result which is consistent with previously described fosmidomycin inhibition.[8] Furthermore the levels of DXP, an upstream metabolite in the MEP pathway, do not change upon treatment with either fosmidomycin or (1*R*, 3*S*)-MMV008138 (**1a**). In the same experiment the inactive (1*S*, 3*S*)-MMV008138 (**1d**) (Figure 2.2) did not show any change in cMEPP levels, nor did structurally unrelated antimalarial compounds such as chloroquine. Taken all together this data suggests that IspD is a valid drug target and leads to both effective shut down of the MEP pathway, along with loss of parasite viability.[8]

2.1.1 Known SAR around the Tetrahydro-β-carboline Scaffold

With the identification of MMV008138 (**1**), its biological target and stereochemical requirement, we initially focused our research on the development of this novel tetrahydro-β-carboline scaffold by conducting SAR studies at numerous points around the motif with the aim of enhancing phenotypic whole cell activity and / or *Pf*IspD inhibition.

During our initial development around the chemotype Yao *et al*. published their research on the same chemical motif.[9] They focused and evaluated their research on the phenotypic activity of compounds derived from **1** against the *Pf*Dd2 strain, and did not test for IspD activity. Despite this, their research indicated strict structural requirements are needed in order to maintain levels of potency, where even small changes in substituent size can lead to a loss of activity, potentially indicating that the binding side of *Pf*IspD is quite restricted.[9]

2.1.2 Modifications to MMV008138 D-ring

The research conducted by Yao first examined the modification of the D-ring aryl substituent (highlighted green) bound at the C1 position of the tetrahydro-β-carboline core for the (1*R*, 3*S*)-enantiomer and (1*S*, 3*S*)-enantiomers. Their results are summarised in Table 2.3 below, only results for the (1*R*, 3*S*)-enantiomer (**1a**, **2a – j**) are displayed.[9]

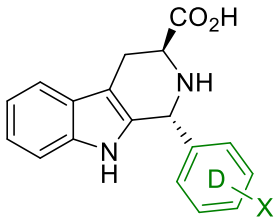

Table 2.3. Inhibitory activities of each D-ring substituent pattern against parasite growth (Dd2). X = substituent pattern.

X	*Pf*Dd2 IC_{50} (nM)
2-Cl, 4-Cl (**1a**)	250 ± 70
3-OMe, 4-OMe (**2a**)	>20,000
2-H, 4-H (**2b**)	>10,000
2-Cl, 4-H (**2c**)	3280 ± 990
2-H, 4-Cl (**2d**)	1170 ± 60
2-Cl, 4-Me (**2e**)	410 ± 40
2-Me, 4-Cl (**2f**)	700 ± 90
2-Me, 4-Me (**2g**)	70 % inhibition at >10,000
2-F, 4-F (**2h**)	780 ± 175
2-OMe, 4-OMe (**2i**)	>20,000
2-CF_3, 4-CF_3 (**2j**)	>10,000

It is apparent that there is a strict spatial and / or electronic requirement for the 2, 4 substitution pattern of this aryl ring. Only one 3, 4 substitution pattern was explored (**2a**), however, it led to complete loss of activity. Similarly removal of all substitution (**2b**) also results in a loss of activity. Activity is regained upon addition of a chlorine atom at either the 2-position (**2c**) or 4-position (**2d**) of the aryl ring, albeit with greatly diminished potency compared to **1a**. Of the substitution patterns explored only the 2-Cl, 4-Me (**2e**) or 2-Me, 4-Cl (**2f**) substitution came close to replicating the potent activity of **1a**, however, they were not as potent as the parent compound. Interestingly the halogens seem to influence the potency greatly, whether this is through steric or electronic effects was not explored in the paper. Substitution of both chlorine atoms with Me groups (**2g**) results in greatly diminished potency, replacement of the chlorine atoms to fluorine atoms (**2h**) retains activity but again is less potent than the parent. Both the 2, 4-bis(methoxy) (**2i**) and 2, 4-bis(trifluoromethyl) (**2j**) analogues show no activity at 20,000 and 10,000 nM, respectively.[9]

It is interesting that even small modifications to this D-ring can influence activity so substantially; Yao *et al*. postulated that there is a very tight binding pocket for this region resulting in potentially limited SAR. They also postulated that the 2-position is required to constrain the D-ring to lie perpendicular to the tetrahydro-β-carboline core, potentially forcing a particular binding mode.[9]

2.1.3 Modifications at the C3 Position

Yao *et al.* also evaluated the effect of substitution of the carboxylate moiety at C3 on the tetrahydro-β-carboline (THBC) core. Similar to their findings on the C1 D-ring, there also appears to be critical steric and electronic constraints for potential SAR. Again it was observed even minor changes appear to dramatically influence potency.[9] Their initial rationale for the substitution of this position was to examine if the carboxylic acid moiety could be replaced.[9] Carboxylic acids are often believed to be non-ideal in a drug development programme as they can exist in their deprotonated form at physiological pH, this can cause issues such as cell permeability as the negatively charged carboxylate cannot cross an also negatively charged phospholipid cell membrane.[10] They can also be susceptible to glucuronidation *via* phase II metabolism which both reduces the amount of available drug in the body, and can cause undesirable side effects.[10] Therefore, the bioisoteric replacement of this moiety can aid in both reducing potential unwanted side effects, and can increase the metabolic half-life of the drug in the body, thus improving the overall pharmacokinetic profile of the compound. Table 2.4 summarises their findings.

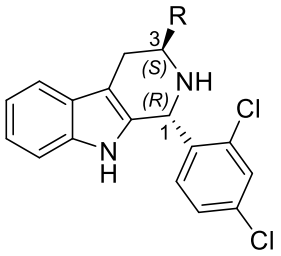

Table 2.4. Inhibitory activities of each C3 substituent against parasite growth (Dd2). R = substituent.

R	*Pf*Dd2 IC_{50} (nM)
H (**3a**)	10,000 ± 1600
$CONH_2$ (**3b**)	1200 ± 100
$CONH^iPr$ (**3c**)	50 % inhibition at 10,000
$CONH^nBu$ (**3d**)	80 % inhibition at 10,000
$^aCONHC_6H_{11}$ (**3e**)	2830 ± 500
CONHNHMe (**3f**)	1940 ± 200
CO_2Me (**4**)	6800 ± 1400
CONHMe (**6**)	190 ± 30

a = Growth inhibition was not rescued by addition of exogenous IPP

Yao *et al.* removed the carboxylate moiety entirely, eliminating the stereogenic centre at C3. They administered the resulting compound **3a** as the C1 (*R* / *S*)-racemic mixture and found loss of activity. Consequently, they switched their attention to amide derivatives of **1a**, interestingly the primary amide (**3b**), similar in size and shape to the acid, led to only moderate inhibitory activity. The group also examined amides with increased steric bulk including NH-^{i}Pr (**3c**), and NH-^{n}Bu (**3d**) and observed greatly diminished activity. Surprisingly NH-cyclohexane (**3e**) maintains moderate potency, examination of the molecule within an IPP rescue screen showed no rescue of parasites, therefore in the absence of an IspD assay it is reasonable to assume this compound shows off target effects. Replacement to the NHNHMe hydrazide (**3f**) showed a reduction in activity; potentially due to extra steric bulk.[9] Yao *et al.* also examined the methyl ester of (1*R*, 3*S*)-MMV008138 (**4**) after separation from its inactive (1*S*, 3*S*)-isomer (**5**). This ester is an intermediate for the synthesis of the parent compound (**1a**) and so if active, it would reduce the number of steps *en route* to the target compound to just one step starting from cheap starting materials, a very desirable trait indeed for any possible novel drug candidate. Unfortunately replacement to the ester displayed weak activity, however, the group postulate this compound could serve as a useful prodrug if the ester functionality is hydrolysed to the acid *in vivo*. Though not reported, the authors state a number of esters were also examined and all were found to be inactive.[9] Using CONHMe (**6**) as the amide, led to improved potency over the parent compound (**1a**). This is interesting as it is a similar size to the methyl ester (**4**), and slightly bigger than acid (**1a**), this indicates that there is a small degree of manipulation that can be tolerated at the C3 position. It does appear that based on these results that the heteroatom directly bonded to the carbonyl must be a hydrogen bond donor.

Figure 2.3 summaries what is known from the template thus far.

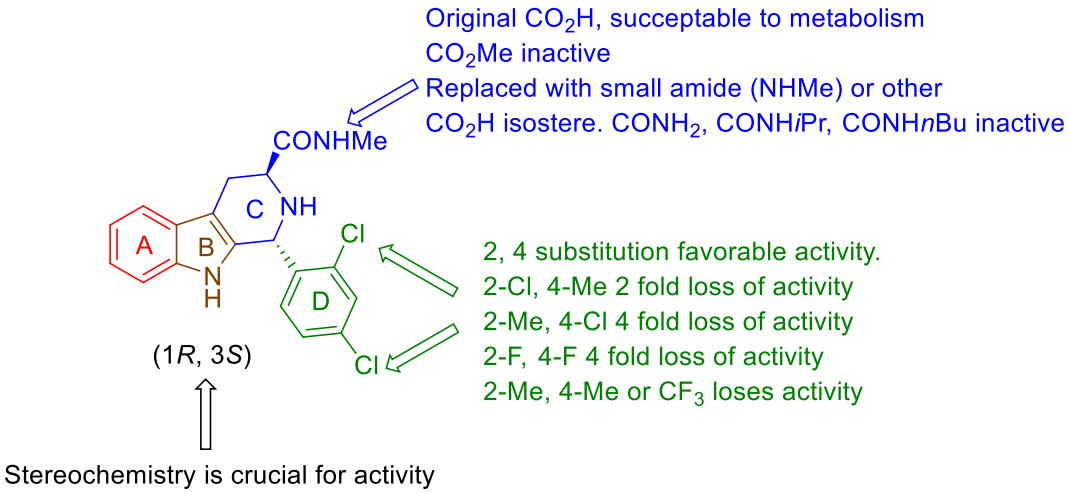

Figure 2.3. Summary of the known SAR of the template.[9]

2.1.4 Is MMV008138 a Good Template?

The MMV008138 compound (**1a**) contains a distinct chemical motif known as a tetrahydro-β-carboline as the core of the molecule. Indeed whilst the compound has strict requirements of the stereochemistry at positions 1 and 3, therefore potentially complicating synthesis, there are a large number of potential drug therapies that utilise not only the tetrahydro-β-carboline (THBC) core, but also the chirality, which can be crucial in delivering chemotherapies with good efficacy.[11] A review of the literature shows that optically active THBC scaffolds are of great pharmacological importance and are present in not only in drugs but also are present in natural products as well.[11] Some examples are given in Figure 2.4.

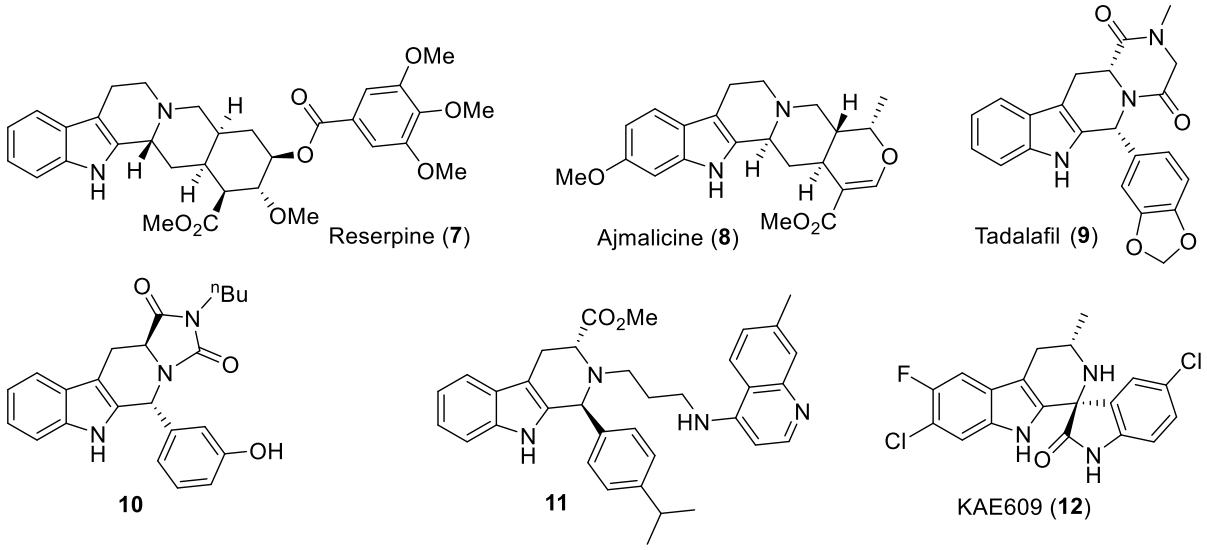

Figure 2.4. Examples of optically active THBC scaffolds that have been used for various chemotherapies.

Reserpine (**7**) and ajmalicine (**8**), are both natural optically active THBC alkaloids which have been used as antihypertensive therapies.[11] Perhaps the most pharmacologically important synthetic THBC to date is tadalafil (**9**) which under the brand name Cialis earns over $2 billion in annual sales; it is used primarily to treat erectile dysfunction but also is used to treat pulmonary arterial hypertension.[12] **9** contains some degree of structural similarity to MMV008138 (**1a**) but bears a diketopiperazine ring. Yao *et al*. even tested it for its antiplasmodial activity, however, the result was disappointing and showed no activity against the parasite. It should be noted, however, that during this test **9** was used as the (1*R*, 3*R*)-stereoisomer, rather than the (1*R*, 3*S*)-stereoisomer, which is required for IspD activity. It also lacks the 2, 4 aryl substitution, and finally the C-ring nitrogen atom is locked as an amide and thus has lost its basicity.[9]

10 has been used also been used as a mitotic spindle protein inhibitor for potential use as a cancer chemotherapy.[13] **11** has also been reported to possess excellent activity against plasmodium

falciparum displaying an minimum inhibitory concentration (MIC) of 50 nM.[14] Perhaps most importantly for this project is the extremely positive results seen from the molecule KAE609 (**12**) also known as Cipargamin. Developed by Novartis, it is another compound with high structural similarity to MMV008138 (**1a**) the molecule is a tetrahydro-β-carboline structure with a fused spiroindalone at its C1 stereogenic centre, and a methyl group at the C3. Since the lead compound was discovered with an *Pf*NF54 EC_{50} value of 9.2 nM it has demonstrated an outstanding safety profile in humans, has a good half-life and as a result has currently completed phase IIa clinical trials.[15–18] Although possessing the formal labels of (1*R*, 3*S*)-configuration, which match **1a**, the spatial arrangement of these substituents does not resemble (1*R*, 3*S*)-MMV008138 (**1a**) but rather the (1*R*, 3*R*)-diastereoisomer **1b**, therefore it is not likely to dual inhibit IspD.

In summary, it has been demonstrated in the literature that compounds harbouring an optically active tetrahydro-β-carboline scaffold have success within drug development programmes, particularly as shown with the success of tadalafil (**9**) and KAE609 (**12**). The fact that one of these compounds has made it to market and the other to human trials demonstrates there is potential for an excellent safety profile working with the MMV008138 template. The specificity of **1a** to a parasite specific pathway would also reduce the potential of unwanted side effects. Whilst SAR has been carried out on the MMV008138 template by Yao, there is more than can be explored around the C and D-ring, and the as of yet unexplored A-ring. The aim of our work is to expand on the known SAR to deliver a compound with improved activity against the malaria parasite, and ideally have that same compound as an inhibitor as *Pf*IspD with the ultimate aim of producing a new lead compound to be taken forward to *in vivo* studies.

2.2 Results and Discussion

2.2.1 General Synthesis of Compounds Exploring C and D-ring Modification

The generation of most compounds in the series was successfully achieved from a two-step synthesis, and any deviations from this route will be discussed as appropriate (Scheme 2.1). The first and most crucial step in the reaction pathway involved utilising the well-established Pictet-Spengler reaction between the aldehyde of choice (to set the D-ring functionalisation) and L-tryptophan methyl ester (**13**). Classically the Pictet-Spengler reaction is known as an acid-catalysed transformation between a β-aryl amine and an aldehyde or ketone.[19–21] In the case of tryptamine, the reaction with the desired carbonyl compounds generates a tetrahydro-β-carboline scaffold with a stereogenic centre at C1 that exists as a mixture of enantiomers (unless formaldehyde is used as the carbonyl source). In the case of tryptophan derivatives, a stereogenic centre is also present at C3. Provided that

starting tryptophan is optically pure; the result of the Pictet-Spengler reaction is a mix of two diastereoisomers. The C3 stereogenic centre does not racemise under standard reaction conditions thus allowing for ease of isolation of optically pure products.[20,21] Tryptophan ester products were expected to be easier to isolate and handle than their carboxylic acid counter parts, and for these reasons we chose L-tryptophan methyl ester (**13**) as the starting point for our synthesis. The final step in the general synthetic scheme involves a simple amide coupling from the desired (1*R*, 3*S*)-isomer (from here on stated as *trans*) *via* direct displacement of the ester in a large excess of the desired amine. Compounds were then successfully recrystallised from methanol (Scheme 2.1).[9]

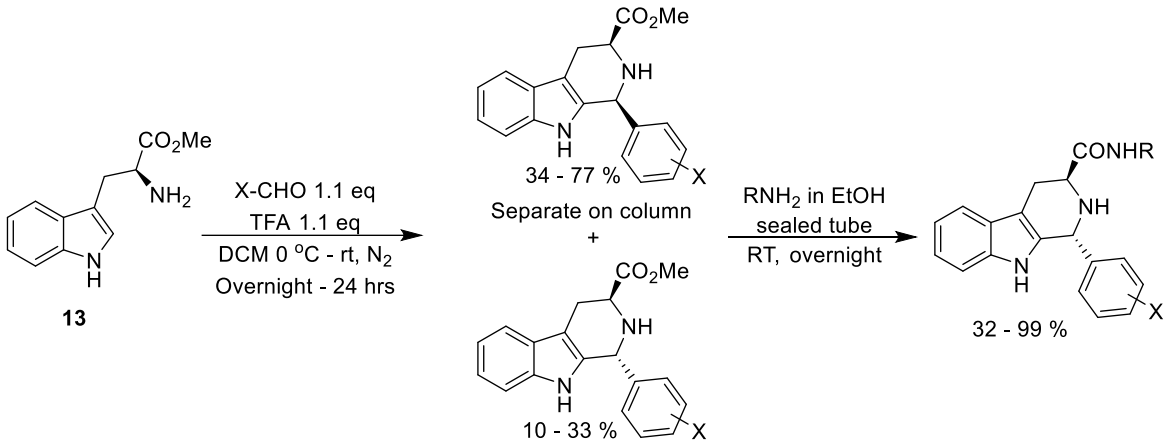

Scheme 2.1. General synthesis for final targets.

2.2.2 Pictet-Spengler Reaction Mechanisms

The Pictet-Spengler reaction can be regarded as a reaction similar to a Mannich type reaction. The detailed reaction mechanism remains a topic of debate with two possible courses the reaction can take (Figure 2.5). In both cases the first step of the mechanism is believed to be the same. First, the acid catalyst acts to protonate the carbonyl source (**B**) which facilitates the nucleophilic attack of the amine (**A**) to the protonated carbonyl forming intermediate **C** before loss of H_2O. The resulting iminium ion (**D**) causes the sp^2 carbon to become sufficiently electrophilic for ring closure.[22] It is this ring closing step that is debated in the literature, the reaction can proceed either *via* nucleophilic attack of the indole 3-position resulting in the formation of a 5-membered spiroindolenine intermediate (**E**) (Figure 2.5 route a). Migration of the highlighted bond onto the 2-position of the indole results in the formation of a 6-membered ring (**F**), following proton loss aromaticity is restored and the tetrahydro-β-carboline core is completed (product **G**). Alternatively the reaction can proceed *via* direct attack of the 2-position of the indole, presumably *via* delocalisation into the A-ring, forming the 6-membered ring (**F**) immediately without the need to pass through the spiroindolenine intermediate (**E**) (Figure 2.5 route b, for clarity, the delocalisation is omitted), again proton loss restores aromaticity and completes the reaction (**G**) . There is currently no compelling evidence either

way for which mechanism is in operation, literature presents evidence both for and against either pathway.[20,23–25]

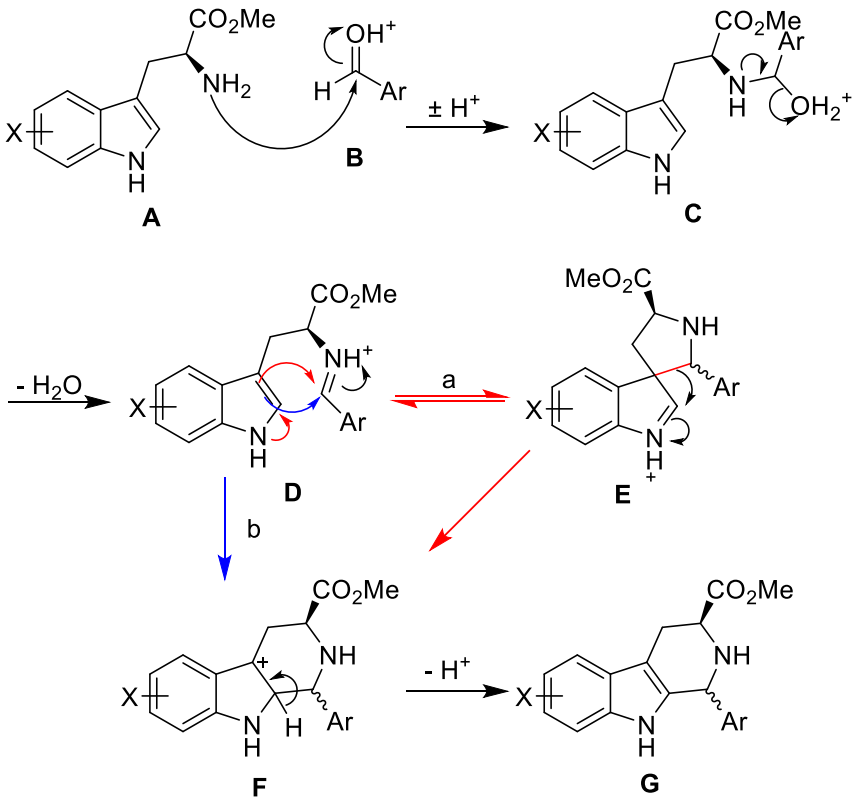

Figure 2.5. Proposed reaction mechanisms of the Pictet-Spengler reaction, route a is depicted with red arrows, route b is depicted with blue arrows.

As tryptophan derivatives are used as part of this project, we generate two diastereoisomers whenever a Pictet-Spengler reaction is carried out with optically pure starting materials. Fortuitously in most cases the ease of isolation of both diastereoisomers along with sufficient generation of material for the desired *trans* product meant that this was not a problem. In general *cis* to *trans* selectivity was approximately 2 : 1 to 3 : 1. However, this is slightly problematic for a waste perspective as a substantial amount of reaction product can be discarded.

The use of a *trans*-selective Pictet-Spengler reaction would be very beneficial indeed. Cook *et al*. report of two ways to achieve *trans*-product, and both involved a benzylation protocol. They demonstrated that carrying out the reaction with *N*-benzyl tryptophan derivatives yields highly selective *trans* product.[24,26–28] Alternatively benzylating any isolated *cis* isomer and exposing it to an acidic environment leads to ring opening, bond rotation and ring closing forming the desired *trans* isomer.[29–31] The drawback of this protocol, however, is the benzyl group cannot be easily removed without running the risk of affecting other parts of the MMV008138 derived compound, such as dehalogenation of the D-ring. Therefore no final target was made using this protocol, however, it

should be noted that all *cis* isomers were isolated in case new methods to carry out this isomerisation were discovered or were needed.

2.2.3 Confirming Series Activity and Introducing Drug Metabolism and Pharmacokinetic (DMPK) Properties.

To order to confirm activity of the series, **1a** was resynthesised by our research group following the procedure reported by Yao *et al*. The group used an amberlyst catch and release protocol to generate the COOH functionality from the methyl ester (synthesis was specifically carried out by a postdoctoral research assistant in the group Dr Chandrakala Pidathala. Note, unless otherwise stated all reported compounds have been made by myself).[9] The assessment of biological activity for final compounds was generously undertaken by members of the Odom group. We also decided to resynthesise and reconfirm the activity of **6** also following the reported procedure by Yao *et al.* following Scheme 2.2.[9]

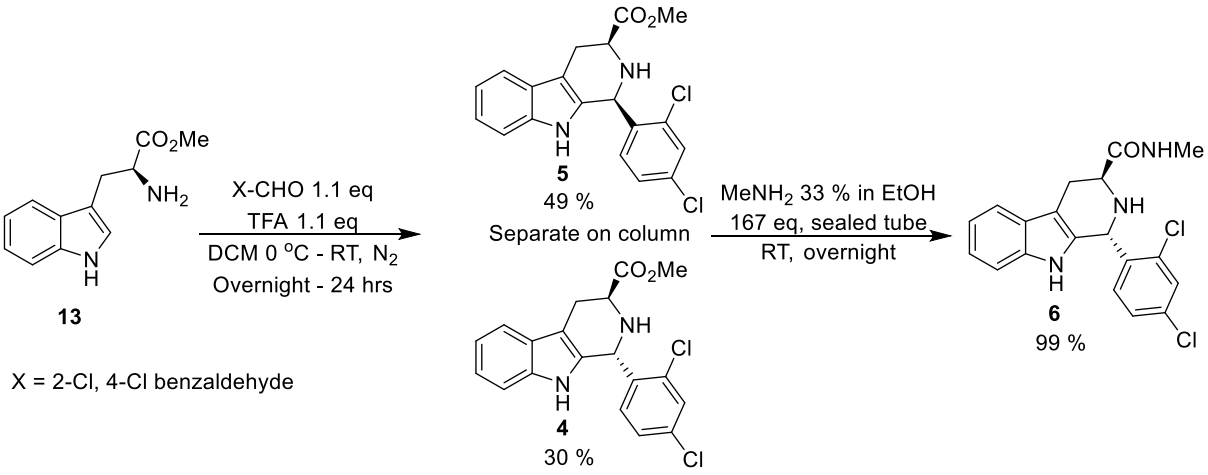

Scheme 2.2. Synthetic route to compound 6.

L-Tryptophan methyl ester (**13**) was purchased as the hydrochloride salt and was isolated as the free base by stirring in a biphasic solution of saturated $NaHCO_3$ and EtOAc. Following extraction and isolation, the free-base L-tryptophan methyl ester (**13**) was carried forward into the Pictet-Spengler reaction using 1.1 equivalents of trifluoroacetic acid. Isolation of the *cis* and *trans* diastereoisomers from column chromatography, gradient elution from 100 % DCM to 2 % EtOAc in DCM, results in the isolation of **4** and **5**. After recrystallisation from hot methanol **5** was isolated as long transparent needles in 49 % yield, and the **4** was isolated as transparent crystals in 30 % yield. Reacting **4** in the presence of a large excess of methylamine gave the final product **6** in 99 % yield following recrystallisation from methanol.

In order to determine unambiguously which compound from **4** and **5** is *cis* and which is *trans*, 2D Nuclear Overhauser Effect Spectroscopy (NOESY) experiments were carried out on each diastereoisomer. As it is impossible to determine which diastereoisomer will come off the column first when substituents are varied, NOESY experiments provide an efficient method to differentiate *cis* from *trans*. The NOE is an effect that monitors through space coupling; this is particularly useful for ring systems as it allows the determination of which protons are near each other, but not necessarily coupling through traditional through-bond coupling, for example 1, 3 diaxial interactions can be observed *via* the NOE, as these protons are near each other occupying the same face.[32] For this template we can use NOE to assess whether or not the C1 and C3 protons interact, in the case of the *cis* isomer a correlation will be observed in the spectrum as the substituents occupy the same face and are therefore near each other. This can then be confirmed by analysing the *trans* isomer, which will show an absence of through space coupling between the same protons (Figure 2.6 and 2.7, **Appendix 1**). Final confirmation that the correct diastereoisomer and enantiomer was isolated, was carried out *via* X-ray crystallography.[33–35] The *trans* product **4** was crystallised from hot methanol and examined for its crystal structure by Dr Craig Robertson and images visualised in OLEX2 (Figure 2.8).[36] The *trans* product was confirmed clearly demonstrating the C1 and C3 substituents on differing faces.

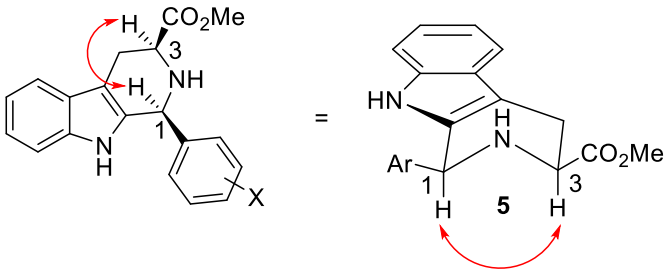

Observable NOE correlation of hydrogens at positions 1 and 3 on same face, substituents are *cis*

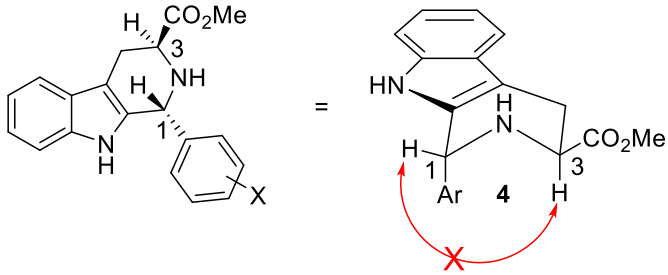

No observable NOE correlation of hydrogens at positions 1 and 3 on differing faces, substituents are *trans*

Figure 2.6. Identification of 4 and 5 by NOESY. Protons on the same face show a correlation as displayed in the top portion of the diagram, which indicate a *cis* isomer and therefore compound 5. Protons on differing faces show an absence of a correlation as displayed in the bottom portion of the diagram which indicates a *trans* isomer and therefore compound 4.

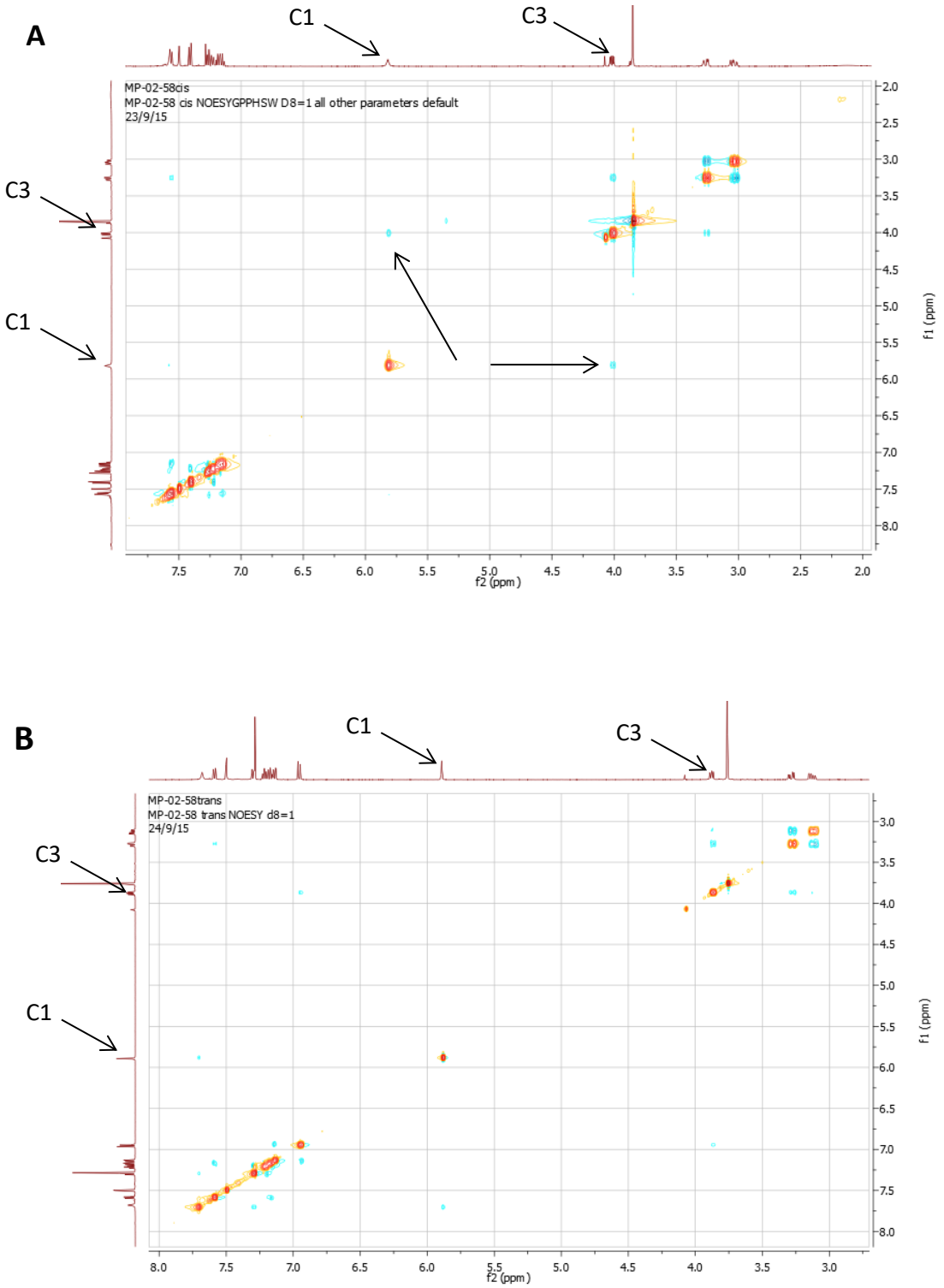

Figure 2.7. Representative NOESYs for compounds 4 and 5. A, shows a correlation between C1 and C3 hydrogens, product is most likely *cis* (5), B shows no correlation between C1 and C3 hydrogens, product is most likely *trans* (4).

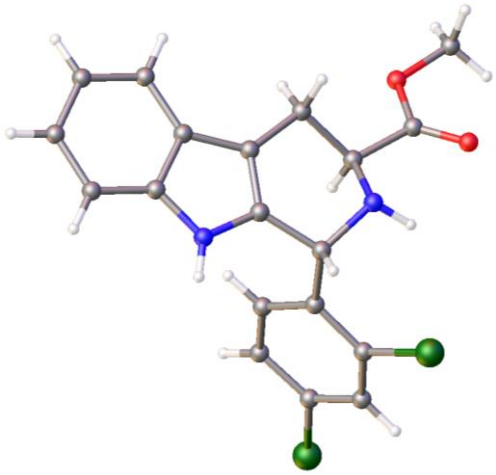

Figure 2.8. X-ray crystal structure of 4, Flack parameter = -0.002 (9). Image is rendered as ball and stick, carbon, coloured in grey, chlorine in green, hydrogen in white, nitrogen in blue and oxygen in red. Compound was visualised using OLEX2.[36]

To confirm series activity the biochemical and cellular assays undertaken as part of this project were carried out by our collaborators at the University of Washington Department of Molecular Microbiology in the Odom group.

To determine enzyme activity, the Odom lab developed an enzyme-linked assay to detect the release of pyrophosphate by the *Pf*IspD enzyme. IspD reacted in the presence of its substrates MEP and CTP yields the product CDPME and inorganic pyrophosphate. The assay utilises the generation of inorganic phosphate (iP) formed from inorganic pyrophosphate (iPP) by reaction of iPP with an inorganic phosphatase enzyme iPPTase. The generated iP can then be monitored by subsequent reaction with the synthetic substrate 2-amino-6-mercapto-7-methylpurine (MESG) (**14**) (Figure 2.9) in the presence of the enzyme PNP (purine nucleoside phosphorylase), which releases ribose-1-phosphate (**15**) and 2-amino-6-mercapto-7-methylpurine (**16**) a product with a well-defined characteristic maximal absorption at 360 nm wavelength.[37] The assay is linear with respect to time and enzyme concentration and activity is dependent on concentrations of *Pf*IspD, MEP and CTP. Upon inhibition, the generation of iPP is reduced, thus the generation of the observed product from the linked assay is reduced, allowing for calculation of IC_{50} values (Figure 2.9).

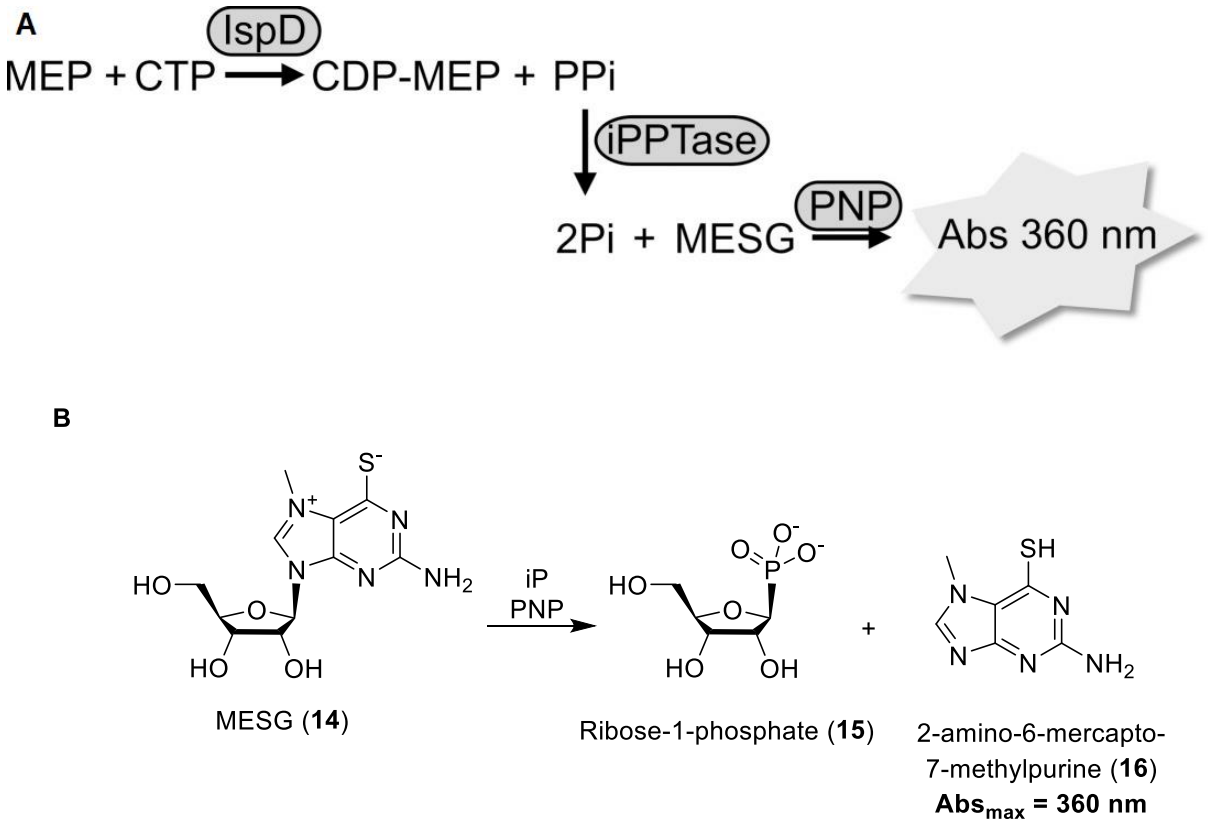

Figure 2.9. Representation of pyrophosphate release assay.

The *P. falciparum* cellular assay was carried out on the intraerythrocytic stage of the parasite using standard methods, which involved intercalation of *P. falciparum* DNA with the fluorophore PicoGreen – an ultrasensitive nucleic acid stain for measurement of double stranded DNA in solution.[38] Erythrocyte cells do not contain DNA whereas *P. falciparum* does, therefore fluorescence can be detected in infected erythrocyte cells, and effective concentration (EC_{50}) values can be calculated based on the drug concentration that yields 50 % of the net fluorescence compared with untreated infected erythrocyte cells. The strain of *P. falciparum* that is used as part of the essay is a chloroquine resistant strain known as 3D7, and the erythrocyte cells are from human.

Selected compounds also had their DMPK profiles analysed for certain parameters including $LogD_{7.4}$, aqueous solubility, and metabolic stability. Each of these parameters is especially important, and certain requirements from these parameters need to be met for a hit drug to become a lead candidate and are discussed below.

i) LogD

LogD, (the distribution coefficient of a compound between an organic (octanol) phase and aqueous phase at a specific pH), is a measure of the pH dependent lipophilicity of a molecule, i.e. the affinity a molecule has for a non-polar hydrophobic (lipophilic) environment. Lipophilicity is a

physiochemical property can influence numerous factors of a drug including; the distribution across a phospholipid bilayer of cells; the absorption and binding of a drug; and also the solubility of the drug in aqueous or organic environments.[39]

The rule of five set by Lipinski is a set of parameters that are used to predict oral bioavailability of orally administered compounds,[40] in particular for predicting the adsorption of a drug. These rules assist in the knowledge of whether a drug is likely to succeed or fail in the clinic.[40] The rule itself is based on the properties of hundreds of drugs were a trend was found with successful drug compounds. Many successful drug compounds shared the following parameters.[39,40]

i) ≤ 5 hydrogen bond donors
ii) ≤ 500 $gmol^{-1}$
iii) LogP ≤ 5 (related to LogD)
iv) ≤ 10 hydrogen bond acceptors

A drug is more likely to fail in the clinic if two or more of these parameters are not met.[40] As LogP (the partition coefficient of a compound between an organic (octanol) and an aqueous phase were all molecules are in neutral form), is related to LogD clearly lipophilicity is an important parameter in the success of a drug compound.[39] As a general rule for $LogD_{7.4}$ a value between 1 and 3 is considered as the optimal point for a drug to possess good oral bioavailability. $LogD_{7.4}$ can be seen to influence other DMPK properties for values outside of this range, for example, $LogD_{7.4}$ <1 has an advantage of low metabolic liability, but may suffer from poor permeability and rapid *in vivo* renal clearance. A $LogD_{7.4}$ >5 would likely possess low aqueous solubility, poor oral bioavailability and high metabolic liability.[39,41,42]

There is increasing evidence that clinical drug candidates are overly hydrophobic, which may be responsible for the high rates of attraction observed during the drug development process.[43] Though $LogD_{7.4}$ can be used to estimate the likelihood of a particular drug compound to be soluble in an aqueous environment, work undertaken by Hill and Young show that measured and calculated $Log_{7.4}$ values of tens of thousands of compounds show poor correlation.[43] This was particularly true when they analysed compounds based on aqueous solubility. Poorly aqueous soluble compounds showed the poorest measured to calculated $LogD_{7.4}$ correlation, while this correlation was improved with highly aqueous soluble compounds, it was still statistically poor.[43]

Using solubility categorised box plots, Hill and Young demonstrated that for poorly soluble compounds, if calculated $logD_{7.4}$ is predicted between 3 and 7, then there was no statistical difference between measured values of the same compounds, which gave average measured $logD_{7.4}$ values

between 2.5 and 3.5.[43] The observations suggest that the factors causing poor aqueous solubility may be perturbing the octanol / water system preventing true equilibrium from being obtained.[43] This can possibly be explained through the tendency of poorly soluble compounds to form aggregates (discussed in the next section on aqueous solubility).[43,44] The data presented by Hill and Young shows therefore, that the measured $logD_{7.4}$ value should only be used in context of the aqueous solubility of the molecule in question, or, that the calculated $logD_{7.4}$ value may be a better indicator of hydrophobicity than a measured value.[43]

Hill and Young, amongst others, have highlighted the negative impact of aromaticity on solubility.[43–47] This effect can be explained by an increase in lattice energy, and melting point caused by π-stacking of the planar aromatic rings, or by a reduction of entropy contribution in the free energy of solvation due to the molecules being more rigid.[43,48,49] Hill and Young therefore, demonstrated in their review, that the proportion of poorly soluble compounds increases as either hydrophobicity increases, or the number of aromatic rings increases.[43] From this, they formulated the solubility forecast index (SFI), which is the sum of $ClogD_{7.4}$ + the number of aromatic rings, were bi- or tri-fused rings count as two and three rings, respectively.[43] They demonstrated that if the SFI is <5, (instead of $CLogD_{7.4}$ <5) then there is an enhanced chance of compounds possessing good aqueous solubility, rather than just taking $ClogD_{7.4}$ into account alone.[43] From the equation, it is implied that for each aromatic ring there is a penalty equal to one log unit of hydrophobicity. Each compound within this chapter will have its SFI calculated, compared with measured $logD_{7.4}$ and measured aqueous solubility where appropriate. To calculate SFI $Clog_{7.4}$ was first calculated using the estimation method developed by Csizmadia *et al*. and pipeline pilot.[50,51]

ii) Aqueous solubility

Solubility is defined the maximum dissolved concentration of a drug in a particular solvent at a particular temperature.[39] Aqueous solubility is important because poorly aqueous soluble compounds result in limited absorption from the gastrointestinal tract further resulting in poor oral bioavailability. Therefore, lead candidates with poor solubility can require special formulation in order to remain efficacious which can be both costly and can result in delays.[39] There are numerous factors that affect solubility, such as molecular weight, lipophilicity, pKa, temperature and many more. In general compounds possessing high molecular weight, high degree of lipophilicity, used in their neutral forms and used at lower temperatures will all suffer poor solubility. Introducing compounds as salts can aid in increasing aqueous solubility as can increasing the temperature, thus the temperature in solubility assessments should be kept constant.[39] In addition, the solid form of a compound can also affect solubility. Using compounds in crystal form can result in increased time it

takes for a compound to dissolve, as the compound exists as a highly ordered lattice with low surface area. Using amorphous solids, however, means that this ordered lattice is not present and thus a compound can be easier to dissolve in this form due to the presence of a higher surface area and ease of access of solvent to solute.[39] A compound is considered to be poorly soluble for values <30 μM, and considered to possess good solubility for values >200 μM.[43]

Aqueous solubility also is an increasingly important parameter for the correct interpretation of data resulting from enzymatic biochemical assays and high-throughput screens (HTS). Enzymatic HTSs are dominated by false positives, many of which are due to inhibition by colloidal aggregates.[46] It is known that there is a tendency for poorly aqueous soluble compounds to form aggregates, and many organic molecules form submicrometer aggregates at μM concentrations in aqueous solution.[45] These aggregates are known to cause unusual nonspecific inhibition of enzymes in biochemical assays.[44–46,52] The interference of aggregates in biochemical assays has known characteristics, these include, reversal of inhibition by non-ionic detergent, steep dose response curves, and acute sensitivity to enzyme concentration, and these attributes aid in the identification of aggregate based inhibition.[45,46,52]

Coan *et al*. examined aggregate formation and found that for seven aggregate forming molecules, aggregates were not observed until the concentration of monomer passed a certain threshold known as the critical aggregate concentration (CAC).[46] They elucidated that aggregates behave in a similar manor to micelles, and that above the CAC, the concentration of monomer units and the size of aggregate particles is constant above the CAC. In addition to this, aggregate count increases linearly with added organic material above the CAC, and when the particles are diluted below the CAC the aggregates redissolve back into solution.[46] Using a flow cytometer, the group were able to determine aggregate concentration of two known aggregate molecules, nicardipine and miconazole, and found the concentration in solution to be between 5 – 30 fM.[46] The group then measured the stoichiometry of the aggregate enzyme interaction for the two aggregators, and discovered a surprising stoichiometric ratio of the number of bound enzyme molecules per aggregate. This was determined to be 12,850 ± 875 for nicardipine, and 10,040 ± 440 for miconazole.[46] Though surprising, this data is consistent with known aggregate behaviour, aggregate inhibition is sensitive to changes in enzyme concentration and increasing enzyme concentration 10 fold eliminated observed inhibition.[46,52] As aggregates are only present at the fM range, increasing enzyme concentration overwhelms the ability of the aggregate to sequester enzyme. The group also elucidated that these aggregates are composed of 10^8 monomer units, that these aggregates are densely packed and that

the surface of the aggregates is large enough to accommodate all of the calculated bound enzyme molecules.[46]

McGovern *et al*. uncovered three mechanistic features of aggregate molecules.[52] First, inhibition occurs through direct binding of the enzyme to the aggregate, as observed by the ability to sediment protein-aggregate complexes *via* centrifugation, the punctate fluorescence as seen in microscopy in mixtures of aggregates with green fluorescent protein, and direct observation of protein-aggregate complexes by electron transmission microscopy. Second, addition of non-ionic detergent results in reversal of aggregate based inhibition. Third, several experiments rule out full denaturation of the enzyme. Coan *et al*. used these concepts to uncover a proposed mechanism of aggregate particles on enzymes.[52] Using ^{1}H – ^{2}H exchange mass spectrometry and proteolysis of enzyme-aggregate complexes, the group proposed that aggregate inhibition is due to partial unfolding of the enzyme when bound to an aggregate particle.[45]

In 2007, a HTS identified 95 % of hits showed aggregate based behaviour, this represents an overwhelming amount of molecules that may be false positives, and thus substantially reduces the hit rate of non-aggregating specific inhibitors.[53] Another major issue with poorly aqueous soluble compounds is the tendency of the compound to precipitate out of solution during biological assays which causes difficulties in the interpretation of activity values.[54] The above mentioned research exemplifies the importance of aqueous solubility on the interpretation of biological data resulting from biochemical assays. If poor aqueous solubility tracks with increased enzyme activity, care must be taken to ensure this activity is not from false readout through aggregate based inhibition.

iii) Drug metabolism

Drug metabolism is an enzymatic chemical biotransformation of a drug compound to more hydrophilic water soluble metabolites to aid excretion from the body. In humans the liver is the most important site of drug metabolism. Drug metabolism is split into two phases.[39]

i) Phase I metabolism. Involves reduction, oxidation and hydrolysis reactions of a particular compound. One of the major routes of metabolism of numerous compounds is through cytochrome P (CYP) metabolism, specifically *via* the CYP450 superfamily.[39]

ii) Phase II metabolism. Involves the additions of highly polar molecules to the drug. An example of phase II metabolism is glucuronidation. Note phase I and II metabolism do not have to be sequential. A drug can be metabolised by phase I followed by phase II, phase I exclusively, phase II exclusively, or phase II followed by phase I.[39]

Drug metabolism affects numerous parameters such as oral bioavailability, clearance time, and half-life. This can then have significant impact of toxicity and efficacy of a drug. As a chemical transformation of a drug takes place its structure is inadvertently altered. This can result in a loss of therapeutic effect, or in some cases a gain of therapeutic effect, compounds that are metabolised to an active drug in this manner are known as prodrugs. Further to the alteration of a therapeutic effect, the drug metabolite can become toxic to the host *via* affecting off-target biochemical pathways, something which of course is highly disfavoured.[39]

In terms of entering the clinic, drug metabolism and efficacy affect the dosing regimen. Drugs that are metabolised quickly can require multiple dosings per day or higher dosing to show a desirable therapeutic effect.[39] Drugs that are metabolised slowly are ideal, however, too slow can also be problematic as a drug that bio-accumulates can itself then become toxic over a certain concentration threshold.[39]

The gold standard for a drug is a half-life at a point where a once daily dosing regimen can be taken with no issues of toxicity.[39] A perfect drug would ideally be administered as single dose cure. Dosing in this manner holds a major advantage in patient compliance and in the case of pathogens this can help slow the spread of resistance.

To examine the metabolic stability of a particular drug *in vitro*, subcellular fractions such as liver microsomes are used to predict the hepatic clearance of a drug as they contain many of the phase I metabolising enzymes found in the liver but do not have an intact cell membrane. A down side to microsomes, however, is that metabolism can be underestimated especially if the primary metabolism route is *via* phase II. To this end hepatocytes have an advantage of possessing an intact cell membrane, and hold all enzymes from phase I and phase II metabolism, therefore they more accurately represent an *in vivo* system. As mentioned above compounds that are metabolised (or cleared) quickly are discouraged as upon entering an *in vivo* model the compounds will be cleared rapidly giving a poor half-life and thus poor therapeutic window.[39]

Selected compounds have been tested for human microsomal (mics) stability to assess the stability of a compound when it enters CYP450 oxidation *via* phase I metabolism. The same compounds have also been tested in the presence of rat hepatocyte cells (heps) to assess the potential situation should the compound enter *in vivo* studies. Some selected compounds were also been tested for mouse microsomal (mics) stability as the majority of early *in vivo* models for malaria are examined in mouse. Table 2.5 below indicates the rate when a compound is considered to be metabolically

cleared slowly or quickly. As mentioned above selected compounds were also examined for their $LogD_{7.4}$ and aqueous solubility profiles.[39,55]

Table 2.5. Criteria to assess the rate of metabolic clearance. High clearance is shown in red (poor), low clearance is shown in green (good).

Clearance Catagory	*In vitro* microsomal intrinsic clearance mL / min / mg protein		*In vitro* hepatocyte intrinsic clearance mL / min / 10^6 cells
	Human	Mouse	Rat
Low	≤ 8.6	≤ 8.8	≤ 5.1
High	≥ 47	≥ 48	≥ 28

In vitro testing of **1a** and **6** with both *Pf*IspD using a pyrophosphate release assay, and *Pf*3D7 whole cell assay gave respective IC_{50} values and EC_{50} values of 25.3 ± 5.6 nM and 349 ± 30 nM for **1a**, and 21.6 ± 2.7 nM and 373 ± 86 nM for **6**. This is encouraging as both **1a** and **6** yield similar activities as observed by Yao *et al*. as summarised in Table 2.6 below. Note there are some minor discrepancies between the values, and this is likely due to the slightly different *Pf* strains used between our group and Yao *et al*.

Table 2.6. Inhibitory activities of 1a and 6 against *Pf*IspD, parasite growth (3D7 our work) and (Dd2 Yao *et al*. work).[9]

Compound	*Pf*IspD IC_{50} (nM)	*Pf*3D7 EC_{50} (nM)	Yao *Pf*Dd2 IC_{50} (nM)
1a	25.3 ± 5.6 n = 3	349 ± 30 n = 6	250 ± 70
6	21.6 ± 2.7 n = 3	373 ± 86 n = 4	190 ± 30

It was our initial goal to synthesise both acid and methylamide derivatives of the majority of compounds, however, for three reasons we changed this strategy to synthesise amide derivatives solely. Firstly, upon exploring C-ring modifications, the amberlyst catch and release protocol reported by Yao *et al*. failed, and no reactions were observed.[9] Although this ester can be hydrolysed easily in the presence of base, the zwitterionic nature of the final compounds made removal of salt contamination difficult even after column chromatography; this was noticeable as CHN analysis was consistently and considerably out of the target range. Furthermore, there was concern that addition of hydroxide as the base and long reaction times could run the risk of epimerisation of the C3 stereogenic centre, potentially further complicating purification procedures. Therefore these compounds were not tested and are not included as part of this work. Secondly, synthesising amide derivatives possessed numerous advantages; purification was trivial with most reactions progressing to completion with little to no side products. Thirdly, the amides are considered less susceptible to drug-metabolism, therefore, are likely to increase the half-life and pharmacokinetic profile of the drug. The amides had also already demonstrated potential improved potency over the hit molecule. Finally, crystallisation was simple, all compounds could be successfully recrystallised from neat methanol, in

some cases these recrystallisations gave rise to X-ray quality crystals, and as such X-ray analyses on these compounds were used as structural characterisation. X-ray analysis gives us extra confidence that the correct stereoisomers were indeed used in our studies as absolute stereochemistry can be determined.[33–35]

2.2.4 C-ring Modifications

We began our SAR of the template first investigating exploration of the C ring asking three questions.

i) Can the C-ring nitrogen be substituted?

ii) Is basicity of the C-ring nitrogen required?

iii) Are there alternatives to the NHMe amide?

To answer the first question intermediate **17** was prepared. This was accomplished in good yield of 67 % through simple addition of MeI to **4** in the dark Scheme 2.3. The same reaction in light led to highly diminished yields and side products that needed to be removed on column. The final compound 1**8** was then successfully synthesised from the direct amide coupling of $MeNH_2$ following Scheme 2.3 in excellent an yield 99 %.

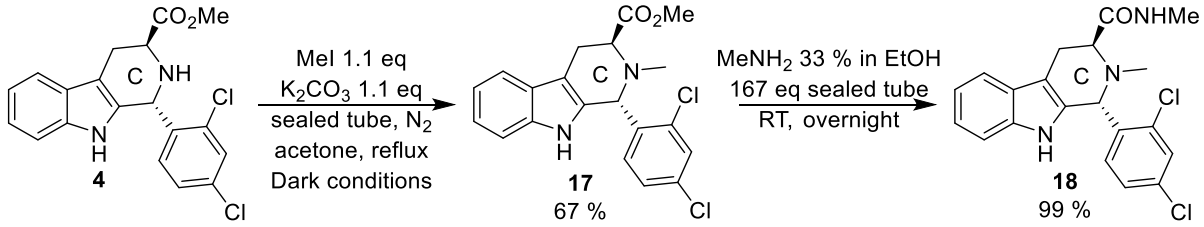

Scheme 2.3. Synthesis of compound 18.

To answer the second question molecules **20** and **21** were generated through slightly different procedures. A further rationale behind the synthesis of **20** was to investigate if a compound mirroring tadalafil (**9**) could target *Pf*IspD and be antiplasmodial. Unlike the investigation using (1*R*, 3*R*)-tadalafil (**9**) by Yao *et al*., we conducted this study with (1*R*, 3*S*)-configuration. We also replaced the aryl ring with that of the MMV template with the required 2-Cl, 4-Cl substitution pattern. This compound was generated *via* the addition of bromoacetyl bromide to **4** forming **19** in 80 % yield. Cyclisation to **20** was successfully achieved in the presence of 5 equivalents of $MeNH_2$ in moderate yield of 57 % (Scheme 2.4). We reduced the number of equivalents of $MeNH_2$ substantially to overcome the potential of the addition of two molecules of $MeNH_2$, one into the ester, and the other into the alkyl bromide side chain.

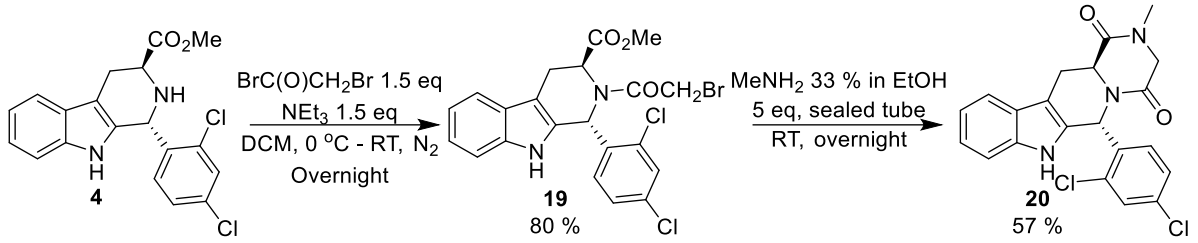

Scheme 2.4. Synthesis of compound 20.

Finally, **21** was designed to see if activity benefited from being cyclic or not as **21** is essentially a ring-opened form of **20**. **21** was initially planned to be generated following a similar route to **20**, reacting **4** in the presence of AcCl and NEt_3 before amide coupling to the final target. However, this first reaction despite apparent full conversion to a single spot *via* TLC resulted in an NMR spectrum that was difficult to interpret. We initially believed that the reaction conditions had epimerised the carboxylate group at C3 as this would explain the presence of extra peaks due to the formation of a diastereoisomer, but no separation on TLC could be observed. We instead resynthesised compound **6**, and performed the coupling of AcCl at this stage as the final step giving a yield of 60 % (Scheme 2.5). Similar to the reaction with the ester the NMR led to broadened signals and more peaks than expected. We postulated that this compound therefore existed as a rotamer, as we did not expect epimerisation of the C3 stereogenic centre with either the ester or the amide. Analytical chiral HPLC of **21** appears to back this postulation up as only one peak is seen using the protocol described in the experimental section (**Section 2.5.2**).

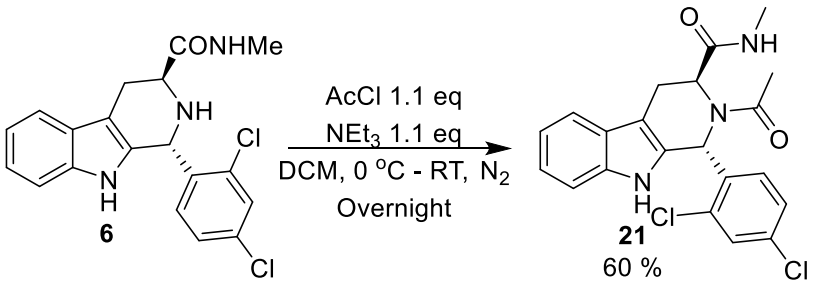

Scheme 2.5. Synthesis of 21.

To answer question three we examined the SAR from Yao *et al.* and noticed two molecules of interest that they had not tested. These include utilising a two other alkyl amides, the first cyclopropyl and the second ethyl. We are interested in cyclopropyl amide as it is sterically smaller than the tested ^{i}Pr and thus offers renewed chance to regain activity if it spatially complements the fit of the IspD active site. The second amide, an ethyl amide would be the smallest straight chain alkyl tested after methyl amide. Yao *et al.* did not test smaller than ^{n}Bu and thus it was possible that a methyl amide is not the best fit for the IspD active site, therefore there is a chance of improving potency by testing longer chain alkyls bigger than Me, but smaller than ^{n}Bu.

Generation of the two alkyl amides **22** and **23** followed a similar procedure to that described for the hit molecule (Scheme 2.6). In the case of **22** the reaction required heating to 50 °C likely due to the extra steric demand the cyclopropyl amine compared with methyl amine. This reaction required purification by column chromatography due to the formation of unknown side products, however, the reaction yield was moderate of 49 %. **23** was synthesised following a similar protocol to **6** in also in moderate yield of 51 % Further to these two alkyl based amides, we also tested an unsubstituted hydrazide moiety (synthesised by 4th year project student Lauren Wray) **24** and a hydroxamic acid moiety (synthesised by 4th year project student Lauren Wray and Erasmus student Giacomo Paloscia) **25** as potential bioisosteres (Scheme 2.6).

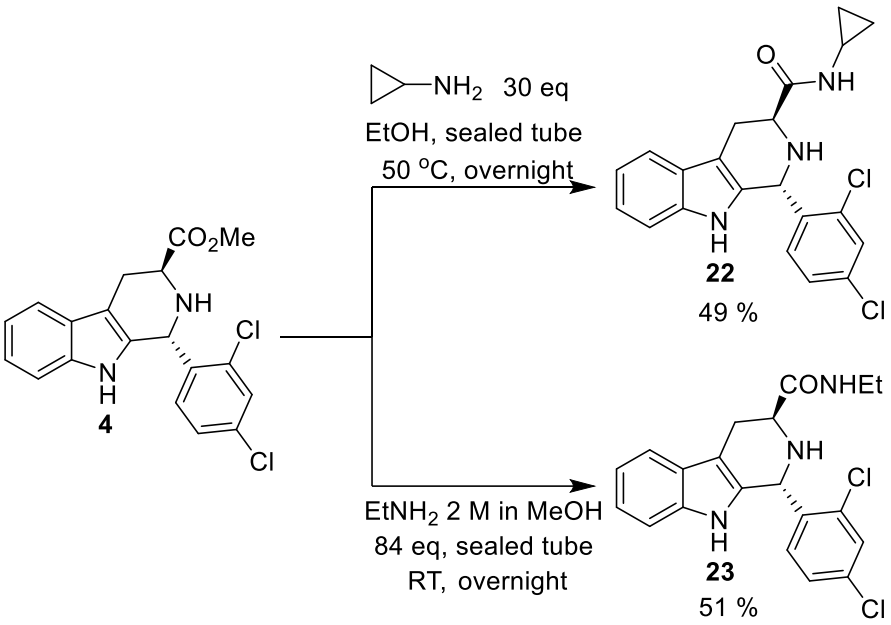

Scheme 2.6. Synthesis of compounds 22 and 23.

2.2.4.1 Biological Activity of C-Ring Modifications against *Pf*IspD and *Pf*3D7

C-ring modifications of **1a** were tested *in vitro* for their inhibitory activity against *Pf*IspD and were also tested against *Pf*3D7 cells as displayed in Table 2.7 (for direct comparison **1a** and **6** are also displayed). Table 2.7 reveals that optimal activity was achieved from **1a** and **6.** It is apparent that potency is dramatically affected by the incorporation of substituents at the C-ring nitrogen. The incorporation of a simple Me group as seen with **18** retains basicity of this nitrogen atom, however, this still results in the loss of potency of approximately 100 fold *vs* the IspD enzyme and approximately 50 fold in the cellular assay. Similarly compounds **20** and **21**, were the C-ring nitrogen atom has greatly reduced basicity, exhibit complete loss of potency against both enzyme and cell. Based on the values obtained it appears that there is at least one of the following requirements: i) the nitrogen must be unsubstituted due to a strict spatial requirement of the active site, ii) the nitrogen atom must be a

hydrogen bond donor as activity is lost with substitution, iii) the nitrogen must also be basic as activity is further reduced *via* amide incorporation.

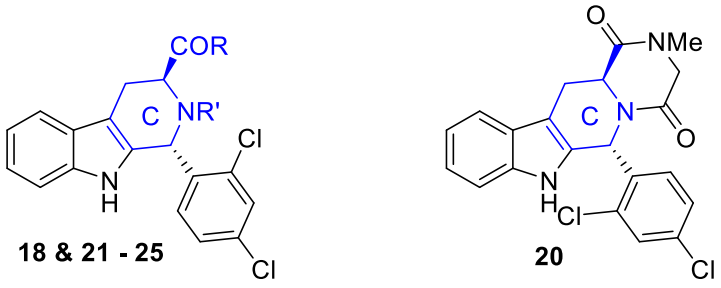

Table 2.7. Inhibitory activities of C-ring modifications against *Pf*IspD, and *Pf*3D7, values are colour coded with a traffic lights system according to how good or bad a specific value is. Green = good, amber = acceptable, red = poor.

Entry	R	R'	*Pf*IspD IC_{50} (nM)	*Pf*3D7 EC_{50} (nM)	$ClogD_{7.4}$	Aq. Sol. (μM)	SFI
1a	OH	H	25.3 ± 5.6 n = 3	349 ± 30 n = 6	2.9	N/A	5.9
6	NHMe	H	21.6 ± 2.7 n = 3	373 ± 86 n = 4	4.1	16	7.1
18	NHMe	Me	>2000 n = 2	8070 ± 115 n = 4	4.6	9	7.6
20	N(Me)R'	$COCH_2R$	>5000 n = 1	>10000 n = 3	3.7	N/A	6.7
21	NHMe	Ac	>5000 n = 1	>10000 n = 3	3.9	N/A	6.9
22	NH-^{cyc}Pr	H	594 ± 178 n = 2	6000 ± 341 n = 4	4.5	N/A	7.5
23	NHEt	H	>1000 n = 2	8110 n = 1	4.4	N/A	7.4
24	$NHNH_2$	H	83 n = 1	4920 n = 1	3.4	N/A	6.4
25	NHOH	H	Not tested	1000 ± 90 n = 3	3.9	N/A	6.9

Of the whole series only two compounds (**6** and **18**) had aqueous solubility measured. Compound **6** possessed a lower $ClogD_{7.4}$ value and SFI than **18**, as can be predicted from this, compound **6** demonstrates higher aqueous solubility than **18**. When comparing the enzyme activities of these two compounds, the activity is substantially dropped with decreased solubility. When considering compound **1a**, the SFI is lower than **6** or **18**, therefore, it would be predicted to possess improved aqueous solubility in comparison to **6** or **18**. Comparing SFI to activity, **1a** is still active when it has the highest predicted solubility, this could back up that the activity of this series is not due to aggregate formation. However, for future work a measured solubility assessment of **1a** would be required. Despite these trends suggesting non-aggregate behaviour, the SFI of all compounds (including **1a**) is higher than ideal, the predicted aqueous solubility of **1a** will likely still be low, and the aqueous solubility is low for compound **6**. Therefore, aggregate formation of **1a** and **6** cannot be ruled out. For future work regarding all compounds, assays could be repeated with non-ionic detergent, if activity is retained in the presence of non-ionic detergent it is likely the activity is not due to aggregate formation.

Upon examination of potential replacements of NHMe as the amide from **6**, again we can see a clear trend that **6** retains the best potency against both enzyme and cell assays. Replacement to the

cyclopropyl amide **22** results in approximately 30 fold drop in activity against IspD and this result is mirrored by poor potency *vs Pf*3D7. Surprisingly the NHEt amide demonstrates a 45 fold drop in potency against IspD. We would have expected that **22** and **23** would possess similar activity, as sterically they are not too different and both possess a similar $ClogD_{7.4}$, similar SFI value, and thus, similar predicted aqueous solubility. We postulate that the terminal CH_3 of the ethyl is bound by a rotatable bond and is not constrained in a ring like is seen with the equivalent carbon atom in the cyclopropyl derivative. This free rotation could cause unfavourable steric clashes in a small binding pocket.

Compound **24** bearing a hydrazide moiety regains activity *vs* IspD but surprisingly suffers poor cell potency, this could be due to poor membrane permeability but it is not related to lipophilicity (measured as $ClogD_{7.4}$ defined in **Section 2.2.3**) or aqueous solubility. As can be seen in Table 2.7, **1a** and **6** both possess lower and higher $ClogD_{7.4}$ values, respectively when compared with **24** and aqueous solubility would be predicted to be in between the **1a** and **6**. Again, aggregate formation in the enzyme assay cannot be ruled out at this time. Finally, though not yet tested *vs* IspD, compound **25** displays moderate potency against *Pf*3D7 cells. We believe that in the IspD assay the compound should possess good inhibitory activity, as **25** was designed to act as a potential metal chelator to bind to Mg^{2+} in the IspD active site in a similar manner to how fosmidomycin binds within IspC. Indeed the moderate activity seen in cell is promising and therefore may back this postulation up. However, we were disappointed with the cell activity of **25**, it appears that there is also a potential issue with membrane permeability of this compound, but again, if that is the case it is not related to $ClogD_{7.4}$.

2.2.4.2 Analysis of the Drug Metabolism and Pharmacokinetic (DMPK) Properties of the Hit 6 and Compound 18

To date an *in vitro* DMPK assessment of **1a** and **6** had not been carried out in the literature. Thus as part of the programme we also analysed compound **6**, for its DMPK profile in order to see if the MMV template had any metabolic short-comings. As part of C-ring optimisation we also decided to take compound **18** forward for DMPK testing to examine what effect increasing $ClogD_{7.4}$ or SFI has on the DMPK profile.

It is clear from Table 2.8 below that the template needs major improvement of DMPK properties. **6** has a measured $LogD_{7.4}$ just outside the desirable 1 – 3 range. SFI is larger than the upper threshold of 5 and thus solubility is predicted to be low. Compound **6** is also classified as possessing increased metabolic liability, as shown in the metabolic stability profile it has medium clearance from human microsomes and rapid clearance from rat hepatocytes. A major drawback for **6** is its metabolic

stability when exposed to mouse microsomes. **6** possesses an extremely high rate of clearance; because of this it is unlikely that it would show efficacy in *in vivo* testing within the mouse malaria model. As expected, **18** has an increased measured $LogD_{7.4}$ when compared with **6**, it is more lipophilic and therefore, has lower aqueous solubility than **6**. Furthermore, as the $LogD_{7.4}$ value for **18** is higher than that of **6**, this suggests that **18** may be highly susceptible to metabolism compared with compound **6**. Examination of the metabolic stability profile confirms that **18** is highly susceptible to metabolism as this compound possesses clearance rates almost twice as fast as **6** against human microsomes, and rat hepatocytes. As a result, this compound was not tested for mouse clearance which we also expect to be further diminished in comparison to **6**.

Table 2.8. DMPK profiles of compounds 6 and 18. Green = good, amber = acceptable, red = poor.

Entry	$LogD_{7.4}$	$ClogD_{7.4}$	Aq. Sol. (μM)	SFI	Human Mics CL_{int} (mL / min / mg)	Rat Heps CL_{int} (mL / min / 10^6)	Mouse Mics CL_{int} (mL / min / mg)
6	3.8	4.1	16	7.1	30.17	44.26	202.4
18	4.8	4.6	9	7.6	76.40	76.43	Not tested

2.2.4.3 Conclusion of C-ring Series SAR

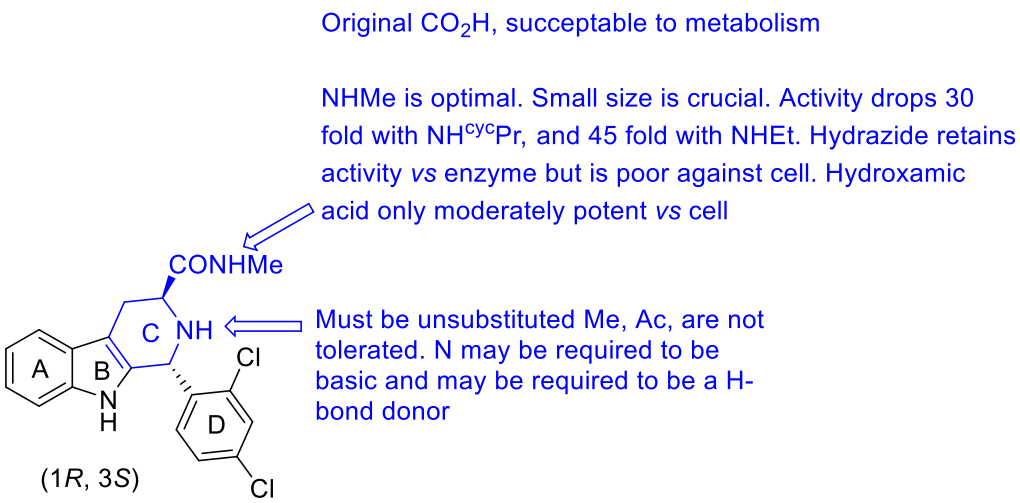

Figure 2.10. Conclusion of C-ring SAR.

Compound **6** remains optimal for activity against both IspD and 3D7. It appears as though any extra steric demand of the carboxylate group after NHMe significantly drops inhibitory activity, indicating that this moiety fits within a tight binding pocket. Substitution of the C-ring N atom of any kind is not tolerated at all as part of the SAR; incorporation of a Me group leads to greatly diminished potency whilst incorporation of amide functionality results in complete loss of potency. Examination of the DMPK profile of **6** gave concern for the metabolic stability of the compound in rat hepatocytes, human microsomes, and mouse microsomes. Compound **6** exhibits extremely rapid clearance times,

potentially hampering any future *in vivo* testing of the compound in the mouse model of malaria. Finally, all compounds possess high a SFI value, and when measured, also possess poor aqueous solubility leading to difficulties in the interpretation of the SAR. Due to the results of the C-ring SAR presented here all compounds retain the optimal C-ring core (presented in Figure 2.10).

2.2.5 D-ring modifications

2.2.5.1 D-ring Di-substitution

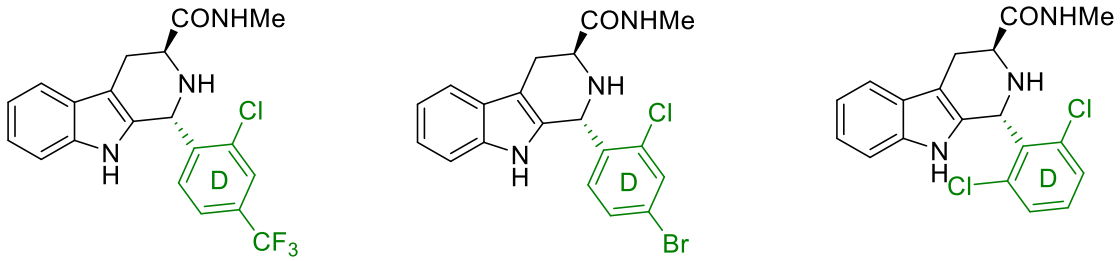

Figure 2.11. Explored D-ring di-substitution patterns.

Regarding D-ring functionalisation we focused our SAR on numerous substitution patterns. Initially, we examined further the effect of di-substituted ring motifs on activity to gain further knowledge of the specific requirements of this ring. Based on work by Yao *et al*. the 2-Cl seems to be a requirement when a substituent is at the 4-position of the aromatic ring. Therefore in our SAR this 2-Cl substitution was always kept in place. We found it very unusual that the loss of potency against cell observed with 2, 4-bisCF_3 substitution had occurred in the SAR studies carried out by Yao *et al*.[9] We therefore wanted to examine the effect of 2-Cl, 4-CF_3-substitution on IspD and cellular potency, and thus generated compound **28** (Figure 2.11).

In addition we wanted to explore the steric demand around the 4-position; the active site itself appears to tolerate sterically demanding groups, as 2-Cl, 4-Cl is already relatively large from a steric point of view. Of commercially available aldehydes at the time, we located and obtained 2-Cl, 4-Br benzaldehyde. The incorporation of an even bigger halogen allows us to assess what we can manipulate around this aryl ring. Furthermore, the bromine atom is essentially acting as a source of lipophilicity allowing us to probe not only steric demand, but electronics of the D-ring as-well. From this benzaldehyde compound **29** was generated (Figure 2.11).

As the last of the di-substitution patterns explored we deviated away from a 2, 4-di-substitution pattern and instead wanted to probe the 6-position generating compound **30** (Figure 2.11). As of yet this position on the molecule had not been explored, this allows us to probe the steric demand of the other half of the D-ring, and if the substituent is big enough this should force without

ambiguity the D-ring to lie perpendicular to the tetrahydro-β-carboline core. In order to nullify the potential effect of atropisomerism, 2-Cl, 6-Cl was chosen as the substitution pattern. Furthermore this pattern is more suitable for a direct comparison with 2-Cl, 4-Cl substitution.

2.2.5.2 D-ring Tri-substitution

Following from the exploration of di-substituted patterns we were also interested in looking at tri-substitution. As previously mentioned the D-ring appears to tolerate relatively sterically demanding substitution, it can therefore be proposed that additional small or even large substituents could optimise potency. The first logical course of action to take was the exploration of 2, 3, 4-substitution were the 2, and 4-positions remained as Cl atoms. We chose to generate compounds **31** and **32** baring F and Cl atoms, respectively (Figure 2.12). **31** baring small functionality (Van der Waals radius of F = 1.47 Å *vs* H = 1.20 Å) and a potential H-bond acceptor in fluorine could improve potency if the fluorine atom is in proximity to a hydrogen bond donor in the active site.[56,57] The small size of fluorine should not have a big impact in terms of steric requirements and thus should still fit within the IspD binding pocket. **32** on the other hand allows us to probe steric demand, if activity is improved, **32** may indicate some flexibility within the binding site to accommodate the change. The advantage of incorporating halogens in this way means that metabolic stability can potentially be improved, especially in the case of fluorine incorporation. The fluorine atom is highly electronegative and furthermore the C-F bond has very high bond strength (C-F strength = 513.8 $KJmol^{-1}$ vs C-H = 338.4 $KJmol^{-1}$); the advantage of this is that positions occupied by fluorine become less metabolically labile as biological transformations become less favoured compared with the same position occupied with a hydrogen atom.[57,58]

In addition to halogen substitution, the 3-position carbon was also replaced with a nitrogen atom (Figure 2.12), i.e. turning the D-ring into a pyridyl aromatic ring (**34a**) (Synthesised by 4th year project student Lauren Wray). This holds three advantages in comparison to the addition of substituents to the C3 carbon. Firstly, steric demand is not a factor, in effect what we really have is a 2, 4-di-substituted pyridyl, rather than a tri-substituted Ar-ring. In terms of comparison to compound **6** there should be very little difference from a steric point of view. Secondly, similar to fluorine, the nitrogen atom has the ability to pick up an extra hydrogen bond in the active site, nitrogen is more prone to hydrogen bonding than fluorine, which may enhance binding energy within the enzyme; in turn this could lead to enhanced potency.[57,59,60] Thirdly, another major advantage of using a nitrogen atom in this way is that because of the increased polarity of nitrogen, the $LogD_{7.4}$ will drop, as a consequence, aqueous solubility should increase and metabolic liability should decrease. For this reason this compound and derivatives of it are very interesting to explore.

In addition to 2, 3, 4-substitution 2, 4, 5-substitution and 2, 4, 6-substitution has also been examined. The rationale for exploring these positions is the same as it was for 2, 3, 4-substitution. The advantage with 2, 4, 5 and 2, 4, 6-substitutions is that we can explore the other side of the D-ring, allowing us to determine if substituents can be either sterically or electronically tolerated in the active site. For 2, 4, 5-substitution, due to the commercial availability of the aldehydes only compounds **35** (5-F) and **36a** (5-N in place of 5-C) were examined. For 2, 4, 6-substitution, (synthesis carried out by former PhD student Dr Kathyrn Price) compounds **37** (6-F), **38** (6-Cl), **39** (6-OH), **40** (6-OMe), **41** (6-N in place of 6-C) were examined. Compound **38** is interesting to explore as like **30** a chlorine atom is at both 2 and 6-positions, however, if activity is also dependent on a 4-position substituent, any loss of activity for 2, 6-di-substitution could be regained with 2, 4, 6-tri-substitution. For compound **39**, in contrast to halogen substitution which acts as a potential hydrogen bond acceptor, a hydroxyl derivative examines the effect of a hydrogen bond donor. Examining the methoxy derivative **40** then allows us to probe the steric demand again around the active site (Figure 2.12).

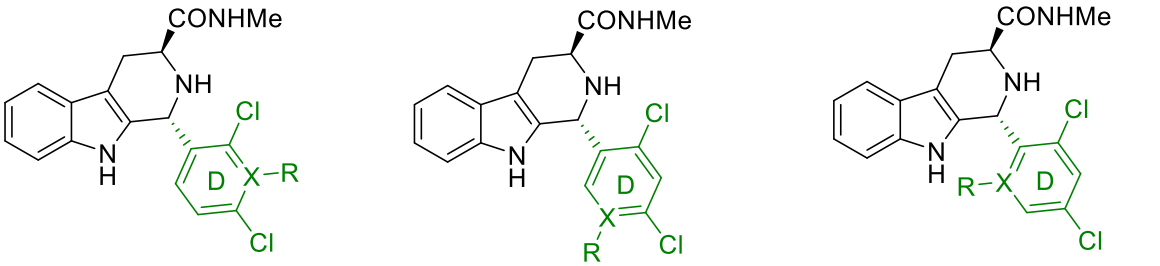

32, 33, 34

31 X = C, R = F
32 X = C, R = Cl
34a X = N, R = Null

35, 36

35 X = C, R = F
36a X = N, R = Null

37 - 41

37 X = C, R = F
38 X = C, R = Cl
39 X = C, R = OH
40 X = C, R = OMe
41 X = N, R = Null

Figure 2.12. Differing substation patterns explored as part of the SAR of the D-ring.

With the exception of **34a** and **36a** all compounds were synthesised following Scheme 2.7. The free base of L-tryptophan methyl ester (**13**) was coupled with various di-and tri-substituted aldehydes utilising the Pictet-Spengler reaction yielding **26a – l** as *trans* isomers and **27a – l** as *cis* isomers. With the exception of **26c** and **27c**, all diastereomers could be separated at the ester stage. **26c** and **27c** were taken forward to the amide coupling forming **30a** (*trans*) plus **30b** (*cis*) which were then separated at this stage.

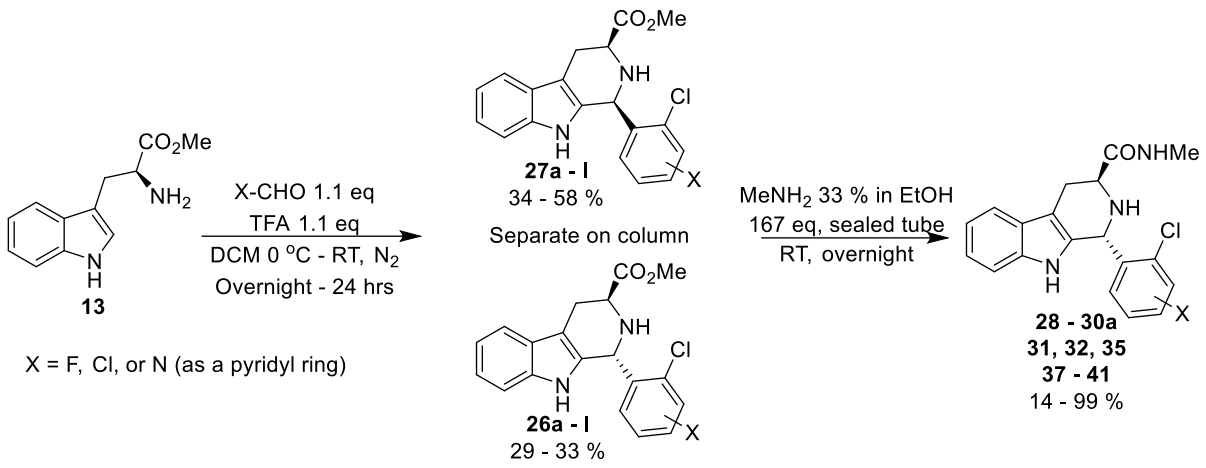

Scheme 2.7. Synthesis of D-ring modifications.

Isolated reactions yields of both *trans* and *cis* isomers from the Pictet-Spengler reactions of each differing substitution pattern from Scheme 2.7 are displayed in Table 2.9 below, subsequent Table 2.10 displays yields for the final amide couplings, all yields are reported after recrystallisation. Note only compounds synthesised by myself are included in the data tables. Therefore please also note compounds not displayed are **26g – l**, **27g – l**, and **37** – **41**, and that **37** – **41** are synthesised chronologically from **26g – l** (Synthesis carried out by former PhD student Dr Kathryn Price).

Table 2.9. Yields of the Pictet-Spengler reaction with various different aldehydes.

Compound	X	% Yield
26a	4-CF_3	33
26b	4-Br	17
26c & 27c	6-Cl	80
26d	3-F, 4-Cl	26
26e	3-Cl, 4-Cl	29
26f	4-Cl, 5F	29
27a	4-CF_3	55
27b	4-Br	34
27d	3-F, 4-Cl	60
27e	3-Cl, 4-Cl	48
27f	4-Cl, 5F	58

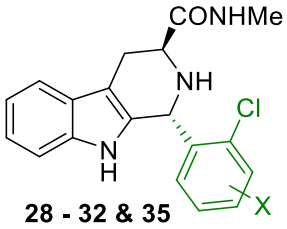

28 - 32 & 35

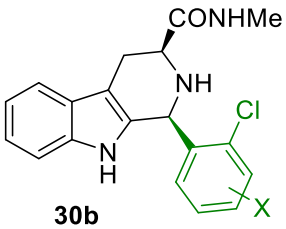

30b

Table 2.10. Yields of the final amide couplings.

Starting material	Product	X	% Yield
26a	**28**	4-CF_3	91
26b	**29**	4-Br	87
26c & 27c	**30a (*trans*)**	6-Cl	14
26c & 27c	**30b (*cis*)**	6-Cl	34
26d	**31**	3-F, 4-Cl	99
26e	**32**	3-Cl, 4-Cl	88
26f	**35**	4-Cl, 5F	87

In general the combined *cis* and *trans* Pictet-Spengler reaction yields were very good ranging from 77 % to 88 %, with the exception of 4-Br substitution giving a yield of 51 %. Generally *cis* to *trans* ratio was 2 : 1. Compounds of interesting note are **26c** and **27c**. There are two reported cases in the literature which state that **26c** cannot be observed and that *cis* selectivity is 100 %.[61,62] The general procedure for this compound differed slightly to what was described in literature, the difference being that at the time of reaction for this compound lab temperature was 12 °C not standard room temperature. Therefore at least for this substitution pattern, cooler temperatures seemed to lead to higher *trans* selectivity. Unfortunately, as described above the compounds could not be separated at ester stage, the presence of the *trans* product needed to be confirmed by NOESY of the combined diastereoisomers, fortuitously, the C1 and C3 hydrogen atoms of the two diastereoisomers have differing chemical shifts which allowed the determination of the *cis* and *trans* product. As can be observed from Table 2.10, amide couplings generally proceeded well, with the exception of **30a** and **30b**. Although separation could be achieved on column, it was minimal, and some fractions remained mixed. Reported in Table 2.10 are the isolated yields only.

The synthesis of **34** and **36** required alternate approach. It was observed that reacting the *trans* ester of 2-Cl, 4-Cl, 5-N, with $MeNH_2$ led to substitution of one of the chlorine atoms with $MeNH_2$ along with amide formation. Unfortunately we could not determine which chlorine had been substituted and is not included as part of the reported data. (Out of interest, however, it was tested anyway and proved to be inactive). As we did not know whether the 2-chlorine atom (*para* to the pyridine nitrogen atom) or 4-chlorine atom (*ortho* to the pyridine nitrogen atom) had been substituted we did not want to run the risk of having the same side reaction occur again when pyridine nitrogen

atom was at the 3-position, in this case both chlorine atoms are *ortho* to the pyridine nitrogen atom and either one could be substituted. We instead carried out the reactions in reverse order, amide coupling $MeNH_2$ into L-tryptophan methyl ester (**13**) first forming **33** in 99 % yield, and then carried out the Pictet-Spengler reaction as the last step yielding the **36a** and **36b** in yields of 6 % and 31 %, respectively (Scheme 2.8). When a nitrogen atom is at the 6-position as displayed in **41** this approach is not necessary as Cl atoms are *meta* and cannot be easily substituted (Note **34a** and **34b** synthesised by 4th year project student Lauren Wray, compounds not shown).

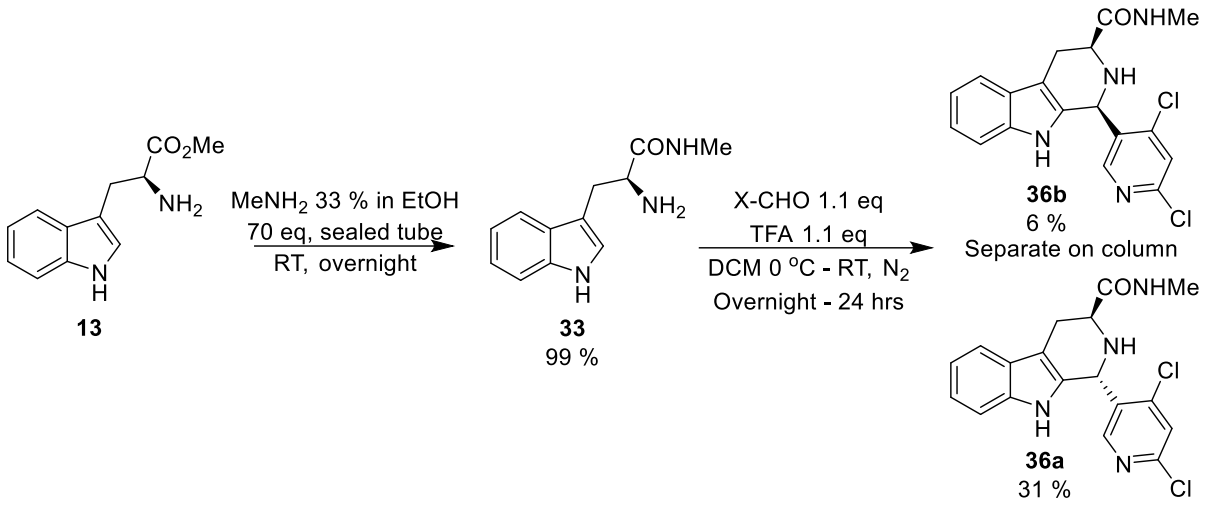

Scheme 2.8. Alternative synthesis for the generation of compounds 36a.

2.2.5.3 Biological Activity of D-Ring Modifications against *Pf*IspD and *Pf*3D7

Most D-ring modifications of **6** were tested *in vitro* for their inhibitory activity against *Pf*IspD and against *Pf*3D7 cells as displayed in Table 2.11 and selected compounds were also assessed for aqueous solubility. For direct comparison **1a** and **6** are also displayed.

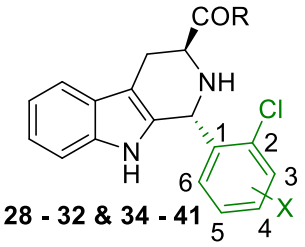

28 - 32 & 34 - 41

Table 2.11. Inhibitory activities of D-ring modifications against *Pf*IspD, and *Pf*3D7 Green = good, amber = acceptable, red = poor.

Entry	R	R'	*Pf*IspD IC_{50} (nM)	*Pf*3D7 EC_{50} (nM)	$ClogD_{7.4}$	Aq. Sol. (μM)	SFI
1a	OH	4-Cl	25.3 ± 5.6 n = 3	349 ± 30 n = 6	2.9	N/A	5.9
6	NHMe	4-Cl	21.6 ± 2.7 n = 3	373 ± 86 n = 4	4.1	16	7.1
28	NHMe	4-CF_3	80.2 ± 18.3 n = 4	3730 ± 534 n = 3	4.3	N/A	7.3
29	NHMe	4-Br	160 ± 24.2 n = 3	248 n = 1	4.1	10	7.1
30a	NHMe	6-Cl	>5000 n = 2	>250000 n = 1	4.1	19	7.1
31	NHMe	3-F, 4-Cl	1140 ± 241 n = 3	3260 n = 1	4.3	0.5	7.3
32	NHMe	3-Cl, 4-Cl	2530 ± 161 n = 2	598 n = 1	4.7	6	7.7
34	NHMe	3-aza, 4-Cl	Not tested	8960 ± 2380 n = 3	3.3	N/A	6.3
35	NHMe	4-Cl, 5-F	>5000 n = 1	>100000 n = 1	4.3	3	7.3
36a	NHMe	4-Cl, 5-aza	>5000 n = 2	>250000 n = 1	3.1	9	6.1
37	NHMe	4-Cl, 6-F	2220 n = 1	Not Tested	4.3	N/A	7.3
38	NHMe	4-Cl, 6-Cl	>5000 n = 1	Not Tested	4.7	N/A	7.7
39	NHMe	4-Cl, 6-OH	>5000 n = 1	Not Tested	3.6	N/A	6.6
40	NHMe	4-Cl, 6-OMe	>5000 n = 1	Not Tested	4.0	N/A	7.0
41	NHMe	4-Cl, 6-aza	>2000 n = 1	Not Tested	3.3	N/A	6.3

From the results displayed around the SAR in the D-ring it is apparent that there appears to be restricted requirements in order to maximise potency. The first compound from the di-substituted series examined was **28** to see what effect CF_3 substitution on the aryl ring has on potency. Our initial thoughts on the Yao *et al.* study showing a loss of cellular potency with 2, 4-bisCF_3 substitution were that this was unusual. While we looked only at the 4-substitution it is clear that the compound inhibits IspD effectively as we believed it should, bearing only a 4 fold loss of potency. However, our poor whole cell potency seems to mirror the result observed by Yao *et al*.[9] Similar to the C-ring optimisation, cell activity does not correlate with $CLogD_{7.4}$ or SFI values, as **28** is almost identical to **6**. We then examined the steric effect by adding Br to the 4-position in **29**. Much to our delight, and also surprise, this compound is still potent against IspD, whilst it is 8 fold less potent then the hit, the cellular potency though only tested once, very much to our surprise, is our current most active compound in the phenotypic assay, which also shows potency against IspD. We can deduce that there is a range of steric tolerance at the 4-position; it could be therefore a place of chemical manipulation. It may possibly be that the 4-position of the D-ring is pointing out into solvent exposed space. For future work it would be ideal to examine the effect of adding a potential solubilising group at this position, to explore steric

demand while also attempting to reduce the $LogD_{7.4}$ of the template as a whole. This should aid in reducing the potential for aggregate formation and may improve the DMPK profile of the series. The final di-substitution pattern with 2-Cl, 6-Cl **30a** unfortunately showed complete loss of activity suggesting that the 6-position cannot be substituted.

From the di-substituted series compounds **6**, **29**, and **30a** were assessed for their aqueous solubility. The SFI is >7 for all compounds in this series and this translates to the poor aqueous solubility of these compounds. Compounds **6** and **29** both possess potent enzyme and cell activity, the SFI value of these two compounds is also the same (SFI = 7.1 for **6**, and **29**). However, compound **6** shows slightly improved aqueous solubility compared with **29**. Due to the compounds both possessing the same SFI value and similar aqueous solubility values, aggregate formation cannot be ruled out for either of these compounds due to the poor aqueous solubility observed. Compound **30a** is inactive in both the enzyme and phenotypic assay despite possessing the same SFI, but has improved aqueous solubility over compound **6**. Compound **28** was not sent for aqueous solubility assessment, but of the di-substituted series it possess the highest SFI, and so is predicted to possess the lowest aqueous solubility of the series, it is active in the enzyme assay but not in the phenotypic assay.

It is clear is that steric demands around the D-ring cannot be the only determining factor for potency. In all examples of tri-substitution, only the 3-F substituent (compound **31**) gives moderate enzyme potency, all other compounds are considered inactive. But again on transferring to the cell, all compounds including fluorine substitutions are inactive, with the exception of 2, 3, 4 tri-chloro substitution (compound **32**), which is only moderately active against enzyme, but displays good activity in cell. Therefore, it is highly likely this compound is exhibiting off target effects and this could be confirmed with an IPP rescue screen in the future. It is odd that the incorporation of one fluorine affects activity so substantially. As previously mentioned, sterically it is not much larger than a hydrogen atom.[56,57] Therefore, it should exhibit very little extra steric clashes in the active site, and any steric effect that may occur does not seem enough to explain the amount of potency loss we observe. In the case of 3-position substitution the fluorine is shielded by the much larger chlorine atoms, therefore steric demand does not account for the loss of potency. It does appear that there is a very strict but not fully understood electronic requirement for this D-ring that determines optimal potency.

Examination of the compounds with measured aqueous solubility data and comparing with activity values also yields results that are difficult to interpret. Compounds **31**, **32**, **35**, and **36a** were assessed for their aqueous solubility, all compounds show poor aqueous solubility vales of less than 10 μM. **31** is practically insoluble in an aqueous environment, yet still shows some moderate enzyme

activity and cell activity. Whether this is due to aggregate formation or not is not clear, and as previously mentioned, this can be assessed through the addition of non-ionic detergent to the assay in the future. However, if the compound is precipitating out of solution, then this could explain why this compound appears to show reduced activity when compared with **1a** and **6**, as what precipitates will not interact with the enzyme. Compound **32** has a higher SFI value than **31**, however, it was determined to show enhanced aqueous solubility when compared with **31** (6 μM). **32** showed a 2 fold loss of potency in the enzyme assay, but as mentioned above it, is more potent than **31** in the phenotypic assay. Whether this result is due to enhanced solubility of this compound in comparison to **31**, or due to off target effects is not clear at this stage. An off target effect could be examined with an IPP rescue screen as previously mentioned. Compound **35** was expected to possess similar activity to **31**, however, complete loss of activity is observed in both enzyme and phenotypic assays. Compound **35** also possesses poor aqueous solubility (3 μM) and its loss of activity may be accounted for if it precipitated during the course of the biological assays.

Perhaps most disappointingly is the loss of potency observed with all pyridyl analogues. These analogues should not have any significant effect on steric requirements in the active site compared with compound **6**, and yet potency across all three differing substitutions is lost. Compound **36a**, despite having a lower SFI value, was determined to possess poorer aqueous solubility than the hit compound (**6**) and lost potency. Clearly there are effects in the D-ring binding site that disfavour either polar interactions or an electron deficient aromatic ring. Using a ring with electron donating substituents may lead to improvement of potency. Other than methyl, all substitutions have been based around heteroatoms within the known SAR. To date larger chain alkyl chains have not been examined at the 4-position of the D-ring, it could be that branched alkyl chains may also lead to improved potency, however, from a DMPK point of view; this could make the molecule less drug-like and should be considered before further drug design.

As a concluding remark on the SAR of the D-ring another point to consider is; is the template a substrate for an uncharacterised transporter into the apicoplast in cell? A specific transporter could explain why some compounds that are potent IspD inhibitors are inactive against 3D7 cells, especially when structures are only minimally varied. At present the answer to this question is not known, however, if the drug requires a transporter of some kind to reach its target, then any future SAR may have to cater for the binding mode in another protein potentially complicating design.

2.2.5.4 Analysis of the DMPK Properties of selected D-Ring Compounds

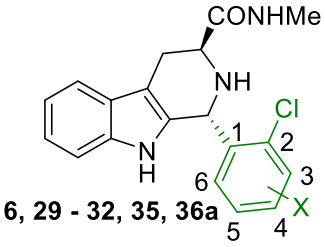

6, 29 - 32, 35, 36a

6 X = 4-Cl
29 X = 4-Br
30a X = 6-Cl
31 X = 3-F, 4-Cl
32 X = 3-Cl, 4-Cl
35 X = 4-Cl, 5-F
36a X = 4-Cl, 5-aza

Table 2.12. DMPK profiles of selected modified D-ring compounds. Green = good, amber = acceptable, red = poor.

Entry	$LogD_{7.4}$	$ClogD_{7.4}$	Aq. Sol. (μM)	SFI	Human Mics CL_{int} (mL / min / mg)	Rat Heps CL_{int} (mL / min / 10^6)	Mouse Mics CL_{int} (mL / min / mg)
6	3.8	4.1	16	7.1	44.26	30.17	202.4
29	4.1	4.1	10	7.1	35.40	42.40	Not tested
30a	2.7	4.1	19	7.1	21.10	49.20	Not tested
31	3.9	4.3	0.5	7.3	51.90	22.70	Not tested
32	> 4.4	4.7	6	7.7	64	64.50	Not tested
35	4	4.3	3	7.3	25.90	39.70	Not tested
36a	2.9	3.1	9	6.1	Not tested	4.07	Not tested

We selected several compounds for DMPK interrogation to assess if any substitution led to improvements in the DMPK profile (Table 2.12). In order for a compound to be sent for mouse microsomal screening our own criteria of potent inhibitory activity against at least cell and an acceptable DMPK profile needed to be met. Unfortunately no compound met these criteria and none of the D-ring substitution patterns were explored for mouse microsomal stability. Again, the SFI values of all compounds is above 5. Therefore as predicted, the solubility of this series is poor, similar to the C-ring series. Despite this, examination of Table 2.12 demonstrates some interesting results, the only compound showing improved cell potency (**29**) harbours a bromine atom which is more lipophilic than the chlorine atom that is present in the hit molecule **6**. As expected, the aqueous solubility has dropped as a consequence. Interestingly, though displaying an increased $LogD_{7.4}$, human microsomal clearance time has reduced vs **6**, however, examination of clearance within rat hepatocytes shows an increased clearance rate. As this compound showed little improvement over **6** in terms of its DMPK profile it was not sent for mouse microsomal screening.

30a is a compound that though inactive, shows an interesting DMPK profile. The incorporation of a chlorine atom at the 6-position has pushed $LogD_{7.4}$ within a target range. The improvement in $LogD_{7.4}$ is mirrored by improvements to aqueous solubility and a promising two-fold improvement for

human microsomal clearance time *vs* **6**. However, the rat hepatocyte assay demonstrates that this compound is rapidly cleared and unfortunately is cleared faster than **6**.

31 contains a 3-F substituent and therefore has slightly increased lipophilicity as demonstrated by the slight increase of $LogD_{7.4}$ vs **6**. This small structural change renders **31** a very insoluble compound which leads to activity values that are difficult to interpret. Metabolic clearance times for this compound are interesting, human microsomal clearance has moved into an undesirable range, however, rat hepatocyte clearance has improved over **6**. Based on the results obtained thus far it seems that along with interesting specific SAR for IspD and cell potency, there is also a species specific requirement of SAR when testing DMPK properties.

32 is the only other compound from the D-ring series possessing cell potency. However, it demonstrates a poor DMPK profile. Due to the presence of 3 chlorine atoms, the $LogD_{7.4}$ and SFI value are significantly higher *vs* **6**, and as a result aqueous solubility has dropped. In addition, **32** shows rapid clearance times in both human microsomes and rat hepatocytes. **35** is similar to **31** possessing fluorine substituent but at the 5-position of the D-ring. Unlike **31** it has far improved human mic clearance times *vs* **6**, surprisingly, however, its rat hep clearance time is significantly higher compared with **31**. Examining **35** and **30a** which are substituted at the 5 and 6-positions, both compounds demonstrate improved human mic stability. This raises the question of; is one or both of these positions a potential site of metabolism in human?

Perhaps the most interesting DMPK data came from compound **36a** which belonged to the pyridyl series specifically where the nitrogen atom is at the 5-position. As expected, the increased polarity of nitrogen has dropped the $LogD_{7.4}$ into a good range and thus also reduced the SFI value, however, SFI is still unfortunately higher than 5. Interestingly, the aqueous solubility was slightly decreased *vs* **6**, however, very interestingly the rat hep clearance time improved almost 10 fold making this our most metabolically stable compound. Unfortunately, human microsomal clearance was not be determined. These more positive results of the DMPK profile made the loss of potency observed against the IspD and 3D7 assays somewhat frustrating. However, the DMPK assessments gave us a new avenue to explore further optimisation of the template see **Section 2.2.6.7**.

2.2.5.5 Conclusion of D-ring series SAR

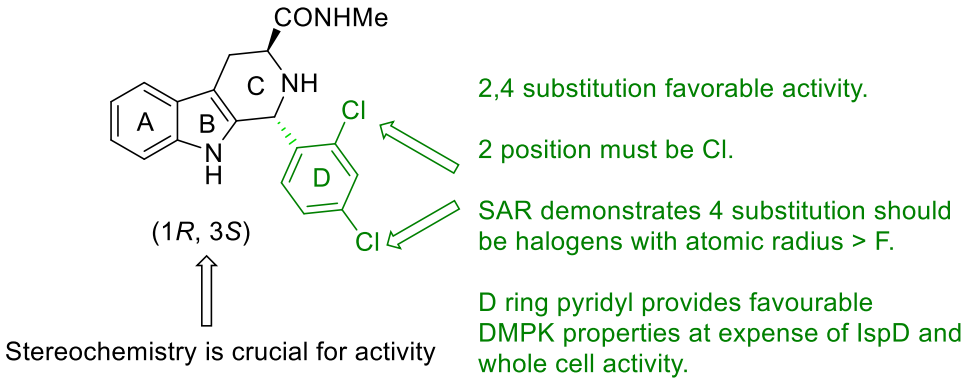

Figure 2.13. Conclusion of D-ring SAR.

Compound **6** remains optimal for activity against IspD, however, at present compound **29** with a bromine substituent at the 4-position of the D-ring is optimal for 3D7 activity. Examination of the DMPK properties of **6** and **29**, yields a similar result, **29** is more stable than **6** in human microsomes, but less stable than **6** in rat hepatocytes, however, **6** has slightly improved aqueous solubility and thus may possess a better profile. Electronics of the D-ring clearly play a significant role enzyme and cell potency. Incorporation of small atoms such as fluorine in any position exhibits a detrimental effect on potency; therefore steric demand alone cannot determine activity. Furthermore, incorporation of a pyridyl ring also leads to loss of potency. It could therefore be argued that the D-ring is bound within a lipophilic environment, where the presence of hydrogen bond donors or acceptors is disfavoured. Alternatively, there may be a requirement for an electron rich aromatic ring, instead of an electron withdrawing one. The aqueous solubility of the whole D-ring series is poor, and again this makes SAR interpretation unclear. As previously stated, aggregate formation cannot be ruled out, however, in the case of compound **31** and **35** aqueous solubility values are very low. Therefore, these compounds may precipitate during the course of the biological assay, which could explain the observed activities. The presence of halogens in the D-ring and the 5-pyridyl D-ring in some cases yielded to improved metabolic stability. Therefore, we used these results to explore SAR around the unexplored A-ring to examine if metabolic stability can be improved, without the loss of activity. Figure 2.13 summarises our findings of SAR of the D-ring.

2.2.6 A-ring modifications

The incorporation of A-ring modifications was driven by two crucial reasons. Firstly, the incorporation of halogens and heteroatoms in the D-ring in some cases had a positive impact on metabolic stability and in some cases a negative effect on metabolic stability. This could suggest that the D-ring is a site of metabolism but the data is inconsistent. Therefore, while the D-ring could be a

site of metabolism, other areas such as the A-ring could not be ruled out, especially considering that sterically the A-ring quite exposed. Secondly, examination of the development of KAE609 (**12**) (Figure 2.4) showed similar issues with metabolic stability of this template. A-ring 6-F, 7-F and 6-F, 7-Cl modifications in this case not only solved the issue of metabolism but also improved the antiparasitic potency of the molecule.[15] It was therefore our goal to examine if this success could be replicated with similar modifications to our template of interest.

Our homology modelling data (see **Section 2.3**) indicated that the *Pf*IspD binding site is small, so we initially carried out A-ring modification in a step wise manner. First we examined the effect of mono-substitutions in the 6 and 7-positions of the tetrahydro-β-carboline A-ring, before examining the effect of di-substitutions so as to not interfere with potential steric clashes too much. One major drawback of examining the A-ring substitutions was that because the starting materials became more complex, this in turn reduced commercial availability. As such some enantiopure derivatives of tryptophan were synthesised from the corresponding starting indoles. In some cases we also purposely synthesised racemic forms of A-ring final compounds, to provide standards for chiral HPLC. In total three racemic targets were synthesised and are discussed in the following sections, all three show separation on a chiral column and two of which were later resynthesised in enantiopure form. This approach gave us confidence that our asymmetric synthesis led to enantiopure final compounds. In some cases X-ray crystallography was also carried out to confirm compound stereochemistry. Similar to the D-ring substitutions we explored both F and Cl substitutions within the A-ring, and as a potential metabolite, we synthesised one hydroxylated A-ring to examine if this metabolite might still possess activity.

2.2.6.1 A-ring Modifications: Mono-substitutions at the 6, and 7-position

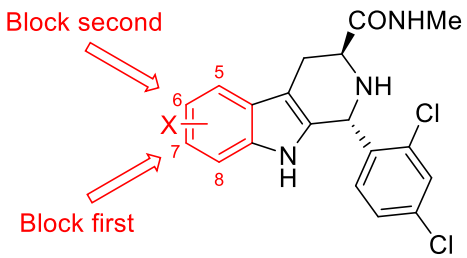

Figure 2.14. Positions of potential metabolic liability in the A-ring.

Building from the development of KAE609 (**12**) (Figure 2.4), it was apparent to us that the 7-position was the likely major position of metabolism within the MMV008138 template (Figure 2.14). During the development of **12**, mono-Cl substitution at the 7-position led to improved metabolic stability in both human and mouse hepatocytes. Mono-substitution of the 6-position also improved metabolic stability, finally, blocking 6 and 7-positions both then gave the molecule its optimal

properties.[15] Following on from this, as we did not want to cause potential unnecessary steric clashes we wanted to examine the effect of fluorine substitution at the 7-position first before moving onto chlorine. Fluorine , as in the D-ring SAR, has a major advantage here as it is small and is effective at blocking potential sites of metabolism due to the high strength of the C-F bond.[58] Therefore if activity is retained and metabolic stability is improved, we can then justify examining chlorine substitution, which also allows us to probe steric demand, and also examine the 6-position.

The 7-F substitution of the THBC A-ring was the first molecule examined and this was first synthesised in racemic form starting from 6-F DL-tryptophan (**42a**) (ideally we wanted to start from the methyl ester (**43a**), however, this was not commercially available). Synthesis of **43a** was straightforward, exposing a suspension of **42a** in methanol to thionyl chloride at 0 °C and leaving overnight at room temperature formed **43a** in good yield of 88 %. Though in this case it does not matter, this reaction proceeds without racemising the stereogenic centre, therefore it is applicable for use when converting all L-amino acids to their corresponding methyl esters.[63] The following Pictet-Spengler reaction also proceeded well, yielding 22 % racemic *trans* **44a** product and 77 % racemic *cis* **45a**, both of which were isolated and characterised by NOESY NMR. The *trans* isomer was reacted with methyl amine, which after recrystallisation gave the final product **46** in 61 % yield.

Activity of **46** was confirmed with an activity parasite EC_{50} value of 730 ± 10 nM. However, for reasons unknown, IspD values were exhibiting highly variable results after multiple assays and are not reported. Bearing in mind that this cellular activity is from a racemic molecule, it was thought that the activity would be notably improved through synthesising the enantiopure form **47**. We initially planned to generate compound **43b** using α-chymotrypsin to enantioselectively cleave **43a** to its L-amino acid, however, when attempting this reaction no reaction was observed and was not repeated.[64,65] Instead, 6-F L-tryptophan (**42b**) was purchased in order to synthesise **47**. Compounds **48 – 51** were generated analogous to Scheme 2.9 with yields for each step reported in Table 2.13 below. (Note for clarity, only chirality *en route* to enantiopure products is displayed).

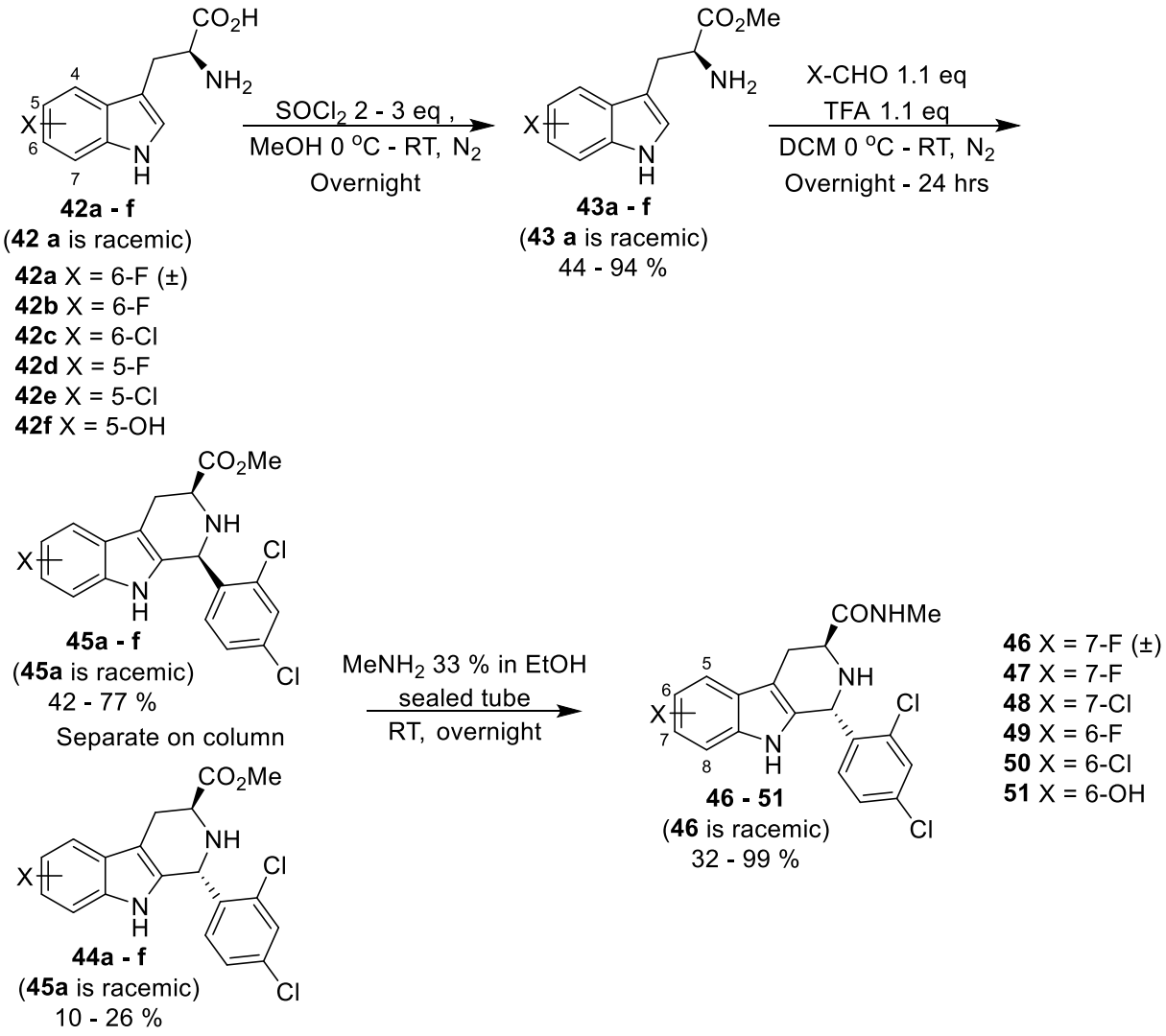

Scheme 2.9. Synthesis of compounds 46 – 51.

Table 2.13. Yields of the Pictet-Spengler reaction and final amide coupling for mono-substituted A-ring compounds.

Final Compound	X (In final compound)	% yield **43 a - f**	% yield **44 a – f** ***trans***	% yield **45 a – f** ***cis***	% yield **46 – 51**
46 (±)	7-F	88	22	77	61
47	7-F	44	25	57	98
48	7-Cl	85	21	42	32
49	6-F	94	10	42	99
50	6-Cl	87	26	59	82
51*	6-OH	70	15*	56	89*

* Contaminated with 16 % of *cis* isomer by NMR

In general yields throughout the synthetic scheme were acceptable; the only anomaly was the esterification reaction to form **43b** which was low yielding (Table 2.13). Interestingly this was repeated twice and gave the same result; it is not clear why there is such a drop of yield on switching from **43a** to **43b**. The Pictet-Spengler reactions all proceeded as previously described, yielding the *cis* isomer as

the major product in all cases with a *cis* to *trans* ratio generally between 2 : 1 and 4 : 1. All final amide couplings also proceeded well, it is of note that all reported final yields are after recrystallisation only.

In addition to previous NOESY experiments confirming *trans* products were isolated, X-ray crystallography was obtained on **47** and **48** to determine if compound chirality was correct. The crystal structures are displayed below in Figure 2.15 which confirm (1*R*, 3*S*)-configuration.

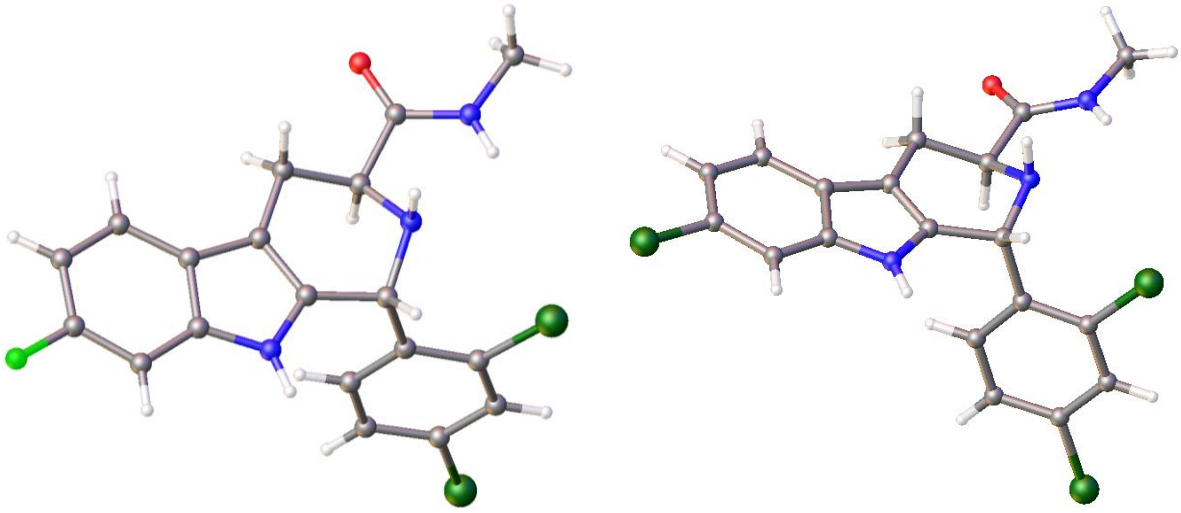

Figure 2.15. X-ray crystal structure of 47 (left), Flack parameter = 0.094 (5) and 48 (right) Flack parameter = 0.034 (7). Image is rendered as ball and stick, carbon, coloured in grey, chlorine in green, fluorine in light green, hydrogen in white, nitrgoen in blue and oxygen in red. Compound was visualised using OLEX2.[36]

2.2.6.2 Biological Activity of Mono-A-Ring Modifications against *Pf*IspD and *Pf*3D7

Similar to C and D-ring modifications most A-ring analogues of **6** were tested *in vitro* for their inhibitory activity against *Pf*IspD and *Pf*3D7 cells. Results are displayed in Table 2.14; again for comparison **1a** and **6** are also displayed.

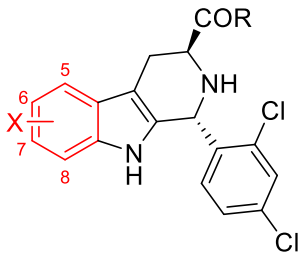

Table 2.14. Inhibitory activities of mono-substituted A-ring modifications against *Pf*IspD, and *Pf*3D7 Green = good, amber = acceptable, red = poor.

Entry	R	X	*Pf*IspD IC_{50} (nM)	*Pf*3D7 EC_{50} (nM)	$ClogD_{7.4}$	Aq. Sol. (µM)	SFI
1a	OH	H	25.3 ± 5.6 n = 3	349 ± 30 n = 6	2.9	N/A	5.9
6	NHMe	H	21.6 ± 2.7 n = 3	373 ± 86 n = 4	4.1	16	7.1
46 (±)	NHMe	7-F	Highly variable	730 ± 10 n = 4	4.3	N/A	7.3
47	NHMe	7-F	117 ± 11.2 n = 4	275 ± 10.5 n = 4	4.3	10	7.3
48	NHMe	7-Cl	1110 ± 389 n = 3	381 ± 57 n = 4	4.7	0.6	7.7
49	NHMe	6-F	Awaiting data	1038 ± 163 n = 3	4.3	36	7.3
50	NHMe	6-Cl	>5000 n =1	>10000 n = 3	4.7	0.4	7.7
51	NHMe	6-OH	148 n = 1	5450 n = 1	3.8	N/A	6.8

Compound **46** was initially synthesised to confirm if substitution on the A-ring is tolerated. Even with a racemic mixture, an EC_{50} value of 730 ± 10 nM was obtained, confirming that the A-ring could be manipulated chemically without sacrificing activity. Unfortunately, IspD activity did not give a consistent value which can be attributed to either interference of the assay by the other enantiomer, through potential aggregate formation, or potential precipitation of the compound within the assay (aqueous solubility of enantiopure version of this compound (**47**) has low aqueous solubility value of 10 µM). The enantiopure molecule **47** was subsequently synthesised and the IspD assay gave us a consistent IC_{50} value against the enzyme, with a 4 fold loss of potency compared with **6**. This loss of potency could be attributed to a lower aqueous solubility value, or suggests a minor electronic or steric requirement around the A-ring in the active site. **47** in comparison to **6**, yielded improvement of potency against growth inhibition of 3D7 cells. We then interrogated the steric demand of the 7-position by the incorporation of a chlorine atom instead of a fluorine atom. It appears that there is still a strict steric requirement around this area of the molecule as **48** demonstrates only moderate potency against the enzyme. However, compound **48** has a very poor aqueous solubility value of 0.6 µM, this compound is practically insoluble in an aqueous environment and may precipitate during the course of the biological assay. Alternatively, because in the whole cell assay compound **48** is still very good (Table 2.14), this suggests that this molecule may have another target. A similar effect was observed with compound **32** from the D-ring series, it would be interesting to know if either one of these compounds cause parasite rescue in the presence of IPP which could be carried out as future work. If they do show rescue, it could be that these compounds are able to inhibit another MEP

pathway enzyme. It is also possible that the increase in lipophilicity of these compounds could enhance apicoplast penetration.

In an analogous study, we also examined the effect of incorporating halogens at the 6-position. We are currently waiting for IspD data for compound **49**, however, it is only moderately active against 3D7 growth. Further to this, compound **50**, which contains a chlorine atom, loses potency against both the enzyme and parasite. This suggests that there is an unfavourable steric clash in the active site from substituents with a Van der Walls radius > F. For the two mono-substituted studies, aqueous solubility and activity in some cases do not correlate well, as compounds **48** and **50** share similar solubility values and the same SFI value, but **48** is active whilst **50** is inactive. Though enzyme data is missing for compound **49** a similar effect is seen between compounds **47** and **49** in the phenotypic assay. However, even though these compounds share the same SFI value, the aqueous solubility of **49** is just over 2 fold higher than **47**, but **49** only shows moderate whole cell potency. This again makes SAR interpretation unclear.

In this series, we wanted to prepare potential metabolite to see if hydroxylation is tolerated. Unfortunately 6-hydroxy-L-tryptophan is not commercially available to synthesise the corresponding 7-substituted tetrahydro-β-carboline from. Instead 5-hydroxy-L-tryptophan **42f** was purchased and from this **51** was synthesised. Interestingly this compound retains IspD activity, giving an impressive IspD activity of 148 nM especially given that it contains 16 % of the inactive *cis* isomer. Unfortunately, however, cell potency is lost, as with other compounds from all the SAR explored so far, there may be an issue with influx or penetration of certain compounds into the apicoplast. Alternatively examination of the SFI of this compounds gives a value of 6.8 which indicates that this compound too may suffer from poor solubility which may explain the unclear SAR.

2.2.6.3 Analysis of the DMPK Properties of selected mono-substituted A-Ring Compounds

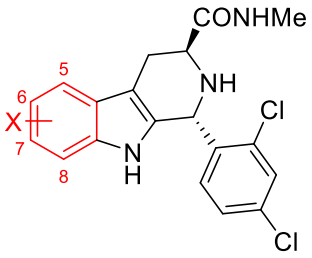

6 X = H
47 X = 7-F
48 X = 7-Cl
49 X = 6-F
50 X = 6-Cl

Table 2.15. DMPK profiles of selected mono-substituted A-ring compounds. Green = good, amber = acceptable, red = poor.

Entry	$LogD_{7.4}$	$ClogD_{7.4}$	Aq. Sol. (μM)	SFI	Human Mics CL_{int} (mL / min / mg)	Rat Heps CL_{int} (mL / min / 10^6)	Mouse Mics CL_{int} (mL / min / mg)
6	3.8	4.1	16	7.1	44.26	30.17	202.4
47	4.2	4.3	10	7.3	23.30	23.31	147.5
48	> 5.0	4.7	0.6	7.7	20.99	21.00	109.4
49	3.7	4.3	36	7.3	45.50	46.10	Not tested
50	4.4	4.7	0.4	7.7	17.60	44.80	155.4

Selected mono-substituted compounds have been screened for their DMPK profile to assess whether any of them could be taken forward to *in vivo* studies (Table 2.15). Compounds **47** and **48** were of most interest to us, as they possessed potent cell activity. Compound **51** was not tested as since it expressed a substantial loss of potency. Incorporation of 7-F in **47** and 7-Cl in **48** both increase $LogD_{7.4}$ in comparison to **6**, the compounds are in an undesirable $LogD_{7.4}$ range, and as expected aqueous solubility has been reduced when compared with **6**. However, in the case of both **47** and **48** metabolic stability in human microsomes and rat hepatocytes are both improved over **6**; in both cases these values are acceptable though still not ideal. Most importantly, the clearance in mouse microsomes has also decreased in both cases, however, the clearance rate is still higher than desired.

Examination of the 6-position with F (**49**) and Cl (**50**) yielded interesting results; the metabolism of **49** was similar to **6** in human microsomes, however, in rat hepatocytes, the rate of metabolism was observed to increase. This is curious and suggests that in both human and rat the 6-position is not a primary site of metabolism, though in the case of rat it does effect the rate of metabolism possibly indicating a switch in the route of metabolism. **50** in human microsomes showed much improved metabolic stability, however, again this is curious, if we say the 6-position is not the site of metabolism does the Cl effectively block access to the site of metabolism in human microsomes? For future work metabolite ID should be performed to examine the sites of metabolism within this series. Another interesting observation of the 6-position series was the observed values for

measured $LogD_{7.4}$ in comparison to the analogous compounds from the 7-position series. The measured $LogD_{7.4}$ of compound **49** was lower than analogous compound **47**, it is also lower than the hit compound **6**, this accounts for the improvement to aqueous solubility observed. A similar effect was seen with compounds **50** and **48** for the measured $LogD_{7.4}$ values, however, in this case aqueous solubility was not improved for **50**, it was in fact slightly worse. We next decided to see if we could maintain activity and further reduce metabolism rates by examining A-ring di-substitution.

2.2.6.4 A-ring Modifications: Di-substitutions

Based on the results from the mono-A-ring substitutions it is clear that the incorporation of halogens at the 7-position maintains potency against *Pf*3D7 parasites. When fluorine is the halogen, IspD activity is also retained. Further to this its metabolic stability is also improved over the hit molecule **6**. In slight contrast, substitution at the 6-position leads to a small loss of potency in the case of fluorine substitution, and a large loss in the case of chlorine substitution. However, metabolic stability at these positions is also improved *vs* **6**. Therefore we decided to examine A-ring di-substitution.

We examined fluorine substitution at the 6 and 7-positions together first, followed by 5 and 7 together. We also examined 6-F, 7-Cl substitution to give a molecule that looks similar to KAE609 (**12**). It may appear strange to include 6, 7-di-substitution if we say that 6 substitution leads to loss of potency. However, if only a small loss of potency is observed when combining the two substitutions together; and a large improvement of the DMPK profile is also observed, then from a hit to lead perspective, this characteristic is favourable as a compound with a poor DMPK profile is more likely to fail in the clinic.

The di-substitutions complicated the synthesis as racemic or enantiopure tryptophan derivatives were not commercially available. Therefore the each A-Ring di-substitution was synthesised from the respective indole as the starting material. Enantiopure final targets can be successfully synthesised in five steps following Scheme 2.10.

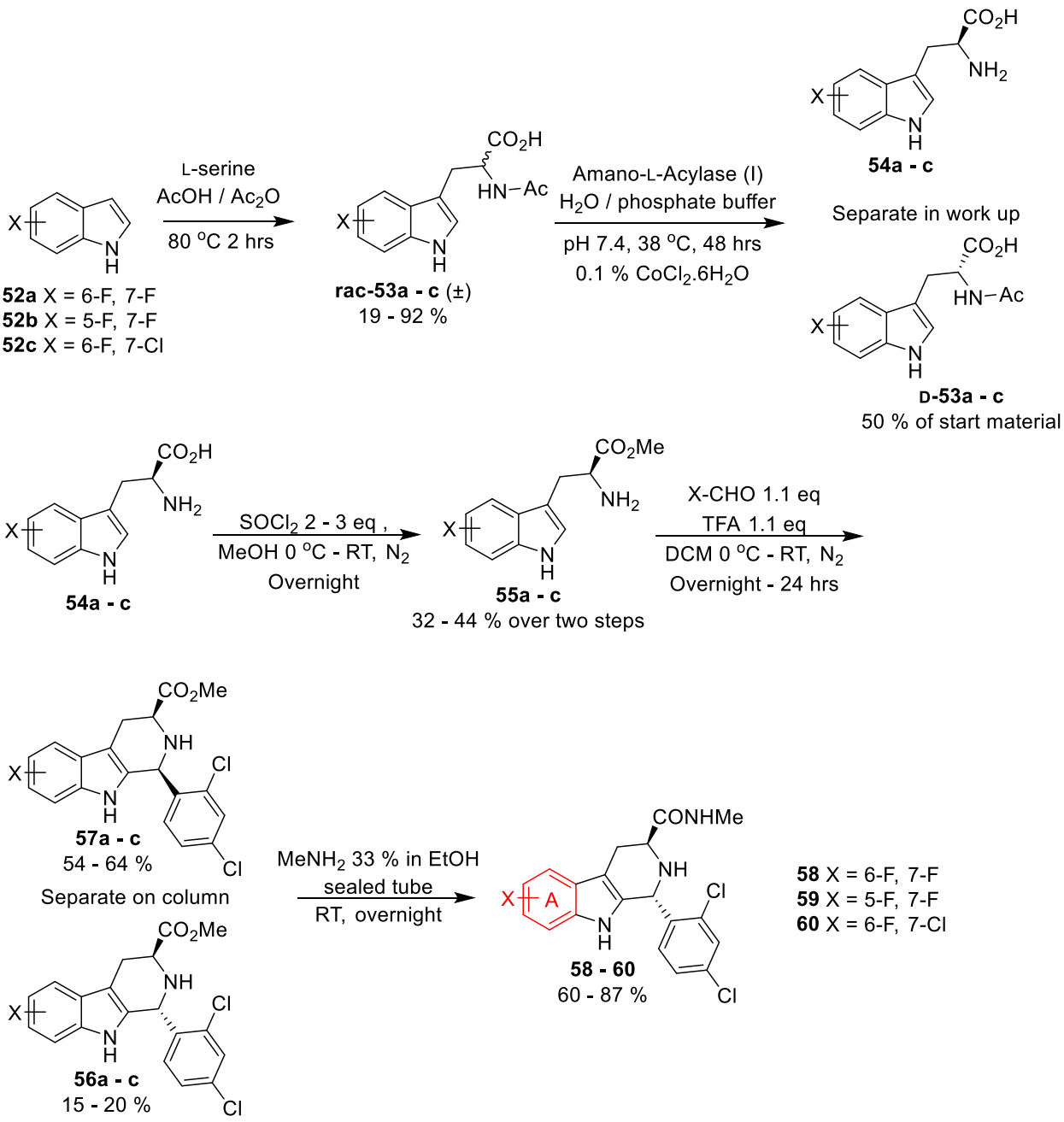

Scheme 2.10. Synthesis of 58 – 60.

Table 2.16 Yields of the reaction steps for di-substituted A-ring compounds

Final Compound	X (In final compound)	% yield **rac-53a - c**	% yield **55a – d** (2 steps)	% yield **56a – d** ***trans***	% yield **57a – d** ***cis***	% yield **58 - 61**
58	6-F, 7-F	91	33	20	54	60
59	5-F, 7-F	19	32	15	64	87
60	6-F, 7-Cl	92	44	19	61	68
61 (±)	6-F, 7-Cl	-	39	16	47	69

From substituted indoles *N*-Acetylated tryptophan derivatives (**rac-53a – c**) were successfully synthesised *via* reaction with L-serine in acetic acid and acetic anhydride. It is worth noting that L-

serine is not strictly required to be optically pure as the reaction racemises under the reaction conditions as reported by the literature.[66] Compounds **rac-53a** – **c** were then subjected to a kinetic enzymatic resolution adapted from literature procedures, allowing for the selective cleavage of the L-enantiomer acetyl group only.[66–68] This was achieved using Amano-L-acylase (I) a highly active amino acylase. This then allowed easy extraction of the D-*N*-acetyl derivatives (**D-53a** – **c)** into an organic phase in an acidic work up. However, this reaction came with its own drawbacks, the L-amino acids (**54a – c**) could not be extracted into an organic phase after work up. This meant that the water layers had to be evaporated to dryness, leaving behind undesired inorganic impurities. In order to remove as many inorganics as possible, the inorganics were crushed into a fine powder and MeOH was added and the reaction flask swirled vigorously. The MeOH was decanted off and analysed for UV activity by TLC, this process was repeated until the MeOH additions showed no UV activity by TLC, all washings possessing UV activity were combined and taken to the next step crude. Similar to the mono-substitutions, the next step was simple esterification using thionyl chloride in MeOH, forming compounds **55a - c**. Once the ester functionality was installed, the organic products could be easily extracted from residual inorganic impurities from the previous step during work up. Pictet-Spengler reactions were then carried out forming **56a – c** (*trans*) and **57a – c** (*cis*) before final amide coupling with methyl amine forming **58 – 60**.

We explored the possibility of using a D-amino acylase, however, this was not pursued for two reasons; firstly the D-amino acylase was much less active than the L-counterpart, as a result this will lead to increased reaction times. In addition the D-amino acylase was much more expensive, and the scales we would work on made this enzyme not commercially viable.[67] Secondly though the resulting L-acetylated tryptophan derivative is easily isolated, cleavage of the resulting acetyl group requires very harsh conditions, and it was not known if this would lead to racemisation or not, we deemed it was not worth it to run the risk of any potential racemisation.

In addition to the enantiopure molecules, one racemic molecule **61** was also synthesised, which was the racemate of **60**. This was synthesised for the purpose of ensuring separation on analytical chiral column was visible to determine if the amino acylase had generated enantiopure L-amino acids. HPLC traces containing only one peak for final compounds could be reasonably argued to be a pure enantiomer. The synthesis of the racemic form was almost identical to Scheme 2.10, however, instead of using L-amino acylase, **rac-53c** was deprotected in the presence of 6 M HCl for three days at 120 °C forming **54d**. **54d** was then esterified to form **55d**, which was reacted through the Pictet-Spengler coupling procedure forming **56d** (*trans*) and **57d** (*cis*), **56d** was separated and

coupled with methyl amine forming **61**. Table 2.16 displays the yields for all steps except **54a – d** which were all used as crude intermediates.

The yields of the addition of the side chain to the indole proceed well, with the exception of **53b**. For reasons unknown, the reaction yielded unidentified impurities and required column chromatography whereas the other reactions did not. It is possible that the reaction did not go to completion and the observed side products may have been intermediates. The products **55a – d** were all relatively low yielding (yields reported are over two steps), however, considering that the crude **54a – d** intermediates had inorganic impurities in them these low yields were expected. Pictet-Spengler cyclisation forming compounds **56a – d** (*trans*) and **57a – d** (*cis*) proceeded as expected generating *cis* and *trans* isomers in approximately 3 : 1 to 4 : 1 ratios. Final amide couplings to the desired targets **58 – 61** also proceeded well in good yields after recrystallisation from hot methanol.

2.2.6.5 Biological Activity of Di-A-Ring-Modifications against *Pf*IspD and *Pf*3D7

The di-substituted A-ring modifications of **6** were tested *in vitro* for their inhibitory activity against *Pf*IspD and *Pf*3D7 cells. Results are displayed in Table 2.17; again for comparison **1a** and **6** are also displayed.

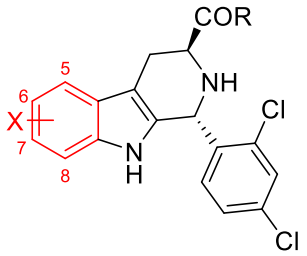

Table 2.17. Inhibitory activities of di-substituted A-ring modifications against *Pf*IspD, and *Pf*3D7 Green = good, amber = acceptable, red = poor.

Entry	R	X	*Pf*IspD IC_{50} (nM)	*Pf*3D7 EC_{50} (nM)	$ClogD_{7.4}$	Aq. Sol. (μM)	SFI
1a	OH	H	25.3 ± 5.6 n = 3	349 ± 30 n = 6	2.9	N/A	5.9
6	NHMe	H	21.6 ± 2.7 n = 3	373 ± 86 n = 4	4.1	16	7.1
58	NHMe	6-F, 7-F	1355 n = 1	3110 n = 1	4.5	4	7.5
59	NHMe	5-F, 7-F	1980 n = 1	Awaiting data	4.5	<1	7.5
60	NHMe	6-F, 7-Cl	Awaiting data	2339 ± 177 n = 3	4.9	1	7.9
61 (±)	NHMe	6-F, 7-Cl	>2000 n = 3	>10000 n = 3	4.9	<0.4	7.9

It is clear from the data that all di-substitutions lead to loss of potency in both enzyme and cell assays. Comparison of **58** to the mono-substituted compound **47** shows 10 fold loss of potency *vs* the enzyme and 11 fold loss of potency *vs* cell. When comparing **58** to mono-substituted **49** a 3 fold loss of cell potency is observed. We had hoped that **58** would have had cell potency in between **47**

and **49**, but it demonstrates reduced potency compared to either compound. A similar loss of potency against enzyme is seen with **59**, we are currently awaiting cell data for this compound, but based on observed IspD inhibitory activity, we also expect this compound to be inactive. **60** in comparison to mono-substituted compound **48** shows a 6 fold loss of cell potency, incorporation of halogens into the 6-position appears to have a substantial negative effect on potency. As expected **61** showed no inhibitory activity in comparison to **60** as it was administered in racemic form. One observation of this di-substituted series is the very poor aqueous solubility observed for all compounds. These compounds may be precipitating during the biochemical assays and this may account for the poor activities observed. Curiously, the racemic mixture compound **61** shows a lower aqueous solubility value compared with enantiopure version (**60**), these values were expected to be the same. Regardless of this, both are very insoluble in an aqueous environment.

2.2.6.6 Analysis of the DMPK Properties of selected Di-substituted A-Ring Compounds

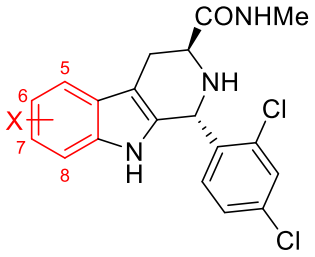

6 X = H
58 X = 6-F, 7-F
59 X = 5-F, 7-F
60 X = 6-F, 7-Cl
61 (±) X = 6-F, 7-Cl

Table 2.18. DMPK profiles of selected di-substituted A-ring compounds. Green = good, amber = acceptable, red = poor.

Entry	$LogD_{7.4}$	$ClogD_{7.4}$	Aq. Sol. (μM)	SFI	Human Mics CL_{int} (mL / min / mg)	Rat Heps CL_{int} (mL / min / 10^6)	Mouse Mics CL_{int} (mL / min / mg)
6	3.8	4.1	16	7.1	44.26	30.17	202.4
58	>4.4	4.5	4	7.5	27.90	21.50	Awaiting data
59	3.9	4.5	<1	7.5	27.60	25.60	290.4
60	>4.2	4.9	1	7.9	22.40	23.10	Not tested
61 (±)	>4.3	4.9	<0.4	7.9	18.60	17.80	9.6

Selected di-substituted compounds have been screened for their DMPK profile to assess whether there was any improvement of the DMPK profile in comparison to mono-substituted A-ring derivatives. As can be seen in Table 2.18 there is little difference in most cases between mono and di-substituted A-rings in terms of measured $logD_{7.4}$, SFI, aqueous solubility, or metabolic profile. **58** is cleared slightly faster than **47** in human microsomes but slightly slower in rat hepatocytes, we are currently awaiting data for mouse microsomes. **59** demonstrated a relatively similar profile to **58**, however, this has been tested in mouse microsomes and curiously is cleared even faster than the hit **6**. Mouse microsome readout appears to be very sensitive to this molecular template. **60** in

comparison to its mono-substituted counterpart **48** had a comparable profile and was not tested within mouse microsomes. The racemic version **61** has a profile that is very similar to **60**, however, mouse microsomal turnover was tested and appears to show a remarkable improvement in metabolic stability. It should be noted though that this is not unusual, a similar situation was observed during the development of KAE609 (**12**), were differing stereoisomers had radically different clearance times. It is likely that the other enantiomer is causing this apparent spike in stability. This of course is unfortunate, as the other enantiomer shows little activity against IspD.[15]

2.2.6.7 A-ring modifications: Incorporation of an aza A-ring

As discussed as part of the D-ring modifications we noticed that incorporation of an aza group into the D-ring led to improvement of rat hepatocyte clearance times. We decided to explore if it was possible to synthesise one or more A-ring substituents containing a nitrogen atom at any position. The rationale behind this was firstly; a reduction in $logD_{7.4}$ from this compound is likely able to increase metabolic stability; secondly the reduction of $logD_{7.4}$ should also improve aqueous solubility; thirdly the nitrogen atom should have very little impact on steric demand within the IspD active site; and fourthly the nitrogen atom has a chance to pick up a hydrogen bond in the active site increasing binding energy and thus potentially potency.

Examination of the literature showed that little research had been done to make an aza-mimic of MMV008138, aza-tetrahydro-β-carbolines possessing (1*R*, 3*S*)-substituents were also scarce. To further complicate matters no aza-tryptophan derivative could be purchased enantiopure, and only 7-aza tryptophan was available as a hydrate with water content not reported. Despite this there is evidence of the synthesis of enantiopure aza-tryptophan derivatives in the literature.[69,70]

The route we chose to follow (Scheme 2.11) was similar to what was reported in the literature by Talukder *et al*.[70] We purchased the Schölkopf chiral auxillary in methyl ether form (**66**) due to its higher purity. 7-azaindole-3-carboxyladehye (**62**) was allowed to react with TsCl in the presence of DMAP and NEt_3 to yield **63** in 99 % yield. The aldehyde was successfully reduced in the presence of sodium borohydride to **64** in 94 % yield.[70] Compound **64** was converted to the bromide **65** in the presence of PBr_3, **65** was dried immediately after TLC confirmed its formation was complete. During the time that **65** was drying, the auxillary (**66**) deprotonation was set up side by side; **65** could then be added by cannula immediately to the deprotonated auxiliary **67** once it was dry from work up solvents.[70,71] Following this protocol, **68** was formed in 52 % yield over two steps after recrystallisation from 20 % DCM in hexane. Within the literature this compound is reported as a yellow oil, however, in our case all attempts to synthesis this molecule resulted in the formation of a solid.[70] To confirm

compound structure, the X-ray crystal structure of **68** was solved by Dr Craig Robertson and confirms the correct diastereoisomer was synthesised (Figure 2.16).

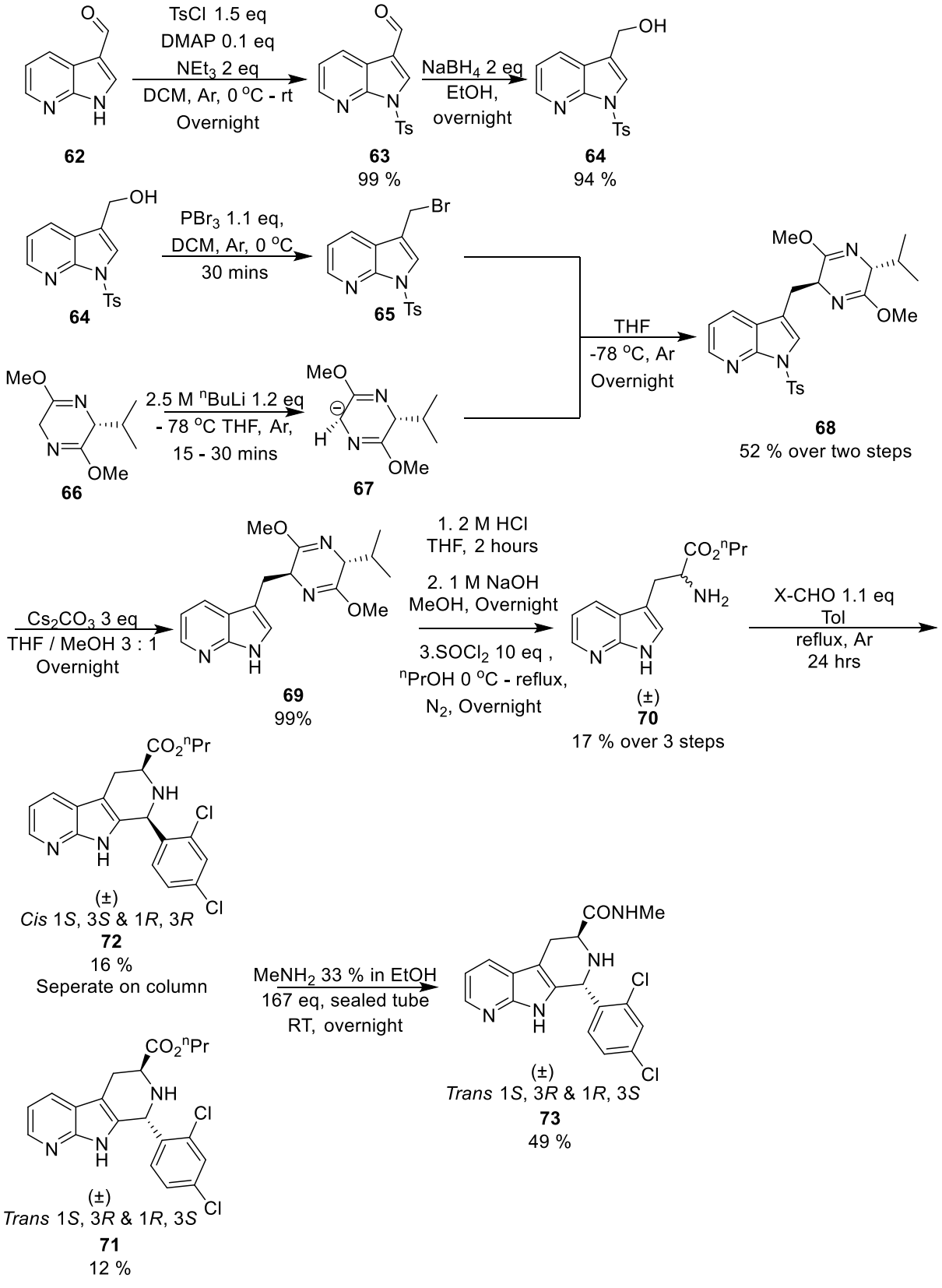

Scheme 2.11. Synthesis of aza-A-ring derivative (73).

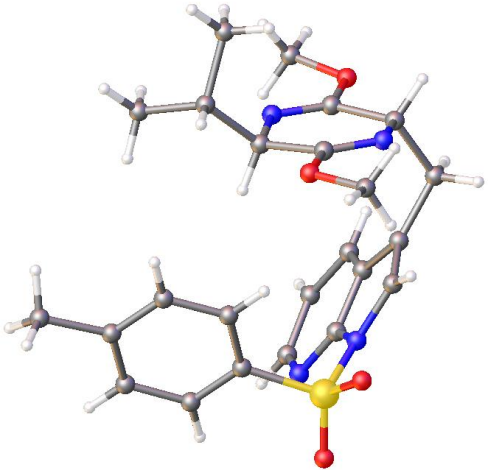

Figure 2.16. Crystal structure of 68 Flack parameter = 0.01 (2). Image is rendered as ball and stick, carbon, coloured in grey, hydrogen in white, nitrogen in blue, oxygen in red and sulfur in yellow. Compound was visualised using OLEX2.[36]

68 was deprotected to **69** using a mixture of Cs_2CO_3 MeOH and THF in 99 % yield.[70,72] To **69** was added 2 M HCl in MeOH to form the methyl ester of 7-aza-L-tryptophan. Attempts to extract this compound again into an organic phase failed, however, the work up procedure did appear to remove the valine methyl ester side product. In order to overcome the issue of extracting the methyl ester into the organic phase we instead cleaved the ester to the carboxylic acid before esterifying again with a more lipophilic ester. To increase the lipophilicity of the intermediate in order to aid extraction an ^{n}Pr ester was chosen first. The methyl ester was hydrolysed to 7-aza-L-tryptophan by stirring in 1 M sodium hydroxide and MeOH overnight. After neutralisation, the crude product (including inorganics) were evaporated to dryness. The crude was suspended in ^{n}PrOH and 10 eq $SOCl_2$ were added dropwise at 0 °C before refluxing overnight. This successfully formed **70** in 17 % yield over three steps, however, chiral HPLC had determined that the molecule racemised under these conditions. The molecule was subjected to a modified Pictet-Spengler procedure; a review of the literature suggests that in the presence of acid, particularly TsOH the molecule will fully aromatise once the Pictet-Spengler reaction completes which was undesired.[73] The reaction instead needed to be carried out in refluxing benzene with no acid (due to the concerns of the health hazard of benzene we instead carried out the reaction in toluene under reflux in an Ar atmosphere for 24 hours). This formed **71** as the *trans* isomer in 16 % yield and **72** as the *cis* isomer in 12 % yield, however, the reaction still appeared to form more products than expected, these were more non polar on TLC and likely belong to oxidised or fully aromatised compounds. After separation **71** was coupled with methyl amine to yield **73** as a racemic molecule in 49 % yield after recrystallisation from MeOH.

Along with chiral HPLC, the X-ray crystal structure of **73** was solved by Dr Craig Robertson. The molecule crystallises in the Pbca space group, which has a centre of inversion. By the virtue of this space group, we can say the compound exists as a racemic mixture of the (1*R*, 3*S*) / (1*S*, 3*R*)-

enantiomers (*trans*). Depicted below is the X-ray image of both enantiomers, forming a hydrogen bond donor / acceptor pair from the A-ring nitrogen atom to the corresponding B-ring indole NH.

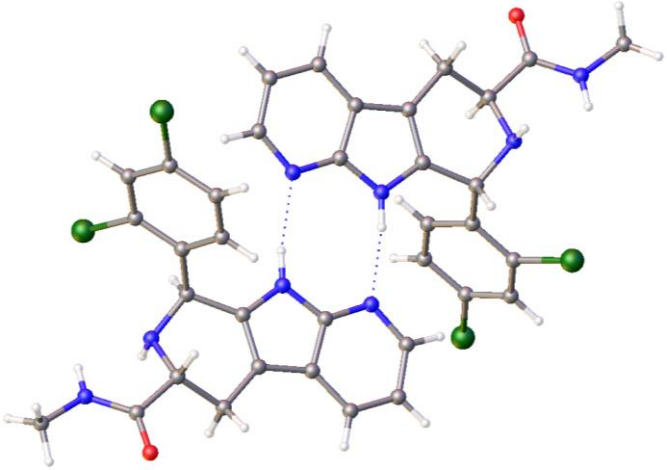

Figure 2.17. Crystal structure of 73. Image is rendered as ball and stick, carbon, coloured in grey, chlorine in green, hydrogen in white, nitrogen in blue and oxygen in red. Compound was visualised using OLEX2.[36]

Once we elucidated that **73** was racemic, and successfully identified the point of racemisation, we decided to see if this could be circumvented. We repeated the synthesis again, but instead of using a propyl ester, we checked to see if an ethyl ester could also be extracted into an organic phase. The ethyl ester is beneficial as the esterification step does not require reflux. The same reaction was carried out and the ethyl ester was isolated and did not racemise (see **Appendix 2** for HPLC trace). However, when we subjected this to the exact same Pictet-Spengler reaction conditions, the reaction was not progressing past the imine after 24 hours. In fact the cyclisation was still not complete after 5-days. The *trans* isomer was isolated anyway in very low yield of 7 %, however, HPLC of this showed that the reaction also racemises at the Pictet-Spengler stage and the synthesis was stopped here (see **Appendix 2**). We tried the reaction again using the methyl amide of aza-tryptophan in place of the ester in case this could overcome the issue of racemisation, however, no reaction past the imine was observed after 5 days and upon leaving the reaction even longer the imine appears to decompose by TLC.

We tested **73** against *Pf*3D7 parasites to see if it demonstrated any potency before deciding whether or not we should send this for DMPK analysis. Upon examination of its *Pf*3D7 growth inhibitory activity, compound **73** gave an EC_{50} value of 6640 ± 903 nM (n = 3). This is unfortunately much less potent than the hit molecule in cell and thus was not sent for DMPK profiling. At present we are awaiting IspD activity values, it may still be that this compound effectively targets IspD, but like many of the other compounds tested for whatever reason it cannot access the apicoplast effectively.

2.2.6.8 Conclusion of A-ring series SAR

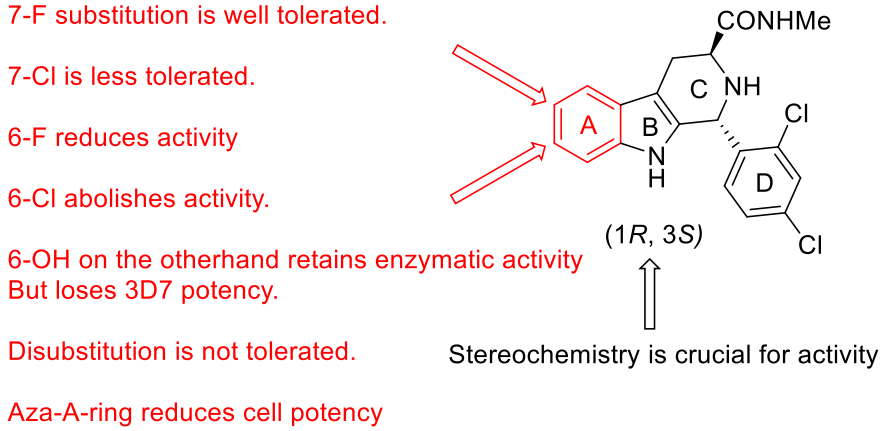

Figure 2.18. Conclusion of A-ring SAR.

It was our aim to design a molecule as part of the A-ring SAR that had improved DMPK properties without the expense of potency in comparison to the hit molecule **6**, which demonstrates rapid metabolic clearance. During A-ring SAR, two compounds were developed that show comparable potency to **6**, **47** and **48**, possessing a 7-F and 7-Cl substitution patterns, respectively. **47** demonstrates a small loss of activity against the IspD enzyme, however, its cell potency and DMPK properties are improved over **6**, therefore this molecule is our current lead compound. **48** on the other hand is only moderately active against the IspD enzyme, but has similar cell potency to **6** and **47**, this compound could be demonstrating off target effects. In terms of clearance rates **48** possesses a similar profile to **47** in human microsomes, and rat hepatocytes, however, it does demonstrate a reduced clearance in mouse microsomes compared to **47** thus this compound could be considered a second lead, even if the primary target is not IspD. It should be noted that **48** possess very poor aqueous solubility and the results of the IspD assay may arise because of this. The 6-position of the THBC A-ring does not appear to tolerate halogen substitution, when a chlorine atom is at this position there is no activity observed. Similarly with a fluorine atom at the 6-position cellular activity is dropped substantially. A hydroxyl group here maintains good IspD activity but unfortunately is poorly potent when it comes to the whole cell assay. Substitution of the A-ring with 2 halogens at all positions explored led only to loss of both enzyme and cell activities with little to no improvement of the DMPK profile. Though only one aza A-ring THBC derivative of the hit was synthesised, and even then only in racemic form, the cell activity is also substantially reduced. Ideally from a drug development perspective for the remainder of this series of compounds to be synthesised effectively, a new method for the synthesis should be uncovered, due to the high cost of some start materials, number of steps involved *en route* to the targets, and the risk of racemisation at the Pictet-Spengler stage. Most compounds of the A-ring series

showed very poor aqueous solubility which could explain the unclear SAR observed, as was similar to the previous two series form the C and D-rings. SAR is summarised is Figure 2.18.

2.3 Molecular Modelling

In order to gain an insight into how the tetrahydro-β-carboline scaffolds bind within the IspD enzyme, and to try to rationalise observed SAR, molecular modelling studies were carried out on our most interesting compounds. To date, no X-ray crystal structure has been elucidated for the *Pf*IspD enzyme, and thus there is no known drug binding pose in the enzyme active site. Therefore work was undertaken by our group to generate a homology model from which molecules could be assessed for the docking pose and potential ligand-enzyme interactions.[74]

Computational docking is used primarily to predict how a drug may bind within a specific protein or receptor and scores how well the molecule fits into a binding site, *i.e.* it assesses the complementary fit of the binding pose to the protein. Predictions of whether a molecule could show activity or not can be made based on the scoring function, as it can be reasoned that molecules with good scores and good complementary binding are more likely to experimentally also show good activity. Using this rationale, virtual screening can be carried out to assess unknown inhibitors of a particular enzyme for their binding affinity, if the complementary fit and scores are good the compounds can be examined experimentally for activity.[75]

Molecular docking involves the exploration of available space within a given bind site, ligands are docked in numerous orientations an conformations and are scored using scoring functions according to the most favourable pose.[75] Docking algorithms are used to generate the poses of the ligand into the active site. They search for the available virtual chemical space to determine if the ligand will fit into the given binding pocket.[75] Here we used a genetic algorithm to explore the docking pose space, exploring the many degrees of freedom of the ligand, and how each ligand conformation may complementarily fit into the active site. Very briefly scoring functions are used to rank different poses based on the number of interactions the ligand has in a particular pose.[75] The scoring function used as part of this research is known as GOLDscore, which is a force-field based function that uses molecular mechanics to quantify the sum of two energies, the receptor-ligand interaction energy and internal energy, this type of scoring considers just one protein conformation in order to simplify scoring by removing the internal protein energy, the programme used for this research was GOLD.[76,77]

2.3.1 Docking Protocol

As the crystal structure of *Pf*IspD was unavailable, a suitable surrogate had to be chosen to identify a docking protocol. This was already undertaken by PhD student Dr Kathryn Price. It was identified that *Ec*IspD shared the most sequence similarity at the active site to the known sequence of *Pf*IspD and thus *Ec*IspD was chosen to be the surrogate protein. A crystal structure with bound CDPME exists for *Ec*IspD, and a protocol was identified that reproduced the crystallographic bind pose of CDPME in the active site. The protocol identified is described in Table 2.19 below.

Table 2.19. Protocol for docking.

Mg^{2+}	Mg^{2+} present, no coordination geometry specified
Protonation	Hydrogens added
Waters	Water molecule HOH1091 extracted, all other waters deleted, water was set as toggle, spin
Ligands	CDPME extracted
Binding site	Defined as 6 Å of the CDPME ligand
Number of GA Runs	10, 50, 100, 500
Scoring Function	GOLDscore

With the protocol in hand it was transferred to the homology model built by our group. In order to undertake docking all compounds were first built in chemdraw and transferred to Spartan, compounds were then energy minimised, Spartan was used to compute local energy minimum geometry using molecular mechanics with the MMFF94 forcefield.[78,79] All images were generated in PyMol.[80]

2.3.2 Modelling of MMV008138 Derived Compounds

The first molecule that we were interested in examining was the hit itself **1a**, shown below in Figure 2.19 firstly with the full *Pf*IspD protein rendered as cartoon, and the binding site surface shown as mesh highlighted in red, images shown display docking both with and without Mg^{2+}, and secondly a zoomed in image of the binding site with binding interactions shown also images both with and without Mg^{2+} are displayed. The previously described docking protocol was run for this compound, however, only one run was carried out using 10 GA runs, curiously all observed poses demonstrated similar scores averaging at 51.0 with a standard deviation (SD) of 1.7, however, many of these poses were in vastly differing orientations, which may suggest the potential for multiple binding modes. One pose in particular with a score of 50.6, caught our attention and is displayed below (Figure 2.19).

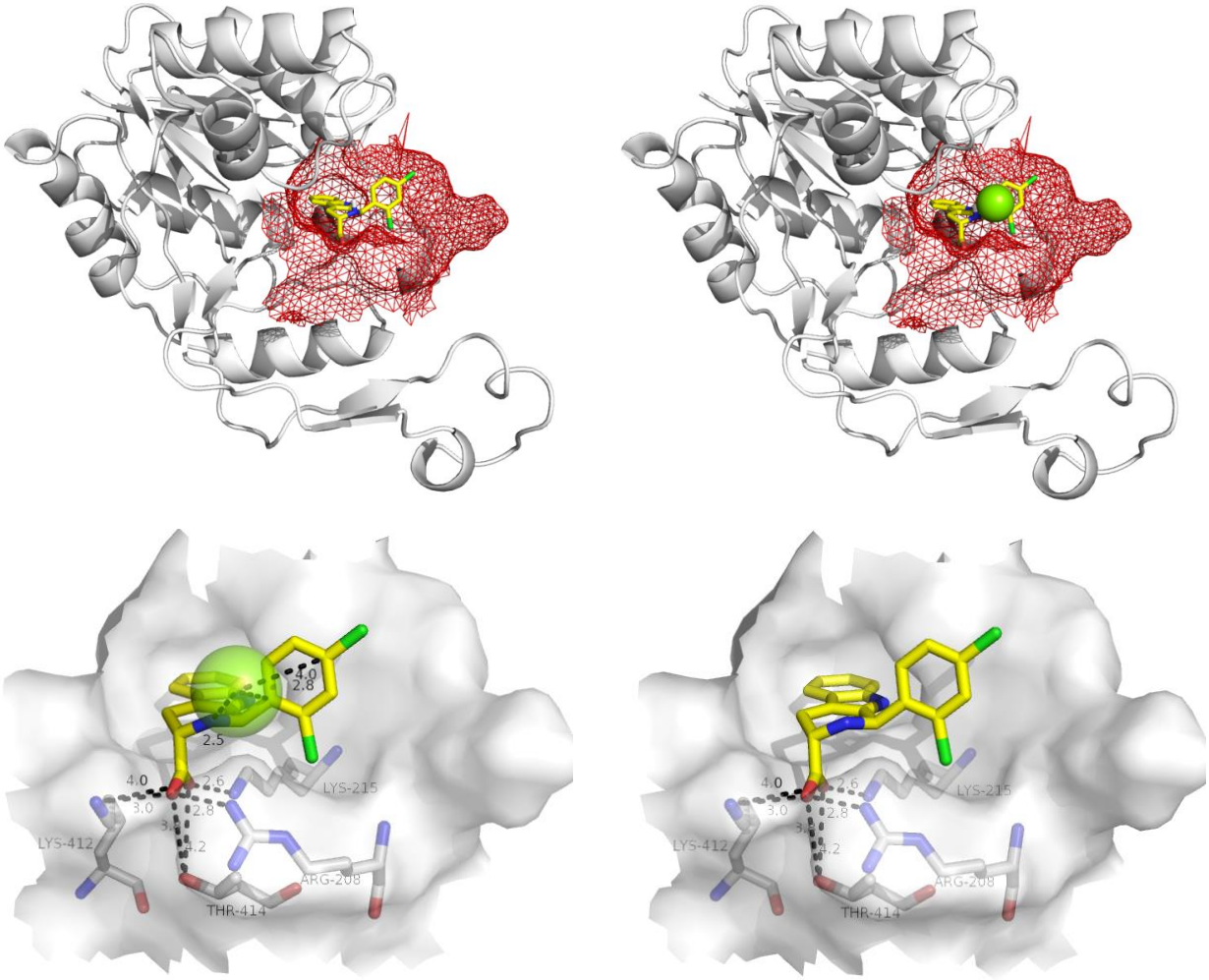

Figure 2.19. Binding pose of 1a. Top diagrams show protein in full view as white cartoon, bind site is highlighted in red depicted as mesh, images are rendered without and with Mg^{2+} for clarity. Bottom two diagrams display the binding site only, rendered as a white surface, Mg^{2+} is depicted and omitted for clarity. Mg^{2+} is rendered as a transparent green sphere, 1a is rendered as sticks, carbon coloured yellow, nitrogen coloured blue, oxygen coloured red, chlorine coloured green. Crucial amino acids are rendered as sticks carbon coloured grey, nitrogen coloured blue, oxygen coloured red.

This pose of **1a** caught our attention for numerous reasons. Firstly as can be seen in the lower images of Figure 2.19, the carboxylic acid moiety of **1a** has the potential to form at least 4 strong hydrogen bonds between Arg-208, Lys-215, Lys-412 and Thr-414 showing interatomic distances of < 3.3 Å (heavy atom to heavy atom). In addition the same moiety has the potential to gain further electrostatic interactions with all but Lys-215, this moiety sits within a tight pocket which could rationalise why any large functionalisation here leads to a loss of potency. Furthermore, the C-ring nitrogen atom appears to be within distance of the Mg^{2+} ion to coordinate with it (2.5 Å) which may aid in the positioning of the inhibitor within the active site, and this could rationalise why simple substitution of this NH to NMe also leads to the loss of potency that is observed. Another interesting interaction is the potential for π-cation interactions from the aromatic D-ring, which sits almost directly behind the Mg^{2+} ion at a distance of approximately 3.4 Å. Disruption of this π-cation interaction could cause loss of potency. It is also interesting to note that the *para*-chlorine atom of

the D-ring is pointing out into solvent exposed space, and that the *ortho*-Chlorine atom is proximal to a small cleft which could explain why the substitution of the 4-position appears to be tolerated by the enzyme. Finally, it is clear that the indole A-ring portion of the molecule sits inside a tight binding pocket within the enzyme, though no crucial interactions were observed with neighbouring amino acid residues here, the shape of the molecule does appear to possess a good complementary fit.

We then wanted to interrogate the next most promising hit **6** for its binding poses. Again the same docking protocol was carried out, however, no pose matched that of **1a**. Most of the poses were in a similar orientation and displayed a low SD of the predicted binding strength, therefore the pose displayed in Figure 2.20 was the pose with the highest GOLDscore of 54.9 (mean and SD of 54.2 and 0.5, respectively). With regards to the orientation *vs* **1a**, **6** is rotated approximately 90 ° clockwise (as displayed), this forces the NHMe moiety to point into the back of the enzyme active site were the A-ring of the indole lies, in this pocket the NHMe group can pick up potentially two strong and one weak hydrogen bonds with neighbouring Leu-201, Gly-295, and Ala-296 residues showing interatomic distances of 2.8, 3.3 and 3.7 Å, respectively. This rotation also forces the D-ring into the small cleft were the carboxylic acid moiety of **1a** was situated, here there is a potential for the *ortho*-chlorine atom of the ring to pick up 3 electrostatic interactions with Arg-208, Lys-215, Lys-412 residues, with interatomic distances of 4.0, 3.6, and 3.0 Å, respectively. The C-ring nitrogen atom no longer points at the Mg^{2+} ion but instead has the potential to possess a hydrogen bond and an electrostatic interaction with the carboxylate of Asp-294 with interatomic distances of 3.5 and 4.1 Å. Finally though in a different orientation there appears to be a common π-cation interaction of the D-ring with the Mg^{2+} ion with a interatomic distance of 3.3 Å and instead of the C-ring nitrogen atom interacting with the Mg^{2+} ion, the indole nitrogen can now interact with it at an interatomic distance of 3.4 Å.

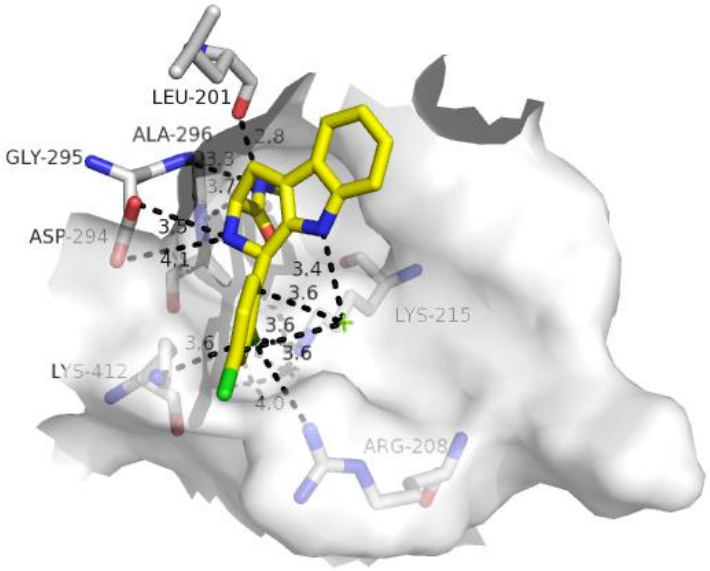

Figure 2.20. Binding pose of 6. Binding site is rendered as a white surface, Mg^{2+} is depicted as a green cross, 6 is rendered as sticks, carbon coloured yellow, nitrogen coloured blue, oxygen coloured red, chlorine coloured green. Crucial amino acids are rendered as sticks carbon coloured grey, nitrogen coloured blue, oxygen coloured red.

In terms of the SAR discussed this pose also justifies some of the results obtained. Substitution of the C-ring nitrogen not only has the potential to cause a steric clash with the surface of the enzyme, but if the C-ring NH is activing as a hydrogen bond donor, then there is a clear disadvantage of the molecule to be substituted as this interaction will be lost. Replacement of the *ortho*-chlorine atom my also disrupt crucial electrostatic interactions, in addition to this, the cleft where the chlorine atom lies is small which may also rationalise some of the SAR observed by Yao *et al.* when substituting this position. Once again it should be noted that the *para*-chlorine atom is also pointing into solvent exposed space which again could indicate why there appears to be some scope for a degree of manipulation here. What is interesting is the indole portion of the ring is also pointing into solvent exposed space, therefore if this is the binding pose it is curious why there is a loss of potency observed in general when substituting the A-ring.

Next we wanted to examine our next most promising lead compound from the A-ring series compound **47**. In order to expand the number of poses available we altered the number of GA runs to 20 to examine if a pose mirroring **1a** could be identified. However, examination of the poses showed that they were all in a similar orientation and the apparent spread of the scores was low, thus the pose displayed below is one with the highest affinity score of 56.3 (mean and SD of 55.0 and 0.7, respectively) (Figure 2.21).

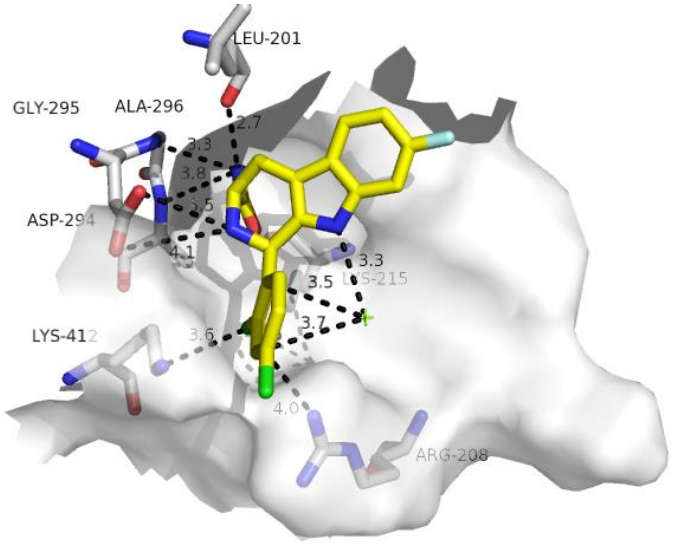

Figure 2.21. Binding pose of 47. Binding site is rendered as a white surface, Mg^{2+} is depicted as a green cross, 47 is rendered as sticks, carbon coloured yellow, nitrogen coloured blue, O coloured red, chlorine coloured green, fluorine coloured sky blue. Crucial amino acids are rendered as sticks carbon coloured grey, nitrogen coloured blue, oxygen coloured red.

In a similar manner to **6**, compound **47** showed no bind pose that matched that of **1a**. Indeed the poses identified by **47** almost perfectly mirror that of **6**. Thus the interactions are summarised in Table 2.20 below.

Table 2.20. Main ligand – protein interactions of 47.

Residue(s)	Moiety	Interaction	Distance Å
Leu-201, Gly-295	NHMe	H-bond	2.7, 3.3
Lys-215, Lys-412	*Ortho*-Cl	Electrostatic	3.6, 3.6
Asp-294	C-ring-NH	Electrostatic	3.5
Mg^{2+}	D-ring	π-cation	~3.3
Mg^{2+}	B-ring-NH	electrostatic	3.3

In terms of the SAR this molecule does not reveal any more potential interactions that have been blocked or gained, however, the pose of **6** and **47** along with the potency of both **6** and **47** appears to back up the bind pose observed.

As we knew that compound **48** though demonstrating cell potency, was only moderately active within the IspD assay, we wanted to use docking studies to explore the possibility of a different binding pose for this compound within the active site. Again the standard docking protocol was ran using only 10 GA runs. Again in general most poses were of similar orientation and the pose with the highest score of 57.6 was chosen to be imaged (mean and SD of 55.8 and 1.3, respectively (Figure 2.22).

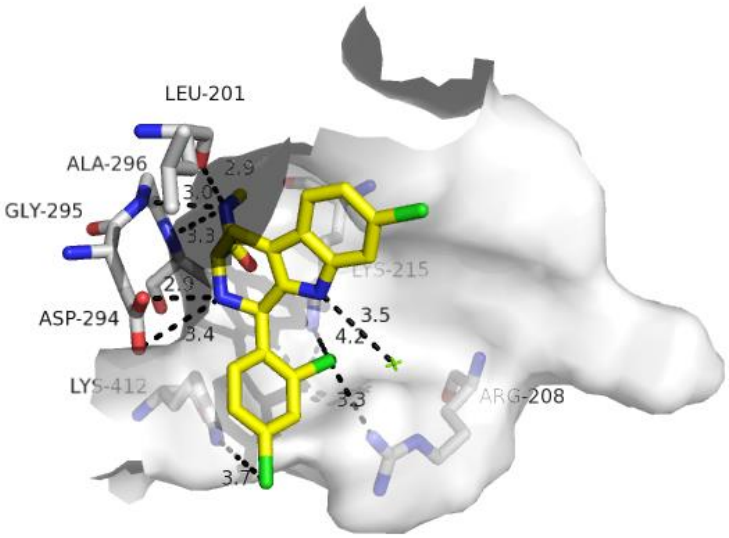

Figure 2.22. Binding pose of 48. Binding site is rendered as a white surface, Mg^{2+} is depicted as a green cross, 48 is rendered as sticks, carbon coloured yellow, nitrogen coloured blue, oxygen coloured red, chlorine coloured green. Crucial amino acids are rendered as sticks carbon coloured grey, nitrogen coloured blue, oxygen coloured red.

At first glance it does appear as though **48** also adopts the same binding pose as **6** and **47**, indeed this was somewhat surprising considering the differing enzyme activities the compounds possess, however, there are some subtle differences in interactions as summarised in Table 2.21 below.

Table 2.21. Main ligand – protein interactions of 48.

Residue(s)	Moiety	Interaction	Distance Å
Leu-201, Gly-295, Ala 296	NHMe	H-bond	2.9, 3.0, 3.3
Arg-208	*Ortho*-Cl	Electrostatic	3.3
Lys-412	*Para*-Cl	Weak electrostatic	3.7
Asp-294	C-ring-NH	H-bond	2.9, 3.4
Mg^{2+}	B-ring-NH	electrostatic	3.5

Both the position and the hydrogen bonding interaction of the NHME moiety of **48** are still in place, however, the D-ring has clearly twisted in comparison to **47**, this twisting motion has resulted in the loss of one potential electrostatic interaction between Lys-412 for the *ortho*-chlorine atom. In doing so, the *ortho*-chlorine atom is in closer proximity to Arg-208. In addition to the loss of the electrostatic interactions, the D-ring is now out of range to efficiently coordinate the Mg^{2+} ion, perhaps to compensate for this, the *para*-chlorine atom is now in proximity to gain an electrostatic interaction from the nearby Lys-412 residue. Another subtle difference is that the C-ring NH is closer to Asp-294 allowed for potential hydrogen bonding to one or both of the carboxylate oxygen atoms. Indeed the loss of activity based on this pose is not expected; therefore we decided to examine the predicted pose of compound **50**, a compound that showed poor activity against the enzyme. The predicted pose

of **50** is displayed below (Figure 2.23), the pose displayed is the best score of 59.0 (mean and SD of 56.7 and 1.0, respectively).

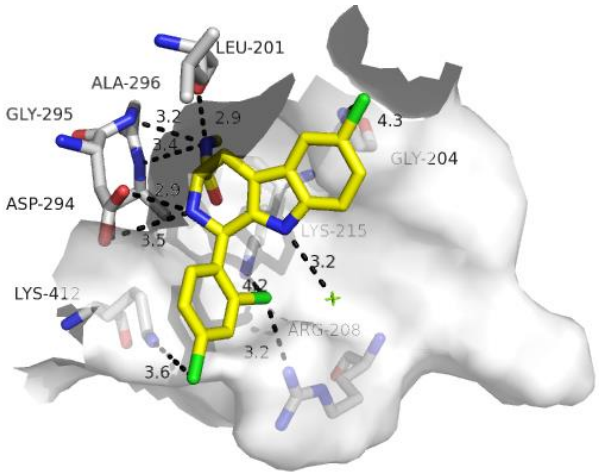

Figure 2.23. Binding pose of 50. Binding site is rendered as a white surface, Mg^{2+} is depicted as a green cross, 50 is rendered as sticks, carbon coloured yellow, nitrogen coloured blue, oxygen coloured red, chlorine coloured green. Crucial amino acids are rendered as sticks carbon coloured grey, nitrogen coloured blue, oxygen coloured red.

Again the predicted pose for this compound mirrors that for all previously described NHMe derivatives of **1a**. The bind pose in this case is almost identical to that of **48**, in fact this compound shows an extra potential electrostatic interaction from the A-ring chlorine atom to the neighbouring Gly-204 residue. All interactions are displayed in Table 2.22.

Table 2.22. Main ligand – protein interactions of 50.

Residue(s)	Moiety	Interaction	Distance Å
Leu-201, Gly-295, Ala-296	NHMe	H-bond	2.9, 3.2, 3.4
Arg-208	*Ortho*-Cl	Electrostatic	3.2
Lys-412	*Para*-Cl	Electrostatic	3.6
Asp-294	C-ring-NH	H-bond	2.9, 3.5
Mg^{2+}	B-ring-NH	electrostatic	3.2

It became apparent at this point that we could not rationalise the loss of enzymatic potency observed with A-ring substituted derivatives of **6**, as it was observed that all A-ring substitutions point out into solvent exposed space, therefore steric effects should not play a role for the inhibition of the enzyme based on the docking poses. We believe therefore that the poses here may not be accurate, this is based on two reasons; firstly, we are using a homology model of *Pf*IspD, we are therefore modelling a model which could lead to the discrepancies we observe, as the actual structure of *Pf*IspD may differ ever so slightly and thus in reality could give a different binding pose. Secondly, the docking procedure used does not allow for protein flexibility, this means that any major steric clash with not be added as a pose as it will give poor docking scores. It is clear that in **1a** there is a very tight pocket for the carboxylic acid moiety to lie in, it may be that the substitution to NHMe amide causes a major

clash in the docking run, therefore in the real situation it is more likely that the enzyme could slightly compensate this extra steric demand as the enzyme will be flexible. We hereby postulate then that the docking poses in reality are more likely to mirror that of **1a**. The location were the A-ring is bound in **1a** is very small, it is unlikely that this pocket could hold a group as large as chlorine and thus we predict that is why we see loss of activity for some A-ring substitutions. For completeness we also docked compounds **29**, **36a**, **51**, and **73** all displayed below sequentially, in all cases the best scores were chosen to image (Figures 2.24 – 2.27 and Tables 2.23 – 2.26).

29 Docking score = 56.0, mean = 54.8, SD = 0.7

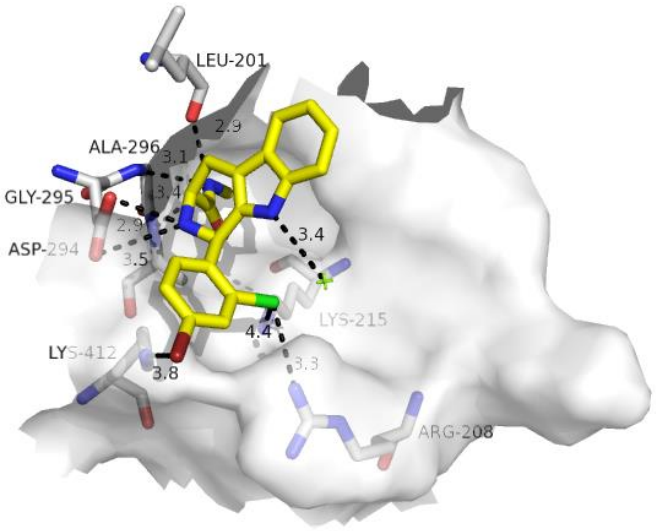

Figure 2.24. Binding pose of 29. Binding site is rendered as a white surface, Mg^{2+} is depicted as a green cross, 29 is rendered as sticks, carbon coloured yellow, nitrogen coloured blue, oxygen coloured red, chlorine coloured green, bromine coloured in dark red. Crucial amino acids are rendered as sticks carbon coloured grey, nitrogen coloured blue, oxygen coloured red.

Table 2.23. Main ligand – protein interactions of 29.

Residue(s)	Moiety	Interaction	Distance Å
Leu-201, Gly-295, Ala-296	NHMe	H-bond	2.9, 3.1, 3.4
Arg-208	*Ortho*-Cl	Electrostatic	3.3
Lys-412	*Para*-Br	Weak electrostatic	3.8
Asp-294	C-ring-NH	H-bond	2.9, 3.5
Mg^{2+}	B-ring-NH	electrostatic	3.4

36a Docking score = 55.78, mean = 54.40, SD = 0.91

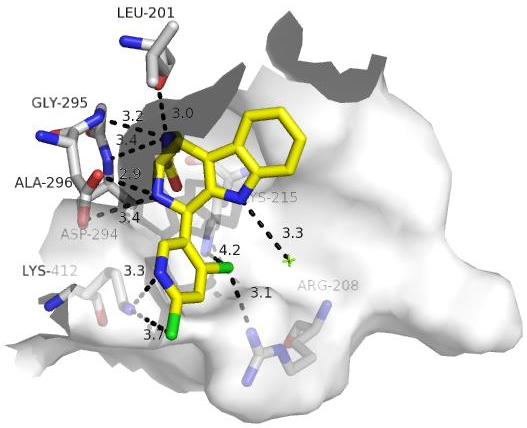

Figure 2.25. Binding pose of 36a. Binding site is rendered as a white surface, Mg^{2+} is depicted as a green cross, 36a is rendered as sticks, carbon coloured yellow, nitrogen coloured blue, oxygen coloured red, chlorine coloured green. Crucial amino acids are rendered as sticks carbon coloured grey, nitrogen coloured blue, oxygen coloured red.

Table 2.24. Main ligand – protein interactions of 36a.

Residue(s)	Moiety	Interaction	Distance Å
Leu-201, Gly-295, Ala-296	NHMe	H-bond	3.0, 3.2. 3.4
Arg-208	*Ortho*-Cl	Electrostatic	3.1
Lys-412	*Para*-Cl	Weak Electrostatic	3.7
Lys-412	D-ring N	H-bond	3.3
Asp-294	C-ring-NH	H-bond	2.9, 3.4
Mg^{2+}	B-ring-NH	electrostatic	3.3

51 Docking score = 58.4, mean = 57.2, SD = 1.0

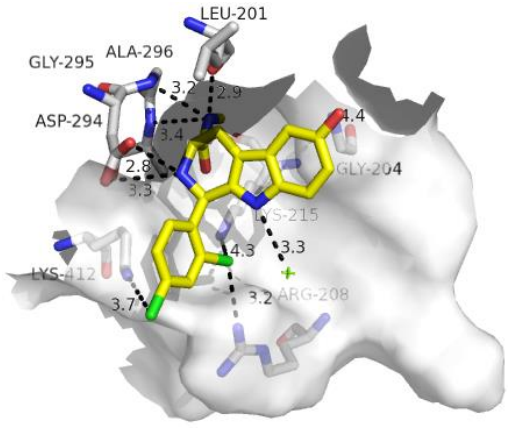

Figure 2.26. Binding pose of 51. Binding site is rendered as a white surface, Mg^{2+} is depicted as a green cross, 51 is rendered as sticks carbon coloured yellow, nitrogen coloured blue, oxygen coloured red, chlorine coloured green, oxygen coloured red. Crucial amino acids are rendered as sticks carbon coloured grey, nitrogen coloured blue, oxygen coloured red.

Table 2.25. Main ligand – protein interactions of 51.

Residue(s)	Moiety	Interaction	Distance Å
Leu-201, Gly-295, Ala-296	NHMe	H-bond	2.9, 3.2. 3.4
Arg-208	*Ortho*-Cl	Electrostatic	3.2
Lys-412	*Para*-Cl	Electrostatic	3.7
Asp-294	C-ring-NH	H-bond	2.8, 3.3
Mg^{2+}	B-ring-NH	electrostatic	3.3

73 Docking score = 56.2, mean = 53.5, SD = 1.1

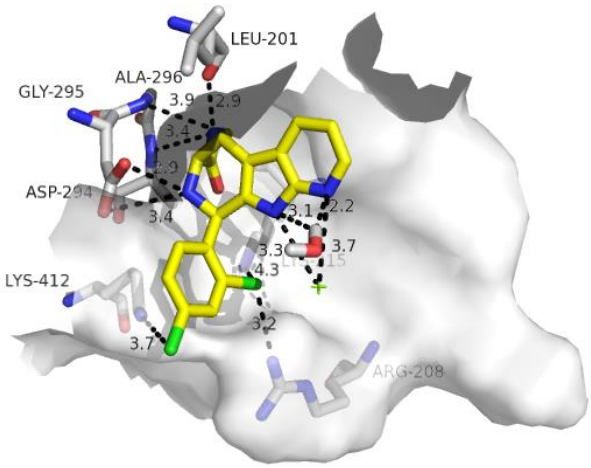

Figure 2.27. Binding pose of 73. Binding site is rendered as a white surface, Mg^{2+} is depicted as a green cross, 73 is rendered as sticks carbon coloured yellow, nitrogen coloured blue, oxygen coloured red, chlorine coloured green. Crucial amino acids are rendered as sticks carbon coloured grey, nitrogen coloured blue, oxygen coloured red.

Table 2.26. Main ligand – protein interactions of 73.

Residue(s)	Moiety	Interaction	Distance Å
Leu-201, Gly-295	NHMe	H-bond	2.9, 3.4
Arg-208	*Ortho*-Cl	Electrostatic	3.2
Lys-412	*Para*-Cl	Weak electrostatic	3.7
H_2O	A-ring-N	H-bond	2.2
H_2O	B-ring-N	H-bond	3.1
Asp-294	C-ring-NH	H-bond	2.9, 3.4
Mg^{2+}	B-ring-NH	electrostatic	3.3
Mg^{2+}	A-ring-NH	Weak electrostatic	3.7

It was observed that the docking pose for all these compounds matched that of all previously described NHMe derivatives. As all compounds have a similar binding pose, it is difficult to rationalise the loss of potency observed with compounds **36a** and **73**, both of these compounds possess and aza moiety, present in the D and A-rings, respectively. Based on their binding interactions both compounds appear to possess the potential to pick up extra interactions from all molecules previously described. Examining these compounds in a similar pose to **1a**, should also yield extra interactions, therefore it is curious as to why a subtle change leads to a loss of inhibitory activity. Again it must be

stressed that as this is a homology model, thus there is the potential for structural variation between the active site of this model, and the real case scenario in *Pf*IspD, therefore it could be reasoned that it is this potential structure change that is responsible for the loss of potency we observe.

2.4 Conclusion and Future Work

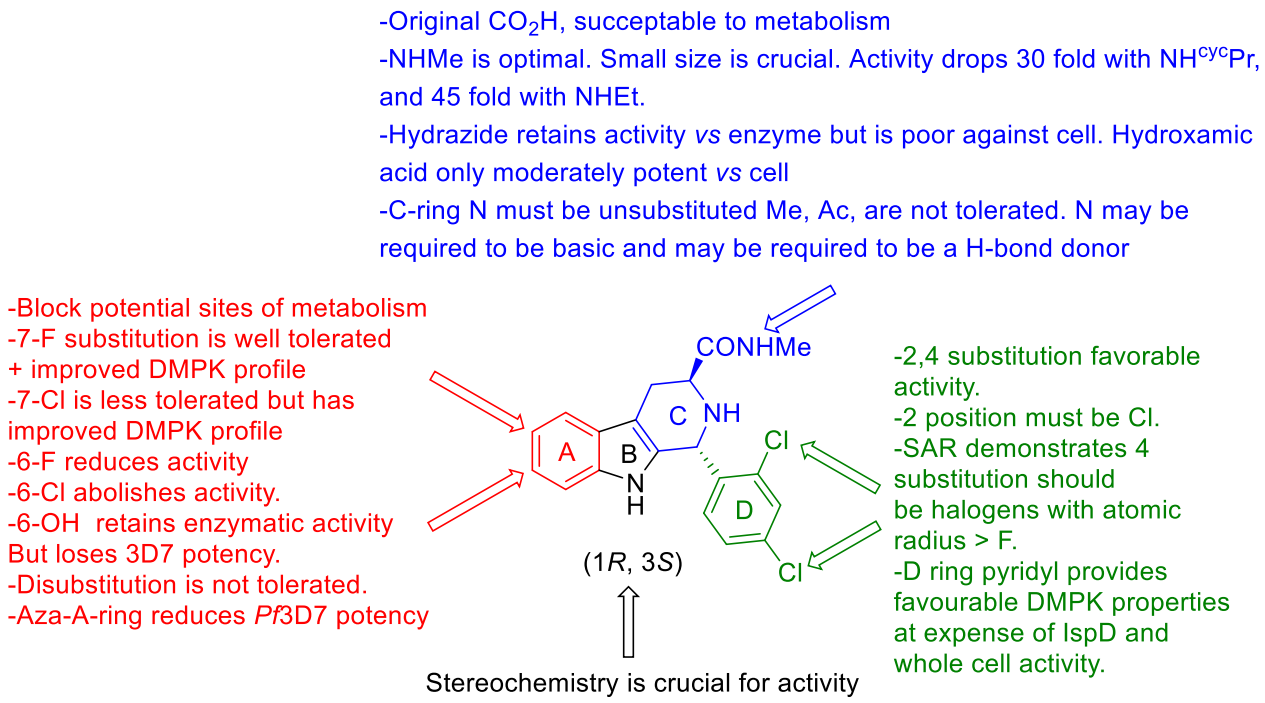

Figure 2.28. Overall SAR conclusion.

To conclude, extensive SAR has been undertaken around the MMV008138 template in order to deliver a compound with improved potency against *Pf*IspD and *Pf*3D7 whole cell parasites (Figure 2.28). We discovered that the C-ring nitrogen could not be substituted and that no improvement to potency could be made over the methyl amide moiety in **6**. We evaluated **6** for DMPK profile and found that the molecule suffered from very fast clearance rates when exposed to human and mouse microsomes, along with rat hepatocytes. We therefore turned our attention to the D-ring and A-rings for SAR and DMPK profiling. We successfully synthesised compounds **29**, **47**, and **48** that have comparable or improved potency *vs* **6**, where **29** is currently our most active compound. Compound **48** displays improved metabolic stability in comparison to **6**; we consider this compound to be a front runner. Finally, **47** shows improved potency in comparison to **6** and **48**, it also shows an improved DMPK profile in comparison to both **29** and **6** and thus we consider this molecule our current lead. Disappointingly, however, the whole template suffers from high SFI values and low aqueous solubility, and these results make SAR interpretation unclear as the most insoluble compounds may either precipitate during the biological assays, or may form enzyme inhibiting aggregates.

With regards to the future of the template we believe that the activity and DMPK profile of the template can be improved further. Whilst this SAR has been extensive, it is still only the initial studies. The discovery that the 4-position of the D-ring can maintain potency with substitutions such as bromine gives us hope that this part of the molecule can be further modified, particularly with solubilising groups. This gives hope for the future of the template, as an improved aqueous solubility profile should make SAR interpretation more clear. In fact, the bromine atom at this position opens many doors in terms of chemical manipulation as we can use Suzuki chemistry and carbonylation chemistry to install new functionalities of our choice. Indeed, with what we have learned, we can begin to combine the most promising optimisation points from each SAR study on each ring together to improve potency and potentially the DMPK profile of the template. In addition, in order to direct future SAR, metabolite identification could be carried out. With this in hand we could block the known site(s) of metabolism directly and with enough SAR knowledge, we may still be able to maintain or improve potency. Based on what we have observed with the DMPK studies, it is possible that the A-ring is not necessarily the only site of metabolism, there are two benzylic positions of the C-ring which may also be prone to metabolism. Blocking groups could be explored here with a chance to improve metabolic stability. In addition, other future work to be carried out is to run biochemical assays in the presence of non-ionic detergent. This will need to be carried out in order to rule out aggregate based nonspecific enzyme inhibition of the template, which may occur due to the poor aqueous solubility profile of the template as a whole. With all of this information taken together, displayed below are compounds within this series which we could potentially synthesise in the future for further hit to lead optimisation (**74 – 81**) (Figure 2.29).

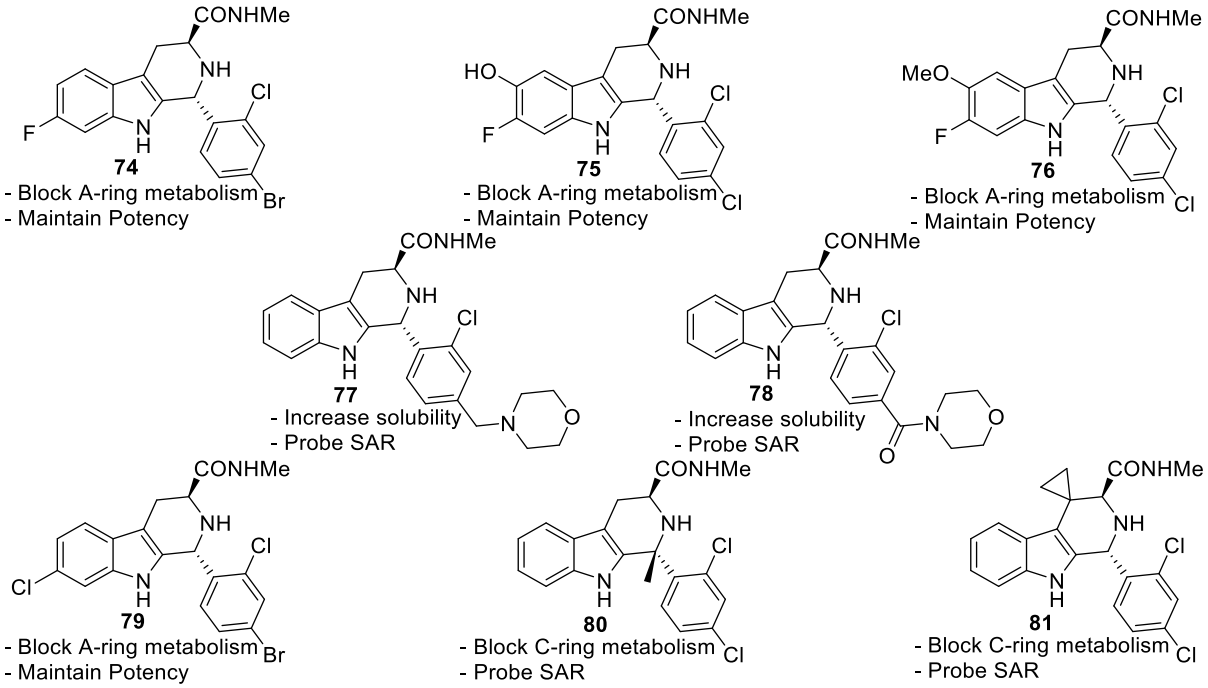

Figure 2.29. Potential future targets.

*Note, after completion of this work we identified that Carlier *et al.* published a patent containing a few of the reported compounds here. We want to disclose that our work was carried out independently of this patent, in some cases using different chemical methods.[81]

2.5 Experimental

2.5.1 General Methodologies

Chemicals

Chemicals and solvents were used as purchased from Sigma Aldrich, Fluorochem, Alfa Aesar, OxChem, BIONET or TCI with no purification needed unless stated. HOBT was bought in from sigma Aldrich containing approximately 12 % impurity of water, reagent values were calculated taking into consideration the water impurity. Anhydrous solvents were bought in or dried and distilled prior to use. Distillation was carried out under the flow of dry nitrogen; THF was distilled from sodium; dichloromethane (DCM) was distilled from calcium hydride. Anhydrous DCM and THF were also obtained from MBRAUN MBSPS5 solvent purification system.

Glassware

For anhydrous reactions, all needles, flasks, stirrer bars and any other required glassware were either flame or oven dried before use. All were cooled in a desiccator containing self-indicating silica gel or were immediately placed under a vacuum.

Thin Layer Chromatography (TLC)

Thin layer chromatography was carried out on Merck silica gel 60 F-254 aluminium backed plates. Compounds were visualised by treatment with potassium permanganate (1 % w/v in water), anisaldehyde, ninhydrin or by exposure to UV light and were developed as appropriate *via* a heat gun.

Flash Column Chromatography

Purification of products was achieved by flash column chromatography unless otherwise stated. Flash column chromatography was performed using the required amount of silica (particle size 40 – 63 µm, supplied by Aldrich) made into a slurry with the appropriate volume of the desired eluent system. The slurry was added to the column over a thin base layer of sand. Crude material was applied to the column, either dissolved in a minimum volume of eluent system or pre-absorbed onto silica. The column was then eluted with the eluent and fractions were collected and analysed by TLC.

Characterisation of compounds

^{1}H (400MHz) and ^{13}C (100MHz) NMR spectra were recorded on a Bruker AMX400 spectrometer (^{1}H 400 MHz; ^{13}C 101 MHz), Bruker DPX400 spectrometer (^{1}H 400 MHz; ^{13}C 101 MHz) or on a Bruker Avance III HD spectrometer (^{1}H 500 MHz; ^{13}C 126 MHz) in deuterated solvents as indicated with the experimental data. Chemical shifts are reported in parts per million (δ, ppm) downfield from the internal standard of TMS. Coupling constants (*J*) are reported in Hz. 2D NOESY experiments were ran with mixing time (d8) = 1 second.

Low Resolution Mass spectrometry (LRMS) and High Resolution Mass Spectrometry (HRMS) were recorded using the analytical service within the Chemistry Department at the University of Liverpool. LRMS and HRMS was conducted on a VG analytical 7070E machine, Frisons TRIO mass spectrometers or Agilent QTOF 7200 using chemical ionisation (CI) or electrospray (ESI). Elemental analysis (%C, %H, %N and %S where specified) were determined by the University of Liverpool Microanalysis Laboratory.

Infra-red spectra were recorded in the range of 4000-600 cm^{-1} using a JASCO FT/IR 4200 spectrometer, or Bruker ALPHA FT-IR platinum ATR spectrometer.

Melting points were carried out using a Gallenkamp melting point machine and values are recorded in degrees Celsius.

Chiral HPLC was carried out using Agilent 1200 HPLC machine equipped with a CHIRACEL OJ column. Flow rate 0.5 ml/min, using neat MeOH as eluent. UV detector recorded signals at wavelength of 254 nm.

2.5.2 Procedures

General Procedure 1: Pictet-Spengler cyclisation

To L-tryptophan methyl ester (**13**) (0.97 g, 4.43 mmol, 1 eq) and 2,4-dichlorobenzaldehyde (0.85 g, 4.87 mmol, 1.1 eq) in a flame dried round bottomed flask under an N_2 atmosphere was added anhydrous DCM (25 cm^3), the resultant solution was cooled to 0 °C and stirred for 10 minutes before the addition of trifluoroacetic acid (0.37 cm^3, 4.87 mmol, 1.1 eq). The reaction was allowed to slowly warm to room temperature and was left to stir for 24 hours. Upon completion, the reaction was quenched with 10 % ammonium hydroxide (25 cm^3), and the product extracted into DCM (3 x 50 cm^3), the combined organics were washed with water (50 cm^3), brine (50 cm^3) and dried over $MgSO_4$. The diastereoisomers and remaining aldehyde were separated by column chromatography, gradient elution from 100 % DCM to 2 % EtOAc in DCM. Recrystallising both diastereoisomers from hot methanol; gave compound **4** as clear see through crystals (0.50 g, 30 %), and compound **5** as white needles (0.82 g, 49 %).

Preparation of methyl (1*R*,3*S*)-1-(2,4-dichlorophenyl)-2,3,4,9-tetrahydro-1*H*-pyrido[3,4-*b*]indole-3-carboxylate (4) and methyl (1*S*,3*S*)-1-(2,4-dichlorophenyl)-2,3,4,9-tetrahydro-1*H*-pyrido[3,4-*b*]indole-3-carboxylate (5)

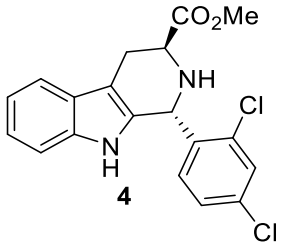

4

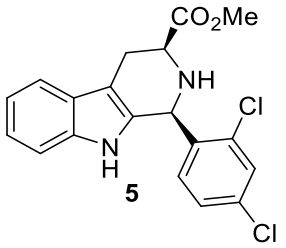

5

L-tryptophan methyl ester **13** (0.97 g, 4.43 mmol, 1 eq), 2,4-dichlorobenzaldehyde (0.85 g, 4.87 mmol, 1.1 eq) and TFA (0.37 cm^3, 4.87 mmol, 1.1 eq) were used in anhydrous DCM (25 cm^3) following **general procedure 1**. Gave **4** as clear see through crystals (0.50 g, 30 %). δ_H (400 MHz, $CDCl_3$) 7.75 (1H, s), 7.55 (1H, d, *J* 7.5 Hz), 7.46 (1H, d, *J* 1.7 Hz), 7.29 – 7.23 (1H, apparent m), 7.20 – 7.13 (3H, m), 6.90 (1H, d, *J* 8.4 Hz), 5.83 (1 H, s), 3.87 – 3.79 (1H, apparent t), 3.72 (3H, s), 3.25 (1H, dd, *J* 15.2, 4.8 Hz), 3.08 (1H, dd, *J* 15.4, 7.8 Hz), 2.77 (1H, s). δ_C (101 MHz, $CDCl_3$) 173.8, 137.9, 136.4, 134.52, 134.48, 131.6, 131.0, 129.9, 127.3, 126.9, 122.4, 119.9, 118.5, 111.1, 109.8, 52.4, 52.3, 51.3, 24.9. **ESI-HRMS**: m/z calculated for $C_{19}H_{17}{}^{35}Cl_2N_2O_2$ $[M+H]^+$ requires 375.0662. Found 375.0664.

Crystal data and structure refinement for 4

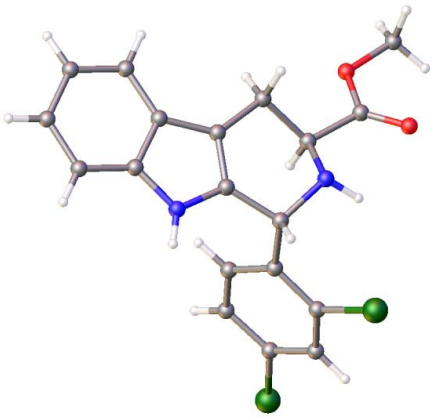

Identification code	**4**
Empirical formula	$C_{19}H_{16}Cl_2N_2O_2$
Formula weight	375.24
Temperature/K	100.0
Crystal system	monoclinic
Space group	$P2_1$
a/Å	9.6151(5)
b/Å	10.6952(5)
c/Å	17.2746(10)
α/°	90
β/°	97.871(2)
γ/°	90
Volume/Å^3	1759.70(16)
Z	4
ρ_{calc}g/cm^3	1.416
μ/mm^{-1}	0.384
F(000)	776.0
Crystal size/mm^3	0.22 × 0.18 × 0.1
Radiation	MoKα (λ = 0.71073)
2Θ range for data collection/°	4.492 to 52.866
Index ranges	-12 ≤ h ≤ 12, -13 ≤ k ≤ 13, -21 ≤ l ≤ 21
Reflections collected	38831
Independent reflections	7193 [R_{int} = 0.0271, R_{sigma} = 0.0198]
Data/restraints/parameters	7193/1/473
Goodness-of-fit on F^2	1.075
Final R indexes [I>=2σ (I)]	R_1 = 0.0294, wR_2 = 0.0705
Final R indexes [all data]	R_1 = 0.0306, wR_2 = 0.0714
Largest diff. peak/hole / e Å^{-3}	0.76/-0.96
Flack parameter	-0.002(9)

The same procedure also gave **5** as white needles (0.82 g, 49 %). **δ_H** (400 MHz, $CDCl_3$) 7.56 (1H, s), 7.53 (1H, d, *J* 7.3 Hz), 7.46 (1H, d, *J* 1.9 Hz), 7.37 (1H, d, *J* 8.5 Hz), 7.26 – 7.09 (4H, m), 5.78 (1H, s), 3.97 (1H, dd, *J* 11.0, 4.1 Hz), 3.81 (3H, s), 3.23 (1H, ddd, *J* 15.1, 4.0, 1.6 Hz), 3.07 – 2.93 (1H, m (overlapped ddd)), 2.61 (1H, s). **δ_C** (101 MHz, $CDCl_3$) 173.1, 137.4, 136.3, 134.8, 134.2, 133.3, 131.6, 129.5, 128.2, 127.0, 122.3, 119.9, 118.4, 111.1, 109.5, 56.7, 52.5, 25.5. **ESI-HRMS**: m/z calculated for $C_{19}H_{17}{}^{35}Cl_2N_2O_2$ $[M+H]^+$ requires 375.0662. Found 375.0665.

General Procedure 2: Amide couplings from tetrahydro-β-carboline methyl ester

To compound **4** (0.12 g, 0.31 mmol, 1 eq) was added methyl amine 33 % in EtOH (6.45 cm^3, 51.77 mmol, 167 eq) and the mixture stirred at RT overnight in a sealed tube. Solvents were removed in *vacuo*, and solid recrystallised from hot methanol to yield the product **6** (0.11 g, 99 %) as transparent crystals.

Preparation of (1*R*,3*S*)-1-(2,4-dichlorophenyl)-*N*-methyl-2,3,4,9-tetrahydro-1*H*-pyrido[3,4-*b*]indole-3-carboxamide (6)

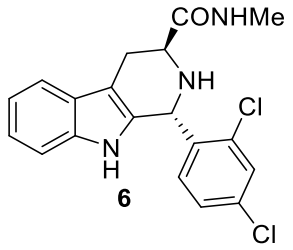

6

Compound **4** (0.12 g, 0.31 mmol, 1 eq) and methyl amine 33 % in EtOH (6.45 cm^3, 51.77 mmol, 167 eq) were used following **general procedure 2**. Gave the desired product **6** as transparent crystals (0.11 g, 99 %). **δ_H** (500 MHz, DMSO) 10.72 (1H, s), 7.72 (1H, apparent q), 7.68 (1H, d, *J* 1.9 Hz), 7.47 (1H, d, *J* 7.7 Hz), 7.30 (1H, dd, *J* 8.3, 1.7 Hz), 7.25 (1H, d, *J* 8.0 Hz), 7.06 (1H, apparent t), 6.99 (1H, apparent t), 6.68 (1H, d, *J* 8.4 Hz), 5.56 (1H, d, *J* 4.7 Hz), 3.39 – 3.33 (1H, m), 3.09 (1H, dd, *J* 9.6, 5.1 Hz), 3.00 (1H, dd, *J* 15.2, 4.4 Hz), 2.69 (1H, dd, *J* 15.1, 10.0 Hz), 2.59 (3H, d, *J* 4.9 Hz). **δ_C** (126 MHz, DMSO) 172.8, 138.9, 136.1, 134.5, 132.6, 132.6, 131.2, 129.1, 126.8, 126.5, 121.1, 118.5, 117.7, 111.1, 109.2, 51.4, 50.8, 25.4, 25.2. **ESI-HRMS**: m/z calculated for $C_{19}H_{18}{}^{35}Cl_2N_3O$ $[M+H]^+$ requires 374.0821. Found 374.0821 **Elemental Analysis** Calculated for $C_{19}H_{17}Cl_2N_3O$ requires C, 60.98 %, H, 4.58 %, N, 11.23 %. Found C, 60.81 %, H, 4.55 %, N, 11.23 %. **IR (neat)**: ν_{max}/cm^{-1}: 3375 (m), 3288 (s), 3065 (m, br), 2937 – 2901 (m, br), 1660 (s), 1588 (m), 1516 (s), 1467 (s), 1449 (vs), 1316 (s), 1258 (s), 825 (s). **Melting Point** ^oC: 248 – 250 (MeOH) **HPLC** (purity analysis %) found: Purity 100 %; Retention time: 10.20 min / 30 min (0.5 ml/min MeOH, Signal = 254 nm, CHIRACEL OJ column).

Preparation of methyl (1*R*,3*S*)-1-(2,4-dichlorophenyl)-2-methyl-2,3,4,9-tetrahydro-1*H*-pyrido[3,4-*b*]indole-3-carboxylate (17)

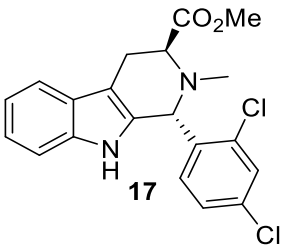

17

To compound **4** (0.26 g, 0.68 mmol, 1eq) was added acetone (5 cm^3), and potassium carbonate (0.10 g, 0.75 mmol, 1.1 eq) in a sealed tube, the tube was purged gently with N_2 before addition of MeI (0.047 cm^3, 0.75 mmol, 1.1 eq). The tube was sealed and covered with aluminium foil to block out light. The reaction was heated to reflux in the dark overnight. The resulting mixture was diluted with brine and product extracted into EtOAc (3 x 50 cm^3), combined organics were dried over $MgSO_4$. The product was purified by column chromatography (10 % EtOAc in hexane) to yield the desired product **17** as yellow crystals (0.16 g, 67 %). δ_H (400 MHz, $CDCl_3$) 7.57 (1H, s), 7.49 (1H, d, *J* 7.4 Hz), 7.45 (1H, s), 7.37 (1H, d, *J* 8.4 Hz), 7.23 – 7.03 (4H, m), 5.88 (1H, s), 4.01 (1H, d, *J* 5.4 Hz), 3.64 (3H, s), 3.35 (1H, dd, *J* 15.4, 6.0 Hz), 3.26 (1H, d, *J* 15.4 Hz), 2.49 (3H, s). δ_C (101 MHz, $CDCl_3$) 173.4, 138.6, 136.6, 134.6, 134.1, 134.0, 131.5, 129.3, 128.1, 126.8, 122.1, 119.6, 118.3, 111.1, 106.1, 61.7, 57.2, 51.6, 40.4, 25.1. **ESI-HRMS**: m/z calculated for $C_{20}H_{19}{}^{35}Cl_2N_2O_2$ $[M+H]^+$ requires 389.0818. Found 389.0821.

Preparation of (1*R*,3*S*)-1-(2,4-dichlorophenyl)-*N*,2-dimethyl-2,3,4,9-tetrahydro-1*H*-pyrido[3,4-*b*]indole-3-carboxamide (18)

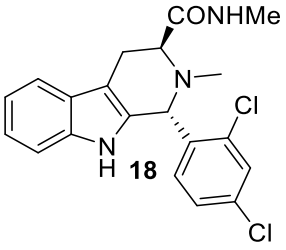

18

Compound **17** (0.07 g, 0.18 mmol, 1 eq) and methyl amine 33 % in EtOH (3.74 cm^3, 30.06 mmol, 167 eq) were used following **general procedure 2**. Gave the desired product **18** as a white solid (0.069 g, 99 %). δ_H (500 MHz, $CDCl_3$) 7.85 (1H, s), 7.65 (1H, d, *J* 7.7 Hz), 7.50 (1H, d, *J* 2.1 Hz), 7.32 (1H, d, *J* 7.9 Hz), 7.24 – 7.21 (1H, m), 7.20 – 7.16 (1H, m), 7.07 (1H, dd, *J* 8.3, 2.1 Hz), 6.70 (1H, d, *J* 4.8 Hz), 6.65 (1H, d, *J* 8.3 Hz), 5.14 (1H, s), 3.50 (1H, dd, *J* 11.5, 4.7 Hz), 3.16 (1H, dd, *J* 16.5, 4.7 Hz), 3.01 (1H, dd, *J* 16.5, 11.6 Hz), 2.79 (3H, d, *J* 5.0 Hz), 2.47 (3H, s). δ_C (126 MHz, $CDCl_3$) 172.4, 137.0, 136.8, 135.9, 134.7, 131.3, 130.2, 129.5, 127.1, 126.9, 122.6, 120.0, 119.0, 111.5, 111.2, 60.9, 56.3, 36.9, 26.1, 17.3.

ESI-HRMS: m/z calculated for $C_{20}H_{20}{}^{35}Cl_2N_3O$ $[M+H]^+$ requires 388.0978. Found 388.0973. **Elemental Analysis** Calculated $C_{20}H_{19}Cl_2N_3O$ requires C, 61.86 %, H, 4.93 %, N, 10.82 %. Found C, 62.02 %, H, 4.96 %, N, 10.81 %. **IR (neat)**: ν_{max}/cm^{-1}: 3390 (m), 3261 (s), 2963 – 2798 (m, br), 1671 (s), 1523 (m), 1467 (s), 1467 (s), 740 (s), 690 (s). **Melting Point** °C: 234 – 235 (MeOH). **HPLC** (purity analysis %) found: Purity 100 %; Retention time: 11.33 min / 30 min (0.5 ml/min MeOH, Signal = 254 nm, CHIRACEL OJ column).

Preparation of methyl (1*R*,3*S*)-2-(2-bromoacetyl)-1-(2,4-dichlorophenyl)-2,3,4,9-tetrahydro-1*H*-pyrido[3,4-*b*]indole-3-carboxylate (19)

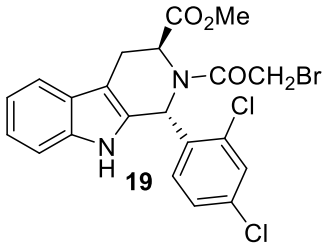

19

To compound **4** (0.20 g, 0.53 mmol, 1 eq) in a flame dried round bottomed flask was added anhydrous DCM (5 cm^3) under a N_2 atmosphere and NEt_3 (0.11 cm^3, 0.80 mmol, 1.5 eq). The reaction mixture was cooled to 0 °C before addition of bromoacetyl bromide (0.07 cm^3, 0.8 mmol, 1.5 eq). The reaction mixture was allowed to slowly warm to room temperature and was left overnight. The resulting reaction was quenched by slow addition of saturated $NaHCO_3$ solution (50 cm^3) and was left to stir until CO_2 production ceased. The product was extracted into DCM (3 x 50 cm^3); combined organics were washed with water (50 cm^3) and brine (50 cm^3) before drying over $MgSO_4$. After filtration the product was purified by column chromatography (100 % DCM) to yield the product **19** as a white solid (0.27 g, 80 %). $\boldsymbol{\delta_H}$ (500 MHz, $CDCl_3$) 8.11 (1H, s), 7.54 (1H, d, *J* 7.8 Hz), 7.43 (1H, s), 7.30 (1H, s), 7. 21 – 7.17 (2H, m), 7.16 – 7.11 (1H, m), 6.59 (1H, s), 5.30 (1H, d, *J* 3.7 Hz), 3.97 (1H, d, *J* 11.4 Hz), 3.85 (1H, d, *J* 11.4 Hz), 3.76 (1H, d, *J* 15.5 Hz), 3.67 (3H, s), 3.49 (1H, dd, *J* 15.5, 4.6 Hz). $\boldsymbol{\delta_C}$ (101 MHz, $CDCl_3$) 171.4, 168.4, 139.3, 136.6, 133.5, 132.7, 132.1, 129.6, 128.3, 126.6, 126.0, 122.9, 120.2, 118.5, 111.4, 105.0, 57.8, 53.4, 53.0, 27.2, 23.8. **ESI-HRMS**: m/z calculated for $C_{21}H_{17}{}^{79}Br^{35}Cl_2N_2NaO_3$ $[M+Na]^+$ requires 516.9692. Found 516.9697.

Preparation of (6*R*,12a*S*)-6-(2,4-dichlorophenyl)-2-methyl-2,3,6,7,12,12a-hexahydropyrazino[1',2':1,6]pyrido[3,4-*b*]indole-1,4-dione (20)

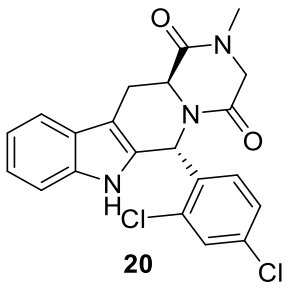

20

Compound **19** (0.078 g, 0.16 mmol) was used following a modified procedure to **general procedure 4**, using methyl amine 33 % in EtOH (0.10 cm^3, 0.80 mmol, 5 eq) and diluting the reaction with EtOH (8 cm^3). δ_H (500 MHz, $CDCl_3$) 8.09 (1H, s), 7.52 (1H, d, *J* 7.8 Hz), 7.46 (1H, d, *J* 2.1 Hz), 7.32 (1H, d, *J* 8.1 Hz), 7.25 – 7.21 (2H, m), 7.19 – 7.14 (1H, m), 7.10 (1H, dd, *J* 8.4, 2.1 Hz), 6.77 (1H, d, *J* 8.4 Hz), 4.25 (1H, dd, *J* 12.0, 4.5 Hz), 4.11 (1H, d, *J* 18.1 Hz), 4.04 (1H, d, *J* 18.1 Hz), 3.48 (1H, dd, *J* 15.6, 4.5 Hz), 3.01 (3H, s), 2.99 – 2.94 (1H, ddd, 15.6, 3.6, 1.36 Hz). δ_C (126 MHz, $CDCl_3$) 166.0, 163.1, 136.5, 135.8, 135.2, 133.9, 131.9, 130.4, 129.2, 127.3, 126.3, 123.2, 120.5, 118.6, 111.5, 109.4, 53.1, 51.6, 49.5, 33.5, 27.3. **ESI-HRMS**: m/z calculated for $C_{21}H_{18}{}^{35}Cl_2N_3O_2$ $[M+H]^+$ requires 414.0771. Found 414.0775. **Elemental Analysis** Calculated for $C_{21}H_{17}Cl_2N_3O_2$ requires C, 60.88 %, H, 4.14 %, N, 10.14 %. Found C, 60.86 %, H, 4.21 %, N, 10.02 %. **IR (neat)**: ν_{max}/cm^{-1}: 3258 (m, br), 3073 (w) 2918 (br) 2855 (m, br), 1666(s), 1648 (s), 1444 (s) 1321 (s), 737 (s). **Melting Point** °C: Did not melt, decomposed above 300 (MeOH).

Preparation of (1*R*,3*S*)-2-acetyl-1-(2,4-dichlorophenyl)-*N*-methyl-2,3,4,9-tetrahydro-1*H*-pyrido[3,4-*b*]indole-3-carboxamide (21)

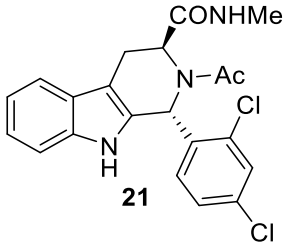

21

In a flame dried round bottom flask was added compound **6** (0.10 g, 0.27 mmol, 1 eq) anhydrous DCM (5 cm^3) and NEt_3 (0.04 cm^3, 0.29 mmol, 1.1 eq) under N_2. The reaction mixture was cooled to 0 °C before addition of AcCl (0.021 cm^3, 0.29 mmol, 1.1 eq). The reaction mixture was allowed to slowly warm to room temperature and left to stir overnight. The resulting reaction was quenched by slow addition of saturated $NaHCO_3$ solution (50 cm^3) and was left to stir until CO_2

production ceased. The product was extracted into DCM (3 x 50 cm^3); combined organics were washed with water (50 cm^3) and brine (50 cm^3) before drying over $MgSO_4$. After filtration the product was purified by column chromatography (30 % EtOAc in DCM) to yield the product **21** as a white solid (0.066 g, 60 %). Note: ^1H and ^{13}C NMR appears to exist as two rotamers with little difference in ratio between major and minor rotamers. In ^1H NMR chemical shifts are reported as the average between any two rotameric peaks. Most signals in ^1H NMR appear as broadened singlets and as such coupling constants are mostly missing. In ^{13}C NMR signals also appear broadened; all observed peaks in ^{13}C are reported. **δ_H** (500 MHz, $CDCl_3$) 8.12 (1H, s, br), 7.50 (1H, d, *J* 7.8 Hz), 7.44 (1H, s, br), 7.27 (1H, d, *J* 8.2 Hz), 7.21 – 7.07 (3H, m, br), 6.63 (1H, s, br), 5.72 (1H, s, br), 5.16 (1H, s, br), 3.75 – 3.26 (2H, m, br), 2.69 (3H, s), 2.12 (3H, s, br). **δ_C** (126 MHz, $CDCl_3$) 171.6, 171.3, 139.7, 139.1, 136.5, 134.7, 133.6, 132.3, 132.2, 132.1, 130.0, 129.7, 129.2, 128.8, 128.3, 126.8, 126.1, 122.9, 120.2, 118.7, 111.4, 107.2, 105.5, 59.0, 55.1, 52.5, 27.0, 26.7, 26.6, 24.3, 23.3, 23.2, 23.0. **ESI-HRMS**: m/z calculated for $C_{21}H_{19}{}^{35}Cl_2N_3NaO_2$ $[M+Na]^+$ requires 438.0747. Found 438.0740. **Elemental Analysis** Calculated for $C_{21}H_{19}Cl_2N_3O_2$ requires C, 60.59 %, H, 4.60 %, N, 10.09 %. Found C, 59.21 %, H, 4.73 %, N, 9.60 %. **IR (neat)**: ν_{max}/cm^{-1}: 3384 (w, br), 3291 (w, br), 3060 (m, br), 2928 (m), 2855 (w), 1644(s), 1384 (s), 741 (s). **Melting Point** °C: 180 – 184. **HPLC** (purity analysis %) found: Purity 100 %; Retention time: 7.28 min / 30 min (0.5 ml/min MeOH, Signal = 254 nm, CHIRACEL OJ column).

Preparation of (1*R*,3*S*)-*N*-cyclopropyl-1-(2,4-dichlorophenyl)-2,3,4,9-tetrahydro-1*H*-pyrido[3,4-*b*]indole-3-carboxamide (22)

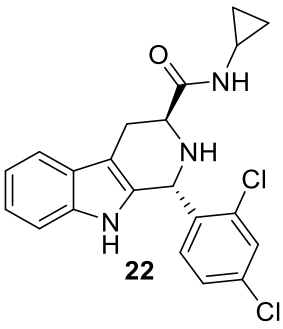

22

Compound **4** (0.12 g, 0.32 mmol, 1eq) was used following a modified procedure to **general procedure 2**. Cyclopropyl amine (0.67 cm^3, 9.60 mmol, 30 eq) was dissolved in EtOH (2 cm^3) and added to compound **4** in a sealed tube. The reaction was heated to 50 °C overnight. Solvents were removed *in vacuo* and product purified by column chromatography (2 % EtOAc in DCM). Recrystallisation from hot methanol gave the desired product **22** as white needles (0.063 g, 49 %). **δ_H** (500 MHz, $CDCl_3$) 7.77 (1H, s), 7.58 (1H, d, *J* 7.8 Hz), 7.48 (1H, d, *J* 2.1 Hz), 7.31 – 7.27 (1H, m), 7.21 (1H, apparent td), 7.15 (1H, apparent td), 7.08 (1H, dd, *J* 8.3, 2.1 Hz), 6.93 (1H, d, *J* 3.0 Hz), 6.74 (1H, d, *J* 8.3 Hz), 5.60 (1H, s), 3.51 (1H, dd, *J* 9.7, 4.9 Hz), 3.30 (1H, dd, *J* 15.9, 4.9 Hz), 2.89 (1 H, ddd, *J* 15.9, 9.8, 1.5 Hz), 2.73 – 2.68

(1H, m), 2.06 (1H, br s), 0.83 – 0.69 (2H, m), 0.55 – 0.43 (2H, m). **δ_C** (126 MHz, $CDCl_3$) 174.1, 136.9, 136.5, 135.2, 134.8, 131.4, 131.2, 130.2, 127.1, 127.0, 122.7, 120.0, 118.8, 111.5, 111.1, 52.6, 51.9, 24.8, 22.5, 6.8, 6.5. **ESI-HRMS**: m/z calculated for $C_{21}H_{20}{}^{35}Cl_2N_3O$ $[M+H]^+$ requires 400.0978. Found 400.0981. **Elemental Analysis** Calculated $C_{20}H_{19}Cl_2N_3O$ requires C, 63.01 %, H, 4.78 %, N, 10.50 %. Found C, 62.70 %, H, 4.77 %, N, 10.34 %. **IR (neat)**: ν_{max}/cm^{-1}: 3364 (m), 3272 (s, br), 3059 (w, br), 2943 (w, br), 2842 (w), 1658 (s), 1507, (s), 1452 (s), 825 (s). **Melting Point** °C: 194 – 196 (MeOH). **HPLC** (purity analysis %) found: Purity 100 %; Retention time: 7.96 min / 30 min (0.5 ml/min MeOH, Signal = 254 nm, CHIRACEL OJ column).

Preparation of (1*R*,3*S*)-1-(2,4-dichlorophenyl)-*N*-ethyl-2,3,4,9-tetrahydro-1*H*-pyrido[3,4-*b*]indole-3-carboxamide (23)

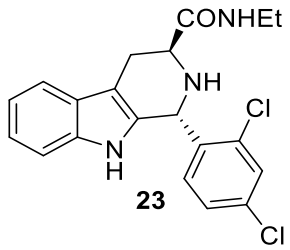

23

Compound **4** (0.10 g, 0.28 mmol, 1 eq) was used following a modified procedure to **general procedure 2**. $EtNH_2$ 2M in MeOH (11.76 cm^3, 23.52 mmol, 84 eq) was used at the nucleophile instead of $MeNH_2$. Yielded the product **23** as a white solid after recrystallisation in hot MeOH (0.055 g, 51 %). **δ_H** (500 MHz, DMSO) 10.70 (1H, s), 7.77 (1H, br t, *J* 5.5 Hz), 7.69 (1H, d, *J* 2.2 Hz), 7.48 (1H, d, *J* 7.8 Hz), 7.30 (1H, dd, *J* 8.3, 2.2 Hz), 7.24 (1H, d, *J* 8.0 Hz), 7.09 – 7.03 (1H, m), 7.02 – 6.96 (1H, m), 6.69 (1H, d, *J* 8.4 Hz), 5.56 (1H, d, *J* 4.6 Hz), 3.36 (1H, apparent td), 3.13 – 3.04 (3H, m), 2.99 (1H, dd, *J* 15.1, 4.5 Hz), 2.70 (1H, ddd, *J* 15.1, 9.8, 1.1 Hz), 1.01 (3H, t, *J* 7.2 Hz). **δ_C** (126 MHz, DMSO) 172.1, 138.9, 136.1, 134.5, 132.6, 132.6, 131.2, 129.1, 126.8, 126.5, 121.1, 118.5, 117.7, 111.1, 109.1, 51.4, 50.6, 33.3, 25.2, 14.7. **ESI-HRMS**: m/z calculated for $C_{20}H_{20}{}^{35}Cl_2N_3O$ $[M+H]^+$ requires 388.0978. Found 388.0972. **Elemental Analysis** Calculated for $C_{20}H_{19}Cl_2N_3O$ requires C, 61.87 %, H, 4.93 %, N, 10.82 %. Found C, 61.21 %, H, 4.92 %, N, 10.63 %. **IR (neat)**: ν_{max}/cm^{-1}: 3358 (m), 3312 (m), 3222 (m, br), 3063 (w, br), 2932 (w), 2874 (w), 2843 (w), 1656 (s), 1519 (s), 1451 (s), 741 (s). **Melting Point** °C: 234 – 236 (MeOH).

Generic structure of compounds 26a – f and 27a – f following general procedure 1

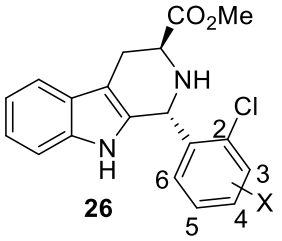

26

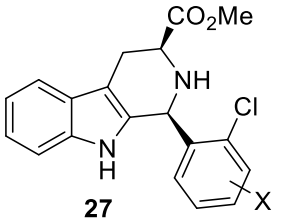

27

26a / **27a**	X = 4-CF_3
26b / **27b**	X = 4-Br
26c / **27c**	X = 6-Cl
26d / **27d**	X = 3-F, 4-Cl
26e / **27e**	X = 3-Cl, 4-Cl
26f / **27f**	X = 4-Cl, 5-F

Preparation of methyl (1*R*,3*S*)-1-(2-chloro-4-(trifluoromethyl)phenyl)-2,3,4,9-tetrahydro-1*H*-pyrido[3,4-*b*]indole-3-carboxylate (26a) and methyl (1*S*,3*S*)-1-(2-chloro-4-(trifluoromethyl)phenyl)-2,3,4,9-tetrahydro-1*H*-pyrido[3,4-*b*]indole-3-carboxylate (27a)

L-tryptophan methyl ester **13** (0.86 g, 3.93 mmol, 1 eq), 2-chloro-4-(trifluoromethyl)benzaldehyde (0.90 g, 4.32 mmol, 1.1 eq), and TFA (0.33 cm^3, 4.32 mmol, 1.1 eq), were used in anhydrous DCM (20 cm^3) following **general procedure 1**. Gave **26a** as white crystals (0.52 g, 33 %). δ_H (400 MHz, $CDCl_3$) 7.73 (1H, d, *J* 1.0 Hz), 7.69 (1H, s), 7.57 (1H, d, *J* 7.5 Hz), 7.38 (1H, d, *J* 8.2 Hz), 7.29 – 7.25 (1H, m), 7.22 – 7.11 (3H, m), 5.93 (1H, s), 3.85 (1H, dd, *J* 7.6, 5.1 Hz), 3.73 (3H, s), 3.32 – 3.24 (1H, ddd, *J* 15.4, 5.1, 0.8 Hz), 3.11 (1H, ddd, *J* 15.4, 7.6, 1.4 Hz), 2.82 (1H, s). δ_C (101 MHz, $CDCl_3$) 173.8, 143.3, 136.4, 134.4, 131.7 (q, *J* 33.1 Hz), 131.2, 130.7, 127.1 (q, *J* 3.8 Hz), 126.9, 123.9 (q, *J* 3.5 Hz), 123.3 (q, *J* 272.7 Hz), 122.6, 120.0, 118.5, 111.2, 109.9, 52.4, 51.5, 24.9. δ_F (376 MHz, $CDCl_3$) -62.8 (3F, s). **ESI-HRMS**: m/z calculated for $C_{20}H_{16}{}^{35}ClF_3N_2O_2$ $[M+H]^+$ requires 409.0925. Found 409.0933.

The same procedure also gave **27a** as white needles (0.88 g, 55 %). δ_H (400 MHz, $CDCl_3$) 7.73 (1H, s), 7.61 (1H, d, *J* 8.1 Hz), 7.57 (1H, s), 7.54 (1H, d, *J* 7.2 Hz), 7.47 (1H, d, *J* 8.1 Hz), 7.26 – 7.22 (1H, m), 7.19 – 7.10 (2H, m), 5.88 (1H, s), 4.00 (1 H, dd, *J* 11.0, 4.1 Hz), 3.82 (3H, s), 3.25 (1H, ddd, *J* 15.1, 4.1, 1.7 Hz), 3.02 (1H, ddd, *J* 15.1, 11.0, 2.4 Hz). δ_C (101 MHz, $CDCl_3$) 173.0, 142.9, 136.4, 134.1, 132.8, 131.9 (q, *J* 33.4 Hz), 131.3, 126.9, 126.8 (q, *J* 3.4), 124.6 (q, *J* 3.5 Hz), 123.3 (q, *J* 272.6 Hz), 122.5, 120.0, 118.5, 111.1, 109.7, 56.6, 52.5, 25.5. δ_F (376 MHz, $CDCl_3$) -62.8 (3F, s). **ESI-HRMS**: m/z calculated for $C_{20}H_{16}{}^{35}ClF_3N_2O_2$ $[M+H]^+$ requires 409.0925. Found 409.0934.

Preparation of methyl (1*R*,3*S*)-1-(4-bromo-2-chlorophenyl)-2,3,4,9-tetrahydro-1*H*-pyrido[3,4-*b*]indole-3-carboxylate (26b) and methyl (1*S*,3*S*)-1-(4-bromo-2-chlorophenyl)-2,3,4,9-tetrahydro-1*H*-pyrido[3,4-*b*]indole-3-carboxylate (27b)

L-tryptophan methyl ester **13** (0.45 g, 2.08 mmol, 1 eq), 2-chloro-4-bromobenzaldehyde (0.50 g, 2.29 mmol, 1.1 eq) and TFA (0.18 cm^3, 2.29 mmol, 1.1 eq), were used in anhydrous DCM (10 cm^3) following **general procedure 1**. Gave **26b** as a white solid (0.15 g, 17 %). **δ_H** (500 MHz, $CDCl_3$) 7.68 (1H, s), 7.61 (1H, d, *J* 2.0 Hz), 7.56 (1H, d, *J* 7.7 Hz), 7.27 – 7.23 (2H, m), 7.20 – 7.16 (1H, m), 7.16 – 7.12 (1H, m), 6.85 (1H, d, *J* 8.3 Hz), 5.83 (1H, s), 3.83 (1H, dd, *J* 7.7, 5.0 Hz), 3.73 (3H, s), 3.25 (1H, ddd, *J* 15.3, 5.0, 1.0 Hz), 3.09 (1H, ddd, *J* 15.3, 7.8, 1.5 Hz), 2.77 (1H, br s). **δ_C** (126 MHz, $CDCl_3$) 173.8, 138.4, 136.4, 134.7, 132.7, 131.6, 131.4, 130.2, 126.9, 122.5, 122.3, 119.9, 118.5, 111.1, 109.8, 52.37, 52.35, 51.4, 24.9. **ESI-HRMS**: m/z calculated for $C_{19}H_{17}{}^{79}Br^{35}ClN_2O_2$ $[M+H]^+$ requires 419.0156. Found 419.0151.

The same procedure also gave **27b** as a white solid (0.29 g, 34 %). **δ_H** (500 MHz, $CDCl_3$) 7.63 (1H, d, *J* 1.8 Hz), 7.56 – 7.52 (2H, m), 7.37 – 7.31 (2H, m), 7.26 – 7.22 (1H, m), 7.18 – 7.11 (2H, m), 5.79 (1H, s), 3.99 (1H, dd, *J* 11.0, 4.1 Hz), 3.83 (3H, s), 3.24 (1H, ddd, *J* 15.0, 4.1, 1.8 Hz), 3.01 (1H, ddd, *J* 15.0, 11.0, 2.5 Hz), 2.63 (1H, s). **δ_C** (126 MHz, $CDCl_3$) 173.1, 137.0, 136.3, 134.5, 133.2, 132.3, 131.9, 131.1, 127.0, 122.5, 122.4, 119.9, 118.4, 111.1, 109.5, 56.7, 52.5, 25.5. **ESI-HRMS**: m/z calculated for $C_{19}H_{17}{}^{79}Br^{35}ClN_2O_2$ $[M+H]^+$ requires 419.0156. Found 419.0151.

Preparation of methyl (1*R*,3*S*)-1-(2,6-dichlorophenyl)-2,3,4,9-tetrahydro-1*H*-pyrido[3,4-*b*]indole-3-carboxylate (26c) and methyl (1*S*,3*S*)-1-(2,6-dichlorophenyl)-2,3,4,9-tetrahydro-1*H*-pyrido[3,4-*b*]indole-3-carboxylate (27c)

Note reported here are the distinguishable *trans* signals first **26c** with the full *cis* isomer reported **27c** separately below. The *cis* isomer in this case is a highly predominant product and could not be separated from *trans* by column. The *trans* isomer was separated at the next step (**see compound 30a and 30b**). All Ar-H corresponding to the *trans* product are lost under *cis* signals as are some Ar-C signals. The aliphatic region is the only part of the spectrum were *trans* signals can be observed unambiguously.

L-tryptophan methyl ester **13** (0.51 g, 2.31 mmol, 1 eq), 2,6-dichlorobenzaldehyde (0.45 g, 2.54 mmol, 1.1 eq) and TFA (0.20 cm^3, 2.54 mmol, 1.1 eq), were used in anhydrous DCM (15 cm^3) following **general procedure 1**. It should be noted in the case of this compound lab temperature was 12 °C throughout the course of the reaction. After column chromatography the mixture of **26c** and **27c** were obtained as a pale yellow solid (0.67 g, 80 %). **26c NMR δ_H** (500 MHz, $CDCl_3$) 6.48 (1H, s), 4.25 (1H, dd, *J* 6.0, 2.7 Hz), 3.72 (3H, s), 3.38 (1H, ddd, *J* 15.4, 2.7, 1.8 Hz), 3.29 – 3.25 (1H, m). **δ_C** (126 MHz,

$CDCl_3$) 174.4, 136.1, 135.7, 132.0, 129.9, 127.2, 121.8, 119.6, 118.3, 111.0, 107.9, 55.0, 51.0, 50.8, 23.7.

27c NMR δ_H (500 MHz, $CDCl_3$) 7.52 – 7.50 (1H, m), 7.48 (1H, s), 7.43 (1H, dd, *J* 7.7, 1.7 Hz), 7.28 – 7.19 (3H, m), 7.16 – 7.10 (2H, m), 6.19 (1H, s), 4.03 (1H, dd, *J* 11.2, 4.2 Hz), 3.82 (3H, s), 3.25 (1H, ddd, *J* 15.2, 4.3, 1.9 Hz), 2.95 (1H, ddd, *J* 15.1, 11.2, 2.7 Hz), 2.71 (1H, s). **δ_C** (126 MHz, $CDCl_3$) 173.4, 137.1, 136.3, 136.0, 134.5, 133.0, 130.6, 130.2, 128.9, 127.2, 122.0, 119.9, 118.1, 111.1, 108.9, 57.5, 54.5, 52.4, 26.0. **ESI-HRMS**: m/z calculated for $C_{19}H_{17}{}^{35}Cl_2N_2O_2$ $[M+H]^+$ requires 375.0662. Found 375.0654.

Preparation of methyl (1*R*,3*S*)-1-(2,4-dichloro-3-fluorophenyl)-2,3,4,9-tetrahydro-1*H*-pyrido[3,4-*b*]indole-3-carboxylate (26d) and methyl (1*S*,3*S*)-1-(2,4-dichloro-3-fluorophenyl)-2,3,4,9-tetrahydro-1*H*-pyrido[3,4-*b*]indole-3-carboxylate (27d)

L-tryptophan methyl ester **13** (0.50 g, 2.29 mmol, 1 eq), 2,4-dichloro-3-fluoro-benzaldehyde (0.49 g, 2.52 mmol, 1.1 eq) and TFA (0.19 cm^3, 2.52 mmol, 1.1 eq), were used in anhydrous DCM (15 cm^3) following **general procedure 1**. Gave **26d** as white crystals (0.24 g, 26 %). **δ_H** (500 MHz, MeOD) 7.48 (1H, d, *J* 7.8 Hz), 7.28 (1H, dd, *J* 8.4, 7.1 Hz), 7.24 (1H, d, *J* 8.0 Hz), 7.11 – 7.06 (1H, m), 7.05 – 7.00 (1H, m), 6.63 (1H, dd, *J* 8.5, 1.7 Hz), 5.84 (1H, s), 3.79 (1H, dd, *J* 8.7, 4.8 Hz), 3.72 (3H, s), 3.21 (1H, dd, *J* 15.3, 4.8 Hz), 2.99 (1H, ddd, *J* 15.3, 8.7, 1.3 Hz). **δ_C** (126 MHz, MeOD) 174.9, 155.6 (d, *J* 248.8 Hz), 141.6 (d, *J* 1.3 Hz), 138.3, 132.1, 129.3, 127.9, 126.8 (d, *J* 4.2 Hz), 123.4 (d, *J* 17.4 Hz), 122.9, 122.4 (d, *J* 18.1 Hz), 120.1, 118.9, 112.1, 109.9, 53.1, 52.7, 52.5 (d, *J* 2.2), 25.8. **δ_F** (376 MHz, MeOD) -116.2 (1F, s). **ESI-HRMS**: m/z calculated for $C_{19}H_{16}{}^{35}Cl_2FN_2O_2$ $[M+H]^+$ requires 393.0567. Found 393.0575.

The same procedure also gave **27d** as white crystals (0.54 g, 60 %). **δ_H** (500 MHz, MeOD) 7.45 (1H, d, *J* 7.7 Hz), 7.37 (1H, dd, *J* 8.5, 7.2 Hz), 7.21 (1H, d, *J* 8.0 Hz), 7.09 – 7.03 (2H, m), 7.02 – 6.98 (1H, m), 5.77 (1H, s), 3.96 (1H, dd, *J* 10.9, 4.3 Hz), 3.78 (3H, s), 3.17 (1H, ddd, *J* 15.1, 4.3, 1.7 Hz), 2.95 (1H, ddd, *J* 15.1, 10.9, 2.4 Hz). **δ_C** (126 MHz, MeOD) 174.5, 155.3 (d, *J* 247.9 Hz), 141.1, 138.3, 133.7, 129.9, 128.0, 127.2 – 126.9 (m), 123.9 (d, *J* 17.7 Hz), 122.6, 122.5 (d, *J* 18.0 Hz), 120.0, 118.7, 112.1, 109.6, 57.8, 55.5 – 55.2 (m), 52.7, 26.2. **δ_F** (376 MHz, MeOD) -115.9 (1F, s). **ESI-HRMS**: m/z calculated for $C_{19}H_{16}{}^{35}Cl_2FN_2O_2$ $[M+H]^+$ requires 393.0567. Found 393.0561.

Preparation of methyl (1*R*,3*S*)-1-(2,3,4-trichlorophenyl)-2,3,4,9-tetrahydro-1*H*-pyrido[3,4-*b*]indole-3-carboxylate (26e) and methyl (1*S*,3*S*)-1-(2,3,4-trichlorophenyl)-2,3,4,9-tetrahydro-1*H*-pyrido[3,4-*b*]indole-3-carboxylate (27e)

L-tryptophan methyl ester **13** (0.51 g, 2.33 mmol, 1 eq), 2,3,4-trichlorobenzaldehyde (0.54 g, 2.56 mmol, 1.1 eq), and TFA (0.20 cm^3, 2.56 mmol, 1.1 eq), were used in anhydrous DCM (15 cm^3)

following **general procedure 1**. Gave **26e** as a white solid (0.28 g, 29 %). **δ_H** (500 MHz, DMSO) 10.64 (1H, s), 7.52 (1H, d, *J* 8.5 Hz), 7.48 (1H, d, *J* 7.8 Hz), 7.26 – 7.23 (1H, m), 7.09 – 7.04 (1H, m), 7.02 – 6.97 (1H, m), 6.81 (1H, d, *J* 8.5 Hz), 5.76 (1H, d, *J* 4.2 Hz), 3.76 – 3.71 (1H, m), 3.63 (3H, s), 3.34 (1H, dd, *J* 6.7, 4.5 Hz), 3.13 – 3.07 (1H, m), 2.88 (1H, ddd, *J* 15.1, 7.9, 1.2 Hz). **δ_C** (126 MHz, DMSO) 173.6, 141.2, 136.2, 133.2, 132.4, 131.7, 130.5, 129.2, 128.3, 126.3, 121.3, 118.6, 117.8, 111.2, 107.9, 51.72, 51.70, 51.6, 24.7. **ESI-HRMS**: m/z calculated for $C_{19}H_{16}{}^{35}Cl_3N_2O_2$ $[M+H]^+$ requires 409.0272. Found 409.0268.

The same procedure also gave **27e** as a white solid (0.45 g, 48 %). **δ_H** (500 MHz, DMSO) 10.43 (1H, s), 7.59 (1H, d, *J* 8.5 Hz), 7.46 (1H, d, *J* 7.7 Hz), 7.26 (1H, d, *J* 8.5 Hz), 7.21 (1H, d, *J* 8.0 Hz), 7.05 – 7.00 (1H, m), 6.99 – 6.95 (1H, m), 5.71 (1H, d, *J* 5.6 Hz), 3.96 (1H, dt, 10.8, 4.2 Hz), 3.70 (3H, s), 3.12 – 3.08 (1H, m), 3.08 – 3.03 (1H, m), 2.87 (1H, ddd, *J* 14.7, 10.9, 2.2 Hz). **δ_C** (126 MHz, DMSO) 172.7, 140.7, 136.3, 133.7, 133.3, 131.9, 130.1, 129.8, 128.8, 126.4, 121.1, 118.6, 117.8, 111.2, 107.5, 56.0, 54.9, 51.8, 25.1. **ESI-HRMS**: m/z calculated for $C_{19}H_{16}{}^{35}Cl_3N_2O_2$ $[M+H]^+$ requires 409.0272. Found 409.0268.

Preparation of methyl (1*R*,3*S*)-1-(2,4-dichloro-5-fluorophenyl)-2,3,4,9-tetrahydro-1*H*-pyrido[3,4-*b*]indole-3-carboxylate (26f) and methyl (1*S*,3*S*)-1-(2,4-dichloro-5-fluorophenyl)-2,3,4,9-tetrahydro-1*H*-pyrido[3,4-*b*]indole-3-carboxylate (27f)

L-tryptophan methyl ester **13** (0.51 g, 2.32 mmol, 1 eq), 2,4-dichloro-5-fluoro-benzaldehyde (0.49 g, 2.55 mmol, 1.1 eq) and TFA (0.20 cm^3, 2.55 mmol, 1.1 eq) were used in anhydrous DCM (15 cm^3) following **general procedure 1**. Gave **26f** as awhite solid (0.26 g, 29 %). **δ_H** (500 MHz, $CDCl_3$) 7.70 (1H, s), 7.56 (1H, d, *J* 7.6 Hz), 7.51 (1H, d, *J* 6.5 Hz), 7.27 (1H, d, *J* 8.0 Hz), 7.22 – 7.18 (1H, m), 7.17 – 7.13 (1H, m), 6.89 (1H, d, *J* 9.5 Hz), 5.85 (1H, s), 3.88 (1H, dd, *J* 7.1, 5.2 Hz), 3.73 (3H, s), 3.27 (1H, ddd, *J* 15.3, 5.1, 0.9 Hz), 3.12 (1H, ddd, *J* 15.4, 7.2, 1.4 Hz), 2.79 (1H, s). **δ_C** (126 MHz, $CDCl_3$) 173.9, 157.1 (d, *J* 250.6 Hz), 140.4 (d, *J* 5.3 Hz), 136.4, 131.4, 131.1, 128.6 (d, *J* 3.7 Hz), 126.8, 122.7, 121.5 (d, *J* 19.3 Hz), 120.0, 118.6, 117.9 (d, *J* 23.4 Hz), 111.2, 109.7, 52.5, 52.4, 51.3, 24.8. **δ_F** (376 MHz, $CDCl_3$) -116.0 (1F, s). **ESI-HRMS**: m/z calculated for $C_{19}H_{16}{}^{35}Cl_2FN_2O_2$ $[M+H]^+$ requires 393.0567. Found 393.0562.

The same procedure also gave **27f** as a white solid (0.53 g, 58 %). **δ_H** (500 MHz, $CDCl_3$) 7.57 (1H, s), 7.55 – 7.51 (2H, m), 7.34 (1H, d, *J* 9.6 Hz), 7.24 (1H, apparent d overlapped with $CDCl_3$), 7.19 – 7.15 (1H, apparent td), 7.15 – 7.09 (1H, apparent td), 5.77 (1H, s), 3.98 (1H, dd, *J* 11.0, 4.0 Hz), 3.83 (3H, s), 3.23 (1H, ddd, *J* 15.0, 4.0, 1.8 Hz), 3.01 (1H, ddd, *J* 15.0, 11.0, 2.4 Hz), 2.69 (1H, s). **δ_C** (126 MHz, $CDCl_3$) 172.9, 157.6 (d, *J* 250.7 Hz), 139.9 (br d, *J* 5.7 Hz), 136.4, 132.7, 131.1, 128.3 (d, *J* 3.5), 126.9, 122.5, 121.9 (d, *J* 19.4 Hz), 120.1, 118.5, 118.3 (d, *J* 23.7 Hz), 111.1, 109.6, 56.6, 54.1 (br s), 52.5, 25.4. **δ_F** (376 MHz, $CDCl_3$) -115.2 (1F, s). **ESI-HRMS**: m/z calculated for $C_{19}H_{16}{}^{35}Cl_2FN_2O_2$ $[M+H]^+$ requires 393.0567. Found 393.0566.

Generic structure of compounds 28 – 32 and 35 following general procedure 2

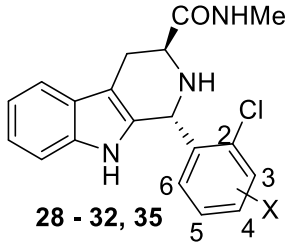

28 - 32, 35

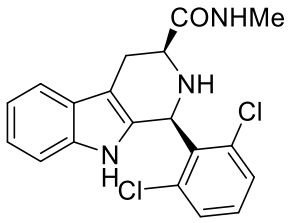

30b

28	X = 4-CF_3
29	X = 4-Br
30a	X = 6-Cl (trans only)
31	X = 3-F, 4-Cl
32	X = 3-Cl, 4-Cl
35	X = 4-Cl, 5-F

Preparation of (1*R*,3*S*)-1-(2-chloro-4-(trifluoromethyl)phenyl)-*N*-methyl-2,3,4,9-tetrahydro-1*H*-pyrido[3,4-*b*]indole-3-carboxamide (28)

Compound **26a** (0.098 g, 0.24 mmol, 1 eq) and methyl amine 33 % in EtOH (4.99 cm^3, 40.08 mmol, 167 eq), were used following **general procedure 2**. Gave **28** a white solid (0.090 g, 91 %). δ_H (500 MHz, DMSO) 10.72 (1H, s), 7.94 (1H, s), 7.74 (1H, apparent q), 7.61 (1H, d, *J* 8.1 Hz), 7.49 (1H, d, *J* 7.8 Hz), 7.25 (1H, d, *J* 8.1 Hz), 7.07 (1H, apparent t), 7.00 (1H, apparent t), 6.90 (1H, d, *J* 8.3 Hz), 5.65 (1H, d, *J* 4.7 Hz), 3.39 – 3.31 (1H, m), 3.19 (1H, dd, *J* 9.5, 5.0 Hz), 3.01 (1H, dd, *J* 15.2, 4.4 Hz), 2.70 (1H, dd, *J* 15.2, 10.2 Hz), 2.59 (3H, d, *J* 4.6 Hz). δ_C (126 MHz, DMSO) 172.8, 144.4, 136.2, 134.4, 132.3, 130.8, 129.4 (q, *J* 32.7 Hz), 126.5, 126.4 (q, *J* 3.6), 123.7 (q, *J* 3.6 Hz), 123.4 (q, *J* 272.5 Hz), 121.2, 118.5, 117.8, 111.2, 109.3, 51.5, 51.0, 25.4, 25.3. δ_F (376 MHz, DMSO) -61.1 (3F, s). **ESI-HRMS**: m/z calculated for $C_{20}H_{18}{}^{35}ClF_3N_3O$ $[M+H]^+$ requires 408.1085. Found 408.1082. **Elemental Analysis** Calculated for $C_{20}H_{17}ClF_3N_3O$ requires C, 58.90 %, H, 4.20 %, N, 10.30 %. Found C, 58.83 %, H, 4.21 %, N, 10.49 %. **IR (neat)**: ν_{max}/cm^{-1}: 3409 (m), 3319 (m), 3251 (br), 3058 (m, br), 2935 – 2841 (m, br), 1672 (m), 1650 (s), 1530 (s), 1315 (vs), 1168 (s), 1127 (s), 740 (s). **Melting Point** °C: 243 – 246 (MeOH). **HPLC** (purity analysis %) found: Purity 100 %; Retention time: 7.98 min / 30 min (0.5 ml/min MeOH, Signal = 254 nm, CHIRACEL OJ column).

Preparation of (1*R*,3*S*)-1-(4-bromo-2-chlorophenyl)-*N*-methyl-2,3,4,9-tetrahydro-1*H*-pyrido[3,4-*b*]indole-3-carboxamide (29)

Compound **26b** (0.14 g, 0.33 mmol, 1 eq) and methyl amine 33 % in EtOH (6.86 cm^3, 55.11 mmol, 167 eq), were used following **general procedure 2**. Gave **29** as a white solid (0.12 g, 87 %). δ_H (500 MHz, DMSO) 10.71 (1H, s), 7.80 (1H, d, *J* 2.0 Hz), 7.72 (1H, q, *J* 4.7 Hz), 7.47 (1H, d, *J* 7.8 Hz), 7.43

(1H, dd, *J* 8.3, 2.0 Hz), 7.25 (1H, d, *J* 8.0 Hz), 7.08 – 7.03 (1H, m), 7.02 – 6.97 (1H, m), 6.62 (1H, d, *J* 8.3 Hz), 5.55 (1H, d, *J* 4.8 Hz), 3.37 – 3.33 (1H, m), 3.09 (1H, dd, *J* 9.6, 5.1 Hz), 3.00 (1H, dd, *J* 15.2, 4.5 Hz), 2.68 (1H, ddd, *J* 15.2, 10.1, 1.2 Hz), 2.59 (3H, d, *J* 4.7 Hz). **δ_C** (126 MHz, DMSO) 172.8, 139.3, 136.2, 134.7, 132.6, 131.7, 131.6, 129.7, 126.5, 121.1, 120.8, 118.5, 117.7, 111.1, 109.2, 51.4, 50.8, 25.4, 25.2. **ESI-HRMS**: m/z calculated for $C_{19}H_{18}{}^{79}Br^{35}ClN_3O$ $[M+H]^+$ requires 418.0316. Found 418.0325. **Elemental Analysis** Calculated for $C_{19}H_{17}BrClN_3O$ requires C, 54.50 %, H, 4.09 %, N, 10.04 %. Found C, 54.39 %, H, 4.09 %, N, 10.03 %. **IR (neat)**: ν_{max}/cm^{-1}: 3385 (m), 3257 (m, br), 3226 (m, br), 3087 (w), 3055 (w), 2933 (w), 2879 (w), 2840 (w), 1650 (s), 1521 (m), 1462 (m), 1450 (m), 745 (s). **Melting Point** °C: 227 – 229 (MeOH). **HPLC** (purity analysis %) found: Purity 100 %; Retention time: 10.85 min / 30 min (0.5 ml/min MeOH, Signal = 254 nm, CHIRACEL OJ column).

Preparation of (1*R*,3*S*)-1-(2,6-dichlorophenyl)-*N*-methyl-2,3,4,9-tetrahydro-1*H*-pyrido[3,4-*b*]indole-3-carboxamide (30a) and (1*S*,3*S*)-1-(2,6-dichlorophenyl)-*N*-methyl-2,3,4,9-tetrahydro-1*H*-pyrido[3,4-*b*]indole-3-carboxamide (30b)

Compound **26c** and **27c** (0.10 g, 0.27 mmol, 1 eq) and methyl amine 33 % in EtOH (5.62 cm^3, 45.09 mmol, 167 eq), were used following **general procedure 2**. *Cis* and *trans* isomers were separated by column chromatography (30 % EtOAc in DCM). Yielded **30a** as a white solid (0.014 g, 14 % isolated yield). **δ_H** (500 MHz, DMSO) 10.51 (1H, s), 7.85 (1H, q, *J* 4.7 Hz), 7.58 (1H, dd, *J* 7.0, 1.9 Hz), 7.40 (1H, d, *J* 7.7 Hz), 7.38 – 7.34 (2H, m), 7.20 – 7.17 (1H, m), 6.98 (1H, apparent td), 6.94 (1H, apparent td), 6.06 (1H, s), 3.91 (1H, br s), 3.11 (2H, ddd, *J* 15.1, 4.3, 1.7 Hz + br peak), 2.92 (1H, ddd, *J* 15.1, 5.7, 1.7 Hz), 2.63 (3H, d, *J* 4.7 Hz). **δ_C** (126 MHz, DMSO) 172.9, 136.4, 136.3, 135.9, 135.2, 132.8, 130.4, 130.0, 128.7, 126.8, 120.4, 118.1, 117.5, 111.0, 106.9, 54.1, 50.3, 25.6, 23.1. **ESI-HRMS**: m/z calculated for $C_{19}H_{18}{}^{35}Cl_2N_3O$ $[M+H]^+$ requires 374.0821. Found 374.0818. **Elemental Analysis** Calculated for $C_{19}H_{17}Cl_2N_3O$ requires C, 60.98 %, H, 4.58 %, N, 11.23 %. Found C, 60.68 %, H, 4.67 %, N, 10.93 %. **IR (neat)**: ν_{max}/cm^{-1}: 3386 (m), 3339 (s), 3226 (m, br), 3069 (m, br), 2926 (m), 2849 (m), 1652 (s), 1527 (m), 1432 (s), 738 (s). **Melting Point** °C: 238 – 240 (MeOH)

30b as a white solid (0.034 g, 34 % isolated yield). **δ_H** (500 MHz, DMSO) 10.54 (1H, s), 7.93 (1H, q, *J* 4.7 Hz), 7.64 – 7.59 (1H, m), 7.43 – 7.39 (3H, m), 7.20 (1H, d, *J* 7.9 Hz), 7.00 (1H, apparent td), 6.97 – 6.93 (1H, m), 6.02 (1H, d, *J* 9.2 Hz), 3.69 (1H, apparent td), 3.03 (1H, ddd, *J* 15.1, 4.1, 1.7 Hz), 2.72 – 2.66 (1H, m), 2.65 (3H, d, *J* 4.7 Hz). **δ_C** (126 MHz, DMSO) 172.5, 136.2, 136.0, 135.1, 134.9, 133.4, 130.5, 130.4, 128.9, 126.7, 120.5, 118.4, 117.5, 111.1, 107.6, 57.5, 54.2, 25.6, 25.4. **ESI-HRMS**: m/z calculated for $C_{19}H_{18}{}^{35}Cl_2N_3O$ $[M+H]^+$ requires 374.0821. Found 374.0821.

Preparation of (1*R*,3*S*)-1-(2,4-dichloro-3-fluorophenyl)-*N*-methyl-2,3,4,9-tetrahydro-1*H*-pyrido[3,4-*b*]indole-3-carboxamide (31)

Compound **26d** (0.10 g, 0.25 mmol, 1 eq) and methyl amine 33 % in EtOH (5.20 cm^3, 41.75 mmol, 167 eq), were used following **general procedure 2**. Gave **31** as white crystals (0.099 g, 99 %). δ_H (500 MHz, DMSO) 10.70 (1H, s), 7.72 (1H, dd, *J* 9.0, 4.4 Hz), 7.52 – 7.42 (2H, m), 7.26 (1H, d, *J* 8.0 Hz), 7.09 – 7.04 (1H, m), 7.02 – 6.97 (1H, m), 6.56 (1H, dd, *J* 8.6, 1.5 Hz), 5.59 (1H, d, *J* 5.0 Hz), 3.36 (1H, td, *J* 10.0, 4.4 Hz), 3.21 – 3.15 (1H, m), 2.99 (1H, dd, *J* 15.2, 4.4 Hz), 2.70 (1H, ddd, *J* 15.2, 10.1, 1.1 Hz), 2.59 (3H, d, *J* 4.7 Hz). δ_C (126 MHz, DMSO) 172.77, 153.4 (d, *J* 246.9 Hz), 141.4 (d, *J* 1.4 Hz), 136.1, 132.2, 127.9, 126.5, 125.7 (d, *J* 3.7 Hz), 121.7 (d, *J* 17.3 Hz), 121.2, 119.6 (d, *J* 17.9 Hz), 118.5, 117.8, 111.2, 109.3, 51.5, 50.8, 25.4, 25.1. δ_F (376 MHz, DMSO) -115.7 (1F, s). **ESI-HRMS**: m/z calculated for $C_{19}H_{17}{}^{35}Cl_2FN_3O$ $[M+H]^+$ requires 392.0727. Found 392.0733. **Elemental Analysis** Calculated for $C_{19}H_{16}{}^{35}Cl_2FN_3O$ requires C, 58.18 %, H, 4.11 %, N, 10.71 %. Found C, 58.16 %, H, 4.08 %, N, 10.71 %. **IR (neat)**: ν_{max}/cm^{-1}: 3376 (w), 3289 (m, br) 2951 (w), 2903 (w), 2857 (w) 1655 (s), 1519 (br), 1451 (s), 1425 (s), 1261 (m), 1217 (m), 811 (s), 745 (s), 589 (s).

Preparation of (1*R*,3*S*)-*N*-methyl-1-(2,3,4-trichlorophenyl)-2,3,4,9-tetrahydro-1*H*-pyrido[3,4-*b*]indole-3-carboxamide (32)

Compound **26e** (0.1 g, 0.24 mmol, 1 eq) and methyl amine 33 % in EtOH (4.99 cm^3, 40.08 mmol, 167 eq), were used following **general procedure 2**. Gave **32** as a white solid (0.088 g, 88 %). δ_H (500 MHz, DMSO) 10.69 (1H, s), 7.72 (1H, q, *J* 4.7 Hz), 7.52 (1H, d, *J* 8.5 Hz), 7.48 (1H, d, *J* 7.8 Hz), 7.25 (1H, d, *J* 8.0 Hz), 7.07 (1H, apparent td), 7.00 (1H, apparent t), 6.66 (1H, d, *J* 8.5 Hz), 5.61 (1H, d, *J* 5.0 Hz), 3.38 – 3.33 (1H, m), 3.18 (1H, dd, *J* 9.9, 5.3 Hz), 2.99 (1H, dd, *J* 15.3, 4.5), 2.69 (1H, dd, *J* 15.3, 10.1 Hz), 2.59 (3H, d, *J* 4.7 Hz). δ_C (126 MHz, DMSO) 172.8, 141.2, 136.1, 133.4, 132.4, 131.6, 130.7, 128.9, 128.0, 126.5, 121.2, 118.5, 117.8, 111.1, 109.3, 51.8, 51.5, 25.4, 25.2. **ESI-HRMS**: m/z calculated for $C_{19}H_{17}{}^{35}Cl_3N_3O$ $[M+H]^+$ requires 408.0432. Found 408.0429. **Elemental Analysis** Calculated for $C_{19}H_{16}Cl_3N_3O$ requires C, 55.84 %, H, 3.95 %, N, 10.28 %. Found C, 55.68 %, H, 3.97 %, N, 10.23 %. **IR (neat)**: ν_{max}/cm^{-1}: 3392 (w), 3290 (m, br), 2922 (w), 2882 (w), 2842 (w), 1666 (s), 1510, (m), 1432 (s), 1172 (s), 746 (s). **Melting Point** °C: 249 – 251 (MeOH)

Preparation of (1*R*,3*S*)-1-(2,4-dichloro-5-fluorophenyl)-*N*-methyl-2,3,4,9-tetrahydro-1*H*-pyrido[3,4-*b*]indole-3-carboxamide (35)

Compound **26f** (0.10 g, 0.25 mmol, 1 eq) and methyl amine 33 % in EtOH (5.20 cm^3, 41.75 mmol, 167 eq), were used following **general procedure 2**. Gave **35** as white crystals (0.087 g, 87 %). δ_H (500 MHz, DMSO) 10.71 (1H, s), 7.90 (1H, d, *J* 6.8 Hz), 7.72 (1H, q *J* 4.7 Hz), 7.49 (1H, d, *J* 7.9 Hz),

7.27 (1H, apparent dt), 7.10 – 7.05 (1H, m), 7.03 – 6.98 (1H, m), 6.58 (1H, d, *J* 9.8 Hz), 5.55 (1H, d, *J* 5.2), 3.42 (1H, td, *J* 9.8, 4.5), 3.15 (1H, dd, *J* 9.8, 5.4 Hz), 3.00 (1H, dd, *J* 15.2, 4.5 Hz), 2.70 (1H, ddd, *J* 15.2, 9.8, 1.2), 2.60 (3H, d, *J* 4.7 Hz). **δ_C** (126 MHz, DMSO) 172.8, 155.6 (d, *J* 247.1 Hz), 141.4 (d, *J* 5.3 Hz), 136.2, 132.1, 131.0, 129.3 (d, *J* 3.4 Hz), 126.4, 121.3, 119.2 (d, *J* 18.9 Hz), 118.6, 117.9, 117.5 (d, *J* 22.9 Hz), 111.2, 109.4, 51.5, 50.9, 25.4, 25.1. **δ_F** (376 MHz, DMSO) -118.2 (1F, s). **ESI-HRMS**: m/z calculated for $C_{19}H_{17}{}^{35}Cl_2FN_3O$ $[M+H]^+$ requires 392.0727. Found 392.0728. **Elemental Analysis** Calculated for $C_{19}H_{16}Cl_2FN_3O$ requires C, 58.18 %, H, 4.11 %, N, 10.71 %. Found C, 58.40 %, H, 4.16 %, N, 10.71 %. **IR (neat)**: ν_{max}/cm^{-1}: 3379 (w), 3293 (m), 3290 (m, br) 3065 (w), 2944 (w), 2902 (w), 2854 (w), 1656 (s), 1520 (m, br), 1464 (s), 1448 (s), 1374 (m), 1357 (m), 1217 (m), 1120 (s), 868 (m), 739 (s), 664 (s), 607 (s). **Melting Point** °C: 256 – 257 (MeOH).

Preparation of (*S*)-2-amino-3-(1*H*-indol-3-yl)-*N*-methylpropanamide (33)

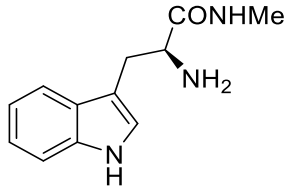

33

L-tryptophan methyl ester **13** (0.5 g, 2.29 mmol, 1 eq) and methyl amine 33 % in EtOH (19.96 cm^3, 160.30 mmol, 70 eq), were used following **general procedure 2**. Gave the desired product **33** as a yellow solid (0.498 g, 99 %). **δ_H** (500 MHz, $CDCl_3$) 8.45 (1H, br s), 7.66 (1H, d, *J* 7.9 Hz), 7.37 (1H, d, *J* 8.1 Hz), 7.28 (1H, s), 7.22 – 7.18 (1H, m), 7.13 – 7.10 (1H, m), 7.06 (1H, d, *J* 2.1 Hz), 3.71 (1H, dd, *J* 9.0, 4.2 Hz), 3.39 (1H, ddd, *J* 14.5, 4.2, 0.8 Hz), 2.92 (1H, dd, *J* 14.5, 9.0 Hz), 2.81 (3H, d, *J* 5.0 Hz). **δ_C** (126 MHz, $CDCl_3$) 175.7, 136.6, 127.6, 123.2, 122.3, 119.7, 119.1, 111.9, 111.4, 55.8, 31.0, 26.0. **CI-HRMS**: m/z calculated for $C_{12}H_{16}N_3O$ $[M+H]^+$ requires 218.1288. Found 218.1292.

Preparation of (1*R*,3*S*)-1-(4,6-dichloropyridin-3-yl)-*N*-methyl-2,3,4,9-tetrahydro-1*H*-pyrido[3,4-*b*]indole-3-carboxamide (36a) and (1*S*,3*S*)-1-(4,6-dichloropyridin-3-yl)-*N*-methyl-2,3,4,9-tetrahydro-1*H*-pyrido[3,4-*b*]indole-3-carboxamide (36b)

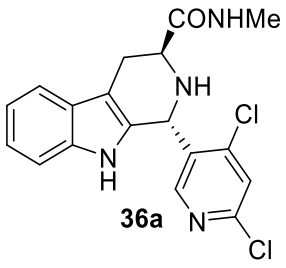

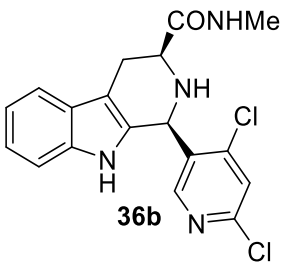

Compound **33** (0.50 g, 2.30 mmol, 1 eq), 4,6-Dichloropyridine-3-carbaldehyde (0.45 g, 2.53 mmol, 1.1 eq), and TFA (0.19 cm^3, 2.53 mmol, 1.1 eq), were used in anhydrous DCM (15 cm^3) following **general procedure 1**. *Cis* and *trans* isomers were separated by column chromatography (50 % EtOAc in DCM). Gave **36a** as a pale yellow solid (0.054 g, 6 % isolated yield). δ_H (500 MHz, DMSO) 10.71 (1H, s), 7.89 (1H, s), 7.74 (1H, br d, *J* 4.7 Hz), 7.61 (1H, s), 7.49 (1H, d, *J* 7.8 Hz), 7.27 (1H, d, *J* 8.0 Hz), 7.08 (1H, apparent t), 7.00 (1H, apparent t), 5.59 (1H, d, *J* 5.2 Hz), 3.40 (1H, td, *J* 10.0, 4.4 Hz), 3.21 (1H, dd, *J* 10.3, 5.5 Hz), 2.98 (1H, dd, *J* 15.2, 4.4 Hz), 2.71 (1H, dd, *J* 15.2, 9.8 Hz), 2.59 (3H, d, *J* 4.7 Hz). δ_C (126 MHz, DMSO) 172.7, 149.8, 149.7, 145.7, 136.1, 135.2, 131.4, 126.5, 124.8, 121.3, 118.6, 117.9, 111.2, 109.6, 51.6, 49.0, 25.4, 25.1. **ESI-HRMS**: m/z calculated for $C_{18}H_{17}{}^{35}Cl_2N_4O$ $[M+H]^+$ requires 375.0774. Found 375.0775. **Elemental Analysis** Calculated for $C_{18}H_{16}Cl_2N_4O$ requires C, 57.61 %, H, 4.30 %, N, 14.93 %. Found C, 57.64 %, H, 4.26 %, N, 15.13 %. **IR (neat)**: ν_{max}/cm^{-1}: 3391 (m), 3318 (m), 3220 (m, br), 3089 (m), 2932 (w), 2895 (w), 2838 (w), 1651 (s), 1567 (s), 1525 (s), 1445 (s), 1329 (m), 834 (s), 751 (s). **Melting Point** °C: 250 – 251 (MeOH). **HPLC** (purity analysis %) found: Purity 100 %; Retention time: 10.18 min / 30 min (0.5 ml/min MeOH, Signal = 254 nm, CHIRACEL OJ column).

36b was isolated as a yellow solid (0.26 g, 31 % isolated yield). δ_H (500 MHz, DMSO) 10.49 (1H, s), 8.27 (1H, s), 7.88 (1H, s), 7.80 (1H, br d, *J* 4.5 Hz), 7.45 (1H, d, *J* 7.7 Hz), 7.22 (1H, d, *J* 8.1 Hz), 7.04 (1H, apparent t), 6.98 (1H,apparent t), 5.59 (1H, d, *J* 5.2 Hz), 3.70 – 3.60 (1H, m), 3.08 – 3.01 (1H, m), 2.97 (1H, s), 2.81 – 2.73 (1H, m), 2.65 (3H, d, *J* 4.7 Hz). δ_C (126 MHz, DMSO) 172.4, 151.7, 149.8, 145.6, 136.3, 134.5, 133.2, 126.6, 124.4, 121.1, 118.6, 117.8, 111.2, 108.6, 57.5, 25.5, 25.3. **ESI-HRMS**: m/z calculated for $C_{18}H_{16}{}^{35}Cl_2N_4NaO$ $[M+H]^+$ requires 397.0593. Found 397.0593.

General Procedure 3: Esterification of amino acids

6-fluoro-DL-tryptophan **42a** (0.50 g, 2.28 mmol, 1 eq) was suspended in anhydrous MeOH (5 cm^3) under an N_2 atmosphere in a flame dried round bottomed flask. The reaction flask was cooled to 0 °C before dropwise addition of thionyl chloride (0.33 cm^3, 4.56 mmol, 2 eq). The reaction vessel was

allowed to slowly warm to room temperature and then stirred overnight. The resulting suspension was basified with the slow addition of saturated sodium bicarbonate solution (50 cm^3) and the resulting solution gently stirred until CO_2 production ceased. The aqueous phase was then extracted with EtOAc (3 x 50 cm^3); combined organics were washed with water (50 cm^3), brine (50 cm^3) and then dried over $MgSO_4$. After filtration the solvents were removed *in vacuo* to yield **43a** as white flakes (0.54 g, 88 %).

Generic structure of compounds 43a – f following general procedure 3

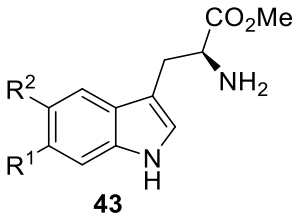

43

43a (racemic)	R^1 = F, R^2 = H
43b	R^1 = F, R^2 = H
43c	R^1 = Cl, R^2 = H
43d	R^1 = H, R^2 = F
43e	R^1 = H, R^2 = Cl
43f	R^1 = H, R^2 = OH

Preparation of methyl 2-amino-3-(6-fluoro-1*H*-indol-3-yl)propanoate (43a)

6-fluoro-DL-tryptophan **42a** (0.50 g, 2.28 mmol, 1 eq) and thionyl chloride (0.33 cm^3, 4.56 mmol, 2 eq), were used in anhydrous MeOH (5 cm^3) following **general procedure 3**. Gave **43a** as white flakes (0.54 g, 88 %). δ_H (400 MHz, DMSO) 10.93 (1H, s), 7.46 (1H, dd, *J* 8.5, 5.7 Hz), 7.15 – 7.07 (2H, m), 6.88 – 6.79 (1H, m), 3.61 (1H, t, *J* 6.3 Hz), 3.54 (3H, s), 2.99 (1H, dd, *J* 14.2, 6.1 Hz), 2.92 (1H, dd, *J* 14.2, 6.4 Hz), 1.77 (2H, br s). δ_C (101 MHz, DMSO) 175.6, 158.8 (d, *J* 233.6 Hz), 135.9 (d, *J* 12.7 Hz), 124.3, 124.2 (d, *J* 3.5 Hz), 119.3 (d, *J* 10.3 Hz), 110.3, 106.7 (d, *J* 24.4 Hz), 97.3 (d, *J* 25.4 Hz), 55.1, 51.3, 30.6. δ_F (376 MHz, DMSO) -122.6 (1F, s). **CI-HRMS**: m/z calculated for $C_{12}H_{14}FN_2O_2$ $[M+H]^+$ requires 237.1034. Found 237.1035.

Preparation of methyl (*S*)-2-amino-3-(6-fluoro-1*H*-indol-3-yl)propanoate (43b)

6-fluoro-L-tryptophan **42b** (0.62 g, 2.84 mmol, 1eq) and thionyl chloride (0.41 cm^3, 5.68 mmol, 2 eq), were used in anhydrous MeOH (5 cm^3) following **general procedure 3**. Gave **43b** as white flakes (0.29 g, 44 %). δ_H (400 MHz, DMSO) 10.91 (1H, s), 7.46 (1H, dd, *J* 8.3, 5.8 Hz), 7.10 (2H, d, *J* 14.4 Hz), 6.88 – 6.79 (1H, apparent t), 3.65 – 3.57 (1H, m), 3.54 (3H, s), 2.99 (1H, dd, *J* 14.2, 6.0 Hz), 2.91 (1H, dd, *J* 14.2, 6.4 Hz), 1.77 (2H, br s). **CI-HRMS**: m/z calculated for $C_{12}H_{14}FN_2O_2$ $[M+H]^+$ requires 237.1034. Found 237.1043

Preparation of methyl (*S*)-2-amino-3-(6-chloro-1*H*-indol-3-yl)propanoate (43c)

6-chloro-L-tryptophan **42c** (0.51 g, 2.11 mmol, 1 eq) and thionyl chloride (0.31 cm^3, 4.23 mmol, 2 eq), were used in anhydrous MeOH (5 cm^3) following **general procedure**. Gave **43c** as white to beige flakes (0.43 g, 85 %). δ_H (400 MHz, DMSO) 11.00 (1H, s), 7.48 (1H, d, *J* 8.4 Hz), 7.37 (1H, s), 7.17 (1H, s), 6.98 (1H, d, *J* 8.4 Hz), 3.61 (1H, t, *J* 6.3 Hz), 3.54 (3H, s), 2.99 (1H, dd, *J* 14.2, 6.1 Hz), 2.92 (1H, dd, *J* 14.2, 6.4 Hz), 1.79 (2H, br s). δ_C (101 MHz, DMSO) 175.6, 136.4, 126.2, 125.6, 124.8, 119.7, 118.6, 110.9, 110.4, 55.1, 51.3, 30.5. **CI-HRMS**: m/z calculated for $C_{12}H_{14}{}^{35}ClN_2O_2$ $[M+H]^+$ requires 253.0738. Found 253.0744

Preparation of methyl (*S*)-2-amino-3-(5-fluoro-1*H*-indol-3-yl)propanoate (43d)

5-fluoro-L-tryptophan monohydrate **42d** (0.50 g, 2.08 mmol, 1eq) and thionyl chloride (0.60 cm^3, 8.32 mmol, 4 eq), were used in anhydrous MeOH (5 cm^3) following **general procedure 3**. Gave **43d** as a white solid (0.47 g, 94 %). δ_H (500 MHz, MeOD) 7.29 (1H, dd, *J* 8.8, 4.4 Hz), 7.18 (1H, d, *J* 9.9 Hz), 7.14 (1H, s), 6.89 – 6.83 (1H, apparent t), 3.75 (1H, t, *J* 6.1 Hz), 3.65 (3H, s), 3.14 (1H, dd, *J* 14.5, 5.9 Hz), 3.08 (1 H, dd, *J* 14.5, 6.5 Hz). δ_C (126 MHz, MeOD) 176.6, 159.0 (d, *J* 232.3 Hz), 134.7, 129.1 (d, *J* 9.6 Hz), 126.7, 113.1 (d, *J* 9.7 Hz), 110.9 (d, *J* 4.8 Hz), 110.6 (d, *J* 26.5 Hz), 103.9 (d, *J* 23.7 Hz), 55.8, 52.4, 31.3. δ_F (376 MHz, MeOD) -129.2 (1F, s). **CI-HRMS**: m/z calculated for $C_{12}H_{14}FN_2O_2$ $[M+H]^+$ requires 237.1034. Found 237.1041.

Preperation of methyl (*S*)-2-amino-3-(5-chloro-1*H*-indol-3-yl)propanoate (43e)

5-chloro-L-tryptophan **42e** (0.50 g, 2.10 mmol, 1 eq) and thionyl chloride (0.31 cm^3, 4.19 mmol, 2 eq), were used in anhydrous MeOH (5 cm^3) following **general procedure 3**. Gave **43d** as brown oil (0.46 g, 87 %). δ_H (500 MHz, $CDCl_3$) 8.25 (1H, s), 7.56 (1H, d, *J* 2.0 Hz), 7.25 (1H, dd, *J* 8.6, 0.5 Hz), 7.13 (1H, dd, *J* 8.6, 2.0 Hz), 7.08 (1H, d, *J* 2.0 Hz), 3.81 (1H, dd, *J* 7.4, 5.0 Hz), 3.72 (3H, s), 3.21 (1H, dd, *J* 14.5, 5.0 Hz), 3.04 (1H, dd, *J* 14.5, 7.4 Hz). δ_C (126 MHz, $CDCl_3$) 175.8, 134.7, 128.7, 125.5, 124.5, 122.6, 118.5, 112.4, 111.1, 54.9, 52.2, 30.6. **CI-HRMS**: m/z calculated for $C_{12}H_{14}{}^{35}ClN_2O_2$ $[M+H]^+$ requires 253.0738. Found 253.0739

Preparation of methyl (*S*)-2-amino-3-(5-hydroxy-1*H*-indol-3-yl)propanoate (43f)

5-hydroxy-L-tryptophan **42f** (0.50 g, 2.28 mmol, 1eq) and thionyl chloride (0.33 cm^3, 4.56 mmol, 2 eq), were used in anhydrous MeOH (5 cm^3) following **general procedure 3**. Gave **43f** pale brown solid (0.37 g, 70 %). δ_H (500 MHz, DMSO) 10.52 (1H, s), 8.58 (1H, s), 7.11 (1H, d, *J* 8.6 Hz), 7.00 (1H, d, *J* 2.3 Hz), 6.79 (1H, d, *J* 2.3 Hz), 6.58 (1H, dd, *J* 8.6, 2.3 Hz), 3.62 – 3.54 (4H, m), 2.93 (1H, dd, *J* 14.2, 6.0 Hz), 2.82 (1H, dd, *J* 14.2, 6.5 Hz), 1.76 (2H, br s). δ_C (126 MHz, DMSO) 175.7, 150.3, 130.7,

128.0, 124.1, 111.6, 111.2, 108.9, 102.2, 55.0, 51.3, 30.9. **CI-HRMS**: m/z calculated for $C_{12}H_{15}N_2O_3$ $[M+H]^+$ requires 235.1077. Found 235.1075.

Generic structure of compounds 44a – f and 45a – f following general procedure 1

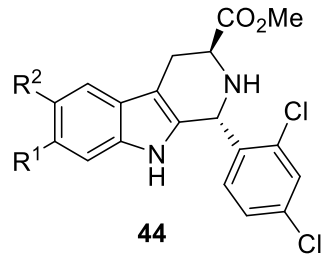

44

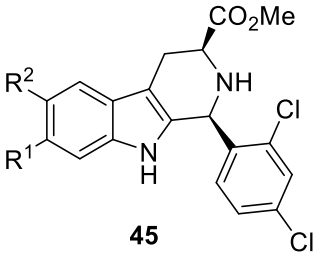

45

44a / 45a (racemic)	R^1 = F, R^2 = H
44b / 45b	R^1 = F, R^2 = H
44c / 45c	R^1 = Cl, R^2 = H
44d / 45d	R^1 = H, R^2 = F
44e / 45e	R^1 = H, R^2 = Cl
44f / 45f	R^1 = H, R^2 = OH

Preparation of methyl (1*R*,3*S* / 1*S*,3*R*)-1-(2,4-dichlorophenyl)-7-fluoro-2,3,4,9-tetrahydro-1*H*-pyrido[3,4-*b*]indole-3-carboxylate (44a) and methyl (1*S*,3*S* / 1*R*,3*R*)-1-(2,4-dichlorophenyl)-7-fluoro-2,3,4,9-tetrahydro-1*H*-pyrido[3,4-*b*]indole-3-carboxylate (45a)

Compound **43a** (0.46 g, 1.93 mmol, 1 eq), 2,4-dichlorobenzaldehyde (0.37 g, 2.12 mmol, 1.1 eq) and TFA (0.16 cm^3, 2.12 mmol, 1.1 eq), were used in anhydrous DCM (10 cm^3) following **general procedure 1**. Gave **44a** as a white solid (0.17 g, 22 %). δ_H (400 MHz, $CDCl_3$) 7.84 (1H, s), 7.49 – 7.41 (2H, m), 7.12 (1H, d, *J* 8.3 Hz), 6.98 – 6.86 (3H, m), 5.80 (1H, s), 3.87 – 3.79 (1H, m), 3.73 (3H, s), 3.21 (1H, dd, *J* 15.4, 4.9 Hz), 3.05 (1H, dd, *J* 15.4, 7.7 Hz), 2.77 (1H, s). δ_C (101 MHz, $CDCl_3$) 173.7, 160.1 (d, *J* 237.9 Hz), 137.7, 136.4 (d, *J* 12.4 Hz), 134.5 (d, *J* 14.0 Hz), 131.9 (d, *J* 3.5 Hz), 130.9, 129.9, 127.3, 123.5, 119.1 (d, *J* 10.2 Hz), 109.7, 108.4 (d, *J* 24.4 Hz), 97.7 (d, *J* 26.3 Hz), 52.4, 52.3, 51.2, 24.8. δ_F (376 MHz, $CDCl_3$) -120.5 (1F, s). **ESI-HRMS**: m/z calculated for $C_{19}H_{16}{}^{35}Cl_2FN_2O_2$ $[M+H]^+$ requires 393.0567. Found 393.0566.

The same procedure also gave **45a** as a white solid (0.55 g, 72 %). δ_H (400 MHz, $CDCl_3$) 7.63 (1H, s), 7.47 (1H, s), 7.45 – 7.36 (2H, m), 7.21 (1H, d, *J* 8.3 Hz), 6.94 – 6.84 (2H, m), 5.79 (1H, s), 3.97 (1H, dd, *J* 10.9, 3.9 Hz), 3.82 (3H, s), 3.19 (1H, dd, *J* 15.1, 2.4 Hz), 3.05 – 2.91 (1H, m), 2.62 (1H, s). δ_C (101 MHz, $CDCl_3$) 173.0, 160.0 (d, *J* 237.8 Hz), 137.2, 136.2 (d, *J* 12.4 Hz), 134.8, 134.2, 133.6 (d, *J* 3.5 Hz), 131.5, 129.5, 128.2, 123.6, 119.0 (d, *J* 10.2 Hz), 109.4, 108.5 (d, *J* 24.4 Hz), 97.7 (d, *J* 26.3 Hz), 56.6,

52.5, 51.0, 25.4. **δ_F** (376 MHz, $CDCl_3$) -120.6 (1F, s). **ESI-HRMS**: m/z calculated for $C_{19}H_{16}{}^{35}Cl_2FN_2O_2$ $[M+H]^+$ requires 393.0567. Found 393.0567.

Preparation of methyl (1*R*,3*S*)-1-(2,4-dichlorophenyl)-7-fluoro-2,3,4,9-tetrahydro-1*H*-pyrido[3,4-*b*]indole-3-carboxylate (44b) and methyl (1*S*,3*S*)-1-(2,4-dichlorophenyl)-7-fluoro-2,3,4,9-tetrahydro-1*H*-pyrido[3,4-*b*]indole-3-carboxylate (45b)

Compound **43b** (0.21 g, 0.91 mmol, 1 eq), 2,4-dichlorobenzaldehyde (0.18 g, 1.00 mmol, 1.1 eq) and TFA (0.08 cm^3, 1.00 mmol, 1.1 eq), were used in anhydrous DCM (5 cm^3) following **general procedure 1**. Gave **44b** as a white solid (0.088 g, 25 %). **δ_H** (500 MHz, MeOD) 7.56 (1H, d, *J* 2.1 Hz), 7.43 (1H, dd, *J* 8.7, 5.3 Hz), 7.21 (1H, dd, *J* 8.4, 2.2 Hz), 6.95 (1H, dd, *J* 10, 2.3 Hz), 6.84 – 6.79 (2H, m), 5.81 (1H, s), 3.79 (1H, dd, *J* 8.6, 4.8 Hz), 3.72 (3H, s), 3.19 (1H, ddd, *J* 15.4, 4.8, 0.8 Hz), 2.98 (1 H, ddd, *J* 15.4, 8.6, 1.4 Hz). **δ_C** (126 MHz, MeOD) 174.8, 161.3 (d, *J* 235.5 Hz), 138.9, 138.3 (d, *J* 12.7 Hz), 135.9, 135.5, 132.9 (d, *J* 3.6 Hz), 132.5, 130.6, 128.2, 124.6, 119.6 (d, *J* 10.0 Hz), 110.0, 108.3 (d, *J* 24.6 Hz), 98.3 (d, *J* 26.2 Hz), 53.0, 52.7, 52.5, 25.6. **δ_F** (376 MHz, MeOD) -123.6 (1F, s). **ESI-HRMS**: m/z calculated for $C_{19}H_{16}{}^{35}Cl_2FN_2O_2$ $[M+H]^+$ requires 393.0567. Found 393.0563.

The same procedure also gave **45b** as a white solid (0.20 g, 57 %). **δ_H** (500 MHz, MeOD) 7.56 (1H, d, *J* 2.0 Hz), 7.40 (1H, dd, *J* 8.6, 5.3 Hz), 7.30 (1H, dd, *J* 8.4, 2.0 Hz), 7.22 (1H, d, *J* 8.4 Hz), 6.92 (1H, dd, *J* 10.0, 2.3 Hz), 6.82 – 6.76 (1H, m), 5.75 (1H, s), 3.96 (1H, dd, *J* 10.8, 4.3 Hz), 3.15 (1H, ddd, *J* 15.2, 4.3, 1.7 Hz), 2.94 (1H, ddd, *J* 15.1, 10.9, 2.4 Hz). **δ_C** (126 MHz, MeOD) 174.4, 161.2 (d, *J* 235.2 Hz), 138.4 (d, *J* 23.4 Hz), 138.2, 136.2, 135.7, 134.6 (d, *J* 2.8 Hz), 133.0 – 132.7 (m), 130.4, 128.9, 124.8, 119.5 (d, *J* 10.1 Hz), 109.7, 108.3 (d, *J* 24.8 Hz), 98.3 (d, *J* 26.2 Hz), 57.7, 52.7, 26.1. **δ_F** (376 MHz, DMSO) -121.9 (1F, s). **ESI-HRMS**: m/z calculated for $C_{19}H_{16}{}^{35}Cl_2FN_2O_2$ $[M+H]^+$ requires 393.0567.

Preparation of methyl (1*R*,3*S*)-1-(2,4-dichlorophenyl)-7-chloro-2,3,4,9-tetrahydro-1*H*-pyrido[3,4-*b*]indole-3-carboxylate (44c) and methyl (1*S*,3*S*)-1-(2,4-dichlorophenyl)-7-chloro-2,3,4,9-tetrahydro-1*H*-pyrido[3,4-*b*]indole-3-carboxylate (45c)

Compound **43c** (0.43 g, 1.70 mmol, 1 eq), 2,4-dichlorobenzaldehyde (0.33 g, 1.87 mmol, 1.1 eq) and TFA (0.14 cm^3, 1.87 mmol, 1.1 eq), were used in anhydrous DCM (10 cm^3) following **general procedure 1**. Gave **44c** as white crystals (0.14 g, 21 %). **δ_H** (500 MHz, $CDCl_3$) 7.77 (1H, s), 7.47 (1H, d, *J* 2.1 Hz), 7.44 (1H, d, *J* 8.4 Hz), 7.24 (1H, d, *J* 1.7 Hz), 7.14 – 7.09 (2H, m) 6.90 (1H, d, *J* 8.4 Hz), 5.81 (1H, s), 3.83 (1H, dd, *J* 7.5, 5.1 Hz), 3.73 (3H, s) 3.21 (1H, ddd, 15.4, 10.4, 0.7 Hz), 3.05 (1H, dd, *J* 15.4, 7.7 Hz), 2.77 (1H, s). **δ_C** (126 MHz, $CDCl_3$) 173.7, 137.6, 136.7, 134.7, 134.5, 132.4, 130.9, 130.0, 128.3, 127.4, 125.5, 120.6, 119.3, 111.2, 109.8, 52.4, 52.3, 51.2, 24.8. **ESI-HRMS**: m/z calculated for $C_{19}H_{16}{}^{35}Cl_3N_2O_2$ $[M+H]^+$ requires 409.0277. Found 409.0272.

The same procedure also gave **45c** as yellow needles (0.29 g, 42 %). δ_H (500 MHz, MeOD) 7.57 (1H, d, *J* 1.7 Hz), 7.40 (1H, d, *J* 8.4), 7.30 (1H, dd, *J* 8.4, 1.8 Hz), 7.25 – 7.20 (2H, m), 6.98 (1H, dd, *J* 8.4, 1.7 Hz), 5.75 (1H, s), 3.96 (1H, dd, *J* 10.9, 4.3 Hz), 3.78 (3H, s), 3.15 (1H, ddd, *J* 15.1, 4.0, 1.3 Hz), 2.93 (1H, ddd, *J* 15.0, 10.9, 2.2 Hz). δ_C (126 MHz, MeOD) 174.3, 138.6, 138.3, 136.2, 135.7, 135.1, 132.9, 130.4, 128.9, 128.4, 126.7, 120.5, 119.8, 112.0, 109.8, 57.7, 52.7, 26.1.

Preparation of methyl (1*R*,3*S*)-1-(2,4-dichlorophenyl)-6-fluoro-2,3,4,9-tetrahydro-1*H*-pyrido[3,4-*b*]indole-3-carboxylate (44d) and methyl (1*S*,3*S*)-1-(2,4-dichlorophenyl)-6-fluoro-2,3,4,9-tetrahydro-1*H*-pyrido[3,4-*b*]indole-3-carboxylate (45d)

Compound **43d** (0.44 g, 1.84 mmol, 1 eq), 2,4-dichlorobenzaldehyde (0.36 g, 2.03 mmol, 1.1 eq) and TFA (0.16 cm^3, 2.03 mmol, 1.1 eq), were used in anhydrous DCM (10 cm^3) following **general procedure 1**. Gave **44d** as a white flakes (0.073 g, 10 %). δ_H (500 MHz, MeOD) 7.58 (1H, d, *J* 2.1 Hz), 7.24 – 7.18 (2H, m), 7.16 (1H, dd, *J* 9.6, 2.5 Hz), 6.85 (1H, apparent td), 6.80 (1H, d, *J* 8.4 Hz), 5.83 (1H, s), 3.80 (1H, dd, *J* 8.6, 4.9 Hz), 3.73 (3H, s), 3.18 (1H, dd, *J* 15.2, 4.9 Hz), 2.97 (1H, ddd, *J* 15.2, 8.6, 1.2 Hz). δ_C (126 MHz, MeOD) 174.8, 159.1 (d, *J* 232.8 Hz), 139.0, 135.9, 135.5, 134.8, 134.6, 132.5, 130.6, 128.24, 128.16, 112.8 (d, *J* 9.6 Hz), 110.7 (d, *J* 26.4 Hz), 110.1 (d, *J* 4.7 Hz), 103.7 (d, *J* 23.6 Hz), 53.0, 52.7, 52.6, 25.6. δ_F (376 MHz, MeOD) -128.9 (1F, s). **ESI-HRMS**: m/z calculated for $C_{19}H_{16}{}^{35}Cl_2FN_2O_2$ $[M+H]^+$ requires 393.0567. Found 393.0569.

The same procedure also gave **45d** as a pale yellow solid (0.30 g, 42 %). δ_H (500 MHz, MeOD) 7.56 (1H, d, *J* 2.1 Hz), 7.30 (1H, dd, *J* 8.4, 2.0 Hz), 7.23 (1H, d, *J* 8.4 Hz), 7.16 (1H, dd, *J* 8.8, 4.4 Hz), 7.12 (1H, dd, *J* 9.6, 2.4 Hz), 6.81 (1H,apparent td), 5.76 (1H, s), 3.96 (1H, dd, *J* 10.9, 4.3 Hz), 3.78 (3H, s), 3.13 (1H, ddd, *J* 15.0, 4.3, 1.6 Hz), 2.93 (1H, ddd, *J* 15.0, 10.9, 2.7 Hz). δ_C (126 MHz, MeOD) 174.4, 159.0 (d, *J* 232.6 Hz), 138.5, 136.2, 136.2, 135.7, 134.8, 132.9 – 132.8 (m), 130.4, 128.8, 128.3 (d, *J* 9.9 Hz), 112.9 (d, *J* 9.7 Hz), 110.4 (d, *J* 26.3 Hz), 109.8 (d, *J* 4.4 Hz), 103.5 (d, *J* 23.6 Hz), 57.7, 55.4, 52.7, 26.2. δ_F (376 MHz, MeOD) -128.9 (1F, s). **ESI-HRMS**: m/z calculated for $C_{19}H_{16}{}^{35}Cl_2FN_2O_2$ $[M+H]^+$ requires 393.0567. Found 393.0564.

Preparation of methyl (1*R*,3*S*)-1-(2,4-dichlorophenyl)-6-chloro-2,3,4,9-tetrahydro-1*H*-pyrido[3,4-*b*]indole-3-carboxylate (44e) and methyl (1*S*,3*S*)-1-(2,4-dichlorophenyl)-6-chloro-2,3,4,9-tetrahydro-1*H*-pyrido[3,4-*b*]indole-3-carboxylate (45e)

Compound **43e** (0.45 g, 1.80 mmol, 1 eq), 2,4-dichlorobenzaldehyde (0.35 g, 1.98 mmol, 1.1 eq) and TFA (0.15 cm^3, 1.98 mmol, 1.1 eq), were used in anhydrous DCM (10 cm^3) following **general procedure 1**. Gave **44e** as a pale to beige solid (0.19 g, 26 %). δ_H (500 MHz, $CDCl_3$) 7.74 (1H, s), 7.51 (1H, d, *J* 2.0 Hz), 7.47 (1H, d, *J* 2.1 Hz), 7.17 (1H, dd, *J* 8.6, 0.5 Hz), 7.15 – 7.10 (2H, m), 6.94 (1H, d, *J* 8.4

Hz), 5.84 (1H, s), 3.86 (1H, dd, *J* 7.2, 5.1 Hz), 3.73 (3H, s), 3.20 (1H, ddd, *J* 15.3, 5.1, 1.1 Hz), 3.06 (1H, ddd, *J* 15.3, 7.3, 1.5 Hz). **δ_C** (126 MHz, $CDCl_3$) 173.7, 137.7, 134.7, 134.4, 133.3, 130.9, 129.9, 128.0, 127.5, 125.7, 122.7, 118.1, 112.1, 109.4, 52.4, 51.2, 24.7. **ESI-HRMS**: m/z calculated for $C_{19}H_{16}{}^{35}Cl_3N_2O_2$ $[M+H]^+$ requires 409.0272. Found 409.0287.

The same procedure also gave **45e** as a pale to beige solid (0.43 g, 59 %). **δ_H** (500 MHz, $CDCl_3$) 7.58 (1H, s), 7.49 (1H, d, *J* 2.0 Hz), 7.48 (1H, d, *J* 2.1 Hz), 7.40 (1H, d, *J* 8.4 Hz), 7.22 (1H, dd, *J* 8.4, 2.1 Hz), 7.14 (1H, dd, *J* 8.6, 0.5 Hz), 7.10 (1H, dd, *J* 8.6, 2.0 Hz), 5.77 (1H, s), 3.97 (1H, dd, *J* 11.0, 4.1 Hz), 3.82 (3H, s), 3.18 (1H, ddd, *J* 15.1, 4.1, 1.8 Hz), 2.97 (1H, ddd, *J* 15.1, 11.0, 2.5 Hz). **δ_C** (126 MHz, $CDCl_3$) 172.9, 134.94, 134.91, 134.6, 134.2, 131.51, 131.47, 129.6, 128.3, 128.2, 125.7, 122.5, 118.0, 112.1, 109.2, 56.6, 52.5, 25.4. **ESI-HRMS**: m/z calculated for $C_{19}H_{16}{}^{35}Cl_3N_2O_2$ $[M+H]^+$ requires 409.0272. Found 409.0263.

Preparation of methyl (1*R*,3*S*)-1-(2,4-dichlorophenyl)-6-hydroxy-2,3,4,9-tetrahydro-1*H*-pyrido[3,4-*b*]indole-3-carboxylate (44f) and methyl (1*S*,3*S*)-1-(2,4-dichlorophenyl)-6-hydroxy-2,3,4,9-tetrahydro-1*H*-pyrido[3,4-*b*]indole-3-carboxylate (45f)

Compound **43f** (0.37 g, 1.59 mmol, 1 eq), 2,4-dichlorobenzaldehyde (0.31 g, 1.75 mmol, 1.1 eq) and TFA (0.13 cm^3, 1.75 mmol, 1.1 eq), were used in anhydrous DCM (10 cm^3) following **general procedure 1**. Gave **44f** as a brown solid (0.093 g, 15 %). **δ_H** (500 MHz, DMSO) 10.32 (1H, s), 8.62 (1H, s), 7.67 (1H, d, *J* 2.1 Hz), 7.31 (1H, dd, *J* 8.4, 2.0 Hz), 7.02 (1H, d, *J* 8.6 Hz), 6.82 (1H, d, *J* 8.4 Hz), 6.76 (1H, d, *J* 2.0 Hz), 6.57 (1H, dd, *J* 8.6, 2.1 Hz), 5.65 (1H, d, *J* 3.3 Hz), 3.69 – 3.64 (1H, m), 3.63 (3H, s) 3.17 (1H, d, *J* 5.2 Hz), 2.99 (1H, dd, *J* 15.0, 4.9 Hz), 2.78 (1H, dd, *J* 15.0, 8.5 Hz). **δ_C** (126 MHz, DMSO) 173.6, 150.5, 139.0, 134.1, 133.0, 132.6, 131.5, 130.6, 128.9, 127.0, 111.5, 111.1, 107.0, 102.0, 51.7, 51.6, 50.6, 24.8. **ESI-HRMS**: m/z calculated for $C_{19}H_{17}{}^{35}Cl_2N_2O_3$ $[M+H]^+$ requires 391.0611. Found 391.0608.

The same procedure also gave **45f** as a brown solid (0.35 g, 56 %). **δ_H** (500 MHz, DMSO) 10.07 (1H, s), 8.59 (1H, s), 7.67 (1H, d, *J* 2.1 Hz), 7.38 (1H, dd, *J* 8.4, 2.0 Hz), 7.26 (1H, d, *J* 8.4 Hz), 7.00 (1H, d, *J* 8.6 Hz), 6.73 (1H, d, *J* 2.1 Hz), 6.54 (1H, dd, *J* 8.6, 2.2 Hz), 5.60 (1H, d, *J* 5.6 Hz), 3.95 – 3.88 (1H, m), 3.69 (3H, s), 2.93 (1H, dd, *J* 14.7, 3.5 Hz), 2.84 (1H, apparent t), 2.82 – 2.75 (1H, m). **δ_C** (126 MHz, DMSO) 172.8, 150.4, 138.4, 134.3, 134.2, 132.8, 130.8, 128.7, 127.5, 127.1, 111.5, 111.0, 106.7, 101.8, 56.1, 51.8, 48.6, 25.2. **ESI-HRMS**: m/z calculated for $C_{19}H_{17}{}^{35}Cl_2N_2O_3$ $[M+H]^+$ requires 391.0611. Found 391.0607.

Generic structure of compounds 46 – 51 following general procedure 2

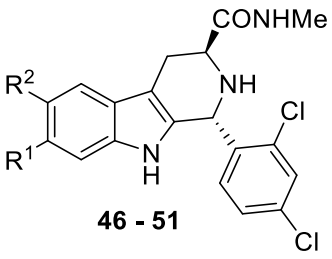

46 - 51

46 (racemic)	R^1 = F, R^2 = H
47	R^1 = F, R^2 = H
48	R^1 = Cl, R^2 = H
49	R^1 = H, R^2 = F
50	R^1 = H, R^2 = Cl
51	R^1 = H, R^2 = OH

Preparation of (1*R*,3*S* / 1*S*,3*R*)-1-(2,4-dichlorophenyl)-7-fluoro-*N*-methyl-2,3,4,9-tetrahydro-1*H*-pyrido[3,4-*b*]indole-3-carboxamide (46)

Compound **44a** (0.17 g, 0.43 mmol, 1 eq) and methyl amine 33 % in EtOH (8.98 cm^3, 71.81 mmol, 167 eq), were used following **general procedure 2**. Gave **46** as white crystals (0.10 g, 61 %). δ_H (500 MHz, DMSO) 10.84 (1H, s), 7.71 (1H, q, *J* 4.7 Hz), 7.68 (1H, d, *J* 2.1 Hz), 7.46 (1H, dd, *J* 8.6, 5.6 Hz), 7.31 (1H, dd, *J* 8.3, 2.1 Hz), 7.03 (1H, dd, *J* 10.1, 2.2 Hz), 6.89 – 6.82 (1H, m), 6.70 (1H, d, *J* 8.3 Hz), 5.54 (1H, d, *J* 3.7 Hz), 3.37 – 3.33 (1H, m), 3.09 (1H, dd, *J* 9.3, 4.9 Hz), 2.98 (1H, dd, *J* 15.3, 4.5 Hz), 2.67 (1H, dd, *J* 15.3, 10.0 Hz), 2.59 (3H, d, *J* 4.7 Hz). δ_C (126 MHz, DMSO) 172.7, 158.9 (d, *J* 233.8 Hz), 138.7, 136.0 (d, *J* 12.6 Hz), 134.5, 133.3 (d, *J* 3.4 Hz), 132.6, 131.2, 129.1, 126.8, 123.4, 118.6 (d, *J* 10.1 Hz), 109.4, 106.7 (d, *J* 24.1 Hz), 97.3 (d, *J* 25.6 Hz). δ_F (376 MHz, DMSO) -121.8 (1F, s). **ESI-HRMS**: m/z calculated for $C_{19}H_{17}{}^{35}Cl_2FN_3O$ $[M+H]^+$ requires 392.0727. Found 392.0727. **Elemental Analysis** Calculated for $C_{19}H_{16}{}^{35}Cl_2FN_3O$ requires C, 58.18 %, H, 4.11 %, N, 10.71 %. Found C, 58.54 %, H, 4.18 %, N, 10.39 %. **IR (neat)**: ν_{max}/cm^{-1}: 3391 (w), 3378 (w), 3288 (m, br), 3241 (m, br), 2919 (w), 2846 (w), 1658 (s), 1531 (m), 1466 (m), 1132 (s), 835 (s), 611(s). **Melting Point** °C: 236 – 238 (MeOH). **HPLC** (purity analysis %) found: Purity peak 1 53 %; Retention time: 8.90 min: Purity peak 2 47 %; Retention time: 17.29 min / 30 min (0.5 ml/min MeOH, Signal = 254 nm, CHIRACEL OJ column).

Preparation of (1*R*,3*S*)-1-(2,4-dichlorophenyl)-7-fluoro-*N*-methyl-2,3,4,9-tetrahydro-1*H*-pyrido[3,4-*b*]indole-3-carboxamide (47)

Compound **44b** (0.11 g, 0.29 mmol, 1 eq) and methyl amine 33 % in EtOH (6.03 cm^3, 48.43 mmol, 167 eq), were used following **general procedure 2**. Gave **47** as white crystals (0.11 g, 98 %). δ_H (500 MHz, DMSO) 10.84 (1H, s), 7.72 (1H, dd, *J* 9.2, 4.5 Hz), 7.68 (1H, d, *J* 2.2 Hz), 7.46 (1H, dd, *J* 8.6, 5.5 Hz), 7.31 (1H, dd, *J* 8.3, 2.2 Hz), 7.03 (1H, dd, *J* 10.1, 2.3 Hz), 6.85 (1H, ddd, *J* 11.0, 8.7, 2.3 Hz), 6.70 (1H, d, *J* 8.4 Hz), 5.54 (1H, d, *J* 4.8 Hz), 3.09 (1H, dd, *J* 9.7, 5.1 Hz), 2.98 (1H, dd, *J* 15.3, 4.5 Hz), 2.67

(1H, ddd, *J* 15.3, 9.9, 1.2 Hz), 2.59 (3H, d, *J* 4.6 Hz). **δ_C** (126 MHz, DMSO) 172.7, 158.9 (d, *J* 233.6 Hz), 138.7, 136.0 (d, *J* 12.5 Hz), 134.5, 133.3 (d, *J* 3.6 Hz), 132.6, 131.2, 129.1, 126.8, 123.4, 118.6 (d, *J* 10.5 Hz), 109.4, 106.7 (d, *J* 24.2 Hz), 97.3 (d, *J* 25.5 Hz), 51.4, 50.7, 25.4, 25.1. **δ_F** (376 MHz, DMSO) -121.8 (1F, s). **ESI-HRMS**: m/z calculated for $C_{19}H_{17}{}^{35}Cl_2FN_3O$ $[M+H]^+$ requires 392.0727. Found 392.0723. **Elemental Analysis** Calculated for $C_{19}H_{16}{}^{35}Cl_2FN_3O$ requires C, 58.18 %, H, 4.11 %, N, 10.71 %. Found C, 58.03 %, H, 4.14 %, N, 10.77 %. **IR (neat)**: ν_{max}/cm^{-1}: 3378 (w), 3355 (w), 3251 (m, br), 3240 (m, br), 2932 (w), 2852 (w), 1668 (s), 1523 (m), 1486 (m), 1133 (s), 826 (s), 794 (s), 611(s). **Melting Point** °C: 236 – 237 (MeOH). **HPLC** (purity analysis %) found: Purity 100 %; Retention time: 8.89 min / 30 min (0.5 ml/min MeOH, Signal = 254 nm, CHIRACEL OJ column).

Crystal data and structure refinement for 47

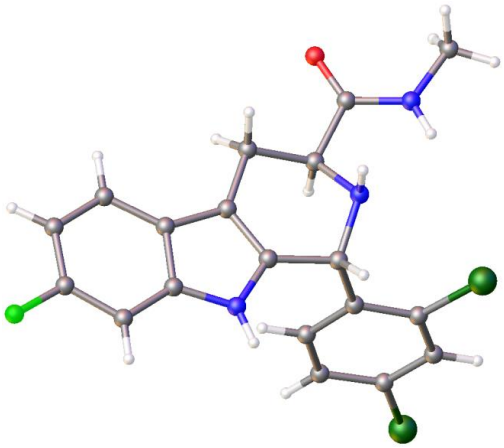

Identification code	**47**
Empirical formula	$C_{19}H_{16}Cl_2FN_3O$
Formula weight	402.16
Temperature/K	150.0
Crystal system	orthorhombic
Space group	$P2_12_12_1$
a/Å	8.3239(5)
b/Å	16.0808(7)
c/Å	27.5875(13)
α/°	90
β/°	90
γ/°	90
Volume/Å^3	3692.7(3)
Z	8
ρ_{calc}g/cm^3	1.447
μ/mm^{-1}	3.681
F(000)	1651.0
Radiation	CuKα (λ = 1.54178)
2Θ range for data collection/°	6.362 to 144.14

Index ranges	$-5 \leq h \leq 9$, $-19 \leq k \leq 19$, $-29 \leq l \leq 34$
Reflections collected	22728
Independent reflections	6865 [R_{int} = 0.0399, R_{sigma} = 0.0454]
Data/restraints/parameters	6865/415/479
Goodness-of-fit on F^2	1.062
Final R indexes [I>=2σ (I)]	R_1 = 0.0439, wR_2 = 0.1106
Final R indexes [all data]	R_1 = 0.0458, wR_2 = 0.1121
Largest diff. peak/hole / e $Å^{-3}$	0.54/-0.52
Flack parameter	0.094(5)

Preparation of (1*R*,3*S*)-1-(2,4-dichlorophenyl)-7-chloro-*N*-methyl-2,3,4,9-tetrahydro-1*H*-pyrido[3,4-*b*]indole-3-carboxamide (48)

Compound **44c** (0.13 g, 0.32 mmol, 1 eq) and methyl amine 33 % in EtOH (6.66 cm^3, 53.44 mmol, 167 eq), were used following **general procedure 2**. Gave **48** as white shards (0.042 g, 32 %). δ_H (500 MHz, DMSO) 10.91 (1H, s), 7.72 (1H, dd, *J* 9.2, 4.5 Hz), 7.69 (1H, d, *J* 2.2 Hz), 7.49 (1H, d, *J* 8.4 Hz), 7.30 (2H, dd, *J* 8.3, 2.2 Hz), 7.01 (1H, dd, *J* 8.4, 1.9 Hz), 6.68 (1H, d, *J* 8.3 Hz), 5.56 (1H, d, *J* 4.9 Hz), 3.38 – 3.33 (1H, m), 3.11 (1H, dd, *J* 9.8, 5.2 Hz), 2.99 (1H, dd, *J* 15.3, 4.5 Hz), 2.67 (1H, ddd, *J* 15.3, 9.9, 1.2 Hz), 2.59 (3H, d, *J* 4.7 Hz). δ_C (101 MHz, DMSO) 172.7, 138.6, 136.5, 134.6, 133.9, 132.7, 131.2, 129.2, 126.9, 125.8, 125.3, 119.1, 118.8, 110.8, 109.5, 51.4, 50.7, 25.5, 25.0. **ESI-HRMS**: m/z calculated for $C_{19}H_{17}{}^{35}Cl_3N_3O$ $[M+H]^+$ requires 408.0432. Found 408.0440. **Elemental Analysis** Calculated for $C_{19}H_{16}Cl_3N_3O$ requires C, 55.84 %, H, 3.95 %, N, 10.28 %. Found C, 55.97 %, H, 3.95 %, N, 10.33 %. **IR (neat)**: ν_{max}/cm^{-1}: 3374 (w), 3281 (m), 3178 (m, br), 2933 (w, br), 1659 (s), 1525 (m), 1466 (s), 794 (s). **Melting Point** °C: 235 – 237 (MeOH) **HPLC** (purity analysis %) found: Purity 100 %; Retention time: 11.09 min / 30 min (0.5 ml/min MeOH, Signal = 254 nm, CHIRACEL OJ column).

Crystal data and structure refinement for 48

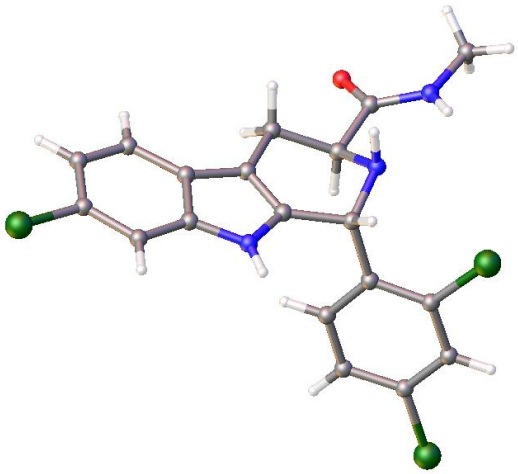

Identification code	**48**
Empirical formula	$C_{19}H_{16}Cl_3N_3O$
Formula weight	408.70
Temperature/K	112.23
Crystal system	orthorhombic
Space group	$P2_12_12_1$
a/Å	8.8830(6)
b/Å	16.1996(7)
c/Å	26.8261(11)
α/°	90
β/°	90
γ/°	90
Volume/Å^3	3860.3(3)
Z	8
ρ_{calc}g/cm^3	1.406
μ/mm^{-1}	4.406
F(000)	1680.0
Radiation	CuKα (λ = 1.54178)
2Θ range for data collection/°	46.552 to 133.17
Index ranges	-6 ≤ h ≤ 10, -19 ≤ k ≤ 12, -30 ≤ l ≤ 31
Reflections collected	6358
Independent reflections	5191 [R_{int} = 0.0254, R_{sigma} = 0.0672]
Data/restraints/parameters	5191/0/479
Goodness-of-fit on F^2	1.034
Final R indexes [I>=2σ (I)]	R_1 = 0.0353, wR_2 = 0.0901
Final R indexes [all data]	R_1 = 0.0369, wR_2 = 0.0912
Largest diff. peak/hole / e Å^{-3}	0.30/-0.36
Flack parameter	0.034(7)

Preparation of (1*R*,3*S*)-1-(2,4-dichlorophenyl)-6-fluoro-*N*-methyl-2,3,4,9-tetrahydro-1*H*-pyrido[3,4-*b*]indole-3-carboxamide (49)

Compound **44d** (0.062 g, 0.16 mmol, 1 eq) and methyl amine 33 % in EtOH (3.32 cm^3, 26.72 mmol, 167 eq), were used following **general procedure 2**. Gave **49** as white crystals (0.050 g, 82 %). δ_H (500 MHz, MeOD) 7.56 (1H, d, *J* 2.1 Hz), 7.22 – 7.17 (2H, m), 7.16 (1H, dd, *J* 9.6, 2.5 Hz), 6.85 (1H, td, *J* 9.2, 2.5 Hz), 6.72 (1H, d, *J* 8.3 Hz), 5.72 (1H, s), 3.53 (1H, dd, *J* 10.2, 4.5 Hz), 3.13 (1H, dd, *J* 15.2, 4.5 Hz), 2.82 (1H, ddd, *J* 15.2, 10.3, 1.0 Hz), 2.75 (3H, s). δ_C (126 MHz, MeOD) 175.8, 159.0 (d, *J* 232.6 Hz), 139.1, 136.3, 135.3, 135.1, 134.7, 132.4, 130.7, 128.3 (d, *J* 9.8 Hz), 127.9, 112.8 (d, *J* 9.7 Hz), 110.9 (d, *J* 4.6 Hz), 110.6 (d, *J* 26.3 Hz), 103.6 (d, *J* 23.6), 53.2, 52.8 (s), 26.3, 26.1. δ_F (376 MHz, MeOD) -127.5 (1F, s). **ESI-HRMS**: m/z calculated for $C_{19}H_{17}{}^{35}Cl_2FN_3O$ $[M+H]^+$ requires 392.0727. Found 392.0730. **Elemental Analysis** Calculated for $C_{19}H_{16}{}^{35}Cl_2FN_3O$ requires C, 58.18 %, H, 4.11 %, N, 10.71 %. Found C, 58.15 %, H, 4.13 %, N, 10.81 %. **IR (neat)**: ν_{max}/cm^{-1}: 3382 (w), 3278 (m, br), 2943 (w), 2903 (w), 2853 (w, br), 1660 (s), 1517 (m), 1489 (s), 1469 (s), 1133 (s), 823 (s), 794 (s). **HPLC** (purity analysis %) found: Purity 100 %; Retention time: 8.11 min / 30 min (0.5 ml/min MeOH, Signal = 254 nm, CHIRACEL OJ column).

Preparation of (1*R*,3*S*)-1-(2,4-dichlorophenyl)-6-chloro-*N*-methyl-2,3,4,9-tetrahydro-1*H*-pyrido[3,4-*b*]indole-3-carboxamide (50)

Compound **44e** (0.12 g, 0.29 mmol, 1eq) and methyl amine 33 % in EtOH (6.03 cm^3, 48.43 mmol, 167 eq), were used following **general procedure 2**. Gave **50** as a white solid (0.12 g, 99 %). δ_H (500 MHz, DMSO) 10.94 (1H, s), 7.72 (1H, q, *J* 4.6 Hz), 7.69 (1H, d, *J* 2.2 Hz), 7.51 (1H, d, *J* 2.0 Hz), 7.31 (1H, dd, *J* 8.3, 2.2 Hz), 7.26 (1H, d, *J* 8.6 Hz), 7.05 (1H, dd, *J* 8.6, 2.1 Hz), 6.68 (1H, d, *J* 8.4 Hz), 5.57 (1H, d, *J* 4.9 Hz), 3.35 (1H, td, *J*, 9.8, 4.5 Hz), 3.12 (1H, dd, *J* 9.8, 5.2 Hz), 2.97 (1H, dd, *J* 15.3, 4.5 Hz), 2.67 (1H, ddd, *J* 15.3, 9.9, 1.0 Hz), 2.59 (3H, d, *J* 4.6 Hz). δ_C (126 MHz, DMSO) 172.7, 138.6, 134.7, 134.6, 134.5, 132.7, 131.2, 129.1, 127.7, 126.8, 123.2, 121.0, 117.1, 112.6, 109.2, 51.4, 50.7, 25.4, 24.9. **ESI-HRMS**: m/z calculated for $C_{19}H_{17}{}^{35}Cl_3N_3O$ $[M+H]^+$ requires 408.0432. Found 408.0434. **Elemental Analysis** Calculated for $C_{19}H_{16}Cl_3N_3O$ requires C, 55.84 %, H, 3.95 %, N, 10.28 %. Found C, 55.81 %, H, 3.94 %, N, 10.28 %. **IR (neat)**: ν_{max}/cm^{-1}: 3377 (w), 3280 (s, br), 3178 (m, br), 2936 (w, br), 2903 (w, br), 2870 (w, br), 2849 (w, br), 1656 (s), 1519 (m), 1449 (s), 827 (s), 801 (s). **Melting Point** ^oC: 243 – 246 (MeOH). **HPLC** (purity analysis %) found: Purity 100 %; Retention time: 9.35 min / 30 min (0.5 ml/min MeOH, Signal = 254 nm, CHIRACEL OJ column).

Preparation of (1*R*,3*S*)-1-(2,4-dichlorophenyl)-6-hydroxy-*N*-methyl-2,3,4,9-tetrahydro-1*H*-pyrido[3,4-*b*]indole-3-carboxamide (51) Contaminated with 16 % *cis* product

Compound **44f** (0.078 g, 0.20 mmol, 1 eq) and methyl amine 33 % in EtOH (4.16 cm^3, 33.4 mmol, 167 eq), were used following **general procedure 2**. Gave **51** as a brown solid (0.069 g, 89 %). δ_H (500 MHz, MeOD) 7.54 (1H, d, *J* 2.1 Hz), 7.17 (1H, dd, *J* 8.3, 2.1 Hz), 7.07 (1H, d, *J* 8.6 Hz), 6.88 (1H, d, *J* 2.3 Hz), 6.72 (1H, d, *J* 8.4 Hz), 6.66 (1H, dd, *J* 8.6, 2.4 Hz), 5.66 (1H, s), 3.49 (1H, dd, *J* 10.4, 4.5 Hz), 3.09 (1H, dd, *J* 15.2, 4.5 Hz), 2.80 – 2.76 (1H, m), 2.74 (3H, s). δ_C (126 MHz, MeOD) 175.9, 151.5, 151.4, 139.2, 136.2, 135.2, 133.6, 133.1, 132.5, 130.6, 128.7, 127.8, 112.5, 110.0, 103.3, 53.2, 52.9, 26.3. **ESI-HRMS**: m/z calculated for $C_{19}H_{18}{}^{35}Cl_2N_3O_2$ $[M+H]^+$ requires 390.0771. Found 390.0771. **Elemental Analysis** Calculated for $C_{19}H_{17}Cl_2N_3O_2$ requires C, 58.48 %, H, 4.39 %, N, 10.77 %. Found C, 56.42 %, H, 4.36 %, N, 10.13 %.

General Procedure 4: Formation of racemic *N*-Ac tryptophan derivatives following published procedure

To 5, 6-difluoroindole **52a** (3.03 g, 19.8 mmol, 1 eq) was added AcOH (50 cm^3). The reaction flask was evacuated and backfilled with N_2, Ac_2O (16 cm^3) followed by L-serine (4.16 g, 39.6 mmol, 2 eq) were added sequentially to the flask. The flask was equipped with a reflux condenser and the system was evacuated again before backfilling with N_2. The reaction mixture was heated to 80 °C for two hours. After the reaction was allowed to cool, the reaction mixture was diluted with Et_2O (150 cm^3) and basified with 30 % NaOH slowly until pH 11 – 12. The aqueous layer was extracted with Et_2O (3 x 150 cm^3), combined organics were washed further with 2 M NaOH (3 x 50 cm^3), the aqueous layers were combined. A few drops of 1 M sodium thiosulfate were added to the aqueous layers before the solution was acidified to pH 7 using 12 M HCl. The volume of the aqueous solution was reduced by 75 %, if precipitates occurred these were collected by filtration and analysed by NMR, if they were deemed to be product they were combined to the total yield at the end of the procedure otherwise they were discarded. The remaining aqueous solution was acidified to approximately pH 3 with 12 M HCl and was extracted with EtOAc (3 x 100 cm^3). Combined organics were washed with water (50 cm^3) followed by brine (50 cm^3). Organics were dried over $MgSO_4$ and filtered; solvents were removed *in vacuo* to yield the product as a thick brown oil. To this oil was added MeOH (20 cm^3) and solvent again removed *in vavuo*, this was repeated until the product **53a** solidified as a dark brown powder (5.10 g, 91 %). Product was used without further purification.

Generic structure of compounds 53a – c following general procedure 4

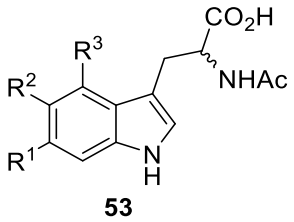

53

53a	R^1 = F, R^2 = F, R^3 = H
53b	R^1 = F, R^2 = H, R^3 = F
53c	R^1 = Cl, R^2 = F, R^3 = H

Preparation of 2-acetamido-3-(5,6-difluoro-1*H*-indol-3-yl)propanoic acid (53a)

5, 6-difluoroindole **52a** (3.03 g, 19.8 mmol, 1 eq), AcOH (50 cm^3), Ac_2O (16 cm^3) and L-serine (4.16 g, 39.6 mmol, 2 eq), were used following **general procedure 4** gave **53a** as a dark brown powder (5.10 g, 91 %). δ_H (500 MHz, MeOD) 10.49 (1H, s), 7.35 (1H, dd, *J* 11.3, 7.9 Hz), 7.16 (1H, dd, *J* 11.1, 6.8 Hz), 7.13 (1H, d, *J* 2.0 Hz), 4.69 (1H, dd, *J* 7.9, 5.3 Hz), 3.27 (1H, ddd, *J* 14.8, 5.3, 0.5 Hz), 3.11 (1H, dd, *J* 14.8, 7.9 Hz), 1.91 (3H, s). δ_C (126 MHz, MeOD) 175.0, 173.2, 149.0 (dd, *J* 206.1, 15.4 Hz), 147.2 (dd, *J* 203.3, 15.5 Hz), 133.0 (dd, *J* 19.3, 10.5 Hz), 126.2 (dd, *J* 20.8, 3.5 Hz), 124.3 (dd, *J* 7.7, 4.4 Hz), 112.2 – 111.1 (m), 105.7 (d, *J* 19.2 Hz), 99.9 (dd, *J* 21.5, 6.2 Hz), 54.6, 28.4, 22.4. δ_F (376 MHz, MeOD) -147.9 (1F, d, *J* 20.2 Hz), -151.2 (1F, d, *J* 20.2 Hz). **ESI-HRMS**: m/z calculated for $C_{13}H_{13}F_2N_2O_3$ $[M+H]^+$ requires 283.0889. Found 283.0893.

Preparation of 2-acetamido-3-(4,6-difluoro-1*H*-indol-3-yl)propanoic acid (53b)

4, 6-difluoroindole **52b** (2.00 g, 13.1 mmol, 1 eq), AcOH (33 cm^3), Ac_2O (11 cm^3) and L-serine (2.75 g, 26.1 mmol, 2 eq), were used following **general procedure 4**, reaction yielded multiple products, and the desired product was purified by column chromatography (100 % EtOAc) gave **53b** as a pale brown powder (0.60 g, 19 %). δ_H (500 MHz, MeOD) 10.67 (1H, s), 7.04 (1 H, d, *J* 1.8 Hz), 6.87 (1H, dd, *J* 9.4, 2.1 Hz), 6.55 (1H, ddd, *J* 11.4, 10.1, 2.0 Hz), 4.74 (1H, dd, *J* 8.9, 5.1 Hz), 3.44 – 3.39 (1H, m), 3.12 (1H, dd, *J* 14.8, 8.9 Hz), 1.90 (3H, s). δ_C (126 MHz, MeOD) 175.1, 173.2, 160.3 (dd, *J* 236.7, 12.1 Hz), 157.7 (dd, *J* 246.4, 14.9 Hz), 140.1 – 139.7 (m), 125.4 – 125.1 (m), 114.1 – 113.8 (m), 110.1 – 110.0 (m), 95.1 (dd, *J* 29.1, 24.4 Hz), 94.6 (dd, *J* 26.0, 4.4 Hz), 54.9 (s), 29.5 (s), 22.3 (s). δ_F (376 MHz, MeOD) -122.1 (1F, d, *J* 4.0 Hz), -123.0 (1F, d, *J* 4.0 Hz). **ESI-HRMS**: m/z calculated for $C_{13}H_{12}F_2N_2NaO_3$ $[M+Na]^+$ requires 305.0708. Found 305.0711.

Preparation of 2-acetamido-3-(6-chloro-5-fluoro-1*H*-indol-3-yl)propanoic acid (53c)

6-chloro-5-fluoroindole **52c** (1.61 g, 9.49 mmol, 1 eq), AcOH (24 cm^3), Ac_2O (8 cm^3) and L-serine (1.99 g, 18.92 mmol, 2 eq), were used following **general procedure 4** gave **53c** as a pale brown powder (2.61 g, 92 %). δ_H (400 MHz, MeOD) 10.56 (1H, s), 7.39 (1H, d, *J* 6.3 Hz), 7.36 (1H, d, *J* 10.2 Hz),

7.18 (1H, s), 4.75 – 4.64 (1H, m), 3.30 – 3.24 (1H, m), 3.12 (1H, dd, *J* 14.7, 7.8 Hz), 1.92 (3H, s). **δ_C** (101 MHz, MeOD) 175.0, 173.2, 153.8 (d, *J* 235.6 Hz), 134.3, 128.0 (d, *J* 8.4 Hz), 127.1, 115.7 (d, *J* 21.4 Hz), 113.4, 111.8 (d, *J* 4.7 Hz), 105.3 (d, *J* 23.4 Hz), 54.6, 28.4, 22.4. **δ_F** (376 MHz, MeOD) -130.2 (1F, s). **ESI-HRMS**: m/z calculated for $C_{13}H_9{}^{35}ClFN_2O_3$ $[M-H]^-$ requires 297.0448. Found 297.0438.

General Procedure 5: Kinetic enzymatic resolution of acetylated unnatural amino acids following literature procedure

To Compound **53a** (2.50 g, 8.86 mmol, 1 eq) was added KH_2PO_4 buffer (525 cm^3, pH 7.4). The reaction flask was left open to air and stirred vigorously at 38 °C until the starting material dissolved. To the reaction mixture was added 1 : 1 w / w of L-amano acylase (2.50 g) (≥30,000 U / g), and a trace amount of $CoCl_2$. 6 H_2O. The mixture stirred gently for 48 hours. The mixture was allowed to cool to room temperature and the enzyme was denatured *via* addition of 12 M HCl to pH 1; the resulting precipitate was filtered through celite and washed with water (20 cm^3). Solvents were removed *in vacuo* until approximately 100 cm^3 remained. The water layer was extracted with EtOAc (3 x 100 cm^3) to ensure removal of unwanted D-*N*-Ac amino acids. After neutralisation L-amino acids could not be extracted into an organic phase and the aqueous phase was evaporated to dryness. To the resulting inorganic salts was added MeOH 75 cm^3 at a time and swirled vigorously ensuring the solid was present as a fine powder. The MeOH was triturated off and the above step repeated until TLC of salt washings showed no UV activity. The MeOH washings were combined, evaporated to dryness and analysed by NMR to indicate if the product was present, mass spectrums were not ran due to high salt contamination. Gave crude **54a** as a pale brown solid, used crude in the next step without purification (see **general procedure 3**). D-*N*-Ac amino derivative D-**53a** was isolated as a brown solid (1.25 g, 50 % of starting racemic *N*-Ac mixture).

Generic structure of compounds 54a – d

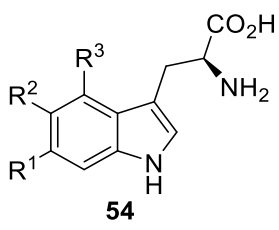

54

54a	R^1 = F, R^2 = F, R^3 = H
54b	R^1 = F, R^2 = H, R^3 = F
54c	R^1 = Cl, R^2 = F, R^3 = H
54d (racemic)	R^1 = Cl, R^2 = F, R^3 = H

Preparation of (*S*)-2-amino-3-(5,6-difluoro-1*H*-indol-3-yl)propanoic acid (54a)

Compound **53a** (2.50 g, 8.86 mmol, 1 eq), L-amano acylase (2.50 g) (≥30,000 U / g), a trace amount of $CoCl_2$. 6 H_2O and KH_2PO_4 buffer (525 cm^3, pH 7.4), were used following **general procedure**

5. Gave crude **54a** as a pale brown solid, used crude in the next step without purification. D-*N*-Ac amino derivative D-**53a** was isolated as a brown solid (1.25 g, 50 % of starting racemic *N*-Ac mixture). δ_H (500 MHz, MeOD) 7.56 (1H, dd, *J* 11.3, 7.9 Hz), 7.26 (1H, s), 7.21 (1H, dd, *J* 11.0, 6.8 Hz), 3.83 (1H, dd, *J* 8.6, 4.2 Hz), 3.41 (1H, ddd, *J* 15.3, 4.2, 0.6 Hz), 3.17 (1H, dd, *J* 15.3, 8.8 Hz). δ_C (126 MHz, MeOD) 174.3, 149.2 (dd, *J* 217.3, 15.4 Hz), 147.3 (dd, *J* 214.0, 15.5 Hz), 133.3 (d, *J* 10.5 Hz), 127.1 (d, *J* 3.4 Hz), 123.9 (d, *J* 8.5 Hz), 110.0 (d, *J* 3.5 Hz), 106.1 (d, *J* 19.6 Hz), 100.1 (d, *J* 21.7 Hz), 56.4, 28.2. δ_F (376 MHz, MeOD) -147.4 (1F, d, *J* 20.3 Hz), -150.7 (1F, d, *J* 20.2 Hz).

Preparation of (*S*)-2-amino-3-(4,6-difluoro-1*H*-indol-3-yl)propanoic acid (54b)

Compound **53b** (0.55 g, 1.96 mmol, 1 eq), L-amano acylase (0.55 g) (≥30,000 U / g), a trace amount of $CoCl_2$. 6 H_2O and KH_2PO_4 buffer (105 cm^3, pH 7.4), were used following **general procedure 5**. Gave crude **54b** as a pale brown solid, used crude in the next step without purification. D-*N*-Ac amino derivative D-**53b** was isolated as a brown solid (0.275 g, 50 % of starting racemic *N*-Ac mixture). Compound too insoluble obtain ^{13}C NMR. δ_H (500 MHz, DMSO) 11.25 (1H, s), 7.40 (2H, s), 7.17 (1H, d, *J* 1.8 Hz), 7.01 (1H, dd, *J* 9.6, 2.1 Hz), 6.81 – 6.72 (1H, m), 3.43 – 3.37 (2H, m), 2.88 (1H, dd, *J* 16.0, 10.9 Hz). δ_F (376 MHz, DMSO) -120.1 (1F, d, *J* 3.7 Hz), -120.9 (1F, d, *J* 3.7 Hz).

Preparation of (*S*)-2-amino-3-(6-chloro-5-fluoro-1*H*-indol-3-yl)propanoic acid (54c) (Only proton ran, data consistent with racemic **54d**)

Compound **53c** (0.38 g, 1.26 mmol, 1 eq), L-amano acylase (0.38 g) (≥30,000 U / g), a trace amount of $CoCl_2$. 6 H_2O and KH_2PO_4 buffer (105 cm^3, pH 7.4), were used following **general procedure 5**. Gave crude **54c** as a pale brown solid, used crude in the next step without purification. D-*N*-Ac amino derivative D-**53c** was isolated as a pale brown solid (0.19 g, 50 % of starting racemic *N*-Ac mixture). δ_H (500 MHz, MeOD) 7.56 (1H, d, *J* 10.2 Hz), 7.43 (1H, d, *J* 6.2 Hz), 7.27 (1H, s), 3.81 (1H, dd, *J* 8.6, 4.3 Hz), 3.40 (1H, dd, *J* 15.3, 4.3 0.7 Hz), 3.16 (1H, dd, *J* 15.3, 8.6 Hz).

Preparation of 2-amino-3-(6-chloro-5-fluoro-1*H*-indol-3-yl)propanoic acid (54d)

Compound **53c** (0.50 g, 1.69 mmol, 1 eq) was placed in a sealed tube, to the flask was added 6 M HCl (7 cm^3) and the tube purged with N_2. The flask was sealed and heated to 120 °C for three days. After cooling the reaction mixture was basified with 30 % NaOH to pH 7. Attempts to extract the product from the aqueous layer were unsuccessful. The organic and aqueous phases were combined and solvents removed *in vacuo*. To the resulting inorganic salts was added MeOH 15 cm^3 at a time and swirled vigorously ensuring the solid was present as a fine powder. The MeOH was triturated off and the above step repeated until TLC of salt washings showed no UV activity. The MeOH washings were combined, evaporated to dryness and analysed by NMR and LRMS to indicate if the product was

present. The crude product **54d** was then used in the next step without further purification. **δ_H** (500 MHz, MeOD) 7.56 (1H, d, *J* 10.1 Hz), 7.43 (1H, d, *J* 6.3 Hz), 7.27 (1H, s), 3.81 (1H, dd, *J* 8.6, 4.3 Hz), 3.40 (1H, dd, *J* 15.3, 11.10 Hz), 3.17 (1H, dd, *J* 15.3, 8.6 Hz). **δ_C** (126 MHz, MeOD) 174.4, 153.9 (d, *J* 235.9 Hz), 134.6, 127.9, 127.6 (d, *J* 8.8 Hz), 116.1 (d, *J* 21.3 Hz), 113.5, 110.2 (d, *J* 4.9 Hz), 105.7 (d, *J* 23.7 Hz), 56.4, 28.3. **ESI-LRMS**: m/z calculated for $C_{11}H_{10}{}^{35}ClFN_2NaO_2$ $[M+Na]^+$ requires 279.0. Found 279.0.

Generic structure of compounds 55a – d following general procedure 3

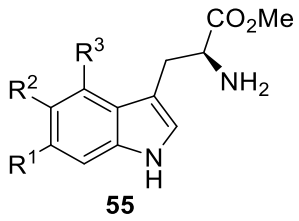

55

55a	R^1 = F, R^2 = F, R^3 = H
55b	R^1 = F, R^2 = H, R^3 = F
55c	R^1 = Cl, R^2 = F, R^3 = H
55d (racemic)	R^1 = Cl, R^2 = F, R^3 = H

Preparation of methyl (*S*)-2-amino-3-(5,6-difluoro-1*H*-indol-3-yl)propanoate (55a)

Compound **54a** (2.22 mmol, 1 eq) was used crude and thionyl chloride (0.32 cm^3, 4.44 mmol, 2 eq), was added to anhydrous MeOH (5 cm^3) following **general procedure 3**. Gave **55a** as a pale brown solid (0.19 g, 33 % over two steps). **δ_H** (500 MHz, $CDCl_3$) 8.34 (1H, s), 7.31 (1H, dd, *J* 10.8, 7.8 Hz), 7.10 (1H, dd, *J* 10.5, 6.6 Hz), 7.06 (1H, d, *J* 2.2 Hz), 3.79 (1H, dd, *J* 7.3, 5.0 Hz), 3.71 (3H, s), 3.18 (1H, ddd, *J* 14.5, 5.0, 0.6 Hz), 3.02 (1H, dd, *J* 14.5, 7.3 Hz), 1.65 (3H, s). **δ_C** (126 MHz, $CDCl_3$) 175.8, 148.4 (dd, *J* 203.8, 15.4 Hz), 146.5 (dd, *J* 200.9, 15.3 Hz), 131.3 (d, *J* 10.3 Hz), 124.4 (d, *J* 3.7 Hz), 122.9 (d, *J* 8.7 Hz), 111.5 (d, *J* 4.4 Hz), 105.5 (d, *J* 19.3 Hz), 99.3 (d, *J* 21.7 Hz), 54.9, 52.2, 30.6. **δ_F** (376 MHz, $CDCl_3$) -143.7 (d, *J* 20.9 Hz), -147.4 (d, *J* 20.9 Hz). **CI-HRMS**: m/z calculated for $C_{12}H_{13}F_2N_2O_2$ $[M+H]^+$ requires 255.0940 Found 255.0933.

Preparation of methyl (*S*)-2-amino-3-(4,6-difluoro-1*H*-indol-3-yl)propanoate (55b)

Compound **54b** (0.98 mmol, 1 eq) was used crude and thionyl chloride (0.21 cm^3, 2.94 mmol, 3 eq), was added to anhydrous MeOH (5 cm^3) following **general procedure 3**. Gave **55b** as a pale brown solid (0.08 g, 32 % over two steps). **δ_H** (500 MHz, MeOD) 7.04 (1H, s), 6.89 (1H, dd, *J* 9.4, 2.1 Hz), 6.55 (1H, ddd, *J* 12.0, 10.1, 2.1 Hz), 3.78 (1H, apparent t), 3.65 (3H, s), 3.23 (1H, dd, *J* 14.3, 6.2 Hz), 3.04 (1H, dd, *J* 14.3, 7.4 Hz). **δ_C** (126 MHz, MeOD) 172.4, 160.4 (dd, *J* 236.8, 12.2 Hz), 157.6 (dd, *J* 246.0, 15.1 Hz), 140.0 (t, *J* 14.5 Hz), 125.6, 113.8 (d, *J* 19.5 Hz), 109.7 (d, *J* 2.6 Hz), 95.4 – 94.6 (2C, m), 56.1 (d, *J* 1.6 Hz), 52.3, 32.6. **δ_F** (376 MHz, MeOD) -121.9 (1F, d, *J* 3.9 Hz), -123.2 (1F, d, *J* 3.9 Hz). **CI-HRMS**: m/z calculated for $C_{12}H_{13}F_2N_2O_2$ $[M+H]^+$ requires 255.0940. Found 255.0947

Preparation of methyl (*S*)-2-amino-3-(6-chloro-5-fluoro-1*H*-indol-3-yl)propanoate (55c) (No Mass spec, data consistent with racemic form **55d**)

Compound **54c** (0.63 mmol, 1 eq) was used crude and thionyl chloride (0.14 cm^3, 1.90 mmol, 3 eq), was added to anhydrous MeOH (5 cm^3) following **general procedure 3**. Gave **55c** as a brown oil (0.075 g, 44 % over two steps). δ_H (500 MHz, MeOD) 7.40 (1H, d, *J* 6.3 Hz), 7.32 (1H, d, *J* 10.1 Hz), 7.17 (1H, s), 3.74 (1H, t, *J* 6.2 Hz), 3.64 (3H, s), 3.11 (1H, dd, *J* 14.5, 5.9 Hz), 3.06 (1H, dd, *J* 14.5, 6.5 Hz). δ_C (126 MHz, MeOD) 176.5, 153.8 (d, *J* 235.7 Hz), 134.3, 127.8 (d, *J* 8.5 Hz), 127.3, 115.9 (d, *J* 21.4 Hz), 113.5, 111.3 (d, *J* 4.7 Hz), 105.3 (d, *J* 23.5 Hz), 55.8, 52.5, 31.1. δ_F (376 MHz, MeOD) -130.1 (s).

Preparation of methyl 2-amino-3-(6-chloro-5-fluoro-1*H*-indol-3-yl)propanoate (55d)

Compound **54d** (1.69 mmol, 1 eq) was used crude and thionyl chloride (0.23 cm^3, 3.16 mmol, 2 eq), was added to anhydrous MeOH (5 cm^3) following **general procedure 3**. Gave **55d** as a brown oil (0.17 g, 39 % over two steps). δ_H (500 MHz, MeOD) 7.40 (1H, d, *J* 6.2 Hz), 7.32 (1H, d, *J* 10.1 Hz), 7.17 (1H, s), 3.79 – 3.72 (1H, m), 3.65 (3H, s), 3.17 – 3.02 (2H, m). δ_C (101 MHz, MeOD) 176.6, 153.8 (d, *J* 235.8 Hz), 134.3, 127.8 (d, *J* 8.4 Hz), 127.3, 115.8 (d, *J* 21.4 Hz), 113.46 (s), 111.3 (d, *J* 4.6 Hz), 105.3 (d, *J* 23.5 Hz), 55.8, 52.4, 31.1. **CI-HRMS**: m/z calculated for $C_{12}H_{13}{}^{35}ClFN_2O_2$ $[M+H]^+$ requires 271.0644. Found 271.0647.

Generic structure of compounds 56a – d and 57a – d following general procedure 1

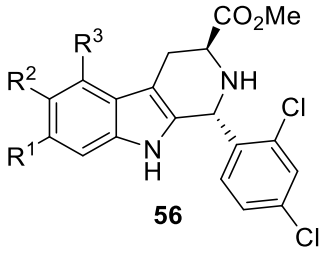

56

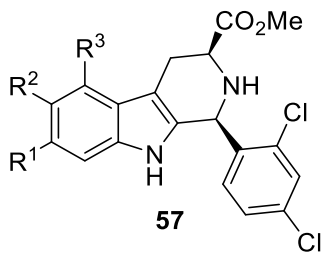

57

56a / 57a	R^1 = F, R^2 = F, R^3 = H
56b / 57b	R^1 = F, R^2 = H, R^3 = F
56c / 57c	R^1 = Cl, R^2 = F, R^3 = H
56d / 57d (racemic)	R^1 = Cl, R^2 = F, R^3 = H

Preparation of methyl (1*R*,3*S*)-1-(2,4-dichlorophenyl)-6,7-difluoro-2,3,4,9-tetrahydro-1*H*-pyrido[3,4-*b*]indole-3-carboxylate (56a) and methyl (1*S*,3*S*)-1-(2,4-dichlorophenyl)-6,7-difluoro-2,3,4,9-tetrahydro-1*H*-pyrido[3,4-*b*]indole-3-carboxylate (57a)

Compound **55a** (0.18 g, 0.69 mmol, 1 eq), 2,4-dichlorobenzaldehyde (0.13 g, 0.76 mmol, 1.1 eq) and TFA (0.06 cm^3, 0.76 mmol, 1.1 eq), were used in anhydrous DCM (5 cm^3) following **general procedure 1**. Gave **56a** as a white solid (0.057 g, 20 %). δ_H (500 MHz, MeOD) 7.58 (1H, d, *J* 2.1 Hz), 7.31 (1H, dd, *J* 11.0, 7.9 Hz), 7.23 (1H, dd, *J* 8.4, 2.1 Hz), 7.10 (1H, dd, *J* 11.0, 6.8 Hz), 6.81 (1H, d, *J* 8.4 Hz), 5.82 (1H, s), 3.80 (1H, dd, *J* 8.3, 4.9 Hz), 3.73 (3H, s), 3.17 (1H, dd, *J* 15.3, 4.9 Hz), 2.96 (1H, ddd, *J* 15.3, 8.4, 1.1 Hz). δ_C (126 MHz, MeOD) 174.7, 149.1 (dd, *J* 206.2, 15.4 Hz), 147.3 (dd, *J* 203.6, 15.3 Hz), 138.9, 135.9, 135.6, 134.5 (d, *J* 3.6 Hz), 133.2 (d, *J* 10.4 Hz), 132.5, 130.6, 128.3, 123.3 (d, *J* 7.8 Hz), 110.2 (d, *J* 3.2 Hz), 105.5 (d, *J* 19.3 Hz), 100.0 (d, *J* 21.8 Hz), 53.0, 52.7, 52.5, 25.5. δ_F (376 MHz, MeOD) -147.2 (1F, d, *J* 20.2 Hz), -151.0 (1F, d, *J* 20.2 Hz). **ESI-HRMS**: m/z calculated for $C_{19}H_{15}{}^{35}Cl_2F_2N_2O_2$ $[M+H]^+$ requires 411.0473. Found 411.0467.

The same procedure also gave **57a** as a white solid (0.15 g, 54 %). δ_H (500 MHz, DMSO) 10.62 (1H, s), 7.69 (1H, d, *J* 2.1 Hz), 7.47 (1H, dd, *J* 11.2, 8.0 Hz), 7.39 (1H, dd, *J* 8.4, 2.1), 7.27 (1H, d, *J* 8.4 Hz), 7.16 (1H, dd, *J* 11.2, 7.0 Hz), 5.61 (1H, s), 3.92 (1H, dd, *J* 10.9, 4.1 Hz), 3.69 (3H, s), 3.02 (1H, ddd, *J* 14.8, 4.1, 1.6 Hz), 2.81 (1H, ddd, *J* 14.8, 10.9, 2.3 Hz). δ_C (126 MHz, DMSO) 172.6, 146.6 (dd, *J* 163.6, 15.3 Hz), 144.7 (dd, *J* 161.3, 15.3 Hz), 138.0, 135.8 (dd, *J* 19.6, 3.5 Hz), 134.2, 133.0, 132.1, 131.2 (dd, *J* 19.4, 10.6 Hz), 128.8, 127.6, 121.8 (d, *J* 8.0 Hz), 108.1, 104.6 (d, *J* 18.7 Hz), 99.1 (d, *J* 21.4 Hz), 55.9, 55.8, 51.8, 24.9. δ_F (376 MHz, DMSO) -145.8 (1F, d, *J* 22.4 Hz), -149.1 (1F, d, *J* 22.4 Hz). **ESI-HRMS**: m/z calculated for $C_{19}H_{15}{}^{35}Cl_2F_2N_2O_2$ $[M+H]^+$ requires 411.0473. Found 411.0466.

Preparation of methyl (1*R*,3*S*)-1-(2,4-dichlorophenyl)-5,7-difluoro-2,3,4,9-tetrahydro-1*H*-pyrido[3,4-*b*]indole-3-carboxylate (56b) and methyl (1*S*,3*S*)-1-(2,4-dichlorophenyl)-5,7-difluoro-2,3,4,9-tetrahydro-1*H*-pyrido[3,4-*b*]indole-3-carboxylate (57b)

Compound **55b** (0.081 g, 0.32 mmol, 1 eq), 2,4-dichlorobenzaldehyde (0.061 g, 0.35 mmol, 1.1 eq) and TFA (0.027 cm^3, 0.35 mmol, 1.1 eq), were used in anhydrous DCM (5 cm^3) following **general procedure 1**. Gave **56b** as a yellow solid (0.020 g, 15 %). δ_H (500 MHz, MeOD) 7.57 (1H, d, *J* 1.8 Hz), 7.24 (1H, dd, *J* 8.4, 1.8 Hz), 6.85 (1H, d, *J* 8.4 Hz), 6.80 (1H, dd, *J* 9.4, 1.5 Hz), 6.57 (1H, dd, *J* 10.6, 1.5 Hz), 5.80 (1H, s), 3.80 (1H, dd, *J* 8.3, 4.9 Hz), 3.73 (3H, s), 3.36 – 3.30 (1H, m, signal obscured by NMR solvent), 3.11 (1H, dd, *J* 15.6, 8.3 Hz). δ_C (126 MHz, MeOD) 174.7, 160.5 (dd, *J* 237.1, 12.1 Hz), 157.4 (dd, *J* 246.3, 15.2 Hz), 139.8 (apparent t, *J* 14.4 Hz), 138.7, 136.0, 135.6, 133.1 (d, *J* 3.0 Hz), 132.5, 130.7, 128.3, 113.3 (d, *J* 20.5 Hz), 108.1, 95.2 (dd, *J* 29.1, 23.6 Hz), 94.7 (dd, *J* 26.2, 4.3 Hz), 52.9, 52.7,

52.3, 26.8. **δ_F** (376 MHz, MeOD) -121.3 (1F, d, *J* 3.6 Hz), -124.5 (1F, d, *J* 3.6 Hz). **ESI-HRMS**: m/z calculated for $C_{19}H_{15}{}^{35}Cl_2F_2N_2O_2$ $[M+H]^+$ requires 411.0473. Found 411.0468.

The same procedure also gave **57b** as a pale yellow solid (0.083 g, 64 %). **δ_H** (500 MHz, MeOD) 7.57 (1H, d, *J* 1.4 Hz), 7.31 (1H, dd, *J* 8.4, 1.4 Hz), 7.24 (1H, d, *J* 8.4 Hz), 6.76 (1H, dd, *J* 9.4, 1.3 Hz), 6.53 (1H, apparent t), 5.73 (1H, s), 3.96 (1H, dd, *J* 10.9, 4.2 Hz), 3.78 (3H, s), 3.31 – 3.26 (1H, m, signal obscured by NMR solvent) 3.11 – 3.00 (1H, m). **δ_C** (126 MHz, MeOD) 174.2, 160.3 (dd, *J* 236.7, 11.9 Hz), 157.3 (dd, *J* 246.1, 15.2 Hz), 139.8 (apparent t, *J* 14.6 Hz), 138.2 (s), 136.2, 135.7, 134.8 (d, *J* 2.7), 133.0 – 132.6 (m), 130.5, 128.9, 113.4 (d, *J* 19.2 Hz), 107.8, 95.1 (dd, *J* 29.1, 23.6 Hz), 94.7 (dd, *J* 26.3, 4.3 Hz), 57.6, 55.4 – 55.0 (m), 52.7, 27.4. **δ_F** (376 MHz, MeOD) -121.6 (1F, br d, *J* 1.6 Hz), -124.7 (1F, br d, *J* 3.3 Hz). **ESI-HRMS**: m/z calculated for $C_{19}H_{15}{}^{35}Cl_2F_2N_2O_2$ $[M+H]^+$ requires 411.0473. Found 411.0471

Preparation of methyl (1*R*,3*S*)-7-chloro-1-(2,4-dichlorophenyl)-6-fluoro-2,3,4,9-tetrahydro-1*H*-pyrido[3,4-*b*]indole-3-carboxylate (56c) and methyl (1*S*,3*S*)-7-chloro-1-(2,4-dichlorophenyl)-6-fluoro-2,3,4,9-tetrahydro-1*H*-pyrido[3,4-*b*]indole-3-carboxylate (57c) No mass spec ran, NMR data consistent with racemic version **56d** and **57d**

Compound **55c** (0.075 g, 0.28 mmol, 1 eq), 2,4-dichlorobenzaldehyde (0.054 g, 0.31 mmol, 1.1 eq) and TFA (0.024 cm^3, 0.31 mmol, 1.1 eq), were used in anhydrous DCM (5 cm^3) following **general procedure 1**. Gave **56c** as a yellow solid (0.022 g, 19 %). **δ_H** (500 MHz, MeOD) 7.57 (1H, d, *J* 2.1 Hz), 7.31 (1H, d, *J* 1.6 Hz), 7.29 (1H, d, *J* 5.3 Hz), 7.22 (1H, dd, *J* 8.4, 2.1 Hz), 6.81 (1H, d, *J* 8.4 Hz), 5.82 (1H, s), 3.81 (1H, dd, *J* 8.3, 4.9 Hz), 3.72 (3H, s), 3.17 (1H, dd, *J* 15.3, 4.9 Hz), 2.96 (1H, ddd, *J* 15.3, 8.3, 1.2 Hz). **δ_C** (126 MHz, MeOD) 174.7, 154.0 (d, *J* 236.2 Hz), 138.7, 135.9, 135.6, 135.5, 134.5, 132.4, 130.6, 128.3, 126.9 (d, *J* 8.6 Hz), 115.9 (d, *J* 21.3 Hz), 113.2, 110.3 (d, *J* 4.5 Hz), 105.0 (d, *J* 23.4 Hz), 53.0, 52.7, 52.4, 25.5. **δ_F** (376 MHz, MeOD) -129.8 (1F, s).

The same procedure also gave **57c** as a pale yellow needles (0.073 g, 61 %). **δ_H** (500 MHz, DMSO) 10.67 (1H, s), 7.70 (1H, d, *J* 2.1 Hz), 7.48 (1H, d, *J* 10.1), 7.39 (1H, dd, *J* 8.4, 2.1 Hz), 7.32 (1H, d, *J* 6.4 Hz), 7.27 (1H, d, *J* 8.4 Hz), 5.62 (1H, apparent d, *J* 6.8 Hz), 3.97 – 3.91 (1H, m), 3.69 (3H, s), 3.19 – 3.15 (1H, m), 3.03 (1H, apparent dd, *J* 14.8, 3.9 Hz), 2.82 (1H, ddd, *J* 14.8, 11.0, 2.1 Hz). **δ_C** (126 MHz, DMSO) 172.6 (s), 151.6 (d, *J* 234.5 Hz), 137.8, 136.9, 134.2, 133.1, 132.7, 132.5, 132.1 (d, *J* 1.7 Hz), 127.7, 125.4 (d, *J* 8.7 Hz), 112.7 (d, *J* 21.2 Hz), 112.0 (d, *J* 5.6 Hz), 108.4 (d, *J* 3.8 Hz), 104.3 (d, *J* 22.9 Hz), 55.84, 55.76, 51.8, 25.0 (s). **δ_F** (376 MHz, DMSO) -128.3 (1F s).

Preparation of methyl (1*R*,3*S* / 1*S*,3*R*)-7-chloro-1-(2,4-dichlorophenyl)-6-fluoro-2,3,4,9-tetrahydro-1*H*-pyrido[3,4-*b*]indole-3-carboxylate (56d) and methyl (1*S*,3*S* /1*R*,3*R*)-7-chloro-1-(2,4-dichlorophenyl)-6-fluoro-2,3,4,9-tetrahydro-1*H*-pyrido[3,4-*b*]indole-3-carboxylate (57d)

Compound **55d** (0.17 g, 0.61 mmol, 1 eq), 2,4-dichlorobenzaldehyde (0.12 g, 0.67 mmol, 1.1 eq) and TFA (0.051 cm^3, 0.67 mmol, 1.1 eq), were used in anhydrous DCM (5 cm^3) following **general procedure 1**. Gave **56d** as a yellow crystals (0.041 g, 16 %). δ_H (500 MHz, $CDCl_3$) 7.89 (1H, s), 7.45 (1H, d, *J* 2.1 Hz), 7.26 – 7.23 (2H, m), 7.12 (1 H, dd, *J* 8.3, 2.1 Hz), 6.89 (1H, d, *J* 8.3 Hz), 5.80 (1H, s), 3.83 (1H, dd, *J* 7.5, 5.1 Hz), 3.73 (3H, s), 3.17 (1H, ddd, *J* 15.4, 5.1, 0.8 Hz), 3.01 (1 H, ddd, *J* 15.4, 7.6, 1.1 Hz). δ_C (126 MHz, $CDCl_3$) 173.6, 153.3 (d, *J* 238.4 Hz), 137.5, 134.8, 134.4, 134.1, 132.5, 130.9, 130.0, 127.5, 125.9 (d, *J* 8.6 Hz), 115.9 (d, *J* 21.3 Hz), 112.3, 109.9 (d, *J* 4.4 Hz), 104.7 (d, *J* 23.5 Hz), 52.5, 52.4, 51.2, 24.6). **ESI-HRMS**: m/z calculated for $C_{19}H_{15}{}^{35}Cl_3FN_2O_2$ $[M+H]^+$ requires 427.0178. Found 427.0179.

The same procedure also gave **57d** as pale yellow needles (0.12 g, 47 %). δ_H (500 MHz, $CDCl_3$) 7.60 (1H, s), 7.47 (1H, d, *J* 2.1 Hz), 7.39 (1H, d, *J* 8.4 Hz), 7.25 – 7.19 (3H, m), 5.75 (1H, s), 3.96 (1H, dd, *J* 11.0, 4.1 Hz), 3.82 (3H, s), 3.14 (1H, ddd, *J* 15.0, 4.1, 1.7 Hz), 2.94 (1H, ddd, *J* 15.0, 11.0, 2.4 Hz), 2.64 (1H, s). δ_C (126 MHz, $CDCl_3$) 172.8, 153.3 (d, *J* 238.5 Hz), 136.9, 135.7, 135.0, 134.2, 132.5, 131.4, 129.6, 128.3, 126.0 (d, *J* 8.6 Hz), 115.7 (d, *J* 21.2 Hz), 112.3, 109.7 (d, *J* 4.4 Hz), 104.6 (d, *J* 23.4 Hz), 56.5, 52.6, 51.0, 25.3. **ESI-HRMS**: m/z calculated for $C_{19}H_{15}{}^{35}Cl_3FN_2O_2$ $[M+H]^+$ requires 427.0178. Found 427.0175.

Generic structure of compounds 58 – 61

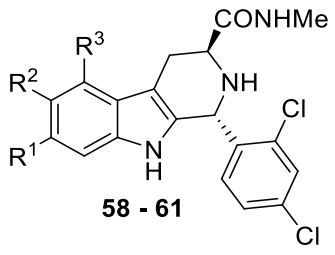

58 - 61

58	R^1 = F, R^2 = F, R^3 = H
59	R^1 = F, R^2 = H, R^3 = F
60	R^1 = Cl, R^2 = F, R^3 = H
61 (±)	R^1 = Cl, R^2 = F, R^3 = H

Preparation of (1*R*,3*S*)-1-(2,4-dichlorophenyl)-6,7-difluoro-*N*-methyl-2,3,4,9-tetrahydro-1*H*-pyrido[3,4-*b*]indole-3-carboxamide (58)

Compound **56a** (0.057 g, 0.14 mmol, 1 eq) and methyl amine 33 % in EtOH (2.91 cm^3, 23.38 mmol, 167 eq), were used following **general procedure 2**. Gave **58** as a white solid (0.034 g, 60 %). δ_H (500 MHz, MeOD) 7.56 (1H, d, *J* 2.1 Hz), 7.31 (1H, dd, *J* 11.0, 7.9 Hz), 7.20 (1H, dd, *J* 8.3, 2.1 Hz), 7.10 (1H, dd, *J* 11.0, 6.8 Hz), 6.73 (1H, d, *J* 8.3 Hz), 5.70 (1H, s), 3.53 (1H, dd, *J* 10.1, 4.6 Hz), 3.11 (1H, dd, *J* 15.3, 4.6 Hz), 2.81 (1H, ddd, *J* 15.3, 10.1, 1.4 Hz), 2.75 (3H, s). δ_C (126 MHz, MeOD) 175.7, 149.1 (dd, *J* 204.9, 15.3 Hz), 147.2 (dd, *J* 202.4, 15.3 Hz), 139.0, 136.3, 135.4, 135.0 (d, *J* 3.6 Hz), 133.2 (d, *J* 10.4

Hz), 132.4, 130.7, 128.0, 123.4 (dd, *J* 7.8, 1.1 Hz), 111.1 (dd, *J* 4.2, 1.3 Hz), 105.4 (dd, *J* 19.1, 0.7 Hz), 99.9 (d, *J* 21.8 Hz), 53.2, 52.7, 26.3, 26.0. **δ_F** (376 MHz, MeOD) -147.2 (1F, d, *J* 20.2 Hz), -151.1 (1F, d, *J* 20.2 Hz). **ESI-HRMS**: m/z calculated for $C_{19}H_{16}{}^{35}Cl_2F_2N_3O$ $[M+H]^+$ requires 410.0633. Found 410.0629. **Elemental Analysis** Calculated for $C_{19}H_{15}{}^{35}Cl_2F_2N_3O$ requires C, 55.63 %, H, 3.69 %, N, 10.24 %. Found C, 54.67 %, H, 3.64 %, N, 9.89 %. **IR (neat)**: ν_{max}/cm^{-1}: 3456 (w), 3368 (w), 3206 (m, br), 2907 (w), 2846 (w), 1667 (s), 1526 (m), 1470 (s), 1308 (s), 1038 (m), 820 (s, br), 618 (s). **HPLC** (purity analysis %) found: Purity 100 %; Retention time: 7.70 min / 30 min (0.5 ml/min MeOH, Signal = 254 nm, CHIRACEL OJ column).

Preparation of (1*R*,3*S*)-1-(2,4-dichlorophenyl)-5,7-difluoro-*N*-methyl-2,3,4,9-tetrahydro-1*H*-pyrido[3,4-*b*]indole-3-carboxamide (59)

Compound **56b** (0.019 g, 0.046 mmol, 1 eq) and methyl amine 33 % in EtOH (4.16 cm^3, 33.4 mmol, 167 eq), were used following **general procedure 2**. Gave **59** as a white solid (0.016 g, 87 %). **δ_H** (500 MHz, MeOD) 7.57 (1H, s), 7.23 (1H, d, *J* 8.4 Hz), 6.79 (2H, apparent t), 6.56 (1H, apparent t, *J* 10.3 Hz), 5.70 (1H, s), 3.53 (1H, dd, *J* 9.9, 4.2 Hz), 2.96 (1H, dd, *J* 15.3, 10.3 Hz), 2.75 (3H, s). (One aliphatic signal is lost under the NMR solvent peak.) **δ_C** (126 MHz, MeOD) 175.7, 160.5 (dd, *J* 237.2, 12.0 Hz), 157.5 (dd, *J* 246.4, 14.9 Hz), 139.7, 138.8, 136.3, 135.4, 133.6 (d, *J* 3.0 Hz), 132.4, 130.8, 128.0, 113.4 (d, *J* 21.3 Hz), 109.0, 95.1 (dd, *J* 29.1, 23.7 Hz), 94.7 (dd, *J* 25.9, 4.2 Hz), 53.1, 52.5, 27.4, 26.3. **δ_F** (376 MHz, MeOD) -121.5 (d, *J* 3.5 Hz), -124.2 (d, *J* 3.5 Hz). **ESI-HRMS**: m/z calculated for $C_{19}H_{16}{}^{35}Cl_2F_2N_3O$ $[M+H]^+$ requires 410.0633. Found 410.0635. **Elemental Analysis** Calculated for $C_{19}H_{15}{}^{35}Cl_2F_2N_3O$ requires C, 55.63 %, H, 3.69 %, N, 10.24 %. Found C, 55.43 %, H, 3.69 %, N, 10.11 %. **IR (neat)**: ν_{max}/cm^{-1}: 3366 (w), 3303 (w), 3368 (w), 3206 (m, br), 2907 (w), 2846 (w), 1667 (s), 1526 (m), 1470 (s), 1308 (s), 1038 (m), 820 (s, br), 618 (s). **HPLC** (purity analysis %) found: Purity 100 %; Retention time: 7.23 min / 30 min (0.5 ml/min MeOH, Signal = 254 nm, CHIRACEL OJ column).

Preparation of (1*R*,3*S*)-7-chloro-1-(2,4-dichlorophenyl)-6-fluoro-*N*-methyl-2,3,4,9-tetrahydro-1*H*-pyrido[3,4-*b*]indole-3-carboxamide (60)

Compound **46c** (0.022 g, 0.051 mmol, 1 eq) and methyl amine 33 % in EtOH (1.07 cm^3, 8.59 mmol, 167 eq), were used following **general procedure 2**. Gave **60** as a white solid (0.015 g, 68 %). **δ_H** (500 MHz, MeOD) 7.57 (1H, d, *J* 2.1 Hz), 7.32 (1H, d, *J* 4.8 Hz), 7.31 (1H, d, *J* 0.9 Hz), 7.22 (1H, dd, *J* 8.3, 2.2 Hz), 6.74 (1H, d, *J* 8.3 Hz), 5.72 (1H, s), 3.54 (1H, dd, *J* 10.0, 4.6 Hz), 3.12 (1H, dd, *J* 15.4, 4.6 Hz), 2.82 (1H, ddd, *J* 15.4, 10.0, 1.4 Hz), 2.75 (3H, s). **δ_C** (126 MHz, MeOD) 175.7, 155.6 (d, *J* 171.4 Hz), 138.9, 136.3, 136.0, 135.4, 134.5, 132.4, 130.8, 128.0, 127.1 (d, *J* 7.8 Hz), 115.8 (d, *J* 21.2 Hz), 113.2, 111.2, 105.0 (d, *J* 23.3 Hz), 53.2, 52.7, 26.3, 25.9. **δ_F** (376 MHz, MeOD) -131.4. **ESI-HRMS**: m/z calculated for

$C_{19}H_{15}{}^{35}Cl_3FN_3NaO$ $[M+Na]^+$ requires 448.0162. Found 448.0155. **Elemental Analysis** Calculated for $C_{19}H_{15}{}^{35}Cl_3FN_3O$ requires C, 53.48 %, H, 3.54 %, N, 9.85 %. Found C, 53.54 %, H, 3.63 %, N, 9.70 %. **IR (neat)**: ν_{max}/cm^{-1}: 3438 (w), 3309 (w), 3234 (m, br), 2906 (w), 2843 (w), 1667 (s), 1643 (m), 1562 (m), 1511 (m), 1347 (s), 1151 (s), 820 (s), 606 (s). **HPLC** (purity analysis %) found: Purity 100 %; Retention time: 9.07 min / 30 min (0.5 ml/min MeOH, Signal = 254 nm, CHIRACEL OJ column).

Preparation of (1*R*,3*S* / 1*S*,3*S*)-7-chloro-1-(2,4-dichlorophenyl)-6-fluoro-*N*-methyl-2,3,4,9-tetrahydro-1*H*-pyrido[3,4-*b*]indole-3-carboxamide (61)

Compound **56d** (0.041 g, 0.096 mmol, 1eq) and methyl amine 33 % in EtOH (2.00 cm^3, 16.03 mmol, 167 eq), were used following **general procedure 2**. Gave **61** as a white solid (0.028 g, 69 %). δ_H (500 MHz, DMSO) 10.99 (1H, s), 7.72 (1H, d, *J* 4.7 Hz), 7.69 (1H, d, *J* 2.2 Hz), 7.49 (1H, d, *J* 10.1 Hz), 7.41 (1H, d, *J* 6.3 Hz), 7.31 (1H, dd, *J* 8.3, 2.2 Hz), 6.67 (1H, d, *J* 8.4 Hz), 5.56 (1 H, d, *J* 5.5 Hz), 3.38 – 3.28 (1H, m (under solvent peak)), 3.13 (1H, dd, *J* 10.0, 5.3 Hz), 2.96 (1H, dd, *J* 15.3, 4.5 Hz), 2.66 (1H, dd, *J* 15.3, 10.0 Hz), 2.59 (3H, d, *J* 4.5 Hz). δ_C (126 MHz, DMSO) 172.6, 151.6 (d, *J* 234.4 Hz), 138.5, 135.8, 134.5, 132.7, 132.5, 131.2, 129.1, 126.9, 125.5 (d, *J* 8.6 Hz), 112.8 (d, *J* 21.1 Hz), 112.0 (s), 109.9 (d, *J* 4.5 Hz), 104.3 (d, *J* 23.0 Hz), 51.3, 50.7, 25.4, 25.0. δ_F (376 MHz, DMSO) -128.5 (1F, s). **ESI-HRMS**: m/z calculated for $C_{19}H_{16}{}^{35}Cl_3FN_3O$ $[M+H]^+$ requires 426.0337. Found 426.0341. **Elemental Analysis** Calculated for $C_{19}H_{15}Cl_2FN_3O$ requires C, 53.48 %, H, 3.54 %, N, 9.85 %. Found C, 53.46 %, H, 3.55 %, N, 9.84 %. **IR (neat)**: ν_{max}/cm^{-1}: 3340 (m, br), 3303 (w, br), 3240 (s, br), 3069 (w, br) 2844 (w), 1666 (s), 1524 (s), 1455 (s), 1222 (s), 835 (s). **HPLC** (purity analysis %) found: Purity peak 1 43 %; Retention time: 9.09 min: purity peak 2 53 %; Retention time: 10.15 / 30 min (0.5 ml/min MeOH, Signal = 254 nm, CHIRACEL OJ column).

Preparation of 1-tosyl-1*H*-pyrrolo[2,3-*b*]pyridine-3-carbaldehyde (63)

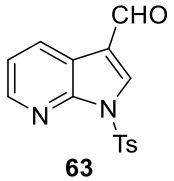

63

To a suspension of 7-azaindole-3-carboxaldehyde **62** (5.00 g, 34.2 mmol, 1 eq), DMAP (0.42 g, 3.42 mmol, 0.1 eq) and TsCl (9.78 g, 51.3 mmol, 1.5 eq) in anhydrous DCM (250 cm^3) contained within a flame dried round bottomed flask, was added NEt_3 (9.53 cm^3, 68.4 mmol, 2 eq) at 0 °C under an argon atmosphere. The reaction was allowed to slowly warm to room temperature and left overnight. To the reaction mixture was added saturated $NaHCO_3$ solution (200 cm^3) and the mixture stirred vigorously for 2 hours. The DCM layer was separated and the aqueous phase extracted with DCM (2 x

100 cm^3). Combined organics were washed with water (2 x 50 cm^3), brine (50 cm^3) and were dried over $MgSO_4$. After filtration solvents were removed *in vacuo* and the product purified by column chromatography (50 % EtOAc in hexane), yielded the product **63** as an off white solid (10.26 g, 99 %). δ_H (500 MHz, $CDCl_3$) 10.04 (1H, s), 8.54 – 8.48 (2H, m), 8.39 (1H, s), 8.18 – 8.13 (2H, m), 7.36 – 7.29 (3H, m), 2.40 (3H, s). δ_C (126 MHz, $CDCl_3$) 185.3, 147.5, 146.8, 146.5, 135.9, 134.4, 131.5, 130.1, 128.82, 120.8, 119.5, 119.1, 21.9. **ESI-HRMS**: m/z calculated for $C_{15}H_{12}N_2NaO_3S$ $[M+Na]^+$ requires 323.0461. Found 323.0462.

Preparation of (1-tosyl-1*H*-pyrrolo[2,3-*b*]pyridin-3-yl)methanol (64)

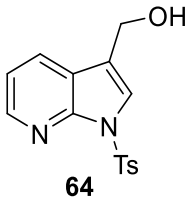

64

To a stirred suspension of compound **63** (10.23 g, 34.1 mmol, 1 eq) in anhydrous EtOH (200 cm^3) was added sodium borohydride (2.58 g, 68.2 mmol, 2 eq) portion wise over the course of approximately one hour. The reaction was stirred overnight monitored by TLC until completion after which was quenched by careful addition of water (100 cm^3); the volume of the solvent was reduced by approximately half *in vacuo*. The product was extracted from the aqueous phase into EtOAc (3 x 100 cm^3). The combined organics were washed with water (100 cm^3), brine (100 cm^3) and were dried over $MgSO_4$. After filtration solvents were removed *in vacuo* to yield the product **64** as a white solid (9.56 g, 94 %). δ_H (500 MHz, $CDCl_3$) 8.44 (1H, dd, *J* 4.8, 1.6 Hz), 8.08 – 8.04 (2H, m), 7.95 (1H, dd, *J* 7.9, 1.6 Hz), 7.69 (1H, s), 7.28 – 7.24 (2H, m), 7.18 (1H, dd, *J* 7.9, 4.8 Hz), 4.82 (2H, s), 2.36 (3H, s), 1.73 (1H, s). δ_C (126 MHz, $CDCl_3$) 147.8, 145.4, 145.3, 135.6, 129.8, 128.7, 128.2, 123.9, 122.0, 119.0, 118.8, 57.4, 21.8. **CI-HRMS**: m/z calculated for $C_{15}H_{15}N_2O_3S$ $[M+H]^+$ requires 303.0798. Found 303.0791.

Preparation of 3-(((2*S*,5*R*)-5-isopropyl-3,6-dimethoxy-2,5-dihydropyrazin-2-yl)methyl)-1-tosyl-1*H*-pyrrolo[2,3-*b*]pyridine (68)

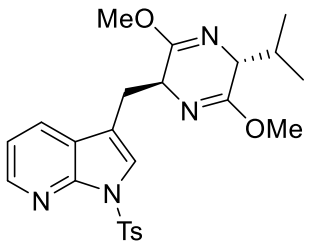

68

To a flame dried round bottom flask, was added compound **64** (5.95 g, 19.7 mmol, 1 eq) along with anhydrous DCM (50 cm^3) and was stirred under argon at 0 °C. To the reaction mixture was added PBr_3 (2.03 cm^3, 21.6 mmol, 1.1 eq) and the reaction left to stir for 30 minutes. Once TLC showed no presence of start material the reaction was stopped immediately and quenched carefully and slowly by addition of saturated $NaHCO_3$ solution (100 cm^3) at 0 °C. Once CO_2 production ceased the product was extracted into EtOAc (3 x 100 cm^3). Combined organics were washed with water (100 cm^3), brine (100 cm^3) and were dried over $MgSO_4$. After filtration solvents were removed *in vacuo*, and the product dried thoroughly on high vacuum. Whist the brominated compound **65** was under vacuum, the deprotonation of the Schöllkopf chiral auxiliary (**66**) was carried out. In a separate flame dried round bottom flask was added anhydrous THF (50 cm^3) and the Schöllkopf chiral auxiliary (**66**) (3.70 cm^3, 21.0 mmol, 1.05 eq) under argon. The reaction mixture was cooled to -78 °C before dropwise addition of ^{n}BuLi 2.5 M (9.4 cm^3, 23.6 mmol, 1.2 eq), the deprotonation was allowed to occur over approximately 25 minutes. During this time the brominated compound **65** was taken off vacuum and dissolved in anhydrous THF (50 cm^3). The flask was placed under argon and cooled to -78 °C. The brominated compound was then transferred by cannula into the vessel containing the deprotonated auxiliary **67** over the course of approximately 10 minutes and reaction was left overnight. The reaction was quenched the following day with saturated NH_4Cl (50 cm^3), most of the THF was removed under vacuum before extraction of the aqueous phase with EtOAc (3 x 50 cm^3). Combined organics were washed with water (50 cm^3), brine (50 cm^3) and dried over $MgSO_4$. The product was purified by column chromatography (50 % EtOAc in hexane) followed by recrystallisation in 15 % DCM in hexane to yield the product **68** as colourless crystals (4.76 g, 52 % isolated yield). δ_H (500 MHz, $CDCl_3$) 8.37 (1H, dd, *J* 4.8, 1.6 Hz), 7.98 – 7.94 (2H, m), 7.83 (1H, dd, *J* 7.9, 1.6 Hz), 7.43 (1H, s), 7.25 – 7.21 (2H, m), 7.12 (1H, dd, *J* 7.9, 4.8 Hz), 4.34 – 4.28 (1H, m), 3.68 (3H, s), 3.65 (3H, s), 3.24 – 3.18 (2H, m), 3.15 (1H, ddd, *J* 14.2, 4.2, 0.7 Hz), 2.35 (3H, s), 2.09 (1H, septd, *J* 6.8, 3.3 Hz), 0.87 (3H, d, *J* 6.9 Hz), 0.60 (3H, d, *J* 6.8 Hz). δ_C (126 MHz, $CDCl_3$) 164.3, 162.1, 147.3, 145.0, 144.8, 135.7, 129.7, 128.4, 127.8, 124.8, 123.9,

118.5, 115.1, 60.6, 55.7, 52.5, 52.4, 31.6, 29.3, 21.7, 19.0, 16.6. **CI-HRMS**: m/z calculated for $C_{24}H_{29}N_4O_4S$ $[M+H]^+$ requires 469.1904. Found 469.1908.

Crystal data and structure refinement for 68

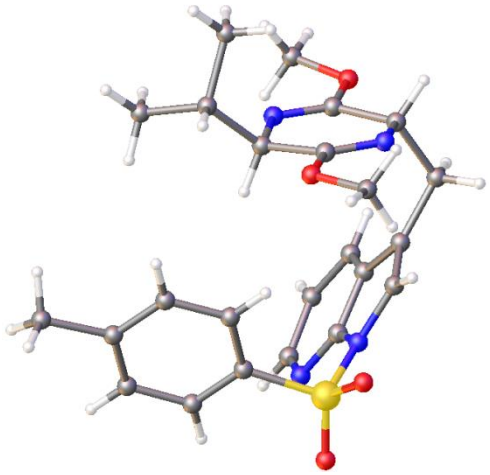

Identification code	**68**
Empirical formula	$C_{24}H_{28}N_4O_4S$
Formula weight	468.56
Temperature/K	150.0
Crystal system	monoclinic
Space group	$P2_1$
a/Å	14.1521(7)
b/Å	9.2610(4)
c/Å	18.1479(8)
α/°	90
β/°	98.786(2)
γ/°	90
Volume/Å^3	2350.60(19)
Z	4
ρ_{calc}g/cm^3	1.324
μ/mm^{-1}	0.176
F(000)	992.0
Radiation	MoKα (λ = 0.71073)
2Θ range for data collection/°	4.95 to 52.882
Index ranges	-17 ≤ h ≤ 17, -11 ≤ k ≤ 11, -22 ≤ l ≤ 22
Reflections collected	27357
Independent reflections	9622 [R_{int} = 0.0373, R_{sigma} = 0.0422]
Data/restraints/parameters	9622/1/605
Goodness-of-fit on F^2	1.042
Final R indexes [I>=2σ (I)]	R_1 = 0.0378, wR_2 = 0.0868
Final R indexes [all data]	R_1 = 0.0487, wR_2 = 0.0926
Largest diff. peak/hole / e Å^{-3}	0.30/-0.35
Flack parameter	0.01(2)

Preparation of 3-(((2*S*,5*R*)-5-isopropyl-3,6-dimethoxy-2,5-dihydropyrazin-2-yl)methyl)-1*H*-pyrrolo[2,3-*b*]pyridine (69)

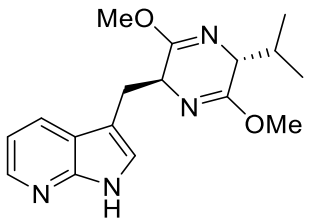

69

To compound **68** (2.53 g, 5.40 mmol, 1 eq) was added THF / MeOH in a 2 : 1 ratio (30 cm^3) and Cs_2CO_3 (3.08 g, 9.46 mmol, 3 eq). The reaction was left to stir overnight at room temperature. Solvents were removed *in vacuo* and the residue dissolved in EtOAc (50 cm^3) and water (50 cm^3). The EtOAc was separated off and the aqueous phase extracted with EtOAc (2 x 50 cm^3) combined organics were washed with water (50 cm^3), brine (50 cm^3) and dried over $MgSO_4$. After filtration solvents were removed *in vacuo* to yield the product **69** as a yellow foam (1.69 g, 99 %). δ_H (500 MHz, $CDCl_3$) 9.54 (1H, s), 8.25 (1H, dd, *J* 4.7, 1.4 Hz), 7.95 (1H, dd, *J* 7.9, 1.4 Hz), 7.07 – 7.00 (1H, m), 4.34 (1H, dd, *J* 8.7, 4.1 Hz), 3.68 (1H, s), 3.65 (1H, s), 3.37 (1H, t, *J* 3.5 Hz), 3.29 (1H, dd, *J* 14.4, 5.0 Hz), 3.24 (1H, dd, *J* 14.3, 4.1 Hz), 2.12 (1H, septd, *J* 6.8, 3.3 Hz), 0.91 (1H, d, *J* 6.8 Hz), 0.61 (1H, d, *J* 6.8 Hz). δ_C (126 MHz, $CDCl_3$) 164.1, 162.8, 148.5, 142.8, 127.9, 123.4, 121.1, 115.4, 110.4, 60.6, 56.7, 52.4, 52.3, 31.5, 29.7, 19.1, 16.6. **CI-HRMS**: m/z calculated for $C_{17}H_{23}N_4O_2$ $[M+H]^+$ requires 315.1816. Found 315.1817.

Preparation of propyl 2-amino-3-(1*H*-pyrrolo[2,3-*b*]pyridin-3-yl)propanoate (70)

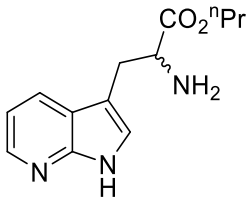

70

To compound **69** (0.98 g, 3.12 mmol, 1 eq) was added THF (20 cm^3) and the solution cooled to 0 °C. To the solution was added 2 M HCl (20 cm^3) and the reaction stirred at room temperature for 2 hours. The reaction was basified to pH 7 using 2 M NaOH. Attempts to extract the product into an organic layer failed. The methyl ester was hydrolysed with 1 M NaOH (10 cm^3) overnight. The solvents were removed *in vacuo*, and the crude amino acid product and salts were then suspended in ^{n}PrOH (10 cm^3) and placed under an argon atmosphere. Thionyl chloride (2.26 cm^3, 31.2 mmol, 10 eq) was added at 0 °C. After warming to room temperature the flask was equipped with a reflux condenser and the system placed under argon. The reaction was the heated to reflux for 12 hours. TLC indicated

the presence of a new spot, the reaction mixture was cooled and quenched with a saturated solution of $NaHCO_3$ (50 cm^3) slowly. Once CO_2 production ceased the product was extracted into EtOAc (3 x 50 cm^3), combined organics were washed with water (50 cm^3), brine (50 cm^3) and dried over $MgSO_4$. After filtration solvents were removed *in vacuo* to yield the product as a white solid **70** (0.13 g, 17 % over 3 steps). HPLC at this stage confirmed racemisation had occurred. δ_H (500 MHz, $CDCl_3$) 9.37 (1H, s), 8.26 (1H, d, *J* 4.4 Hz), 7.95 (1H, d, *J* 8.0 Hz), 7.19 (1H, s), 7.07 (1H, dd, *J* 7.7, 4.8 Hz), 4.08 – 3.99 (2H, m), 3.82 (1H, apparent t), 3.24 (1H, dd, *J* 14.5, 5.2 Hz), 3.09 (1H, dd, *J* 14.5, 7.1 Hz), 2.09 (2H, s), 1.65 – 1.56 (2H, m), 0.87 (3H, t, *J* 7.4 Hz). δ_C (126 MHz, $CDCl_3$) 175.0, 148.7, 142.2, 127.6, 124.3, 120.5, 115.3, 109.1, 66.8, 55.1, 30.5, 21.9, 10.3. **CI-HRMS**: m/z calculated for $C_{13}H_{18}N_3O_2$ $[M+H]^+$ requires 248.1394. Found 248.1398. **HPLC** (purity analysis %) found: Purity peak 1 51 %; Retention time: 8.52 min: purity peak 2 49 %; Retention time: 19.00 / 30 min (0.5 ml/min MeOH, Signal = 254 nm, CHIRACEL OJ column).

Preparation of propyl (6*S*,8*R* / 6*R*,8*S*)-8-(2,4-dichlorophenyl)-6,7,8,9-tetrahydro-5*H*-pyrrolo[2,3-*b*:5,4-*c*']dipyridine-6-carboxylate (71) and propyl (6*S*,8*S* / 6*R*,8*R*)-8-(2,4-dichlorophenyl)-6,7,8,9-tetrahydro-5*H*-pyrrolo[2,3-*b*:5,4-*c*']dipyridine-6-carboxylate (72)

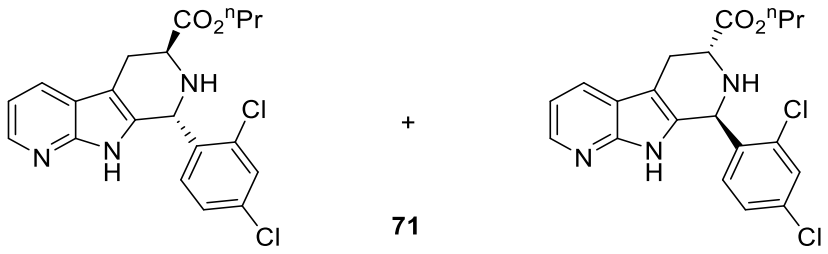

In a flame dried round bottomed flask was added compound **70** (0.13 g, 0.51 mmol, 1 eq) and 2, 4 dichlorobenzaldehyde (0.097 g, 0.56 mmol, 1.1 eq) and anhydrous toluene (5 cm^3) under an argon atmosphere. The reaction was heated to reflux for 24 hours, the dark brown solution was evaporated to dryness and the residue dissolved in EtOAc (50 cm^3) and brine (50 cm^3). The EtOAc was separated and the brine layer extracted with EtOAc (2 x 50 cm^3), combined organics were dried over $MgSO_4$. After filtration, solvents were removed *in vacuo* and the product purified by column chromatography (100 % DCM to 20 % EtOAc in DCM). *Cis* and *trans* isomers were further purified by recrystallisation in MeOH, to yield **71** as a white powder (0.035 g, 16 %). δ_H (500 MHz, $CDCl_3$) 10.72 (1H, s), 7.84 (1H, d, *J* 7.7 Hz), 7.77 (1H, d, *J* 4.8 Hz), 7.52 (1H, d, *J* 1.8 Hz), 7.07 (1H, dd, *J* 8.3, 1.7 Hz), 7.00 (1H, dd, *J* 7.8, 4.9 Hz), 6.90 (1H, d, *J* 8.4 Hz), 5.94 (1H, s), 4.09 (2H, t, *J* 6.7 Hz), 3.85 (1H, dd, *J* 7.4, 5.0 Hz), 3.22 (1H, dd, *J* 15.3, 4.9 Hz), 3.08 (1H, dd, *J* 15.3, 7.6 Hz), 2.85 (1H, s), 1.70 – 1.60 (2H, m), 0.92 (3H, t, *J* 7.4 Hz). δ_C (126 MHz, $CDCl_3$) 173.2, 149.2, 142.1, 137.6, 134.7, 134.7, 132.7, 131.0, 129.9, 127.5, 126.7, 119.8, 115.8, 108.1, 67.0, 52.4, 51.4, 24.7, 22.1, 10.5. **CI-HRMS**: m/z calculated for $C_{20}H_{20}{}^{35}Cl_2N_3O_2$ $[M+H]^+$ requires 404.0927. Found 404.0934.

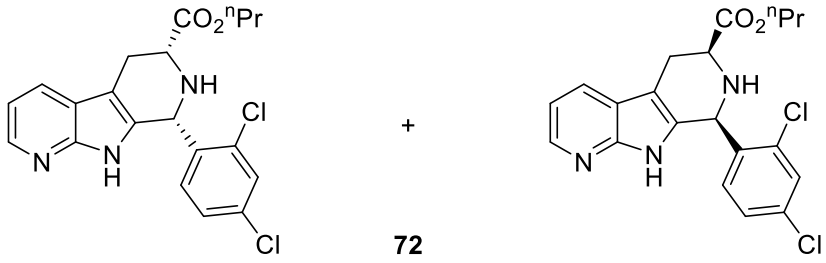

72

The same procedure also gave **72** as a white powder (0.027 g, 12 %). δ_H (500 MHz, $CDCl_3$) 10.61 (1H, s), 7.82 (1H, d, *J* 7.8 Hz), 7.61 (1H, d, *J* 4.4 Hz), 7.49 (1H, s), 7.26 (1H, d, *J* 8.0 Hz), 7.11 (1H, d, *J* 8.1 Hz), 6.97 (1H, dd, *J* 7.6, 4.9 Hz), 5.83 (1H, s), 4.23 – 4.17 (1H, m), 4.17 – 4.11 (1H, m), 3.97 (1H, dd, *J* 10.9, 3.6 Hz), 3.19 (1H, dd, *J* 15.1, 2.9 Hz), 3.04 – 2.94 (1H, m), 2.66 (1H, s), 1.79 – 1.68 (2H, m), 0.99 (3H, t, *J* 7.4 Hz). δ_C (126 MHz, $CDCl_3$) 172.5, 149.2, 142.0, 137.0, 135.0, 134.7, 134.1, 131.6, 129.5, 128.2, 126.6, 119.9, 115.7, 108.0, 67.1, 56.7, 25.3, 22.1, 10.5. **CI-HRMS**: m/z calculated for $C_{20}H_{20}{}^{35}Cl_2N_3O_2$ $[M+H]^+$ requires 404.0927. Found 404.0920.

Preparation of (6*S*,8*R* / 6*R*,8*S*)-8-(2,4-dichlorophenyl)-*N*-methyl-6,7,8,9-tetrahydro-5*H*-pyrrolo[2,3-*b*:5,4-*c*']dipyridine-6-carboxamide (73)

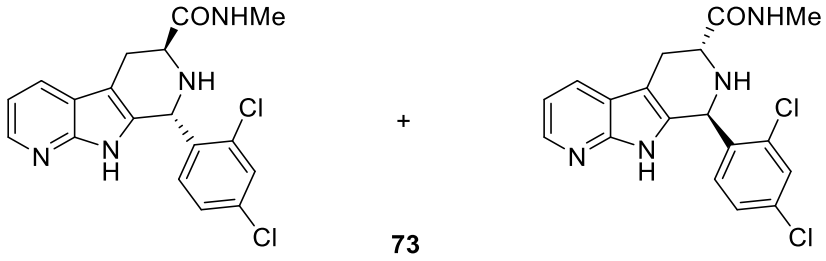

73

Compound **71** (0.035 g, 0.085 mmol, 1 eq) and methyl amine 33 % in EtOH (1.77 cm^3, 14.25 mmol, 167 eq) were used following **general procedure 2**. Gave the desired product **73** as white crystals (0.016 g, 49 %). δ_H (500 MHz, MeOD) 8.14 (1H, d, *J* 4.9 Hz), 7.97 (1H, d, *J* 7.9 Hz), 7.58 (1H, d, *J* 2.0 Hz), 7.21 (1H, dd, *J* 8.3, 2.0 Hz), 7.11 (1H, dd, *J* 7.8, 4.9 Hz), 6.75 (1H, d, *J* 8.3 Hz), 5.77 (1H, s), 3.56 (1H, dd, *J* 10.3, 4.5 Hz), 3.18 (1H, dd, *J* 15.5, 4.5 Hz), 2.85 (1H, dd, *J* 15.5, 10.3 Hz), 2.75 (3H, s). δ_C (126 MHz, MeOD) 175.6, 149.8, 143.2, 138.8, 136.4, 135.4, 134.6, 132.3, 130.8, 128.0, 127.9, 121.4, 116.6, 110.0, 53.0, 52.6, 26.3, 25.7. **CI-HRMS**: m/z calculated for $C_{18}H_{17}{}^{35}Cl_2N_4O$ $[M+H]^+$ requires 375.0774. Found 375.0781. **Elemental Analysis** Calculated for $C_{18}H_{16}Cl_2N_4O$ requires C, 57.61 %, H, 4.30 %, N, 14.93 %. Found C, 57.33 %, H, 4.30 %, N, 14.80 %. **IR (neat)**: ν_{max}/cm^{-1}: 3404 (m), 3381 (m), 3138 (m, br), 3049 (m, br), 2937 (m, br), 2895 (m, br), 2840 (m, br), 1672 (s), 1519 (s), 1409 (s), 1035 (m), 766 (s). **HPLC** (purity analysis %) found: Purity peak 1 53 %; Retention time: 7.65 min: purity peak 2 47 %; Retention time: 21.45 / 30 min (0.5 ml/min MeOH, Signal = 254 nm, CHIRACEL OJ column).

Crystal data and structure refinement for 73

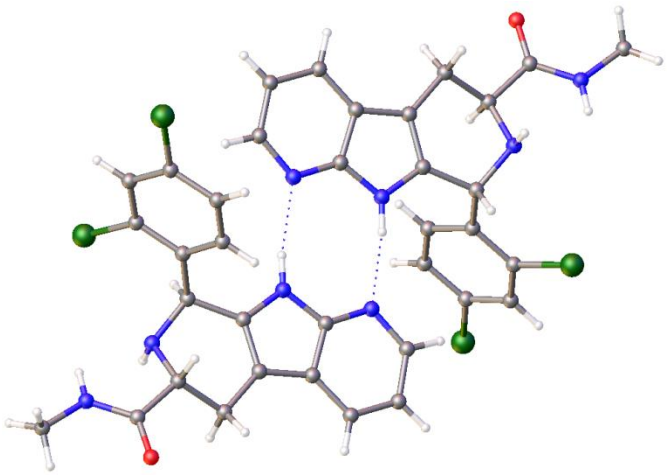

Identification code	**73**
Empirical formula	$C_{18}H_{16}N_4OCl_2$
Formula weight	375.253
Temperature/K	150.0
Crystal system	orthorhombic
Space group	Pbca
a/Å	22.2802(7)
b/Å	13.9229(5)
c/Å	22.3088(6)
α/°	90
β/°	90
γ/°	90
Volume/Å^3	6920.3(4)
Z	8
ρ_{calc}g/cm^3	1.307
μ/mm^{-1}	0.076
F(000)	2920.0
Radiation	MoKα (λ = 0.71073)
2Θ range for data collection/°	4.682 to 52.798
Index ranges	-27 ≤ h ≤ 27, -17 ≤ k ≤ 15, -27 ≤ l ≤ 27
Reflections collected	33085
Independent reflections	7084 [R_{int} = 0.0683, R_{sigma} = 0.0477]
Data/restraints/parameters	7084/0/461
Goodness-of-fit on F^2	1.035
Final R indexes [I>=2σ (I)]	R_1 = 0.0440, wR_2 = 0.0906
Final R indexes [all data]	R_1 = 0.0717, wR_2 = 0.1006
Largest diff. peak/hole / e Å^{-3}	0.33/-0.44

Molecular Modelling Protocol

Compounds were first built in chemdraw and transferred to Spartan, compounds were then energy minimised, Spartan was used to compute local energy minimum geometry using molecular mechanics with the MMFF94 force field. Compounds were then docked in GOLD using the homology model previously built by our group. The docking protocol is outline in the table below. Early termination was not allowed and lone pairs were not saved, all other parameters were left default.

Mg^{2+}	Mg^{2+} present, no coordination geometry specified
Protonation	Hydrogens added
Waters	Water molecule HOH1091 extracted, all other waters deleted, water was set as toggle, spin
Ligands	CDPME extracted
Binding site	Defined as 6 Å of the CDPME ligand
Number of GA Runs	10, 50, 100, 500
Scoring Function	GOLDscore

2.6 References

(1) Gamo, F.-J.; Sanz, L. M.; Vidal, J.; de Cozar, C.; Alvarez, E.; Lavandera, J.-L.; Vanderwall, D. E.; Green, D. V. S.; Kumar, V.; Hasan, S.; Brown, J. R.; Peishoff, C. E.; Cardon, L. R.; Garcia-Bustos, J. F. *Nature* **2010**, *465* (7296), 305–310.

(2) Spangenberg, T.; Burrows, J. N.; Kowalczyk, P.; McDonald, S.; Wells, T. N. C.; Willis, P. *PLoS One* **2013**, *8* (6).

(3) Bowman, J. D.; Merino, E. F.; Brooks, C. F.; Striepen, B.; Carlier, P. R.; Cassera, M. B. *Antimicrob. Agents Chemother.* **2014**, *58* (2), 811–819.

(4) Wu, W.; Herrera, Z.; Ebert, D.; Baska, K.; Cho, S. H.; DeRisi, J. L.; Yeh, E. *Antimicrob. Agents Chemother.* **2015**, *59* (1), 356–364.

(5) Cassera, M. B.; Merino, E. F.; Peres, V. J.; Kimura, E. A.; Wunderlich, G.; Katzin, A. M. *Mem. Inst. Oswaldo Cruz* **2007**, *102* (3), 377–383.

(6) Cassera, M. B.; Gozzo, F. C.; D'Alexandri, F. L.; Merino, E. F.; Del Portillo, H. A.; Peres, V. J.; Almeida, I. C.; Eberlin, M. N.; Wunderlich, G.; Wiesner, J.; Jomaa, H.; Kimura, E. A.; Katzin, A. M. *J. Biol. Chem.* **2004**, *279* (50), 51749–51759.

(7) Fichera, M. E.; Roos, D. S. *Nature* **1997**, *390* (6658), 407–409.

(8) Imlay, L. S.; Armstrong, C. M.; Masters, M. C.; Li, T.; Price, K. E.; Edwards, R. L.; Mann, K. M.; Li, L. X.; Stallings, C. L.; Berry, N. G.; O'Neill, P. M.; Odom, A. R. *ACS Infect. Dis.* **2016**, *1* (4), 157–167.

(9) Yao, Z.; Krai, P. M.; Merino, E. F.; Simpson, M. E.; Slebodnick, C.; Belen, M.; Carlier, P. R. *Bioorg. Med. Chem. Lett.* **2015**, *25* (7), 1515–1519.

(10) Ballatore, C.; Huryn, D. M.; Smith, A. B. *ChemMedChem* **2013**, *8* (3), 385–395.

(11) Laine, A. E.; Lood, C.; Koskinen, A. M. P. *Molecules* **2014**, *19* (2), 1544–1567.

(12) Daugan, A.; Grondin, P.; Ruault, C.; Le Monnier de Gouville, A. C.; Coste, H.; Kirilovsky, J.; Hyafil, F.; Labaudiniere, R. *J Med Chem* **2003**, *46* (21), 4525–4532.

(13) Hotha, S.; Yarrow, J. C.; Yang, J. G.; Garrett, S.; Renduchintala, K. V.; Mayer, T. U.; Kapoor, T. M. *Angew. Chemie - Int. Ed.* **2003**, *42* (21), 2379–2382.

(14) Gupta, L.; Srivastava, K.; Singh, S.; Puri, S. K.; Chauhan, P. M. S. *Bioorganic Med. Chem. Lett.* **2008**, *18* (11), 3306–3309.

(15) Yeung, B. K. S.; Zou, B.; Rottmann, M.; Lakshminarayana, S. B.; Ang, S. H.; Leong, S. Y.; Tan, J.; Wong, J.; Keller-Maerki, S.; Fischli, C.; Goh, A.;; *et al. J. Med. Chem.* **2010**, *53* (14), 5155–5164.

(16) Turner, H. *Future Med. Chem.* **2016**, *8* (2), 227–238.
(17) Rottmann, M.; McNamara, C.; Yeung, B. K. S.; Lee, M. C. S.; Zou, B.; Russell, B.; Seitz, P.; Plouffe, D. M.; Dharia, N. V; Tan, J.; Cohen, S. B.; Spencer, K. R.; *et al. Science* **2010**, *329* (5996), 1175–1180.
(18) Smith, P. W.; Diagana, T. T.; Yeung, B. K. S. *Parasitology* **2014**, *141* (1), 66–76.
(19) Pictet, A.; Spengler, T. *Berichte der Dtsch. Chem. Gesellschaft* **1911**, *44* (3), 2030–2036.
(20) Stöckigt, J.; Antonchick, A. P.; Wu, F.; Waldmann, H. *Angew. Chemie - Int. Ed.* **2011**, *50* (37), 8538–8564.
(21) Maryanoff, B. E.; Zhang, H. C.; Cohen, J. H.; Turchi, I. J.; Maryanoff, C. A. *Chem. Rev.* **2004**, *104* (3), 1431–1628.
(22) Jackson, A. H.; Smith, A. E. *Tetrahedron* **1968**, *24* (1), 403–413.
(23) Cox, E. D.; Cook, J. M. *Chem. Rev.* **1995**, *95* (6), 1797–1842.
(24) Czerwinski, K. M.; Deng, L.; Cook, J. M. *Tetrahedron Lett.* **1992**, *33* (33), 4721–4724.
(25) Liu, J.; Nakagawa, M.; Ogata, K.; Hino, T. *Chem. Pharm. Bull* **1991**, *39* (7), 1672–1676.
(26) Cox, E. D.; Hamaker, L. K.; Li, J.; Yu, P.; Czerwinski, K. M.; Deng, L.; Bennett, D. W.; Cook, J. M.; Watson, W. H.; Krawiec, M. *J. Org. Chem.* **1997**, *62* (1), 44–61.
(27) Deng, L.; Czerwinski, K.; Cook, J. M. *Tetrahedron Lett.* **1991**, *32* (2), 175–178.
(28) Ungemach, F.; Dipierro, M.; Weber, R.; Cook, J. M. **1979**, No. 35, 3225–3228.
(29) Van Linn, M. L.; Cook, J. M. *J. Org. Chem.* **2010**, *75* (11), 3587–3599.
(30) Kumpaty, H. J.; Linn, M. L. Van; Kabir, M. S.; Fo, F. H.; Deschamps, J. R.; Cook, J. M. **2009**, No. 1, 2771–2779.
(31) Han, D.; Försterling, F. H.; Deschamps, J. R.; Parrish, D.; Liu, X.; Yin, W.; Huang, S.; Cook, J. M. *J. Nat. Prod.* **2007**, *70* (1), 75–82.
(32) Anet, F. A. L.; Bourn, A. J. R.; Carter, P.; Winstein, S. *J. Am. Chem. Soc.* **1965**, *87* (22), 5250–5251.
(33) Flack, H. D. *Acta Crystallogr. Sect. A* **1983**, *39* (6), 876–881.
(34) Cecilia Noguez, F. H. *Chirality* **2008**, *20*, 681–690.
(35) Parsons, S.; Flack, H. *Acta Crystallogr. Sect. A Found. Crystallogr.* **2004**, *60*, s61–s61.
(36) Dolomanov, O. V; Bourhis, L. J.; Gildea, R. J.; Howard, J. A. K.; Puschmann, H. *J. Appl. Crystallogr.* **2009**, *42* (2), 339–341.
(37) Webb, M. R. *Proc. Natl. Acad. Sci. U. S. A.* **1992**, *89* (11), 4884–4887.
(38) Corbett, Y.; Herrera, L.; Gonzalez, J.; Cubilla, L.; Capson, T. L.; Coley, P. D.; Kursar, T. A.; Romero, L. I.; Ortega-Barria, E. *Am. J. Trop. Med. Hyg.* **2004**, *70* (2), 119–124.
(39) Cyprotex. *Everything you need to know about ADME*; **2015**.
(40) Lipinski, C. A.; Lombardo, F.; Dominy, B. W.; Feeney, P. J. *Adv. Drug Deliv. Rev.* **1997**, *23*, 3–25.
(41) Hartmann, T.; Schmitt, J. *Drug Discov. Today Technol.* **2004**, *1* (4), 431–439.
(42) Emanuel, H.; Grundschober, A. F.; Leuthold, S.; Meier, P. J.; St-pierre, M. V; Perfetto, S. P.; Chattopadhyay, P. K.; *et al. Functional Analysis of the Extracellular Cysteine Residues in the Human Organic Anion Transporting Polypeptide , OATP2B1*; **2015**; Vol. 63.
(43) Hill, A. P.; Young, R. J. *Drug Discov. Today* **2010**, *15* (15–16), 648–655.
(44) Jadhav, A.; Ferreira, R. S.; Klumpp, C.; Mott, B. T.; Austin, C. P.; Inglese, J.; Thomas, C. J.; Maloney, D. J.; Shoichet, B. K.; Simeonov, A. *J. Med. Chem.* **2010**, *53* (1), 37–51.
(45) Coan, K. E. D.; Maltby, D. A.; Burlingame, A. L.; Shoichet, B. K. *J. Med. Chem.* **2009**, *52* (7), 2067–2075.
(46) Coan, K. E. D.; Shoichet, B. K. *J. Am. Chem. Soc.* **2008**, *130* (29), 9606–9612.
(47) Ritchie, T. J.; Macdonald, S. J. F. *Drug Discov. Today* **2009**, *14* (21–22), 1011–1020.
(48) Sanghvi, T.; Jain, N.; Yang, G.; Yalkowsky, S. *QSAR Comb. Sci.* **2003**, *22* (2), 258–262.
(49) Delaney, J. S. *J. Chem. Inf. Comput. Sci.* **2004**, *44* (3), 1000–1005.
(50) Csizmadia, F.; Tsantili-Kakoulidou, A.; Panderi, I.; Darvas, F. *J. Pharm. Sci.* **1997**, *86* (7), 865–871.
(51) http://accelrys.com/products/collaborative-science/biovia-pipeline-pilot/ (Accessed 22nd

Febrauary **2018**).
(52) McGovern, S. L.; Helfand, B. T.; Feng, B.; Shoichet, B. K. *J. Med. Chem.* **2003**, *46* (20), 4265–4272.
(53) Feng, B. Y.; Simeonov, A.; Jadhav, A.; Babaoglu, K.; Inglese, J.; Shoichet, B. K.; Austin, C. P. *J. Med. Chem.* **2007**, *50* (10), 2385–2390.
(54) Williams, H. D.; Trevaskis, N. L.; Charman, S. A.; Shanker, R. M.; Charman, W. N.; Pouton, C. W.; Porter, C. J. H. *Pharmacol. Rev.* **2013**, *65* (1), 315–499.
(55) Cyprotex. Metabolic stability can be found under http://www.cyprotex.com/admepk/in-vitro-metabolism/microsomal-stability Accessed August 30th **2017**).
(56) Bondi, A. *J. Phys. Chem.* **1964**, *68* (3), 441–451.
(57) Swallow, S. *Prog. Med. Chem.* **2015**, *54*, 65–133.
(58) Luo, Y.-R.; Kerr, J. A. *CRC Handb. Chem. Phys.* **2012**, *89*, 65–98.
(59) Dunitz, J. D.; Taylor, R. *Chem. - A Eur. J.* **1997**, *3* (1), 89–98.
(60) Dunitz, J. D. *ChemBioChem* **2004**, *5* (5), 614–621.
(61) Mohamed, H. A.; Girgis, N. M. R.; Wilcken, R.; Bauer, M. R.; Tinsley, H. N.; Gary, B. D.; Piazza, G. A.; Boeckler, F. M.; Abadi, A. H. *J. Med. Chem.* **2011**, *54* (2), 495–509.
(62) Abadi, Ashraf, H. Tetrahydro-β-carboline derivatives, synthesis and use thereof. WO2011/063223 A1, **2011**.
(63) Tang, J. G.; Wang, Y. H.; Wang, R. R.; Dong, Z. J.; Yang, L. M.; Zheng, Y. T.; Liu, J. K. *Chem. Biodivers.* **2008**, *5* (3), 447–460.
(64) Moon, Y.-C.; Cao, L.; Tamilarasu, N.; Qi, H.; Choi, S.; Lennox, William, J.; Corson, Donald, T. TETRA-CYCLIC CARBOLINE DERIVATIVES FOR INHIBITING ANGIOGENESIS. PCT/US2005/008452, **2005**.
(65) PORTER, J.; DYKERT, J.; RIVIER, J. *Int. J. Pept. Protein Res.* **1987**, *30* (1), 13–21.
(66) Blaser, G.; Sanderson, J. M.; Batsanov, A. S.; Howard, J. A. K. *Tetrahedron Lett.* **2008**, *49* (17), 2795–2798.
(67) Konda-Yamada, Y.; Okada, C.; Yoshida, K.; Umeda, Y.; Arima, S.; Sato, N.; Kai, T.; Takayanagi, H.; Harigaya, Y. *Tetrahedron* **2002**, *58* (39), 7851–7861.
(68) Mollica, A.; Stefanucci, A.; Feliciani, F.; Lucente, G.; Pinnen, F. *Tetrahedron Lett.* **2011**, *52* (20), 2583–2585.
(69) Li, X.; Yin, W.; Sarma, P. V. V. S.; Zhou, H.; Jun Ma; Cook, J. M. *Tetrahedron Lett.* **2004**, *45* (46), 8569–8573.
(70) Talukder, P.; Chen, S.; Liu, C. T.; Baldwin, E. A.; Benkovic, S. J.; Hecht, S. M. *Bioorganic Med. Chem.* **2014**, *22* (21), 5924–5934.
(71) Richelson, E.; Cusack, B. M.; Pang, Y.-P.; McCormick, D. J.; Fauq, A.; Tyler, B. M.; Boules, M. Neo-tryptophan. US2007/0173458 A1, **2007**.
(72) Bajwa, J. S.; Chen, G. P.; Prasad, K.; Repic, O.; Blacklock, T. J. *Tetrahedron Lett.* **2006**, *47* (36), 6425–6427.
(73) Bahekar, R. H.; Jain, M. R.; Jadav, P. A.; Goel, A.; Patel, D. N.; Prajapati, V. M.; Gupta, A. A.; Modi, H.; Patel, P. R. *Bioorganic Med. Chem.* **2007**, *15* (17), 5950–5964.
(74) Sharma, R. *Personal communication* **2013**.
(75) Kitchen, D. B.; Decornez, H.; Furr, J. R.; Bajorath, J. *Nat. Rev. Drug Discov.* **2004**, *3* (11), 935–949.
(76) Jones, G.; Willett, P.; Glen, R. C.; Leach, A. R.; Taylor, R. *J. Mol. Biol.* **1997**, *267* (3), 727–748.
(77) Verdonk, M. L.; Cole, J. C.; Hartshorn, M. J.; Murray, C. W.; Taylor, R. D. *Proteins Struct. Funct. Bioinforma.* **2003**, *623* (January), 609–623.
(78) CambridgeSoft. PerkinElmer Informatics **2016**.
(79) Wavefunction, I. Spartan **2016**.
(80) Schrödinger, LLC. *PyMOL Molecular Graphics, Version~1.8*; **2015**.
(81) Carlier, P. R.; CASSERA, M. B.; MERINO, E. F.; YAO, Z.; GHAVAMI, M. Google Patents May 6, **2016**.

Chapter 3: Development of Ebsulfur, Ebselen and Benzothiazine Analogues as Inhibitors of *Pf*IspD

3.1 Chemotype Identification

In the previous chapter, SAR around the MMV008138 chemical scaffold was presented. As part of a wider research programme, we wanted explore and develop alternative novel inhibitors of *Pf*IspD, and undertake a medicinal chemistry programme to optimise whole cell potency.

In order to identify a template for optimisation and development of SAR, an enzymatic HTS screen was undertaken using a chemoinformatics approach. A series of *in silico* similarity searches were carried out in order to explore chemical space for potential hits around known *Pf*IspD active compounds. In addition scaffold-hopping methods were employed which allowed for identification of novel chemotypes. A compound library held by Biofocus of approximately 500,000 compounds was queried for potential drug molecules that incorporate numerous criteria as displayed below.[1,2]

- Compounds structurally similar to IspD natural substrates (MEP, CTP (see Chapter 2 for structures))
- Compounds structurally similar to IspC natural substrates (DXP)
- Compounds structurally similar to known IspD inhibitors ≤ 1 μM (azolopyrimidines)
- Compounds structurally similar to known IspC inhibitors ≤ 1 μM (Fosmidomycin (FOS) and other FOS mimetics)
- Compounds that possess metal chelating moieties (Hydroxamic acids)
- Compounds possessing biphosphate isosteres

Screening for compounds in this way holds numerous advantages; firstly, using the similarity principle, structurally similar compounds to IspD substrates are more likely to show biological activity,[3,4] therefore mimetics of the natural substrates of IspD could be potent inhibitors, secondly compounds were also cross-examined with structural similarities to both the IspC substrate and inhibitors such as fosmidomycin (FOS) which also shows some activity against IspD (IC_{50} = 20.4 ± 3.3 mM *Ec*IspD).[5] Furthermore FOS and its derived mimics are substrate-like to MEP and therefore structures baring similarity to FOS my also show inhibitory IspD activity. Thirdly, the examination of compounds baring similarity to already known IspD inhibitors also raised the potential of finding a hit molecule, as the chemical space occupied by these ligands is already at least partially suited to the enzyme. Fourthly, all enzymes within the MEP pathway require a divalent metal ion to stabilise and coordinate the substrates and products for catalysis; the IspD enzyme requires Mg^{2+} to function, therefore by employing a strategy that searches for metal chelating moieties, any potential hit could possess enhanced binding energy within the active site *via* coordination to the metal group, which would prevent substrate entry.[6] Finally, the substrates and product of the IspD enzymatic

transformation all have phosphate moieties that possess crucial binding interactions in the active site.[7–10] Replacement of these moieties with potential bioisosteres could lead to reasonable starting points for optimisation.

The compounds were ranked for similarity using the Tanimoto co-efficient; this co-efficient is a similarity metric which takes values between 0 and 1 where 1 classes a compound as identical.[11] For the study undertaken by our group, compounds possessing values greater than 0.7 were selected for further investigation. To incorporate scaffold hopping, compounds also possessing Tanimoto co-efficient values between 0.2 and 0.4 were also selected for further investigation to increase compound diversity.[1]

The end result of this computational screening process was a reduction of 500,000 potential compounds down to 23,000. In order to filter this down further, these 23,000 compounds were docked into the known crystal structures of both IspC and IspD. As the IspD crystal structure is not available for *P. falciparum*, docking was carried out on the active site of *E. coli* IspD and the allosteric binding site of *A. thaliana* IspD. Compounds were assessed and ranked according to their GOLD scores, which is a prediction of the binding affinity within the selected pocket. Compounds with high docking scores were favourable, as these were predicated to be inhibitors. Finally, compounds were also filtered according to their solubility assessment. Solubility was calculated computationally in collaboration with AstraZeneca and compounds were selected with calculated LogS ($moldm^{-3}$) of greater than -3.5.[12,13] Ultimately after the combination of chemoinformatics, computational docking and solubility assessment was undertaken, the 23,000 compounds were filtered into a focused library of 5000 compounds that could be taken forward into a HTS screening programme.[1,2]

The HTS was carried out following the protocol for the IspD pyrophosphate release assay developed by our collaborators at Washington University (Odom group) was transferred to Biofocus.[14] The compounds were tested directly against purified *Pf*IspD in order to determine the enzymatic inhibitory activities. Compounds were classified as hits when IC_{50} values of ≤ 20 μM were observed. The 5000 compounds were successfully evaluated by Biofocus from the 5-point dose response screening of 316 plates. Originally 76 compounds were identified to possess IspD inhibition activity, however, this number was reduced after confirming purity of the compounds by LCMS. For a compound to be classified as active it was required to possess purity greater than 75 %. After purity analysis, the compound set was reduced to 54. Across these 54 compounds there were 10 potential chemotypes identified for additional analysis. Across all the compounds, motifs possessing a benzoisothiazolone (BITZ) chemotype frequently were observed to be active, amongst which

compound **1** was identified as one of the most potent compounds in the series, with an IC_{50} value of 480 nM (Figure 3.1).[1]

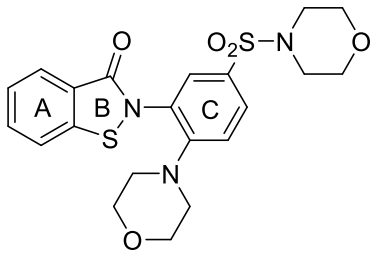

1

Figure 3.1. Hit from HTS screen.

It was observed that all compounds possessing a BITZ core demonstrated good *Pf*IspD activity (<1 μM). Further to this, the synthesis of the BITZ chemotype appeared to possess tractable SAR, and finally, examination of the literature indicated that this compound class has never been used as an inhibitor of *Pf*IspD, as a result, this chemotype was selected for SAR optimisation.

3.2 Known BITZ SAR Exploration and Synthesis

Extensive SAR has been carried out by members of our group and is described briefly in the following sections. Hit **1**, was difficult to synthesise and was replaced with compound **8** with the *ortho* morpholine removed from the C-ring (Scheme 3.1). Further to this compound **9** (also referred to as ebsulfur) was synthesised bearing no C-ring functionality, this molecule was important as it provided a distinct branching point from which further SAR was undertaken. Both compounds were synthesised by former PhD student Dr Kathryn Price following Scheme 3.1.

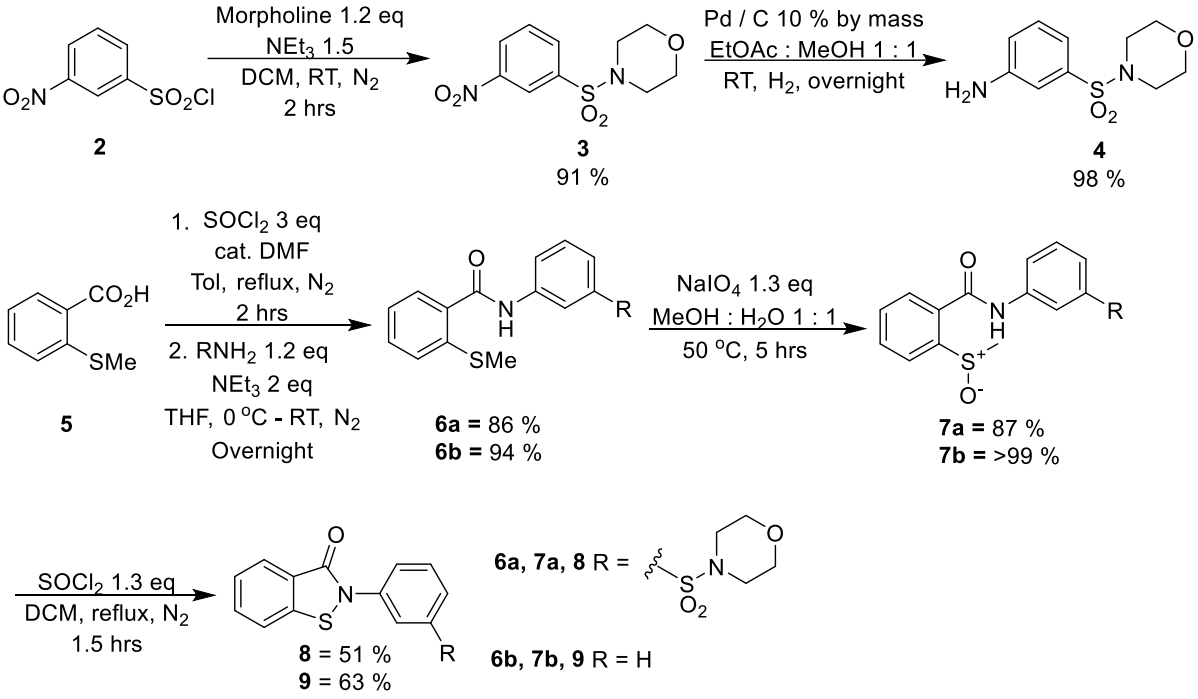

Scheme 3.1. Synthesis of compounds 8 and 9.

Compound **8** was prepared *via* a 5-step synthesis as depicted by Scheme 3.1; first, 3-nitrobenzene sulfonyl chloride (**2**) was coupled with morpholine to form the sulfonamide (**3**). This was followed by nitro group reduction in the presence of H_2 using Pd / C hydrogenation conditions forming **4**.[15,16] **4** was coupled with 2-methylthiobenzoic acid (**5**), *via* $SOCl_2$ mediated peptide coupling procedures which yielded **6a** before sodium periodiate oxidised the thiol group gave the sulfoxide (**7a**), finally reaction of **7a** with $SOCl_2$ promotes ring closure to the desired target **8**.[17–19] Compound **9** was made analogously to **8**, however, aniline could be purchased used directly. Aniline was coupled with **5** to form **6b,** oxidation of **6b** yielded **7b**, which after $SOCl_2$ mediated ring closure yielded **9**. The final step does appear to possess an unusual mechanism and follows a similar reaction to a Pummerer rearrangement as shown below (Figure 3.2) but does not form the Pummerer product.[18]

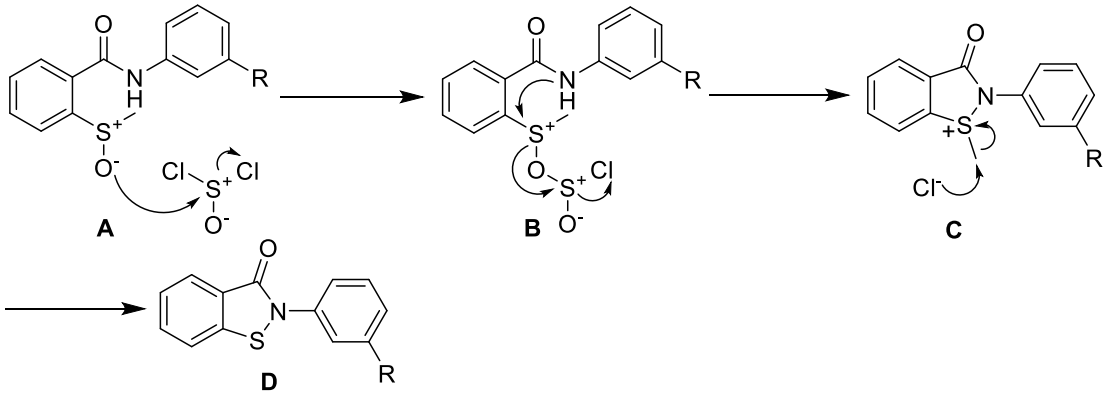

Figure 3.2. Mechanism of sulfoxide ring closure.

In addition to Scheme 3.1, a shorter alternative scheme was also utilised for the synthesis of **8** and **9** (by former PhD student Dr Kathryn Price) using a copper-catalysed heteroatom ring closing reaction for the generation of BITZ compounds (Scheme 3.2).[20]

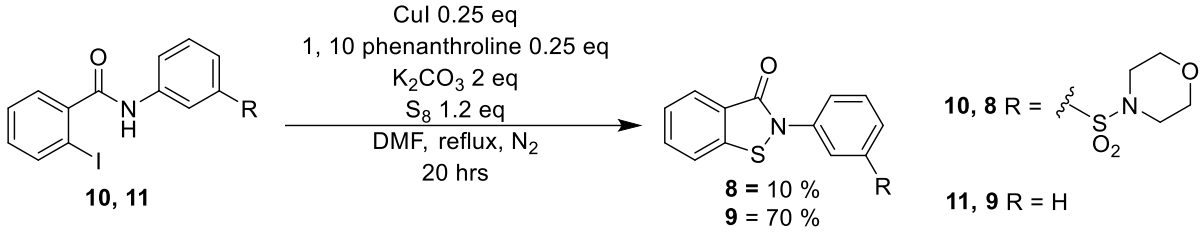

Scheme 3.2. Alternate ring closing route using Cu catalysis.

The reaction utilises *ortho*-iodobenzamide intermediates **10** or **11** as a coordinating group for a Cu(I) species. The mechanism is likely to proceed as follows. First the Cu(I) ligand species (Cu(I)L) is coordinated by the amide nitrogen (**A**), before deprotonation by base (**B**). Elemental sulfur (S_8) then inserts between the Cu-N bond (**C**), the Cu(I) species is then set up for oxidative addition into the C-I bond forming a 6-membered intermediate and a unstable Cu(III) species (**D**), this can then reductively eliminate reforming the catalytic Cu(I) species and releases the product (**E**) (Figure 3.3).

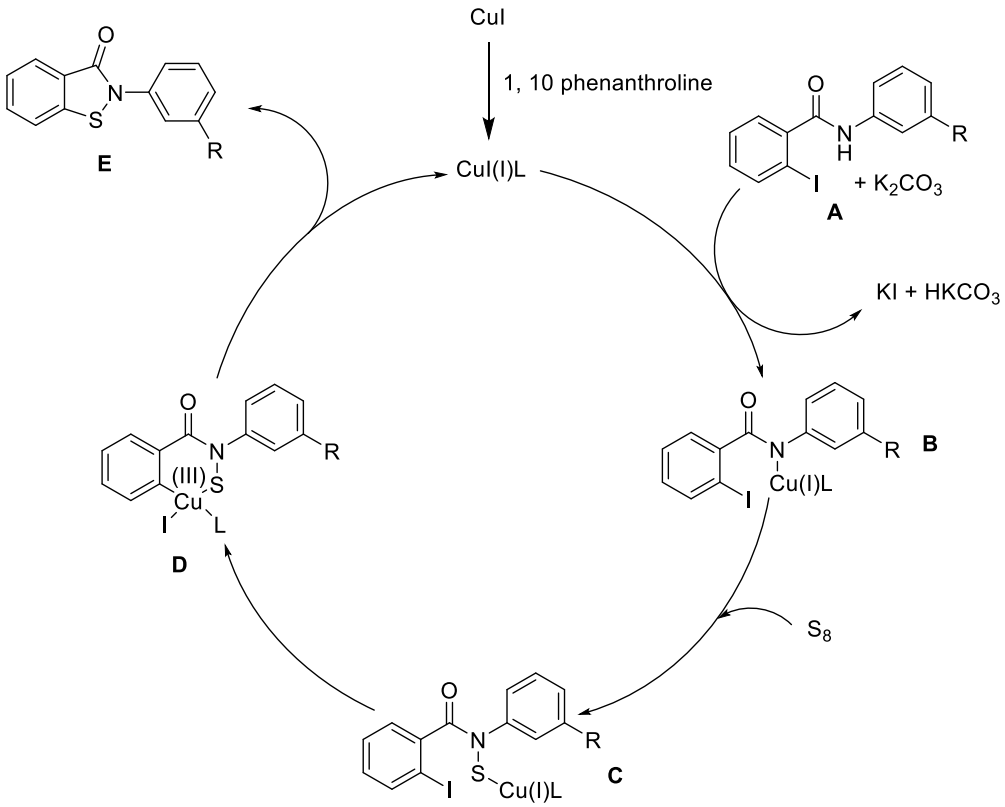

Figure 3.3. Mechanism of Cu promoted ring closure.

The advantage of the approach depicted in Scheme 3.2 *vs* Scheme 3.1 is that it is a shorter synthesis with a better-cost effectiveness in terms of starting materials. Furthermore the authors state

that this method is a more environmentally friendly synthesis than other reported methods for BITZ compound generation.[20] Therefore this makes this route more attractive from a drug-development point of view.

An additional approach that has been studied in detail in the group is depicted in Scheme 3.3. This approach provides a very fast and efficient way to generate BITZ compounds cleanly without the need for metal catalysts. The reaction involves the generation of 2-(chlorocarbonyl)phenyl hypochlorothioite (**14**), which can be successfully synthesised *via* a two-step procedure. Starting from 2,2'-dithiodibenzoic acid (**12**) and refluxing in dichloroethane (DCE) in the presence of $SOCl_2$ forms the acyl chloride intermediate (**13**). The disulfide bridge within **13** can be cleaved *in situ*, the addition of a source of Cl_2 such as SO_2Cl_2 followed by heating generates two equivalents of **14** in quantitative yield.[21] Compound **14** is stable and is a versatile intermediate that can be stored for many months. Reaction with an amine results in ring closure in a two-step process.[22,23] Reactions often proceed cleanly and can occasionally be purified from just a simple work-up (Scheme 3.3).

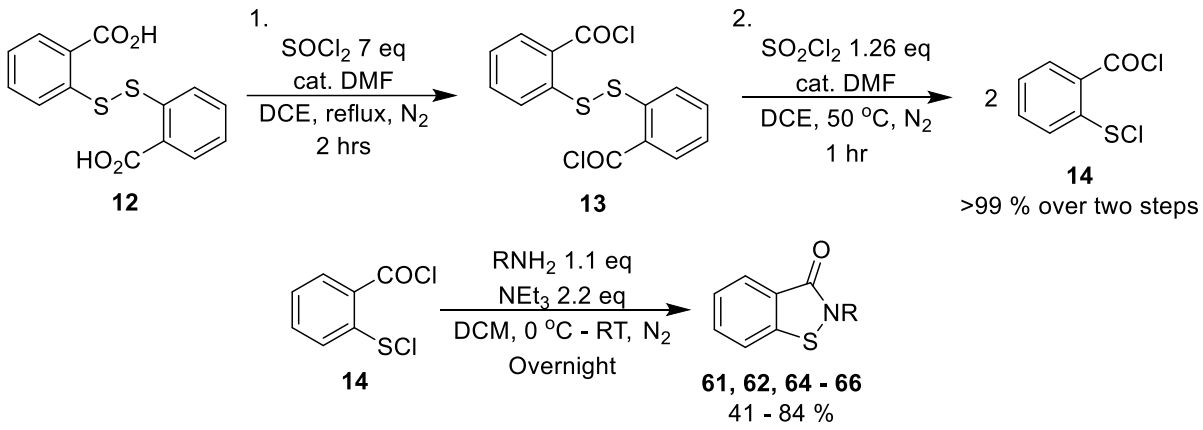

Scheme 3.3. S-Cl / COCl mediated ring closure.

3.2.1 C-ring Modifications

Described below are the biological data that has been previously obtained within our group for the purpose of developing a novel hit that effectively targets both *Pf*IspD and *Pf*3D7 cells.

As previously described compounds **8** and **9** (Figure 3.4) were synthesised according to Schemes 3.1 and 3.2. In order to confirm activity of the series these two compounds were tested against both purified *Pf*IspD and *Pf*3D7 whole cells. **8** expressed comparable activity to **1** with a *Pf*IspD IC_{50} value of 656 nM, however, upon testing *vs Pf*3D7 whole cells, **8** displayed a disappointing EC_{50} value of 8020 nM. **9** was more potent than **8** at 600 nM against enzyme and 5490 nM against *Pf*3D7 malaria parasites.

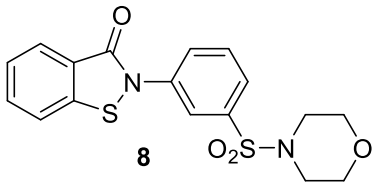

8

*Pf*IspD IC_{50} = 656 nM n = 1
*Pf*3D7 EC_{50} = 8020 nM n = 1

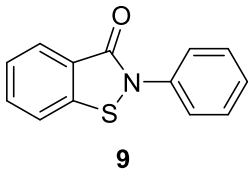

9

*Pf*IspD IC_{50} = 600 nM n = 1
*Pf*3D7 EC_{50} = 5490 nM n = 1

Figure 3.4. Activity of compounds 8 and 9.

The first area of SAR that was explored was modifications to the C-ring. In order to quickly determine a path of SAR that could be developed compounds **15** – **17** were purchased and tested against both enzyme and *Pf*3D7 malaria parasites with activity values shown in Table 3.1 below.

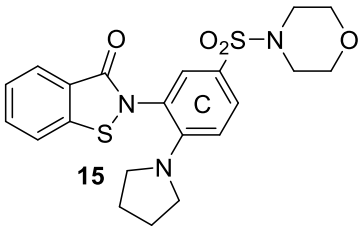

15

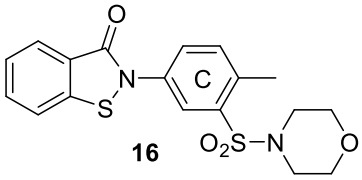

16

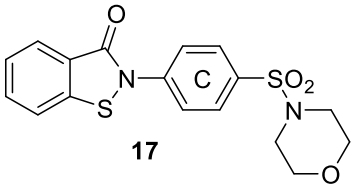

17

Table 3.1. Biological activities of purchased compounds 15, 16 and 17.

Compound	*Pf*IspD IC_{50} (nM)	*Pf*3D7 EC_{50} (nM)
15	9050 ± 2890 n = 4	17100 ± 9400 n = 3
16	445 ± 79 n = 3	4320 ± 183 n = 3
17	>50,000 n = 1	16000 n = 1

It was clear from the data that there was a requirement for the C-ring to be substituted at the *meta*-position as compound **17** possessing *para* substitution displayed a loss of potency against the enzyme. What was also apparent from the limited SAR carried out was that there was a degree of steric manipulation that can also be carried out around the C-ring with potency against enzyme being maintained in compounds **1**, **8**, **9**, and **16**. Despite the loss of potency observed with a change of *ortho*-substituent in **15** when compared to **1**, *ortho*-substituted OH or OMe derivatives possessing various sulfonamides were synthesised in order to examine if potency could be recovered and be comparable to **1** (Synthesis carried out by former Erasmus student Maria Mondini). However, in most cases this led to a loss of IspD activity and thus the decision was taken that for all future SAR only *meta*-substitution would be explored. Further to this, the group decided to move away from sulfonamides as they possessed no advantage in potency in comparison to either **1** or **9**.

3.2.2 D-ring Modifications

The results described above led the group to explore the effect of adding an extra phenyl ring at the *meta*-position of the C-ring; this new D-ring itself had substitution at its *para*-position. Table 3.2 below shows the compounds developed by former PhD student Dr Kathryn Price, and the biological data obtained after testing.[2]

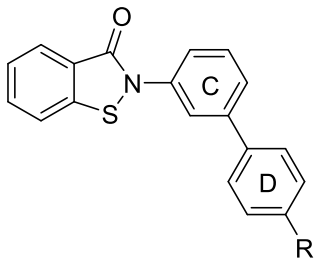

Table 3.2. Biological data of biphenyl BITZ compounds developed by Dr K. Price. Compound properties are ranked using a traffic light system. Green = good, amber = acceptable, red = poor.

Compound	R	*Pf*IspD IC_{50} (nM)	*Pf*3D7 EC_{50} (nM)	CLogP
18	OCH_3	206 ± 89 n = 3	920 ± 66 n = 9	5.16
19	Cl	73 ± 20 n = 3	1080 ± 164 n = 5	5.95
20	CF_3	273 ± 15 n = 3	646 ± 21 n = 6	6.12
21	OCF_3	290 ± 195 n = 3	411 n =1	6.27
22	CO_2CH_3	393 ± 96 n = 3	1000 ± 237 n = 5	5.21
23	OH	660 n = 1	2450 n = 1	4.57
24	3-thiophene	265 ± 21 n = 2	2877 n = 1	6.78

Notably all but compound **23** possessed increased potency *vs Pf*IspD than compounds **1**, **8** and **9**, in addition to this, compounds **18**, **20** and **21**, also displayed cell growth inhibition activities in the sub-micromolar range for the first time with this chemotype. Compound **19** was interesting as it was over 2-fold more potent than the next most active compound (**18**) against the enzyme, however, this promising enzyme activity was not transferred to the whole cell assay. It is evident from the CLogP values that these compounds are very lipophilic and thus would likely show a poor DMPK profile; this was a problem with this series that needed to be addressed. It was clear that there was a large degree of steric manipulation from *meta*-substitution of the C-ring that could be undertaken, it was therefore decided to incorporate solubilising groups at the end of the D-ring, from this compounds **25** – **29** were synthesised (By former PhD student Dr Kathryn Price) and biological activities are shown below (Table 3.3).[2]

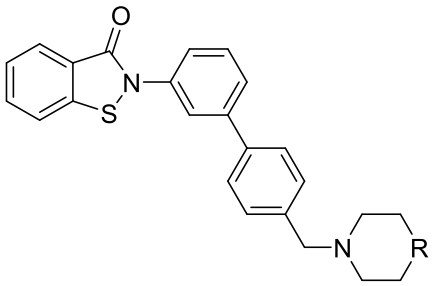

Table 3.3. Biological data of biphenyl BITZ compounds possessing solubilising groups developed by Dr K. Price. Compound properties are ranked using a traffic light system. Green = good, amber = acceptable, red = poor.

Compound	R	*Pf*IspD IC_{50} (nM)	*Pf*3D7 EC_{50} (nM)	CLogP
25	O	400 ± 82 n = 3	413 ± 82 n = 4	4.99
26	CHF	862 ± 107 n = 3	323 ± 92 n = 5	5.96
27	NCH_3	446 ± 75 n = 3	416 ± 6 n = 3	5.55
28	NH	160 ± 7 n = 2	3250 n = 1	4.97
29	NSO_2CH_3	523 ± 90 n = 3	1470 n = 1	4.99

Promisingly the incorporation of sterically demanding solubilising groups did not diminish potency in the cell assay for compounds **25** – **27**, and enzymatic activity was also retained across all compounds. Despite this promising result, the lipophilicity of these compounds is still above an ideal threshold for a drug candidate. Focus was switched from this biphenyl series to a mono-phenyl series with the benzyl-linked solubilising groups attached to the *meta*-position of the C-ring the generic structure of these compounds is displayed below (**30**) (Figure 3.5).

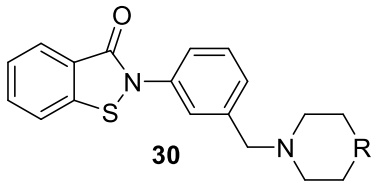

Figure 3.5. Generic structure of mono-phenyl series (30).

The rationale behind these compounds was to further reduce CLogP while also incorporating the desired *meta*-substitution of the C-ring. Analogous mono-phenyl compounds from both Tables 3.2 and 3.3 were synthesised (by former PhD students Dr Kathryn Price and Dr Natalie Roberts) and in general *Pf*IspD activity was comparable to the biphenyl series. However, across the whole mono-substituted series *Pf*3D7 potency was significantly reduced. It appeared as through there was indeed a requirement either for a high CLogP of the compounds, or there was a specific hydrophobic interaction that made this extra phenyl ring favourable for activity.

Alternatively the reactivity of the N-S could be very crucial, and may require strict electronic properties in order to optimise cellular potency. As described in **Section 3.3** below, the proposed

mechanism of action of these compounds involves covalent modification of the enzyme active site. This occurs is by ring opening of the BITZ core *via* nucleophilic attack of a crucial cysteine residue in the IspD active site with the sulfur atom of the BITZ compounds. If this reactivity is too high, the compound may ring open before it is able to reach the apicoplast; if this reactivity is too low it may not react with the cysteine residue once bound in the active site.

3.2.3 Further SAR Investigations

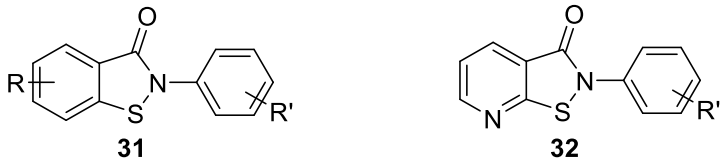

Figure 3.6. Generic structures of further SAR investigations on the BITZ chemotype (31) and (32).

As previously mentioned numerous group members have carried out extensive SAR on this chemotype. With the scope of this thesis it is not possible to disclose all data obtained. A series of A-ring substituted compounds were developed by former PhD student Dr Natalie Roberts for the purpose of improving the DMPK profile of the series as a whole (Figure 3.6). Halogens, OMe, NO_2 and N were incorporated into the A-ring, similar to the MMV008138 template, to block potential sites of metabolism, whilst also exploring the effects of changing the electronics and sterics of the BITZ core. Along with A-ring modifications alterations to the C-ring and its side chain were also synthesised in these series. Unfortunately a general trend across the series was compounds possessed only moderate activity in the *Pf*IspD assay and poor potency in the *Pf*3D7 assay.

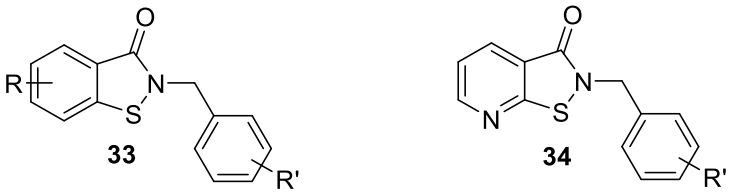

Figure 3.7. Generic structure of CH_2 linked aromatic BITZ compounds (33) and (34).

Other work carried out by the group also involved the incorporation of a CH_2 linker introduced between the B and C-rings (Figure 3.7). This was carried out for the purpose of adding flexibility to the molecule 'side arm' as a study to examine if any extra interactions could be captured within the active site. In a final study a nitrogen atom was also incorporated into both C and D-phenyl rings, this was carried out for the purpose of potentially picking up an extra hydrogen bond in the active site of the enzyme, and attempt to reduce the ClogP of the series as a whole. Again in general across all these series there was a mixture of success with inhibition of the enzyme, but the main drawbacks of all

series investigated was the lack of whole cell potency in comparison to the biphenyl series (EC_{50} = ~ >2000 – 100,000 nM *Pf*3D7).

3.3 BITZ Chemotype Mechanism of Action

Before continuing, it is important to consider the mechanism of action of this series. The BITZ chemotype has an unusual structure, possessing an N-S single bond, which is susceptible to nucleophilic attack. Therefore the proposed mechanism of action for the inhibition of *Pf*IspD *via* the BITZ series is believed to proceed through firstly a non-covalent recognition / docking event followed by a covalent binding mechanism *via* nucleophilic attack from a cysteine residue that is found within the *Pf*IspD active site (**A**). This forms a disulfide bridge and pushes electron density onto the nitrogen atom. The now covalently bound drug is thought to block the binding of substrates in the active site due to the chemical modification of the cysteine residue preventing substrate entry (**B**) (Figure 3.8).

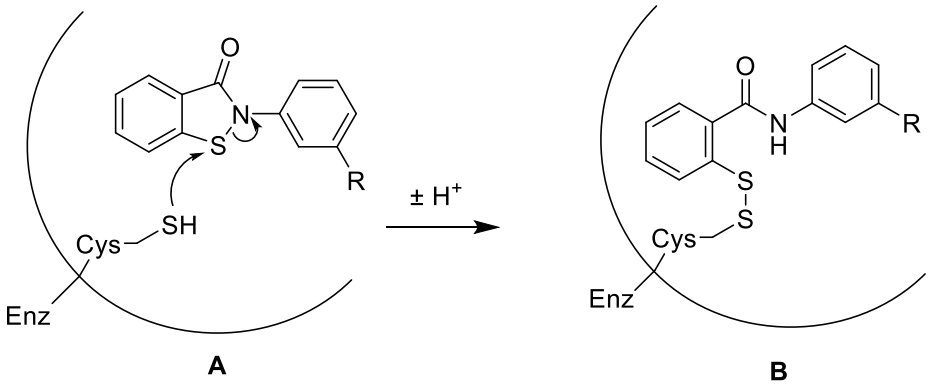

Figure 3.8. Proposed mechanism of action of the BITZ chemotype.

The resulting negative charge on nitrogen can be stabilised before protonation *via* delocalisation into the adjacent aromatic ring system and amide moiety. The stabilisation of charge should favour ring opening and thus the more stable the charge the more active a compound was expected to be following this mechanism. Furthermore the addition of electron withdrawing groups on the aromatic C-ring was expected to also increase the likelihood of ring opening as the N-S bond is be expected to be further weakened as it becomes more polarised.

To examine if the molecule was a covalent inhibitor, compound **20** was examined by our collaborators in Washington University St Louis (Odom group) in a mechanistic study. Wild type *E. coli* IspD (*Ec*IspD) possesses no cysteine residue in the active site, it is instead replaced by an alanine residue denoted A14. Therefore testing **20** against *Ec*IspD should lead too poor potency, which was observed as displayed in Figure 3.9 (IC_{50} > 100,000 nM). Mutating this wild type *Ec*IspD replacing A14 with cysteine (A14C mutation) and retesting **20** for inhibitory activity against mutated *Ec*IspD brought back potency of the compound(IC_{50} ~500 nM), giving an indication that a cysteine residue is crucial for

activity (Figure 3.9 left graph).[24] Note in an analogous study **18** was also examined and gave a concordant result.[2]

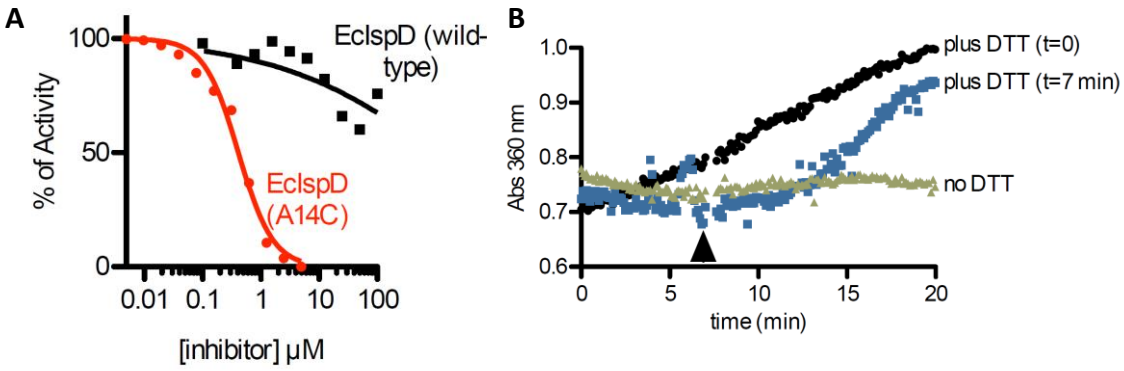

Figure 3.9. Left graph (A), activity of 20 before and after A14C mutation of *E. coli* IspD. Right graph (B), activity of 20 before and after DTT (35) is added to the assay.

A second *in vitro* study to examine if the cysteine covalently binds compound **20** was also carried out by treating the assay with dithiothreitol (DTT) (**35**) a reducing agent (Figure 3.10) When no DTT is added the activity is retained, when DDT is added at 7 minutes, inhibitory activity immediately decreases until **20** is inactive (Figure 3.9 right graph). This suggests that the postulated disulfide formed between **20** and the cysteine residue is being reduced to an inactive thiol derivative of the parent drug (**36**) (Figure 3.10), which could explain the loss of activity.[24]

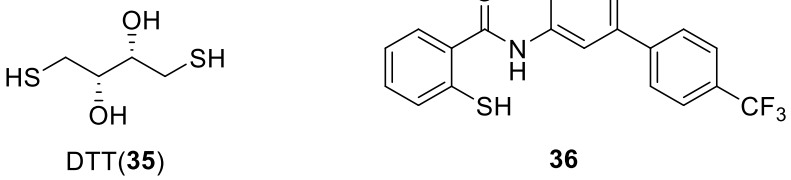

DTT(**35**) **36**

Figure 3.10. Structure of DTT (35) and inactive thiol derivative 36.

Before continuing it is important to point out that the development of drugs whose mechanism of action is *via* covalent modification can pose a risk to off target effects that can cause toxicity problems. During the exploration of the BITZ chemotype, we noticed that it was identified in a publication as a possible pan assay interference compound (PAIN). The paper suggested that medicinal chemistry programmes using this moiety should avoid wasting 'time and research money'.[25] Originally, this chemotype was not defined as a PAIN by the authors of the same commentary in their initial publication.[25–27] In fact they had attempted to use it to target *Trypanosoma brucei* farnesyl pyrophosphate synthase (FPPS). However, the project was unsuccessful, and because of uninterpretable SAR they have since categorised this chemotype as a PAIN.[25,26]

Pan-assay interference compounds (PAINS) are synthetic chemical compounds or natural products that can cause false positive assay signals.[25–33] These compounds can cause false positives due to intrinsic redox activity, chemical reactivity, instability, or they can form aggregates.[25–33] Other false positives can occur due to autofluorescence, metal chelation, membrane disruption, decomposition in buffers, or covalent modification of proteins, which is the proposed mechanism of action of our BITZ chemotype.[2,25–33] Currently, PAINS are identified *via* substructure matching with published moieties.[30]

The term, pan assay interference compounds (PAINS), was first coined by Baell *et al.* after he established a general purpose HTS library consisting of 100,000 compounds that appeared optimisable and lead-like in the year 2003.[26,27,34] The Baell group ran their biochemical assays in the presence of detergent to avoid aggregate formation, and identified numerous potent and selective hits for their various targets.[34] However, within the first few years, the group wasted time on hits that ended up being non-developable.[34] In the simplest case, hits that were resynthesised or repurified did not reproduce biological activity.[34] In more difficult cases the group found that some compounds possessed early SAR, but this eventually ended in flat or uninterpretable SAR.[25–27,29,34] The group noticed that similar looking compounds consistently appeared in different screens, and developed the idea that classes of intrinsically promiscuous compounds share common substructural motifs.[26,27,34] They observed that these problematic compounds possessed different forms of chemical reactivity and could interfere with biochemical assays through the mechanisms mentioned above.[34] Baell collated a list of substructural filters to identify PAINS compounds.[26,27,34] As noted above, the BITZ chemotype was not added to the original published PAINS filters, it was instead branded a PAIN later by the Baell group.[25–27,29,34]

Crucially, it is important to realise that the PAIN nomenclature is class-based and that individual compounds recognised by a PAINS substructure do not necessarily exhibit broad spectrum interference.[27,34] PAINS compounds are present in approximately 6 – 7 % (over 60) FDA approved drugs and so exclusion of these structural classes is not necessarily a good solution.[27,28,31,33,35] Therefore, it is reasonable to say that disregarding all potentially reactive or problematic compounds would be as detrimental to medicinal chemistry just as much as ignoring PAINS classified compounds would be.[30] It is also important to note that no PAINS-containing drug has ever been developed starting from a protein-reactive PAINS target based screening hit.[33,36]

Two subsequent large scale studies of PAINS suggest that the structural context in which PAINS occur play a role in the undesired effects and should be examined.[30,35] It seems reasonable not to discard a template containing a PAINS substructure, but instead perform follow up experiments

and orthogonal assays to determine genuine biological activity.[33,37] Such follow up assays include screening the molecule against unrelated enzyme targets as well as determining whether it competes with a ligand known to bind to the active site.[33,37] Potentially the most important criterion to distinguish a PAIN from a non-PAIN is thorough logical SAR.[33,37]

We have previously stated that we know our BITZ chemotype acts through covalent modification, and that it reacts with a cysteine thiol in the *Pf*IspD.[2] While this may raise questions on whether this chemotype is selective or not, we are confident that it is selective and only reacts with one cysteine residue in the active site of *Pf*IspD. We can justify this through the studies describing the proposed mechanism of action above.[2] Firstly, the BITZ chemotype appears to only modify one cysteine residue in the *Pf*IspD protein, this residue is denoted Cys-202.[2] In *E.coli* IspD this residue is replaced with alanine (denoted A14) (Figure 3.11), and our compounds show no activity against *Ec*IspD.[2] If *Ec*IspD has this A14 residue exchanged with a cysteine residue, and the assay repeated with mutated *Ec*IspD we observe the BITZ chemotype is then active against mutated *Ec*IspD.[2] Secondly, if *Pf*IspD has its Cys-202 exchanged to alanine, we observe loss of potency of the chemotype which again appears to back up our postulation that the BITZ chemotype is showing genuine activity against *Pf*IspD.[2] It is appropriate to note that there is more than one cysteine residue in both *Pf*IspD and *Ec*IspD homologues (Figure 3.11). Therefore, the change of inhibitory activity of the BITZ chemotype observed through subtraction or addition of a single cysteine residue in the active sites of these homologues appears to back up that our compounds are selectively only targeting one cysteine residue. Thirdly, the *Plasmodium vivax* homologue of IspD retains the proposed active cysteine residue (denoted Cys-197) responsible for inhibitor activity in the *Pf*IspD active site (Figure 3.11).[2] In previous research, we have shown that *Pv*IspD is also potently inhibited by our BITZ compounds.[2] Fourthly, in previous research we have shown that the BITZ chemotype is competitive with cytidine triphosphate during short incubation periods, but enzymatic inhibition cannot be out-competed following prolonged incubation of *Pf*IspD with the inhibitor which suggest that a covalent bond is likely formed.[2] This observation meets one of the criteria to rule out potential interference.[33,37] Fifthly, as a control, the original assay to determine *Pf*IspD potency for our HTS was different to that described in Chapter 2. This alternative assay for phosphate release was the BIOMOL Green assay.[38] The difference between the alternate assay and the MESG / PNPase assay described in Chapter 2 is; the MESG / PNPase assay is a continuous assay, while the BIOMOL Green assay is an end point assay only.[2,14] Both assays use fluorescence to measure IC_{50} values, however, the measurement of absorbance of the active ingredient in the BIOMOL Green assay (malachite green) is measured at 620 nm instead of 360 nm for the MESG / PNPase assay.[38,39] This assay has been repeated by our collaborators and has confirmed that the BITZ chemotype is active vs *Pf*IspD.[14] Therefore, we have conducted an orthogonal assay in

order to rule out potential interference from our compounds.[33,37] We acknowledge that to confirm beyond any doubt that the molecules are not interfering in the assay, a counter screen of the compounds against unrelated targets will likely be required, this should be carried out as part of future work. In addition to this, all tested compounds should also be screened within the BIOMOL Green assay or another orthogonal assay.

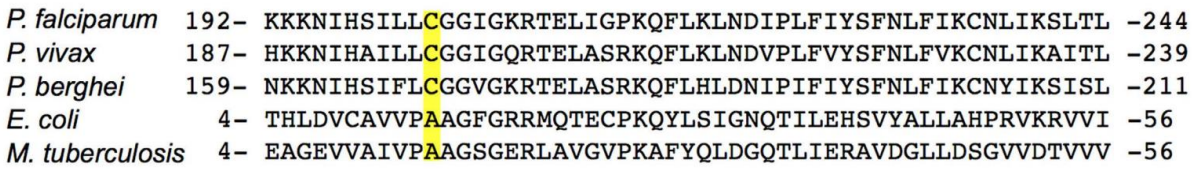

Figure 3.11. Alignment of IspD homologs: active site Cys residue is conserved in *Plasmodium* species, but is absent in bacterial orthologs that are insensitive to BITZ inhibitors. Figure reproduced from Price. K. E. *et al*.[2] Permissions for use are granted under the Creative Commons Attribution 4.0 International License.

There is some concern that the MESG / PNPase assay described in Chapter 2 (Figure 2.9) could cause false readouts when using the BITZ chemotype as the inhibitor, as MESG and its resultant product from the assay contains an aromatic thiol which may be nucleophilic enough to ring open our BITZ compounds before they have a chance to bind to the enzyme (Chapter 2 Figure 2.9). While we have not examined decomposition of our inhibitors by stirring MESG or its assay product in the presence of our BITZ compounds alone, we are confident that our activities are genuine, as the BIOMOL Green assay does not possess a moiety with a potentially reactive thiol, and when measured, BITZ compounds activities were replicated when measured with the BIOMOL Green assay.[14] In addition, as we know *E. coli* IspD is insensitive to inhibition *via* BITZ compounds, our collaborators have compared the pyrophosphate released using *E. coli* IspD in the presence and absence of BITZ inhibitors and there is no difference in pyrophosphate release with or without inhibitor.[14] Therefore, there is no evidence of altered activity and this suggests that there is no reaction of the BITZ compounds with MESG or its assay product.[14] We acknowledge that the control of stirring an active BITZ compound in the presence of MESG and / or its resulting assay product alone will need to be carried out as part of future work.

In summary, we acknowledge that the use of covalent modifiers can be risky and understand that identified PAINS substructures can be a problem and is an important area of research. Recent literature has shown that an identified PAIN substructure does not necessarily mean that any given compound (such as the BITZ chemotype) will result in presumed off target effects. We also note that there is significant evidence that covalent modifiers can be successful in medicinal chemistry programmes. Aspirin for example is one of the world's most widely used drug compounds and its mechanism of action is through covalent modification.[40]

3.4 Results and Discussion

To begin the new SAR on the BITZ compounds we had two main aims. Firstly we wanted to explore new chemical space around the IspD active site, and secondly we wanted to attempt to correlate activity with N-S bond strength. A novel chemotype not yet explored in the group was the 2,1-BITZ chemotype (Figure 3.12), an isomeric variant of the 1,2 BITZ compounds described above.

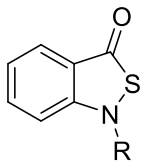

R = H, Aryl or alkyl chain

39, **41 - 45**, **50**

Figure 3.12. 2,1-BITZ template.

The isomeric chemotype has the N-S bond in alternate positions and could lead to interesting SAR. By alternating the N-S, orientation we can probe both reactivity, and steric demands of the drug template within the active site. In addition, by having comparative 1,2 and 2,1 isomers of the same template there is the potential to gain insight of the available chemical space from which new SAR investigations could be developed. To explore the SAR of this template the functionality of the R group on the nitrogen atom was altered using both aliphatic and aromatic side-chains.

3.4.1 Synthesis of 2,1 BITZ Compounds

The production of 2,1-BITZ compounds is not well documented and there are few reports of their generation available in the literature. Despite this there is a general route for their synthesis as depicted by Scheme 3.4. [41–43]

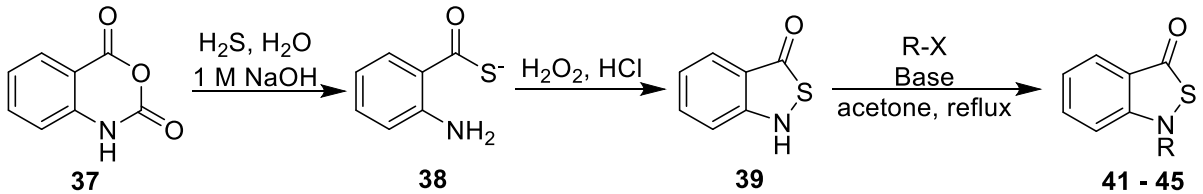

Scheme 3.4. General synthesis of 2,1-BITZ compounds.[43]

The synthesis begins by saturating a solution of water or methanol basified by 1 equivalent of hydroxide with hydrogen sulfide gas.[41–43] Isatoic anhydride (**37**) was then added and the reaction left for one hour allowing ring opening and loss of CO_2 to yield thiolate **38**. **38** is then oxidised *in situ* by hydrogen peroxide, followed by ring closure to the un-substituted 2,1 BITZ intermediate **39**. **39** can

then be coupled with an appropriate halogenated electrophile following S_N2 substitution to yield the desired targets.[43]

We were required to make a modification to step one of the published procedure to avoid the use of H_2S. Examination of the literature elucidated that the reaction could be successfully achieved by dissolving excess Li_2S in a protic solvent in order to generate LiOH and HLiS as the nucleophile. In the same step, a catalytic amount of hydrochloric acid was added before the addition of isatoic anhydride (**37**) (Scheme 3.5), unfortunately a yield is not specified for the reaction in the literature.[44]

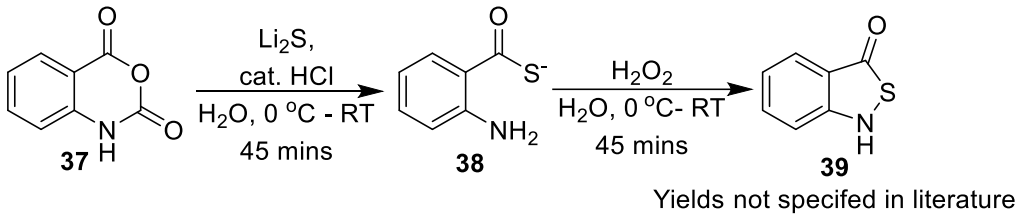

Scheme 3.5. Modified procedure *en route* to 2,1-BITZ compounds.[44]

Following the reported procedure problems were immediately encountered, ^{1}H NMR confirmed the correct number of protons for the isolated product but the mass spectrometry analysis yielded a molecular ion peak that did not correspond to the product. Disappointingly repetition of the reaction varying time and temperature gave the same result.

To determine what the problem was the reaction was repeated using phenyl-isatoic anhydride (**49**), which should yield *N*-phenyl-2,1 benzoisothiazolone (**50**) (see scheme 3.8 below for synthesis), however, again the mass spectrometry analysis was incorrect. The product was further confirmed to be incorrect by IR analysis which indicated the presence of a broad peak across the N-H, O-H stretching frequency range, neither of which should be present in **50**. We suspected that hydroxide generated *in situ* by the reaction of Li_2S with H_2O was acting as the nucleophile instead of the mono-lithium sulfide.

To confirm our suspicions the unsubstituted isatoic anhydride reaction was attempted once more, but using methanol as solvent instead of water. After completion of the reaction, TLC analysis of the reaction mixture showed a non-polar product had developed. After isolation, we saw a new peak in the NMR corresponding to methoxy protons. This is consistent with mono-lithium sulfide not acting as a nucleophile, but rather methoxide exclusively reacting with **37**, yielding methyl 2-aminobenzoate (**40**) (Scheme 3.6). Carrying out the reaction analogously in water results in the production of anthranillic acid.

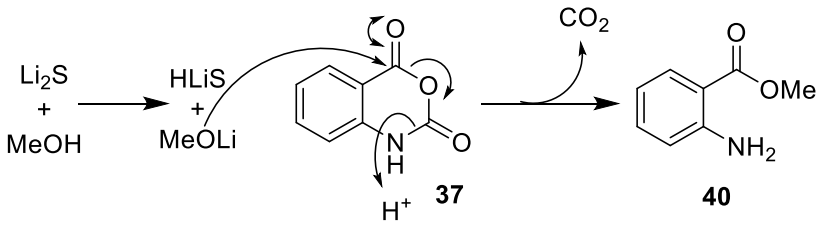

Scheme 3.6. Predominant reaction resulting in the failed synthesis of 2,1-BITZ compounds.

After examination of the procedure we followed we could only conclude that the HCl added was not catalytic, and that the authors had stated 1000 fold fewer equivalents than actually used.[44] This conclusion was supported by the fact that the problem was overcome using ~1.5 eq of HCl with respect to Li_2S. After altering the conditions, using **37** as the starting material, the synthesis of **39** was successful and has been repeated giving consistent yields of ~67 %.

With appropriate amounts of this intermediate available we were able to undertake SAR on this template, synthesising targets that were analogous to those already developed by other group members for the isomeric 1,2-BITZ series. CH_2 linked aromatic side chains (**41 – 44**) were first chosen for the synthesis due to their apparent ease of synthesis (Figure 3.13).[43]

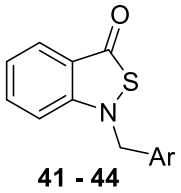

Figure 3.13. Generic structure of CH_2 linked aromatic 2,1-BITZ compounds 41 - 44.

We used molecular modelling studies to guide our SAR in the early stages of compound development; examination of the docking pose of **41** within the homology model of *Pf*IspD developed by our group suggested that CH_2 linked pyridyl substituents could coordinate to the crucial Mg^{2+} ion in the active site which may improve activity (Figure 3.14). From the modelling data it appeared that any of *ortho* (**42**), *meta* (**43**), or *para* (**44**) CH_2 linked pyridyls had a chance of extra coordination and so were synthesised along with the benzyl substituent **41**. Docking was carried out by Dr Alexandre Lawrenson.[45]

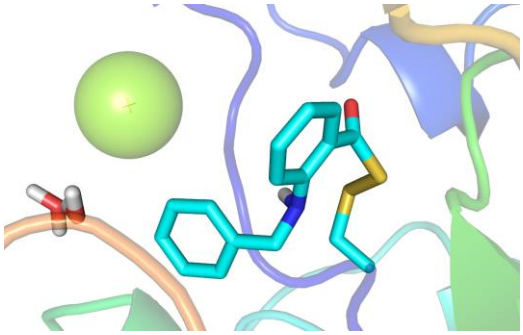

Figure 3.14. Docking pose of covalently bound 23 with cysteine residue in active site, of homology model of *Pf*IspD. Image generated in PyMol[46] by Dr Alexandre Lawrenson.[45] Atoms are coloured by element, carbon in light blue, oxygen in red, nitrogen in blue, hydrogen in white, Mg^{2+} shown as green sphere. Protein backbone rendered as cartoon.

The reaction generating **41** was not carried out under reflux as described by Scheme 3.4, instead **39** was allowed to react overnight at room temperature yielding **41** in near quantitative yields. Problems were encountered when synthesising CH_2 linked pyridyl analogues; it was found that under reflux conditions decomposition was observed by TLC for all three isomers, though to a lesser extent for the *meta* isomer (**43**), which gave enough product for analysis and testing. These reactions were repeated at room temperature and were complete within one to two hours, giving excellent yields of 83 % for *ortho* (**42**) and 87 % for *para* (**44**) substituents (Table 3.4). It is worth noting that TLC had to be used monitor the reaction frequently, as unknown reaction products began to form over time after the reaction was completed.

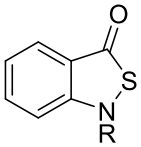

Table 3.4. Yields of S_N2 reactions of 2,1 BITZ compounds.

Compound	R	Yield %
41	Bn	94
42	CH_2-2-pyridyl	83
43	CH_2-3-pyridyl	29
44	CH_2-4-pyridyl	87

The SAR was further explored utilising a benzoyl moiety to potentially pick up an extra hydrogen bond in the active site. Generation of compound **45** was accomplished by allowing the reaction of **39** with benzoyl chloride to yield **45** in 63 % yield (Scheme 3.7). Furthermore, an analogous 1,2 BITZ compound **47** was also synthesised for a comparative study as it was not yet synthesised by the group. Following the same procedure as **45**, 1,2-benzoisothiazolone (**46**) was reacted with benzoyl chloride to form **47** in low yield of 24 % due to suspected double addition of benzoyl chloride.

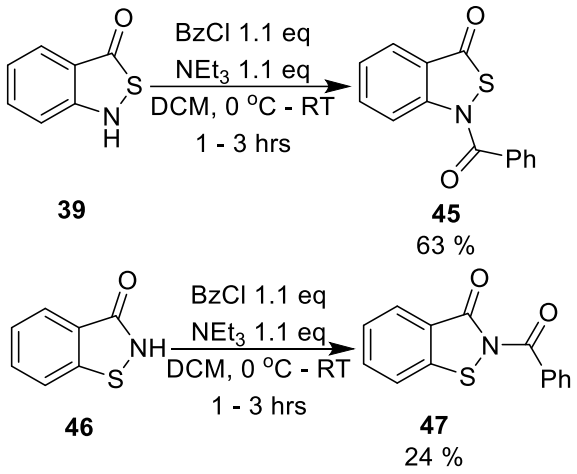

Scheme 3.7. Synthesis of 27 and 28.

Interestingly there was an anomaly regarding **45** in its mass spectrum. An $[M+H]^+$ peak for the product in either ES or CI conditions is not observed, however, 2 peaks are observed one corresponding to $[M+Na]^+$, and the other with a 0.1 increase in mass that seems to correspond to $[M-S+(MeOH+Na^+)]^+$. The reason for this unusual fragment pattern even under ES conditions could be an insight into the liability of the N-S bond in the 2,1 BITZ structure, furthermore, this same pattern is not seen in the 1,2 isomer. Therefore it could be reasonably predicted that **45** could potentially show activity higher than that of **47** if its N-S bond is weaker. It cannot be ruled out that **45** is unstable in aqueous buffer, as it contains a withdrawn thioester bond that may be susceptible to hydrolysis. Therefore, as part of future work, stirring the compound in buffer solution to assess its stability will need to carried out to determine if the activity is true or is the result of a possible decomposition product in the bioassay conditions.

In addition to the benzyl linked 2,1-BITZ series, a phenyl linked series was also investigated. There is very little in the literature as to how to install on aromatic side chain on this template, however, one method is to start the reaction with *N*-functionalisation already attached to isatoic anhydride.[42] *N*-phenyl-isatoic anhydride **49** was synthesised in 75 % yield from the reaction between *N*-phenylanthranilic acid (**48**) and diphosgene (Scheme 3.8). **49** was then reacted analogously to compound **37** to yield compound **50** in low isolated yield of 26 %. It should be noted that there was a side product very close to the product on TLC that was difficult to separate, which was a contributing factor to the low yield. This product was not able to be isolated but it is reasonable to assume this could be a disulfide, as a similar reaction using H_2S gas and sodium hydroxide as the reagents has been attempted in the literature once, and the group yielded exclusive disulfide formation, something not observed using our modified procedure.[42] In order to confirm whether the isolated product was correct and not a disulfide, we carried out IR analysis on the product. IR gives us a clear determination

on whether cyclisation had occurred, as an N-H peak would be observed if it had not, crucially no N-H peak was observed for **50** confirming its structure to be correct.

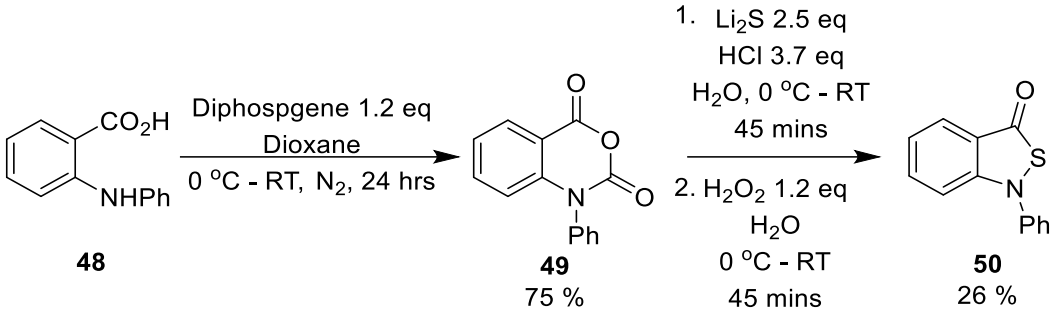

Scheme 3.8. Synthesis of 49 and 50.

Because of the difficulties in the synthesis and purification of 2,1 BITZ compounds directly bound to aromatic rings this compound series was abandoned as it became apparent we could not easily generate an array of compounds mimicking compounds from the 1,2 series.

3.4.2 Biological Activity of 2,1-BITZ Compounds

All synthesised 2,1-BITZ compounds were tested *in vitro* for their inhibitory activity against *Pf*IspD and were also tested against *Pf*3D7 cells as displayed in Table 3.5. As a direct comparison compounds from the 1,2-BITZ chemotype are also displayed in the table.

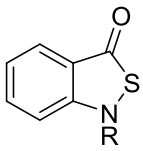

39, 41 - 45, 50

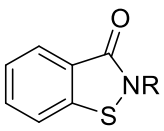

9, 47, 51, 52

Table 3.5. Biological data comparison of 2,1 and 1,2-BITZ compounds. Compound properties are ranked using a traffic light system. Green = good, amber = acceptable, red = poor.

Compound	Chemotype	R	*Pf*IspD IC_{50} (nM)	*Pf*3D7 EC_{50} (nM)	CLogP
39	2,1-BITZ	H	>100,000 n = 1	41,000 n = 1	1.69
41	2,1-BITZ	Bn	>25,000 n = 2	28,000 n = 1	4.03
42	2,1-BITZ	CH_2-2-pyridyl	>50,000 n = 1	>50,000 n = 1	2.53
43	2,1-BITZ	CH_2-3-pyridyl	>100,000 n = 1	>50,000 n = 1	2.53
44	2,1-BITZ	CH_2-4-pyridyl	>100,000 n = 1	>50,000 n = 1	2.53
45	2,1-BITZ	Bz	303 n = 1	>50,000 n = 1	4.31
50	2,1-BITZ	ph	4140 ± 441 n = 2	23,600 n = 1	4.01
9	1,2-BITZ	Ph	600 n = 1	5490 n = 1	3.35
47	1,2-BITZ	Bz	4346 n = 1	>100,000 n = 1	3.39
51*	1,2-BITZ	Bn	2430 n = 1	46,450 n = 1	2.90
52*	1,2-BITZ	CH_2-2-pyridyl	1900 n = 1	>25,000 n = 1	1.41

*** Compounds synthesised by Dr Natalie Roberts**

A clear trend across the series as a whole is that the 2,1-BITZ chemotype holds no advantages over its 1,2-BITZ counterpart. In **39** the compound holds no functionality on the nitrogen atom and thus, its inactivity can be attributed to a potential loss of crucial binding interactions in the IspD active site. Interestingly the compound is more active in the whole cell assay than against the enzyme, which suggests this compound may show off target effects. **41** is also inactive, this was disappointing considering that its 1,2-BITZ counterpart **51** through only weakly active, did show IspD activity. Much to our surprise all the pyridyl analogues **42** – **44** showed poor potency in both enzyme and cell assays, this was unexpected considering a close analogue from the 1,2-BITZ series **52** displayed moderate activity against *Pf*IspD. Perhaps most disappointingly from the series was compound **50**, which though weakly active against *Pf*IspD was 7 fold less active than its regioisomer **9**, and was over 4-fold less active against *Pf*3D7 whole cells. These results suggest that the 2,1 series is not optimal for further SAR development using the same strategies as employed for the 1,2 series.

Despite these negative results from the 2,1-BITZ series, there was one compound in the series **45** of comparable potency to other 1,2-BITZ analogues. **45** displayed excellent potency giving an IC_{50} value of 303 nM against *Pf*IspD. **45** was also 2-fold more potent than **9**. It appears that for the 2,1-BITZ series there is a specific requirement within the active site of the enzyme for an amide bond directly linked to the BITZ core for this series to show activity. It is reasonable to assume that this could be due to conformational locking and / or the potential for the carbonyl oxygen to pick up a hydrogen bond. Interestingly compound **47** the regioisomer of **45**, displayed weak potency *vs Pf*IspD.

As this result was curious, we were interested in docking compounds **45** and **47** into the homology model following the protocol outlined in Chapter 2 to examine if there is a major difference in their binding modes. Displayed below are the two poses for **45** and **47**, for **45** there were numerous potential poses, with a standard deviation (SD) in docking scores of 2.1 and an average score of 43.1, thus we chose a pose close to this average with a score of 42.7 (Figure 3.15 and Table 3.6). For **47** there was very little difference between the most of the poses observed, only two poses did not match the others and one of these possessed a significantly lower score that will have affected the SD and mean (2.24, 45.48, respectively). Therefore the pose selected was the one with the best docking score of 47.32 (Figure 3.16 and Table 3.7).

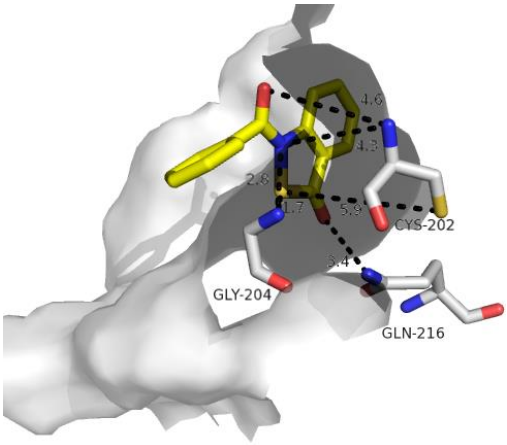

Figure 3.15. Binding pose of 45. Binding site is rendered as a white surface, 45 is rendered as sticks, carbon coloured yellow, nitrogen in blue, oxygen in red, sulfur in dark yellow. Crucial amino acids are rendered as sticks carbon coloured grey, nitrogen in blue, oxygen in red, sulfur in yellow.

Table 3.6. Main ligand – protein interactions of 45.

Residue(s)	Moiety	Interaction	Distance Å
Cys-202, Gly-204	B-ring-S	Electrostatic	1,7
Gln-216	B-ring-C=O	H-bond	3.4
Gly-204	B-ring-N	Electrostatic	2.6

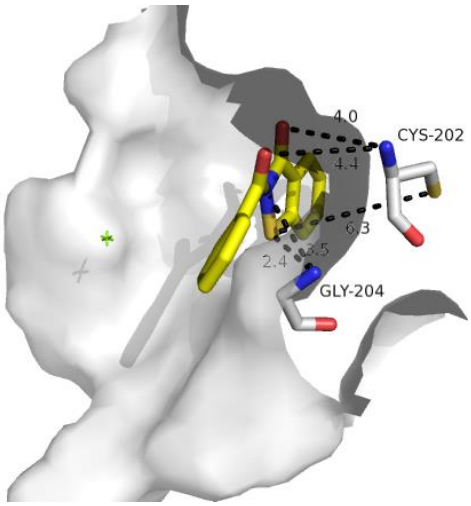

Figure 3.16. Binding pose of 47. Binding site is rendered as a white surface, Mg^{2+} is depicted as a green cross, 47 is rendered as sticks, carbon coloured yellow, nitrogen in blue, oxygen in red, sulfur in dark yellow. Crucial amino acids are rendered as sticks carbon coloured grey, nitrogen in blue, oxygen in red, sulfur in yellow.

Table 3.7. Main ligand – protein interactions of 47.

Residue(s)	Moiety	Interaction	Distance Å
Gly-204	B-ring-S	Electrostatic	2.4
Gly-204	B-ring-N	Weak electrostatic	3.5

In terms of the available interactions of the two molecules, it appears as though compound **45** has more potential interactions that it can make with the enzyme active site compared with **47**, forming a potential hydrogen bond with Gln-296 and two close electrostatic interactions with Gly-204. In addition it is in close proximity to the crucial cysteine thiol at 5.9 Å which as described in **Section 3.3** is thought to form a covalent adduct with the BITZ inhibitors. The sulfur atom is very close to the nitrogen atom of Gly-204 potentially favourable interaction. **47**, on the other hand does not form similar hydrogen bonds and therefore may potentially lose some potency because of this, however, it is also further away from the cysteine thiol at 5.9 Å. Therefore it could be rationalised that this molecule shows weaker activity than **45** as it is less likely to interact with the cysteine residue. The binding poses of the two molecules are similar where both the A and B-rings are bound within a small cavity close to the cysteine residue whilst the benzoyl portion points out into solvent exposed space.

Based on the weak activity seen for the series, the overall comparative high lipophilicity and challenging restrictive chemistry, we made the decision to terminate studies on the 2,1-BITZ chemotype.

3.4.3 Conclusion of 2,1-BITZ Compounds

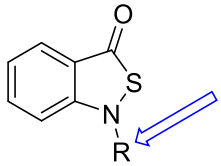

Benzoyl derivative is optimal for enzyme activity, however is poorly active agsint *Pf*3D7 cells.

CH_2 linked Ar groups are not tolerated all 4 compounds of this series were inactive against enzyme and cell.

No substitution is also not tolerated, and unfortunately Ph substitution did not mirror the success of the 1,2 BITZ isomer **3**

Figure 3.17. Conclusion of 2,1 BITZ SAR.

Of all tested compounds from the 2,1-BITZ series only **45** showed very good activity against *Pf*IspD. There seems to be a strict spatial and / or electronical requirement in the active site for the series, as CH_2 linked compounds are not tolerated and show little to no activity against the enzyme and cell. Compound **50** possessed weak activity *vs* the enzyme but was much less potent than its regioisomer **9** suggesting there is an unfavourable interaction with the phenyl ring. The observation that **45** is active suggests that the IspD binding pocket is very tight, as there is an unexpectedly large gain of potency on alternating from benzyl derivatives to benzoyl. The conformational locking properties that an amide bond gives could give rise to a favourable binding pose; in addition the potential gain of a hydrogen bonding interaction could contribute to this large gain in potency of this

compound. All compounds, however, are poorly active against cell and are at a disadvantage *vs* the 1,2 BITZ chemotype as their CLogP is higher than the analogous regioisomers (Figure 3.17). As **45** is more potent than its regioisomer **47**, this series of compounds could be worth revisiting in the future adding solubilising groups to the phenyl ring in an attempt to reduce CLogP. Prior to examining further benzoyl derivatives, stability assessment in aqueous buffer must first be carried out in order to determine if activity is genuine or is the result of a decomposition product resulting from potential hydrolysis of the thioester bond.

3.4.4 Returning to SAR on 1,2-BITZ Compounds

We decided to return to further explore the 1,2-BITZ chemotype; most of the compounds generated within the group had focused on installing aromatic or CH_2-linked aromatic side arms (C-ring onwards) to the BITZ core. With the exception of the biphenyl series of compounds previously mentioned, all compounds failed to show desirable *Pf*3D7 activity even if they showed excellent *Pf*IspD activity. We postulated that there was a requirement of specific reactivity of the N-S bond that needed to be met in order to for a compound to show cell activity. In addition to the biphenyl series, we also needed to reduce the CLogP of the active compounds as a whole. As a result the aim for the new 1,2-BITZ SAR is described in Figure 3.18.

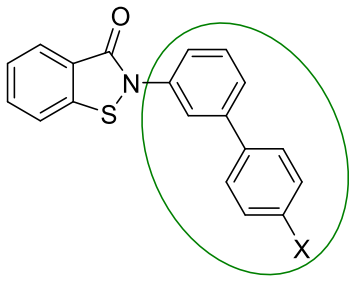

Remove direct and one carbon linked planar aromatic side arm to alter electronics reduce rigidity and lipophilicity

Replace with urea moiety, aliphatic side arms and direct linked aliphatic ring systems, to explore enzyme chemical space, modulate and protect N-S bond

Figure 3.18. Aim for new 1,2 BITZ SAR.

3.4.5 Synthesis of 1,2-BITZ Compounds

In order to address these two problems we decided to move away from planar aromatic compounds with either a direct link or one carbon link to the nitrogen atom of the BITZ core. We began our SAR studies by installing a urea like moiety to the molecule in order to modulate the characteristics of the N-S bond, and to add a hydrogen bond donor accepter pair to molecule to potentially increase binding energy within the IspD active site. This moiety was introduced into the molecule following the reported procedure by Liu *et al*.[47] (Scheme 3.9).

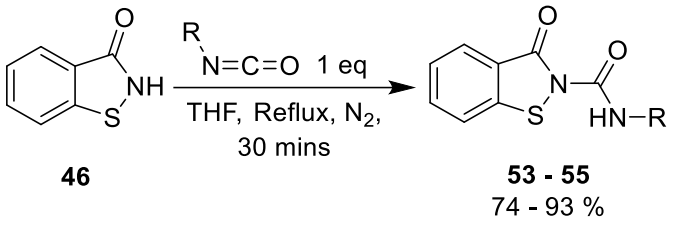

46 **53 - 55**
74 - 93 %

Scheme 3.9. Installation of urea moiety into the 1,2-BITZ chemotype.

The synthetic route was a one step process taking commercially available 1,2 benzoisothiazolone (**46**) and reacting with the relevant isocyanate to yield the target compounds in one-step in excellent yields. In order to create a comparative study from similar molecules other group members previously had synthesised in the mono-phenyl series, our R groups were chosen to be phenyl (**53**), 4-chloro-phenyl (**54**), and benzyl (**55**). The synthesis was carried out according to Scheme 3.9 and the reaction yields are summarised in Table 3.8 below.

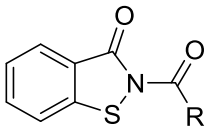

Table 3.8 Yields of urea linked 1,2 BITZ compounds

Compound	R	Yield %
53	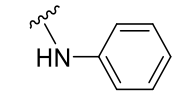	74
54	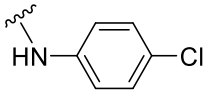	93
55	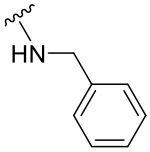	92

The targets were successfully obtained with full data and good purity by elemental analysis, but suffered a drawback of poor solubility in all common solvents. ^{1}H NMR could be successfully achieved in $CDCl_3$ as the solvent, however, in order to get a ^{13}C NMR we required the use d^{6} DMSO. Upon re-examining the ^{1}H NMR spectra in DMSO new peaks emerged in the spectra and the relative proportions of these peaks changed over time (within one hour). The identity of the structure corresponding to these peaks was unknown. It may be possible that the molecules are reactive and decompose readily in solvents with any possible nucleophilic centre, as the same effect was observed when the solvent was altered to methanol. This was only observed for **53** and **54** but not **55**.

The issues in solubility and apparent instability in DMSO, led us to pursue other final targets. In sticking with a non-aromatic linked compounds; compounds **61** – **66**, were synthesised again to modulate the N-S bond strength and to interrogate the available sterics in the active site of the enzyme.

Compounds **61** and **63** (Scheme 3.10 and 3.11), were already discovered from the HTS carried out by Biofocus described in **Section 3.1**.[48] Both compounds were shown to be active possessing *Pf*IspD activities of 165 nM and 356 nM, respectively. In addition, in collaboration with Astra-Zeneca (AZ) LogD values of **61** and **63** were calculated based on prediction software provided by AZ.[12,13] Both compounds displayed $ClogD_{7.4}$ values of 3.55 and 2.99, respectively. These values are in an acceptable to desirable range. This ideally means that for these compounds aqueous solubility and metabolic stability data are more likely to also be in a desirable range. As previously mentioned in Chapter 2 a compound possessing an optimal DMPK profile is less likely to fail in the clinic, therefore these two molecules provided a good starting point for further SAR.

In order to reconfirm activity compounds **61** and **63** were synthesised *via* two differing routes as described below in Scheme 3.10 and Scheme 3.11. The synthesis of **61** began through coupling *N*-Boc-Glycine (**56**) *via* standard peptide coupling procedures with 2-adamantylamine to give **57a** in 62 % yield. The Boc group was then deprotected in the presence of TFA in DCM giving **58a** in 79 % yield, **58a** can then be coupled into intermediate **14**, resulting in the formation of **61** in 84 % yield. We were interested in investigating the effect of changing the substituent position of the adamantyl ring on biological activity, thus compound **62** was synthesised analogously to **61**. *N*-Boc-Glycine (**56**) was coupled with 1-adamantylamine to yield **57b** in 76 % yield. **57b** was then deprotected in the presence of TFA in DCM to form **58b** in 74 % yield before final coupling into intermediate **14** to form **62** in 80 % yield. To examine an alternate synthesis, the route towards **63** began through coupling 2,4-dimethyl aniline with bromoacetyl bromide (**59**) giving **60** in 70 % yield. 1,2-benzoisothiazolinone (**46**) was then deprotonated in the presence of NaH and then coupled to **60** to yield **63** in a low yield of 15 %.[49]

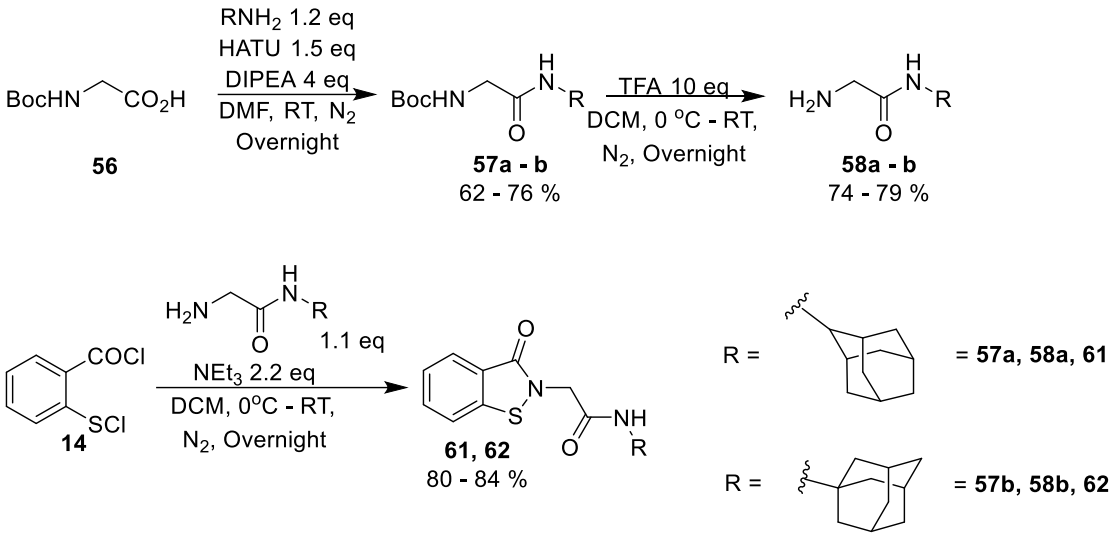

Scheme 3.10 Synthesis of 61 and 62

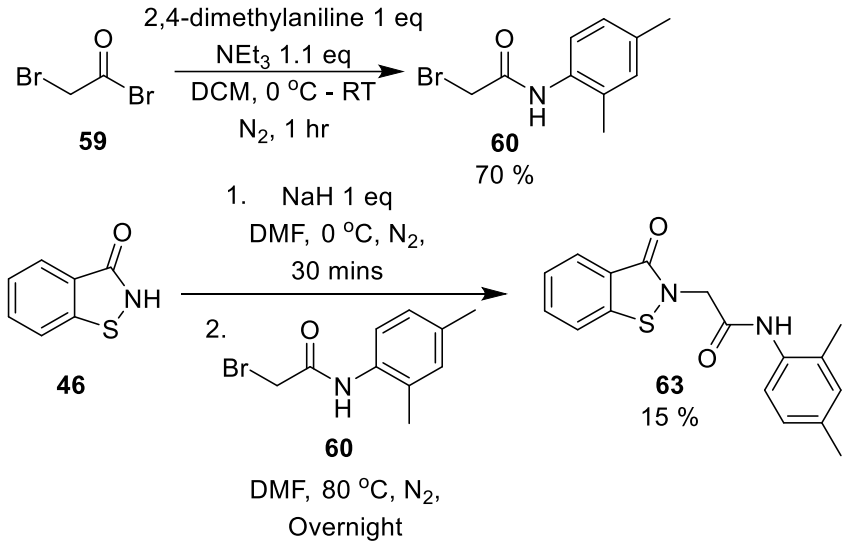

Scheme 3.11. Synthesis of 63.

In an analogous study we also examined if both 2-adamantyl and 1-adamantyl rings could be tolerated directly bound to the BITZ core, in addition to this we also wanted to examine what effect using a smaller ring system such as cyclohexyl has on activity. In the group no SAR had been undertaken on aliphatic C-rings attached directly to the BITZ core and so if this compound showed good activity, it could allow another avenue of SAR to begin. Compounds **64 – 66** were synthesised from direct coupling of 2-adamantylamine, 1-adamantylamine, and cyclohexylamine into intermediate **14** (Scheme 3.12) in 41 %, 80 % and 74 % yield, respectively.

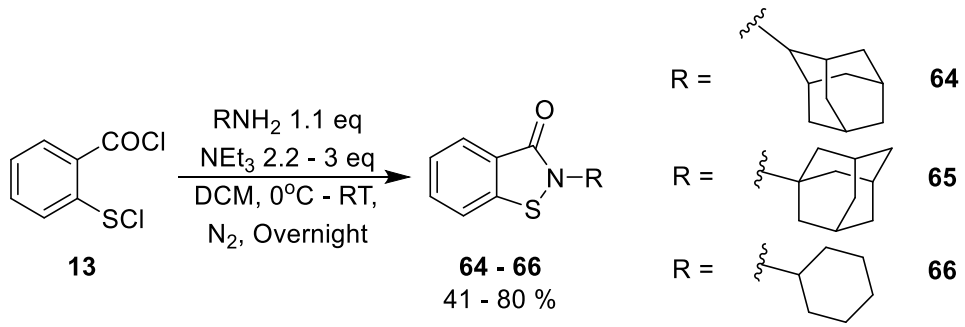

Scheme 3.12. Synthesis of 64 - 66.

3.4.6 Biological Activity of 1,2-BITZ Compounds

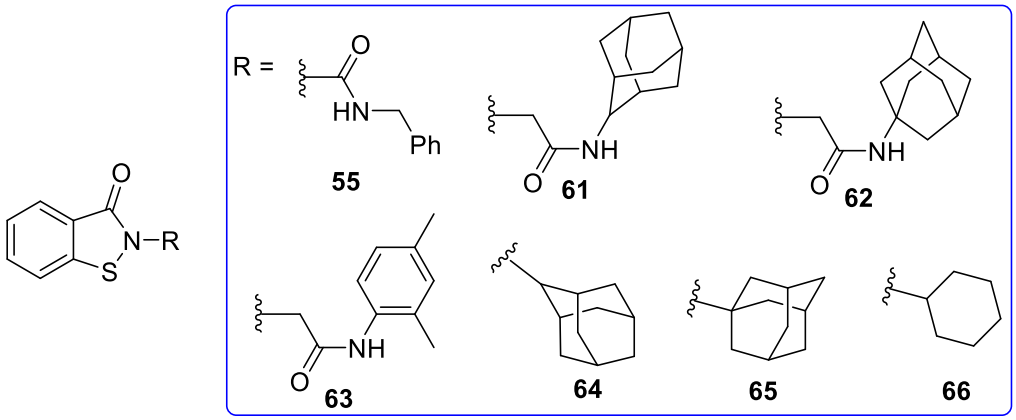

Table 3.9. Biological data of 55 and 61 – 66. Compound properties are ranked using a traffic light system. Green = good, amber = acceptable, red = poor.

Compound	*Pf*IspD IC_{50} (nM)	*Pf*3D7 EC_{50} (nM)	CLogP
55	6170 ± 32 n = 2	26,400 n = 1	3.54
61	~20,000 n = 1	Not tested	4.92
62	>10,000 n = 1	Not tested	3.52
63	No inhibition n = 1	Not tested	2.80
64	No inhibition n = 1	Not tested	5.18
65	>10,000 n = 1	Not tested	4.14
66	No inhibition n = 1	Not tested	3.52

All compounds were screened for at least *Pf*IspD activity (Table 3.9). A trend across all compounds is that they are poorly potent or show no inhibitory activity against the enzyme. **55** displayed the highest potency of all the compounds but was only weakly potent against both enzyme and cell. Disappointingly the activity of **61** and **63** was not reconfirmed from the HTS carried out by Biofocus indicating that these two compounds from the screen were unfortunately false positives. **62** also showed poor activity against the enzyme.

From the analogous study, compounds **64** – **66** also displayed poor to no activity against the enzyme. In the case of **64** and **65**, the inactivity could be attributed to sterics, as the adamantyl group is very large and may not fit into the active site. Alternatively the adamantyl group may be acting as a protecting group for the N-S bond. Due to the size of the adamantyl moiety, the crucial cysteine residue responsible for activity may not be able bypass this bulky group to attack the sulfur atom of the BITZ core. This would therefore, prevent disulfide formation.

Most surprisingly from the study was the result obtained from **66**. Comparing the cyclohexane ring to the phenyl ring in **9**, the steric effects are not significantly different between the two molecules. This suggests three possibilities; firstly a tight bonding pocket were the phenyl ring of **9** resides; secondly a specific requirement for a planar aromatic ring at this position; or thirdly a specific electronical requirement for a phenyl ring, or an electron withdrawing moiety to be present either directly linked, or close to the nitrogen atom harbouring the N-S bond. This would likely be required in order to sufficiently weaken this bond so that it may be cleaved *via* nucleophilic attack of the cysteine thiol. As a final remark, due to the disappointing activities of all compounds against *Pf*IspD, compounds **61 – 66**, were not tested against *Pf*3D7 whole cells.

To try to rationalise these results we examined the binding poses of three of the molecules **61**, **65**, and **66** again following the protocol described in Chapter 2, in each case the pose with best fitness score was chosen for display. Poses and interactions are shown in Figures 3.19 – 3.21 and Tables 3.10 – 3.12.

61 Docking score = 54.2, mean = 52.0, SD = 2.1

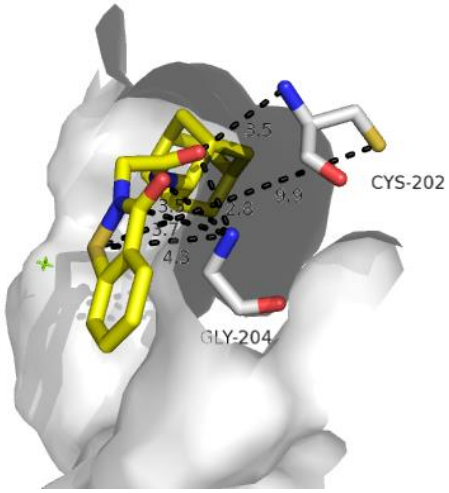

Figure 3.19. Binding pose of 61. Binding site is rendered as a white surface, Mg^{2+} is depicted as a green cross, 61 is rendered as sticks, carbon coloured yellow, nitrogen in blue, oxygen in red, sulfur in dark yellow. Crucial amino acids are rendered as sticks carbon coloured grey, nitrogen in blue, oxygen in red, sulfur in yellow.

Table 3.10. Main ligand – protein interactions of 61.

Residue(s)	Moiety	Interaction	Distance Å
Cys-202, Gly-204	$CH_2C=O$	Weak electrostatic, H-bond	3.5, 2.8
Gly-204	B-ring-C=O	H-bond	3.5

65 Docking score = 47.2, mean = 46.3, SD = 0.8

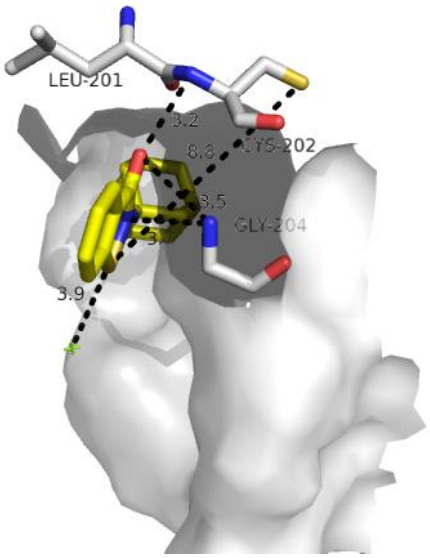

Figure 3.20. Binding pose of 65. Binding site is rendered as a white surface, Mg^{2+} is depicted as a green cross, 65 is rendered as sticks, , carbon coloured yellow, nitrogen in blue, oxygen in red, sulfur in dark yellow. Crucial amino acids are rendered as sticks carbon coloured grey, nitrogen in blue, oxygen in red, sulfur in yellow.

Table 3.11. Main ligand – protein interactions of 65.

Residue(s)	Moiety	Interaction	Distance Å
Cys-202	B-ring-C=O	Electrostatic	3.2
Gly-204	B-ring-C=O	weak electrostatic	3.5

66 Docking score = 44.3, mean = 44.1, SD = 0.1

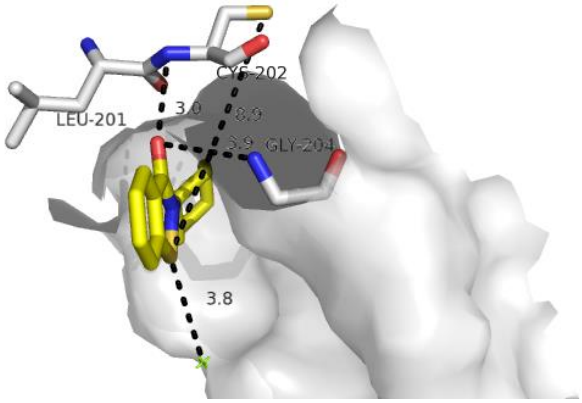

Figure 3.21. Binding pose of 66. Binding site is rendered as a white surface, Mg^{2+} is depicted as a green cross, 66 is rendered as sticks, , carbon coloured yellow, nitrogen in blue, oxygen in red, sulfur in dark yellow. Crucial amino acids are rendered as sticks carbon coloured grey, nitrogen in blue, oxygen in red, sulfur in yellow.

Table 3.12. Main ligand – protein interactions of 66.

Residue(s)	Moiety	Interaction	Distance Å
Cys-202	B-ring-C=O	H-Bond	3.0
Mg^{2+}	B-ring-S	Very weak electrostatic	3.8

The docking runs of compounds **61**, **65**, and **66** show that the A and B-rings of these structures do not reside in the same pocket as the previously docked compounds **45** and **47**. Instead the bulky adamantyl rings in both **61** and **65** and the cyclohexyl ring in **66** are predicted to bind in the pocket where the A and B-rings of **45** and **47** lie, most likely forming Van der Waals interactions with the nearby Leu-201 residue. In this pose the carbonyl groups form hydrogen bonds with nearby Cys-202 and Gly-204 residues. In **61** and **65** the B-ring nitrogen atom can also weakly interact with with Gly-204 at 3.7 Å. Finally in **65** and **66** the sulfur atom can potentially electrostatically coordinate weakly to the Mg^{2+} ion at 3.8 to 3.9 Å. In all cases from the modelling studies, there is a clear trend that the sulfur atom is now bound between 8.8 and 9.9 Å. This is out of proximity of the cysteine residue responsible for the ring opening of the BITZ compounds. Therefore, it can be rationalised that the lack of inhibitory activity of these compounds is due to no disulfide formation in the active site.

3.4.7 Conclusion of 1,2-BITZ Compounds

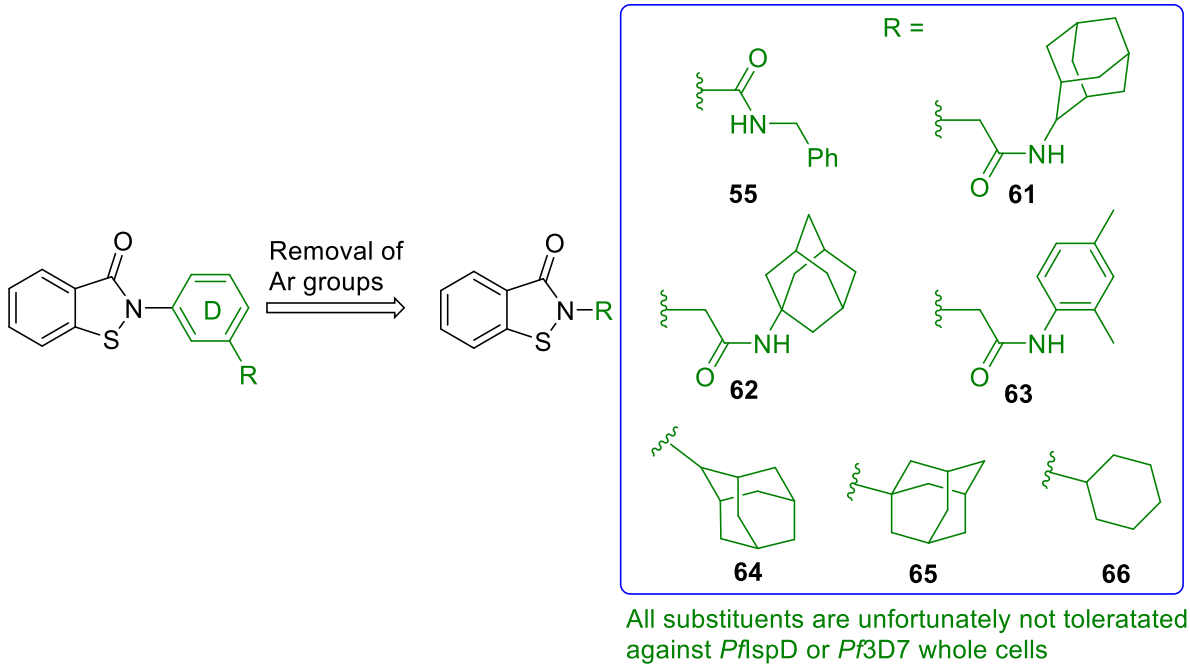

Figure 3.22. Conclusion of D-ring SAR.

Re-examination of the 1,2-BITZ chemotype was largely disappointing (Figure 3.22). Unfortunately no compound showed significant inhibition of the *Pf*IspD enzyme, and because of this lack of potency, most compounds were not tested for the whole cell growth inhibitory activity.

From the HTS screen carried out by Biofocus two compounds came out as active against the IspD enzyme compounds **61** and **63**. To reconfirm activity both compounds were resynthesised, re-examination of their activity showed them to be inactive, suggesting that these two hits from the screen were unfortunately false positives. As could be expected, structurally related **62** was also inactive. We also carried out an analogous study, synthesising compounds **64** – **66** that possessed 2-adamantyl, 1-adamantyl, and cyclohexyl groups bound to the nitrogen atom of the BITZ core, respectively. Unfortunately all of these compounds were also inactive, which was surprising particularly in the case of **66**. It apears that there is a specific requirement for either sterics and / or electronics of this chemotype, as comparing **66** to **9** it is unexpected to see such a loss of potency based on sterics alone from alternating from a phenyl ring to a cyclohexyl ring.

3.5 B-ring Modification, Compounds Representing Organoselenium Drug Ebselen

It is clear from examination of the literature that the use of organoselenium compounds for use in the pharmaceutical industry has in the past been severely disfavoured by the apparent lack of available drugs containing a selenium moiety there are in the literature. This is understandable, as

selenium has long been considered toxic, even if it is an essential element for the body.[50] Unfortunately the required therapeutic doses of most drugs would far exceed the expected safe level of selenium intake, therefore, are postulated to be toxic, preventing their development.[50] However, as is now known, the key for a successful non-toxic organoselenium compound is to stop the selenium atom becoming bioavailable, a good way to do this is to lock the element within a heterocycle.[50–55]

More recently there is evidence in the literature where selenium has replaced its counterpart sulfur to yield improved biological activity and in some cases a better toxicity profile. Wiles *et al*. were successful in the development of a piperidinyl quinolone with fused selenophene moiety which displayed improved activity against its target DNA gyrase, improved activity against a panel of clinical MRSA isolates, and importantly a reduced hERG channel inhibition than its thiophene counterpart.[51]

Since the reactivity of Ebselen (**67**) with cysteine thiols has been widely documented, we reasoned that a seleno series of analogues might express activity *vs Pf*IspD.[52,55,56] The organoselenium drug ebselen (**67**) (rat oral $LD_{50} \geq 6810$ mgkg^{-1}), is the seleno-version of our BITZ compound **9** (Ebsulfur) (Figure 3.23).[51,57]

Ebselen (**67**) **9**

Figure 3.23. Structure of Ebselen (67) *vs* 9.

Ebselen (**67**) was designed for the treatment of ischaemic stroke *via* the inhibition of lipid peroxidation, however, it was halted in the final stage of clinic trials due to poor efficacy.[58] Since its abandonment the drug was rescued after it was discovered that the trial data showed it was clinically safe. It is now being tested for a new treatment of bipolar disorder, hearing loss, as an anticancer drug, as an antiviral, and as an antibiotic.[56,59–64] With this in mind we decided to examine modification of the B-ring of the biaryl BITZ series of compounds, *via* replacement of sulfur with selenium.

3.5.1 Synthesis of Ebselen Derived Compounds

5 compounds were successfully synthesised, namely **77** – **81**, and these were compared with their sulfur analogues compounds **20**, **21**, **25 – 27**. In addition one compound, **82** from the mono-phenyl series was also synthesised and compared with its sulfur analogue **83** (compound synthesised by Dr Kathryn Price).

All the requisite side chains required syntheses, and this was successfully carried out according to Scheme 3.13 below. First, the desired amines were coupled into (4-(bromomethyl) phenyl) boronic acid (**68**) to produce **69a** – **69c** in varying yields (see Table 3.13).[65] These boronic acids were then coupled with 3-bromoanline (**70**) using Suzuki chemistry to form **71a – e** .[2,66]

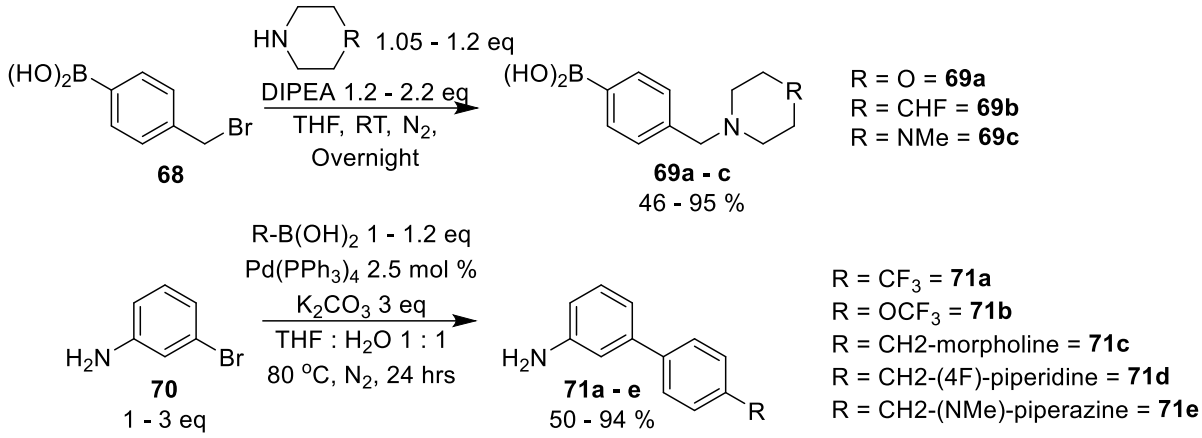

Scheme 3.13 Synthesis of 71a – e.

In order to synthesise the side chain of the mono-phenyl compound, first morpholine was coupled into 1-(bromomethyl)-3-nitrobenzene forming **73** in 99 % yield.[65] We attempted a Pd / C hydrogenation reaction to reduce the nitro group to the amine **74**, however, when we did this, what we isolated was morpholine and *m*-toluidine by C-N bond cleavage.[67] To circumvent this problem, we instead synthesised **74** through a Fe / AcOH single electron transfer reduction in 96 % yield (Scheme 3.14).[68]

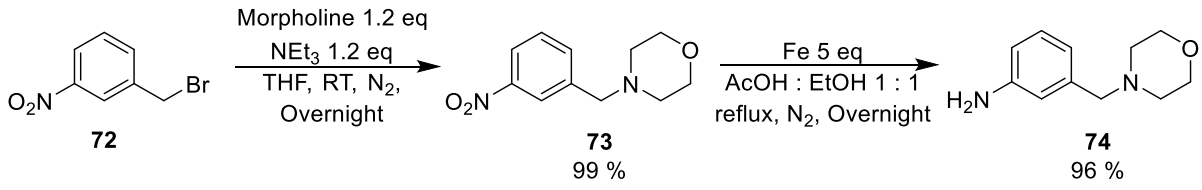

Scheme 3.14. Synthesis of 74.

We then investigated how best to carry out the ring closing reactions. We first examined the possibility of preparing **77** – **82** through analogous procedures to Scheme 3.3, through a Se-Cl / acid chloride mediated ring closure. However, the desired starting material 2,2'-diselanediyldibenzoic acid, was not commercially available. We investigated methods to synthesise this starting material, however, it required the use of Na_2Se_2, which also was not commercially available. There are procedures reported for the synthesis of Na_2Se_2, however, some of them reported H_2Se gas release as a side product. H_2Se gas is highly poisonous and we deemed it too dangerous to attempt the synthesis of Na_2Se_2 even *via* the procedures not reporting H_2Se in the absence of a glovebox.[69–72] Therefore, all compounds were synthesised according to the ring closure analogous to Scheme 3.2. Intermediates

76a – **f** were first synthesised using peptide coupling procedures, reacting 2-iodobenzoic acid (**75**) in the presence of oxalyl chloride followed by amines **71a – e** and **74**. Ring closure to compounds **77 – 82** was then accomplished *via* the replacement of elemental sulfur for elemental selenium as depicted below (Scheme 3.15).[56,73,74]

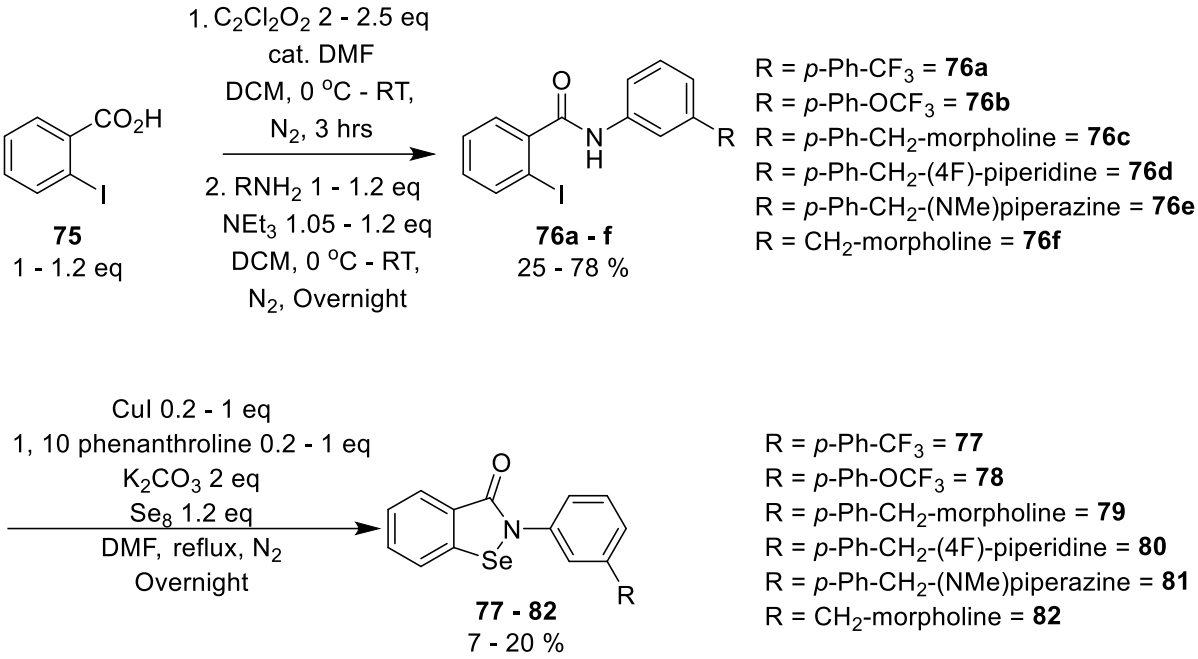

Scheme 3.15. Synthesis of 77 – 82.

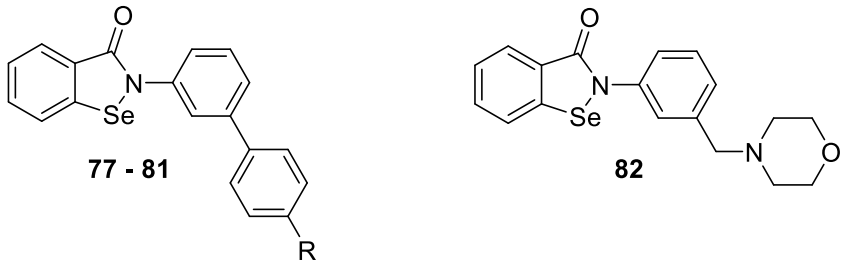

Table 3.13. Summary of yields obtained synthesising mono-phenyl and biphenyl targets.

Final Compound	R (In final compound)	% yield **69a – c**	% yield **71a – e**	% yield **76a – f**	% yield **77 – 82**
77	CF_3	-	75	25	7
78	OCF_3	-	82	35	20
79	CH_2-morpholine	87	90	58	18
80	CH_2-(4F)-piperidine	95	50	53	11
81	CH_2-(NMe)piperazine	46	94	74	7
82	-	-	-	78	15

The yields of steps *en route* to final compounds are reported in Table 3.13. As can be seen the amine couplings gave good yields with the exception of **69c** which was difficult to isolate and extract

due to the high polarity of the compound, and its tendency to stay in an aqueous phase. Nevertheless, the low yield of 46 % was acceptable to carry on the synthesis. In general, the synthesis of intermediates **71a** – **e** proceeded very well following Suzuki coupling procedures, generally giving high yields. The synthesis of **76a** – **f** *via* amide coupling procedures gave a high degree of variation with yields. Interestingly the final ring closing step to compounds **77 – 82** consistently produced low yields; this is in contradiction to the literature method which is reported to give high yields.[73] It should be noted, however, that the substrates used here are larger and more complex than those reported in the literature, and perhaps this could justify these results. In some cases we varied the loading of CuI, however, this had little impact on yields obtained.

3.5.2 Biological Data of Ebselen Derived Compounds

All compounds were screened for *Pf*IspD and *Pf*3D7 activity and are summarised in Table 3.14 below. For direct comparison, data for the sulfur analogues are also displayed.

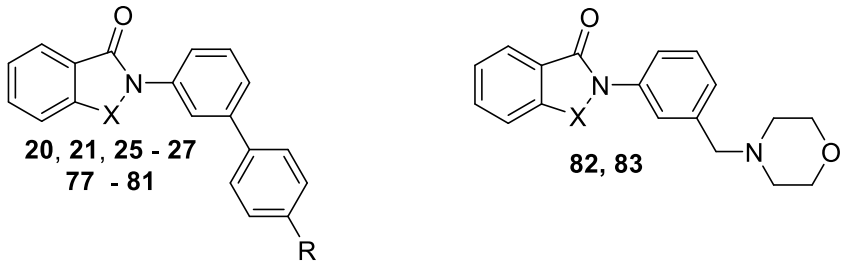

Table 3.14. Biological data comparison of Ebselen mimetics and 1,2-BITZ compounds. Compound properties are ranked using a traffic light system. Green = good, amber = acceptable, red = poor. 1,2 BITZ compounds were synthesised by former PhD student Dr Kathryn Price.

Compound	R	X	*Pf*IspD IC_{50} (nM)	*Pf*3D7 EC_{50} (nM)	CLogP
20	CF_3	S	273 ± 15 n = 3	646 ± 21 n = 6	6.12
21	OCF_3	S	290 ± 195 n = 3	411 n = 1	6.27
25	CH_2-morpholine	S	400 ± 82 n = 3	413 ± 82 n = 4	4.99
26	CH_2-(4F)-piperidine	S	862 ± 107 n = 3	323 ± 92 n = 5	5.96
27	CH_2-(NMe)piperazine	S	446 ± 75 n = 3	416 ± 6 n = 3	5.55
77	CF_3	Se	11900	3010	6.48
78	OCF_3	Se	>50000	3250 ± 1340	6.62
79	CH_2-morpholine	Se	132	3040	5.34
80	CH_2-(4F)-piperidine	Se	160	2834 ± 373	6.31
81	CH_2-(NMe)piperazine	Se	133	5250	5.9
82	-	Se	281 ± 4	14900	3.45
83*	-	S	540 n = 1	5710 n = 1	3.10

*** Compound synthesised by Dr Kathryn Price**

The results from the testing data are very interesting, replacing the sulfur atom to selenium in **20** and **21**, forming **77** and **78**, led to a large loss of potency against the enzyme and a loss of potency against 3D7 whole cells. It is interesting to note that the potency in the cellular assay is greater than

that for the IspD assay; this suggests that these two compounds demonstrate off target effects, and this can be confirmed in the future through an IPP rescue screen. Comparing **20** and **21** to **77** and **78**, it is unexpected to see such a drop in potency, we postulate this could be due to the increased lipophilicity, poorer aqueous solubility and greater reactivity for these matched pairs.

When solubilising groups were incorporated into the structure, as can be seen in compounds **79** – **81**, *Pf*IspD activity was regained and demonstrated excellent activity. Comparing these compounds to the sulfur analogues **25** – **27**, all variants displayed improved potency. However, the drawback of the series again was the loss of potency observed in the cellular assay; unfortunately these compounds are either too reactive and ring open before reaching the apicoplast, or alternatively, are not able to penetrate the apicoplast. One thing to note is that if transportation into the apicoplast is the issue, it is not related to CLogP entirely. When comparing the CLogP of **79** to **26**, **79** possesses a lower CLogP than **26**, however, **26** is still potent in the whole cell assay. Therefore, this could be an indication that electronics and reactivity play a crucial role in determining whole cell activity.

We also investigated one compound possessing a mono-phenyl ring with a morpholine group amended *meta* to the ring by a methyl linker **82**. Similar to above, **82** displayed improved potency against the enzyme, however, the compound again lost activity in the cellular assay in comparison to sulfur analogue **83**. Furthermore, **82** was the least potent compound against *Pf*3D7 cells in the selenium analogue series. It should be noted that this loss of potency here was in part expected, as **83** was also weakly potent in the cell assay. This compound backed up our hypothesis that compounds possessing a biphenyl moiety are required for cell activity.

As part of other work within the group, former PhD student Dr Natalie Roberts also synthesised ebselen related compounds based on other areas of SAR around the BITZ chemotype. As part of this study ebselen (**67**) itself was also synthesised and displayed poorer enzyme and whole cell activity than **9**. Other than **67**, in general, the findings from this analogous study elucidated that selenium analogues display improved enzyme activity when comparing to the analogous BITZ compounds with variable effects on whole cell activity.

We investigated the docking poses of compounds **77** and **79**, respectively into the active site of our IspD homology model to shed some light on why **77** demonstrated poor activity whilst **79** demonstrated good enzymatic potency. Again the protocol in Chapter 2 was followed once more. For compound **77**, most poses were in similar orientation and the SD of the data was low, giving mean and SD values of 53.4 and 0.8, respectively, thus we selected the best binding score (53.9) for the pose of this compound (Figure 3.24, Table 3.15). **79**, however, had many varying poses giving mean and SD

values of 52.6 and 2.7, respectively. One pose, though being the second lowest fitness score (51.4), was in close proximity to the crucial Cys-202 residue, and this was selected for display (Figure 3.25, Table 3.16). Finally for completeness a covalently bound docking pose was generated for **79** showing how the pose may look once the Cys-202 residue has been chemically modified. The covalent docking was carried out in GOLD though linking the C-α carbon of Cys-202 to **79** (Figure 3.26, Table 3.17).

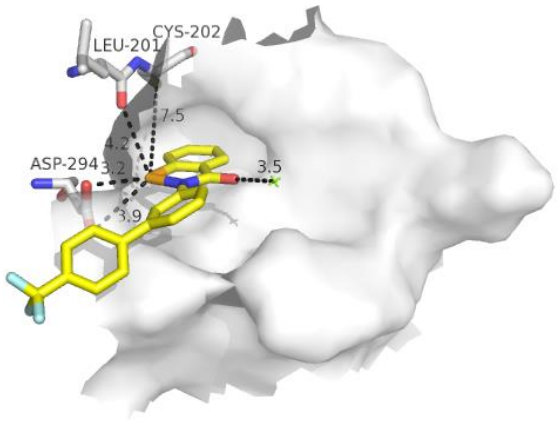

Figure 3.24. Binding pose of 77. Binding site is rendered as a white surface, Mg^{2+} is depicted as a green cross, 77 is rendered as sticks, carbon coloured yellow, fluorine in sky blue, nitrogen in blue, oxygen in red, selenium in orange. Crucial amino acids are rendered as sticks carbon coloured grey, nitrogen in blue, oxygen in red, sulfur in yellow.

Table 3.15. Main ligand – protein interactions of 77.

Residue(s)	Moiety	Interaction	Distance Å
Asp 294	B-ring-Se	Electrostatic	3.2
Mg^{2+}	B-ring-C=O	Weak electrostatic	3.5

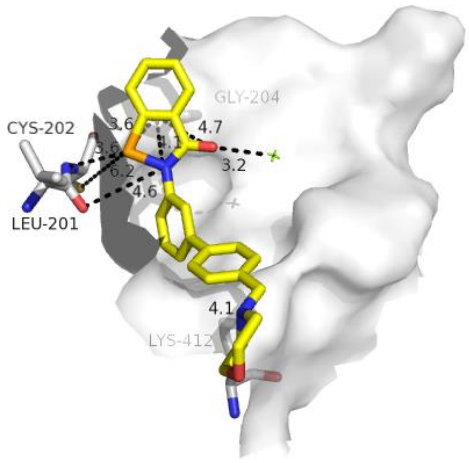

Figure 3.25. Binding pose of 79. Binding site is rendered as a white surface, Mg^{2+} is depicted as a green cross, 79 is rendered as sticks, carbon coloured yellow, fluorine in sky blue, nitrogen in blue, oxygen in red, selenium in orange. Crucial amino acids are rendered as sticks carbon coloured grey, nitrogen in blue, oxygen in red, sulfur in yellow.

Table 3.16. Main ligand – protein interactions of 79.

Residue(s)	Moiety	Interaction	Distance Å
Cys-202, Gly-204	B-ring-Se	Weak electrostatic	3.6, 3.6
Mg^{2+}	B-ring-C=O	Electrostatic	3.2

Examination of the pose of **77** reveals that the A and B-rings are buried within the same binding pocket that the same ring system of MMV008138 is bound within. This allows for one strong and two weak potential electrostatic interactions of the selenium atom with neighboring Leu-201 and Gly-204 residues whilst the carbonyl of the B-ring is able to coordinate the Mg^{2+} ion, the remaining biphenyl moiety is pointing into solvent exposed space picking up no notable further interactions. The Se atom is located quite far away from the cysteine thiol in this pose at 7.5 Å, which may account for the lack of activity observed with **77** as it is not in suitable proximity for covalent modification to occur.

In contrast, **79** shows a pose closer the cysteine thiol at 6.2 Å. In this pose the Se atom can form weak electrostatic interactions with the Cys-202 and Gly-204 nitrogen atoms, which may bring the molecule within close proximity to the thiol of Cys-202 to allow for covalent modification. In addition the B-ring carbonyl can coordinate with the Mg^{2+} ion and Gly-204 suitably anchoring the molecule for covalent modification. Finally the morpholine ring may also pick up a weak electrostatic interaction with Lys-412 at 4.1 Å; such an interaction is not present in **77**. Taken all together this pose could explain why the analogues possessing solubilising groups are able to demonstrate *Pf*IspD potency. After covalent modification of Cys-202 occurs we were interested to examine what other interactions may be gained from the now bound inhibitor, displayed below is the docking pose of **79** after covalent modification (Figure 3.26 and Table 3.17).

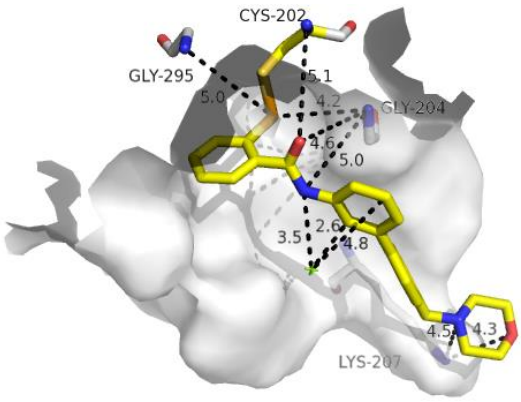

Figure 3.26. Covalent binding pose of 79. Binding site is rendered as a white surface, Mg^{2+} is depicted as a green cross, 79 is rendered as sticks, , carbon coloured yellow, fluorine in sky blue, nitrogen in blue, oxygen in red, selenium in orange. Crucial amino acids are rendered as sticks carbon coloured grey, nitrogen in blue, oxygen in red, sulfur in yellow.

Table 3.17. Main ligand – protein interactions of ring opened 79.

Residue(s)	Moiety	Interaction	Distance Å
Mg^{2+}	Ex-B-ring N	Electrostatic	3.5
Mg^{2+}	C-ring	π-cation	~3.5

Interestingly after covalent docking **79** in *Pf*IspD active site and choosing a suitable docking pose, the molecule picks up different interactions to that prior to covalent binding. The molecule has

altered orientation which allows for the Cys-202 and Gly-204 to weakly interact with the ring opened B-ring carbonyl, the Se is flanked by two Glycine residues which may also pick up weak electrostatic interactions. The ring opened nitrogen atom can coordinate the Mg^{2+} ion and may pick up a weak interaction with the neighboring Gly-204 residue. In addition the C-ring can also form a π-cation interaction with the Mg^{2+}, however, the angle of the ring is skewed from the Mg^{2+} slightly. Finally, the morpholine ring can be anchored with Lys-207, now forming two weak interactions *vs* the one from Lys-412 in the previous pose. These poses potentially indicate that the mechanism of these compounds is first through non-covalent recognition, which then drives the covalent bond formation between protein and ligand.

3.5.3 Conclusion of Ebselen Derived Compounds

Altering the B-ring of the BITZ core *via* the substitution of the sulfur atom to selenium yielded interesting results. Of the biphenyl series, compounds **79** – **81** demonstrated potent activity against *Pf*IspD giving IC_{50} values <200 nM. In these cases enzymatic potency was improved over the corresponding BITZ compounds. Interestingly all of these compounds harboured a solubilising 6-membered amine ring liking to the aromatic D-ring through a methyl linker. If this ring was removed as in the case of compounds **77** and **78** activity against the enzyme is lost, this was surprising considering in this case the equivalent BITZ compounds retain activity. At this time the reason for loss of activity is unknown, we postulate that the lipophilicity of the compounds are too high and thus cannot pass inside the polar enzyme active site.

One mono-phenyl compound **82** was also made with the C-ring substituted at the *meta*-position by a methyl linked morpholine ring. Similar to the biphenyl series this compound also showed improved *Pf*IspD activity over the analogous BITZ compound **83**. However, both chemotypes were poorly potent against *Pf*3D7 whole cells.

Similar to the mono-phenyl series the biphenyl series also demonstrated a loss of potency in the whole cell assay. The reasons for this unexpected loss of cellular potency are not clear, however, we can postulate two reasons for their inactivity; i) the ebselen series is too reactive, and thus ring open before entering the apicolplast resulting in an inactive compound; ii) the compounds are not transported or able to penetrate the apicoplast.

3.6 Future Work of all Investigated Series

2.1-BITZ Series

For future work, as compound **45** was the only compound possessing enzymatic potency in the series, it could be worth examining other benzoyl derivatives in order to further explore chemical space, or to incorporate solubilising groups. However, it cannot be ruled out that **45** is unstable in aqueous buffer. Therefore assessment of the stability of **45** aqueous buffer will need to carried out to determine if the activity is true, or is the result of a possible decomposition product resulting from bioassay conditions. This will need to be undertaken before examining further benzoyl derivatives. Examples of future compounds are displayed below (**84 – 88**) (Figure 3.27). In addition to benzoyl compounds one compound possessing an *N*-linked thiophene moiety (**88**) demonstrated good *Pf*3D7 potency and was identified in the Tres-Cantos antimalarial set (TCAMS).[32] Unfortunately it is not known if this compound targets IspD to date and a method for its synthesis has not yet been identified by us or released into the literature.

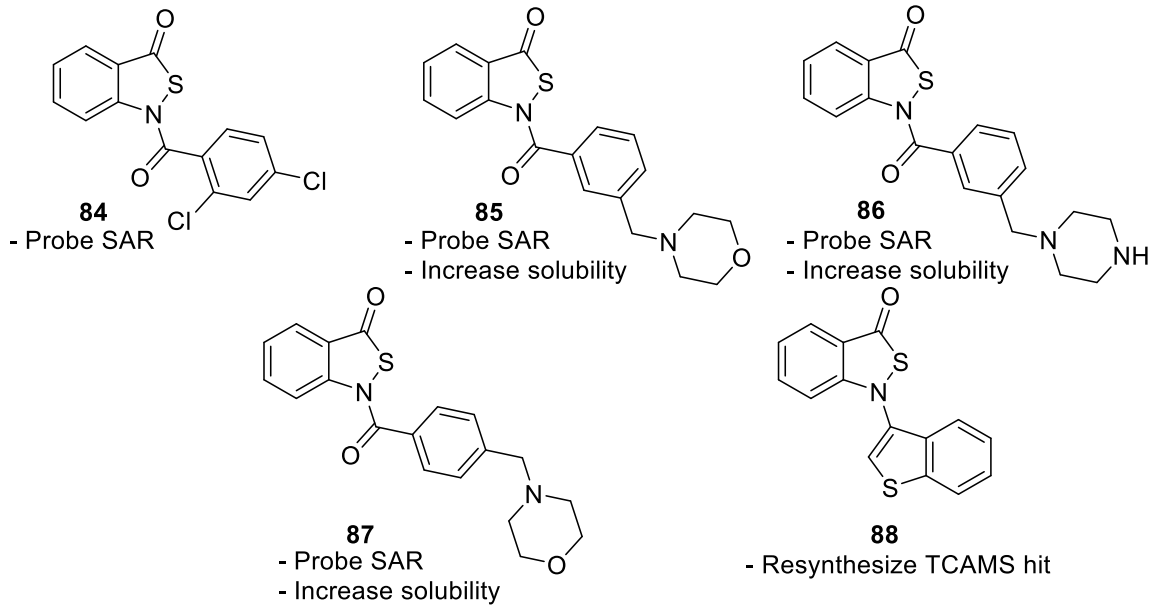

Figure 3.27. Potential future targets from the 2,1-BITZ series.

1,2-BITZ Series and Ebselen Series

With regards to future work of both series it is not clear what else could be synthesised to regain cellular potency. The ebselen biphenyl series does not mirror the *Pf*3D7 whole cell potency of the analogous BITZ chemotype. However, it could be worth examining further substitution of the D-ring as to date, substitution has focused mainly on methyl linked 6-membered tertiary amine rings. Rings of differing sizes (compounds **89**, **90**) and altered to secondary amines such as compound **91**

could provide us with the cell activity that we are aiming to achieve (Figure 3.28). With regards to the future work of the 1,2-BITZ series, the analogous compounds can also be tested for potency.

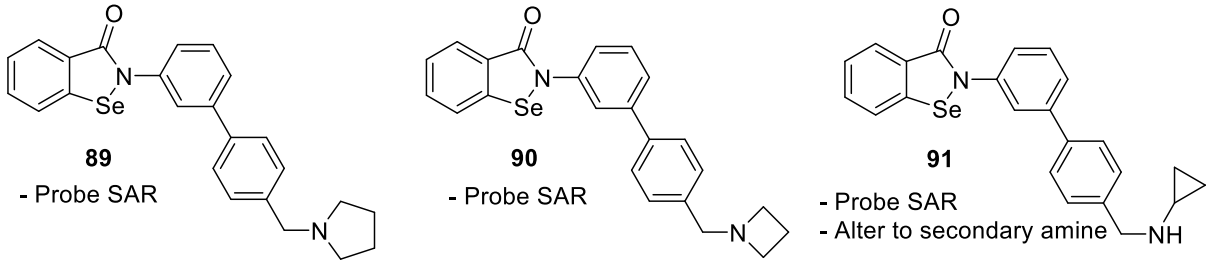

Figure 3.28. Potential future targets for the ebselen series.

Towards the end of the project on the BITZ compounds we noticed that the class had been identified as a PAIN. While we are confident our molecules are not interfering in the assay, we acknowledge that to confirm beyond any doubt that this is the case, a counter screen of the compounds against unrelated targets will be required to be carried out as part of future work along with any added orthogonal assay. In addition to this, all tested compounds should also be screened within the alternate BIOMOL Green assay (see **Section 3.3**). The control experiment of stirring an active BITZ compound in the presence of MESG and / or its resultant product will also be carried out as part of future work.

3.7 Benzothiazines as Potential Inhibitors of *Pf*IspD

Following on from the HTS carried out by Biofocus a second HTS (HTS2) was undertaken following similar methods to those described in **Section 3.1**. In HTS2, 5000 compounds were selected *via* computational testing and were interrogated for potency against *Pf*IspD by Biofocus. From all 5000 compounds screened 17 of them were identified to possess reproducible IspD potency of < 1 μM along with good purity. Of greatest interest from the screen was a related series of 3 compounds, two of which demonstrated potency of <1 μM.[75]

These three identified compounds were of great interest as they already showed early indications of SAR, furthermore the chemistry *en route* to the compounds seemed straightforward, cheap, and scalable, potentially allowing for rapid compound generation. The compounds belong to a benzothiazinone (BTZ) chemotype, and are displayed below (Figure 3.29).

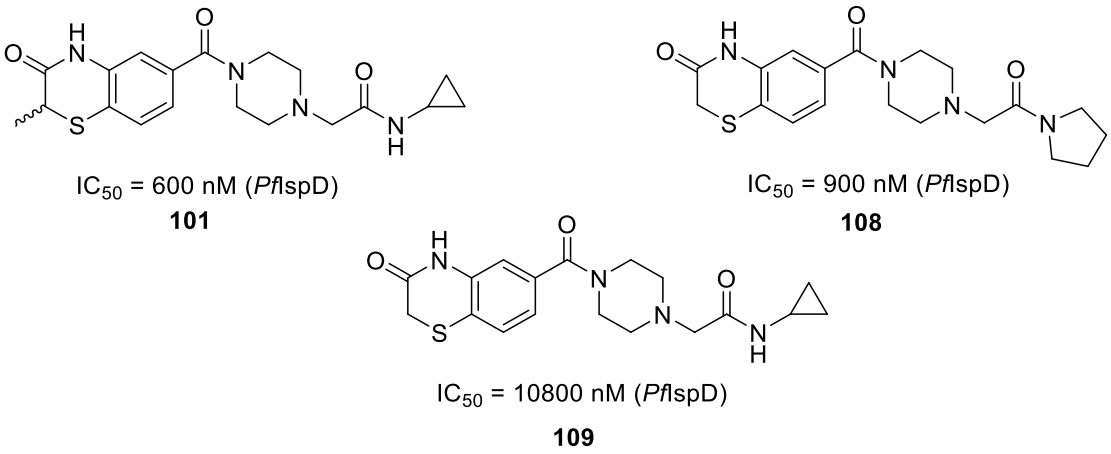

Figure 3.29. Compounds of interest from HTS2.

The early SAR looked very interesting; with regards to the left hand side of the molecule there seems to be a specific requirement for the incorporation of the methyl adjacent to the sulfur atom when the right hand side of the molecule harbours a secondary amide. Removal of this methyl results in an 18 fold drop of activity, however, if this secondary amide is replaced with a tertiary amide, activity returns in the absence of the methyl on the BTZ core. It may be the case that reincorporation of the methyl could boost activity even further. As a starting point we focused on the development **101** was it showed the most potent inhibitory activity.

There are many possible sites within the template which can be manipulated which made it an exciting template to work on. The main goal of the SAR was to focus on the right hand side of the molecule by examining the effect of substituting the terminal amide ring system with rings of altering sizes in order to probe sterics. In addition to this promising line of SAR, the molecules look favourable in terms of their drug like properties, with **101** possessing a promising ClogP value of 1.28.

3.7.1 Synthesis of BTZ Compounds

The route to the targets is shown below (Scheme 3.16); the chemistry towards the BTZ core was adapted from work published by Yamamoto *et al*. followed by standard peptide coupling and de-protection strategies to yield the final compounds.[76] Note the starting thiol is racemic as the chirality of the methyl group was not deemed important at this stage.

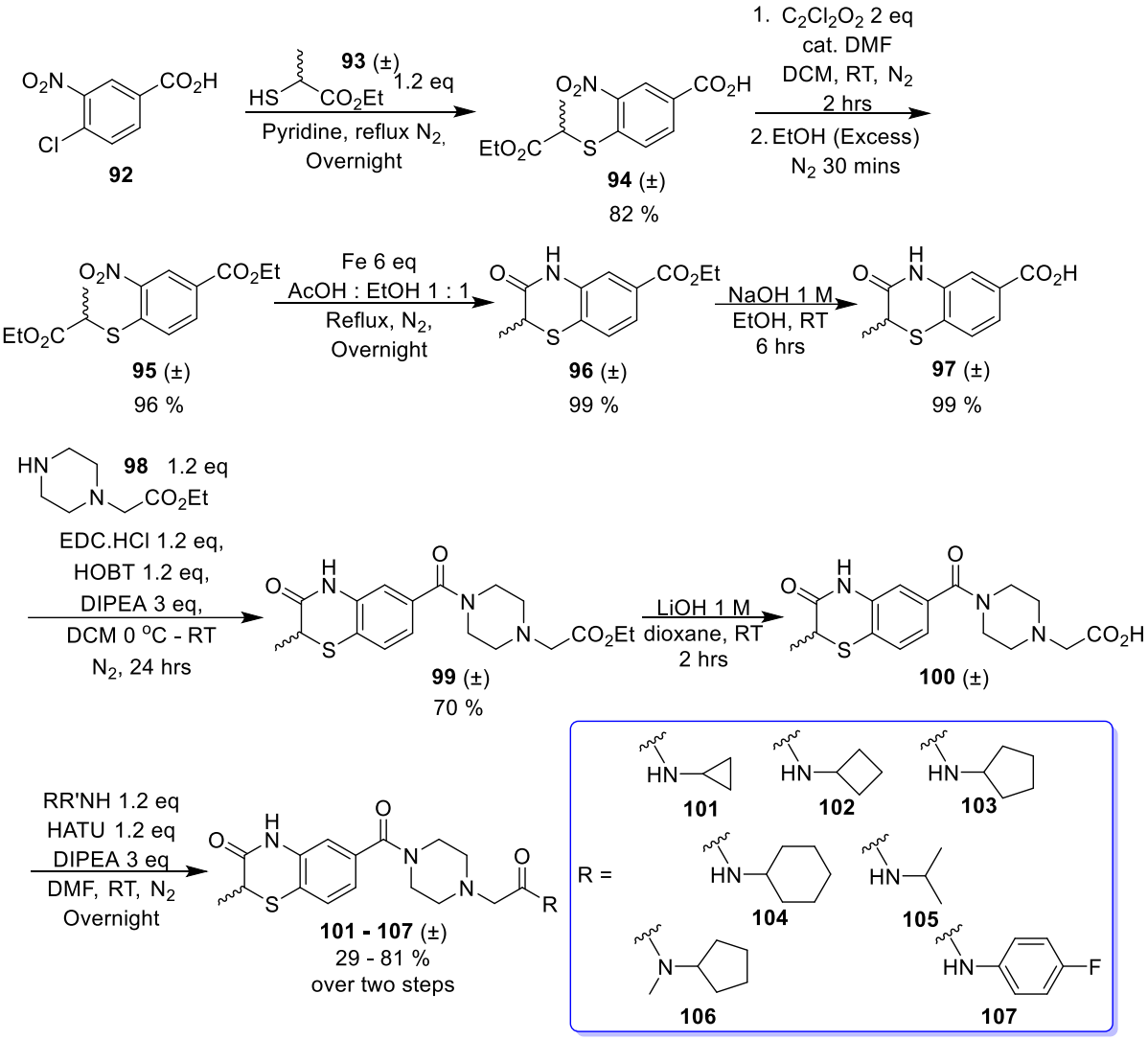

Scheme 3.16. Synthesis of 101 – 107.

The synthesis begins with the nucleophilic aromatic substitution reaction of 4-chloro-3-nitrobenzoic acid (**92**) with ethyl 2-mercaptopropanoate (**93**) forming **94**. The acid moiety of **94** is then esterified *via* the formation of an acyl chloride, which can then be quenched with excess EtOH forming the desired ethyl ester **95**. The next step involved reduction of the nitro group followed by *in situ* ring closure to the BTZ ethyl ester core **96**. The initial reduction route planned was through Pd / C conditions under a H_2 atmosphere as reported by the literature.[76] However, upon repetition of this, the reaction constantly failed yielding only starting materials, this is likely due to catalyst poisoning by the sulfur atom. Therefore we decided to utilise the SET reduction method using Fe and AcOH as previously used for ebselen series of compounds, this reaction successfully formed the BTZ ethyl ester core **96**.[68]

We next installed the amide functionality of the molecule, in order to do this, however, **96** was hydrolysed to its acid form **97** *via* basic hydrolysis in the presence of 1 M NaOH. As **97** was an

important intermediate it was subsequently stockpiled. To install amide functionality we decided to utilise peptide coupling reagents that would generate an activated ester *in situ* which can be sequentially attacked by the amine nucleophile forming the amide bond. This reaction was carried out using EDC.HCl and HOBT as reagents to form the activated ester before addition of the desired amine, ethyl 2-(piperazin-1-yl)-acetate (**98**), which successfully yielded intermediate **99**. It should be noted that this compound can synthesised *via* the generation of an acyl chloride as the electrophile for the amine, however, when we used this method we found that reaction yields were low and purification was more difficult therefore we preferred to use peptide coupling reagents.

Again we wanted to install amide functionality for the right hand side of the molecule; therefore the ethyl ester of **99** was hydrolysed to its acid **100** in the presence of 1 M LiOH which was found to proceed faster than using 1 M NaOH for the same reaction. Unfortunately **100** could not be isolated successfully, during work up it was found that it remained in the water layer at various pH values, this is likely due to the presence of amphoteric sites. After formation of **100** was confirmed by TLC, the aqueous phase was neutralised to approximately pH 7 and solvents were removed under vacuum. After mass spectrometry and ^{1}H NMR confirmed the correct product, **100** was used crude directly in the next step.

The final step of the reaction was again an amide coupling reaction, however, this was our branching point for SAR. From intermediate **100** we generated final compounds **101 – 107**, using a slightly different peptide coupling procedure were HATU was used as the peptide coupling reagent to generate the activated ester. We chose this method as it was believed that reactions occur faster and any side products would be easier to remove.[77] The yields for the final peptide coupling steps are summarised in Table 3.18. Note that yields are reported over two steps as **100** could not be isolated.

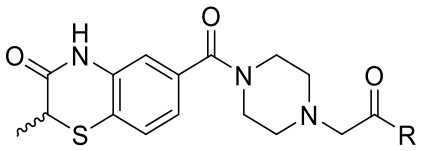

Table 3.18. Yields of final coupling steps.

Final Compound	R (In final compound)	% Yield over 2-steps
101	NH-cyclopropyl	36 %
102	NH-cyclobutyl	27 %
103	NH-cyclopentyl	29 %
104	NH-cyclohexyl	81 %
105	NH-^{i}Pr	63 %
106	NMe-cyclopentyl	66 %
107	NH-(4F)-Ph	52 %

In general all yields for all steps up to the final coupling proceed very well giving yields between 70 and 99 %. However, the final couplings gave a large degree of variation to the yields, we propose that this is related to how efficiently the previous step is neutralised, as any residual lithium carboxylate salts are less likely to react with the peptide coupling reagents, resulting in the failure to generate the activated ester required for peptide coupling.

3.7.2 Biological Data of BTZ Compounds

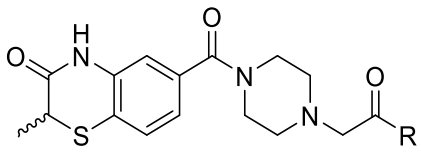

Table 3.19. Biological data of BTZ compounds. Compound properties are ranked using a traffic light system. Green = good, amber = acceptable, red = poor.

Compound	R	IC_{50} *Pf*IspD (nM)	EC_{50} *Pf*3D7 (nM)	ClogP
99*	OEt	>100,000 n = 1	>100,000 n = 1	2.14
101	NH-cyclopropyl	>100,000 n = 1	>50,000 n = 1	1.28
102	NH-cyclobutyl	>100,000 n = 1	>50,000 n = 1	1.61
103	NH-cyclopentyl	>100,000 n = 1	>50,000 n = 1	2.16
104	NH-cyclohexyl	>100,000 n = 1	48,000 n = 1	2.72
105	NH-^{i}Pr	>100,000 n = 1	>100,000 n = 1	1.60
106	NMe-cyclopentyl	>100,000 n = 1	>100,000 n = 1	2.59
107	NH-(4F)-Ph	>100,000 n = 1	>100,000 n = 1	2.95

*** Compound sent for testing was synthesised by former masters student Charles Evans**

The results from the biological data set were disappointing (Table 3.19). It is clear that none of the compounds possess potency against enzyme or *Pf*3D7 cells and unfortunately no compound is of comparable activity to the assay conducted by BioFocus. Therefore, this suggests that there were at least 2 false positives from the HTS. Interestingly compounds **101 – 104** did show some minor activity against *Pf*3D7 cells but again the activity is poor and is suggestive that the compounds demonstrate off target effects as the inhibition of IspD is lower than that of the cellular assay. A small trend that can be observed from compounds **101 – 104** is that as lipophilicity increases *Pf*3D7 potency slightly increases. However, this trend fails when taking **106** and **107** into account. For **106** the methylated tertiary amide may be too hindered to allow any possible binding which could explain the loss of activity. For **107** this loss could be due to the electron withdrawing nature of the aromatic ring causing delocalisation of nitrogen lone pairs which may be crucial to any minor activity.

We do not yet understand exactly why there are differences between the BioFocus and Washington University assay results; LCMS data for the molecule looked correct and had good purity so this issue requires investigation. To confirm the correct structure of **101**, we successfully crystallised

compound **101** and determined its relative structure by X-ray crystallography. The crystal structure of **101** was resolved by Dr Craig Robertson and imaged in OLEX2 (Figure 3.30).[78]

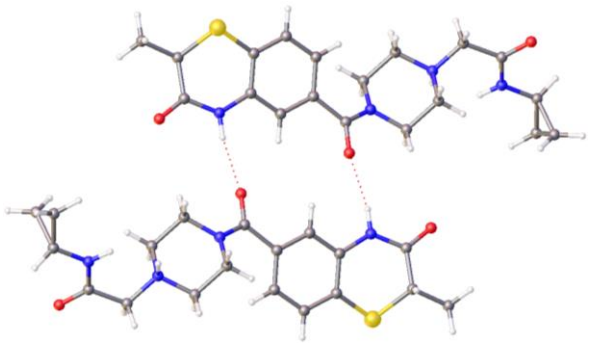

Figure 3.30. X-ray structure of 101. Image is rendered as ball and stick, carbon, coloured in grey, hydrogen in white, nitrogen in blue, oxygen in red, sulfur in yellow. Compound was visualised using OLEX2.[78]

The crystal structure confirmed the correct structure for **101**. Depicted below is the X-ray image of both enantiomers together forming a hydrogen bond donor / accepter pair between the BTZ ring nitrogen atom and the carbonyl oxygen linking the piperazine ring. The confirmation of the correct structure gave us confidence that the discrepancies observed between the two assays carried out by BioFocus and the Odom group was not due to any mistake on our part.

3.7.3 Conclusion of BTZ Compounds

Unfortunately all compounds from the BTZ series of compounds demonstrated poor potency against both *Pf*IspD and *Pf*3D7 cells. This was disappointing; especially considering all compounds possessed attractive CLogP values. Due to the results from the Biofocus assay, we decided to focus on substituting the amide moiety at the right hand side of the hit molecule **101**, and as protocol, we resynthesised **101** and sent it for biological evaluation. All compounds from this series were inactive in both enzyme and cellular assays and unfortunately, did not mirror the results from the Biofocus assay, suggesting that **101** was a false positive. Ester **99** was also sent for evaluation and was also inactive.

Within the group an analogous study was also undertaken (by former Masters student Charles Evans). Compound **110** was successfully synthesised to mirror the second BTZ hit **108** from the Biofocus screen, but included the methyl group within the BTZ core (Figure 3.31). This compound did demonstrate improved potency against IspD than the analogous study, however, potency is still poor, and *Pf*3D7 activity is comparable to that described above. With regards to any future work it is important to understand if **101** was a *Pf*IspD false positive before synthesising anymore derivatives, however, as cell potency is poor anyway this series is not likely worth expanding upon.

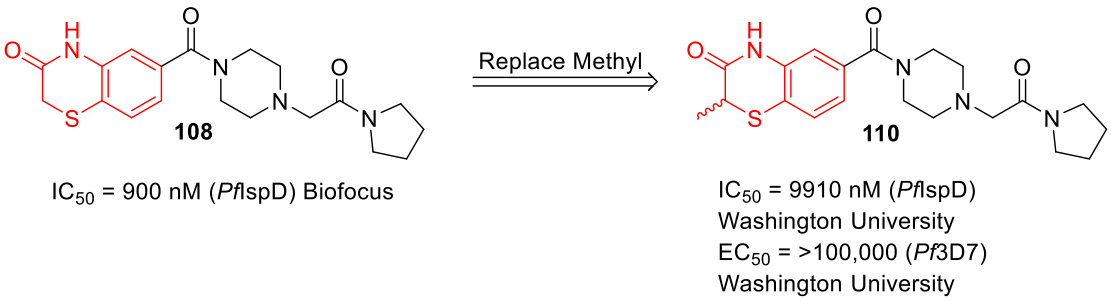

Figure 3.31. Biological data of 108 compared with 110.

3.8 Experimental Procedures

General Procedure 1: 2,1 benzoisothiazolinone synthesis.

Lithium sulfide (1.06 g, 23.00 mmol, 2.5 eq) was added to water (100 cm^3) at 0 °C, to the stirred solution was added 1 M HCl (34.2 cm^3, 34.20 mmol, 3.7 eq) dropwise over 15 minutes. Isatoic anhydride (**37**) (1.50 g, 9.2 mmol, 1 eq) was added portion wise over 15 minutes and the solution allowed to stir for a further 45 minutes at room temperature. The reaction mixture was filtered and purged with N_2 for one hour before cooling to 0 °C. To the solution was added hydrogen peroxide (1.13 cm^3, 11.04 mmol, 30 % w / w 1.2 eq) dropwise, the solution was allowed to warm to room temperature followed by stirring for 45 minutes. The mixture was filtered and to the filtrate was adjusted to pH 6. The desired product precipitated out and was filtered under vacuum to give the product **39** as a light brown solid (0.93 g, 67 %).

Preparation of benzo[*c*]isothiazol-3(1*H*)-one (39)

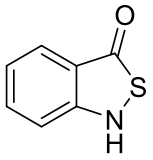

39

Isatoic anhydride (**37**) (1.50 g, 9.2 mmol, 1 eq), lithium sulfide (1.06 g, 23.00 mmol, 2.5 eq), 1 M HCl (34.2 cm^3, 34.20 mmol, 3.7 eq), and hydrogen peroxide (1.13 cm^3, 11.04 mmol, 1.2 eq) were used in water (100 cm^3) following **general procedure 1** to give the product **39** as a light brown solid (0.93 g, 67 %). δ_H (400 MHz, $CDCl_3$) 7.84 (1H, d, *J* 8.0 Hz), 7.58 – 7.53 (1H, m), 7.26 (1H, d, *J* 8.4 Hz), 7.14 (1H, t, *J* 7.5 Hz), 5.87 (1H, br s). δ_C (101 MHz, $CDCl_3$) 192.9, 154.4, 133.5, 123.2, 121.1, 120.5, 115.4. **CI-HRMS**: m/z calculated for C_7H_6NOS $[M+H]^+$ requires 152.0165. Found 152.0166. **Elemental Analysis** Calculated for C_7H_5NOS requires, C, 55.61; H, 3.33; N, 9.26; S, 21.21, found, C, 55.58; H, 3.32;

N, 9.19; S, 21.26. **IR (neat)**: ν_{max}/cm^{-1}: 3069 (br), 2843 (br), 1615 (s), 1593 (s), 1474 (m), 1341 (w). **Melting Point** °C: 134 – 136 (H_2O).

General Procedure 2: 2, 1 benzoisothiazolone S_N2 reactions

To benzo[*c*]isothiazol-3(1*H*)-one (**39**) (0.10 g, 0.65 mmol, 1 eq) was added acetone (10 cm^3), benzyl bromide (0.10 cm^3, 0.85 mmol, 1.3 eq) and potassium carbonate (0.18 g, 1.30 mmol, 2 eq) sequentially, and the reaction left to stir at room temperature under a N_2 atmosphere overnight. Solvents were removed *in vacuo* and to the residue was added water (50 cm^3). The product was extracted into ethyl acetate (3 x 50 cm^3), the organics were washed with water (50 cm^3), brine (50 cm^3) and dried over $MgSO_4$. The product was purified by flash column chromatography (10 % EtOAC / Hex – 100% EtOAc) to yield the product **41** as a yellow oil (0.16 g, 94 %).

Generic structure of compounds 41 – 45

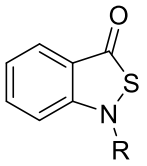

41 R = Bn

42 R = 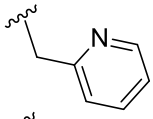

43 R = 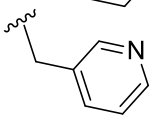

44 R = 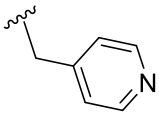

45 R = Bz

Preparation of 1-benzylbenzo[*c*]isothiazol-3(1*H*)-one (41)

Compound **39** (0.10 g, 0.65 mmol, 1 eq), benzyl bromide (0.10 cm^3, 0.85 mmol, 1.3 eq) and potassium carbonate (0.18 g, 1.30 mmol, 2 eq), were used in acetone (10 cm^3) following **general procedure 2** to give **41** as a yellow oil (0.16 g, 94 %). δ_H (400 MHz, $CDCl_3$) 7.83 (1H, dd, *J* 8.0, 0.4 Hz), 7.56 – 7.50 (1H, m), 7.39 – 7.32 (3H, m), 7.30 – 7.26 (2H, m), 7.24 (1H, d, *J* 8.6 Hz), 7.04 (1H, t, *J* 7.4 Hz), 4.99 (2H, s). δ_C (101 MHz, $CDCl_3$) 189.6, 153.8, 135.7, 134.1, 129.1, 128.6, 127.6, 124.4, 122.5, 120.0, 112.6, 52.7. **ESI-HRMS**: m/z calculated for $C_{14}H_{12}NOS$ $[M+H]^+$ requires 242.0634. Found 242.0641 **Elemental Analysis** Calculated for $C_{14}H_{11}NOS$ requires, C, 69.68; H, 4.59; N, 5.80; S, 13.29, found, C, 70.03; H, 4.66; N, 5.78; S, 13.24. **IR (neat)**: ν_{max}/cm^{-1}: 3062 (br), 2916 (br), 1647 (s), 1597 (s), 1471 (s), 1332 (m), 1158 (m).

Preparation of 1-(pyridin-2-ylmethyl)benzo[*c*]isothiazol-3(1*H*)-one (42)

Compound **39** (0.061 g, 0.41 mmol, 1 eq), 2-(bromomethyl)pyridine hydrobromide (0.10 g, 0.41 mmol, 1.0 eq) and potassium carbonate (0.18 g, 1.22 mmol, 3 eq), were used in acetone (10 cm^3) following a modified **general procedure 2**. Reaction was complete within 2 hours at room temperature rather than left overnight. This gave **42** as a yellow oil (0.082 g, 83 %). **δ_H** (400 MHz, $CDCl_3$) 8.62 (1H, s), 7.86 (1H, d, *J* 7.9 Hz), 7.68 (1H, apparent t), 7.54 (1H, apparent t), 7.30 – 7.22 (2H, m), 7.16 (1H, d, *J* 7.7 Hz), 7.07 (1H, apparent t), 5.15 (2H, s). **δ_C** (101 MHz, $CDCl_3$) 189.5, 155.7, 153.6, 149.9, 137.3, 134.3, 124.4, 123.3, 122.1, 121.5, 120.0, 112.6, 54.0. **ESI-HRMS**: m/z calculated for $C_{13}H_{10}N_2NaOS$ $[M+Na]^+$ requires 265.0406. Found 265.0408. **Elemental Analysis** Calculated for $C_{13}H_{10}N_2OS$ requires C, 64.44, H, 4.16, N, 11.56, S, 13.23, found C, 64.17, H, 4.28, N, 11.45, S, 13.10. **IR (neat)**: ν_{max}/cm^{-1}: 3064 (br), 2923 (br), 1631 (s), 1597 (s), 1472 (s), 1332 (m), 1159 (m).

Preparation of 1-(pyridin-3-ylmethyl)benzo[*c*]isothiazol-3(1*H*)-one (43)

Compound **39** (0.081 g, 0.54 mmol, 1 eq), 3-(bromomethyl)pyridine hydrobromide (0.18 g, 0.70 mmol, 1.3 eq) and potassium carbonate (0.22 g, 1.61 mmol, 3 eq), were used following a modified **general procedure 2**. Reaction was refluxed in acetone (10 cm^3) and was complete within 2 hours rather than left overnight. This gave **43** as a yellow semi solid / paste (0.037 g, 29 %). **δ_H** (400 MHz, $CDCl_3$) 8.61 – 8.57 (2H, m), 7.83 (1H, d, *J* 8.0 Hz), 7.60 (1H, apparent dt), 7.58 – 7.54 (1H, m), 7.29 (1H, dd, *J* 7.9, 4.9 Hz), 7.25 (1H, d, *J* 7.7 Hz), 7.07 (1H, t, *J* 7.5 Hz), 5.01 (2H, s). **δ_C** (101 MHz, $CDCl_3$) 189.3, 153.7, 150.1, 149.1, 135.4, 134.4, 131.3, 124.6, 124.0, 122.7, 120.5, 112.6, 50.4. **CI-HRMS**: m/z calculated for $C_{13}H_{11}N_2OS$ $[M+H]^+$ requires 243.0587. Found 243.0592. **Elemental Analysis** Calculated for $C_{13}H_{10}N_2OS$ requires C, 64.44, H, 4.16, N, 11.56, S, 13.23, found, C, 63.27, H, 4.34, N, 10.87, S, 12.45. **IR (neat)**: ν_{max}/cm^{-1}: 3040 (br), 2923 (br), 1642 (s), 1598 (s), 1469 (s), 1325 (m).

Preparation of 1-(pyridin-4-ylmethyl)benzo[*c*]isothiazol-3(1*H*)-one (44)

Compound **39** (0.083 g, 0.55 mmol, 1 eq), 4-(bromomethyl)pyridine hydrobromide (0.14 g, 0.55 mmol, 1.0 eq) and potassium carbonate (0.23 g, 1.64 mmol, 3 eq), were used in acetone (10 cm^3) following a modified **general procedure 2**. Reaction was complete within 2 hours at room temperature rather than left overnight. This gave **44** as a yellow solid (0.12 g, 87 %). **δ_H** (400 MHz, $CDCl_3$) 8.59 (2H, s), 7.85 (1H, d, *J* 7.8 Hz), 7.59 – 7.48 (1H, m), 7.17 (2H, s), 7.15 – 7.04 (2H, m), 5.00 (2H, s). **δ_C** (101 MHz, $CDCl_3$) 189.1, 153.6, 150.8, 150.4, 145.0, 134.5, 124.6, 122.3, 121.9, 120.5, 112.3, 51.5. **ESI-HRMS**: m/z calculated for $C_{13}H_{11}N_2OS$ $[M+H]^+$ requires 243.0587. Found 243.0596. **Elemental Analysis** Calculated for $C_{13}H_{10}N_2OS$ requires C, 64.44, H, 4.16, N, 11.56, S, 13.23, found C, 64.38, H, 4.12, N, 11.56, S, 13.30.

IR (neat): ν_{max}/cm^{-1}: 3150 (br), 3084 (br), 2981 (br), 2923 (br), 1624 (s), 1599 (s), 1480 (m), 1277 (m). **Melting Point** °C: 157 – 158 (melted and decomposed) (EtOAC / Hex).

General Procedure 3: Peptide coupling *via* acyl halide

To benzo[*c*]isothiazol-3(1*H*)-one (**39**) (0.082 g, 0.54 mmol, 1 eq) was added anhydrous DCM (10 cm^3), triethylamine (0.083 cm^3, 0.60 mmol, 1.1 eq), and benzoyl chloride (0.07 cm^3, 0.60 mmol, 1.1 eq). The reaction was stirred for two hours to overnight under a N_2 atmosphere. The organic layer was washed with 2 M HCl (50 cm^3), saturated sodium bicarbonate solution (3 x 50 cm^3), water (50 cm^3) and brine (50 cm^3), then dried over $MgSO_4$. Solvents were removed in *vacuo* and product purified by column chromatography using 50 % DCM in hexane, followed by recrystallisation in the same system, to yield **45** as white needles (0.14 g, 63 %).

Preparation of 1-benzoylbenzo[*c*]isothiazol-3(1*H*)-one (45)

Compound **39** (0.082 g, 0.54 mmol, 1 eq), triethylamine (0.083 cm^3, 0.60 mmol, 1.1 eq), and benzoyl chloride (0.07 cm^3, 0.60 mmol, 1.1 eq), were used in anhydrous DCM (10 cm^3) following **general procedure 3**. Column purification using 50 % DCM in hexane, followed by recrystallisation in the same system yielded **45** as white needles (0.14 g, 63 %). δ_H (400 MHz, $CDCl_3$) 8.47 (1H, d, *J* 8.6 Hz), 7.95 – 7.90 (1H, m), 7.76 – 7.68 (3H, m), 7.66 – 7.59 (1H, m), 7.57 – 7.48 (2H, m), 7.41 – 7.33 (1H, m). δ_C (101 MHz, $CDCl_3$) 187.7, 168.2, 148.4, 135.1, 134.7, 132.7, 128.9, 128.3, 125.5, 125.2, 123.9, 120.2. **ESI-HRMS**: m/z calculated for $C_{14}H_9NNaO_2S$ $[M+Na]^+$ requires 278.0246. Found 278.0256, and 278.0724 $[(M-S)+MeOH+Na]^+$. **Elemental Analysis** Calculated for $C_{14}H_9NO_2S$ requires: C, 65.87, H, 3.55, N, 5.49, S, 12.56, found, C, 65.85, H, 3.54, N, 5.50, S, 12.68. **IR (neat)**: ν_{max}/cm^{-1}: 3104 – 2922 (br), 1760 (s), 1609 (m), 1597 (m), 1461 (m), 1308 (m). **Melting Point** °C: 91 – 92 (DCM / Hex).

Preparation of 2-benzoylbenzo[*d*]isothiazol-3(2*H*)-one (47)

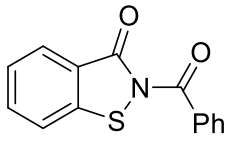

47

Benzo[*d*]isothiazol-3(2*H*)-one (**46**), triethylamine (0.083 cm^3, 0.60 mmol, 1.1 eq), and benzoyl chloride (0.07 cm^3, 0.60 mmol, 1.1 eq), were used in anhydrous DCM (10 cm^3) following **general procedure 3**. Column purification using 50 % DCM in hexane, following recrystallisation in the same system yielded **47** as white needles (0.044 g, 24 %). δ_H (400 MHz, $CDCl_3$) 7.96 (1H, d, *J* 7.9 Hz), 7.77 – 7.69 (3H, m), 7.62 – 7.54 (2H, m), 7.48 (2H, apparent t), 7.40 (1H, t, *J* 7.6 Hz). δ_C (101 MHz, $CDCl_3$)

169.1, 163.3, 141.6, 134.7, 133.1, 132.7, 129.2, 128.2, 128.1, 126.2, 125.3, 120.8. **CI-HRMS**: m/z calculated for $C_{14}H_{10}NO_2S$ $[M+H]^+$ requires 256.0427. Found 256.0423. **Elemental Analysis** Calculated for $C_{14}H_9NO_2S$ requires: C, 65.87, H, 3.55, N, 5.49, S, 12.56, found, C, 65.64, H, 3.56, N, 5.57, S, 12.83. **IR (neat)**: ν_{max}/cm^{-1}: 3091 – 3026 (br), 1708 (s), 1664 (s), 1579 (m), 1447 (m), 1273 (s). **Melting Point** ^oC: 163 – 164 (DCM / Hex).

Preparation of 1-phenyl-2H-benzo[*d*][1,3]oxazine-2,4(1*H*)-dione (49)

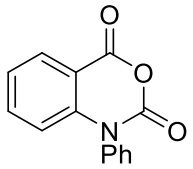

49

To *N*-phenylanthranilic acid (**48**) (2.01 g, 9.41 mmol 1 eq) was added anhydrous dioxane (25 cm^3). The solution was put under an N_2 atmosphere and cooled to 0 °C. Diphosgene (1.7 cm^3, 14.1 mmol, 1.5 eq) was added dropwise over five minutes and the solution stirred for one hour before warming to room temperature and stirring for a further 23 hours. Solvents were removed in *vacuo*, the solid washed with diethyl ether and dried by filtration, yielding the product as a brown solid (2.25 g, 75 %). δ_H (400 MHz, DMSO) 8.07 (1H, dd, *J* 7.8, 1.1 Hz), 7.69 – 7.55 (4H, m), 7.53 – 7.46 (2H, m), 7.32 (1H, t, *J* 7.6 Hz), 6.41 (1H, d, *J* 8.4 Hz). δ_C (101 MHz, DMSO) 159.2, 147.0, 143.4, 136.8, 136.0, 130.3, 129.5, 129.2, 128.8, 123.7, 115.3, 111.3. **CI-HRMS**: m/z calculated for $C_{14}H_{10}NO_3$ $[M+H]^+$requires 240.0655. Found 240.0659.

Preparation of 1-phenylbenzo[*c*]isothiazol-3(1*H*)-one (50)

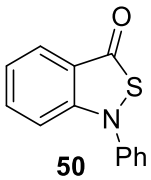

50

Compound **49** (1.00 g, 4.19 mmol, 1 eq) lithium sulfide (0.48 g, 10.48 mmol, 2.5 eq), 1 M HCl (15.5 cm^3, 15.5 mmol, 3.7 eq), and hydrogen peroxide (0.51 cm^3, 5.03 mmol, 1.2 eq) were used in water (50 cm^3) following a modified **general procedure 1**. No precipitation occurred after adjusting the pH to 6. The product was extracted into ethyl acetate (3 x 100 cm^3) washed with water (3 x 50 cm^3) basified by DIPEA (1 %). Organics were washed with brine (50 cm^3) , dried over $MgSO_4$, solvents removed *in vacuo* and product purified *via* purified by column chromatography (0.1 % DIPEA / 4.9 % EtOAc / 95 % hex) to give the product **50** as a dark yellow oil (0.25 g, 26 %). δ_H (400 MHz, $CDCl_3$) 7.89

(1H, d, *J* 8.0 Hz), 7.52 – 7.42 (5H, m), 7.41 – 7.35 (1H, m), 7.24 (1H, d, *J* 8.6 Hz), 7.08 (1H, t, *J* 7.5 Hz). **δ_C** (101 MHz, $CDCl_3$) 190.1, 152.7, 139.5, 134.1, 130.1, 128.1, 126.6, 124.2, 122.6, 120.5, 113.5. **CI-HRMS**: m/z calculated for $C_{13}H_{10}NOS$ $[M+H]^+$ requires 228.0478. Found 228.0483. **Elemental Analysis** Calculated for $C_{13}H_9NO_2S$ requires, C, 68.70; H, 3.99; N, 6.16; S, 14.11, found, C, 68.81; H, 4.05; N, 6.11; S, 14.08. **IR (neat)**: ν_{max}/cm^{-1}: 3062 (br), 1651 (s), 1588 (s), 1460 (s), 1325 (s).

General Procedure 4: Installation of urea moiety into 1,2 benzoisothiazolinone

To benzo[*d*]isothiazol-3(2*H*)-one (**46**) (0.30 g, 1.98 mmol, 1 eq) was added anhydrous THF (5 cm^3) and phenylisocyanate (0.22 cm^3, 1.98 mmol, 1 eq). The reaction was refluxed for one hour, solvents were removed in *vacuo* and the residue suspended in acetone (7 cm^3) and water (7 cm^3), precipitates were filtered by vacuum and washed with 1 : 1 water / acetone (3 x 5 cm^3) to give **53** as white crystals (0.53 g, 74 %).

Generic structure of 33 – 35 following general procedure 4

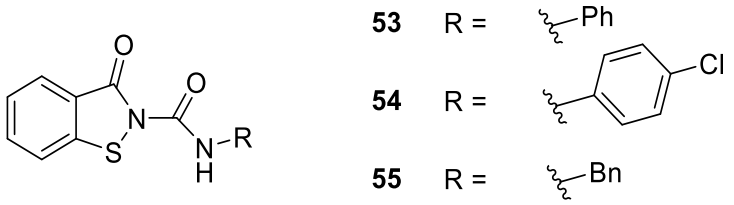

Preparation of 3-oxo-*N*-phenylbenzo[*d*]isothiazole-2(3*H*)-carboxamide (53)

Benzo[*d*]isothiazol-3(2*H*)-one (**46**) (0.30 g, 1.98 mmol, 1 eq) and phenylisocyanate (0.22 cm^3, 1.98 mmol, 1 eq) were used in anhydrous THF (5 cm^3) following **general procedure 4** to give **53** as white crystals (0.53 g, 74 %). **δ_H** (400 MHz, $CDCl_3$) 10.99 (1H, s), 8.08 (1H, d, *J* 7.9 Hz), 7.79 – 7.71 (1H, m), 7.67 – 7.55 (3H, m), 7.51 – 7.42 (1H, m), 7.42 – 7.36 (2H, m), 7.17 (1H, t, *J* 7.4 Hz). **δ_C** (100 MHz, $CDCl_3$) 165.3, 148.4, 140.8, 136.8, 134.1, 129.2, 127.4, 126.0, 124.9, 124.8, 120.6, 120.2. **ESI-HRMS**: m/z calculated for $C_{14}H_{10}N_2NaO_2S$ requires 293.0355. Found 293.0370. **Elemental Analysis** Calculated for $C_{14}H_{10}N_2O_2S$ requires, C, 62.21; H, 3.73; N, 10.36; S, 11.86, found, C, 61.95; H, 3.83; N, 10.32; S, 11.95. **IR (neat)**: ν_{max}/cm^{-1}: 3133 (br, N-H amide), 3076 (br, C-H aromatic), 1709, (s, C=O amide), 1592 (s, C=O amide), 1592 (s, C-C aromatic). **Melting Point** °C: 199 – 201 (Acetone / H_2O).

Preparation of *N*-(4-chlorophenyl)-3-oxobenzo[*d*]isothiazole-2(3*H*)-carboxamide (54)

Benzo[*d*]isothiazol-3(2*H*)-one (**46**) (0.15 g, 0.99 mmol, 1 eq) and 4-chlorophenylisocyanate (0.13 cm^3, 0.99 mmol, 1 eq) were used in anhydrous THF (5 cm^3) following **general procedure 4** to give **54** as white crystals (0.28 g, 93 %). **δ_H** (400 MHz, $CDCl_3$) 11.09 (1H, s), 8.07 (1H, d, *J* 8.0 Hz), 7.81 – 7.70

(1H, m), 7.62 (1H, d, *J* 8.1 Hz), 7.61 – 7.53 (2H, m), 7.51 – 7.43 (1H, m), 7.38 – 7.30 (2H, m). **ESI-HRMS**: m/z calculated for $C_{14}H_{10}ClN_2NaO_2S$ requires 326.9965, found 326.9959. **Elemental Analysis** Calculated for $C_{14}H_9ClN_2O_2S$ requires, C, 55.18; H, 2.98; N, 9.19; S, 10.52, found, C, 55.21; H, 3.13; N, 9.28; S, 10.03. **IR (neat)**: ν_{max}/cm^{-1}: 3225 (br), 3116 (br), 1708 (s), 1650 (s), 1595 (s). **Melting Point** °C: 204 – 205 (Acetone / H_2O).

Preparation of *N*-benzyl-3-oxobenzo[*d*]isothiazole-2(3*H*)-carboxamide (55)

Benzo[*d*]isothiazol-3(2*H*)-one (**46**) (0.15 g, 0.99 mmol, 1 eq) and benzylisocyanate (0.12 cm^3, 0.99 mmol, 1 eq) were used in anhydrous THF (5 cm^3) following **general procedure 4** to give **55** as white crystals (0.25 g, 92 %). δ_H (400 MHz, DMSO) 9.29 (1H, t, *J* 5.9 Hz), 8.02 (1H, d, *J* 8.2 Hz), 7.95 (1H, d, *J* 7.9 Hz), 7.82 – 7.76 (1H, m), 7.52 – 7.46 (1H, m), 7.39 – 7.33 (4H, m), 7.30 – 7.25 (1H, m), 4.55 (2H, d, *J* 6.0 Hz). δ_C (101 MHz, DMSO) 164.4, 150.9, 140.8, 138.5, 134.0, 128.5, 127.4, 127.2, 126.5, 126.0, 124.7, 122.1, 43.5. **ESI-HRMS**: m/z calculated for $C_{15}H_{12}N_2NaO_2S$ $[M+Na]^+$ requires 307.0512. Found 307.0516. **Elemental Analysis** Calculated for $C_{15}H_{12}N_2O_2S$ requires, C, 63.36; H, 4.25; N, 9.85; S, 11.28, found, C, 63.44; H, 4.31; N, 9.92; S, 11.59. **IR (neat)**: ν_{max}/cm^{-1}: 3252 (br), 3090 (w), 3063 (w), 1704 (s), 1650 (s), 1530 (s), 1445 (s), 1300 (s), 1178 (br, s). **Melting Point** °C: 170 – 171 (Acetone / H_2O).

General Procedure 5: Amide coupling *via* HATU

To desired *N*-Boc-glycine (**56**) (0.50 g, 2.85 mmol, 1 eq) was added HATU (1.63 g, 4.28 mmol, 1.5 eq) DIPEA (1.99 cm^3 11.42 mmol, 4 eq) and DMF (10 cm^3). The resulting solution was stirred for 5 minutes before addition of the 2-adamantylamine hydrochloride (0.64 g, 3.43 mmol, 1.2 eq). The solution was placed under an N_2 atmosphere and stirred overnight. Solvents were removed in *vacuo* and organics taken back into EtOAc (50 cm^3). Organics were washed with 2 M HCl (50 cm^3), saturated sodium bicarbonate solution (50 cm^3), water (50 cm^3), brine (50 cm^3) and dried over $MgSO_4$. Solvents were removed in *vacuo* and purified *via* column chromatography 25 % EtOAc in hexane yields **57a** as a white solid (0.55 g, 62 %).

Generic structure of compounds 57a and 57b

Preparation of tert-butyl (2-(adamantan-2-yl)amino)-2-oxoethyl)carbamate (57a)

N-Boc-glycine (**56**) (0.50 g, 2.85 mmol, 1 eq), HATU (1.63 g, 4.28 mmol, 1.5 eq) DIPEA (1.99 cm^3 11.42 mmol, 4 eq), and 2-adamantylamine hydrochloride (0.64 g, 3.43 mmol, 1.2 eq), were used in DMF (10 cm^3) following **general procedure 5** column chromatography in 25 % EtOAc in hexane yields **57a** as a white solid (0.55 g, 62 %). δ_H (400 MHz, $CDCl_3$) 6.71 (1H, br s), 5.31 (1H, br s), 4.03 (1H, br d, *J* 7.7 Hz), 3.77 (2H, d, *J* 5.9 Hz), 1.91 (2H, s), 1.88 – 1.79 (7H, m), 1.75 (3H, d, *J* 12.8 Hz), 1.63 (2H, d, *J* 13.1 Hz), 1.46 (9H, s). δ_C (101 MHz, $CDCl_3$) 168.8, 156.5, 80.4, 53.4, 45.2, 37.6, 37.2, 32.0, 31.9, 28.4, 27.3, 27.2. **ESI-HRMS**: m/z calculated for $C_{17}H_{28}N_2NaO_3$ $[M+Na]^+$ requires 331.1992. Found 331.1990.

Preparation of tert-butyl (2-adamantan-1-yl)amino)-2-oxoethyl)carbamate (57b)

N-Boc-glycine (**56**) (0.50 g, 2.85 mmol, 1 eq), HATU (1.63 g, 4.28 mmol, 1.5 eq) DIPEA (1.99 cm^3 11.42 mmol, 4 eq), and 1-adamantylamine (0.52 g, 3.43 mmol, 1.2 eq), were used in DMF (10 cm^3) following **general procedure 5** column chromatography in 25 % EtOAc in hex yields **57b** as a white solid (0.67 g, 76 %). δ_H (400 MHz, $CDCl_3$) 5.69 (1H, s), 5.18 (1H, s), 3.66 (2H, d, *J* 5.3 Hz), 2.07 (3H, s), 1.98 (6H, d, *J* 2.5 Hz), 1.67 (6H, s), 1.45 (9H, s). δ_C (101 MHz, $CDCl_3$) 168.3, 156.2, 80.2, 52.1, 45.2, 41.7, 36.4, 29.5, 28.4. **ESI-HRMS**: m/z calculated for $C_{17}H_{28}N_2NaO_3$ $[M+Na]^+$ requires 331.1992. Found 331.1988.

General Procedure 6: Boc deprotection in TFA

To compound **57a** (0.55 g, 1.77 mmol, 1 eq) was added DCM (5 cm^3) the solution was placed under an N_2 atmosphere and cooled to 0 °C before addition of TFA (1.36 cm^3, 17.71 mmol, 10 eq). The solution was allowed to warm to room temperature and left to stir overnight. The reaction was quenched by slow addition of saturated sodium bicarbonate solution (50 cm^3) and the organics extracted into DCM (3 x 50 cm^3). Combined organics were washed with water (50 cm^3), brine (50 cm^3) and dried over $MgSO_4$. Solvents removed in *vacuo* to yield and product purified by trituration with Et_2O, to yield **58a** as a white solid (0.37 g, 79 %).

Generic structure of compounds 58a and 58b

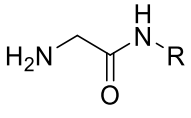

58a R = 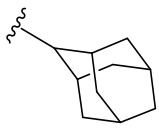

58b R = 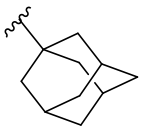

Preparation of *N*-(adamantan-2-yl)-2-aminoacetamide (58a)

Compound **57a** (0.55 g, 1.77 mmol, 1 eq) and TFA (1.36 cm^3, 17.71 mmol, 10 eq), were used in DCM (5 cm^3) following **general procedure 6**. Purified by trituration with Et_2O, to yield **58a** as a white solid (0.37 g, 79 %). δ_H (400 MHz, $CDCl_3$) 7.79 (1H, s), 4.08 (1H, d, *J* 8.6 Hz), 3.36 (2H, s), 1.94 – 1.79 (10H, m), 1.75 (2H, s), 1.65 (2H, d, *J* 12.4), 1.50 (2H, s). δ_C (101 MHz, $CDCl_3$) 171.7, 52.6, 45.1, 37.7, 37.3, 32.3, 32.1, 27.4, 27.3. **CI-HRMS**: m/z calculated for $C_{12}H_{21}N_2O$ $[M+H]^+$ requires 209.1654. Found 209.1658.

Preparation of *N*-(adamantan-1-yl)-2-aminoacetamide (58b)

Compound **57b** (0.67 g, 2.17 mmol, 1 eq) and TFA (1.66 cm^3, 21.72 mmol, 10 eq), were used following **general procedure 6**. Purified by trituration with Et_2O, to yield **58b** as a white solid (0.45 g, 74 %). δ_H (400 MHz, $CDCl_3$) 6.89 (1H, s), 3.22 (2H, s), 2.08 (3H, s), 2.02 (6H, d, *J* 2.6 Hz), 1.74 – 1.65 (6H, m), 1.44 (2H, s). δ_C (101 MHz, $CDCl_3$) 171.7, 51.3, 45.6, 41.8, 36.5, 29.6. **CI-HRMS**: m/z calculated for $C_{12}H_{21}N_2O$ $[M+H]^+$ requires 209.1654. Found 209.1652

Preparation of 2-bromo-*N*-(2,4-dimethylphenyl) acetamide (60)

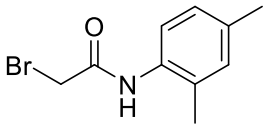

60

2,4 Dimethylaniline (0.10 cm^3, 0.84 mmol, 1 eq), bromoacetyl bromide (**59**) (0.074 cm^3, 0.84 mmol, 1 eq) and triethylamine (0.13 cm^3, 0.93 mmol, 1.1 eq), were used in anhydrous DCM (15 cm^3) following **general procedure 3** to give the product **60** as a white solid (0.14 g, 70 %). This was used in the next step without purification. δ_H (400 MHz, $CDCl_3$) 8.06 (1H, s), 7.65 (1H, d, *J* 8.2 Hz), 7.06 – 7.01 (2H, m), 4.07 (2H, s), 2.30 (3H, s), 2.26 (3H, s). δ_C (101 MHz, $CDCl_3$) 163.4, 135.8, 132.4, 131.4, 129.6, 127.5, 122.9, 30.0, 21.1, 17.7. **CI-HRMS**: m/z calculated for $C_{10}H_{13}{}^{79}BrNO$ $[M+H]^+$ requires 242.0175. Found 242.0174

Preparation of 2-(chlorocarbonyl)phenyl hypochlorothioite (14)

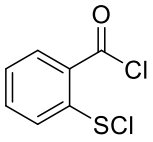

14

To 2,2'-dithiodibenzoic acid (**12**) (3.00 g, 9.80 mmol, 1 eq) was added DCE (20 cm^3) and placed under a N_2 atmosphere. To the reaction mixture was added thionyl chloride (5.00 cm^3, 7 eq) dropwise followed by the addition of DMF (0.20 cm^3). The resulting solution was refluxed at 80 °C for two hours after which the reaction suspension turned into a brown solution. The solution was cooled to 50 °C before addition of sulfuryl chloride (1.00 cm^3, 1.3 eq), the reaction was left to stir at this temperature for one hour, the reaction mixture was cooled and solvents removed in *vacuo* to yield **14** as a bright yellow solid (4.1 g, >99 %). δ_H (400 MHz, $CDCl_3$) 8.33 (1H, s), 7.92 (1H, s), 7.76 (1H, d, *J* 4.5 Hz), 7.42 (1H, d, *J* 4.9 Hz). δ_C (101 MHz, $CDCl_3$) 169.6, 146.1, 135.9, 134.8, 127.5, 125.9, 124.5. **CI-LRMS**: m/z calculated for C_7H_3ClOS $[M\text{-}HCl]^+$ requires 170.0. Found 170.0.

Generic structure of compounds 61 – 66

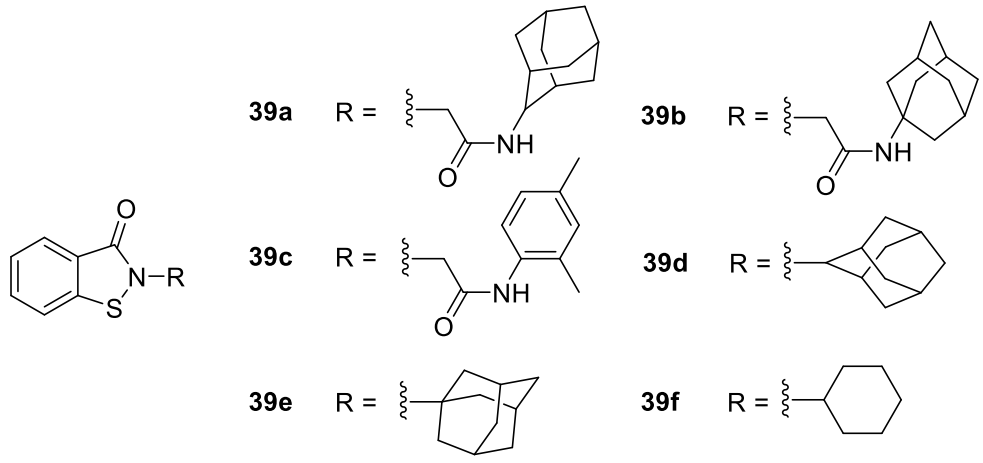

Preparation of *N*-(adamantan-2-yl)-2-(3-oxobenzo[*d*]isothiazol-2(3*H*)-yl)acetamide (61)

Compound **14** (0.14 g, 0.66 mmol, 1 eq), compound **58a** (0.15 g, 0.72 mmol, 1.1 eq) and triethylamine (0.20 cm^3, 1.44 mmol, 2.2 eq), were used in anhydrous DCM (10 cm^3) following **general procedure 3**, the compound was purified by recrystallisation in DCM to yield **61** as a pale yellow solid (0.19 g, 84 %). δ_H (400 MHz, $CDCl_3$) 8.07 (1H, d, *J* 7.9 Hz), 7.69 – 7.62 (1H, m), 7.59 (1H, d, *J* 8.1 Hz), 7.43 (1H, dd, *J* 16.1, 8.5 Hz), 6.86 (1H, d, *J* 6.9 Hz), 4.50 (1H, s), 4.03 (1H, br d, *J* 8.0 Hz), 1.89 (1H, s), 1.83 – 1.75 (3H, m), 1.71 – 1.65 (2H, m), 1.56 (1H, br d, *J* 13.0 Hz). δ_C (101 MHz, $CDCl_3$) 166.3, 166.2, 141.1, 132.6, 127.0, 126.0, 123.5, 120.6, 53.8, 48.5, 37.6, 37.1, 31.9, 31.9, 27.21, 27.15. **ESI-HRMS**:

m/z calculated for $C_{19}H_{22}N_2NaO_2S$ $[M+H]^+$ requires 365.1294. Found 365.1288. **Elemental Analysis** Calculated for $C_{19}H_{12}N_2O_2S$ requires C, 66.64; H, 6.48; N, 8.18; S, 9.36 found C, 66.83; H, 6.57; N, 8.29; S, 9.08. **IR (neat)**: ν_{max}/cm^{-1}: 3335 (m), 3223 (w), 3062 (w), 2907 (m), 2851 (m), 1647 (s), 1609 (s), 1547 (s), 1445 (m), 1343 (m). **Melting Point** °C: 202 – 204 (DCM).

Preparation of *N*-(adamantan-1-yl)-2-(3-oxobenzo[*d*]isothiazol-2(3*H*)-yl)acetamide (62)

Compound **14** (0.14 g, 0.66 mmol, 1 eq), compound **58b** (0.15 g, 0.72 mmol, 1.1 eq) and triethylamine (0.20 cm^3, 1.44 mmol, 2.2 eq), were used in anhydrous DCM (10 cm^3) following **general procedure 3**, the compound was purified by recrystallisation in DCM to yield **62** as a yellow solid (0.18 g, 80 %). δ_H (400 MHz, $CDCl_3$) 8.05 (1H, d, *J* 7.9 Hz), 7.64 (1H, apparent t), 7.57 (1H, d, *J* 8.1), 7.42 (1H, t, *J* 7.5 Hz), 5.96 (1H, s), 4.40 (2H, s), 2.07 – 2.02 (3H, m), 1.97 (6H, d, *J* 2.3 Hz), 1.64 (6H, br s). δ_C (101 MHz, $CDCl_3$) 166.0, 165.9, 141.3, 132.5, 127.0, 125.8, 123.6, 120.6, 52.6, 48.6, 41.5, 36.4, 29.5. **ESI-HRMS**: m/z calculated for $C_{19}H_{22}N_2NaO_2S$ $[M+H]^+$ requires 365.1294. Found 365.1292. **Elemental Analysis** Calculated for $C_{19}H_{12}N_2O_2S$ requires C, 66.64; H, 6.48; N, 8.18; S, 9.36 found C, 66.54; H, 6.45; N, 8.24; S, 9.47. **IR (neat)**: ν_{max}/cm^{-1}: 3290 (m), 3067 (w), 2916 (m), 2882 (s), 2851 (m), 1643 (s), 1593 (m), 1448 (s), 1417 (s), 1342 (m), 1234 (m). **Melting Point** °C: 222 – 213 (DCM).

Preparation of *N*-(2,4-dimethylphenyl)-2-(3-oxobenzo[*d*]isothiazol-2(3*H*)-yl)acetamide (63)

Benzo[*d*]isothiazol-3(2*H*)-one (**46**) (0.07 g, 0.46 mmol, 1 eq) was dissolved in anhydrous DMF (5 cm^3) and the solution cooled to 0 °C. To the solution was added sodium hydride 60 % in mineral oil (0.018 g, 0.46mmol, 1 eq) and the solution was stirred for 30 mins under a N_2 atmosphere. To the reaction mixture was added compound **60** (0.11 g, 0.46 mmol, 1 eq) pre-dissolved in DMF (1 cm^3) and the reaction mixture heated to 80 °C overnight. Solvents were removed in *vacuo* and the residue taken into EtOAc (50 cm^3), organics were washed with 2 M HCl (50 cm^3), saturated $HNaCO_3$ solution (50 cm^3), water (50 cm^3) and brine (50 cm^3). The organics were dried over $MgSO_4$, solvents removed in *vacuo* and the compound was purified by column chromatography (20 % EtOAc in Hexane) followed by recrystallisation in DCM to yield **63** as a white solid (0.021 g, 15 %). δ_H (400 MHz, $CDCl_3$) 8.06 (1H, s), 7.96 (1H, d, *J* 8.0 Hz), 7.84 (1H, d, *J* 8.2 Hz), 7.79 (1H, d, *J* 8.1 Hz), 7.59 (1H,apparent t), 7.46 (1H, apparent t), 7.04 (1H, d, *J* 8.3 Hz), 7.01 (1H, s), 5.22 (2H, s), 2.30 (3H, s), 2.20 (3H, s). δ_C (101 MHz, $CDCl_3$) 165.8, 160.9, 152.6, 135.4, 132.3, 131.3, 129.2, 129.0, 127.6, 125.1, 124.5, 122.9, 122.5, 120.7, 67.9, 21.0, 17.6. **ESI-HRMS**: m/z calculated for $C_{17}H_{16}N_2NaO_2S$ $[M+Na]^+$ requires 335.0825. Found 335.0827. **Elemental Analysis** Calculated for $C_{17}H_{16}N_2O_2S$ requires C, 65.36; H, 5.16; N, 8.97; S, 10.26 found C, 65.31; H, 5.26; N, 8.69; S, 10.17. **IR (neat)**: ν_{max}/cm^{-1}: 3241 (m), 3020 (w), 2920 (w), 1669 (s), 1534 (m), 1511 (m), 1360 (s). **Melting Point** °C: 177 – 178 (DCM).

Preparation of 2-(adamantan-2-yl)benzo[*d*]isothiazol-3(2*H*)-one (64)

Compound **14** (0.13 g, 0.60 mmol, 1 eq), 2-adamantylamine hydrochloride (0.12 g, 0.66 mmol, 1.1 eq) and triethylamine (0.25 cm^3, 1.80 mmol, 3 eq), were used in anhydrous DCM (10 cm^3) following **general procedure 3**, the compound was purified by recrystallisation in DCM to yield **64** as a pale yellow solid (0.071 g, 41 %). **δ_H** (400 MHz, $CDCl_3$) 8.02 (1H, d, *J* 7.9 Hz), 7.60 – 7.50 (2H, m), 7.36 (1H, apparent t), 4.73 (1H, s), 2.39 (2H, s), 2.27 (2H, d, *J* 13.2 Hz), 2.04 – 1.88 (6H, m), 1.82 – 1.69 (4H, m). **δ_C** (101 MHz, $CDCl_3$) 166.1, 140.4, 131.5, 126.4, 125.3, 124.8, 119.9, 61.0, 38.3, 37.7, 32.5, 32.2, 27.5, 27.1. **CI-HRMS**: m/z calculated for $C_{17}H_{20}NOS$ $[M+H]^+$ requires 286.1260. Found 286.1264. **Elemental Analysis** Calculated for $C_{17}H_{19}NOS$ requires C, 71.54; H, 6.70; N, 4.95; S, 10.71 found C, 71.54; H, 6.71; N, 4.95; S, 10.90. **IR (neat)**: ν_{max}/cm^{-1}: 2905 (m), 2848 (m), 1630 (s), 1592 (m), 1446 (s), 1296 (m). **Melting Point** °C: 148 – 150 (DCM).

Preparation of 2-(adamantan-2-yl)benzo[*d*]isothiazol-3(2*H*)-one (65)

Compound **14** (0.13 g, 0.60 mmol, 1 eq), 1-adamantylamine (0.10 g, 0.66 mmol, 1.1 eq) and triethylamine (0.17 cm^3, 1.20 mmol, 2 eq), were used in anhydrous DCM (10 cm^3) following **general procedure 3**, the compound was purified by recrystallisation in DCM to yield **65** as a white solid (0.14 g, 80 %). **δ_H** (400 MHz, $CDCl_3$) 7.95 (1H, d, *J* 7.9 Hz), 7.58 – 7.53 (1H, m), 7.50 (1H, d, *J* 8.0 Hz), 7.38 – 7.33 (1H, m), 2.45 (6H, d, *J* 2.6 Hz), 2.20 (3H, s), 1.84 – 1.70 (6H, m). **δ_C** (101 MHz, $CDCl_3$) 165.5, 140.0, 131.3, 127.3, 126.2, 125.2, 119.9, 59.9, 40.7, 36.3, 30.1. **CI-HRMS**: m/z calculated for $C_{17}H_{20}NOS$ $[M+H]^+$ requires 286.1260. Found 286.1264. **Elemental Analysis** Calculated for $C_{17}H_{19}NOS$ requires C, 71.54; H, 6.70; N, 4.95; S, 10.71 found C, 71.36; H, 6.80; N, 4.90; S, 11.18. **IR (neat)**: ν_{max}/cm^{-1}: 2898 (m), 2849 (m), 1630 (s), 1446 (m), 1300 (m). **Melting Point** °C: 178 – 180 (DCM).

Preparation of 2-cyclohexylbenzo[*d*]isothiazol-3(2*H*)-one (66)

Compound **14** (0.13 g, 0.60 mmol, 1 eq), cyclohexylamine (0.07 cm^3, 0.66 mmol, 1.1 eq) and triethylamine (0.17 cm^3, 1.20 mmol, 2 eq) was used following **general procedure 3**, the compound was purified by recrystallisation in DCM to yield **66** as a yellow solid (0.10 g, 74 %). **δ_H** (400 MHz, $CDCl_3$) 8.03 (1H, d, *J* 7.9 Hz), 7.61 – 7.53 (2H, m), 7.41 – 7.35 (1H, m), 4.60 (1H, tt, *J* 11.5, 3.9 Hz), 2.04 (2H, apparent d, *J* 11.7 Hz), 1.87 (2H, apparent d, *J* 13.0 Hz), 1.78 – 1.68 (1H, m), 1.62 – 1.40 (4H, m), 1.26 – 1.14 (1H, m). **δ_C** (101 MHz, $CDCl_3$) 164.9, 140.4, 131.5, 126.6, 125.6, 125.4, 120.5, 53.3, 33.0, 25.7, 25.4. **CI-HRMS**: m/z calculated for $C_{13}H_{16}NOS$ $[M+H]^+$ requires 234.0947. Found 234.0952. **Elemental Analysis** Calculated for $C_{13}H_{16}NOS$ requires C, 69.92; H, 6.48; N, 6.00; S, 13.74 found C, 66.56; H, 6.45; N, 6.03; S, 13.30. **IR (neat)**: ν_{max}/cm^{-1}: 2927 (m), 2854 (m), 1639 (s), 1446 (m), 1332 (m). **Melting Point** °C: 78 – 81 °C (DCM).

General Procedure 7: Preparation of amine coupled aryl side chains

To (4-(bromomethyl)phenyl)boronic acid (**68**) (1.01 g, 4.71 mmol, 1 eq) was added THF (10 cm^3), DIPEA (0.98 cm^3, 5.65 mmol, 1.2 eq) and morpholine (0.62 cm^3, 7.06 mmol, 1.5 eq). The reaction was stirred at room temperature under a N_2 atmosphere overnight. The reaction was diluted with brine (50 cm^3) and extracted into ethyl acetate (3 x 50 cm^3), dried with $MgSO_4$ and solvents removed in *vacuo* to yield the product **69a** as an off white solid (0.91 g, 87 %). Which was used without further purification.

Generic structure of compounds 69a –c following general procedure 7

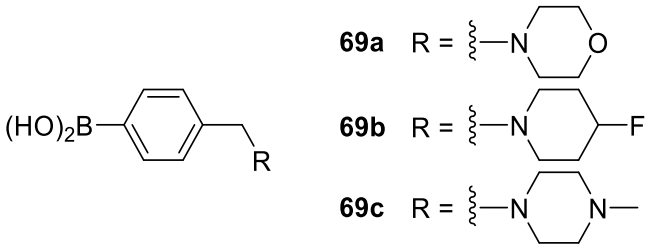

Preparation of (4-(morpholinomethyl)phenyl)boronic acid (69a)

(4-(bromomethyl)phenyl)boronic acid (**68**) (1.01 g, 4.71 mmol, 1 eq), morpholine (0.62 cm^3, 7.06 mmol, 1.5 eq), and DIPEA (0.98 cm^3, 5.65 mmol, 1.2 eq), were used in THF (10 cm^3) following **general procedure 7** to give **69a** as an off white solid (0.91 g, 87 %). δ_H (400 MHz, $CDCl_3$) 8.07 – 7.68 (2H, m), 7.29 (2H, d, *J* 6.9 Hz), 3.77 – 3.65 (4H, m), 3.53 (2H, s), 2.46 (4H, s). δ_C (101 MHz, $CDCl_3$) 134.1, 128.6, 67.0, 63.7, 53.7. **CI-HRMS**: m/z calculated for $C_{11}H_{15}NO$ $[M-(BO_2H)+H]^+$ requires 178.1226. Found 178.1232.

Preparation of (4-((4-fluoropiperidin-1-yl)methyl)phenyl)boronic acid (69b)

(4-(bromomethyl)phenyl)boronic acid (**68**) (0.52 g, 2.41 mmol, 1 eq) 4-fluoropiperidine hydrochloride (0.36 g, 2.53 mmol, 1.05 eq), and DIPEA (0.92 cm^3, 5.30 mmol, 2.2 eq), were used in THF (5 cm^3) following **general procedure 7** to give **69b** as a white foam (0.54 g, 95 %). δ_H (400 MHz, DMSO) 8.05 (2H, s), 7.71 (2H, d, *J* 7.8 Hz), 7.24 (2H, d, *J* 7.8 Hz), 3.44 (2H, s), 3.38 – 3.12 (2H, m), 2.45 (1H, s), 2.25 (1H, br s), 1.90 – 1.60 (2H, m). δ_C (101 MHz, DMSO) 140.4, 134.3, 128.3, 88.8 (d, *J* 168.6 Hz), 62.2, 49.3, 31.3 (d, *J* 19.0 Hz). **CI-HRMS**: m/z calculated for $C_{12}H_{16}FN$ $[M-(BO_2H)+H]^+$ requires 194.1340. Found 194.1334, and 176.1436 $[(M-BO_2H-F)+H]^+$.

Preparation of (4-((4-methylpiperazin-1-yl)methyl)phenyl)boronic acid (69c)

(4-(bromomethyl)phenyl)boronic acid (**68**) (1.01 g, 4.71 mmol, 1 eq), *N*-methylpiperazine (0.63 cm^3, 5.65 mmol, 1.2 eq), and DIPEA (0.98 cm^3, 5.65 mmol, 1.2 eq), were used in THF (10 cm^3) following **general procedure 7** to give **69c** as a white solid (0.51 g, 46 %). δ_H (400 MHz, MeOD) 7.60 (2H, d, *J* 6.9 Hz), 7.30 (2H, d, *J* 7.8 Hz), 3.57 (1H, s), 2.57 (8H, s), 2.34 (3H, s). δ_C (101 MHz, DMSO) 140.5, 140.2, 134.1, 133.9, 128.0, 127.9, 62.2, 54.7, 52.6, 45.7. **CI-HRMS**: m/z calculated for $C_{12}H_{19}N_2$ [M-(BO_2H)+H]$^+$ requires 191.1543. Found 191.1547.

General Procedure 8: Suzuki couplings

To a mixture of THF (5 cm^3) and water (5 cm^3) was added 3-bromoaniline (2.18 cm^3, 20.01 mmol, 3 eq) and potassium carbonate (2.78 g, 20.01 mmol, 3 eq) the flask was evacuated and backfilled with N_2. (4-(Trifluoromethyl)phenyl)boronic acid (1.27 g, 6.67 mmol, 1 eq) was added, the flask evacuated and backfilled with N_2. Finally palladium tetrakis (0.19 g, 0.17 mmol, 0.025 eq) was added and the reaction vessel was evacuated and backfilled with N_2 before refluxing at 80 °C overnight. The reaction mixture was diluted with brine (50 cm^3) and product extracted into ethyl acetate (3 x 50 cm^3). Organics were dried with $MgSO_4$ and product purified by column chromatography (20 % EtOAc in Hex) to give **71a** as a white solid (1.58 g, 75 %).

Generic structure of compounds 71a – e following general procedure 8

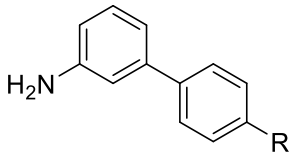

71a R = CF_3

71b R = OCF_3

71c R =

71d R =

71e R =

Preparation of 4'-(trifluoromethyl)-[1,1'-biphenyl]-3-amine (71a)

(4-(Trifluoromethyl)phenyl)boronic acid (1.27 g, 6.67 mmol, 1 eq), 3-bromoaniline (**70**) (2.18 cm^3, 20.01 mmol, 3 eq), potassium carbonate (2.78 g, 20.01 mmol, 3 eq), and palladium tetrakis (0.19 g, 0.17 mmol, 0.025 eq), were used in THF (5 cm^3) and water (5 cm^3) following **general procedure 8**, purified by column chromatography (20 % EtOAc in Hexane) to give **71a** as a white solid (1.58 g, 75 %). δ_H (400 MHz, $CDCl_3$) 7.69 – 7.62 (4H, m), 7.25 (1H, apparent t), 6.98 (1H, d, *J* 7.6 Hz), 6.89 (1H, s), 6.72 (1H, dd, *J* 7.9, 1.8 Hz), 3.76 (2H, br s). δ_C (101 MHz, $CDCl_3$) 146.9, 144.9, 141.0, 129.9, 129.3 (q, *J*

32.4 Hz), 127.4, 125.6 (q, *J* 3.8 Hz), 124.4 (q, *J* 271.8 Hz), 117.7, 114.9, 113.9. **CI-HRMS**: m/z calculated for $C_{13}H_{11}F_3N$ $[M+H]^+$ requires 238.0838. Found 238.0845.

Preparation of 4'-(trifluoromethoxy)-[1,1'-biphenyl]-3-amine (71b)

(4-(Trifluoromethoxy)phenyl)boronic acid (0.36 g, 1.74 mmol, 1.2 eq), 3-bromoaniline (**70**) (0.16 cm^3, 1.45 mmol, 1 eq), potassium carbonate (0.60 g, 4.35 mmol, 3 eq), and palladium tetrakis (0.043 g, 0.036 mmol, 0.025 eq) were used in THF (5 cm^3) and water (5 cm^3) following **general procedure 8**, purified by column chromatography (20 % EtOAc in Hex) to give **71b** as a brown oil (0.30 g, 82 %). δ_H (400 MHz, $CDCl_3$) 7.58 – 7.54 (2H, m), 7.28 – 7.19 (3H, m), 6.94 (1H, ddd, *J* 7.6, 1.5, 0.9 Hz), 6.86 (1H, apparent t), 6.69 (1H, ddd, *J* 7.9, 2.3, 0.8 Hz), 3.75 (2H, br s). δ_C (101 MHz, $CDCl_3$) 148.7 (q, *J* 1.6 Hz), 147.0, 141.2, 140.3, 130.0, 128.5, 121.2, 120.7 (q, *J* 257.1 Hz), 117.7, 114.6, 113.9. δ_F (375 MHz, $CDCl_3$) -57.8 (3F, s). **CI-HRMS**: m/z calculated for $C_{13}H_{11}F_3NO$ $[M+H]^+$ requires 254.0787. Found 254.0789.

Preparation of 4'-(morpholinomethyl)-[1,1'-biphenyl]-3-amine (71c)

Compound **69a** (0.91 g, 4.09 mmol, 1 eq), 3-bromoaniline (**70**) (1.32 cm^3, 12.27 mmol, 3 eq), potassium carbonate (0.57 g, 12.27 mmol, 3 eq), and palladium tetrakis (0.12 g, 0.10 mmol, 0.025 eq), were used following **general procedure 8** purified by column chromatography (40 % EtOAc in Hex) to give **71c** as a yellow to orange oil (0.98 g, 90 %). δ_H (400 MHz, $CDCl_3$) 7.52 (2H, d, *J* 8.1 Hz), 7.37 (2H, d, *J* 8.1 Hz), 7.22 (1H, apparent t, *J* 7.8 HZ), 6.99 (1H, d, *J* 7.7 Hz), 6.90 (1H, apparent t), 6.67 (1H, dd, *J* 7.9, 1.6 Hz), 3.76 – 3.70 (4H, apparent t), 3.53 (2H, s), 2.48 (4H, br s). δ_C (101 MHz, $CDCl_3$) 146.8, 142.2, 140.4, 136.8, 129.8, 129.7, 127.1, 117.7, 114.2, 113.9, 67.1, 63.3, 53.8. **ESI-HRMS**: m/z calculated for $C_{17}H_{21}N_2O$ $[M+H]^+$ requires 269.1648. Found 269.1647.

Preparation of 4'-((4-fluoropiperidin-1-yl)methyl)-[1,1'-biphenyl]-3-amine (71d)

Compound **69b** (0.54 g, 2.29 mmol, 1 eq), 3-bromoaniline (**70**) (0.75 cm^3, 6.87 mmol, 3 eq), potassium carbonate (0.95 g, 6.87 mmol, 3 eq), and palladium tetrakis (0.066 g, 0.057 mmol, 0.025 eq) were used in THF (5 cm^3) and water (5 cm^3) following **general procedure 8** purified by column chromatography (40 % EtOAc in Hex) to give **71d** as a clear yellow oil (0.32 g, 50 %). δ_H (400 MHz, $CDCl_3$) 7.52 (2H, d, *J* 8.1 Hz), 7.36 (2H, d, *J* 8.1 Hz), 7.22 (1H, t, *J* 7.8 Hz), 6.99 (1H, d, *J* 7.7 Hz), 6.91 (1H, apparent t), 6.67 (1H, dd, *J* 7.9, 2.2 Hz), 4.79 – 4.59 (1H, m), 3.54 (2H, s), 2.68 – 2.55 (2H, m), 2.46 – 2.36 (2H, m), 2.00 – 1.81 (4H, m). δ_C (101 MHz, $CDCl_3$) 146.9, 142.3, 140.3, 137.5, 129.8, 129.5, 127.1, 117.7, 114.2, 113.9, 88.9 (d, *J* 171.6 Hz), 62.8, 49.7 (d, *J* 5.8 Hz), 31.7 (d, *J* 19.4 Hz). **ESI-HRMS**: m/z calculated for $C_{18}H_{22}FN_2$ $[M+H]^+$ requires 285.1762. Found 285.1772.

Preparation of 4'-((4-methylpiperazin-1-yl)methyl)-[1,1'-biphenyl]-3-amine (71e)

Compound **69c** (0.89 g, 3.80 mmol, 1 eq) 3-bromoaniline (**70**) (1.24 cm^3, 11.41 mmol, 3 eq), potassium carbonate (1.58 g, 11.41 mmol, 3 eq), and palladium tetrakis (0.11 g, 0.095 mmol, 0.025 eq) were used in THF (5 cm^3) and water (5 cm^3) following **general procedure 8** purified by column chromatography (5 % MeOH in EtOAc) to give **71e** as a clear orange oil (1.01 g, 94 %). δ_H (400 MHz, $CDCl_3$) 7.50 (2H, d, *J* 8.1 Hz), 7.36 (2H, d, *J* 8.1 Hz), 7.21 (1H, apparent t, *J* 7.8 Hz), 6.98 (1H, d, *J* 7.7 Hz), 6.90 (1H, apparent t), 6.67 (1H, dd, *J* 7.8, 1.8 Hz), 3.73 (2H, br s), 3.54 (2H, s), 2.48 (8H, s, *J* 11.3 Hz), 2.29 (3H, s). δ_C (101 MHz, $CDCl_3$) 146.8, 142.3, 140.3, 137.3, 129.8, 129.6, 127.0, 117.7, 114.1, 113.9, 62.9, 55.3, 53.2, 46.2. **ESI-HRMS**: m/z calculated for $C_{18}H_{24}N_3$ $[M+H]^+$ requires 282.1965. Found 282.1969.

Preparation of 4-(3-nitrobenzyl)morpholine (73)

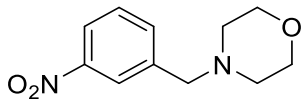

73

1-(bromomethyl)-3-nitrobenzene (**72**) (2.00 g, 9.27 mmol, 1 eq), morpholine (0.81 cm^3, 9.27 mmol, 1 eq), and DIPEA (1.94 cm^3, 11.12 mmol, 1.2 eq) were used in THF (20 cm^3) following **general procedure 7** to give **73** as a white solid (2.04 g, 99 %). δ_H (400 MHz, $CDCl_3$) 8.22 (1H, s), 8.12 (1H, d, *J* 8.2 Hz), 7.68 (1H, d, *J* 7.6 Hz), 7.49 (1H, apparent t, *J* 7.9 Hz), 3.76 – 3.69 (4H, m apparent t), 2.50 – 2.42 (4H, apparent t). δ_C (101 MHz, $CDCl_3$) 148.5, 140.4, 135.2, 129.4, 123.9, 122.5, 67.0, 62.5, 53.7. **CI-HRMS**: m/z calculated for $C_{11}H_{15}N_2O_3$ $[M+H]^+$ requires 223.1077. Found 223.1086.

General procedure 9: Reduction of nitro group *via* Fe AcOH

To compound **73** (2.04 g, 9.16 mmol, 1 eq) was added ethanol (20 cm^3), acetic acid (20 cm^3) and iron powder (2.56 g, 45.79 mmol, 5 eq). The reaction was refluxed overnight under an N_2 atmosphere. Reaction mixture was filtered through celite, and washed with EtOAc (50 cm^3), solvents were removed in *vacuo*. Water (100 cm^3) was added and the product extracted into EtOAc (3 x 100 cm^3), organics washed with saturated $HNaCO_3$ (100 cm^3), water (100 cm^3), brine (100 cm^3) and dried over $MgSO_4$. Solvents removed in *vacuo* to give the product as a brown oil (1.68 g, 96 %).

Preparation of 3-(morpholinomethyl)aniline (74)

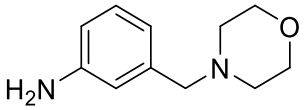

74

Compound **73** (2.04 g, 9.16 mmol, 1 eq) and iron powder (2.56 g, 45.79 mmol, 5 eq) were used in ethanol (20 cm^3) and acetic acid (20 cm^3) following **general procedure 9** to give **74** as a brown oil (1.68 g, 96 %). δ_H (400 MHz, $CDCl_3$) 7.09 (1H, apparent t), 6.72 – 6.68 (2H, m), 6.60 – 6.56 (1H, m), 3.77 – 3.59 (6H, m), 3.40 (2H, s), 2.48 – 2.38 (4H, m). δ_C (101 MHz, $CDCl_3$) 146.5, 139.1, 129.2, 119.7, 115.9, 114.1, 67.1, 63.6, 53.8. **CI-HRMS**: m/z calculated for $C_{11}H_{17}N_2O$ $[M+H]^+$ requires 193.1335. Found 193.1340.

General Procedure 10: Amide couplings *via* oxalyl chloride

To desired 2-iodobenzoic acid (**75**) (1.50 g, 6.04 mmol, 1.2 eq) was added anhydrous DCM (10 cm^3) under a N_2 atmosphere. The resulting solution was then cooled to 0 °C before the addition of oxalyl chloride (1.06 cm^3, 12.58 mmol, 2.5 eq) and a catalytic amount of DMF (1 drop). The resulting solution was stirred for 3 hours, after this time solvents were removed in *vacuo* to yield the acyl chloride, this is then used immediately *via* re-dissolving in anhydrous DCM (10 cm^3) under a N_2 atmosphere before addition of compound **71a** (1.19 g, 5.03 mmol, 1 eq), and triethylamine (0.84 cm^3, 6.04 mmol, 1.2 eq). The solution is then left to stir overnight. The organics were washed with 2 M HCl (50 cm^3), a saturated solution of $HNaCO_3$ (50 cm^3), water (50 cm^3) and brine (50 cm^3) and dried over $MgSO_4$. Solvents were removed *in vacuo* to yield **76a** as a white solid (1.38 g, 49 %). Compound used in the next step without further purification.

Generic structure of compounds 76a – f following general procedure 10

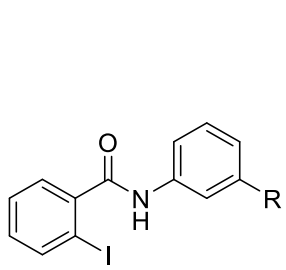

76a R = 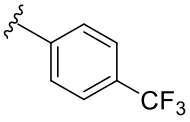

76b R = 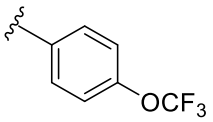

76c R = 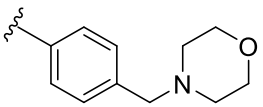

76d R = 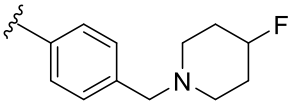

76e R = 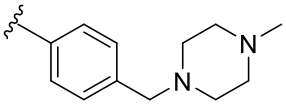

76f R = 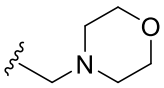

Preparation of 2-iodo-*N*-(4'-(trifluoromethyl)-[1,1'-biphenyl]-3-yl)benzamide (76a)

Compound **71a** (1.19 g, 5.03 mmol, 1 eq), 2-iodobenzoic acid (**75**) (1.50 g, 6.04 mmol, 1.2 eq), oxalyl chloride (1.06 cm^3, 12.58 mmol, 2.5 eq), triethylamine (0.84 cm^3, 6.04 mmol, 1.2 eq), and catalytic DMF (1 drop) were used in anhydrous DCM (10 cm^3) following **general procedure 10** to give **76a** as a white solid (1.38 g, 49 %). Compound used in the next step without further purification. δ_H (400 MHz, $CDCl_3$) 7.97 (1H, s), 7.92 (1H, d, *J* 7.9 Hz), 7.75 – 7.67 (4H, m), 7.65 – 7.57 (2H, m), 7.56 – 7.52 (1H, m), 7.50 – 7.38 (3H, m), 7.16 (1H, apparent td). δ_C (101 MHz, $CDCl_3$) 167.5, 144.2, 142.1, 141.0, 140.3, 138.3, 132.3 – 131.9 (m), 129.9, 129.8 (q, *J* 33.0 Hz), 128.7, 128.6, 127.7, 125.9 (q, *J* 3.8 Hz), 124.4 (q, *J* 272.1 Hz), 123.9, 119.8, 119.1, 92.5. δ_F (375 MHz, $CDCl_3$) -62.4 (3F, s). **ESI-HRMS**: m/z calculated for $C_{20}H_{13}F_3INNaO$ $[M+Na]^+$ requires 489.9886. Found 489.9890.

Preparation of 2-iodo-*N*-(4'-(trifluoromethoxy)-[1,1'-biphenyl]-3-yl)benzamide (76b)

Compound **71b** (0.27 g, 1.07 mmol, 1.2 eq), 2-iodobenzoic acid (**75**) (0.22 g, 0.89 mmol, 1 eq), oxalyl chloride 2 M solution in DCM (0.89 cm^3, 1.78 mmol, 2 eq), triethylamine (0.15 cm^3, 1.07 mmol, 1.2 eq), and catalytic DMF (1 drop) were used in anhydrous DCM (5 cm^3) following **general procedure 10** to give **76b** as an off white to yellow powder (0.15 g, 35 %). Used in the next step without further purification. δ_H (400 MHz, $CDCl_3$) 7.95 – 7.88 (2H, m), 7.66 – 7.57 (4H, m), 7.54 (1H, dd, *J* 7.6, 1.3 Hz), 7.48 – 7.41 (2H, m), 7.37 (1H, d, *J* 7.7 Hz), 7.28 (2H, d, *J* 8.2 Hz), 7.16 (1H, apparent td). δ_C (101 MHz, $CDCl_3$) 167.4, 149.0, 142.1, 141.1, 140.3, 139.5, 138.2, 131.8, 129.8, 128.8, 128.6, 123.8, 121.4, 119.4, 119.0, 92.5. **ESI-HRMS**: m/z calculated for $C_{20}H_{13}F_3INNaO_2$ $[M+Na]^+$ requires 505.9835. Found 505.9847.

Preparation of 2-iodo-*N*-(4'-(morpholinomethyl)-[1,1'-biphenyl]-3-yl)benzamide (76c)

Compound **71c** (1.07 g, 3.98 mmol, 1 eq), 2-iodobenzoic acid (1.19 g, 4.78 mmol, 1.2 eq), oxalyl chloride (0.67 cm^3, 7.96 mmol, 2 eq), triethylamine (0.67 cm^3, 4.48 mmol, 1.2 eq), and catalytic DMF (1 drop) were used in anhydrous DCM (10 cm^3) following **general procedure 10**, note HCl not used in workup. Purified by column chromatography (50 % EtOAc in Hex) to give **76c** as a white solid (1.15 g, 58 %). δ_H (400 MHz, $CDCl_3$) 7.94 – 7.88 (2H, m), 7.66 – 7.59 (2H, m), 7.59 – 7.52 (3H, m), 7.47 – 7.38 (5H, m), 7.15 (1H, apparent td), 3.75 – 3.69 (4H, apparent t), 3.54 (2H, s), 2.51 – 2.44 (4H, apparent t). δ_C (101 MHz, $CDCl_3$) 167.4, 142.3, 142.2, 140.2, 139.6, 138.1, 137.4, 131.7, 129.8, 129.7, 128.7, 128.5, 127.3, 123.7, 119.0, 118.9, 92.5, 67.2, 63.2, 53.8. **ESI-HRMS**: m/z calculated for $C_{24}H_{27}IN_2O_2$ $[M+H]^+$ requires 499.0877. Found 499.0877.

Preparation of *N*-(4'-((4-fluoropiperidin-1-yl)methyl)-[1,1'-biphenyl]-3-yl)-2-iodobenzamide (76d)

Compound **71d** (0.32 g, 1.12 mmol, 1 eq), 2-iodobenzoic acid (0.29 g, 1.18 mmol, 1.05 eq), oxalyl chloride (0.19 cm^3, 2.24 mmol, 2 eq), triethylamine (0.16 cm^3, 1.18 mmol, 1.05 eq), and catalytic DMF (1 drop) were used in anhydrous DCM (5 cm^3) following **general procedure 10**, note HCl not used in workup. Purified by column chromatography (100 % EtOAc) to give **76d** as a white solid (0.31 g, 53 %). δ_H (400 MHz, $CDCl_3$) 7.95 – 7.86 (2H, m), 7.69 – 7.59 (2H, m), 7.59 – 7.49 (3H, m), 7.47 – 7.33 (5H, m), 7.14 (1H, t, *J* 7.4 Hz), 4.79 – 4.55 (1H, m), 3.55 (2H, s), 2.69 – 2.54 (2H, m), 2.50 – 2.32 (2H, m), 2.01 – 1.74 (4H, m). δ_C (101 MHz, $CDCl_3$) 167.4, 142.2, 142.2, 140.2, 139.5, 138.1, 137.9, 131.7, 129.7, 128.7, 128.5, 127.2, 123.7, 119.0, 118.9, 92.5, 88.8 (d, *J* 170.1 Hz), 62.7, 49.6 (d, *J* 6.0 Hz), 31.6 (d, *J* 19.4 Hz). **ESI-HRMS**: m/z calculated for $C_{25}H_{25}FIN_2O$ $[M+H]^+$ requires 515.0990. Found 515.0978.

Preparation of 2-iodo-*N*-(4'-((4-methylpiperazin-1-yl)methyl)-[1,1'-biphenyl]-3-yl)benzamide (76e)

Compound **71e** (0.74 g, 2.64 mmol, 1 eq), 2-iodobenzoic acid (0.72 g, 2.90 mmol, 1.1 eq), oxalyl chloride (0.45 cm^3, 5.27 mmol, 2 eq), triethylamine (0.40 cm^3, 2.90 mmol, 1.2 eq), and catalytic DMF (1 drop) were used in anhydrous DCM (5 cm^3) following **general procedure 10**, note HCl not used in workup. Purified by column chromatography (10 % MeOH in EtOAc and a few drops of NEt_3) to give **76e** as a sticky off white to light yellow foam (1.00 g, 74 %). δ_H (400 MHz, $CDCl_3$) 7.92 (1H, d, *J* 7.9 Hz), 7.87 (1H, s), 7.66 – 7.60 (2H, m), 7.58 – 7.53 (3H, m), 7.48 – 7.42 (2H, m), 7.42 – 7.37 (3H, m), 7.16 (1H,apparent td), 3.55 (2H, s), 2.51 (8H, s), 2.31 (3H, s). δ_C (101 MHz, $CDCl_3$) 167.4, 142.2, 142.2, 140.2, 139.5, 138.1, 137.7, 131.7, 129.8, 129.7, 128.7, 128.5, 127.2, 123.8, 119.0, 118.9, 92.5, 62.8, 55.2, 53.1, 46.1. **ESI-HRMS**: m/z calculated for $C_{25}H_{26}IN_3O$ $[M+H]^+$ requires 512.1193. Found 512.1197.

Preparation of 2-iodo-*N*-(3-(morpholinomethyl)phenyl)benzamide (76f)

Compound **74** (1.01 g, 5.23 mmol, 1 eq), 2-iodobenzoic acid (1.56 g, 6.27 mmol, 1.2 eq), oxalyl chloride (0.88 cm^3, 10.45 mmol, 2 eq), triethylamine (0.88 cm^3, 5.23 mmol, 1.2 eq), and catalytic DMF (1 drop) were used in anhydrous DCM (10 cm^3) following **general procedure 10**, note HCl not used in workup. To give **76f** as a white to yellow semi solid (1.71 g, 78 %). Compound used without further purification. δ_H (400 MHz, $CDCl_3$) 7.90 (1H, d, *J* 7.8 Hz), 7.65 (1 H, s), 7.59 – 7.55 (2H, m), 7.50 (1H, dd, *J* 7.6, 1.5 Hz), 7.44 – 7.39 (1H, m), 7.32 (1H, apparent t), 7.17 – 7.11 (2H, m), 3.72 – 3.66 (4H, m), 3.50 (2H, s), 2.50 – 2.40 (4H, m). δ_C (101 MHz, $CDCl_3$) 167.4, 142.2, 140.2, 139.2, 137.7, 131.6, 129.1, 128.6, 128.5, 125.7, 120.7, 119.1, 92.5, 67.1, 63.3, 53.7. **ESI-HRMS**: m/z calculated for $C_{18}H_{20}IN_2O_2$ $[M+H]^+$ requires 423.0564. Found 423.0568.

General Procedure 11: Cyclisation to 1,2 benzoisoselenazoles

To a stirred solution of DMF (5 cm^3) was added copper(I) iodide (0.28 g, 1.46 mmol, 1 eq) and 1, 10-phenanthroline (0.26 g, 1.46 mmol, 1 eq) and was stirred for five minutes. Selenium powder (0.14 g, 1.76 mmol, 1.2 eq), potassium carbonate (0.32 g, 2.34 mmol, 1.6 eq) and compound **76a** (0.68 g, 1.46 mmol, 1 eq), were added sequentially. The reaction mixture was heated under reflux at 120 °C for 20 hours under a N_2 atmosphere. The mixture was poured into brine (50 cm^3) and stirred for three hours. The product was filtered under vacuum and extracted into ethyl acetate (3 x 50 cm^3) washed with brine (50 cm^3) and dried with $MgSO_4$. Solvents removed *in vacuo* and the product purified by column chromatography (20 % EtOAc in Hex). Solvents were removed *in vacuo* and the residue was recrystallised from ethyl acetate to give **77** as white crystals (0.042 g, 7 %).

Generic structure of compounds 77 – 82

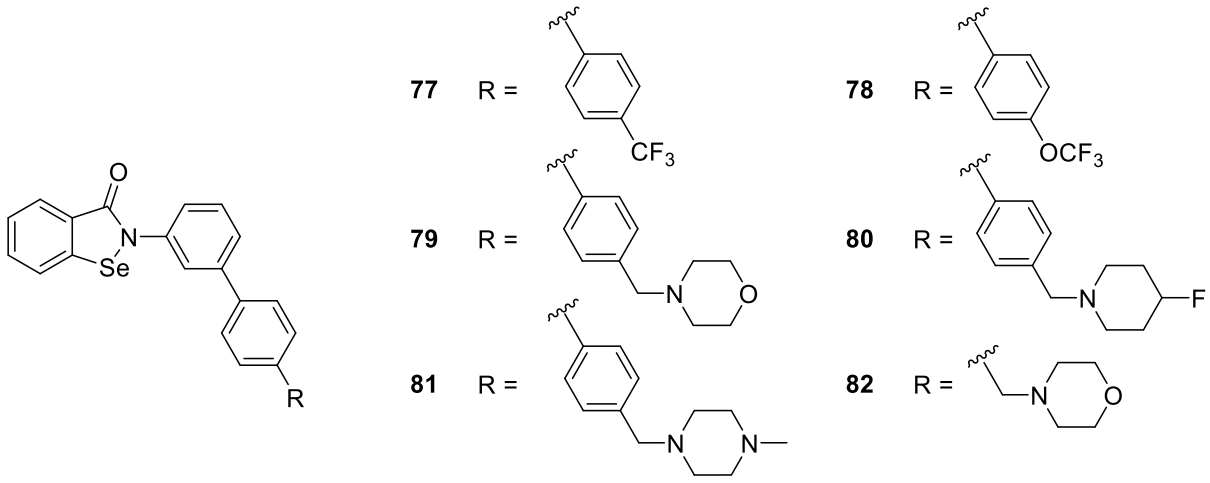

Preparation of 2-(4'-(trifluoromethyl)-[1,1'-biphenyl]-3-yl)benzo[*d*][1,2]selenazol-3(2*H*)-one (77)

Compound **76a** (0.68 g, 1.46 mmol, 1 eq), CuI (0.28 g, 1.46 mmol, 1 eq), 1,10-phenanthroline (0.26 g, 1.46 mmol, 1 eq), potassium carbonate (0.32 g, 2.34 mmol, 1.6 eq) and selenium powder (0.14 g, 1.76 mmol, 1.2 eq), were used in DMF (5 cm^3) following **general procedure 11**, product purified by column chromatography (20 % EtOAc in hexane). Solvents were removed *in vacuo* and the residue was recrystallised from ethyl acetate to give **77** as white crystals (0.042 g, 7 %). δ_H (400 MHz, $CDCl_3$) 8.14 (1H, d, *J* 7.8 Hz), 7.94 (1H, s), 7.76 – 7.65 (6H, m), 7.62 (1H, br d, *J* 7.3 Hz), 7.58 – 7.45 (3H, m). δ_C (101 MHz, $CDCl_3$) 166.0, 143.9, 141.2, 140.0, 137.7, 132.9, 130.1, 129.8, 129.6, 127.8, 127.6, 126.9, 126.0 (q, *J* 3.7 Hz), 125.7, 125.1, 124.5, 123.9. δ_F (375 MHz, $CDCl_3$) -62.5 (3F, s). **ESI-HRMS**: m/z calculated for $C_{20}H_{12}F_3NNaOSe$ $[M+Na]^+$ requires 441.9928. Found 441.9929. **Elemental Analysis** Calculated for $C_{20}H_{12}F_3NOSe$ requires C, 57.43; H, 2.89; N, 3.35, found C, 57.46; H, 2.83; N, 3.28. **IR**

(neat): ν_{max}/cm^{-1}: 3088 (w), 3052 (w), 1599 (s), 1563 (s), 1485 (m), 1326 (s), 1305 (s), 1125 (s), 1108 (s). **Melting Point** °C: 223 – 224 °C (EtOAc).

Preparation of 2-(4'-(trifluoromethoxy)-[1,1'-biphenyl]-3-yl)benzo[*d*][1,2]selenazol-3(2*H*)-one (78)

Compound **76b** (0.14 g, 0.28 mmol, 1 eq), CuI (0.026 g, 0.14 mmol, 0.5 eq), 1,10-phenanthroline (0.025 g, 0.14 mmol, 0.5 eq), potassium carbonate (0.077 g, 0.56 mmol, 2 eq) and selenium powder (0.027 g, 0.34 mmol, 1.2 eq) were used in DMF (3 cm^3) following **general procedure 11**, product purified by column chromatography (25 % EtOAc in hexane). Solvents were removed *in vacuo* and the residue was recrystallised from ethyl acetate to give **78** as a static white solid (0.024 g, 20 %). δ_H (400 MHz, $CDCl_3$) 8.14 (1H, d, *J* 7.8 Hz), 7.89 (1H, apparent t, *J* 1.8), 7.69 – 7.66 (2H, m), 7.66 – 7.62 (2H, m), 7.62 – 7.58 (1H, m), 7.54 – 7.45 (3H, m), 7.30 (2H, d, *J* 8.1 Hz). δ_C (101 MHz, $CDCl_3$) 166.0, 149.1, 141.3, 139.8, 139.1, 137.7, 132.9, 130.0, 129.6, 128.8, 127.6, 126.8, 125.6, 124.6, 124.3, 123.9, 121.5. **ESI-HRMS**: m/z calculated for $C_{20}H_{12}F_3NNaO_2Se$ $[M+Na]^+$ requires 457.9878. Found 457.9881. **Elemental Analysis** Calculated for $C_{20}H_{12}F_3NO_2Se$ requires, C, 55.31; H, 2.79; N, 3.23, found, C, 54.79; H, 2.71; N, 3.09. **IR (neat)**: ν_{max}/cm^{-1}: 3088 (w), 3053 (w), 1597 (s), 1563 (s), 1483 (m), 1443 (m), 1269 (s, br), 1204 (s, br), 1154 (s, br). **Melting Point** °C: 204 – 205 (EtOAc).

Preparation of 2-(4'-(morpholinomethyl)-[1,1'-biphenyl]-3-yl)benzo[*d*][1,2]selenazol-3(2*H*)-one (79)

Compound **76c** (0.58 g, 1.16 mmol, 1 eq), CuI (0.22 g, 1.16 mmol, 1 eq), 1,10-phenanthroline (0.21 g, 1.16 mmol, 1 eq), potassium carbonate (0.26 g, 1.86 mmol, 1.6 eq) and selenium powder (0.11 g, 1.39 mmol, 1.2 eq), were used in DMF (5 cm^3) following **general procedure 11**, product purified by column chromatography (50 % EtOAc in hexane). Solvents were removed *in vacuo* and the residue was recrystallised from ethyl acetate to give **79** as a white solid (0.094 g, 18 %). δ_H (400 MHz, $CDCl_3$) 8.14 (1H, d, *J* 7.8 Hz), 7.87 (1H, s), 7.71 – 7.63 (2H, m), 7.61 – 7.54 (3H, d + another m underneath, *J* 8.0 Hz), 7.53 – 7.46 (3H, m), 7.41 (2H, d, *J* 8.0 Hz), 3.78 – 3.69 (4H, apparent t), 3.54 (2H, s), 2.48 (4H, br s). δ_C (101 MHz, $CDCl_3$) 165.9, 142.5, 139.7, 139.3, 137.8, 137.6, 132.8, 129.83, 129.81, 129.6, 127.7, 127.3, 126.8, 125.6, 124.3, 124.2, 123.9, 67.2, 63.2, 53.8. **ESI-HRMS**: m/z calculated for $C_{24}H_{23}N_2O_2Se$ $[M+H]^+$ requires 451.0919. Found 451.0906. **Elemental Analysis** Calculated for $C_{24}H_{22}N_2O_2Se$ requires, C, 64.14; H, 4.93; N, 6.23, found C, 63.73; H, 4.82; N, 6.09. **IR (neat)**: ν_{max}/cm^{-1}: 3088 (w), 3053 (w), 2856 (w), 2800 (w), 1587 (s), 1561 (s), 1441 (m), 1307 (s), 1108 (s). **Melting Point** °C: 179 – 180 (EtOAc).

Preparation of 2-(4'-((4-fluoropiperidin-1-yl)methyl)-[1,1'-biphenyl]-3-yl)benzo[*d*][1,2]selenazol-3(2*H*)-one (80)

Compound **76d** (0.31 g, 0.60 mmol, 1 eq), CuI (0.11 g, 0.60 mmol, 1 eq), 1,10-phenanthroline (0.11 g, 0.60 mmol, 1 eq), potassium carbonate (0.13 g, 0.95 mmol, 1.6 eq) and selenium powder

(0.056 g, 0.71 mmol, 1.2 eq), were used in DMF (5 cm^3) following **general procedure 11**, product purified by column chromatography (100 % EtOAc). Solvents were removed *in vacuo* and the residue was recrystallised from ethyl acetate to give **80** as a white solid (0.030 g, 11 %). δ_H (400 MHz, $CDCl_3$) 8.14 (1H, d, *J* 7.8 Hz), 7.87 (1H, s), 7.70 – 7.63 (2H, m), 7.62 – 7.54 (3H, m), 7.53 – 7.45 (3H, m), 7.40 (2H, d, *J* 8.0 Hz), 4.81 – 4.57 (1H, m), 3.55 (2H, s), 2.69 – 2.56 (2H, m), 2.45 – 2.32 (2H, m), 2.00 – 1.83 (4H, m). δ_C (101 MHz, $CDCl_3$) 165.9, 142.5, 139.7, 139.1, 138.3, 137.8, 132.8, 129.8, 129.7, 129.6, 127.7, 127.3, 126.8, 125.6, 124.3, 124.2, 123.9, 88.9 (d, *J* 169.9 Hz), 62.8, 49.7 (d, *J* 6.0 Hz), 31.7 (d, *J* 19.4 Hz). **ESI-HRMS**: m/z calculated for $C_{25}H_{23}FN_2OSe$ $[M+H]^+$ requires 467.1032. Found 467.1028. **Elemental Analysis** Calculated for $C_{25}H_{23}FN_2OSe$ requires C, 64.52; H, 4.98; F, 4.08; N, 6.02, found C, 64.70; H, 4.90; N, 5.97. **Melting Point** °C: 181 – 182 °C (EtOAc).

Preparation of 2-(4'-((4-methylpiperazin-1-yl)methyl)-[1,1'-biphenyl]-3-yl)benzo[*d*][1,2]selenazol-3(2*H*)-one (81)

Compound **76e** (0.19 g, 0.38 mmol, 1 eq), CuI (0.036 g, 0.19 mmol, 0.5 eq), 1,10-phenanthroline (0.034 g, 0.19 mmol, 0.5 eq), potassium carbonate (0.11 g, 0.73 mmol, 2 eq) and selenium powder (0.036 g, 0.45 mmol, 1.2 eq), were used in DMF (3 cm^3) following **general procedure 11**, product purified by column chromatography (20 % MeOH in EtOAc with a few drops of NEt_3) to give **81** as a yellow to off white foam (0.012 g, 7 %). δ_H (400 MHz, $CDCl_3$) 8.13 (1H, d, *J* 7.8), 7.86 (1H, s), 7.72 – 7.64 (2H, m), 7.61 – 7.54 (3H, m), 7.52 – 7.46 (3H, m), 7.39 (2H, d, *J* 8.0), 3.57 (2H, s), 2.60 (8H, br s), 2.38 (3H, s). δ_C (101 MHz, $CDCl_3$) 165.9, 142.4, 139.7, 139.2, 137.83, 137.81, 132.7, 129.8, 129.5, 127.7, 127.2, 126.7, 125.5, 124.3, 124.2, 124.0, 62.7, 55.1, 52.9, 46.0. **ESI-HRMS**: m/z calculated for $C_{25}H_{26}N_3OSe$ $[M+H]^+$ requires 464.1236. Found 464.1243. **Elemental Analysis** Calculated for $C_{25}H_{25}N_3OSe$ requires, C, 64.93; H, 5.45; N, 9.09, found, C, 61.78; H, 5.25; N, 8.60.

Preparation of 2-(3-(morpholinomethyl)phenyl)benzo[*d*][1,2]selenazol-3(2*H*)-one (82)

Compound **76f** (0.65 g, 1.53 mmol, 1 eq), CuI (0.15 g, 0.77 mmol, 0.5 eq), 1,10-phenanthroline (0.14 g, 0.77 mmol, 0.5 eq), potassium carbonate (0.34 g, 2.45 mmol, 1.6 eq) and selenium powder (0.12 g, 1.84 mmol, 1.2 eq), were used in DMF (5 cm^3) following **general procedure 11**, product purified by column chromatography (100 % EtOAc). Solvents were removed *in vacuo* and the residue was recrystallised from ethyl acetate to give **82** as a white Solid (0.088 g, 15 %). δ_H (400 MHz, $CDCl_3$) 8.11 (1H, d, *J* 7.9 Hz), 7.69 – 7.62 (3H, m), 7.53 – 7.45 (2H, m), 7.38 (1H, t, *J* 7.8 Hz), 7.27 – 7.23 (1H, m), 3.76 – 3.68 (4H, apparent t), 3.53 (2H, s), 2.47 (4H, br s). δ_C (101 MHz, $CDCl_3$) 165.8, 139.6, 139.2, 137.7, 132.7, 129.5, 129.3, 127.7, 127.6, 126.7, 126.1, 124.2, 123.9, 67.2, 63.1, 53.7. **ESI-HRMS**: m/z calculated for $C_{18}H_{19}N_2O_2Se$ $[M+H]^+$ requires 375.0606. Found 375.0615. **Elemental Analysis** Calculated for $C_{18}H_{18}N_2O_2Se$ requires, C, 57.91; H, 4.86; N, 7.50, found, C, 57.77; H, 4.79; N, 7.42. **IR**

(neat): ν_{max}/cm^{-1}: 3087 (w), 3054 (w), 2972 (w), 2858 (w), 2801 (w), 1590 (s), 1561 (s), 1442 (s), 1330 (s), 1087 (s). **Melting Point** °C: 179 – 180 (EtOAc).

Preparation of 4-((1-ethoxy-1-oxopropan-2-yl)thio)-3-nitrobenzoic acid (94)

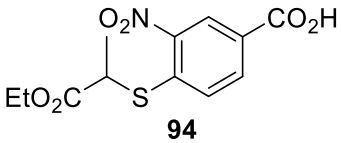

94

To 4-chloro-3-nitrobenzoic acid (**92**) (2.01 g, 9.97 mmol, 1 eq), pyridine (15 cm^3) was added under an N_2 atmosphere. To the resultant viscous fluid ethyl-2-mercaptopropionate (**93**) (1.61 cm^3, 12.4 mmol, 1.2 eq) was added and stirred under reflux overnight. The resultant solution was acidified with 2 M hydrochloric acid, extracted with ethyl acetate (3 x 50 cm^3) the organic layers were collected, dried with magnesium sulfate and the solvent removed in *vacuo*. The resultant brown oil was left overnight and solidified. The brown solid was washed with hexane and diethyl ether, the mixture of solvents was pipetted out of the flask and excess solvents removed in *vacuo* to give **94** as a yellow brown solid (2.46 g, 82 %). δ_H (400 MHz, $CDCl_3$) 8.91 (1H, d, *J* 1.8 Hz), 8.22 (1H, dd, *J* 8.5, 1.8 Hz), 7.73 (1H, d, *J* 8.6 Hz), 4.26 – 4.16 (2H, m), 4.12 (1H, q, *J* 7.3 Hz), 1.68 (3H, d, *J* 7.2 Hz), 1.25 (3H, t, *J* 7.1 Hz). δ_C (101 MHz, $CDCl_3$) 171.9, 169.7, 145.6, 143.3, 134.1, 128.0, 127.7, 126.5, 62.3, 43.4, 17.2, 14.2. **ESI-HRMS**: m/z calculated for $C_{12}H_{13}NNaO_6S$ $[M+Na]^+$ requires 322.0256. Found 322.0359.

Preparation of ethyl 4-((1-ethoxy-1-oxopropan-2-yl)thio)-3-nitrobenzoate (95)

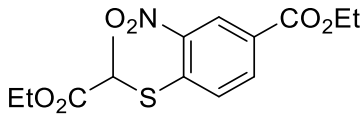

95

To **94** (6.75 g, 23 mmol, 1 eq) was added 2 M oxalyl chloride (22.5 cm^3, 45 mmol, 2 eq) in a N_2 atmosphere. Four drops of DMF was added and the reaction left to stir for two hours. Solvents were removed *in vacuo*, product re-dissolved ethanol was added and stirred under an N_2 atmosphere for 30 minutes. Solvents were concentrated in *vacuo* and ethyl acetate (25 cm^3) was added to the residue. This was washed with saturated $HNaCO_3$ solution (3 x 50 cm^3) and brine (50 cm^3). Organic layer was collected and solvents removed in *vacuo* to yield **95** as a brown oil (7.53 g, 96 %). δ_H (400 MHz, $CDCl_3$) 8.81 (1H, d, *J* 1.9), 8.17 (1H, dd, *J* 8.5, 1.9), 7.67 (1H, d, *J* 8.6), 4.41 (2H, q, *J* 7.1), 4.24 – 4.14 (2H, m), 4.09 (1H, q, *J* 7.2), 1.65 (3H, d, *J* 7.2), 1.41 (3H, t, *J* 7.1), 1.23 (3H, t, *J* 7.1). δ_C (101 MHz, $CDCl_3$) 171.8, 164.4, 145.7, 141.7, 133.7, 127.9, 127.6, 127.2, 62.1, 61.9, 43.4, 17.1, 14.4, 14.2. **CI-HRMS**: m/z calculated for $C_{14}H_{18}NO_6S$ $[M+H]^+$ requires 328.0849. Found 328.0858.

Preparation of ethyl 2-methyl-3-oxo-3,4-dihydro-2*H*-benzo[*b*][1,4]thiazine-6-carboxylate (96)

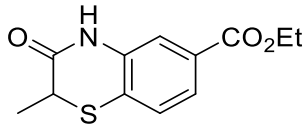

96

Compound **95** (1.30 g, 3.98 mmol, 1 eq) and iron powder (1.33 g, 23.88 mmol, 6 eq), were used in acetic acid (10 cm^3) and water (10 cm^3) following **general procedure 9**. Reduction and cyclisation occurs *in situ* to give **96** as pale yellow crystals (0.99 g, 99 %). δ_H (400 MHz, $CDCl_3$) 8.57 (1H, s), 7.68 (1H, dd, *J* 8.1, 1.6 Hz), 7.58 (1H, d, *J* 1.5 Hz), 7.37 (1H, d, *J* 8.1 Hz), 4.39 (2H, q, *J* 7.1 Hz), 3.60 (1H, q, *J* 7.1 Hz), 1.51 (3H, d, *J* 7.1 Hz), 1.39 (3H, t, *J* 7.1 Hz). δ_C (101 MHz, $CDCl_3$) 168.2, 165.9, 136.1, 129.5, 128.0, 125.6, 124.7, 117.9, 61.5, 37.0, 15.7, 14.4. **CI-HRMS**: m/z calculated for $C_{12}H_{14}NO_3S$ $[M+H]^+$ requires 252.0689. Found 252.0693.

Preparation of 2-methyl-3-oxo-3,4-dihydro-2*H*-benzo[*b*][1,4]thiazine-6-carboxylic acid (97)

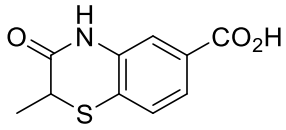

97

To compound **96** (0.93 g, 3.71 mmol, 1 eq) sodium hydroxide (1 M, 10 cm^3) and ethanol (10 cm^3) was added and stirred overnight under a N_2 atmosphere. Solvents where removed in *vacuo,* residue acidified with HCl (2 M), washed with ethyl acetate (3 x 50 cm^3) and dried with $MgSO_4$. Solvents removed in *vacuo* to give **97** as pale yellow crystals (0.83 g, 99 %). δ_H (400 MHz, DMSO) 13.01 (1H, s), 10.75 (1H, s), 7.57 (1H, d, *J* 1.5), 7.52 (1H, dd, *J* 8.1, 1.6), 7.43 (1H, d, *J* 8.1), 3.73 (1H, q, *J* 7.0), 1.32 (3H, d, *J* 7.0). δ_C (101 MHz, DMSO) 167.2, 166.7, 137.0, 129.4, 127.7, 124.3, 123.6, 117.4, 35.5, 15.3. **CI-HRMS**: m/z calculated $C_{10}H_{10}NO_3S$ $[M+H]^+$ requires 224.0376. Found 224.0384.

Preparation of ethyl 2-(4-(2-methyl-3-oxo-3,4-dihydro-2*H*-benzo[*b*][1,4]thiazine-6-carbonyl)piperazin-1-yl)acetate (99)

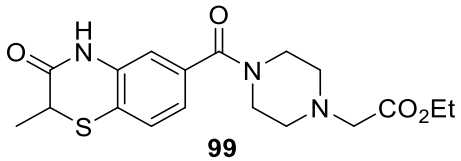

99

Compound **97** (3.01 g, 13.47 mol, 1 eq), was suspended in DCM (50 cm^3), this was cooled to 0 °C and placed under an N_2 atmosphere. EDC . HCl (3.10 g, 16.16 mmol, 1.2 eq), HOBT (2.46 g, 16.16

mmol, 1.2 eq) and DIPEA (7.04 cm^3, 40.40 mmol, 3 eq) were added. The reaction was allowed to stir until the suspension dissolved, after which ethyl 2-(piperazin-1-yl)acetate (**98**) (2.51 cm^3, 14.81 mmol, 1.1 eq) was added and the reaction allowed to warm to room temperature and was left to stir overnight. The reaction mixture was washed with saturated $HNaCO_3$ solution (50 cm^3), followed by 2 M HCl (50 cm^3) the organic phase was disposed of and the acidified product neutralised with 1 M NaOH and extracted back into DCM (3 x 50 cm^3). Organics were washed with brine (50 cm^3), and dried over $MgSO_4$. Solvents were removed *in vacuo* and the product purified by trituration with Et_2O to give **99** as faded white crystals (3.56 g, 70 %). δ_H (400 MHz, $CDCl_3$) 8.64 (1H, s), 7.32 (1H, d, *J* 8.3 Hz), 7.04 – 6.97 (2H, m), 4.19 (2H, q, *J* 7.1 Hz), 3.84 (2H, br s), 3.63 – 3.46 (3H, m), 3.27 (2H, s), 2.64 (4H, br s), 1.50 (3H, d, *J* 7.1 Hz), 1.28 (3H, t, *J* 7.1 Hz). δ_C (101 MHz, $CDCl_3$) 170.1, 169.3, 168.4, 136.7, 134.3, 127.8, 122.1, 121.7, 116.4, 60.9, 59.2, 53.1 (br), 52.6 (br), 47.8 (br), 42.3 (br), 36.9, 15.7, 14.3. **ESI-HRMS**: m/z calculated for $C_{18}H_{23}N_3NaO_4S$ $[M+Na]^+$ requires 400.1301. Found 400.1300. **Elemental Analysis** Calculated for $C_{18}H_{23}N_3O_4S$ requires, C, 57.28; H, 6.14; N, 11.13; S, 8.49, found, C, 57.11; H, 6.12; N, 10.97; S, 7.86. **IR (neat)**: ν_{max}/cm^{-1}: 3217 (br), 3147 (br), 2931 (s), 1739 (s), 1682 (s), 1597 (s), 1562 (s), 1184 (s), 1022 (s). **Melting Point** °C 182 – 184 °C (Et_2O).

Preparation of 2-(4-(2-methyl-3-oxo-3,4-dihydro-2*H*-benzo[*b*][1,4]thiazine-6-carbonyl)piperazin-1-yl)acetic acid (100)

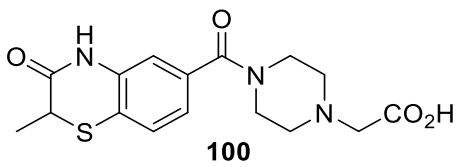

100

To compound **99** (0.20 g, 0.54 mmol, 1 eq) in dioxane (6 cm^3) was added and LiOH 1 M (2 cm^3). The solution was stirred at room temperature for 2 hours. After completion of the reaction extraction into organic phase using ethyl acetate (50 cm^3) failed, aqueous phase was removed *in vacuo* to give **100** as a hydroscopic orange solid used crude in the next step. δ_H (400 MHz, MeOD) 7.42 (1H, d, *J* 8.0 Hz), 7.12 (1H, dd, *J* 8.0, 1.7 Hz), 7.06 (1H, d, *J* 1.6 Hz), 3.83 (4H, br s), 3.65 – 3.58 (3H, m), 3.20 (4H, br s), 1.43 (3H, d, *J* 7.1 Hz). **ESI-LRMS**: m/z calculated for $C_{18}H_{23}N_3NaO_4S$ $[M-H]^-$ requires 348.1. Found 348.1.

Generic structure of compounds 101 – 107 following general procedure 5

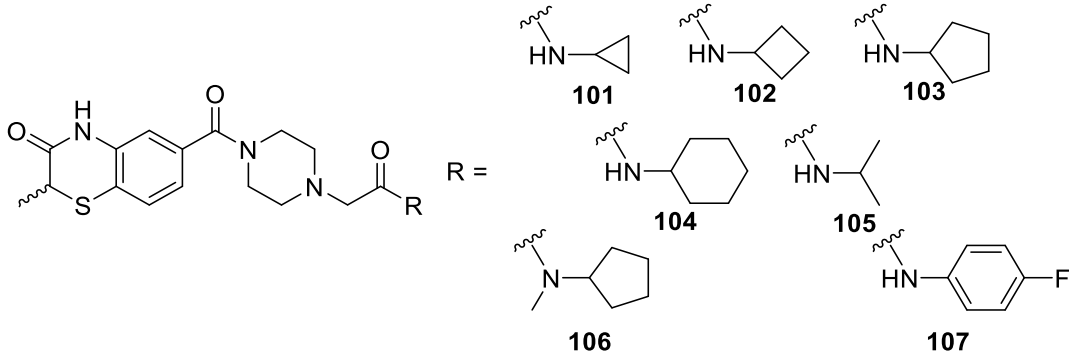

Preparation of *N*-cyclopropyl-2-(4-(2-methyl-3-oxo-3,4-dihydro-2*H*-benzo[*b*][1,4]thiazine-6-carbonyl)piperazin-1-yl)acetamide (101)

Compound **100** (0.54 mmol, 1 eq), HATU (0.25 g, 0.65 mmol, 1.2 eq), DIPEA (0.37 cm^3, 2.16 mmol, 4 eq) and cyclopropylamine (0.05 cm^3, 0.64 mmol, 1.2 eq), were used in DMF (5 cm^3) following **general procedure 5**, purified by column chromatography (100 % EtOAc to 5 % MeOH in EtOAc) followed by trituration with Et_2O to give **101** as a white solid (0.075 g, 36 % over two steps). X-ray crystal was generated through slow recrystallisation from EtOAc. δ_H (400 MHz, $CDCl_3$) 9.49 (1H, s), 7.30 (1H, d, *J* 7.9 Hz), 7.10 (1H, s), 7.04 (1H, s), 6.98 (1H, d, *J* 7.9 Hz), 3.78 (2H, s), 3.61 – 3.40 (3H, m), 3.02 (2H, s), 2.77 – 2.66 (1H, m), 2.51 (4H, s), 1.48 (3H, d, *J* 7.0 Hz), 0.83 – 0.77 (2H, m), 0.55 – 0.44 (2H, m). δ_C (101 MHz, $CDCl_3$) 171.1, 169.5, 168.4, 136.8, 134.0, 127.9, 122.0, 121.9, 116.4, 61.6, 53.4 (br), 47.9 (br), 42.6 (br), 36.9, 22.2, 15.7, 6.7. **CI-HRMS**: m/z calculated for $C_{19}H_{25}N_4O_3S$ $[M+H]^+$ requires 389.1642. Found 389.1656. **Elemental Analysis** Calculated for $C_{19}H_{24}N_4O_3S$ requires, C, 58.74; H, 6.23; N, 14.42; S, 8.25, found, C, 57.85; H, 6.31; N, 14.02; S, 7.97. **IR (neat)**: ν_{max}/cm^{-1}: 3289 (br), 3146 (br), 2933 (s), 1687 (s), 1666 (s), 1598 (s), 1567 (s). **Melting Point** °C: 190 – 192 (Et_2O).

Crystal data and structure refinement for 101.

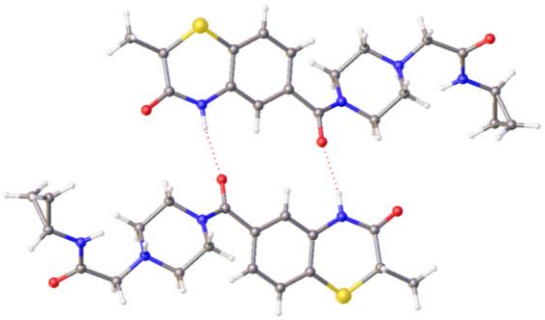

Identification code	**101**
Empirical formula	$C_{19}H_{25}N_4O_3S$
Formula weight	388.48
Temperature/K	100.02
Crystal system	monoclinic
Space group	$P2_1/c$
a/Å	6.1643(5)
b/Å	29.893(2)
c/Å	10.3248(8)
α/°	90
β/°	101.291(3)
γ/°	90
Volume/Å^3	1865.7(3)
Z	4
ρ_{calc}g/cm^3	1.383
μ/mm^{-1}	1.779
F(000)	824.0
Radiation	CuKα (λ = 1.54178)
2Θ range for data collection/°	5.912 to 83.972
Index ranges	-5 ≤ h ≤ 5, -24 ≤ k ≤ 25, -8 ≤ l ≤ 4
Reflections collected	2684
Independent reflections	1214 [R_{int} = 0.0184, R_{sigma} = 0.0265]
Data/restraints/parameters	1214/0/245
Goodness-of-fit on F^2	1.097
Final R indexes [I>=2σ (I)]	R_1 = 0.0537, wR_2 = 0.1143
Final R indexes [all data]	R_1 = 0.0615, wR_2 = 0.1184
Largest diff. peak/hole / e Å^{-3}	0.76/-0.39

Preparation of *N*-cyclobutyl-2-(4-(2-methyl-3-oxo-3,4-dihydro-2*H*-benzo[*b*][1,4]thiazine-6-carbonyl)piperazin-1-yl)acetamide (102)

Compound **100** (0.50 mmol, 1 eq)**,** HATU (0.23 g, 0.60 mmol, 1.2 eq), DIPEA (0.33 cm^3, 1.89 mmol, 4 eq) and cyclobutylamine (0.06 cm^3, 0.75 mmol, 1.5 eq), were used in DMF (5 cm^3) following **general procedure 5**, purified by column chromatography (2 % MeOH in EtOAc) followed by trituration with Et_2O to give **102** as a white solid (0.054 g, 27 % over two steps). **δ_H** (400 MHz, $CDCl_3$) 7.31 (1H, d, *J* 7.9 Hz), 7.13 (1H, d, *J* 8.0 Hz), 6.97 (1H, d, *J* 7.9 Hz), 6.93 (1H, s), 4.44 – 4.30 (1H, m), 3.76 (2H, s), 3.64 – 3.43 (3H, m), 2.99 (2H, s), 2.53 (4H, br, s), 2.38 – 2.27 (2H, m), 1.91 – 1.79 (2H, m), 1.76 – 1.65 (2H, m), 1.46 (3H, d, *J* 7.1 Hz). **δ_C** (101 MHz, MeOD, 2 drops of $CDCl_3$) 170.9, 170.6, 169.6, 137.6, 134.7, 128.8, 122.8, 122.7, 116.4, 61.6, 54.1, 53.6, 45.2, 43.0, 37.4, 31.2, 15.9, 15.7. **CI-HRMS**: m/z calculated for $C_{20}H_{27}N_4O_3S$ $[M+H]^+$ requires 403.1798. Found 403.1782. **Elemental Analysis** Calculated for $C_{20}H_{26}N_4O_3S$ requires, C, 59.68; H, 6.51; N, 13.92; S, 7.97, found, C, 58.37; H, 6.46; N, 13.51; S, 7.90. **IR (neat):** ν_{max}/cm^{-1}: 3218 (br), 2969 (br), 2943 (s), 1685 (s), 1653 (s), 1612 (s), 1568 (s). **Melting Point** °C: 208 – 210 °C (diethyl ether).

Preparation of *N*-cyclopentyl-2-(4-(2-methyl-3-oxo-3,4-dihydro-2*H*-benzo[*b*][1,4]thiazine-6-carbonyl)piperazin-1-yl)acetamide (103)

Compound **100** (0.49 mmol, 1 eq), HATU (0.28 g, 0.74 mmol, 1.5 eq), DIPEA (0.34 cm^3, 1.96 mmol, 4 eq) and cyclopentylamine (0.07 cm^3, 0.74 mmol, 1.5 eq), were used in DMF (5 cm^3) following **general procedure 5**, purified by column chromatography (100 % EtOAc) followed by trituration with Et_2O to give **103** as a white solid (0.059 g, 29 % over two steps). **δ_H** (400 MHz, $CDCl_3$) 9.29 (1H, s), 7.31 (1H, d, *J* 7.9), 7.07 (1H, s), 6.99 (1H, d, *J* 7.9), 6.93 (1H, d, *J* 7.6), 4.28 – 4.17 (1H, m), 3.92 – 3.57 (3H, m), 3.51 – 3.40 (2H, m), 3.03 (2H, s), 2.55 (4H, s), 2.03 – 1.93 (2H, m), 1.72 – 1.55 (4H, m), 1.48 (3H, d, *J* 7.1), 1.43 – 1.31 (2H, m). **δ_C** (101 MHz, $CDCl_3$) 169.5, 168.9, 168.4, 136.8, 134.1, 128.0, 122.1, 122.0, 116.3, 61.6, 53.7 – 53.3 (m), 50.7, 36.9, 33.3, 23.8, 15.7. **CI-HRMS**: m/z calculated for $C_{21}H_{29}N_4O_3S$ $[M+H]^+$ requires 417.1955. Found 417.1960. **Elemental Analysis** Calculated for $C_{21}H_{28}N_4O_3S$ requires, C, 60.55; H, 6.78; N, 13.45; S, 7.70, found, C, 59.80; H, 6.75; N, 13.24; S, 7.50. **IR (neat)**: ν_{max}/cm^{-1}: 3286 (br), 3217 (br), 2947 (s), 1686 (s), 1652 (s), 1612 (s), 1568 (s). **Melting Point** °C: 216 – 218 (diethyl ether).

Preparation of *N*-cyclohexyl-2-(4-(2-methyl-3-oxo-3,4-dihydro-2*H*-benzo[*b*][1,4]thiazine-6-carbonyl)piperazin-1-yl)acetamide (104)

Compound **100** (0.40 mmol, 1 eq), HATU (0.23 g, 0.59 mmol, 1.5 eq), DIPEA (0.21 cm^3, 1.19 mmol, 3 eq) and cyclohexylamine (0.05 cm^3, 0.44 mmol, 1.1 eq), were used in DMF (5 cm^3) following

general procedure 5, purified by column chromatography (100 % EtOAc) to give **104** as a white solid (0.14 g, 81 % over two steps). **δ_H** (400 MHz, $CDCl_3$) 8.19 (1H, s), 7.34 (1H, d, *J* 7.9 Hz), 7.02 (1H, dd, *J* 7.9, 1.2 Hz), 6.97 (1H, s), 6.88 (1H, s), 3.88 – 3.68 (3H, m), 3.65 – 3.46 (3H, m), 3.04 (2H, s), 2.56 (4H, s), 1.94 – 1.85 (2H, m), 1.75 – 1.66 (2H, m), 1.66 – 1.53 (2H, m + H_2O), 1.50 (3H, d, *J* 7.1 Hz), 1.45 – 1.33 (2H, m), 1.23 – 1.15 (2H, m). **δ_C** (101 MHz, $CDCl_3$) 169.5, 168.5, 136.7, 134.1, 127.9, 122.0, 121.9, 116.3, 61.6, 53.9 – 53.1 (br, m), 47.6, 42.9 – 42.0 (br, m), 36.9, 33.2, 25.6, 24.8, 15.7. **ESI-HRMS**: m/z calculated for $C_{22}H_{30}N_4NaO_3S$ $[M+Na]^+$ requires 453.1931. Found 453.1925. **Elemental Analysis** Calculated for $C_{22}H_{30}N_4O_3S$ requires, C, 61.37; H, 7.02; N, 13.01; S, 7.45, found, C, 60.82; H, 6.86; N, 12.61; S, 6.80. **IR (neat)**: ν_{max}/cm^{-1}: 3216 (br), 3144 (br), 2931 (s), 1686 (s), 1660 (s), 1611 (s), 1567 (s). **Melting Point** ^oC: 196 – 198 (EtOAc).

Preparation of *N*-isopropyl-2-(4-(2-methyl-3-oxo-3,4-dihydro-2*H*-benzo[*b*][1,4]thiazine-6-carbonyl)piperazin-1-yl)acetamide (105)

Compound **100** (0.40 mmol, 1 eq), HATU (0.23 g, 0.60 mmol, 1.5 eq), DIPEA (0.21 cm^3, 1.20 mmol, 3 eq) and isopropylamine (0.11 cm^3, 1.24 mmol, 3.1 eq), were used in DMF (5 cm^3) following **general procedure 5**, purified by column chromatography (100 % EtOAc) to give **105** as a white solid (0.098 g, 63 % over two steps). **δ_H** (400 MHz, $CDCl_3$) 9.28 (1H, s), 7.31 (1H, d, *J* 7.9 Hz), 7.07 (1H, d, *J* 1.2 Hz), 7.00 (1H, dd, *J* 7.9, 1.3 Hz), 6.80 (1H, d, *J* 8.2 Hz), 4.15 – 4.04 (1H, m), 3.80 (2H, br s), 3.65 – 3.43 (3H, m), 3.02 (2H, s), 2.55 (4H, br s), 1.49 (3H, d, *J* 7.1 Hz), 1.16 (6H, d, *J* 6.6 Hz). **δ_C** (101 MHz, $CDCl_3$) 169.5, 168.6, 168.4, 136.7, 134.1, 128.0, 122.1, 122.0, 116.3, 61.6, 54.8 – 51.9 (m), 41.0, 36.9, 23.0, 15.7. **ESI-HRMS**: m/z calculated for $C_{19}H_{26}N_4NaO_3S$ $[M+Na]^+$ requires 413.1618. Found 413.1627. **Elemental Analysis** Calculated for $C_{19}H_{26}N_4O_3S$ requires, C, 58.44; H, 6.71; N, 14.35; S, 8.21, found, C, 57.83; H, 6.85; N, 13.62; S, 7.80. **IR (neat)**: ν_{max}/cm^{-1}: 3217 (br), 2969 (br), 2932 (s), 1677 (s), 1624 (s), 1566 (s). **Melting Point** ^oC: 110 – 112 (Et_2O)

Preparation of *N*-cyclopentyl-*N*-methyl-2-(4-(2-methyl-3-oxo-3,4-dihydro-2*H*-benzo[*b*][1,4]thiazine-6-carbonyl)piperazin-1-yl)acetamide (106)

Compound **100** (0.54 mmol, 1 eq), HATU (0.31 g, 0.81 mmol, 1.5 eq), DIPEA (0.28 cm^3, 1.62 mmol, 3 eq) and *N*-methylcyclopentylamine (0.07 cm^3, 0.59 mmol, 1.1 eq), were used in DMF (5 cm^3) following **general procedure 5**, purified by column chromatography (100 % EtOAc) to give **106** as a white solid (0.15 g, 66 % over two steps). Note: Peaks around the terminal amide bond appear to be rotameric. The major rotamer contributes approximately 55 %, whilst the minor contributes 45 % in the ^1H NMR. The chemical shifts of the molecule on the left hand side are unaffected by the rotamer. Reported below is the proton spectrum where major and minor rotamers will be noted as appropriate. All observable ^{13}C peaks are reported, it was not possible to identify clearly which peaks belonged to

rotamers or other ^{13}C chemical shifts nor was it clear in all cases which peak was major or minor. **δ_H** (400 MHz, $CDCl_3$) 9.19 (1H, d, *J* 11.7 Hz), 7.30 (1H, d, *J* 7.9 Hz), 7.08 (1H, s), 7.00 (1H, d, *J* 7.9 Hz), 4.92 (1H, apparent p (Minor), 4.39 – 4.27 (1H, m (Major)), 3.81 (2H, s), 3.60 – 3.41 (3H, m), 3.30 (2H, s (Major)), 3.22 (2H, s (Minor)), 2.87 (3H, s (Minor)), 2.79 (3H, s (Major)), 2.57 (4H, br, s), 1.89 – 1.53 (8H, m), 1.48 (3H, d, *J* 7.1 Hz). **δ_C** (101 MHz, $CDCl_3$) 169.34, 169.31, 168.9, 168.8, 168.3, 136.7, 134.5, 134.4, 127.9, 122.1, 121.71, 121.69, 116.3, 60.9, 60.7, 58.1, 54.5, 53.6 – 52.3 (m), 37.0, 29.4, 29.3, 28.3, 27.6, 24.6, 24.4, 15.7. **ESI-HRMS**: m/z calculated for $C_{22}H_{31}N_4O_3S$ $[M+H]^+$ requires 431.2111. Found 431.2112. **Elemental Analysis** Calculated for $C_{22}H_{30}N_4O_3S$ requires, C, 61.37; H, 7.02; N, 13.01; S, 7.45, found, C, 60.86; H, 6.90; N, 12.69; S, 7.31. **IR (neat)**: ν_{max}/cm^{-1}: 3222 (br), 3183 (br), 2953 (s), 1688 (s), 1634 (s), 1600 (s), 1567 (s). **Melting Point** °C: 174 – 175 (EtOAc).

Preparation of *N*-(4-fluorophenyl)-2-(4-(2-methyl-3-oxo-3,4-dihydro-2*H*-benzo[*b*][1,4]thiazine-6-carbonyl)piperazin-1-yl)acetamide (107)

Compound **100** (0.54 mmol, 1 eq), HATU (0.31 g, 0.81 mmol, 1.5 eq), DIPEA (0.28 cm^3, 1.62 mmol, 3 eq) and 4-fluoroaniline (0.06 cm^3, 0.59 mmol, 1.1 eq), was used in DMF (5 cm^3) following **general procedure 5**, purified by column chromatography (100 % EtOAc) to give **107** as a white solid (0.12 g, 52 % over two steps). **δ_H** (400 MHz, $CDCl_3$) 9.09 (1H, s), 8.92 (1H, s), 7.52 (2H, dd, *J* 8.8, 4.7 Hz), 7.33 (1H, d, *J* 7.9 Hz), 7.08 (1H, s), 7.07 – 6.97 (3H, m), 3.99 – 3.61 (4H, m), 3.56 (2H, q, *J* 7.1 Hz), 3.21 (2H, s), 2.67 (4H, s), 1.50 (3H, d, *J* 7.1 Hz). **δ_C** (101 MHz, $CDCl_3$) 169.5, 168.3, 159.6 (d, *J* 244.0 Hz), 136.8, 134.0, 133.5 (d, *J* 2.8 Hz), 128.0, 122.2, 122.1, 121.5 (d, *J* 7.9 Hz), 116.3, 115.9 (d, *J* 22.5 Hz), 62.0, 53.9 – 53.3 (m), 37.0, 15.7. **δ_F** (376 MHz, $CDCl_3$) -117.60 (1F, s). **ESI-HRMS**: m/z calculated for $C_{22}H_{23}FN_4O_3S$ $[M+Na]^+$ requires 465.1367. Found 465.1371. **Elemental Analysis** Calculated for $C_{22}H_{23}FN_4O_3S$ requires, C, 59.71; H, 5.24; N, 12.66; found, C, 58.67; H, 5.15; N, 12.32. **IR (neat)**: ν_{max}/cm^{-1}: 3219 (br), 3180 (br), 2936 (s), 1685 (s), 1612 (s), 1567 (s). **Melting Point** °C: 186 – 187 °C (EtOAc).

Molecular Modelling Protocol

Compounds were first built in chemdraw and transferred to Spartan, compounds were then energy minimised, Spartan was used to compute local energy minimum geometry using molecular mechanics with the MMFF94 forcefield. Compounds were then docked in GOLD using the homology model previously built by our group. The docking protocol is outlined in the below. Early termination was not allowed and lone pairs were not saved, all other parameters were left default. Covalent docking was carried by linking the Cα of the Cys-202 with the ring opened form of **79**.

Mg^{2+}	Mg^{2+} present, no coordination geometry specified
Protonation	Hydrogens added
Waters	Water molecule HOH1091 extracted, all other waters deleted, water was set as toggle, spin
Ligands	CDPME extracted
Binding site	Defined as 6 Å of the CDPME ligand
Number of GA Runs	10, 50, 100, 500
Scoring Function	GOLDscore

3.9 References

(1) Berry, N. G. Personal Communication. **2016**.
(2) Price, K. E.; Armstrong, C. M.; Imlay, L. S.; Hodge, D. M.; Pidathala, C.; Roberts, N. J.; Park, J.; Mikati, M.; Sharma, R.; Lawrenson, A. S.; Tolia, N. H.; Berry, N. G.; Neill, P. M. O.; John, A. R. O. *Nat. Publ. Gr.* **2016**, *6* (November), 1–12.
(3) Maggiora, G.; Vogt, M.; Stumpfe, D.; Bajorath, J. *J. Med. Chem.* **2014**, *57* (8), 3186–3204.
(4) Vogt, M.; Stumpfe, D.; Geppert, H.; Bajorath, J. *J. Med. Chem.* **2010**, *53* (15), 5707–5715.
(5) Zhang, B.; Watts, K. M.; Hodge, D.; Kemp, L. M.; Hunstad, D. A.; Hicks, L. M.; Odom, A. R. *Biochemistry* **2011**, *50* (17), 3570–3577.
(6) Kuzuyama, T.; Takagi, M.; Kaneda, K.; Seto, H. *Tetrahedron Lett.* **2000**, *41*, 703–706.
(7) Frank, A.; Groll, M. *Chem. Rev.* **2017**, *117* (8), 5675–5703.
(8) Richard, S. B.; Lillo, A. M.; Tetzlaff, C. N.; Bowman, M. E.; Noel, J. P.; Cane, D. E. *Biochemistry* **2004**, *43* (38), 12189–12197.
(9) Richard, S. B.; Bowman, M. E.; Kwiatkowski, W.; Kang, I.; Chow, C.; Lillo, a M.; Cane, D. E.; Noel, J. P. *Nat. Struct. Biol.* **2001**, *8* (7), 641–648.
(10) Hale, I.; O'Neill, P. M.; Berry, N. G.; Odom, A.; Sharma, R. *Medchemcomm* **2012**, *3* (4), 418.
(11) Willett, P.; Barnard, J. M.; Downs, G. M. *J. Chem. Inf. Comput. Sci.* **1998**, *38* (6), 983–996.
(12) Stålring, J. C.; Carlsson, L. A.; Almeida, P.; Boyer, S. *J. Cheminform.* **2011**, *3* (7), 1–10.
(13) Wood, D. J.; Buttar, D.; Cumming, J. G.; Davis, A. M.; Norinder, U.; Rodgers, S. L. *Mol. Inform.* **2011**, *30* (11–12), 960–972.
(14) Odom, A. Personal Communication. **2018**.
(15) Qandil, A. M.; Hassan, M. A.; Al-Shar'i, N. A. *Arch. Pharm. (Weinheim).* **2008**, *341* (2), 99–112.
(16) Anandan, S. K.; Gless, R. D. *Bioorganic Med. Chem. Lett.* **2010**, *20* (9), 2740–2744.
(17) Mohammed, I.; Parai, M. K.; Jiang, X.; Sharova, N.; Singh, G.; Stevenson, M.; Rana, T. M. *ACS Med. Chem. Lett.* **2012**, *3* (6), 465–469.
(18) Uchida, Y.; Kozuka, S. *Bull. Chem. Soc. Jpn* **1982**, *55*, 1183–1187.
(19) Kagano, H.; Goda, H.; Yoshida, K.; Yamamoto, M.; Sakaue, S. Google Patents 1997.
(20) Bhakuni, B. S.; Balkrishna, S. J.; Kumar, A.; Kumar, S. *Tetrahedron Lett.* **2012**, *53* (11), 1354–1357.

(21) Aprile, S.; Del Grosso, E.; Grosa, G. *Xenobiotica* **2011**, *41* (3), 212–225.
(22) Pietka-Ottlik, M.; Potaczek, P.; Piasecki, E.; Mlochowski, J. *Molecules* **2010**, *15* (11), 8214–8228.
(23) Baggaley, K. H.; English, P. D.; Jennings, L. J. A.; Morgan, B.; Nunn, B.; Tyrrell, A. W. R. *J. Med. Chem.* **1985**, *28* (11), 1661–1667.
(24) Berry, N. G. Personal Communication. **2014**.
(25) Baell, J.; Walters, M. A. *Nature* **2014**, *513* (7519), 481–483.
(26) Baell, J. B. *Future Med. Chem.* **2010**, *2* (10), 1529–1546.
(27) Baell, J. B.; Holloway, G. A. *J. Med. Chem.* **2010**, *53* (7), 2719–2740.
(28) Lagorce, D.; Oliveira, N.; Miteva, M. A.; Villoutreix, B. O. *Drug Discov. Today* **2017**, *22* (8), 1131–1133.
(29) Baell, J. B.; Ferrins, L.; Falk, H.; Nikolakopoulos, G. *Aust. J. Chem.* **2013**, *66* (12), 1483–1494.
(30) Jasial, S.; Hu, Y.; Bajorath, J. *J. Med. Chem.* **2017**, *60* (9), 3879–3886.
(31) Willem, J.; Nissink, M.; Blackburn, S. *Future Med. Chem.* **2014**, *6* (10), 1113–1126.
(32) Almela, M. J.; Lozano, S.; Lelièvre, J.; Colmenarejo, G.; Coterón, J. M.; Rodrigues, J.; Gonzalez, C.; Herreros, E. *PLoS One* **2015**, *10* (8), 1–18.
(33) Kenny, P. W. *J. Chem. Inf. Model.* **2017**, *57* (11), 2640–2645.
(34) Baell, J. B.; Nissink, J. W. M. *ACS Chem. Biol.* **2018**, *13* (1), 36–44.
(35) Capuzzi, S. J.; Muratov, E. N.; Tropsha, A. *J. Chem. Inf. Model.* **2017**, *57* (3), 417–427.
(36) Baell, J. B. *J. Nat. Prod.* **2016**, *79* (3), 616–628.
(37) Dahlin, J. L.; Walters, M. A. *Assay Drug Dev. Technol.* **2016**, *14* (3), 168–174.
(38) http://www.enzolifesciences.com/BML-AK111/biomol-green/ (last accessed 18th March **2018**).
(39) Webb, M. R. *Proc. Natl. Acad. Sci. U. S. A.* **1992**, *89* (11), 4884–4887.
(40) De Cesco, S.; Kurian, J.; Dufresne, C.; Mittermaier, A. K.; Moitessier, N. *Eur. J. Med. Chem.* **2017**, *138*, 96–114.
(41) Albert, A. H.; O'Brien, D. E.; Robins, R. K. *J. Heterocycl. Chem.* **1978**, *15* (4), 529–536.
(42) Faust, J.; Mayer, R. *J. f. Prakt. Chemie* **1976**, *318* (1), 161–167.
(43) Kharul, R. K.; Prajapati, P. N.; Thorave, A. A.; Shah, H. A.; Dhar, A.; Joshi, D. A.; Jain, M. R.; Patel, P. R.; Pancholi, S. S. *Synth. Commun.* **2011**, *41* (22), 3265–3279.
(44) Beard, R. L.; Liu, X.; Donello, J. E.; Viswanath, V. Benzoisothiazol-3(1H)-one-5-sulfonyl Derivatives as Chemokine Receptor Modulators. PCT/US2012/068873, **2012**.
(45) Lawrenson, A. Peronsal Communication. **2014** .
(46) Schrödinger, L. *PyMOL Molecular Graphics, Version~1.8*; **2015**.
(47) Liu, D.; Tian, Z.; Yan, Z.; Wu, L.; Ma, Y.; Wang, Q.; Liu, W.; Zhou, H.; Yang, C. *Bioorganic Med. Chem.* **2013**, *21* (11), 2960–2967.
(48) Berry, N. G. Personal Communication. **2015**.
(49) Lai, H.; Dou, D.; Aravapalli, S.; Teramoto, T.; Lushington, G. H.; Mwania, T. M.; Alliston, K. R.; Eichhorn, D. M.; Padmanabhan, R.; Groutas, W. C. *Bioorg Med Chem* **2013**, *21* (1), 102–113.
(50) Lowe, D. Selenium In a Drug Structure: Why Not?
(51) Wiles, J. A.; Phadke, A. S.; Bradbury, B. J.; Pucci, M. J.; Thanassi, J. A.; Deshpande, M. *J. Med. Chem.* **2011**, *54* (9), 3418–3425.
(52) Nogueira, C. W.; Zeni, G.; Rocha, J. B. T. *Chem. Rev.* **2004**, *104* (12), 6255–6285.
(53) Ivanenkov, Y. A.; Veselov, M. S.; Rezekin, I. G.; Skvortsov, D. A.; Sandulenko, Y. B.; Polyakova, M. V.; Bezrukov, D. S.; Vasilevsky, S. V.; Kukushkin, M. E.; Moiseeva, A. A.; Finko, A. V.; Koteliansky, V. E.; Klyachko, N. L.; Filatova, L. A.; Beloglazkina, E. K.; Zyk, N. V.; Majouga, A. G. *Bioorganic Med. Chem.* **2016**, *24* (4), 802–811.
(54) Garud, D. R.; Koketsu, M.; Ishihara, H. *Molecules* **2007**, *12* (3), 504–535.
(55) Mugesh, G.; Du Mont, W. W.; Sies, H. *Chem. Rev.* **2001**, *101* (7), 2125–2179.
(56) Mukherjee, S.; Weiner, W. S.; Schroeder, C. E.; Simpson, D. S.; Hanson, A. M.; Sweeney, N. L.; Marvin, R. K.; Ndjomou, J.; Kolli, R.; Isailovic, D.; Schoenen, F. J.; Frick, D. N. *ACS Chem. Biol.*

2014, *9* (10), 2393–2403.
(57) Maruyama, I.; Abeyama, K.; Masayasu, H. Preventive or Therapeutic Drug for Alzheimer's Disease. US5948800 A, 1999.
(58) Yamaguchi, T.; Sano, K.; Takakura, K.; Saito, I.; Shinohara, Y.; Asano, T.; Yasuhara, H. *Stroke* **1998**, *29* (1), 12–17.
(59) Singh, N.; Sharpley, A. L.; Emir, U. E.; Masaki, C.; Herzallah, M. M.; Gluck, M. A.; Sharp, T.; Harmer, C. J.; Vasudevan, S. R.; Cowen, P. J.; Churchill, G. C. *Neuropsychopharmacology* **2016**, *41* (7), 1768–1778.
(60) Kil, J.; Pierce, C.; Tran, H.; Gu, R.; Lynch, E. D. *Hear. Res.* **2007**, *226* (1–2), 44–51.
(61) Prevention and Treatment of Chemotherapy Induced Hearing Loss. Can be found at Https://clinicaltrials.gov/show/NCT01451853. SPI-1005 Prevention and Treatment of Chemotherapy Induced Hearing Loss (Accessed 4th September **2017**)
(62) Madhunapantula, S. V; Desai, D.; Sharma, A.; Huh, S. J.; Amin, S.; Robertson, G. P. **2008**, *7* (May), 1297–1308.
(63) Zhang, L.; Zhou, L.; Du, J.; Li, M.; Qian, C.; Cheng, Y.; Peng, Y.; Xie, J.; Wang, D. *Biomed Res. Int.* **2014**, *2014*.
(64) Thangamani, S.; Younis, W.; Seleem, M. N. *Sci. Rep.* **2015**, *5*, 11596.
(65) Moore, J. L.; Taylor, S. M.; Soloshonok, V. A. *Arkivoc* **2005**, *2005* (vi), 287–292.
(66) Miyaura, N.; Yamada, K.; Suzuki, A. *Tetrahedron Lett.* **1979**, *20* (36), 3437–3440.
(67) Kinney, W. A.; Lee, N. E.; Blank, R. M.; Demerson, C. A.; Sarnella, C. S.; Scherer, N. T.; Mir, G. N.; Borella, L. E.; Dijoseph, J. F.; Wells, C. *J. Med. Chem.* **1990**, *33* (1), 327–336.
(68) Nakahira, H.; Ikuma, Y.; Fukuda, N.; Kobayashi, T.; Tozaki, S. Preparation of amide compounds as renin inhibitors. JP 2010037276, **2008**.
(69) He, J.; Li, D.; Xiong, K.; Ge, Y.; Jin, H.; Zhang, G.; Hong, M.; Tian, Y.; Yin, J.; Zeng, H. *Bioorganic Med. Chem.* **2012**, *20* (12), 3816–3827.
(70) Pietka-Ottlik, M.; Wojtowicz-Mlochowska, H.; Kolodziejczyk, K.; Piasecki, E.; Mlochowski, J. *Chem. Pharm. Bull. (Tokyo).* **2008**, *56* (10), 1423–1427.
(71) Yang, X.; Wang, Q.; Tao, Y.; Xu, H. *J. Chem. Res.* **2002**, No. 1, 160–161.
(72) Krief, A.; Derock, M. *Tetrahedron Lett.* **2002**, *43* (16), 3083–3086.
(73) Balkrishna, S. J.; Bhakuni, B. S.; Kumar, S. *Tetrahedron* **2011**, *67* (49), 9565–9575.
(74) Bhabak, K. P.; Mugesh, G. *Acc. Chem. Res.* **2010**, *43* (11), 1408–1419.
(75) Berry, N. G. Personal Communication. **2013**.
(76) Yamamoto, T.; Hori, M.; Watanabe, I.; Harada, K.; Ikeda, S.; Ohtaka, H. *Chem. Pharm. Bull. (Tokyo).* **2000**, *48* (6), 843–849.
(77) Carpino, L. A.; Imazumi, H.; Foxman, B. M.; Vela, Mi. J.; Henklein, P.; El-Faham, A.; Klose, J.; Bienert, M. *Org. Lett.* **2000**, *2* (15), 2253–2256.
(78) Dolomanov, O. V; Bourhis, L. J.; Gildea, R. J.; Howard, J. A. K.; Puschmann, H. *J. Appl. Crystallogr.* **2009**, *42* (2), 339–341.

Appendix 1

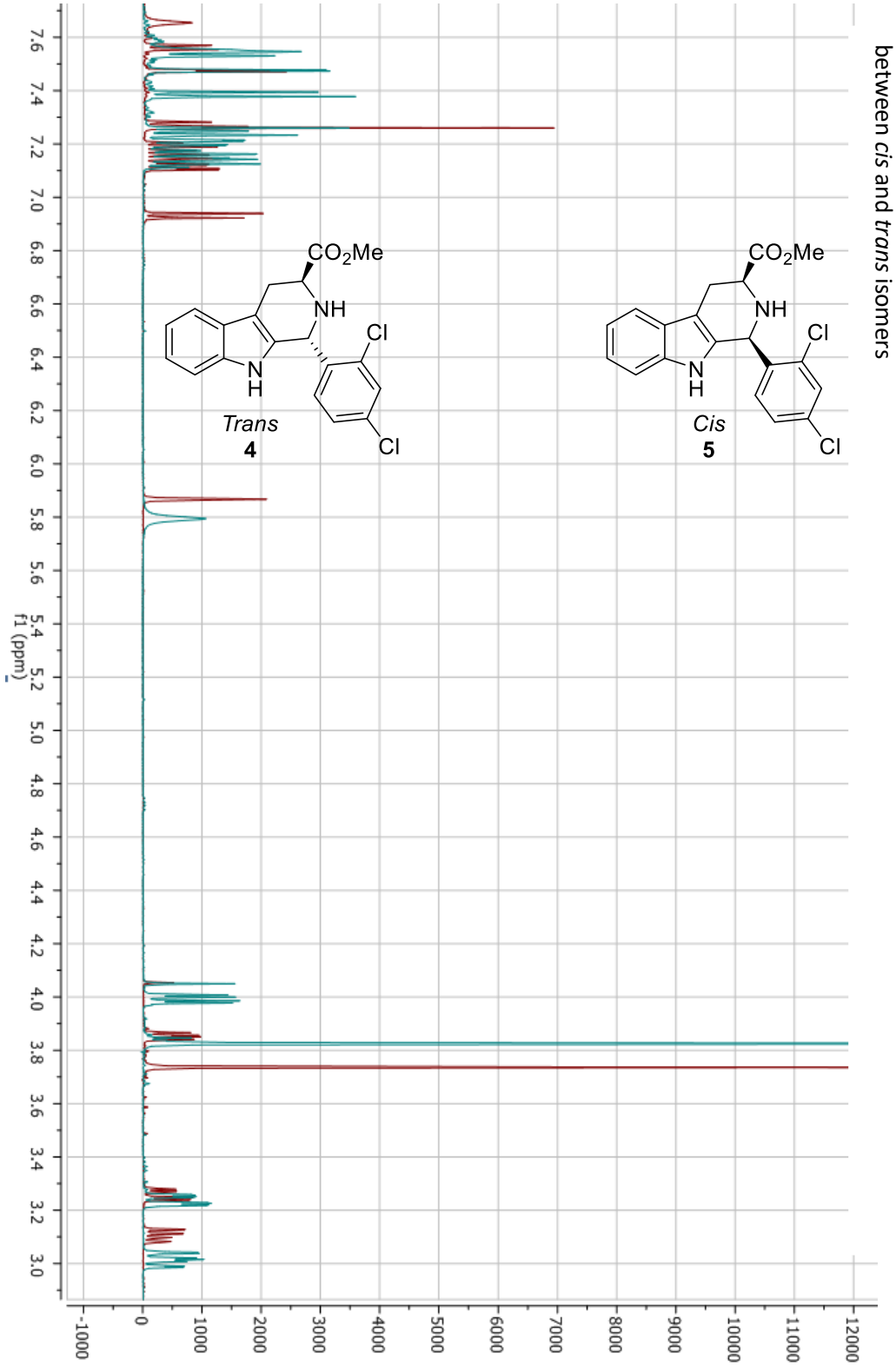

^{1}H spectra overlay of compound **4** (*trans*, red) and **5** (*cis* blue) isomers, demonstrating separate chemical shifts between *cis* and *trans* isomers

Appendix 1

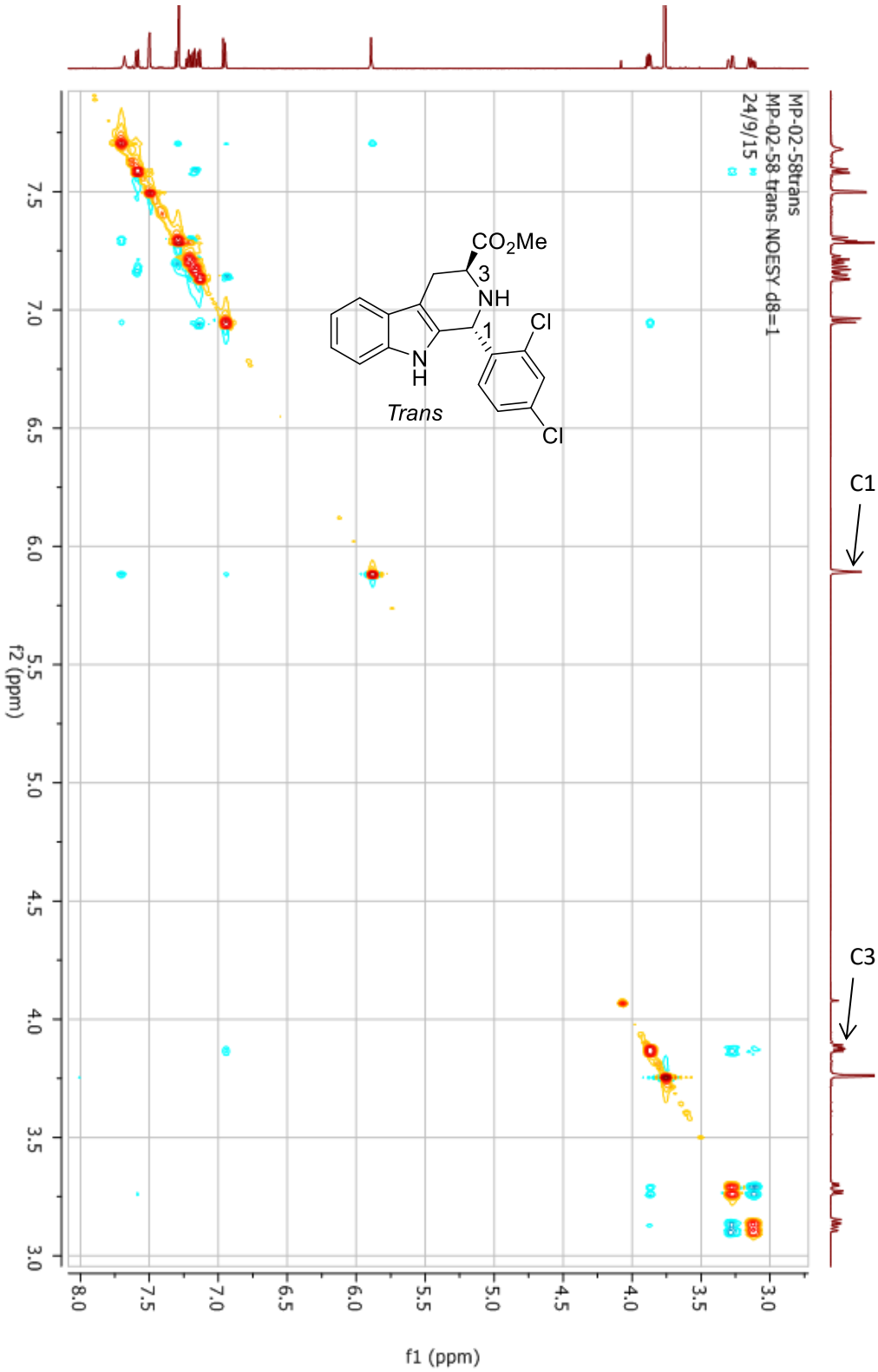

Generic appearance of NOESY NMR of *trans* isomer (compound **4** displayed as representative structure), no correlation of C1 and C3 protons confirms structure. Note NOESY mixing time (d8) = 1 second

Appendix 1

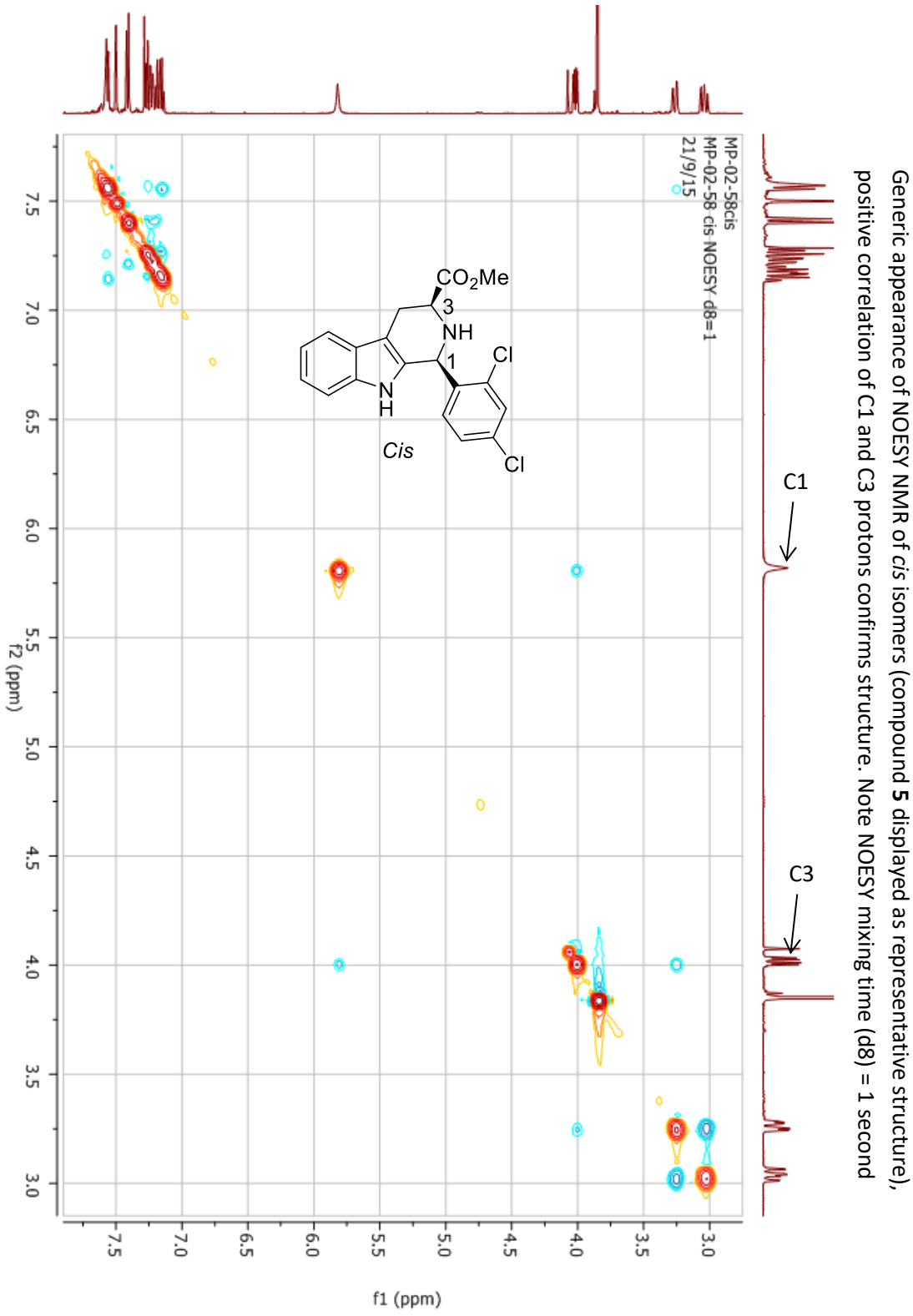

Generic appearance of NOESY NMR of *cis* isomers (compound **5** displayed as representative structure), positive correlation of C1 and C3 protons confirms structure. Note NOESY mixing time (d8) = 1 second

Appendix 2

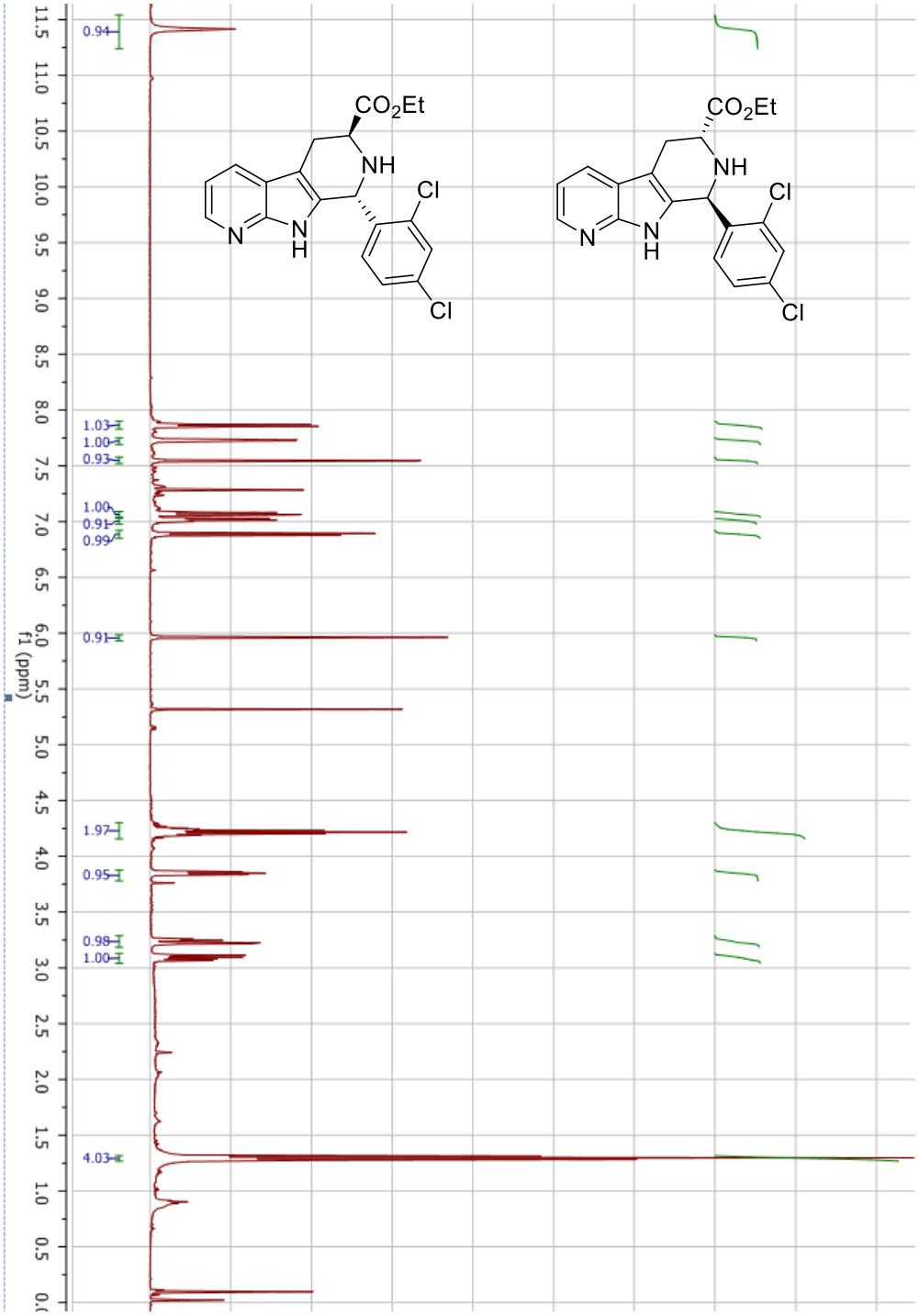

^{1}H NMR of racemised ethyl ester derivative of compound **71**

Appendix 2

NOESY NMR of racemised ethyl ester derivative of compound **71**, confirming *trans* isomer

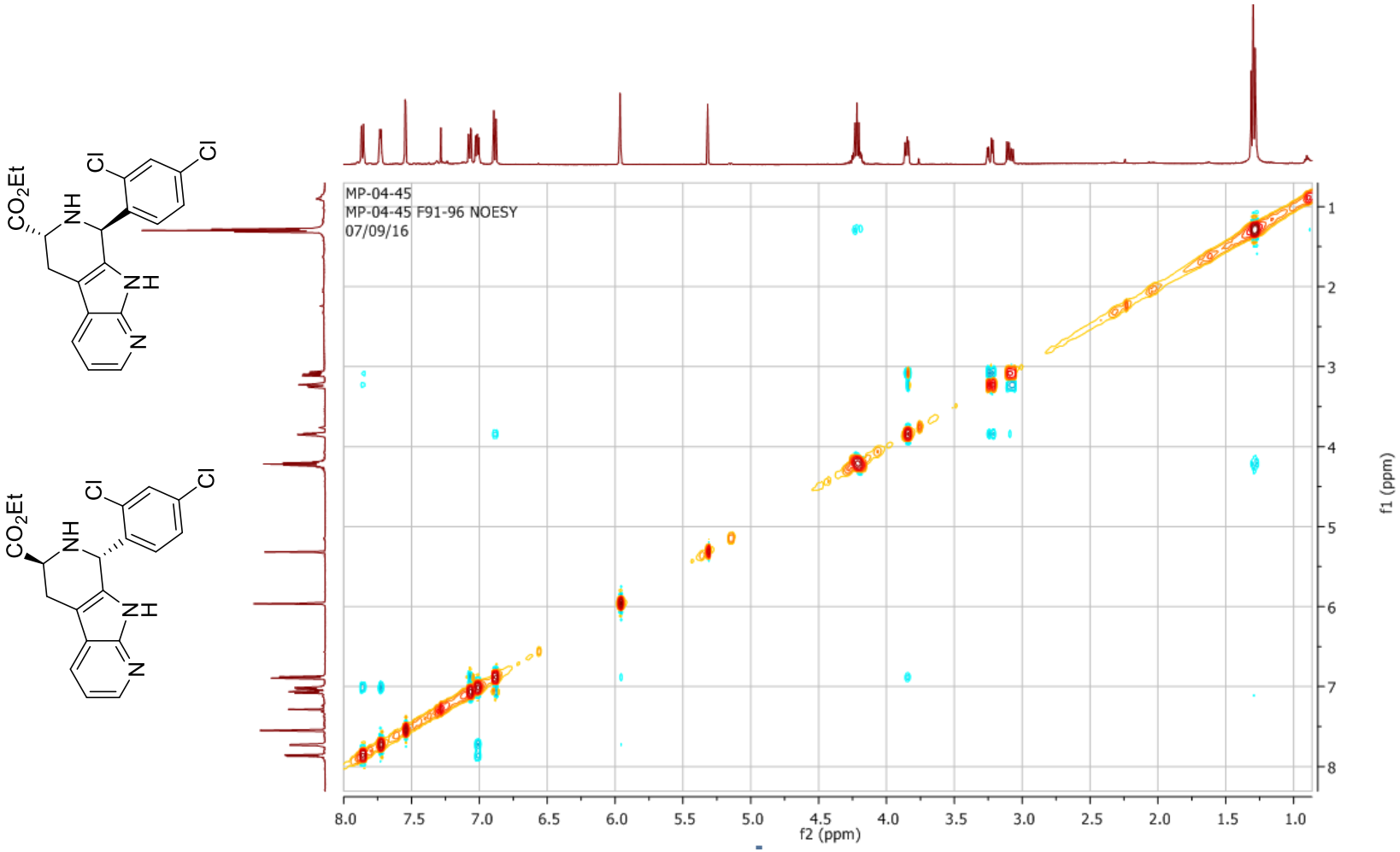

Appendix 2

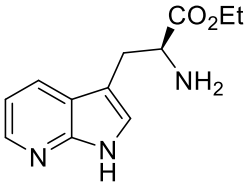

HPLC traces of ethyl ester derivative of compound **70** as chirally pure starting material (top), followed by ethyl ester derivative of **71** showing racemisation from Pictet-Spengler reaction.